PATRICK ANDRIEUX

APPLICATION OF ROCK ENGINEERING SYSTEMS TO LARGE-SCALE CONFINED DESTRESS BLASTS IN UNDERGROUND MINE PILLARS

Thèse présentée
à la Faculté des études supérieures de l'Université Laval
dans le cadre du programme de doctorat en Génie minier
pour l'obtention du grade de Philosophiæ Doctor (Ph.D.)

DÉPARTEMENT DE GÉNIE DES MINES, DE LA MÉTALLURGIE ET DES MATÉRIAUX
FACULTÉ DES SCIENCES ET DE GÉNIE
UNIVERSITÉ LAVAL
QUÉBEC

2005

RÉSUMÉ

Cette thèse décrit le développement d'une nouvelle méthodologie qui quantifie les chances de succès d'un tir confiné à grande échelle de relâchement des contraintes dans un pilier de mine souterraine, pour une masse rocheuse et un régime de contraintes donnés.

L'approche est basée sur huit paramètres qui sont considérés comme contrôlant ultimement le processus, et dont l'influence et les interactions ont été quantifiées dans un premier temps avec la méthode des Systèmes d'ingénierie du roc ("Rock Engineering Systems"). Ces interactions et degrés d'influence ont ensuite été utilisés pour élaborer la nouvelle méthodologie, qui est basée sur un nouveau paramètre appelé l'Indice de relâchement, qui peut être 'Faible', 'Moyen', 'Bon' ou 'Excellent'.

Il est conclu que cette méthodologie a une valeur pratique élevée de par sa capacité à concevoir adéquatement un tir confiné à grande échelle de relâchement des contraintes dans un pilier de mine, en prenant simplement des mesures qui résultent en une augmentation de l'Indice de relâchement et, donc, des chances de succès du tir.

SOMMAIRE

L'objectif de cette thèse était de développer une nouvelle méthodologie pour quantifier les chances de succès d'un tir confiné à grande échelle de relâchement des contraintes dans un pilier de mine souterraine, pour une masse rocheuse et un régime de contraintes donnés. Huit paramètres ont été retenus comme contrôlant ultimement le processus, les quatre premiers considérant le massif rocheux et les quatre autres divers aspects du sautage. Étant donné la quantité limitée de travaux accomplis dans ce domaine, il a été nécessaire de déterminer en premier lieu comment et dans quelle mesure ces paramètres interactent, et lesquels dominent le processus. L'approche des Systèmes d'ingénierie du roc ("Rock Engineering Systems", ou RES), une technique matricielle qui permet de quantifier systématiquement l'interaction entre chaque paire de paramètres identifiés comme jouant un rôle dans un processus d'ingénierie, a été utilisée pour aborder cette question. Ces interactions et degrés d'influence ont ensuite été appliqués à l'élaboration de la nouvelle méthodologie, basée sur un nouveau paramètre appelé l'Indice de relâchement.

Cette approche consiste à quantifier dans un premier temps la mesure dans laquelle chacun des huit paramètres est favorable à la réussite d'un tir de relâchement des contraintes. Basé sur un éventail de seuils développé dans ces travaux, un simple indice de 0 (non favorable), 1 (relativement favorable) ou 2 (favorable) est assigné, qui est ensuite multiplié par l'influence qu'a le paramètre sur l'ensemble du système, telle que quantifiée par la méthode des RES. Cela donne un score pour chaque paramètre. Les scores de tous les paramètres sont ensuite additionnés, puis divisés par le score total maximum possible, ce qui donne un score total normalisé à partir duquel un Indice de relâchement de 'Faible', 'Moyen', 'Bon' ou 'Excellent' est obtenu. La rétro-analyse de deux récentes études de cas bien documentées a démontré que cette approche est valide et peut indiquer de manière fiable si une situation de hautes contraintes est susceptible d'être relaxée efficacement par un tir

confiné à grande échelle de relâchement des contraintes, et, le cas échéant, si la conception du tir est adéquate à cette fin.

Il est conclu que cette méthodologie a une valeur pratique élevée de par sa capacité à concevoir adéquatement un tir confiné à grande échelle de relâchement des contraintes dans un pilier de mine, en prenant simplement des mesures qui résultent en une augmentation de l'Indice de relâchement et, donc, des chances de succès du tir. Ces mesures n'incluent pas seulement l'optimisation des paramètres de tir, mais également le choix du moment propice auquel le tir devrait être tenté. Des modifications successives peuvent être apportées et l'Indice de relâchement réévalué, ce qui permet au design d'être éventuellement optimisé, de manière itérative.

SUMMARY

The objective of this thesis was to develop a novel methodology to quantify the likelihood of a large-scale confined destress blast in an underground mine pillar being successful, for a given rock mass condition and stress regime. Eight parameters were argued to ultimately control the process, the first four being related to the rock in which the destress blast is attempted, the last four to blasting issues. Given the limited amount of background work completed in this field, it was necessary to first determine how and to which extent these parameters interact, and which ones dominate the process. The Rock Engineering Systems (RES) approach, a matrix-based technique that allows to quantify in a systematic manner the interaction between each pair of parameters known to play a role in an engineering process, was applied to address this issue. These interactions and degrees of influence were then applied to derive the new methodology, based upon a new parameter named the "Destressability Index".

The Destressability Index approach consists in first quantifying how conducive each of the eight parameters is to a successful choked destress blast. Based upon thresholds developed in this work, a simple rating of 0 (not conducive), 1 (somewhat conducive) or 2 (conducive) is first assigned, which is then multiplied by the influence of the parameter on the whole system, as quantified with the RES methodology. This provides a score for each parameter. The scores from all the parameters are then added and divided by the maximum possible total arithmetical score in order to produce a normalised total score from which a 'Low', 'Medium', 'Good', or 'Excellent' Destressability Index can be obtained. The back-analysis of two recent well-documented case studies have demonstrated that this approach is sound and can reliably indicate whether a high stress situation is conducive to being destressed by means of a large-scale confined destress blast, and, if so, whether the blast design itself is appropriate to achieve this goal.

It is argued that this methodology has a high practical value by allowing one to adequately design a large-scale confined panel destress blast by simply taking steps that result in an increase in the Destressability Index and, hence, in the chance of success. Such steps include not only optimising the blasting parameters, but also choosing when in the mining sequence the blast should be implemented. Successive changes can be proposed and the Destressability Index re-assessed, which allows the design to be eventually optimised in an iterative manner.

ACKNOWLEDGEMENTS

A number of individuals and organisations must be thanked for the support they generously provided throughout the completion of this work. First and foremost, the guidance and support offered by Professor John Hadjigeorgiou must be acknowledged. He made it possible for the author to pursue doctorate studies on a part-time basis while working full-time on demanding jobs at Brunswick Mine in Bathurst, then at Itasca Consulting Canada, Inc. in Sudbury. Many thanks, John, for a wisely established progress strategy, well-planned milestones, your patient guidance and the countless suggestions you provided over the six years it took to complete this work. The help of Professor Jacek Paraszczak with many of the administrative issues has also greatly facilitated this project, and is thankfully acknowledged.

Invaluable technical discussions were held during the preparation of this thesis with a number of outstanding engineers who provided much appreciated input, suggestions and help. Among them are, alphabetically, Dr. Richard Brummer, Professor John Hadjigeorgiou, Dr. Qian (Ken) Liu, Mrs. Anneta Sampson-Forsythe, Mr. Brad Simser and Dr. Graham Swan. The feedback provided by Professor John Hudson of Imperial College on the application of the Rock Engineering Systems methodology to large-scale confined panel destress blasts is also greatly appreciated.

Thanks must also be directed at Noranda, Inc., Falconbridge, Ltd. and Itasca Consulting Canada, Inc. More specifically to the Brunswick Mine management for their support during the early stages of this project – in this note, the author feels particularly indebted to Mr. Jean Desrosiers, Mr. Bill Rogers and Mr. Glen Crowther. Many thanks also to the Fraser Mine management for allowing unpublished data from the December 2001 destress blast in the A5-Right pillar to be used in a case history in this thesis. The support and

encouragement of the Itasca Consulting Canada, Inc. management during the redaction of this thesis is also gracefully acknowledged.

Finally, the author would like to express his appreciation to Dr. Cameron McKenzie, Dr. John Heilig and Mr. David Sprott who made him realise during field work campaigns in the early 1990's how much enjoyment rock engineering can provide. Last but not least, the author is grateful to his family for putting up with the great deal of supplemental work the completion of this degree has meant.

Sunday 6 March 2005
Sudbury, Ontario, Canada.

TABLE OF CONTENTS

LIST OF FIGURES

Page

LIST OF TABLES

Page

LIST OF FORMULAE AND EQUATIONS

LIST OF SYMBOLS

a	Intercept of the Gutenberg-Richter plot
a	Exponent of the generalised Hoek-Brown failure criterion
A	Rock Stress Factor, or area
ABS	Absolute Bulk Strength of an explosive product
A_i	Activity Index
AWS	Absolute Weight Strength of an explosive product
b	Slope of the Gutenberg-Richter plot
B	Burden in front of a blasthole
B_1	Rock mass brittleness index
B_I, B_{II}	Fragility ratings of an intact rock sample
B_{er}	Burst Efficiency Ratio
BIM	Brittleness Index Modified
BPR	Bursting Potential Ratio
β	Attenuation factor in the USBM blast-induced vibration scaling relationship
c	Cohesion, or cohesive strength
C	Unloaded length at the collar of a blasthole
d	Diameter of an explosive charge
D	Diameter of a blasthole
d_f	Dimension of a fractal distribution
D_f	Similarity dimension (of a self-similar fractal distribution)
D_{mi}	Decrease Modulus Index
δ	Displacement, or infinitesimally small variation (of a quantity)
Δ	(Large) variation (of a quantity)
Δ*A*i	Transformation area of a given rock mass subjected to a given

blast design, for the purpose of assessing its blastability

$\Delta\sigma$ Stress drop associated with a seismic event

E Young's modulus (also called the elastic modulus), or energy

Ea Average seismic energy liberated by a seismic event of a given seismic moment Mo

E_c Energy available in one explosive charge

E_d Static energy dissipated by the failure of a pillar

E_D Energy dissipated in the Bursting Liability Index test

EI Energy Index of a seismic event

E_p Potential energy that must be dissipated by a system at failure

Ep Net change in potential energy in the system after a destress blast

E_R Elastic energy recovered in the Bursting Liability Index test

ERP Evaluation of Rockburst Potential

ERR Energy Release Rate

Es Seismic energy liberated by a seismic event

ESQ Expert Semi-Quantitative (matrix coding) method

ESS Excess Shear Stress on a fault (also referred to as τ_e)

Ex Explosive energy used to push back the pillar walls during a large destress blast

E'_m Post-peak stiffness of the encasing rock mass

ε Strain

ε_r Axial deformation at failure of a sample subjected to a uniaxial compressive test

ϕ Friction angle

ϕ_0 Maximum energy stored inside a sample during the loading phase of a uniaxial compressive test

ϕ_1 Energy of the particles ejected at failure from a sample subjected to a uniaxial compressive test

G Rigidity of the rock mass (stiffness modulus)

GSI Geological Strength Index of a rock mass

H Height

H-B Hoek-Brown failure criterion

Ja Joint alteration number

Jn Joint set number

Jr Joint roughness number

Jv Volumetric joint count

Jw Joint water reduction factor

K Amplitude factor in the USBM blast-induced vibration scaling relationship

k_1 Ratio of $(\Delta\sigma_1 / \Delta\sigma_3)$

k_2 Ratio of $(\Delta\sigma_2 / \Delta\sigma_3)$

k_e Stiffness of a loading system

k'_{pr} Equivalent post-peak stiffness of a pillar

l Length of an explosive charge

L Length

m Hoek-Brown constant related to the degree of block interlocking in the rock

$m_{Laboratory}$, or m_i Value of the Hoek-Brown constant m at the

laboratory, or intact rock material scale

$m_{Rock\ Mass}$, or m_b Value of the Hoek-Brown constant m at the rock mass scale

M "Generic" magnitude of a seismic event (either Richter or Nuttli)

M_e External zone of influence of a destress blast

M_N Nuttli Magnitude of a seismic event

Mo Moment of a seismic event

M_R Richter Magnitude of a seismic event

M_T Total mass, or "effective" mass, targeted by a destress blast

M(r) Total number of seismic events within a counting sphere

μ_d Dynamic coefficient of friction

μ_s Static coefficient of friction

N Number of blasting rings in a destress blast

P_i Parameter i of a Rock Engineering System interaction matrix

Pn Clustering index (of seismic events)

PPV Peak Particle Velocity of a vibration

PTF_{Intact} Proximity To (static) Failure of an intact sample of rock

$PTF_{Rock\ Mass}$ Proximity To (static) Failure of a rock mass

Q Rock tunnelling Quality index

Q' Modified rock tunnelling Quality index

RBS Relative Bulk Strength of an explosive product

RES Rock Engineering Systems

RMR Rock Mass Rating

RQD Rock Quality Designation

RWS Relative Weight Strength of an explosive product

ρ_e Density of an explosive product

ρ_r Density of rock

s Hoek-Brown constant associated with the degree of fracturing of the rock

$s_{Laboratory}$ Value of the Hoek-Brown constant s at the scale of the intact rock material (always = 1.000)

$s_{Rock\ Mass}$ Value of the Hoek-Brown constant s at the scale of the rock mass

S Spacing between blastholes on the same row

S_f Self-similar fractal distribution

SRF Stress Reduction Factor

σ Stress

σ_1 Major principal stress component

σ_2 Intermediate principal stress component

σ_3 Minor principal stress component

σ'_1 Effective major principal stress component at failure

σ'_2 Effective intermediate principal stress component at failure

σ'_3 Effective minor principal stress component at failure

$\sigma_{1\ Actual}$ Mining-induced major principal stress component at a time of interest.

$\sigma_{2\ Actual}$ Mining-induced intermediate principal stress component at a time of interest

$\sigma_{3\ Actual}$ Mining-induced minor principal stress component at a time of interest

σ_a Apparent stress of a seismic event

σ_c Compressive strength (unconfined, or uniaxial) of the intact rock material (also sometimes referred to as σ_{ci})

σ_{ci} Compressive strength (unconfined, or uniaxial) of the intact rock material (more often referred to as σ_c)

σ_{cR} Unconfined (or uniaxial) compressive strength at the rock mass scale (same as $\sigma_{c\ Rock\ Mass}$)

$\sigma_{c\ Rock\ Mass}$ Unconfined (or uniaxial) compressive strength at the rock mass scale (same as σ_{cR})

σ_N Normal stress

σ_T Tensile strength (also sometimes referred to as T_o)

Σ Summation (of quantities)

T Unloaded length at the toe of a blasthole

T_o Tensile strength of the intact rock material

τ Shear stress

τ_d Dynamic shear stress on a fault

τ_e Excess shear stress on a fault (also referred to as ESS)

τ_s Static shear strength of a fault

U_c Stored static strain energy increase in the remaining (un-mined) rock, after mining

U_C Increase in strain energy in the surrounding rock after a destress blast

UCS Unconfined Compressive Strength, or Uniaxial Compressive Strength (also referred to as σ_c or σ_{cR}, depending upon the scale considered)

Ue Excess energy

U_f Energy consumed in fracturing the rock mass (either naturally, around an excavation, and/or artificially, by blasting)

Um Strain energy that was stored in material that has been mined (removed)

Um_1 Strain energy stored in a system before a destress blast

Um^1 Strain energy originally stored in the failed rock material around an excavation

Um_2 Strain energy stored in a system after a destress blast

Ur Energy released by the excavation of a void in rock

Us Energy consumed by the ground support system

Uv Vibrational energy released at failure in a rock mass in the case of a rapid excavation

V Volume, or source volume of a seismic event

Va Apparent volume of a seismic event

VOD Velocity Of Detonation of an explosive product

Vp Velocity of propagation of P (compressive) seismic waves

Vs Velocity of propagation of S (shear) seismic waves

υ Poisson's ratio

W Width

W_{et} Bursting Liability Index

Wk Dynamic (seismic) energy released by the mining process

W_K Dynamic (seismic) energy that vibrates the rock mass after a destress blast

Wr Energy released, or dissipated, in the mining process

Wt Change in potential energy of the system as a result of mining

W_T Change in the potential energy of a system from before and after a destress blast

CHAPTER I

1. INTRODUCTION

Few mine discoveries in Canada nowadays involve large high-grade ore bodies located at shallow depths, as, over the past few years, many of the significant projects in terms of size and grades have been located at great depth. This has certainly been the case for the Falconbridge Kidd Mine D and Onaping Deep Project, as well as for the Agnico-Eagle Laronde Deep Project, amongst others. The technical risks associated with mining at great depth, combined with the costs involved, are significant for most of these projects, which also sometimes compete for capital funding with much larger and shallower deposits located in countries where they can be mined at a much lower cost. Furthermore, an increasing number of underground mines still in operation in Canada are pushing operations at depths in excess of 2,000 metres, as is the case for some of the Sudbury Basin nickel mines, for example. In many instances, these ageing deep mines are also extracting sill pillars and other difficult regions – the resulting combination of high in situ stress levels, high extraction ratios and "tired" ground can become insurmountable for some of them.

If the Canadian underground hard rock mining industry is to succeed in the twenty-first Century and compete with countries with huge near-surface deposits and cheaper labour, the problems related with mining hard rock at great depth need to be resolved. Indeed, if the associated risks and uncertainties could be reduced, and the difficulties surmounted, the

high grades associated with some of the deep projects in Canada would make them much more attractive than they currently are. Mining at depth typically results in additional costs due to the longer rate of return of the initial investment, the extra development required to reach the ore, the logistics of bringing air, workers and materials down to the work faces and ore back to surface, and the difficult ground conditions that are typically encountered, amongst others.

Some of the major challenges associated with mining at depth – and also often with mining under high extraction ratios – are related to the resulting high levels of ground stress. This, in turn, can lead to the failure and collapse of the rock mass that surrounds the excavations. This failure can either be progressive, or sudden and violent. The latter case probably represents the highest degree of difficulty in terms of underground personnel exposure, erratic and unpredictable production, ground rehabilitation requirements (which displace resources, cause delays and bring about additional costs), possible reserve losses, and overall mining costs.

There are a number of proactive measures that can be implemented to alleviate the problems associated with mining under high stress levels. As discussed in Andrieux & Simser (2001) the mining method can be modified (to a pillarless procedure, for example, or a non-entry approach); the mining sequence can be altered in order to avoid pinching stress in shrinking pillars; alternative ground support systems better adapted to the expected conditions can be used; and, destressing techniques can be attempted. Reactive measures can also be implemented, essentially in the form of modifications to the ground support system already installed, and destressing attempts.

This thesis concentrates on the destressing option – either proactive or reactive – and, in particular, on large-scale confined destress blasts in underground mine pillars. The work described in this document attempts to contribute to the development of a rational destress blasting approach that will be both accessible and useful to practitioners such as site engineers, technologists and consultants.

As it will be demonstrated through the review of numerous case studies, there are currently no well-established guidelines to 1) decide at which point a large-scale confined destress blast should be attempted in an underground mine pillar; and, 2) design such a blast taking into consideration rock mechanics *and* blasting issues. In general, a trial and error approach is used, with the best "recipe" at a given site being retained as the standard for subsequent blasts. Furthermore, it should be pointed out that it is difficult to quantitatively assess the results of a confined destress blast in a large pillar – results are usually described in a highly qualitative manner.

An important aspect of this thesis is the application of the relatively new Rock Engineering Systems (RES) approach (Hudson, 1992) to the issue of large-scale confined destress blasting in large underground pillars. The RES methodology uses a matrix-based technique to quantify in a systematic manner the interaction between each pair of parameters known to play a role in a given engineering process. The RES technique is used in this thesis to weigh the individual influence of a series of parameters that are argued to have a significant impact on the destress blasting process. This weighing is then used to derive a methodology to assess the likelihood of a given destress blast design – implemented in a given rock mass subjected to a given stress regime – being successful. This methodology is based upon a new parameter called the "Destressability Index".

The overall Destressability Index approach developed in this work can be summarised as follows. A calculated value is assigned to the property associated with each of the eight governing parameters chosen for the large-scale choked pillar destressing RES interaction matrix. Each value is compared to various thresholds, in order to assess how conducive it is to a successful choked destress blast – a simple rating of 0 (not conducive), 1 (somewhat conducive) or 2 (conducive) is assigned. For each parameter this 0, 1 or 2 rating is then multiplied by its cause (which represents its influence on the whole system, as identified with the RES methodology) in order to provide a measure of how favourable it is to a successful destress blast. This provides a score for each parameter. All the scores are then added and divided by the maximum possible arithmetical score in order to produce a

normalised total score from which the Destressability Index can be obtained, which can land in one of four categories: 'Low', 'Medium', 'Good', or 'Excellent'.

As mentioned, a total of eight parameters will be considered in the Destressability Index approach, the rationale for this being discussed in detail in the thesis. The first two parameters, related to the rock in which the destress blast is attempted, are the stiffness and the brittleness. These can conceivably be considered either at the intact rock material scale, or at that of the rock mass. The first approach is intrinsically simpler because both parameters can then be represented by properties that are somewhat easily derived in the laboratory – it however needs to be adjusted for the fact that it is the rock mass properties that are ultimately pertinent in the case of a large-scale destress blast. The second approach is more complicated because both parameters must then be represented by properties either extrapolated to, or measured directly at, the rock mass scale – its main advantage however resides in the scientific relevance of this larger scale to the problem at hand. Because the simplicity associated with the first approach might be more conducive to a routine usage, it will be assessed along with the second one, and tested against documented case studies.

The third parameter considered in the methodology is the degree of fracturing of the rock mass. This parameter, also rock-related, needs to be treated differently depending upon the scale at which it is considered. At the rock mass scale the weakening effect of the geological structures is already accounted for to a certain extent in the other rock-related parameters. As a result, the degree of fracturing is not required to downgrade the mechanical properties as much as at the intact rock material scale. The fourth parameter, the last rock-related one, considers how close the rock (prior to destressing) is to static failure due to the stress regime it is subjected to (as determined either analytically or numerically). This parameter as well needs to be treated differently depending upon whether the intact rock material or the rock mass scale is considered.

Parameters five to eight are related to the proposed destress blast design and consider: the orientation of the blast with regard to the major principal stress component (argued to be

the driving component); the width of the destress blast; the explosive energy per tonne of targeted rock mass; and, the confinement of the explosive charges, respectively.

Two recent well-documented and comprehensively-instrumented case studies are provided to demonstrate that the Destressability Index methodology is sound at both the intact rock material and the rock mass scales, and that it can indicate whether a given high stress situation is conducive to being destressed by means of a large-scale confined destress blast, and, if so, whether the blast design itself is appropriate to achieve this goal. Based upon the back-analysis of these two case histories, the approach that considers the rock parameters at the rock mass scale is eventually retained.

The proposed procedure is not a direct design methodology, but rather an assessment of the likelihood of success of a proposed design in a given situation. Although one cannot modify the intrinsic rock parameters, one can choose to a certain extent the stress state that will prevail at the time of the destress blast (by choosing the step in the mining sequence at which the destress blast will be implemented) and alter the blasting parameters in order to increase the Destressability Index and, hence, the chance of success. The blast parameters can be modified a number of times and the Destressability Index re-assessed, which allows the design to eventually become optimised, in an iterative manner. It is therefore argued that the proposed approach has a high practical value as it can allow one to properly design a large-scale confined panel destress blast simply by taking steps that result in an increase in the Destressability Index. A particular appeal of this approach is that it provides a series of easily implemented steps, based upon readily available input data, that result is a rational assessment of the chance of success of a given destress blast design in a given situation of rock mass conditions and stress regime.

A rather wide array of topics are discussed in this work. In a first step, ground stress considerations are presented due to their importance in the topic at hand. Following this, the geomechanical conditions associated with violent rock mass failure are examined. The various types of rockbursts are then reviewed. The methods most commonly used to assess the bursting potential of a rock mass are presented (with the details given in appendix) –

these methods are deemed important within the framework of this work because they allow one to gauge to a certain extent how necessary it is to take action at a given time. Possible measures to alleviate violent rock mass failure are then discussed, which include destress blasting in underground mine pillars, as well as means of reporting the relevant data.

The second main body of this thesis starts with a description of the various confined destress blast design philosophies. A review of the various blasting engineering methodologies currently used is presented next, which shows that none is at present ideal to describe large-scale confined destress blasts. Rock Engineering Systems are then introduced, followed by a discussion on their potential application to blasting at large, and destress blasting in particular. The development of the two interaction matrices that describe the large-scale confined destress blasting process (one at the intact rock material scale and one at the rock mass scale) is then described in detail. Some blasting mechanics considerations are addressed in this part of the thesis because of their influence on how large-scale choked blasts work. The thinking process behind the development of the Destressability Index is then presented in detail, as well as two recent case studies with which the author was heavily involved. A general conclusion follows, in which guidelines for future work are suggested.

CHAPTER II

2. VIOLENT ROCK FAILURE CONSIDERATIONS

SOMMAIRE DU CHAPITRE. Avant d'adresser les tirs de relâchement des contraintes, il est nécessaire de décrire les conditions qu'ils sont destinés à combattre. Cela est fait dans ce chapitre qui commence par l'examen des diverses conditions géomécaniques associées à la rupture violente du roc. Trois aspects contrôlent essentiellement ce type de rupture, qui sont les niveaux de contraintes, les propriétés du roc et les caractéristiques du système de chargement. Ces aspects sont définis, décrits et discutés dans la première partie de ce chapitre. Des considérations énergétiques sont également présentées qui donnent un aperçu supplémentaire de la mesure dans laquelle ces facteurs contrôlent la rupture violente du roc.

Une fois établies les conditions géomécaniques associées à la rupture violente du roc, les divers types de ce genre de rupture sont décrits, qui sont les coups de terrain de déformation ("strain rockbursts"), de pilier ("pillar rockbursts") et de glissement ("fault-slip rockbursts"). Diverses méthodologies d'évaluation du potentiel de coup de terrain sont ensuite présentées, leurs détails étant donnés aux annexes A (à l'échelle du roc intact) et B (à l'échelle du massif). Il est jugé important dans le contexte de cette thèse de présenter des mesures de reconnaissance de ce potentiel afin de pouvoir correctement identifier les situations où des tirs de relâchement des contraintes pourraient s'avérer utiles.

L'étendue de la manipulation des diverses conditions géomécaniques susceptible de réduire les risques de coup de toit est ensuite discutée. Certaines approches sont de nature stratégique et regroupent des mesures telles qu'un changement de méthode de minage ou de séquence d'extraction. D'autres approches sont de nature tactique et concernent des mesures telles que le renforcement du système de support artificiel ou le tir de sautages de relaxation des contraintes ou de préconditionnement.

CHAPTER SUMMARY. Prior to discussing destress blasting, there is a need to describe the conditions that it is meant to alleviate – this is done in this chapter, which first reviews the various geomechanics conditions associated with the occurrence of violent rock failure. There are three aspects that essentially control this occurrence, which are stress levels, rock properties and loading system characteristics. These are defined, described and discussed in the first part of this chapter. Energy-based considerations are also provided that offer additional insight into how these factors control the violent failure of rock.

Once the geomechanical conditions associated with the occurrence of violent rock failure are established, the various types of such failure are described, which are strain rockbursts, pillar rockbursts and fault-slip rockbursts. Methodologies to assess the bursting potential of rock are then provided, with their details given in appendices A (at the intact rock material scale) and B (at the rock mass scale). It is deemed important within the context of this thesis to provide the ability to recognise this bursting potential in order to properly identify situations that may warrant destress blasting.

The extent to which the various geomechanical conditions identified can be manipulated in order to alleviate the risk of violent rock failure are then discussed. Some approaches are strategic by nature and involve such steps as altering the mining method and/or sequence, whereas some are more tactical, and involve measures such as supplemental ground support and destress blasts.

2.1. STRESS ISSUES

Ground stresses are an essential component of rock mass failure because they largely govern the rupture mode of the intact rock material and geological structures in it.

2.1.1. General stress considerations

The in situ stress in a rock mass is caused principally by the weight of the overlying material and by tectonic forces, which themselves result from the movement of the continental plates on the surface of the Earth. Stress is ground pressure and, as such, is expressed in units of pressure, i.e., in units of force per area. As for any other pressure, stress is defined in one direction, as the ratio of the force acting in this direction divided by the surface normal to this direction. A major difference between the stress regime inside a

solid and that inside a fluid (either liquid or gaseous) is that the stress regime inside a solid body is not necessarily iso-static – in other words, whereas the pressure at a given point inside a fluid is equal in all directions, the pressure at a given point inside a solid can be (and generally is) different in different directions. As a result, the stress state at a given point inside a solid needs to be expressed as a tensor, which can be rotated to provide stress magnitudes in any direction desired. As shown in Figure 1a, a stress tensor is expressed in the form of a 3×3 matrix, in which the direct (either compressive or tensile) stresses – those acting perpendicularly to the faces of a unit volume aligned along the reference system chosen – are placed in the leading diagonal, and the shear components acting along these faces are placed in the off-diagonal cells. The reference system often used for the generalised stress tensor is Northing (either true, magnetic, or local grid), Easting and elevation. Under static conditions, a stress tensor matrix is necessarily symmetrical.

For any given stress tensor there is always one – and only one – rotation possible that results in the shear stresses acting along the faces of a unit volume aligned with the rotated reference system to be zero. In this case, the direct stresses acting perpendicularly to these faces are said to be the principal stress components, referred to as the major principal stress component (by convention the largest of the three components, represented by σ_1), the minor principal stress component (by convention the smallest of the three components, represented by σ_3), and the intermediate principal stress component (the third component, represented by σ_2). Figure 1b shows the stress tensor matrix associated with the principal stresses, with zero values in the shear stress components off the leading diagonal.

$$\begin{pmatrix} \sigma_{xx} & \tau_{xy} & \tau_{xz} \\ \tau_{yx} & \sigma_{yy} & \tau_{yz} \\ \tau_{zx} & \tau_{zy} & \sigma_{zz} \end{pmatrix} \qquad \begin{pmatrix} \sigma_1 & 0 & 0 \\ 0 & \sigma_2 & 0 \\ 0 & 0 & \sigma_3 \end{pmatrix}$$

(a) Generalised stress tensor. ***(b) Principal stress tensor.***

Figure 1. (a) Generalised stress tensor; and, (b) principal stress tensor.

Figure 2 schematically illustrates two stress tensors: a general one (Figure 2a), whereby shear stresses are required on the faces of the unit solid to maintain equilibrium and prevent

a moment-induced rotation; and, the principal one (Figure 2b), whereby the stresses acting perpendicularly to the faces of the unit solid provide equilibrium by themselves.

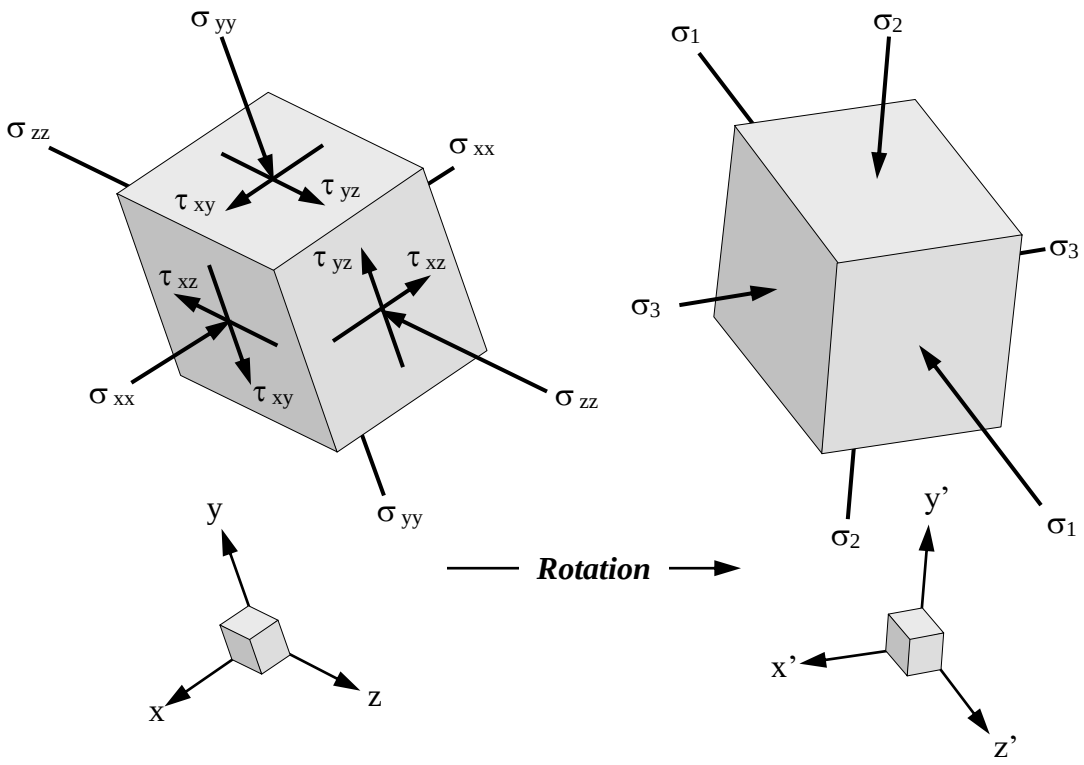

(a) General reference system. ***(b) Principal stresses reference system.***

Figure 2. (a) General reference system; and, (b) rotated reference system that corresponds to the major (σ_1), intermediate (σ_2) and minor (σ_3) principal stress components.

In summary, the stress regime at a point inside a solid body can be entirely defined by: 1) a tensor regrouping in a matrix form the magnitude of each of the six stress components (three direct and three in shear); and, 2) a complete description of the orientation of the reference grid along which these components are defined.

2.1.2. Variation of stress with depth

The stress magnitude (or intensity) inside a rock mass increases with depth, as the weight of the overlying material increases (the density of the various strata hence plays a role).

Figure 3 illustrates this point. As can be seen, the vertical stress component σ_V (in MPa) averages about 0.027 times the depth expressed in metres.

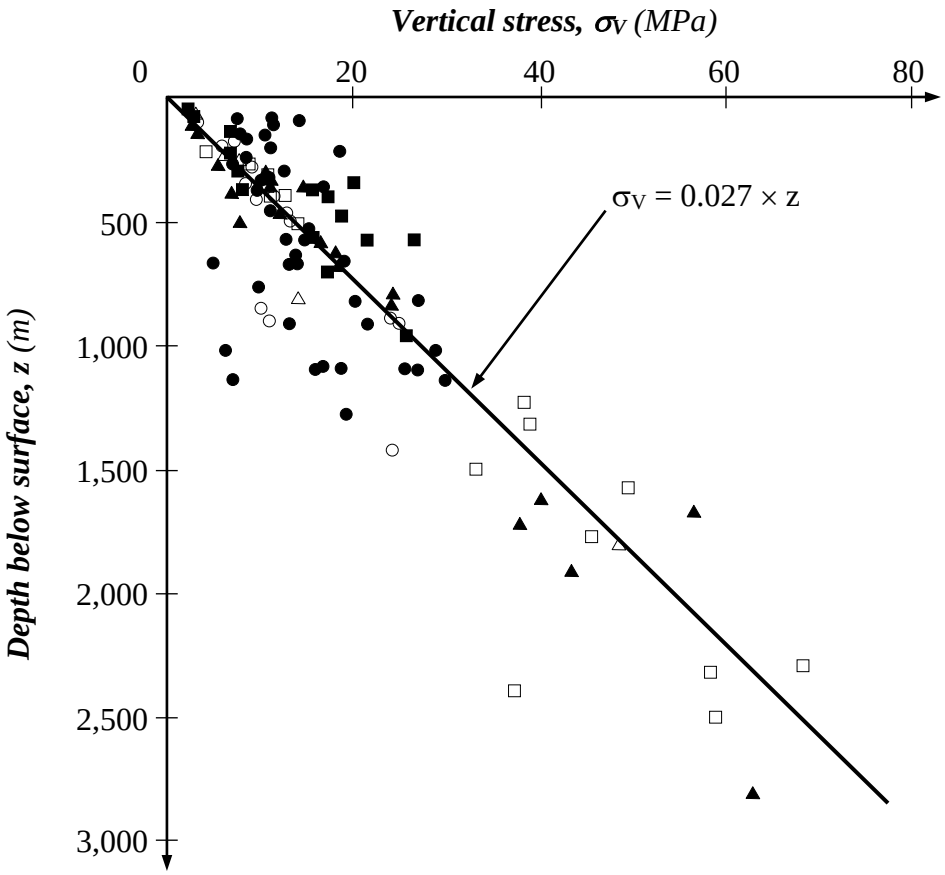

Figure 3. Vertical stress measurements from mining and civil engineering projects around the world. (After Hoek *et al*., 1995.)

The manner in which the magnitude of a given stress component varies with depth is usually expressed mathematically as a stress gradient of the following form:

$$\sigma_{i\text{-}i} = \sigma_{\text{Ref. } i\text{-}i} - [\, \textit{Elevation} \times \Delta\sigma_{i\text{-}i} \,] \qquad \text{..... Eq. (1)}$$

With: $\sigma_{i\text{-}i}$ the stress component of interest (either a principal component, or any component aligned with a given reference grid); $\sigma_{\text{Ref. } i\text{-}i}$ the reference stress magnitude (to account for the fact that the magnitude of a stress component is not necessarily zero on the surface of the Earth); *Elevation* the vertical distance (up from a reference point located deep underground) at which the magnitude of the stress component of interest is sought

after; and, $\Delta\sigma_{i\text{-}i}$ the stress gradient (the variation of magnitude with elevation). Equation (1) can be re-arranged to express stress as a function of depth instead of elevation. Reference stresses are expressed in units of pressure (typically MPa for underground mining applications), whereas stress gradients are expressed in units of pressure per distance (usually MPa per metre for underground mining applications).

The manner in which the stress regime varies with depth inside a solid body can thus be entirely defined by: 1) the reference stress magnitude of each component; and, 2) the stress gradient with depth (or elevation) of each component.

The ratios $(\Delta\sigma_1 / \Delta\sigma_3)$ and $(\Delta\sigma_2 / \Delta\sigma_3)$ are defined as k_1 and k_2, respectively. Throughout the Canadian Shield the sub-horizontal stress components typically exceed the sub-vertical one due to tectonic history. As the k_1 and k_2 ratios increase, and particularly k_1, a more highly deviatoric stress regime prevails whereby the solid is subjected to stresses of increasingly different magnitudes in different directions. (A deviator of stress at a given point is defined as the stress tensor obtained by subtracting from a principal stress tensor $[\sigma_1, \sigma_2, \sigma_3]$ an isotropic tensor of principal stress values equal to a third of $[\sigma_1 + \sigma_2 + \sigma_3]$. In other words, it is the stress tensor obtained by subtracting the mean of the normal stress components of a principal stress tensor from each normal stress component.) The practical issue associated with highly deviatoric stress regimes is that abnormally high stress levels are encountered in one direction, which can cause the rock mass to reach failure relatively quickly (at relatively shallow depths – failure considerations are discussed later in this chapter).

2.1.3. In situ vs. mining-induced stresses

The in situ stress regime (also referred to as “regional”, “virgin” or “natural”) in a rock mass can be locally affected and distorted by the presence of adjacent materials of different stiffnesses, neighbouring formations of widely different mechanical properties and/or geological discontinuities in this rock mass. The geometrical extent of these elements, as well as their shape, orientation, location with regard to each other, and the order and

manner in which they were placed or created, all impact the actual stress regime that prevails locally in a volume of rock that will be mined – such local stress regimes are also referred to as "pre-mining" stresses.

Once mining starts, the excavations created will distort the local stress regime, sometimes very significantly. The size, shape and orientation of these voids, their location with regard to each other and the order in which they are excavated will all have an effect on where the ground stresses will be diverted and concentrated. The reason why excavations have such a strong influence on the distribution of stresses within a solid is that stress essentially "flows" in a solid body, very much like a fluid or a gas flows inside a conduit. One difference, though, is that the stress flow inside a solid body does not result in a transfer of material. If one considers fluid flow, it is easy to see that an obstacle along its path will constrict this flow, creating regions of low flow (behind the obstacle) and high flow velocity (around the obstacle), and possibly resulting in zones of turbulence. Figure 4 illustrates this point with the example of the airflow in a mine drift, without obstruction (Figure 4a) and obstructed by a bulkhead (Figure 4b) – anyone who has ever walked through the man door of a mine ventilation bulkhead has experienced the increase in air speed through the open door, and the absence of airflow behind the bulkhead.

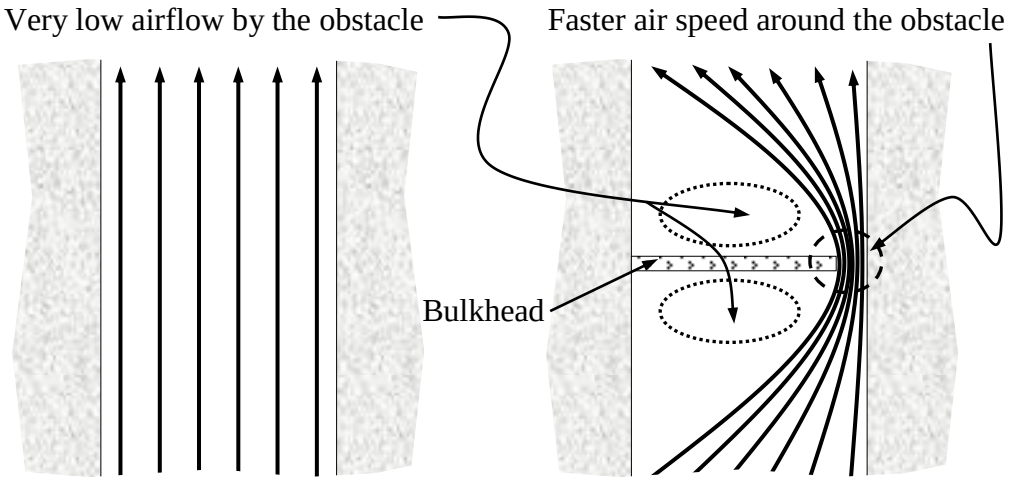

Figure 4. Conceptual sketch illustrating how an obstacle alters the airflow in a wind tunnel.

In the case of a "stress flow" inside a solid body, a void will act as the obstacle, with the stress being diverted around it. Figure 5 illustrates this behaviour: if no void is present, the stress flow inside the solid (far from its boundaries) will be steady (Figure 5a), whereas a void will create zones of high stress and regions of low stress (Figure 5b) around it.

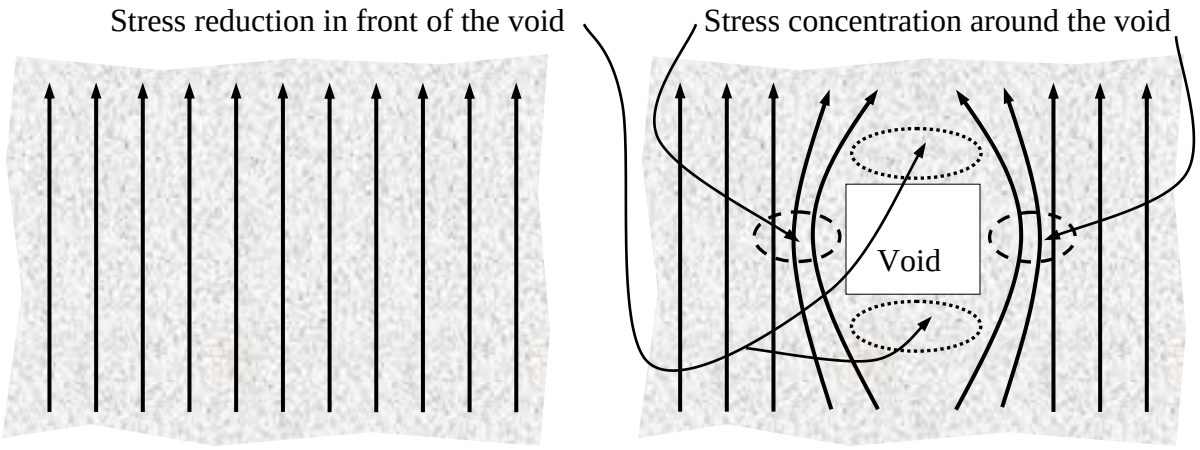

(a) Unobstructed stress flow. ***(b) Stress flow obstructed by a void.***

Figure 5. Conceptual sketch illustrating how an excavation alters the stress flow inside a solid body.

If one was to compare the conceptual example of airflow in Figure 4 with the one of stress flow in Figure 5, air speed would essentially correspond to stress magnitude. The tri-dimensionality of a solid substantially complicates the matter, and it can become extremely difficult to intuitively assess where stresses are redirected and concentrated, and where low stresses will prevail when complex shapes are involved and located near each other. Numerical modelling analyses are generally required to address this question when complicated geometries and close proximities are involved.

2.2. GEOMECHANICAL CONDITIONS FOR THE VIOLENT FAILURE OF ROCK

Understanding the conditions that can lead to the violent failure of a rock mass is of paramount importance if one is to design destress blasts that will accomplish their stress

relaxation objective. A violent failure can be broadly defined as a failure that is accompanied by a sudden and substantial release of strain energy. Although destressing can conceptually be attempted under conditions of non-violent rock mass failure (when large plastic deformations occur, or drifts are aseismically squeezed, for example), it is generally implemented under conditions of violent failure. The main reason is the safety aspect associated with such collapses, whereby the inherent risk they expose the underground personnel to (and their equipment as well), is much greater. Furthermore, violent failures are generally sudden and difficult to predict.

Three components need to be simultaneously present in order for large-scale violent failure to occur in a rock mass. Firstly, certain stress conditions are required, secondly, the rock mass must have certain mechanical characteristics, and, thirdly, the loading system needs to be soft. Each of these points will be discussed in detail in the following sections.

2.2.1. Stress conditions required for violent failure

The first stress-related requirement for violent failure to occur is a high stress magnitude (a rock mass subjected to low stress conditions is unlikely to fail in the first place). The second stress-related requirement is associated with the manner in which failure is reached. The strength of a volume of rock subjected to stress can be expressed as a function of the stress magnitudes it can withstand under various levels of confinement. There are many failure criteria, both linear and non-linear, that describe the strength of rock. A commonly used linear failure criterion is the Mohr-Coulomb one, in which strength is defined as the amount of shear stress the material can withstand at various levels of normal stress (normal to the shear plane). The following equation describes this failure criterion:

$$\tau = c + (\sigma_N \times \tan \phi) \qquad \text{..... Eq. (2)}$$

With: τ the shear strength (in Pa); c the cohesion (in Pa); σ_N the normal stress (in Pa); and, ϕ the friction angle. A graphical representation of this failure criterion is shown in Figure 6a.

Alternatively, a widely used non-linear empirical failure criterion is the Hoek-Brown one (Hoek & Brown, 1980), whereby strength is represented by the amount of driving stress σ_1 the material can sustain at various levels of confinement σ_3. This criterion has the following mathematical formulation:

$$\sigma_1 = \sigma_3 + \sigma_{ci} \times ([\{ m \times \sigma_3 \} / \sigma_{ci}] + s)^a \quad \text{..... Eq. (3)}$$

With: σ_1 and σ_3 the major and minor principal stresses at failure, respectively; σ_{ci} the uniaxial compressive strength of the intact rock material; m and s the Hoek-Brown parameters; and, *a* an exponent that depends upon the rock mass characteristics. The graphical aspect of this criterion is shown in Figure 6b.

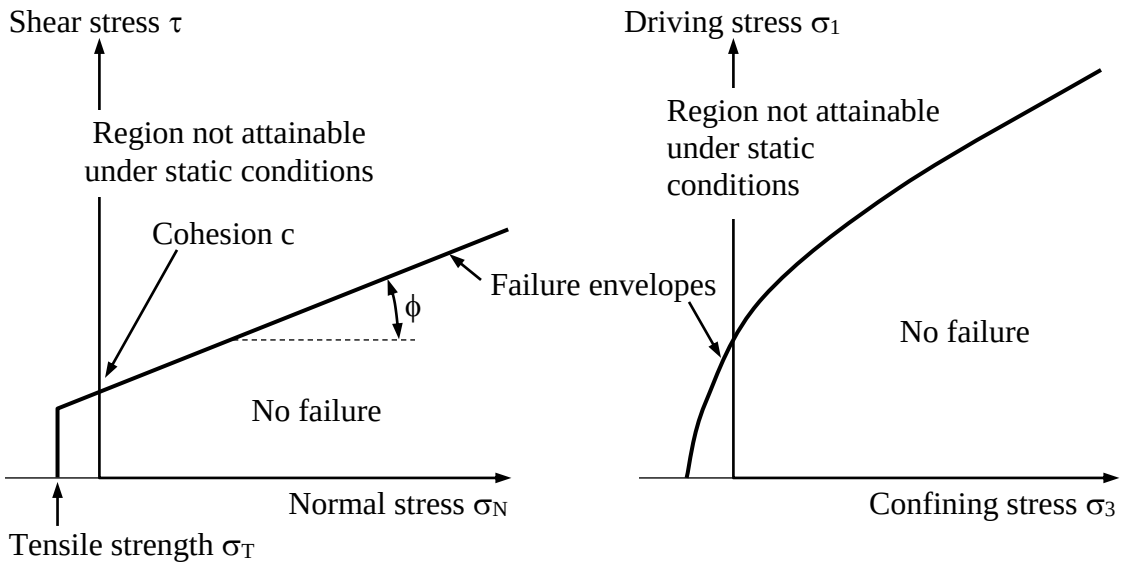

(a) Linear Mohr-Coulomb failure criterion.

(b) Non-linear Hoek-Brown failure criterion.

Figure 6. (a) Linear Mohr-Coulomb; and, (b) non-linear Hoek-Brown failure criteria for rock.

Each of these two criteria can also be expressed in the units normally used for the other one: the Mohr-Coulomb one can be expressed in the $[\sigma_1 - \sigma_3]$ space, whereas the Hoek-Brown one can be expressed in the $[\tau - \sigma_N]$ space. Both are usually derived in the laboratory through series of triaxial loading tests performed under various levels of confinement, the results of which are extrapolated to the rock mass scale using a number of

alternative approaches. In all cases, the region above the failure envelope is not attainable under static conditions – at the rock mass scale once the failure envelope is reached locally, the material starts to yield inelastically and begins to shed stress towards neighbouring regions that are still intact. This holds true for all hard rocks, which typically behave as strain-softening materials. Importantly, it is recognised in all failure criteria that the strength of rock increases with confinement – in other words, a given rock mass can withstand significantly higher stress levels when it is subjected to a higher degree of confinement. As a consequence, a rock mass that is highly confined can accumulate much greater levels of elastic strain energy than if it were under low confinement, which, under certain conditions, could be suddenly released at failure with devastating effects.

The manner in which the $(\sigma_1 - \sigma_3)$ – or the $(\tau - \sigma_N)$ – stress regime evolves and approaches the failure envelope as mining progresses can be indicative of the type of failure to expect. Figure 7 shows various possible such paths to failure in the $(\sigma_1 - \sigma_3)$ space with a Mohr-Coulomb failure criterion. (In this figure ϕ is again the friction angle of the rock material, and c is its cohesion.)

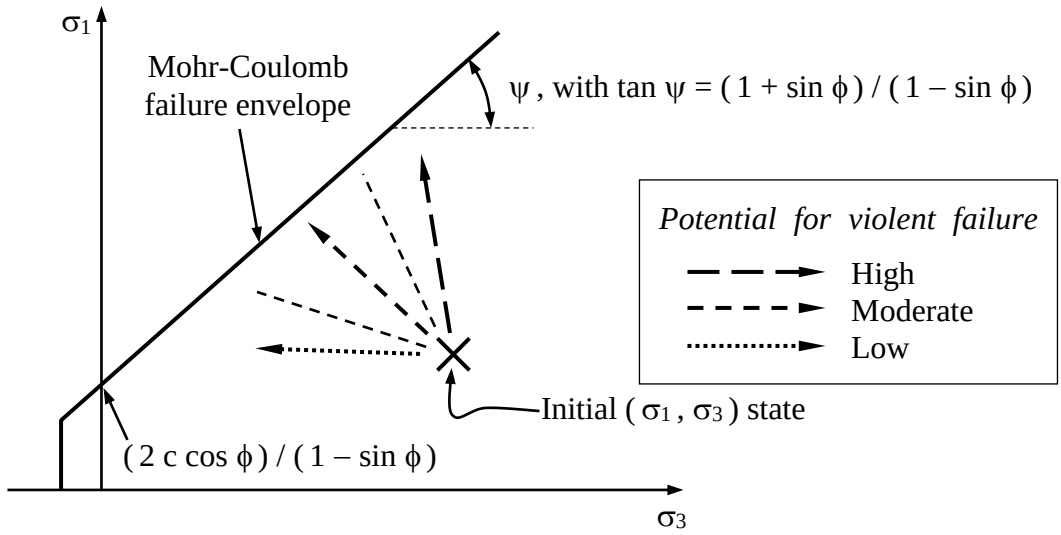

Figure 7. Schematic illustration in the $(\sigma_1 - \sigma_3)$ space with a Mohr-Coulomb failure criterion of various possible stress paths to failure, and their consequences on the type of failure to expect. (Adapted from Andrieux *et. al*., 2003.)

A stress path represented by the long dash arrow, whereby the major principal stress increases and reaches high levels while the confining stress remains essentially constant, would be associated with a large accumulation of strain energy that has the potential to be suddenly released at failure, which could result in seismic or even rockbursting conditions. Please note that within the frame of this thesis a rockburst will be defined according to the terminology suggested in the draft version of the Canadian Rockburst Support Handbook (Kaiser *et al*., 1996), as follows: *a rockburst is defined as damage to an excavation that occurs in a sudden or violent manner and is associated with a seismic event*.

The stress path associated with the dotted arrow, whereby the failure envelope is being approached under near constant or reducing σ_1 and reducing σ_3 magnitudes – hence with a significant loss of confinement – would typically be associated with unravelling conditions that would likely result in aseismic gravity-driven structurally-controlled ground failures. This type of gravity-driven instability can be very much intensified if the rock mass has previously undergone a stress cycle, whereby it has first been subjected to a stress increase while it sat in a high stress abutment ahead of mining, followed by a stress decrease once mining progressed past it and put it in the stress shadow of the excavations. The high stress phase tends to break up the rock mass, prior to it being de-clamped by the subsequent confinement stress decrease. As the amplitude of the stress cycle increases (i.e., as the difference between the highest and the lowest driving stress magnitudes increases), the likelihood of ground instability increases as well. The third stress path, represented by the short dash arrow in Figure 7, would correspond to an intermediate scenario.

The stress path approach has been shown to give reasonably good insight into the potential for strain bursting and pillar bursting to occur (these two types of rockburst are defined in sections 2.3.1 and 2.3.2, respectively). It was, for example, used by Board & Brummer (1998) to assess the bursting potential associated with the deep production stopes at Kidd Mine D. It has also been successfully applied at Brunswick Mine to estimate the bursting potential of large secondary stopes in the lower part of the mine (Simser & Andrieux, 1999), as well as at the Bell-Allard Mine in Matagami to investigate the bursting potential in the central Retreat Zone (Falmagne *et al*., 2003).

The approach has however shown limitations with regard to the assessment of fault-slip bursting potential (this form of rockburst is defined in Section 2.3.3 further down). Although the analysis principle conceptually applies to slipping along a discontinuity, the approach has shortcomings. The main difficulty is that the actual location, extent and geometry of the discrete lock-up points along the discontinuity, which correspond to the areas where the elastic strain energy is being built-up, are largely unknown. This results in the need to derive sets of "equivalent" mechanical properties for the discontinuity that aim at somehow considering the characteristics of these lock-up points, while also describing the "regular" properties of the discontinuity, away from these points. These properties are often unrealistic because they end up being much too strong for the "regular" conditions, while still being too weak for the actual lock-up points. In other words, the compromise in properties is often poor at describing the field behaviour of the discontinuity due to its objective of trying to describe some sort of "average" behaviour over the full extent of the feature.

2.2.2. Rock mass properties required for violent failure

Besides being subjected to high stress levels and a particular stress path, the rock mass itself needs to be made of stiff, strong and brittle material in order for a violent collapse to occur. The stress-strain curve characteristic of a typical strain-softening hard rock sample submitted to a compressive force under low confinement in a stiff laboratory press is shown in Figure 8.

Such a curve has two principal domains: the elastic one, during which the deformation imparted to the rock sample is reversible (i.e., if the compressive force is removed, the sample returns to its original shape, without any permanent damage having occurred), and the inelastic one, which is characterised by a level of permanent deformation (i.e., if the compressive force is removed, the sample does not return to its original shape, but rather retains some level of permanent deformation due do the occurrence of irreversible damage within its matrix). All rocks start to exhibit an inelastic behaviour at some level of deformation, which is typically fairly small. The elastic portion of the response is where

the stiffness of the material is defined, as the ratio of stress over strain – as this ratio increases, the material becomes stiffer.

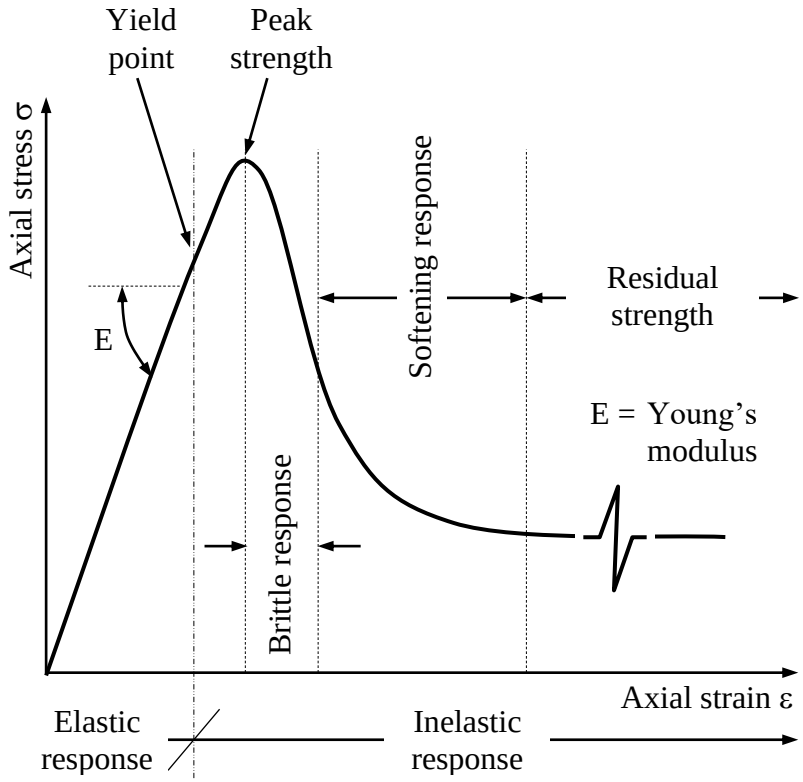

Figure 8. Idealised characteristic compressive stress-strain curve for a typical strain-softening hard rock at a given (low) level of confinement.

As shown in Figure 8, the inelastic portion of the stress-strain curve can itself be subdivided into distinct areas, which are as follows:

- *The pre-peak inelastic response*, characterised by the onset of damage (formation and propagation of micro-fractures), and the accumulation of irreversible degradation within the sample. The yield point is defined as the point where the inelastic behaviour begins.
- *The peak strength*, which represents the maximum load the sample can carry under the level of confinement considered.
- *The brittle response*, characterised by a sudden drop in the load-bearing capacity of the sample immediately after reaching its peak strength. This sudden stress reduction is accompanied by only a small deformation, and is the result of the sudden rapid extension and networking of the micro-fractures within the sample. As the deformation associated

with the brittle response decreases and the drop in axial stress increases, the material is said to be more brittle. A highly brittle material, such as glass, typically breaks apart and shatters at failure.

- *The softening response*, associated with a continued and more progressive reduction of the load-bearing capacity of the sample as it further deforms and degrades.
- *The residual strength*, which corresponds to the load the sample can continue to sustain "indefinitely", or, in other words, the minimum and constant level of stress it can continue to carry as the deformation in it continues to increase. It is clear that in a compressive laboratory test the residual strength of a sample is not constant forever.

At the rock mass scale, however, the failed rock can retain a certain level of minimum load-bearing capacity if it is completely surrounded by solid material, does not have the kinetic freedom to completely collapse and continues to occupy a certain volume. The residual values of the friction angle, cohesion and tensile strength define another strength curve, that can also be expressed either in the $(\sigma_1 - \sigma_3)$ or the $(\tau - \sigma_N)$ space, and which describes the strength of the failed material under various states of confinement, as illustrated in Figure 9.

Intermediate envelopes between the intact and the completely failed material can be described by the combination of the friction angle, cohesion and tensile strength values at the corresponding intermediate levels of accumulated plastic strain.

Failed rock is unlikely to undergo violent failure as its much lower mechanical properties simply do not allow large energy build-ups to take place in the material, which are necessary for violent failure to occur.

Brittle materials generally have a limited softening response and low residual properties. On the other hand, materials that are not brittle (such as highly schistose rock units, or poorly consolidated sedimentary formations, for example), commonly have a more dominant softening response and proportionally higher residual properties.

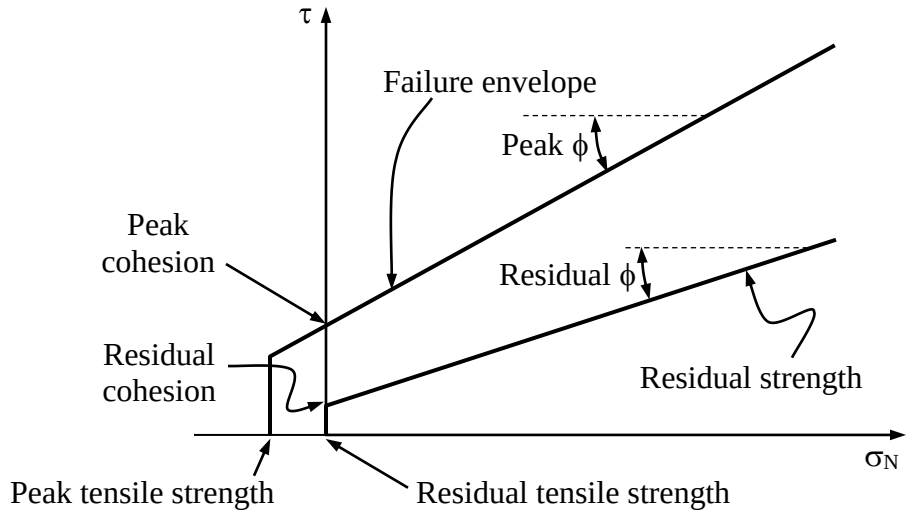

Figure 9. Failure and residual envelopes in the ($\tau - \sigma_N$) space that describe the strength of the intact and failed material under various levels of confinement.

As mentioned earlier, a stiff, strong and brittle rock mass is more conducive to violent failure. Firstly, for the same amount of deformation, a stiff rock will accumulate more strain energy than a soft one. Secondly, once failure occurs, a more brittle rock will tend to release more rapidly and to a greater extent part of the strain energy it had accumulated. Thirdly, the high strength that usually accompanies high stiffness and high brittleness increases the level of elastic strain energy accumulated in the material prior to failure, which, in turn, increases the energy that can be released at failure.

2.2.3. Loading system characteristics required for violent failure

Further to the rock mass being subjected to high stress levels and a stress path conducive to failure, and comprising stiff, strong and brittle material, a soft loading system is also required for large-scale violent failure to occur. Because the concept of a soft *vs.* stiff loading system will be discussed in some detail in this section, a clear understanding of the notion is required. Figure 10a shows an idealised soft press, whereby the load applied onto the sample is the parameter directly controlled during the test (in this conceptual setup, more load is incrementally applied by adding weights on top of the press platen). It can clearly be seen that once a brittle sample will fail in such a press, the failure will likely be

complete because the load will continue to be exerted onto the failing sample, further crushing it. Figure 10b shows an idealised stiff press, whereby the deformation exerted onto the sample is the parameter directly controlled during the test (as the threaded rods are turned by a servo-controlled motor, the distance between the press base and the top platen is reduced, squeezing the sample). If controlled sufficiently precisely, the deformation rate can be slowed down at the onset of failure, then subsequently re-increased in a managed fashion in order to progressively complete the failure process, without violently collapsing the sample.

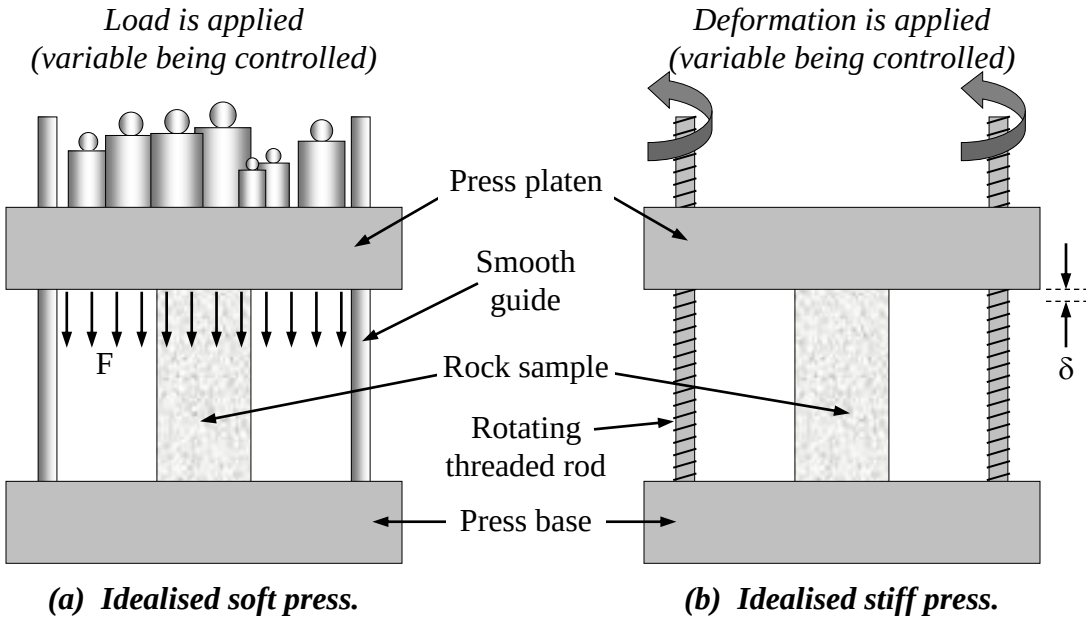

Figure 10. (a) Idealised soft press; and, (b) idealised stiff press, showing which variable is controlled in each case.

Figure 11 illustrates how the stiffness of the loading system will have an influence on whether the post-peak load shedding process of a rock sample under uniaxial compression will be sudden and violent, or progressive. Consider a sample of "typical" hard rock (relatively stiff, strong and brittle) subjected to a uniaxial compressive test, as shown on the left hand side of the figure. In the case of a soft loading system, the post-peak stress reduction in the sample will correspond to the path ADS. In this particular case, the press has stored, and is releasing, more energy than the sample can dissipate at failure. This excess energy, similarly to what was shown in Figure 10a, leads to the sudden and

complete destruction of the sample, without any supplemental external energy having to be supplied to the system. The excess energy at failure – represented by area ADE in Figure 11) – is converted into kinetic energy, which accelerates the failure process and results in the violent and total collapse of the sample.

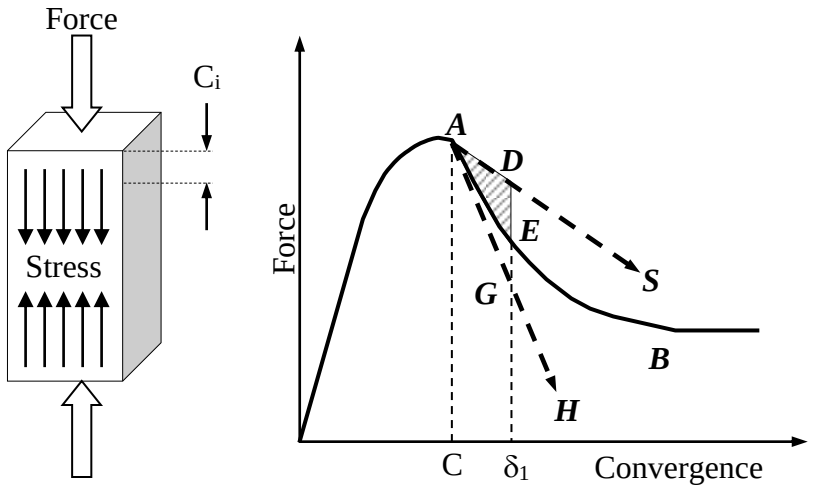

Figure 11. Brittle rock specimen deformation in a soft *vs*. stiff testing machine. (Adapted from Blake *et al*., 1998.)

In the case of a rigid press, less energy is accumulated in the system for a similar level of deformation, and additional external energy is needed in order to sustain the failure process in the sample. In other words, additional external energy is needed to fill the deficit between paths AGH and AB (the energy deficit at point δ_1 is represented by the area AEG in Figure 11). This situation results in a more progressive and stable failure mechanism, in which energy is dissipated in a more stable manner, than in the case of the soft press discussed earlier. In the case of a mine pillar, the press can be taken to represent the encasing rock mass that surrounds this pillar and transfers load onto it – this rock mass can be either soft or stiff. In summary, the ADS path shown in Figure 11 corresponds to a ductile unloading process at failure (associated with a soft press), whereas path AGH corresponds to a stiff unloading process at failure (associated with a stiff press). As the rock mass strength increases the process occurs under higher stress conditions, which further increases the potential for a violent failure. Table 1 summarises the general potential for violent failure to occur for various conceptual combinations of stress

conditions, rock properties and loading system stiffness, as discussed in the previous sections.

Table 1. Summary of the general potential for violent failure to occur for various conceptual combinations of stress conditions, rock properties and loading system stiffness.

<table>
<tr><th colspan="2">Stress regime change</th><th colspan="3">Rock properties</th><th>Loading system stiffness</th><th>Potential for violent failure</th></tr>
<tr><th>σ_1</th><th>σ_3</th><th>Stiffness</th><th>Strength</th><th>Brittleness</th><th></th><th></th></tr>
<tr><td>Increasing severely</td><td>Near constant</td><td rowspan="4">High</td><td rowspan="4">High</td><td rowspan="4">High</td><td rowspan="4">Soft</td><td>Extreme</td></tr>
<tr><td>Increasing progressively</td><td>Decreasing progressively</td><td>High</td></tr>
<tr><td>Increasing slowly</td><td>Decreasing progressively</td><td>Moderate</td></tr>
<tr><td>Near constant</td><td>Decreasing rapidly</td><td>Low</td></tr>
<tr><td colspan="2">High stress build up unlikely</td><td>Low</td><td colspan="2">–</td><td rowspan="2">–</td><td rowspan="2">Moderate to low</td></tr>
<tr><td colspan="5">When a rock unit is soft, large deformations are required to reach the high stress levels necessary for violent failure. These high deformations usually result in neighbouring stiffer geological horizons to attract most of the load, effectively shielding the softer unit from reaching high stress levels itself.</td></tr>
<tr><td colspan="2">High stress build up unlikely</td><td>–</td><td>Low</td><td>–</td><td rowspan="2">–</td><td rowspan="2">Moderate to low</td></tr>
<tr><td colspan="5">When a rock unit is weak, the failure envelope sits low on the y-axis and there is no opportunity for the high stress levels necessary for violent failure to build-up</td></tr>
<tr><td colspan="2">–</td><td colspan="2">–</td><td>Low</td><td rowspan="2">–</td><td rowspan="2">Moderate to low</td></tr>
<tr><td colspan="5">When a rock unit exhibits a more plastic behaviour it releases energy at failure in a more progressive manner, which results in a less violent breakdown of the matrix</td></tr>
<tr><td>Increasing severely</td><td>Near constant</td><td rowspan="4">High</td><td rowspan="4">High</td><td rowspan="4">High</td><td rowspan="4">Stiff</td><td>High to moderate</td></tr>
<tr><td>Increasing progressively</td><td>Decreasing progressively</td><td>Moderate</td></tr>
<tr><td>Increasing slowly</td><td>Decreasing progressively</td><td>Low</td></tr>
<tr><td>Near constant</td><td>Decreasing rapidly</td><td>Low</td></tr>
</table>

2.2.4. Idealised energy considerations

In an idealised case of pillar bursting whereby violent failure would be triggered by a high near-uniaxial static load, the mechanical behaviour of the system can be simplified as shown in Figure 12. In this figure it is assumed that the pillar fails completely (i.e., retains no residual strength) between points A and B, and that the loading system "platens" converge to point C after the failure of the pillar. In this figure k'_{pr} and k_e represent the post-peak stiffness of the pillar and the stiffness of the loading system, respectively.

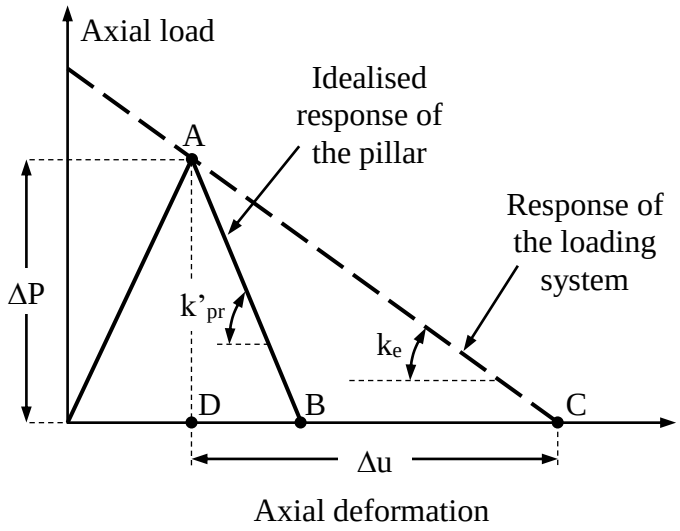

Figure 12. Idealised load-deformation behaviour of a pillar under uniaxial compressive load. (After Simon *et al*., 1998.)

As previously discussed, the area ABC in Figure 12 represents the excess energy available to "power" the failure. On the one hand, the potential energy E_p that must be dissipated by the system at failure is given by area ACD, as follows:

$$E_p = 0.5 \times \Delta u \times \Delta P \qquad \text{..... Eq. (4)}$$

With Δu and ΔP as defined in Figure 12. Given that the system stiffness $|k_e|$ is given by $(\Delta P / \Delta u)$, Equation (4) becomes:

$$E_p = (\Delta P)^2 / (2 \times |k_e|) \qquad \text{..... Eq. (5)}$$

On the other hand, the static energy E_d dissipated by the failure of the pillar is given by area ABD, as follows:

$$E_d = (\Delta P)^2 / (2 \times |k'_{pr}|) \quad \text{..... Eq. (6)}$$

The minimum excess energy $E_{x\,(min)}$ in the system is thus the difference between E_p and E_d, as follows:

$$E_{x\,(min)} = [(\Delta P)^2 / 2] \times [(1 / |k_e|) - (1 / |k'_{pr}|)] \quad \text{..... Eq. (7)}$$

Equation (7) indicates that the potential for violent failure increases as the amount of excess energy in the system increases, i.e., as $|k'_{pr}|$ becomes increasingly larger than $|k_e|$.

Since we assumed that the pillar has no post-peak residual strength (i.e., that the load drop ΔP is equal to the maximum load it can carry), we have that:

$$\Delta P = \sigma_{cR} \times A \quad \text{..... Eq. (8)}$$

With: σ_{cR} the uniaxial compressive strength of the pillar at the rock mass scale (in Pa) and A the area over which the uniaxial load is applied onto it (in m^2). Also assuming that the pillar has a perfectly brittle behaviour (i.e., that $|k'_{pr}| = \infty$), and combining equations (7) and (8), the *maximum* excess energy $E_{x\,(max)}$ in the system is given by:

$$E_{x\,(max)} = [(\sigma_{cR})^2 \times A^2] / [2 \times |k_e|] \quad \text{..... Eq. (9)}$$

Furthermore, if the strength of the rock mass is assumed to be governed by a Hoek-Brown failure criterion, then we have that:

$$\sigma_{c\,\text{Rock Mass}} = (s_{\text{Rock Mass}})^{0.5} \times \sigma_c \quad \text{..... Eq. (10)}$$

With: $\sigma_{c\,\text{Rock Mass}}$ the uniaxial compressive strength of the pillar at the rock mass scale (similar to σ_{cR} defined in Equation [8]); $s_{\text{Rock Mass}}$ the parameter in the Hoek-Brown failure criterion (at the rock mass scale); and, σ_c the uniaxial compressive strength of the intact rock material comprising the pillar (at the laboratory sample scale).

Combining equations (9) and (10) yields Equation (11).

$$E_{x\,(max)} = [\, s_{\text{Rock Mass}} \times (\sigma_c)^2 \times A^2 \,] / [\, 2 \times |k_e| \,] \qquad \text{..... Eq. (11)}$$

Equation (11) states that the upper bound of the excess energy available when a pillar fails under axial compressive load, and which can contribute to a rockburst, is dependent upon the following parameters:

- *The uniaxial compressive strength of the intact rock material*. The excess energy $E_{x\,(max)}$ increases with the square of σ_c .
- *The competency of the rock mass*. The excess energy $E_{x\,(max)}$ increases as parameter s increases, i.e., as the rock mass becomes more massive and encompasses fewer geological discontinuities. Parameter s is 1.00 for a Rock Mass Rating (RMR [Bieniawski, 1976] – this methodology is described in detail in Appendix E) value of 100, and decreases with decreasing values of RMR.
- *The area of the pillar*. The excess energy $E_{x\,(max)}$ increases with the square of the area over which the uniaxial compressive load is applied. In other words, as the pillar becomes larger it will release more energy at failure.
- *The stiffness of the loading system*. The excess energy $E_{x\,(max)}$ increases as $|k_e|$ decreases, i.e., as the loading system becomes softer.

This simplified energy-based analysis supports the conclusions previously reached. Firstly, it agrees that rockbursting is more likely to occur in a rock mass that is stiff (in which case the idealised response curve of the pillar shown in Figure 12 moves to the left, thus increasing the post-failure areas involved), strong (with a high σ_c value) and brittle (with a high $|k'_{pr}|$ value).

The required degree of massiveness of the rock mass indicated by Equation (11) is also well in accordance with these stiffness, strength and brittleness issues. This energy approach also confirms that the risk of rockbursting increases when the loading system is soft, i.e., when $|k_e|$ is low, and the difference between $|k'_{pr}|$ and $|k_e|$ is large.

2.3. THE VARIOUS TYPES OF ROCKBURSTS

Hedley (1992) proposed that there are three types of rockbursts, which he described as violent failures with ejection of material. Each type is described in the following sections.

2.3.1. Strain bursts

Strain burst type failures are essentially caused by instabilities in the vicinity of a free face, which has little confinement but can be located near a region of high stress concentration, a short distance inside the rock mass. Figure 13 schematically illustrates the mechanism – a very stiff, strong and brittle rock mass is generally involved in this type of failure.

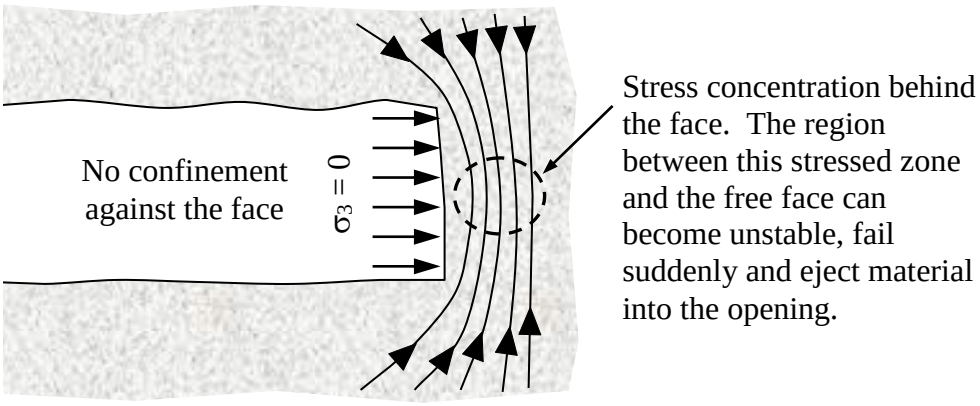

Figure 13. Schematic side view of a conceptual drift illustrating the mechanism of strain bursting.

This type of instability can be in the form of spalling at the face, which, although generally limited in terms of the quantity of material ejected, can have serious safety implications. Excavation surfaces subjected to somewhat higher levels of confinement – such as drift shoulders (because of their geometry), for example – can also be prone to this type of failure. The propagation of shear fractures ahead of the mining front can also trigger this type of failure (Brummer, 1987).

2.3.2. Pillar bursts

Pillar burst type failures are the violent rupture of a largely intact and massive volume of rock inside a pillar, as a result of high stress levels having concentrated in it. Figure 14 schematically illustrates the mechanism.

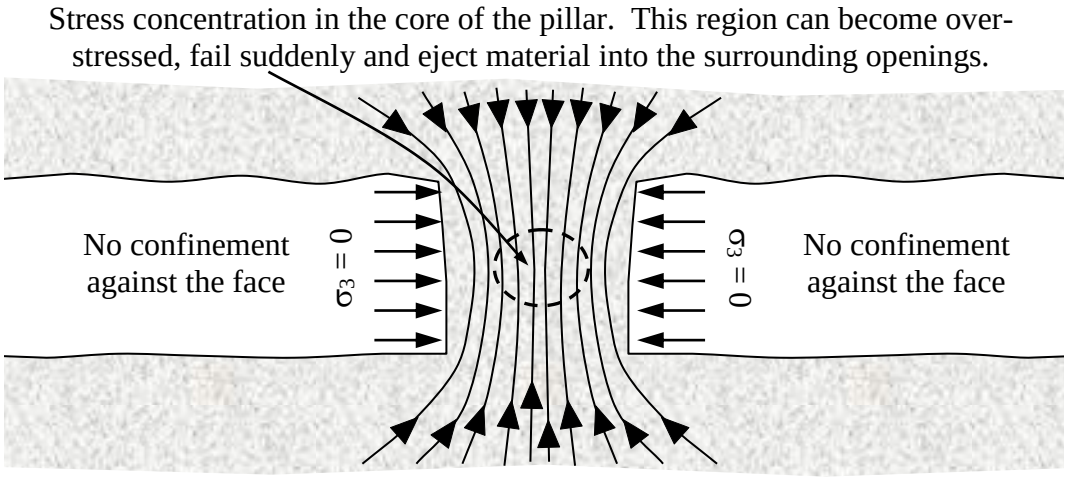

Figure 14. Schematic side view of a conceptual pillar illustrating the mechanism of pillar bursting.

Again, a stiff, strong and brittle rock mass is generally involved in this type of failure, which can result in large quantities of material being ejected, and be associated with sizeable seismic events (over a Richter Magnitude 1.0).

2.3.3. Fault-slip bursts

Fault-slip type bursts are violent failures along adversely oriented large-scale sub-planar geological discontinuities. These discontinuities are generally natural and pre-date mining, and can locally affect significantly both the magnitude and orientation of the stress field. As mining progresses it changes the stress regime acting upon the geological structure, by locally increasing the driving shear stress acting upon it and/or decreasing the normal clamping stress it is subjected to. Figure 15 illustrates the concept. This stress change can eventually overcome the strength of the geological structure and cause it to fail locally.

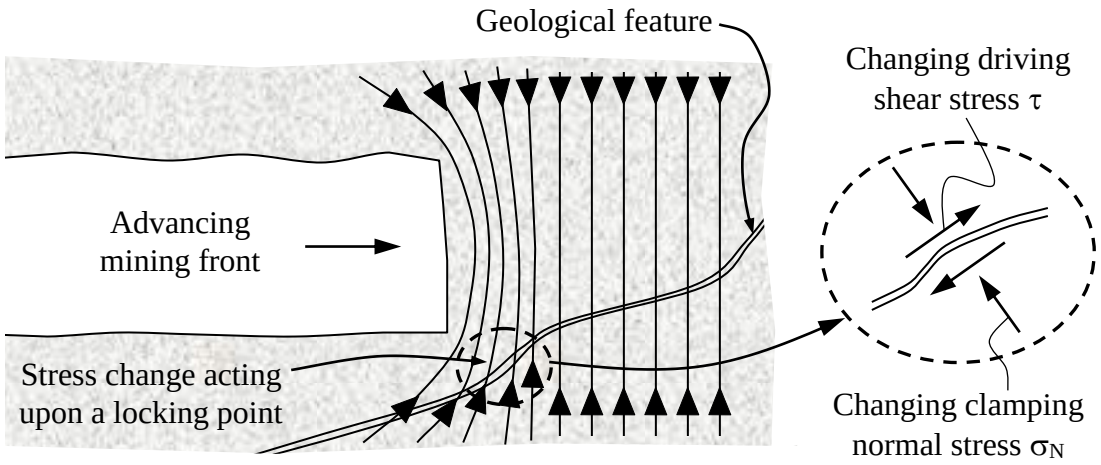

Figure 15. Schematic view of a conceptual advancing mining front illustrating the mechanism of fault-slip type bursting.

Very large seismic events (over a Richter Magnitude 2.0) are often associated with this type of failure because it takes very large amounts of energy to force displacement along a strong and stiff discontinuity that: 1) is not perfectly planar and resists movement in regions where undulations lock it in place; and, 2) is completely surrounded and confined by rock and has no degree of freedom to accommodate the deformation the stress regime is forcing upon it. Depending upon the location and orientation in relation to the mining fronts of other fractures in the rock mass, a particular discontinuity can be mobilised and brought to failure by mining carried out quite a distance away. As more mining fronts advance in the vicinity of a discontinuity, the stress regime acting upon it becomes more complex.

2.4. METHODOLOGIES TO ASSESS THE ROCKBURST POTENTIAL OF ROCK

Although the prediction of rockbursting conditions does not constitute the core of this thesis, it was deemed important to describe some of the more commonly encountered methods used for this purpose, in order to provide some means of assessing whether or not violent failure is likely to occur, and, ultimately, whether or not destressing should be considered. A number of methodologies have been derived to assess the rockburst

potential of rock. Some only consider the characteristics of the intact rock material, and, hence, only provide an indication on whether or not the rock has a tendency to fail violently, if other conditions are present as well. These methods are summarised in Appendix A. Other approaches are based upon in situ conditions and apply more readily to the rock mass. These are summarised in Appendix B.

2.5. GEOMECHANICS-BASED MEASURES TO ALLEVIATE VIOLENT ROCK MASS FAILURE

In previous sections the necessary geomechanical conditions that can lead to the violent failure of rock have been discussed, as follows:

1. A high magnitude stress regime, as well as a stress path to failure under increasing driving stress and near-constant / increasing confining stress;
2. A stiff, strong and brittle rock mass; and,
3. A soft loading system.

One could argue that if these conditions could be altered, one could somewhat control the occurrence of violent rock mass failure. Although there is little one can do to artificially stiffen the loading system, items 1 and 2 can be addressed to a certain extent. The high stress regime, for one, can sometimes be alleviated by modifying the mining method (to a pillarless approach, for example) or implementing a different mining sequence (one that manages stress differently and avoids pinching stress in shrinking pillars). Extracting a piece of ground for the purpose of diverting stresses away and putting a mining block in a stress shadow can also be contemplated, so can a destressing approach, to weaken the rock mass and prevent the accumulation of large stress levels in it.

Note: Destress blasting can be broadly defined as the process of detonating confined explosive charges for the purpose of damaging a rock mass, thus softening its behaviour, reducing its capacity to sustain high stresses, and, hence, its potential to undergo violent failure. Destress blasting will be discussed in detail in Chapter III.

The stress path to failure can also be managed to a certain extent through the implementation of alternative mining sequences, which would result in lower driving stresses developing and allow confinement to be dissipated (usually towards open excavations). Of particular importance in this work, destressing techniques can also be used for this purpose, as they reduce the stress levels under which failure can occur. Item 2 can also be addressed, by implementing a destressing approach that would modify the mechanical properties of the rock mass.

These comments are in agreement with a series of three strategies that Oliver *et al*. (1987) outlined to combat the occurrence of rockbursting at INCO's Creighton Mine, as follows. Firstly, "ensure that the pillars are weak, with low lateral confinement so that they fail under low levels of stress" – this essentially addresses items 2 and 1, respectively. Secondly, "modify the behaviour of the rock in the pillar by destress blasting" – this deals with item 2. (The third strategy put forth, which consists of attempting to induce the sudden failure at blast time, when no one is exposed underground, is tactical in nature and based on common sense.)

These comments are also in agreement with a summary proposed by Singh (1987), in which he stated that the purposes of destressing in Ontario mines were to:

- Divert the high stress fronts away from the mining faces; distribute the stress more evenly over a wider area than before destressing; and, lower the stress levels and the stored strain energy. These steps all relate to item 1.
- Modify the failure mode from brittle to plastic and promote gradual yielding of the fracture zone. This relates to item 2.
- Try to generate a number of minor rockbursts, rather than fewer larger ones. Although this point does not specifically relate to any of the items stated, it constitutes an end-result of those. (If the rock mass cannot be made softer, a stress path that will fail it under both lower driving and confining stresses will result in smaller, but more numerous, instantaneous energy releases.)

Blake *et al*. (1998) noted that the strain energy inside a rock mass is accumulated and stored within the solid volume, but dissipated along surfaces, essentially by frictional sliding. Hence, the potential violence of failure increases for homogeneous materials in which little natural fracturing and/or variation in mineralogy occur. On the other hand, as a rock mass becomes less homogeneous, it becomes easier for micro-fractures to develop and propagate along the pre-existing discontinuities – this softens the behaviour of the material, promotes a more even and progressive energy dissipation process, and changes the failure mode of the system towards plasticity. This is well in accordance with item 2, because stiff, strong and brittle rock masses are usually quite massive, and encompass few discontinuities and weakening features. This reasoning provides justification for destress blasting, which increases the degree of inhomogeneity of the rock mass. Blake *et al*. (1998) further argued that promoting shearing deformation on existing fractures is highly beneficial for destressing purposes because it results in energy dissipation via gouge formation and heating due to frictional sliding.

CONCLUSION DU CHAPITRE. Le Chapitre II a défini le concept de rupture violente du roc ainsi que les conditions nécessaires pour qu'elle survienne, qui sont reliées au régime de contraintes et à leur cheminement vers l'enveloppe de rupture, aux caractéristiques mécaniques du massif rocheux et à la rigidité du système de chargement. La discussion s'est ensuite orientée vers les conditions qui peuvent être manipulées de manière à réduire les risques de coups de terrain. Il a été montré que la plupart peuvent être altérées à divers degrés par l'application d'une gamme de procédures. L'une de ces procédures consiste en l'utilisation de tirs de préconditionnement et de relâchement des contraintes, qui peuvent modifier le régime de contraintes auquel un certain volume de roc est soumis, ainsi que les propriétés mécaniques de la zone ciblée.

Le prochain chapitre va examiner plus en détail les tirs de préconditionnement et de relâchement des contraintes, et décrire comment ces techniques fonctionnent.

CHAPTER CONCLUSION. Chapter II defined violent rock mass failure and identified the conditions necessary for it to occur, which are related to the stress regime and stress path to failure, the mechanical characteristics of the rock mass, and the stiffness of the loading system. The discussion then concentrated on those conditions that can be manipulated in order to lower the risk of rockbursting to occur. It was shown that most can be altered to various extents by the implementation of a range of procedures. One of these procedures is

destress blasting, which can modify the stress regime a particular volume of rock is subjected to, as well as the mechanical properties of the targeted volume.

The next chapter will focus on the mechanics of destress blasting and describe how these techniques work.

CHAPTER III

3. DESTRESS BLASTING MECHANISMS

SOMMAIRE DU CHAPITRE. Ce chapitre traite des mécanismes de tir de relâchement des contraintes et montre que, bien que des explications raisonnables aient été proposées, il n'existe pas de description unique du procédé qui soit universellement acceptée. La principale raison en est la grande difficulté associée à l'observation et à la mesure de la rapide succession d'événements qui se produisent dans ce type de sautage fortement confiné. Certaines explications reposent sur un raisonnement analytique, tandis que d'autres sont basées sur des considérations énergétiques. D'une manière générale, le mécanisme des tirs de relâchement des contraintes le plus largement accepté consiste en un affaiblissement du massif rocheux et une réduction de son module effectif d'élasticité. Une discussion est également effectuée concernant les critères de performance des tirs de relaxation des contraintes – ici également, il n'existe pas de critère unique qui soit universellement accepté et pas de seuil quantitatif bien établi qui définisse le succès de manière inéquivoque.

L'objectif principal de ce chapitre est de fournir une compréhension du processus des tirs de relâchement des contraintes, qui sera utilisée plus tard pour aider à définir les paramètres des matrices d'interaction de Systèmes d'ingénierie du roc qui seront construites pour décrire ce processus.

CHAPTER SUMMARY. This chapter discusses the mechanisms of destress blasting and shows that, even though reasonable explanations have been proposed, there is still no universally accepted detailed description of the process. The main reason for this is the great difficulties associated with observing and measuring the rapid succession of events that

occur in this type of confined blast. Some explanations rely on an analytical thinking process, whereas others rely on energy considerations. Overall, the most widely accepted destressing mechanism consists in the softening of the rock mass and the reduction of its effective elastic modulus. A discussion is also presented on adequate performance criteria for destress blasts – again, no single criterion is universally accepted and no well-established quantitative threshold exists to define success.

The main objective of this chapter is to provide insight into the destress blasting process, which will be used later to help define adequate parameters for the Rock Engineering Systems interaction matrices that will be constructed to describe this process.

3.1. GENERAL DEFINITION OF DESTRESS BLASTING

For the purpose of this thesis destress blasting is broadly defined as any attempt involving the usage of confined explosive charges to reduce the ground stresses in a particular region, and in which the blasted material is left in place (i.e., not mined). From a more mechanistic point of view it can be defined as the process of using confined explosive charges in order to damage a rock mass, thus softening its behaviour, reducing its capacity to bear high stresses, and, hence, the potential for it to undergo violent failure. (Although the technique would conceptually work in soft rock masses in which high stress levels would induce large-scale deformations under quasi-static and aseismic conditions, it will be discussed later that a requirement for it to work is for the rock mass to be brittle, which is rarely the case for soft rock units.)

3.2. THE MECHANISMS OF DESTRESS BLASTING

At the time this thesis was prepared there was no universally accepted explicit description of the detailed mechanisms involved in destress blasting. A number of authors have however proposed reasonable explanations of the process.

3.2.1. Destress blasting mechanism as per Crouch

Crouch (1974) expressed destressing in terms of where the elastic modulus line of the destressed region intersects the local mine stiffness line. Crouch defined the elastic modulus line of the destressed region, which he also refers to as the "destress line modulus", as a line that intersects the origin of the stress-strain graph (at coordinates [0,0]) and has a slope equal to the elastic modulus of the region of interest after the destress blast has been detonated in it. The local mine stiffness line, on the other hand, is defined as a line that 1) intersect the y-axis of the stress-strain graph at the stress level initially applied to the region of interest (prior to any deformation occurring in it); and, 2) has a slope equal to the stiffness of the loading system. It hence represents the stiffness of the loading "platens" (the mine abutments) acting upon the zone targeted for destressing (typically a pillar), similarly to lines ADS and AGH in Figure 11. In other words it corresponds to the reduction of load (imparted to the region of interest by the mine abutments) that will be achieved for a given amount of deformation in the system.

As illustrated in Figure 16, Crouch defined three possible destress blasting outcomes, which are "critical", "subcritical" and "supercritical". "Critical" and "supercritical" results, whereby the intersection of the elastic modulus line of the destressed region and the local mine stiffness line lies on or outside the stress-strain envelope of the rock mass, are postulated to result in a successful destressing effect, i.e., in a destress blast that effectively lowers the risk of rockbursting occurring. "Subcritical" results, on the other hand, are considered to be ineffective in reducing the stress level in the targeted region.

The reasoning is as follows, based upon the conceptual physical arrangement shown in Figure 16d. The initial situation corresponds to a high stress level (point A) being applied to a pillar, which has not yet started to deform in response to the load. An equilibrium will eventually be reached at point B, where 1) enough deformation ε_i will have occurred in the pillar to increase the load in it to σ_i; and, 2) the mine abutments will have converged also by ε_i and will be applying a load of σ_i to the pillar. The problem is that this equilibrium sits near the peak strength of the pillar and that any additional load (due to further mining in the

region, for example) will push it over its peak strength and into its brittle response phase. According to Crouch, destress blasting is meant to damage the rock mass in order to change its stiffness and avoid the occurrence of this brittle phase. After destressing, the pillar stiffness will be modified and will be reduced to the slopes of lines OC, OD or OE, depending upon the outcome of the blast.

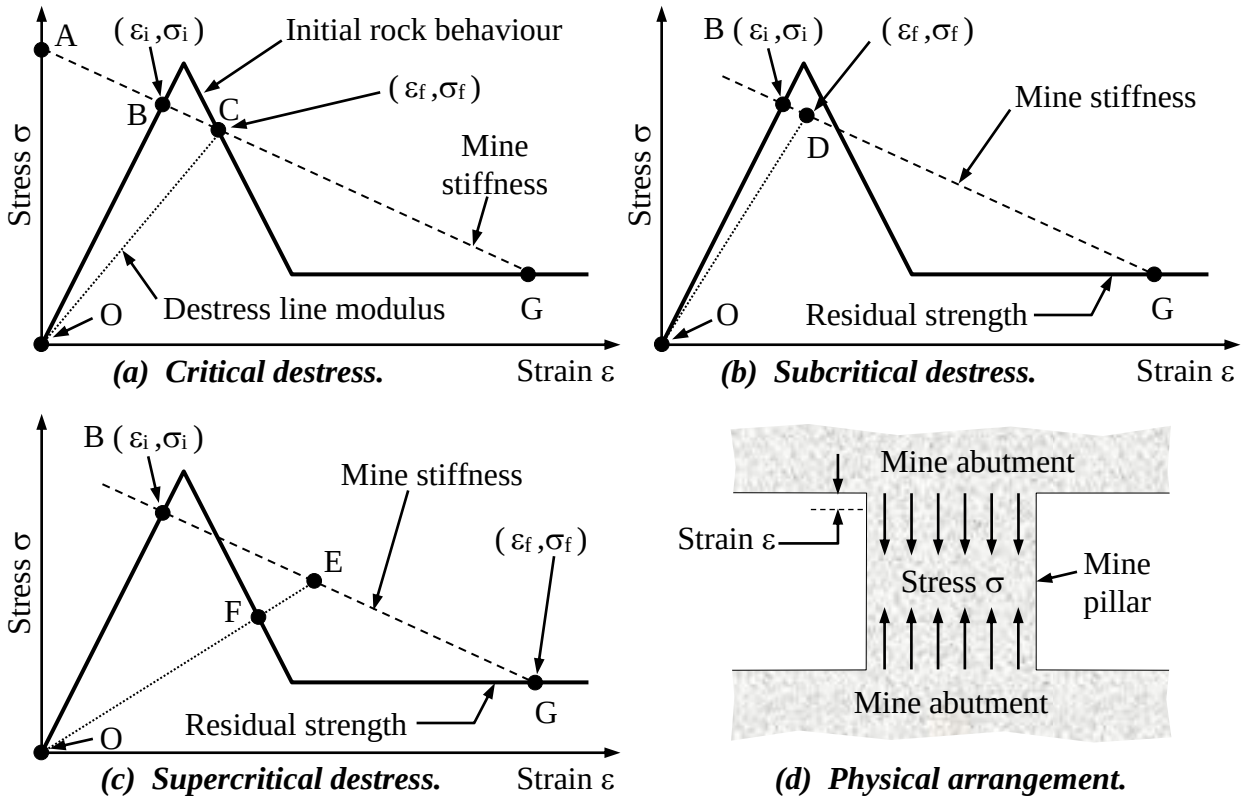

Figure 16. The possible outcomes of a destress blast. (Adapted from Crouch, 1974.)

In the case of a critical outcome (Figure 16a) the destress line modulus of the pillar will intersect the local mine stiffness line at point C, which sits right on the stress-strain curve of the pillar – although the worst possible situation has been avoided by avoiding the peak load, much of the brittle response remains before the residual strength of the pillar can be reached, which can still result in violent behaviour.

In the case of a subcritical outcome (Figure 16b) the destress line modulus of the pillar will intersect the local mine stiffness line at point D, which is inside the stress-strain curve of

the pillar. As a result, additional loading will bring the pillar to failure and into its brittle response – this does not constitute the destressing effect sought after.

In the case of a supercritical destress blast (Figure 16c) the intersection of the pillar destress line modulus and the local mine stiffness line lies at point E, outside the stress-strain envelope. As a result, the remainder of the path along the stress-strain curve (from point F to point G, which corresponds to the ultimate state of equilibrium) occurs under relatively low stress levels and along the last leg of the brittle response of the pillar. Much of the problem area – near peak strength and at the beginning of the brittle response, where large amounts of strain energy are rapidly dissipated – is hence avoided. As a pillar is destressed and its load bearing capacity is reduced, the local ground stresses are redistributed elsewhere in the rock mass, in regions where the load bearing capacity remains higher. Crouch pointed out that destressing works best when the targeted pillar is nearing its peak strength and relatively little additional energy is required to bring it to failure (i.e., past its peak strength).

3.2.2. Destress blasting mechanism as per Hedley

Whereby Crouch (1974) investigated the conditions of stress and strain before and after a destress blast, Hedley (1992) has proposed one description of the rapid chain of events that happen inside a pillar when a destress blast is fired in it. Figure 17, and in particular the load-displacement curve shown in Figure 17c, summarises this succession of events.

Based upon this description, at the instant the destress blast is fired the pillar experiences a near-instantaneous increase in load (due to the blast) that forces apart its hanging wall and footwall abutments (which represent the “platens” acting upon the pillar) along the local mine stiffness slope AB. This dynamic load is represented schematically in Figure 17a – a mechanical analogy is shown in Figure 17b, whereby a high pressure uncompressible gas would be near-instantaneously injected in a flat-jack positioned between two statically-loaded platens in order to separate them very rapidly.

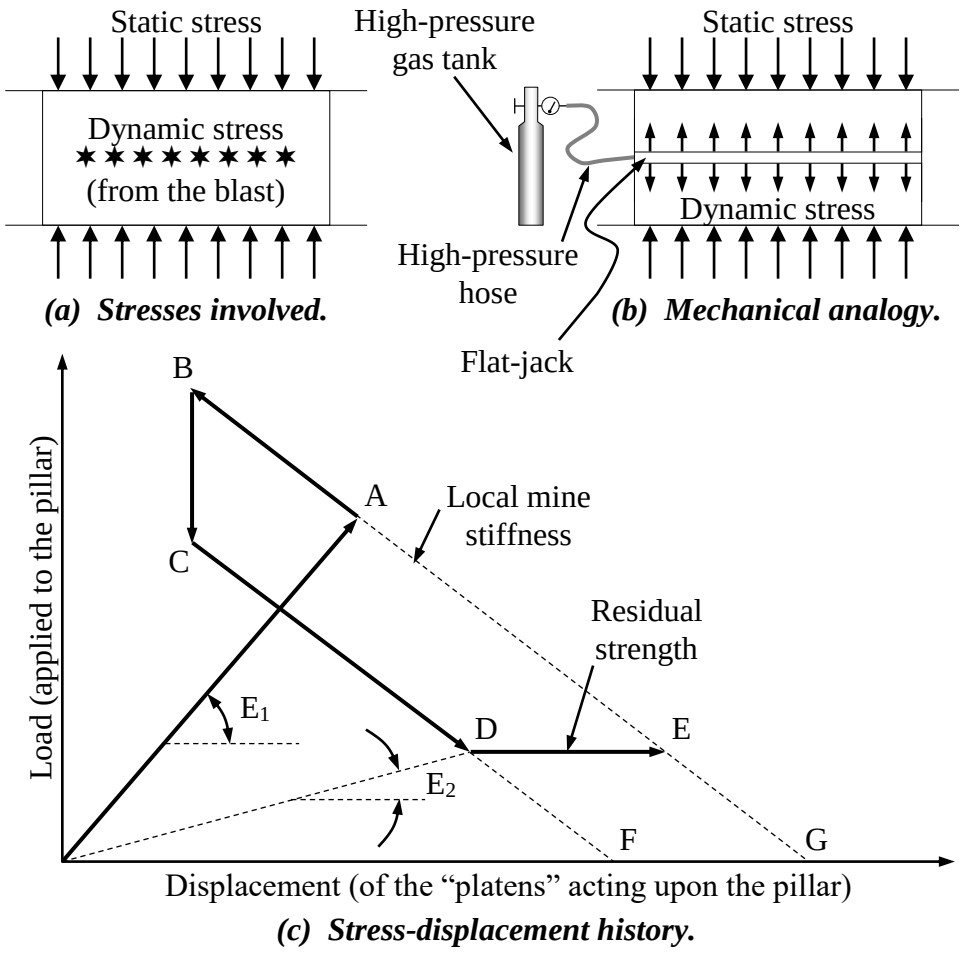

Figure 17. Stress-displacement history of a pillar during a destress blast. (After Hedley, 1992.)

Once the pressure wave has passed and the detonation gases have started to vent, the load suddenly drops to C, too quickly for the hanging wall and footwall to converge again. The analogy would be the sudden failure of the high pressure hose of Figure 17b. A further load reduction (to point D) follows very rapidly, due to the convergence of the hanging wall and footwall. At this point the pillar will have a reduced elastic modulus E_2. Equilibrium is eventually reached at point E once the hanging wall and footwall have converged enough to intersect the local mine stiffness line.

This explanation is plausible. Although there are no field measurements that undisputedly corroborate it, it explicitly accounts for many of the known contributing factors to the process (such as the progression of the explosive energy input and dissipation, and the

eventual convergence of the hanging wall and footwall, for example), and is in accordance with post-blast observations. It however considers that because of the high level of confinement generally associated with a pillar destress blast most of the detonation gases are vented through the blasthole collar, effectively playing only a limited role in the process, and that, as a result, the shock wave is the major source of rock fragmentation under these circumstances. This, as will be discussed later, is debatable and illustrates that, overall, there still does not seem to be a consensus on exactly how destress blasting works.

3.2.3. Energy considerations

Salamon (1974) expressed the energy balance due to mining (i.e., the creation or enlargement of an excavation in solid rock) as follows:

$$Wt + Um = U_c + Wr \qquad \text{..... Eq. (12)}$$

With: Wt the change in potential energy of the system (i.e., the total amount of energy available in the system); Um the strain energy that was originally stored in the rock that has been mined (removed from the system); U_c the increase in stored strain energy in the un-mined rock (remaining in the system); and, Wr the energy released, or dissipated, in the process. All these energy components are expressed in Joules. The left hand side of Equation (12) corresponds to the energy components that are generated by the creation or enlargement of the excavation, whereas the right hand side of this equation corresponds to the energy that is dissipated in the excavation process. The energy released in the process, Wr, has two components: the strain energy that was originally stored in the rock that has been mined, Um, and a dynamic component, Wk. We have that:

$$Wr = Um + Wk \qquad \text{..... Eq. (13)}$$

Equation (13) holds true if no artificial support is involved, which would contribute to the energy balance. When the effect of ground support and the stress-induced failure of the region immediately surrounding the mined area are considered, the energy balance becomes:

$$Wt = U_c + Us + Wr + Um + Um^1 \qquad \text{..... Eq. (14)}$$

With: Us the energy absorbed by the ground support system; Um^1 the strain energy that was originally stored in the failed rock material around the excavation (and which has been shed towards intact rock further away); and, Wt, U_c, Wr and Um as previously defined. (Additional energy considerations are discussed in Appendix B-4.)

The energy balance becomes more complex in the case where a destress blast is detonated in the rock mass and explosive energy is injected into the system. Hedley (1992) proposed the following energy balance for this situation, based upon the reasoning associated with Figure 17:

$$W_T + Um_1 + Ex = U_C + Um_2 + U_f + W_K \quad \text{..... Eq. (15)}$$

With: W_T the change in the potential energy of the system from before and after the destress blast; Um_1 and Um_2 the stored strain energy before and after the destress blast, respectively; Ex the explosive energy used to push back the pillar walls; U_C the increase in strain energy in the surrounding rock after the destress blast; U_f the energy consumed in fracturing the rock mass; and, W_K the dynamic energy that vibrates the rock mass after the destress blast. Combining equations (12) and (13) gives:

$Wt + Um = U_c + Wr$, and $Wr = Um + Wk$

Hence, $Wt + Um = U_c + (Um + Wk)$, which results in $Wt = U_c + Wk$, or,

For the case of a destress blast, $W_T = U_C + W_K$

Considering Equation (15) $W_T + Um_1 + Ex = U_C + Um_2 + U_f + W_K$

We have $(U_C + W_K) + Um_1 + Ex = U_C + Um_2 + U_f + W_K$, which results in:

$$Um_1 + Ex = Um_2 + U_f \quad \text{..... Eq. (16)}$$

Equation (16) provides a balance between the static strain energy stored in the system before and after the blast, and the dynamic energy injected in and consumed by the system. The energy components involved are shown graphically in Figure 18, with Ep the net change in potential energy in the system. Figure 18d, in particular, illustrates how the load in the targeted zone is reduced after the blast (from point A to point E) and how the elastic modulus of the blasted region has decreased, from E_1 to E_2.

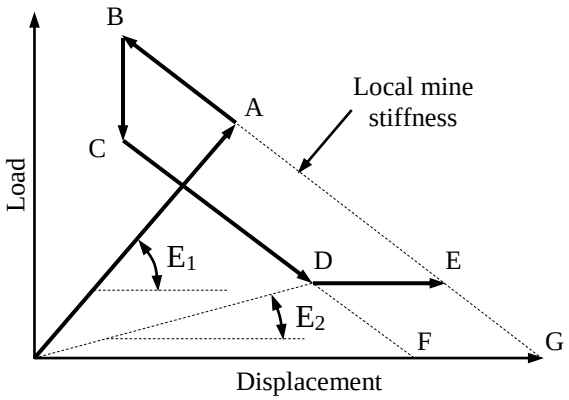

(a) General load-displacement path.

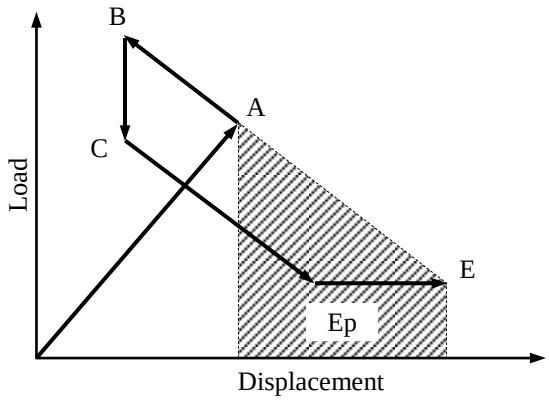

(b) Net change in potential energy.

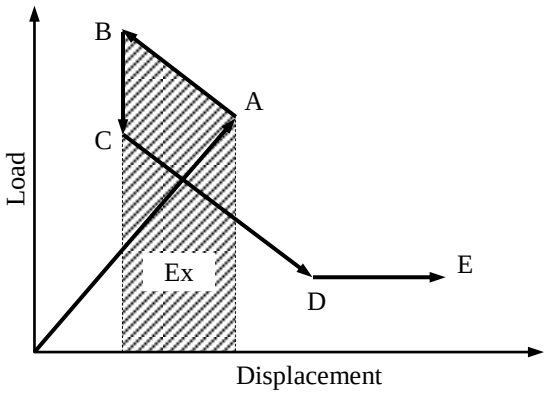

(c) Explosive energy (walls push back).

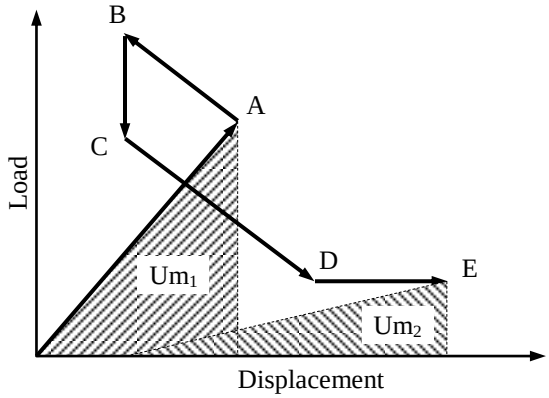

(d) Stored strain energy before and after destressing.

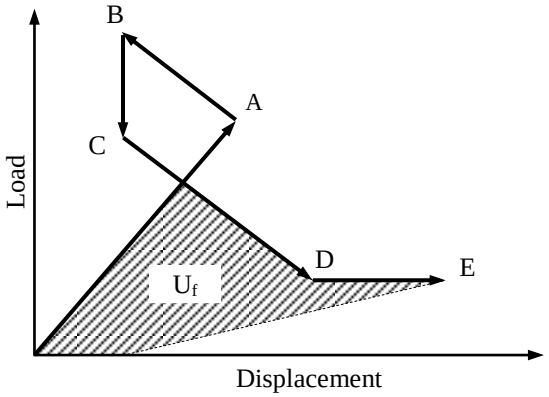

(e) Consumed energy (excluding the explosive energy) to fracture the pillar.

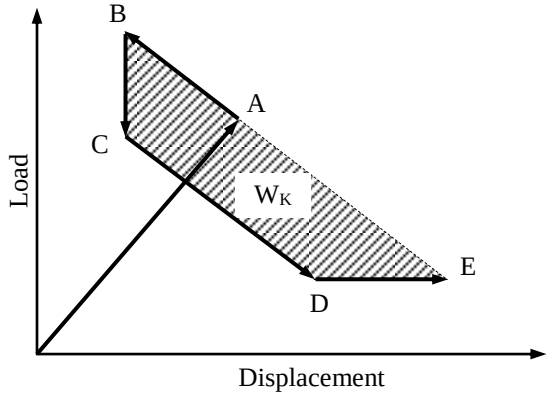

(f) Seismic energy released.

Figure 18. Energy components involved during a pillar destress blast. (Adapted from Hedley, 1992.)

Hedley drew a number of important conclusions from this reasoning, as follows:

- The principal mechanism of stress reduction that results from a destress blast is a lowering of the potential energy of the local rock mass, i.e., of the total amount of energy available to drive failure – this is in accordance with what was stated by Crouch (1974).
- This is accomplished by the decrease in elastic modulus and the load reduction shown in Figure 18d. An additional potential energy reduction can be achieved if point G in Figure 18a can be reached, which can occur only if the blasted material is removed (in which case no load can remain). The effectiveness of a destress blast hence increases as point E moves towards point G, i.e., downwards and/or towards the right hand side. Hedley however pointed out that as the effectiveness of the destress blast increases, the practical difficulties associated with mining this heavily fractured ground will also rapidly increase.
- The strain energy stored inside the targeted region prior to the destress blast is used in the fracturing process, rather than liberated as seismic energy. This seismic energy, released late in the process, is considered to result from both the explosive energy and the variation in potential energy.

  As far as the explosive energy is concerned, it is considered in this approach to be used essentially in pushing apart the walls of the pillar and initiating the fracture process – it is not considered to be the main fracture contributor.

Hedley also stated that the most widely accepted destressing mechanism consists in the softening of the rock mass and the reduction of its effective elastic modulus.

Similarly to what was discussed at the end of the previous section, this energy-based explanation of the destress blasting mechanisms is quite reasonable, although difficult to prove with field measurements and hard data.

3.2.4. Additional comments on the destress blasting mechanisms

Importantly, the occurrence during a destress blast of some level of rock ejection and material dislodging can be argued to result in a further reduction of the local stress levels. Such ejection and dislodging of rock generally occurs in the regions of least confinement – usually around the blastholes collar area, and/or near the toe of the blastholes when they break through into other cavities – when high powder factors are implemented. These ejections provide void inside the targeted volume, which, in turn, provide kinetic freedom for the blasted pieces of rock to displace, shift and rotate relative to each other. This results in much more significant levels of disturbance being attained inside the rock mass after blasting, and in a larger reduction of its load bearing capacity, as illustrated in Figure 19.

In the case of a blasted rock mass that sustains little ejection and is left essentially undisturbed (Figure 19a), the stress reduction is provided by the movement that occurs along the surfaces of the many discrete blocks created by the destress blast. In a confined environment where no material ejection has happened, and in which some bulking of the rock mass has occurred as a result of the extension of existing, and the creation of new, fractures, the possible extent of this movement is limited.

In the case of a rock mass that has been disturbed as the result of material ejection during the blast (Figure 19b), the load must be transferred through fewer contacts having a smaller surface area and relatively little confinement – this results in very large stress levels developing locally, which further fail the rock in the contact regions. This impedes the load transfer process, and, hence, further reduces the load bearing capacity of the rock mass. Ejection of material also results in additional convergence of the walls.

Ejection is an important issue that is not directly accounted for in the explanations proposed by Crouch (1974) and Hedley (1992). The C-D displacement in Figure 17 and Figure 18 due to the convergence of the hanging wall and footwall can however be argued to indirectly account for such ejection. From a practical point of view, preventing ejection from occurring is quite difficult when large quantities of explosives are involved.

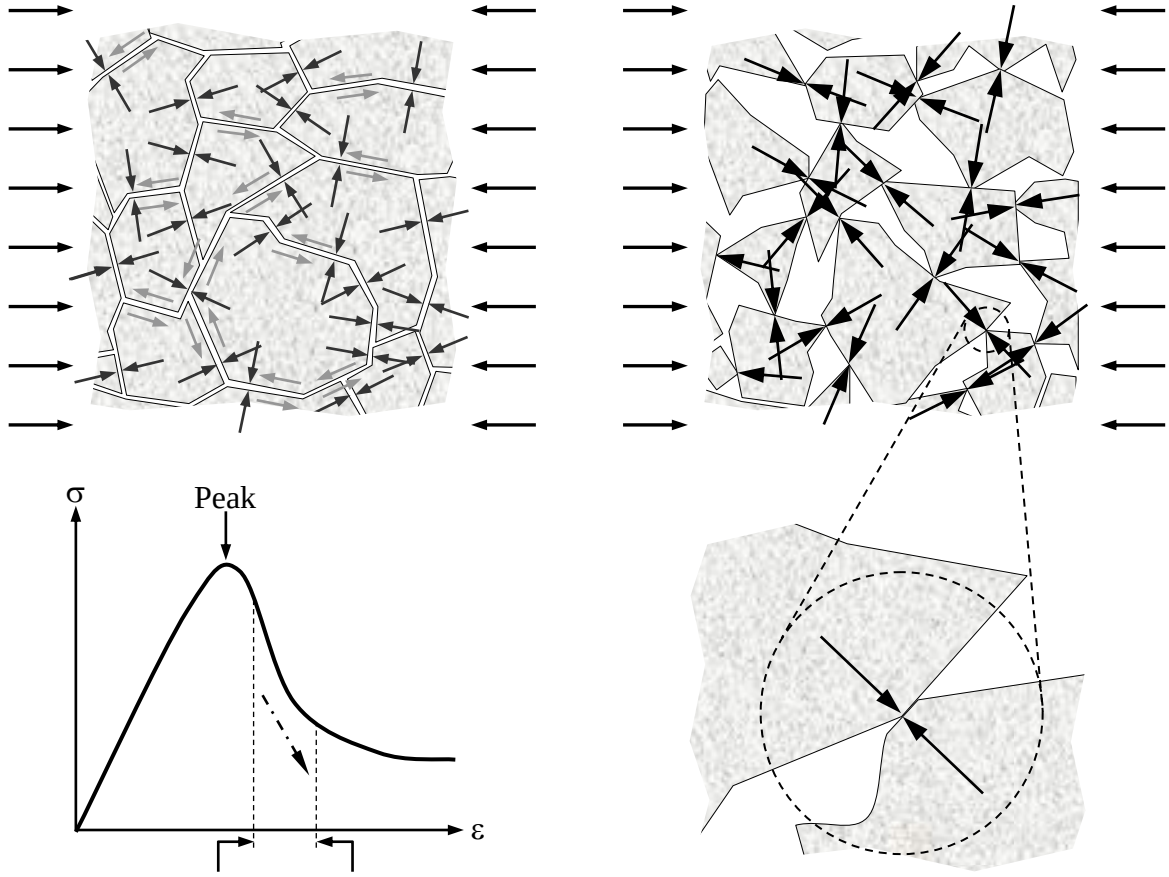

Additional deformation and movement in post-peak conditions further reduce the stress level.

Very large stress levels developing locally along small surface area contacts, with little confinement, resulting in further failure and an increased inability to carry load.

(a) Broken, but undisturbed rock mass. ***(b) Broken and disturbed rock mass.***

Figure 19. Difference in the load bearing capacity of a blasted rock mass that is (a) undisturbed *vs*. (b) disturbed. (Adapted from Andrieux *et al*., 2003.)

3.3. PERFORMANCE CRITERIA FOR DESTRESS BLASTING

As it will be seen later when historical practices will be reviewed, there is no unique and universally accepted criterion to assess the performance of a destress blast – success however implies that a stress reduction has been achieved in the targeted region. From a field perspective, such a blast can be considered successful when it results in safer

conditions for the underground workers and in “easier” mining, i.e., in a more predictable and reliable production output. Any means of assessing such improvements can conceivably be used as a success criterion – as it will be seen later during the review of historical practices, qualitative evaluations in the form of general statements are often used.

Many quantitative assessments can however be made to evaluate the extent of the stress reduction achieved. This reduction could conceivably be represented by any of the properties shown in Figure 20, which are known to vary with the axial deformation of a rock sample (Bieniawski, 1967) and, hence, with the compressive stress it is subjected to.

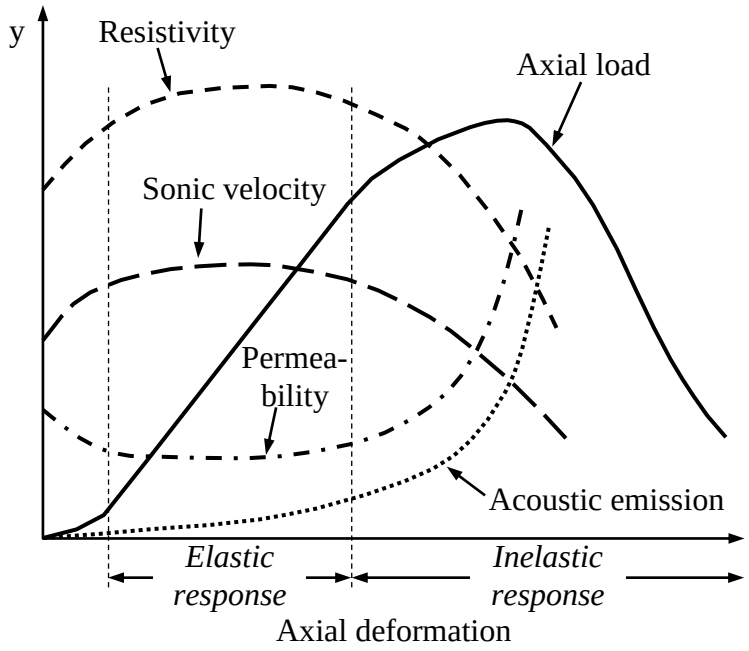

Figure 20. Schematic representation of the behaviour of the resistivity, sonic velocity, permeability and acoustic emission as a function of axial deformation in an axially loaded intact sample of brittle hard rock. (After Bieniawski, 1967.)

Of these properties, the resistivity, permeability and acoustic emission should really be monitored by specialised personnel, which, from a practical point of view, precludes most resident engineering personnel at the mine sites from carrying these measurements. Sonic velocity surveys (as described in Figure 108a and b in Appendix B.2) are somewhat simpler to perform, but can give results that are difficult to interpret by a neophyte.

Convergence measurements can also be performed (with contractometers, for example, which are extensometers that can measure both extension and contraction [Bawden & Lausch, 2000]) near the targeted zone, in order to track the ground deformations that result from a destress blast. A reduction of the microseismic activity in the region of interest can also be indicative of lower stress levels.

It can however be argued that the most direct method to quantify the results of a destress blast consists in performing direct stress measurements, by means of load cells. These have the advantage of providing a direct assessment of the stress level changes in the region of interest.

Regardless of the method retained to assess the results of a destress blast, there are no well-established or universally-accepted threshold values above or below which success is considered to have been achieved. As more stress reduction has been attained, more success can be considered to have been accomplished. Destress blasting performance criteria will be discussed further in Section 7.4.2.10.

CONCLUSION DU CHAPITRE. Une revue de divers mécanismes proposés pour les tirs de relaxation des contraintes a été effectuée dans ce chapitre qui a montré que, bien que des explications raisonnables aient été mises de l'avant, il n'existe pas de description détaillée du processus qui soit universellement acceptée. De plus, il n'y a pas de critère unique qui soit communément accepté et pas de seuil bien établi qui définisse quantitativement le succès d'un tel tir.

Bien que ces conclusions soulignent le besoin en recherche qui subsiste dans le domaine des tirs de relâchement des contraintes, les explications proposées sont néanmoins utiles dans la mesure où elles fournissent une base qui peut aider à déduire quels paramètres jouent un rôle dans le procédé.

Le prochain chapitre va examiner plus en détail les divers types de tirs de relâchement des contraintes couramment appliqués dans les mines souterraines. Les pratiques historiques de tirs de relaxation des contraintes vont être également examinées dans le prochain chapitre, de manière à cerner davantage quels paramètres ont été historiquement considérés comme jouant un rôle dans le procédé. (L'identification de ces paramètres est

fondamentale pour la construction des matrices d'interaction recherchées dans le cadre de ces travaux.)

CHAPTER CONCLUSION. This chapter has reviewed proposed destress blasting mechanisms and showed that, although reasonable explanations have been put forth, there is still no universally accepted detailed description of the process. Also, no single criterion is universally accepted and no well-established quantitative threshold exists to define success.

Even though these findings underline the need for further research in the field of destress blasting, the proposed explanations are still valuable as they provide a basis that can help deduce which parameters play a role in the process.

The next chapter will examine in more detail the various types of destress blasts commonly implemented in underground mines. Historical destress blasting practices will also be reviewed in the next chapter, in order to further investigate which parameters have been historically considered to play a role in the destress blasting process. (The identification of these parameters is central to the construction of the Rock Engineering Systems interaction matrices sought after in this work.)

CHAPTER IV

4. DESTRESS BLASTING TYPES AND HISTORICAL PRACTICES

SOMMAIRE DU CHAPITRE. Considérant que cette thèse concerne spécifiquement les tirs de relâchement des contraintes de gros piliers de mines dans des conditions complètement confinées, il est nécessaire d'établir clairement qu'ils ne constituent qu'un type particulier de tirs de relaxation des contraintes. Pour ce faire, les quatre types de tirs de relâchement des contraintes qui sont généralement utilisés dans les mines souterraines sont décrits en détail dans ce chapitre, qui sont: 1) dans les faces de développement, horizontales ou verticales; 2) dans des volumes de roc qui seront éventuellement minés; 3) dans des horizons où aucune opération de minage n'est prévue, mais qui redirigent et concentrent de hauts niveaux de contraintes vers des zones de production active ou des infrastructures à long terme; et, 4) près de failles actives qui ont un potentiel de glissement violent.

Une trentaine d'études de cas, provenant d'Afrique du Sud, des États-Unis, du Canada, d'Australie, de Suède, d'Allemagne et de Pologne, sont ensuite présentées dans ce chapitre. Ces cas adressent un vaste éventail d'approches et ont été sélectionnés dans le but d'identifier quels paramètres gouvernent principalement le processus de relâchement des contraintes. Bien qu'ils ne constituent pas le sujet principal de cette thèse, des exemples de tirs de préconditionnement ainsi que de relâchement des contraintes dans des faces de développement sont brièvement présentés, de manière à 1) démontrer que l'approche fonctionne à diverses échelles; et, 2) augmenter les chances d'identifier quels paramètres jouent un rôle prépondérant dans le procédé.

La revue des études de cas indique clairement qu'il n'existe pas actuellement de procédure d'ingénierie formelle et bien établie pour la conception de tirs de relâchement des contraintes – ces sautages sont encore largement conçus par essai et erreur, et basés sur

l'expérience passée (généralement spécifique à un site particulier). Il existe peu de données consistantes qui expliquent de manière rationnelle les choix effectués concernant la localisation, la géométrie et les dimensions d'un sautage donné de relâchement des contraintes, ainsi que le choix du diamètre des trous, du fardeau et de l'espacement, des types d'explosifs, et des autres paramètres de tir. De plus, beaucoup d'observations différentes ont historiquement été effectuées suite aux essais de tirs de relâchement des contraintes – ce manque de consistance rend difficile la comparaison quantitative des diverses études de cas et l'établissement de conclusions fermes concernant le succès réel atteint par les diverses approches essayées. Ce problème est compliqué par le peu de data de haute qualité qui permettraient de quantifier de manière non équivoque le degré de succès atteint (c'est-à-dire l'ampleur de la réduction de contrainte réalisée dans la zone ciblée) par les tirs confinés à grande échelle de relâchement des contraintes détonés dans des piliers de mine décrits dans les études de cas examinées.

Cette revue démontre clairement qu'un besoin existe pour une approche plus scientifique pour la conception de tels sautages (approche qui sera entreprise plus tard dans cette thèse).

CHAPTER SUMMARY. Considering that this thesis addresses specifically the destress blasting of large pillars under completely choked conditions, it is necessary to clearly establish that this constitutes only a particular type of destress blast. For this purpose, the four types of destress blasting situations that are usually implemented in underground mines are described in some detail in this chapter, which are: 1) in development headings, either horizontal or vertical; 2) in volumes of rock that will eventually be mined; 3) in remnant pillars and panels that are not intended to be mined, but that redirect and concentrate problematic high stresses towards active mining areas or long-term infrastructures; and, 4) near active faults that have a potential to slip violently.

Over thirty destress blasting case studies, from the Republic of South Africa, the United States, Canada, Australia, Sweden, Germany and Poland, are then presented and reviewed in this chapter. These encompass a wide array of approaches, and were selected with the objective of trying to identify which parameters govern the destressing process the most. Although not the core subject of this thesis, examples of development destressing and preconditioning are included, essentially in order to: 1) demonstrate that destressing has been shown to work at various scales; and, 2) increase the chances of properly identifying all the parameters that play a significant role in the process.

The literature review clearly indicated that there are essentially no common and well-established "formal" engineering procedures that are used to design destress blasts – destressing with explosives is still largely a trial and error procedure based upon past (and generally site-specific) experience. Little consistent data exist that rationally explain the chosen location, shape and size of a given destress blast, as well as the choice of blasthole diameter, burden and spacing, explosive types, and other design parameters. Furthermore, a wide variety of parameters have historically been recorded during destress blasting trials – this lack of consistency makes it difficult to quantitatively compare case histories and draw definitive conclusions concerning the success of various design approaches. This

issue is compounded by a limited amount of high quality data that would allow one to unequivocally quantify the actual degree of success – i.e., the extent of the stress reduction that was achieved in the targeted volumes of ground – reached by the large-scale choked panel destress blasts described in the case studies examined.

This literature review clearly highlights the need for a more scientific approach to designing such large-scale choked panel destress blasts. (Such an approach will be pursed later in the thesis.)

4.1. THE VARIOUS TYPES OF DESTRESS BLASTING

There are essentially four types of destress blasting situations encountered in the mining industry, as follows:

1. in development headings, either horizontal or vertical;
2. in volumes of rock that will eventually be mined;
3. in remnant pillars and panels that are not intended to be mined, but that redirect and concentrate problematic high stresses towards active mining areas or long-term infrastructures; and,
4. along sub-planar geological features, such as faults, for example, that have the potential to slip suddenly and violently.

Each type has its peculiarities and historical background, as discussed in the following sections. As far as historical background is concerned, numerous case studies of each type of destress blast have been described in the literature at various levels of detail over the past fifty years or so. Tran & Liu (1997), Blake *et al*. (1998), O'Donnell (1999) and Mitri (2000) have compiled a large number of such case studies. One point that comes across when studying these case histories is the difficulty to directly compare them to each other, due to a lack of consistency in the parameters recorded and the effects observed and/or measured. As a result, and as it will be demonstrated, the comparison between various documented destressing experiments can often only be largely qualitative.

4.1.1. Destress blasting in development headings

Destressing in development headings typically involves relatively small quantities of explosives that are detonated ahead of the face – this is in order to minimise the creation of severe blast-induced damage that may result in ground instabilities in the future. Destress blasting in development headings is routinely done in many mining countries where high stress levels are an issue. In most instances, the practice is perceived as being successful, i.e., as resulting in safer development, a reduction of the risk of violent failure, more stable conditions and less rehabilitation work being required in the drifts. Interestingly, Blake *et al*. (1998) have noticed that destressing ahead of an advancing face has been deemed unsuccessful at some United States mines, not so much due to a lack of destressing effect, but rather out of concerns that destress blastholes detonated in the walls might cause enough damage to compromise the long-term stability of the drift. There is also reportedly a general reluctance in the U.S. to drill larger diameter blastholes for destressing purposes, again out of fear that excessive damage will be induced by larger charges. Destress blasting in development headings does not constitute the core subject of this thesis, and will only be discussed in a limited way.

4.1.2. Preconditioning

Within the context of destressing, the etymology of the word "preconditioning" infers the action of conditioning the rock mass prior to a subsequent action taking place, which is mining. More precisely, preconditioning is the action of rendering the rock mass more conducive to mining, prior to mining actually taking place in it. Preconditioning, also sometimes referred to as "face destressing", hence implies that mining will be carried out directly inside the volume that is to be preconditioned.

Preconditioning typically targets volumes of rock that are not yet subjected to extremely high stress levels, but that will eventually reach that stage, as mining progresses towards them. Blake (1982) first used the word "preconditioning" to specifically indicate that the rock to be conditioned was treated prior to high stresses being forced onto it. The South

African experience in longwall mining, a method widely used in the deep narrow tabular shallow-dipping gold reefs, typically refers to preconditioning because, in this context, the objective is to weaken the rock mass in advance of mining. German coal mines are also using preconditioning on a routine basis (Bräuner, 1983). The practice appears to have a routine connotation to it: based upon the literature it seems to be done often, and sometimes even routinely as an intricate part of the normal mining cycle.

As with development headings, destressing future mining horizons does require some level of "restraint" in the blasting approach, as excessive blast-induced damage and remnant explosive products (that can result from excessive powder factors and the interaction between charges that are located too close to each other) are not desirable with respect to the re-entry of personnel and future production drilling, respectively.

Toper (2002) described two general preconditioning approaches widely used in South Africa – both of them reportedly aim more at inducing slip on pre-existing fractures than at shattering the rock mass. The first approach, illustrated in Figure 21a, consists in drilling preconditioning blastholes that are parallel to the face, whereas the other approach (Figure 21b) involves preconditioning blastholes that are drilled perpendicularly to the face.

Toper (2002) clearly stated that, regardless of the methodology implemented, the objective of preconditioning is to push the stress peak ahead of the mining face and further into the solid rock mass behind it, by releasing some of the strain energy locked-up near the face in the asperities of pre-existing geological features and/or mining-induced fractures. This is consistent with Blake *et al*. (1998), which pointed out that accumulated strain energy inside a rock mass can be relieved in a stable manner by means of shear on existing fractures and the formation of gouge, through frictional losses (in the form of heat) and comminution of the rock along these surfaces. Furthermore, Blake *et al*. (1998) stated that movement along existing fractures and the initiation of slip are likely to result in a softening of the mechanical behaviour of the rock mass ahead of the face, from a tightly-locked brittle behaviour to a more stable and progressive plastic response.

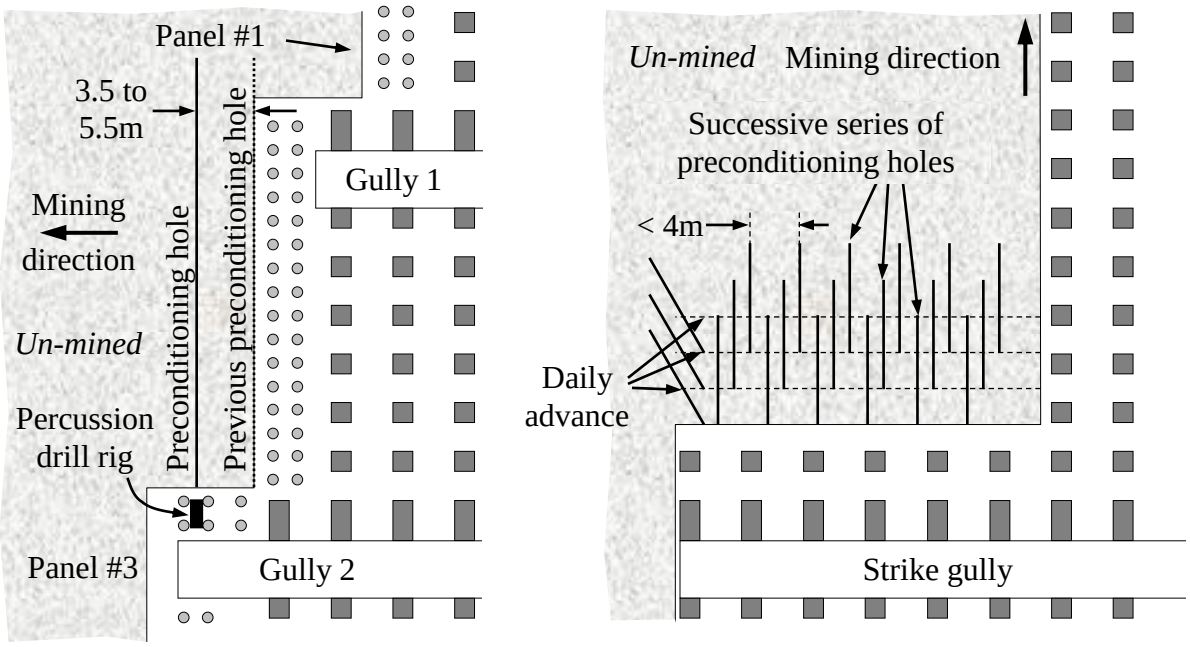

(a) Face-parallel preconditioning.

(b) Face-perpendicular preconditioning.

Figure 21. Conceptual plan views (not to scale) showing layouts for (a) face-parallel; and, (b) face-perpendicular preconditioning in a South African longwall mining sequence. (Adapted from Toper, 2002.)

4.1.3. Destress blasting of remnant pillars

The objectives pursued by the destressing of remnant pillars are the reduction of the stress levels in the targeted volume of rock and the softening of its behaviour. It is typically attempted in remnant rock masses that are subjected to very high stress levels, and which are nearing failure. Contrary to the previous two situations, there are not necessarily personnel re-entry issues or future mining considerations in this case. In the case where no personnel re-entry is planned, the only restricting factors as far as explosive energy levels are concerned are the vibration levels that are produced (and which can destabilise nearby excavations and long-term infrastructures) and the damage to the area from where the destress blastholes were drilled. As a result, large and powerful destress blasts can be implemented, which have the potential to result in significant stress reductions. If personnel re-entry is needed, more moderation is required in order to maintain the integrity

of the excavations – other practical issues, such as subsequent drilling and mining in an area where undetonated explosives might remain, also need to be addressed. (This issue, in Canada, requires the usage of remote drilling.) The destressing of large remnant pillars usually has a "one shot deal" connotation to it, as it is typically aimed at fixing a specific stress issue – it also typically causes enough damage in the blasthole collars area to preclude a second attempt.

Cutting-off and diverting the path of the ground stresses by targeting a volume of rock along this path, whereby deflecting them away from active mining areas, can be considered as pillar destressing. Figure 22 schematically illustrates the principle. This operation essentially seeks to induce a more favourable stress regime (in terms of lower magnitude and/or better orientation) in an active mining horizon.

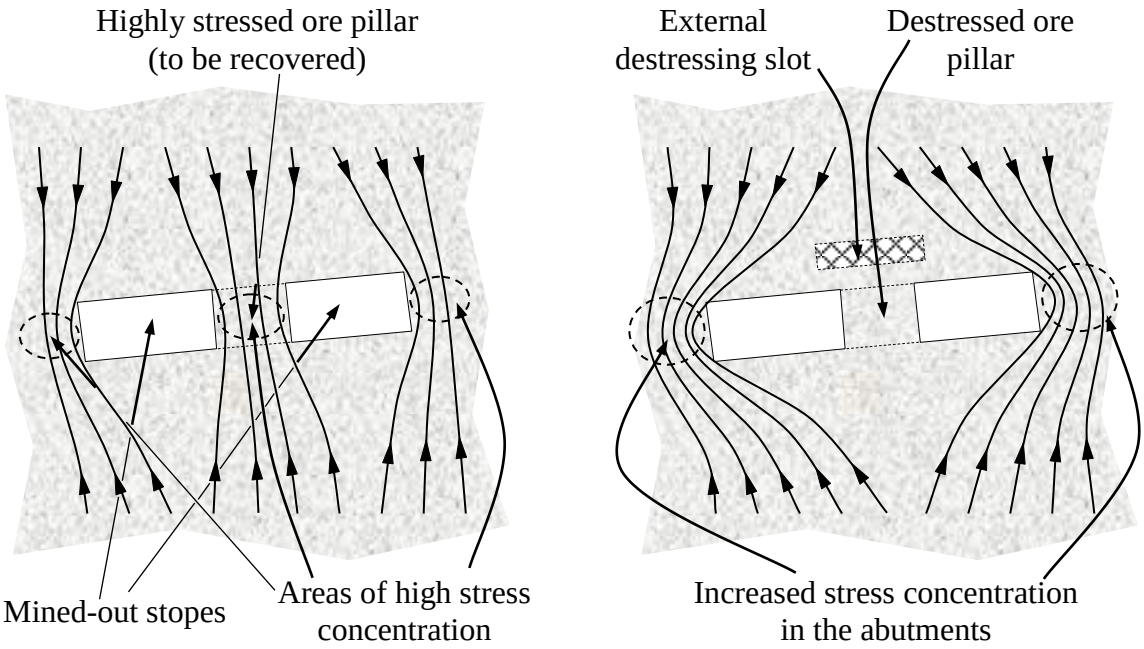

(a) Initial situation. ***(b) Destressed situation.***

Figure 22. The effect of an external destressing slot on a highly stressed ore block.

Such a stress diversion was the objective sought after by the October 1999 blast in the 29-9 Pillar at Brunswick Mine (Andrieux *et al*. [2000]; Brummer *et al*. [2000]), as well as by the December 2001 blast at the Fraser Copper Mine (Andrieux [2001]; Sampson-Forsythe

et al. [2002]), which will both be discussed in detail in later chapters. On the other hand, the large mass-blast of July 2001 in the South Ore Zone at Brunswick Mine (Andrieux & Brummer [2001]; Simser *et al*. [2002]), although implemented principally as a stress control measure, cannot be considered a destress blast because numerous internal voids and free faces had been prepared before-hand, which significantly reduced the level of confinement the targeted volume was subjected to, and because some of the blasted material was planned to be mucked.

Destress blasting large pillars under completely choked conditions (without any free face) constitutes the core subject of this thesis. More specifically, this project will investigate how the relatively new matrix-based Rock Engineering Systems approach can be used to describe more explicitly the level of interaction between various parameters known to play a dominant role in this process.

4.1.4. Destress blasting of active faults

Extensive work has also been done (Hart *et al*., 1988; Last & Harper, 1990; Board *et al*., 1992; Lightfoot & Goldbach, 1995, amongst others) regarding the destressing of highly stressed large-scale sub-planar geological features that have the potential to induce fault-slip seismic events and rockbursts. In this case, the approach generally consists in injecting high pressure fluids (either water, or gases from the detonation of explosive charges) into the fault system with the objective of releasing some of the normal confining stresses that act upon it, in order for the driving stresses that also act upon it to induce movement and release some of the accumulated strain energy.

The fluid can be introduced either progressively, typically by the controlled injection of an incompressible liquid under high pressure, or instantaneously, with the detonation of confined explosive charges. The blasting approach can also aim at softening the rock material in the immediate hanging wall and footwall of the fault, which reduces the capability of the system to clamp it in place and resist slip movement. Triggering movement along active faults at a chosen moment in order to destress them is still the

subject of considerable research, particularly in the field of earthquakes and ultra deep mining.

One problem with large fault-slip type events is the current lack of success in predicting them, both in space and time. Some success has been achieved in anticipating large strain-burst type events by conducting advanced analyses of seismic source parameters, such as tracking cumulative apparent volume *vs*. average energy index, for example. No such progress has been achieved to date for fault-slip type events whereby the nucleation of the process is not necessarily concentrated in one area, but rather occurs over a number of yielding lockup points, each releasing in the process relatively little precursory seismic energy, often not large enough to be detected. The difficulty in predicting such fault-slip events makes it very challenging to decide where along a highly stressed fault a destress blast should be attempted.

4.2. SELECTED CASE HISTORIES

A comprehensive review of over thirty destress blasting case studies was completed within the framework of this project. These constitute by no means an exhaustive description of all the destressing field trials done to date world-wide – rather, they were selected because they encompass a wide array of approaches, with the objective of trying to identify which parameters govern the destressing process the most. Although not the core subject of this thesis, examples of development destressing and preconditioning are also presented, essentially in order to: 1) demonstrate that destressing has been shown to work at various scales; and, 2) increase the chances of properly identifying all the parameters that play a significant role in the process.

The detailed review of these case histories, from South Africa, the United States, Canada, Australia, Sweden, Germany and Poland, is presented in Appendix C.

One point that comes out of the literature review is that large-scale panel destressing is generally regarded as a last resort option, which is only contemplated when it is clear that mining cannot continue safely without some control over local stress levels, and when all other stress control approaches have either failed or could not be implemented.

There seems to be some variation in the terminology used for describing past destressing attempts, particularly between the terms “preconditioning” and “destressing”, which are not always used as per the definitions proposed in Section 4.1. In particular, underground personnel in the Coeur d’Alene district has often returned and worked directly into areas that had been “violently” destressed.

Table 2 compares twenty-one of the most relevant case histories reviewed in Appendix C (those that pertain to large-scale choked destress blasts in large underground pillars, and have the most quantitative data). These were selected in an attempt to compare the various approaches implemented and designs retained. Please note that in this table the term “success” is based upon the assessment of the results, as reported by the mine personnel.

As can be seen, quite a bit of variation exists in the design parameters, including in the degree of “violence” – in terms of the explosive energy per unit volume or unit mass of targeted ground – of the blast (represented by the powder factor in Table 2). This energy aspect is discussed in greater detail in subsequent sections of this thesis.

The literature review clearly indicated that there are essentially no common and well-established “formal” engineering procedures that are used to design destress blasts, regardless of the scale at which they are carried out – destressing with explosives seems to still be largely a trial and error procedure based upon past (and generally site-specific) experience. Little consistent data exist that rationally explain the chosen location, shape and size of a given destress blast, as well as the choice of blasthole diameter, burden and spacing, explosive types, and other design parameters. Furthermore, a wide variety of parameters have historically been recorded during destress blasting trials.

Table 2. Comparative reported data from 21 selected large-scale choked destress blasts in underground pillars.

Mine	Galena Mine	Crescent Mine	Lucky Friday	Lucky Friday	Lucky Friday	Star Mine
Year	1970	1972	1985	Post '85	1990	1976
Panel depth *(m)*	1,135	945–1,065	1,415	N/R	1,500	2,350
Mining method [1]	OC&F	OC&F	OC&F	N/R	UC&F	OC&F
Pillar(s) type	Sill	Sills [× 3]	Sill	N/R	Sill	Sills [× 2]
Length [2] *(m)*	30.0	75.0	~ 45	N/R	180.0	~ 40
Width [2] *(m)*	3.0	N/R	N/R	N/R	3.0	3.0
Height [2] *(m)*	6.0	10–15	~ 25	N/R	28.0	20.0
Volume [2, 3] *(m^3)*	860	N/R	N/R	N/R	32,505	~ 4,720
Density *(kg/m^3)*	3,200	3,200	3,200	3,200	3,200	3,200
Mass [3] *(tonnes)*	2,745	N/R	N/R	N/R	104,020	~ 15,110
Hole depth *(m)*	6.0	2.1	12–15	N/R	25.0	18
Blastholes [4] *(#)*	18	73	19	N/R	58	685m
Diameter *(mm)*	48	41	63.5	127	127	92–101
Spacing *(m)*	1.50	2.1	3.0	3.0	3.0	N/R
Collar *(m)*	N/R	N/R	N/R	6.0	10.0	Variable
Stemm. material	N/R	N/R	N/R	N/R	N/R	N/R
Explosives type	ANFO	ANFO	ANFO	N/R	Watergel	N/R
Total charge(*kg)*	230	275	400	N/R	6,300	4,000
Powder factor*(kg/t)*	0.08	N/R	N/R	N/R	0.06	0.26
Reported results	Success	Success	Success	N/R	Success	Success

Table 2 (continued). Comparative reported data from 21 selected large-scale choked destress blasts in underground pillars.

Mine	Star Mine	Star Mine	Star Mine	Falcon-bridge #5	Strathcona Mine	Strathcona Mine [5]
Year	1979	1974–77	1979	C. 1968	1991	2001
Panel depth *(m)*	2,430	Variable	2,040	N/R	1,190	1,260
Mining method [1]	OC&F	OC&F	OC&F	OC&F	OC&F	OC&F
Pillar(s) type	Sill	Next cut	Sill	Sills	Sill	Rib
Length [2] *(m)*	125.0	Variable	N/R	N/R	N/R	27.5
Width [2] *(m)*	3.0	Variable	N/R	~ 5–6	N/R	3.0
Height [2] *(m)*	28.0	Variable	15.0	17.0	N/R	18.0
Volume [2, 3] *(m³)*	21,295	Variable	N/R	N/R	N/R	3,735
Density *(kg/m³)*	3,200	3,200	3,200	3,600	3,150	2,800
Mass [3] *(tonnes)*	86,140	Variable	N/R	N/R	N/R	10,455
Hole depth *(m)*	28.0	6.0	5–8	3–18	5.5	13–33
Blastholes [4] *(#)*	2,200m	Variable	29	N/R	66	28
Diameter *(mm)*	92	N/R	50–57	N/R	64	114
Spacing *(m)*	N/R	2.0	2–3	6.0	N/R	3.0
Collar *(m)*	Variable	3.0	1.0	N/R	N/R	Variable
Stemm. material	N/R	N/R	Clay	N/R	N/R	Air
Explosives type	Emulsion	N/R	Variable	N/R	N/R	Emulsion
Total charge*(kg)*	4,500	4.5 / hole	180	N/R	N/R	4,485
Powder factor*(kg/t)*	0.07	Variable	N/R	N/R	N/R	0.45
Reported results	Success	Partial	Success	Success	Partial	Success

Table 2 (continued). Comparative reported data from 21 selected large-scale choked destress blasts in underground pillars.

Mine	Lake Shore	Macassa Mine	Red Lake Mine	Red Lake Mine [6]	Red Lake Mine [6]	Sigma Mine
Year	1965	1987	Mid '80s	1984	1984	1996
Panel depth *(m)*	N/R	1,750	1,600	820	820	1,500
Mining method [1]	N/R	OC&F	OC&F	OC&F	OC&F	OS
Pillar(s) type	Remnant	Sill	Sill	Crown	Sill	Sill
Length [2] *(m)*	~ 55	70.0	~ 38	45.0	25.0	~ 17
Width [2] *(m)*	N/R	3.0	N/R	4.5	4.5	1.2
Height [2] *(m)*	~ 23	20.0	~ 10	6.0	7.5	8.5
Volume [2, 3] *(m^3)*	N/R	7,275	N/R	1,380	940	~ 375
Density *(kg/m^3)*	2,700	2,700	2,800	2,800	2,800	2,700
Mass [3] *(tonnes)*	N/R	19,640	N/R	3,860	2,640	~ 1,010
Hole depth *(m)*	11–31	16–21	2.5	5.0	6.0	8.5
Blastholes [4] *(#)*	7	28	22	18	19	15
Diameter *(mm)*	38	64	45	45	45	38
Spacing *(m)*	Variable	3.0	Variable	1.8	1.8	1.2
Collar *(m)*	N/R	2.5	1.5	1.5	1.5	3.0
Stemm. material	N/R	N/R	N/R	Air	Air	Cement
Explosives type	N/R	ANFO	ANFO	ANFO	ANFO	ANFO
Total charge*(kg)*	N/R	630	N/R	245	N/R	90
Powder factor*(kg/t)*	N/R	0.03	N/R	0.06	N/R	~ 0.09
Reported results	Failed	Partial	N/R	Partial	Success	Success

Table 2 (continued). Comparative reported data from 21 selected large-scale choked destress blasts in underground pillars.

Mine	Stobie Mine	Brunswick Mine [7]	Mount Charlotte
Year	1998	1999	1995
Panel depth *(m)*	550	1,015	950
Mining method [1]	SC	OS	OS
Pillar(s) type	Regional	Remnant	Rib
Length [2] *(m)*	47.0	30.0	36.0
Width [2] *(m)*	1.8	2.4	3.5
Height [2] *(m)*	21.0	25.0	55.0
Volume [2, 3] *(m^3)*	5,070	6,275	16,175
Density *(kg/m^3)*	3,600	4,300	3,200
Mass [3] *(tonnes)*	18,250	26,980	51,755
Hole depth *(m)*	21.3	24–31	53.0
Blastholes [4] *(#)*	54	32	17
Diameter *(mm)*	102	165	140
Spacing *(m)*	1.2	2.4	6.4
Collar *(m)*	2.1	Variable	4.5
Stemm. material	Air	Gravel	Gravel
Explosives type	Emulsion	Emulsion	Emulsion
Total charge*(kg)*	10,045	8,880	3,480
Powder factor*(kg/t)*	0.55	0.33	0.07
Reported results	Success	Success	Success

Notes:

1 *"OC&F" stands for overhand cut-and-fill, "UC&F" for underhand cut-and-fill, "OS" for open stoping and "SC" for sublevel caving.*

2 *When multiple pillars were blasted, quantities are reported per individual pillar.*

3 *The calculation of the targeted volume and mass includes, when appropriate, outside zones of influence off the width and length of the pillar that are equal to 16 times the blasthole diameter. Figure 23 illustrates these outside zones. Which of these zones were considered in each case depends upon the geometry of the destress blast, as discussed in the next paragraph. This approach was implemented in order to consider the external zone of influence of a blasthole reported by Blake* et al. *(1998). Additional comments on this issue are provided in sections 5.2.2, 8.2 and 8.3, as well as in Appendix C.*

4 *Some quantities of drilling are reported in the table in metres drilled, rather than in number of blastholes.*

5 *Blast described in detail in Chapter X.*

6 *As reported by O'Donnell (1999).*

7 *Blast described in detail in Chapter IX.*

N/R stands for "not reported" in (or not deducible from) the documentation examined.

As mentioned in the comments at the end of Table 2, the external zones of influence considered in the calculation of the effective volume and mass of the targeted zone in the various case studies summarised in this table, as per note [3], are based upon the actual geometry and location of the blast in each case.

Conceptually, a destress blast has up to four external zones of influence outside the volume outlined by the peripheral blastholes: one on either side of its length, and one on either side of its width, as illustrated in Figure 23.

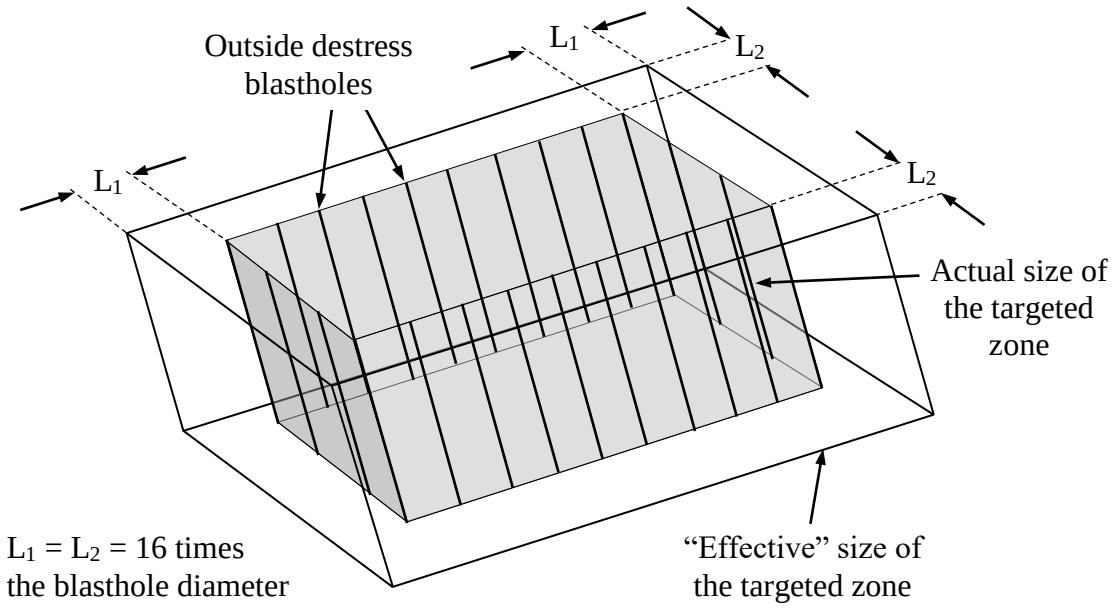

Figure 23. Conceptual representation of the outside zones of influence that can be considered around a large-scale choked pillar destress blast.

Since within the context of large-scale choked pillar destress blasts the explosive charges are generally cylindrical (their length over diameter ratio is larger than 7), no external zone of influence is considered in the direction of their long axis, above and below the blast. (The energy from a cylindrical charge radiates outwards in an essentially cylindrical manner, in a direction perpendicular to the long axis of the charge.) In the unlikely case where spherical charges would be used in a large-scale choked pillar destress blast, whereby the length over diameter ratio of these charges would be under 7, outside zones of influence along this third direction should be considered as well.

Figure 24 shows various conceptual views of possible outside zones of influence – some of which were considered in the case histories of Table 2 – depending upon the location of the destress blast in relation to neighbouring voids or filled areas.

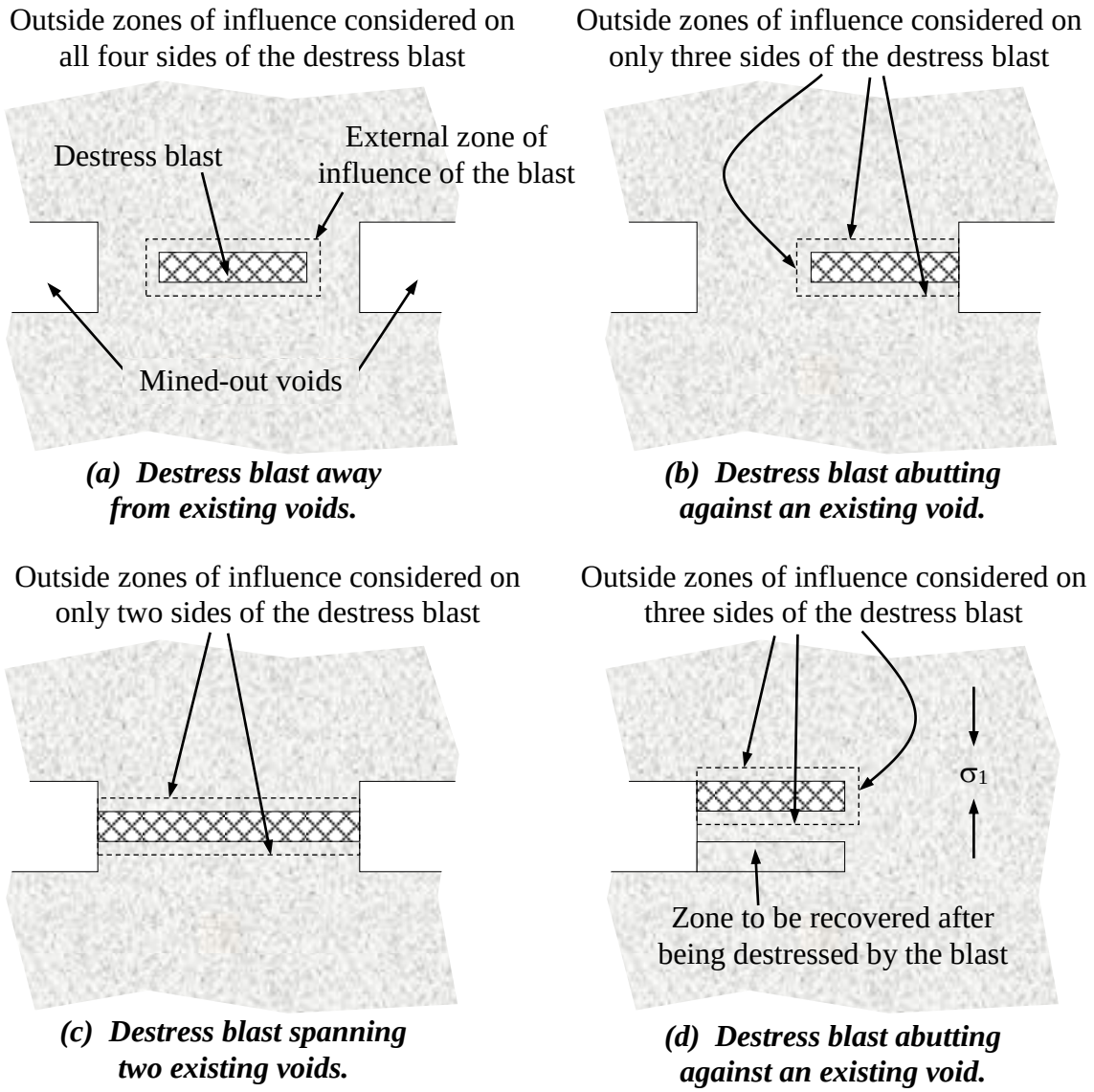

Figure 24. Examples of various destress blast situations and the corresponding outside zones of influence considered. (Schematic plan views, not to scale.)

Overall, there are little high quality data that would allow one to quantify the actual degree of success – i.e., the extent of the stress reduction that was achieved in the targeted volumes of ground – associated with the large-scale choked panel destress blasts described in the

case studies examined. The results of most of the early attempts are assessed qualitatively, essentially based upon the ease of the mining operations that were carried out after the blast – little instrumentation was used (and available) in these early trials, which would allow a more reliable assessment of their effect. This is however understandable given the difficulties in collecting the information and the need to respond to pressing operational problems. Overall, it is however clear from the literature review performed and the experience of the author that large-scale confined destress blasts can be successful if properly done – in particular, two clearly successful case histories will be discussed in detail in chapters IX and X.

The literature review also indicates that the time at which large-scale destress blasts are detonated in pillars is a critical parameter – the best results seem to have been attained when stress levels in the targeted pillars were reportedly nearing their ultimate capacity.

Also, very few of the reviewed case histories addressed the issue of stress transfer following a successful destress blast, and discussed precautions undertaken to prepare for this transfer (ground reinforcement, proactive closures, etc.). Certainly, numerous case studies mentioned that the destress blast triggered large seismic events in neighbouring regions.

This literature review also clearly highlights the need for a more scientific approach to designing large-scale choked panel destress blasts. (Such an approach will be pursed later in the thesis.)

CONCLUSION DU CHAPITRE. Les études de cas présentées dans ce chapitre et à l'annexe C montrent clairement qu'il n'existe actuellement pas de procédure d'ingénierie formelle et bien établie qui soit appliquée à la conception de tirs de relâchement des contraintes, et que ces sautages sont encore largement conçus par essai et erreur, en se basant sur l'expérience passée spécifique à un site donné. Peu de data consistants existent dans les études de cas examinées qui expliquent de manière rationnelle les choix effectués concernant la localisation, la géométrie et les dimensions d'un tir confiné de relâchement des contraintes

dans un pilier de mine, ainsi que le choix du diamètre des trous, du fardeau et de l'espacement, des produits explosifs, et des autres paramètres de tir. La revue des études de cas démontre clairement qu'un besoin existe pour une approche plus scientifique de la conception des tirs de relaxation des contraintes. Les méthodologies existantes de conception générale des sautages vont être examinées dans le prochain chapitre afin d'évaluer si celles-ci peuvent être adaptées aux tirs de relâchement des contraintes et servir de base à une telle approche scientifique.

CHAPTER CONCLUSION. The case histories presented in this chapter and in Appendix C clearly indicate that there is no well-established formal engineering procedure that is applied to the design of destress blasts, and that these are still largely conceived by trial and error, based upon site-specific past experience. Few consistent data can be found in the reviewed case histories that rationally explain the choices made concerning the location, geometry and size of a given choked destress blast in a mine pillar, or the choice of hole size, burden and spacing, explosive products, and other design parameters. The review of the case studies clearly shows that a need exists for a more scientific approach to designing destress blasts. Existing design methodologies for general blasting operations will be reviewed in the next chapter to assess whether they can be adapted to destress blasts and constitute a basis to such a scientific approach.

CHAPTER V

5. POTENTIAL DESTRESS BLAST DESIGN METHODOLOGIES

RÉSUMÉ DU CHAPITRE. Ce chapitre débute par une description des diverses philosophies de design associées aux tirs confinés à grande échelle de relaxation des contraintes dans des piliers de mine qui ont été décelées durant la revue d'études de cas du chapitre précédent. Deux principales approches ont été identifiées: l'une favorise des tirs hautement énergétiques, l'autre préconise des sautages plus faibles.

Une revue des diverses méthodologies de conception couramment utilisées en forage-sautage est ensuite présentée, qui sont de simples règles de base, des approches empiriques, des méthodes analytiques, des techniques numériques et des concepts hybrides. L'objectif de cette revue est d'évaluer: 1) si chacune de ces méthodologies peut être aisément appliquée aux sautages confinés à grande échelle de relâchement des contraintes dans des piliers de mine; et, 2) dans le cas contraire, leur potentiel à adresser de tels tirs.

Ce chapitre va montrer qu'il n'y a actuellement pas de méthodologie standard de conception des sautages qui décrive de manière satisfaisante les tirs confinés à grande échelle de relaxation des contraintes dans des piliers de mine, et qu'il existe un besoin: 1) d'identifier de manière fiable les paramètres qui jouent un rôle dominant dans ce type de tir; 2) de quantifier leur importance relative; et, 3) de développer une technique de conception basée sur ces paramètres.

CHAPTER SUMMARY. This chapter starts with a description of the large-scale confined pillar destress blast design philosophies that emerged during the literature review of the previous

chapter. Two broad schools of thoughts came across in this review: one that favours highly energetic blasts, and one that supports lighter blasts.

A review of the various engineering methodologies currently used in drilling and blasting is then presented, which are rules-of-thumb, empirical approaches, analytical methods, numerical techniques and hybrid schemes. The objective of this review is to assess whether each methodology can be readily applied to large-scale confined destress panel blasts; and, if not, what its potential is to address such blasts.

This chapter will show that there is currently no standard blasting design methodology that satisfactorily describes large-scale confined destress pillar blasts, and that there is a need to 1) reliably identify the parameters that play a dominant role in this type of blast; 2) quantify their relative importance; and, 3) develop a design technique based upon these parameters.

5.1. CURRENT CHOCKED DESTRESS BLAST DESIGN PHILOSOPHIES

When examining large-scale confined panel destress blast case studies reported in the technical literature, it appears that two "schools of thoughts" exist on the design of such blasts. The first one consists in blasting the targeted volume extremely violently, with the objective of creating the maximum possible level of damage in it (i.e., creating as dense a zone of microfracturing as possible), in order to maximise the softening effect in the rock mass. It is interesting to note that, as pointed out by Blake *et al*. (1998), the extreme case of this philosophy is a regular production blast, which creates many new fractures through intact rock and essentially reduces the rock mass strength and stiffness to zero. This first approach seems to be often implemented in situations where remnant pillars must be significantly destressed and/or no personnel re-entry is sought after. This philosophy is the one that seems to have been generally implemented in the Coeur d'Alene mining camp in later attempts. In that sense Karwoski *et al*. (1979) pointed out that the distance between the blastholes was small enough in many of the massive destress blasts detonated there over later years to result in extensive fracturing between them, undoubtedly changing the response of the rock mass to loading from brittle to plastic.

The second design philosophy advocates the implementation of much less violent destress blasts, whereby low powder factors are maintained, which damage the ground to a much smaller extent. This approach is often applied in face destressing and preconditioning situations, as well as in pillars that require full personnel re-entry. It relies essentially on the mobilisation of a shear component along fractures – mainly pre-existing, but also, to a lesser extent, generated by the blast itself – in order to facilitate slippage along these surfaces and, hence, reduce the stress levels. A key premise of this reasoning is that widely-spaced destress blastholes cannot possibly fracture the targeted ground sufficiently to result in a significant change in its stiffness, and, hence, some other dominant mechanism must be at play. Brummer & Rorke (1988) postulated that a key energy dissipation mechanism in destress blasting results from shear on pre-existing fractures and geological structures, induced principally by the high pressure detonation gases. This effect was also discussed by Lightfoot (1993), whose work with a distinct element numerical method indicated that the penetration of the detonation gases into a jointed rock mass resulted in a significant shearing effect along pre-existing fractures, by instantaneously wedging them open and reducing the normal stress clamping them shut and maintaining them frictionally-locked. Toper *et al*. (1997) also observed that, following preconditioning blasts detonated deep at the Western Deep Levels Mine, few new fractures were created, and that pre-existing fractures – and mainly those sub-parallel to the major principal stress component – were increased. Ground penetrating radar measurements confirmed that for relatively widely spaced blastholes (i.e., for conditions of light blasting) the primary destressing effect (which was reportedly quite successful) seemed to have resulted more from shear on existing fractures than from the creation of extensive new ones. The usage of an explosive product as gaseous as possible was thus advocated, in order to enhance this structure wedging effect rather than pulverise the rock immediately around the blastholes, as a high shock energy product would tend to do. (Blake *et al*. [1998] however pointed out that the overall world-wide success of destressing does not seem to be heavily linked to the type of explosive products used.)

Overall, there however seems to be some correlation – at least in the case of large-scale choked panel destress blasts – between the level of success attained and the powder factor

implemented: higher powder factors seem to have been associated with "better" destressing results. Table 2 shows that, although success has been reported in some instances for powder factors as low as 0.06 kg of explosives per "effective" (including the external zones of influence) tonne of targeted rock, good results were more systematically reported when much higher powder factors had been implemented.

Importantly, and as mentioned previously, these design philosophies do not seem to have evolved in the development of versatile, well-established and widely-used design procedures.

5.2. CURRENT BLAST ENGINEERING APPROACHES AND THEIR APPLICABILITY TO DESTRESS BLASTING

A review of existing blasting engineering approaches will be done in this section, with the objective of assessing the extent to which each is, or could conceivably be, applied to large-scale choked panel destress blasting. Despite recent advances over the past fifteen to twenty years, blasting engineering is still often perceived more like an art than a science – certainly, it could not be considered as an exact science at the time this thesis was prepared. Blast design techniques, similarly to geomechanics design procedures, can be grouped in four broad categories, which are, by increasing order of complexity: 1) rules-of-thumb; 2) empirical procedures; 3) analytical approaches; and, 4) numerical methods. A fifth approach can be defined as a combination of the previous four. Each will be discussed in the following sections, again with the objective of assessing its potential to describe large-scale confined pillar destress blasts.

5.2.1. Rules-of-thumb

Rules-of-thumb are simple relations that typically link two blast parameters together. For example, statements such as "burden should be 25 to 30 times the blasthole diameter", or

"spacing should be 1.0 to 1.8 times the burden" are typical rules-of-thumb. Even though useful, these rules are quite crude and simultaneously consider very few of the numerous parameters that play an important role in blasting. Most of the current guidelines concerning destress blasting can probably be categorised as rules-of-thumb – although they are useful, they do not encompass much scientific bases.

5.2.2. Empirical techniques

Empirical techniques attempt to predict the outcome of the blasting process based upon observed past behaviour and readily available input parameters – they are the result of a matching process between the results obtained, the design parameters used and observed prevailing pre-blast conditions. Numerous such empirical schemes have been developed over the years, such as the Kuz-Ram method (Cunningham, 1983 and 1987), the comminution theory-based Da Gama approach (Da Gama, 1983), the Blastability Index concept (Lilly, 1986), and the JKMRC concept (Scott, 1996), to name only a few.

Each empirical technique typically encompasses only some of the numerous parameters known to influence blasting results. The parameters considered in each method are usually a reflection of the governing factors present in the case studies used to derive it. As a result, a given method is generally best-suited at solving specific problems in which only the few parameters it addresses are varying or dominant. The difficulty and tediousness associated with an empirical method often increase with the number of parameters considered in it. Despite some limited theoretical foundations, empirical design techniques are widely used, as they are fast and easy to apply, and typically not too susceptible to small assessment errors in their input parameters. Empirical methods can provide reasonably accurate answers, as long as they are used inside the limits within which they were developed.

At the time this thesis was prepared, no large-scale choked panel destress blast design techniques existed that could be "formally" labelled as empirical – no techniques existed to

the knowledge of the author that manipulated precise and well-defined input parameters to derive in a systematic manner an explicit design.

An indirect energy-based design approach was derived in 2001 at Itasca Canada (Brummer [2001], Andrieux & Brummer [2002], Brummer & Andrieux [2002]), which essentially compares the amount of explosive energy (expressed in calories) available per kilogram of targeted pillar to empirically-derived threshold levels. This approach can be considered indirect because it does not provide a design *per se*, but rather assesses the chances of success of a given design. It was derived from a number of documented case histories – some of which are included in Appendix C – that provided sufficient detail on the blasthole layouts and the explosive products used.

The mass of the targeted pillar was calculated in each case as being the volume included within the blasted volume, plus an outer zone of thickness equal to 16 explosive charge diameters on both sides of the blast width (as per L_2 in Figure 23). As mentioned in the footnotes of Table 2, this external volume was meant to take into account the external zone inferred to be fractured by the peripheral blastholes, as discussed by Blake *et al*. (1998). The explosive energy levels, in calories, were then evaluated for each case, based upon the reported blasthole diameters, drilling geometries, explosive products and loading details.

Figure 25 shows the results obtained from the comparison of the various targeted masses and explosive energy levels in the case histories retained for this analysis. Equal energy lines were added onto this figure, that correspond to levels of 10, 100, 200, 500 and 1,000 cal/kg of rock.

This figure clearly indicates that the majority of the cases examined had energy values in the range between 10 and 100 cal/kg of targeted rock. The best and most convincing results seem however to have been observed in the cases included in the interval between 200 and 500 cal/kg, which corresponds to the hatched zone in Figure 25.

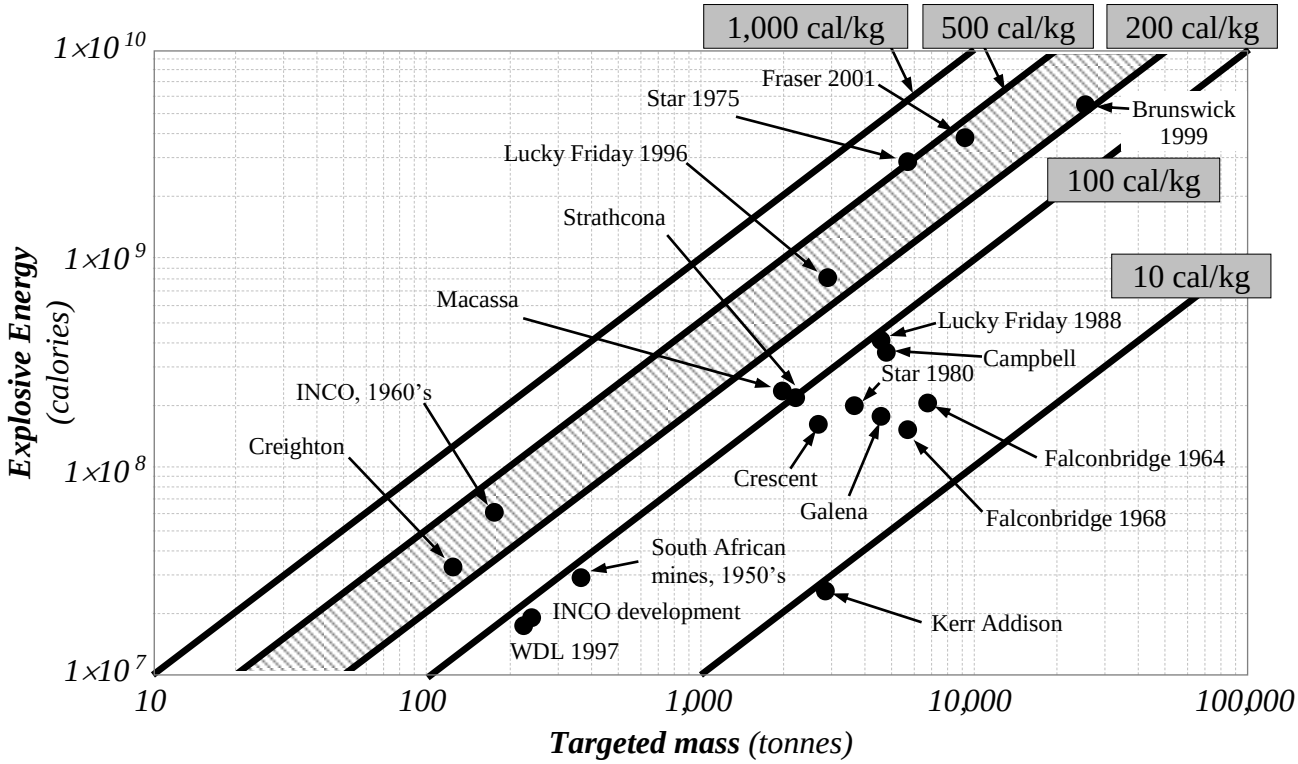

Figure 25. Comparison of the energy levels implemented in various documented destress blasts. (After Brummer, 2001.)

Based upon these results, it was recommended that large-scale confined pillar destress blasts be designed for an explosive energy factor of between 200 and 500 cal/kg of "effective" (considering the external zones of influence) targeted rock.

Also based upon these results, a generic approach was proposed by Brummer & Andrieux (2002). For a regularly shaped destress blast (i.e., one with a rectangular section) the total mass of the external lateral zone of influence (on both sides of the blast), M_e, is calculated first, as follows:

$$M_e = 2 \times (16 \times d) \times H \times L \times \rho_r \qquad \text{..... Eq. (17)}$$

Where M_e is expressed in kg; d is the diameter of the explosive charges (in metres); H and L are the height and length (in metres) of the zone comprised within the blasthole pattern, respectively; and, ρ_r is the density of the rock (in kg/m^3). The factor "16" accounts for the external zone of influence of 16 times the blasthole diameter mentioned earlier, while the

factor "2" results from the need to consider the two external zones, one on each side of the blast. Figure 26 shows these dimensions.

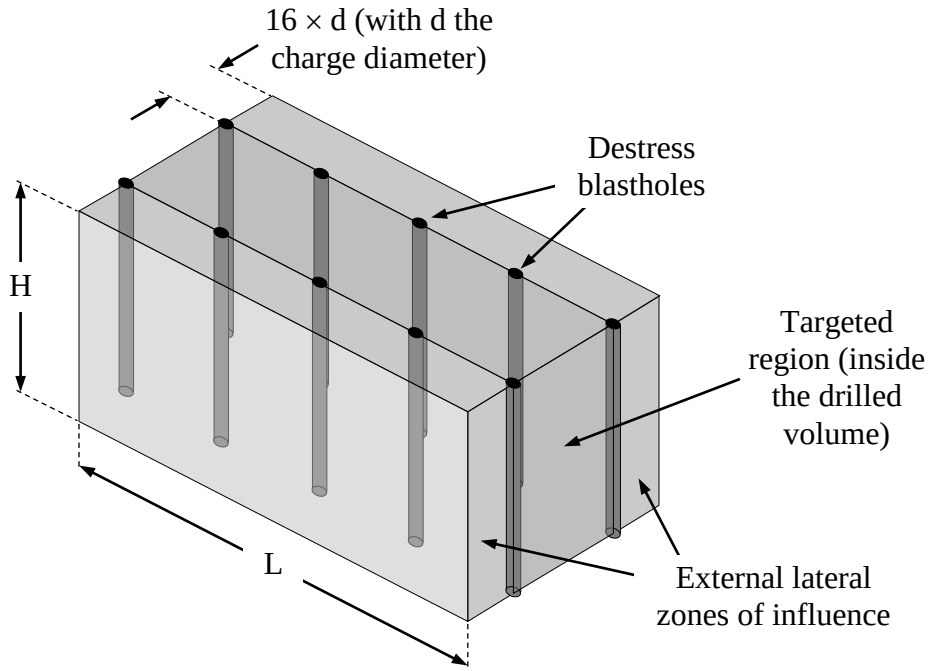

Figure 26. Schematic isometric view (not to scale) showing the external lateral zones of influence considered for a regularly shaped destress blast.

(As discussed in Section 4.2 and shown in Figure 24, the generic case shown in Figure 26 would need to be adapted to the actual geometry and location of the destress blastholes when applied to a real case. Please note also that, contrary to what was done in Table 2, no external zones of influence were considered in this early work at the ends of the destress blast, i.e., along the strike direction, as per L_1 in Figure 23).

The total, or "effective", mass targeted by the choked destress panel blast is then given by:

$$M_T = M_e + (W \times H \times L \times \rho_r) \qquad \text{..... Eq. (18)}$$

With: M_T expressed in kg; M_e as per Equation (17); W, H and L the width, height and length (in metres), respectively, of the volume comprised within the blasthole pattern; and, ρ_r the density of the rock (in kg/m^3).

The total explosive energy E_T in the blast is then calculated by adding the energy available in all the explosive charges in the blast. The explosive energy E_c available in one charge is given by the following expression:

$$E_c = (\pi \times d^2 \times l \times \rho_e \times 1000 \times AWS) \div 4 \qquad \text{..... Eq. (19)}$$

Where: E_c is expressed in calories; d is the diameter of the explosive charge (in metres); l is the length of the explosive charge (in metres); ρ_e is the density of the explosive product (in kg/m^3); and, AWS is the absolute weight strength of the explosive product (in cal/g). Dividing E_T by M_T yields the explosive energy factor of the blast, expressed in calories per effective targeted kilogram (or kcal/tonne) of rock. The result can then be compared to the energy lines of Figure 25 to ensure that it falls within the 200 to 500 cal/kg range.

Further general design guidelines were also provided, to account for the fact that different blast designs can conceptually yield a given explosive energy factor. (Various combinations of blasthole sizes, drilling patterns, loading schemes and explosive products can result in the same energy input per unit mass, with not all such designs being realistic.) Some of the qualitative guidelines provided for large-scale choked pillar destress blasts were as follows (as per Andrieux & Brummer [2002] and Brummer & Andrieux [2002]).

- *Hole size*. Standard production drill holes should be used wherever possible, although larger diameter holes can sometimes be necessary, depending upon hole length, in order to maintain drilling accuracy.
- *Drilling pattern*. A minimum of two parallel lines of blastholes should be used in order to guarantee as much as possible that the volume between these two lines will be significantly fractured over a relatively wide region. A wider fractured area will also delay a possible stress remobilization by requiring it to occur over a much greater number of distinct blocks and edges.

  The drilling lines should as much as possible be perpendicular to the direction of the stress component to be reduced. A square toe spacing of 25 times the blasthole diameter is a good design starting point. A larger hole size may nevertheless be advantageous

since the hole spacing will be increased accordingly, thus further increasing the width of the targeted zone.

- *Collars and stemming of the holes*. An uncharged collar length of at least 40 times the blasthole diameter should be maintained. Wherever possible, an inert stemming material should also be used to provide a high level of confinement to the explosive charges and to maximise the work done in the targeted area – in the case of downholes, crushed minus 20 mm gravel is recommended. The collars should also be adjusted in the case of fanned holes to prevent an excessive concentration of explosive energy at the top of the holes, which could result in cut-offs, sympathetic detonations, charge desensitisation, and/or other malfunctions. Blind holes are ideal from an energy viewpoint since they provide maximum confinement at the bottom of the holes.

- *Explosive products*. The explosives used can be the standard products used at the mine site, usually either an emulsion or ANFO. The explosive columns should ideally be continuous and fully coupled (i.e., decking and/or decoupling should be avoided, if possible with respect to the vibration levels that can be tolerated from the blast).

  If possible, and as discussed previously, an explosive with relatively low shock and strong gas contribution, such as ANFO, should be used, as pressurised detonation gases promote movements along discontinuities and disturb/displace discrete blocks, which is efficient at reducing stress. Furthermore, and as mentioned before, by forcing a path through the rock mass, the detonation gases instantaneously reduce the normal confinement and cause movement along the fractures they encounter – this promotes fracture growth and shearing.

It could be necessary at this stage to adjust the drilling pattern and the loading parameters in order to maintain the explosive energy factor within the 200 to 500 cal/kg range. Other broad guidelines were also provided, concerning initiation and blasting sequences, and the maximum instantaneous charge to fire per delay (as high as possible, but without causing excessive damage to neighbouring infrastructure in the mine). Please refer to Andrieux & Brummer (2002) and Brummer & Andrieux (2002) for additional details.

This empirical approach has the advantage of being specifically aimed at large-scale choked panel destress blasts. It has also been shown to have a certain potential to predict the outcome of a given destress blast design under a given set of circumstances (Sampson-Forsythe *et al*., 2002). This method will be used later in this thesis, and will constitute one of the bases of the "Destressability Index", which is the core of this project.

5.2.3. Analytical techniques

Analytical techniques attempt to analyse blasting by using fundamental principles of physics. In such methodologies, thermodynamics equations and equations of state are generally used to consider detonation energy, fracture mechanics are used to describe how the explosive energy is breaking the material, ballistics are used to study throw and muck pile profile, etc. Such approaches describe the blasting process well, are based upon sound and well-established physics concepts, and treat the problem from the "scientific" point of view.

These methods are however not without limitations, particularly due to their explicit nature. For example, even though they can very well take into account the effect of a given pre-existing fracture within the rock mass, much of this information is, in practice, rarely available beforehand in a detailed way. Furthermore, a number of physical parameters required for such analyses are seldom available, unless extensive site investigations are carried out. Analytical techniques are hence very powerful and thorough, but often require more input data than are usually available. For example, an analytical representation of the geological structural regime is often not possible. This results in the "missing data" being approximated or derived from experience, which undermines some of the credibility of the approach by rendering it more empirical. Another limitation is the near-impossibility to use such techniques on a daily basis, due to their complexity. Even two-dimensional problems usually require the usage of powerful computer codes. The BLASPA programme (Favreau & Favreau, 2002) is probably one of the best examples of an analytical approach.

At the time this thesis was prepared no analytical design techniques existed to the knowledge of the author for large-scale choked panel destress blasting. Analytical approaches however have the potential to help in the identification of the parameters relevant to the process.

5.2.4. Numerical methods

Broadly stated, numerical techniques attempt to resolve the stress-deformation-displacement state through a mathematical representation – or model – of a real-life problem by subdividing this model into small zones on which "manageable" and relatively simple calculations can be applied. By performing a large number of such calculations on each small zone, it becomes possible to study complex mechanical behaviours and derive stress, deformation and displacement information anywhere throughout the zones of interest in the inner part of the model. Rock engineering numerical approaches have made tremendous progress in the past fifteen years, as computing power has become both more powerful and affordable. The numerical modelling of the blasting process has benefited from this advance. Continuum models, whereby the rock mass is considered as a continuous, homogeneous and generally isotropic medium, are usually used to investigate stress wave effects and failure mechanisms inside intact material. Discontinuum models, in which the rock mass is considered as an assembly of discrete blocks, are better adapted to study the impact of structural discontinuities, detonation gases pressurisation and flow, and the movement of the broken material.

These techniques, although very effective, are also not without limitations. Firstly, due to the gigantic amounts of calculations typically involved, the complex numerical models needed to study the blasting process must typically be run on powerful computers over significant periods of time, which all but precludes their routine usage. This issue also limits the size of the problems that can be analysed. Secondly, setting up numerical models takes time, with the amount of time required rapidly increasing with the complexity of the situation to analyse, which further precludes their routine usage.

Importantly, numerical modelling is always a simplification of the real-life situation, and provides only indications on the likely behaviour of the full-scale problem when subjected to the set of conditions considered in the model. Contrary to other engineering disciplines involving well-known processes, like in the field of electronics, for example, the numerical modelling of rock does generally not provide absolute results. The main reasons are the many unknowns involved, such as the rock mass structural characteristics, the exact loading regime applied to it and the actual failure mechanisms involved. The static numerical analysis of stress, deformation and displacement is difficult enough – dynamic analyses are yet more complex, and, in the particular case of blasting, the difficulty is compounded by the fact that blast-related codes must be inelastic and properly capture the behaviour of the blasted material in the post-failure domain. Few commercially-available inelastic numerical codes can reproduce somewhat properly the blast-induced fracturing process, and those that can require so much computing power that only relatively small-scale problems can be addressed in practice, and generally only in two dimensions. Numerical instability can quickly develop with even the most advanced of numerical codes available in geomechanics for quasi-static conditions, due to the tremendous forces acting upon the numerical elements over extremely short periods of time, which create problems such as numerical elements interpenetrating, for example. Material separation is also not easily addressed numerically when starting with a continuum, or even with discrete elements.

The Bedded Crack (Margolin, 1983), NAG-FRAG (McHugh, 1983[a]), SHALE (Adams *et al*., 1983), DDA (Shi, 1992; Mortazavi & Katsabanis, 1998) and MBM2D (Minchinton & Lynch, 1996), models are examples of numerical methods for blasting applications. Katsabanis (2001) provided a summary of some of the numerical methods that were available at that time for blasting engineering applications.

Overall, and despite the promise they hold, numerical methods are not commonly used for actual blast design purposes, and their routine use remains distant to most practitioners. Generally, their use is limited to the investigation of fundamental aspects and/or particular phenomena associated with blasting, which, once better understood, offer additional insight

into the blasting process. There are numerous examples of such focused numerical investigations, which cover a wide range of blasting aspects such as detonation mechanics (Harries 1983; Heuze *et al*., 1990; Braithwaite *et al*., 1996), detonation gases behaviour and effects (McHugh, 1983 [b]; Nilson *et al*., 1985; Haghighi *et al*., 1988; Preece *et al*., 1993; Mortazavi & Katsabanis, 1998), fracture mechanics (Grady & Kipp, 1980; Potyondy & Cundall, 1996), blast-induced ground motion, and wave generation and propagation (Starfield & Pugliese, 1968; Aimone, 1982; Valliappan & Ang, 1988), geological structures behaviour under dynamic loading (Han *et al*., 1986; Cundall, 1988; Cundall & Hart, 1993), cratering (Katsabanis & Liu, 1998), fragmentation (Kleine *et al*., 1990; Minchinton & Lynch, 1996), and burden movement (Yang & Kavetsky, 1990), to name only a few.

One "danger" associated with pushing numerical techniques (and analytical ones as well) far beyond the limits of what is currently understood of the rock blasting process, is that obtaining results that do match field observations is not necessarily a guarantee that the analytical or numerical reasoning is correct. Mortazavi *et al*. (2001) have clearly showed that various widely different logic schemes and reasoning processes can produce results that still closely match such blasting experimental field observations.

Work was under way at the time this thesis was written to develop more powerful numerical models for blasting, including a large-scale project carried out by Itasca for an international consortium of large mining companies in the form of the PFC-based Hybrid Stress Blast Modelling (HSBM) approach (Ruest, 2001; Cundall, 2002).

Aside from somewhat trivial analyses (which concluded, as expected, that a rock formation with a lower modulus of elasticity [as a result of destressing] will be subjected to lower stress levels for similar deformations), no numerical method had been developed at the time this thesis was prepared that addresses destress blasting.

The numerical modelling of destress blasting does not appear to be a straight forward affair. As described in Andrieux *et al*. (2000) and Brummer *et al*. (2000), solely reducing the

mechanical properties of the targeted volume in a model does not always result in the prediction of stress level reductions in accordance with those measured in the field. For a match to occur in the particular case described by Andrieux *et al*. (2000) and Brummer *et al*. (2000), the destressed zone had to be entirely removed from the 3DEC model. Other numerical modelling work, such as the one from Sweden reported in Section 5 of Appendix C and summarised in Figure 141, or the one described by Mitri (2000), has shown more convincing – although only generic – results. Although numerical methods can show to a certain extent the results on the local stress regime of a reduction of the mechanical properties of the targeted zone, they were not, at the time this thesis was prepared, readily adapted to evaluate the effects of various blasting design parameters on these mechanical properties.

5.2.5. Hybrid methods

Hybrid techniques were also developed to address blasting, usually encompassing some physics-based concepts supplemented by empirically-developed relationships. Such approaches constitute an interesting compromise as they provide a better scientific basis than purely empirical methods, while remaining easier to use than full-fledge analytical or numerical techniques. The Orica Sabrex programme (Harries, 1973; Chung, 1997) is one example of a hybrid method. No hybrid scheme existed for destress blasting to the knowledge of the author at the time this thesis was written.

5.3. GENERAL COMMENTS ON THE CURRENT DESTRESS BLAST DESIGN METHODOLOGIES

As discussed throughout the previous sections, the currently available design techniques for large-scale choked panel destress blasts are few and limited. At this stage it is probably fair to state that designing such destress blasts remains just about as much an art as a science, with the engineering approach being essentially a combination of basic rules-of-thumb and empirical approaches based upon previous site-specific field trials. Certainly, little existed

at the time this thesis was prepared for the practitioner to use in order to "rationally" design such blasts or assess their chance of success, other than an empirical approach recently developed by Brummer & Andrieux (2002) that provides some estimation of the likelihood of success of a given design.

Furthermore, it is the author's opinion that there is currently no design technique that exists for "standard" blasting operations (in which free faces are exploited in the fragmentation process and whereby the blasted material is meant to be mucked) that does encompass and consider all the relevant aspects of blasting – certain methods focus on certain aspects of blasting, whereas other methods focus on other aspects. This limitation is yet more stringent in the even less understood field of large-scale choked pillar destress blasting. There is currently a need to: 1) identify the parameters that play a role in large-scale confined destress blasting; and, 2) quantify their relative importance. This would allow the subsequent development of a design methodology that would focus on those dominant parameters that do control the process. The remainder of this thesis will try to address both issues.

Because the basic mechanisms that control destressing are still not fully understood, or, at least, universally accepted, it is difficult to envision how the identification and weighing of the many parameters at play in the process could be done in an entirely formal manner. Instead, the identification of these parameters will be pursued conceptually, based upon basic blasting considerations. The weighing aspect will be subsequently attempted through the application of the relatively new Rock Engineering Systems (RES) methodology developed by Hudson (1992).

CONCLUSION DU CHAPITRE. Une revue des diverses méthodologies de conception actuellement utilisées en forage-sautage a été effectuée dans ce chapitre. Cette revue en est arrivée à la conclusion qu'aucune n'est idéale pour décrire les tirs confinés à grande échelle de relaxation des contraintes dans des piliers de mine, et que les techniques de design actuellement disponibles pour ce type de tirs sont limitées. Il est probablement juste à ce stade-ci de mentionner que la conception de tels tirs relève presque autant d'un art que

d'une science, l'approche d'ingénierie étant essentiellement une combinaison de simples règles de base et de méthodes empiriques spécifiques au site, bâties sur des essais antérieurs. Peu de lignes directrices existaient au moment où cette thèse a été rédigée qu'un ingénieur pouvait utiliser pour concevoir de tels sautages de manière "rationnelle". Une approche empirique récemment développée par Brummer & Andrieux (2002) permet toutefois d'anticiper dans une certaine mesure les résultats auxquels l'on peut s'attendre pour un sautage donné. Bien que cette approche soit encore quelque peu simpliste, elle sera utilisée plus tard dans cette thèse, de concert avec d'autres considérations, et formera la base d'une nouvelle méthodologie.

D'après les data examinés, il existe actuellement un besoin: 1) d'identifier les paramètres qui jouent un rôle dominant dans les tirs à grande échelle de relaxation des contraintes dans des piliers de mine; 2) de quantifier leur importance relative; et, 3) de développer une technique de conception basée sur ces paramètres.

En considérant que les mécanismes complexes qui régissent les tirs de relâchement des contraintes dans les piliers de mine ne sont ni parfaitement compris ni universellement acceptés, il est difficile de concevoir comment l'identification et la pondération des nombreux paramètres impliqués pourraient se faire d'une manière formelle. L'identification de ces paramètres sera plutôt tentée de manière conceptuelle, en se basant sur des considérations de base de dynamitage. La pondération de ces paramètres sera tentée subséquemment via l'application de la méthodologie des Systèmes d'ingénierie du roc ("Rock Engineering Systems", ou RES), récemment développée par Hudson (1992). L'option consistant à utiliser des réseaux neuronaux a été brièvement considérée à ce stade du projet – il a toutefois été estimé qu'il n'existe actuellement pas suffisamment de data pour entraîner un tel réseau avec un haut degré de confiance.

Le prochain chapitre va présenter et décrire la méthodologie des Systèmes d'ingénierie du roc, ainsi que son application au domaine des sautages. Cette approche s'avérera plus tard avoir le potentiel de décrire de manière satisfaisante les interactions entre les nombreux paramètres qui régissent les tirs confinés à grande échelle de relâchement des contraintes sans des piliers de mine.

CHAPTER CONCLUSION. A review of the various engineering methodologies currently used in standard drilling and blasting applications was done in this chapter. This review concluded that none is at present ideal to describe large-scale confined pillar destress blasts and that the currently available design techniques for this type of blasts are few and limited. At this stage it is probably fair to state that designing such blasts remains just about as much an art as a science, with the engineering approach being essentially a combination of basic rules-of-thumb and site-specific empirical approaches derived from previous field trials. Few generic guidelines existed at the time this thesis was prepared for the practitioner to use in order to "rationally" design such blasts. One empirical approach, recently developed by Brummer & Andrieux (2002), allows to anticipate to a certain extent the results that can be expected for a given design, but requires further development – this

methodology will be used later in this thesis, in conjunction with other considerations, and will form the basis of a new approach.

Based upon the data examined, there is currently a need to: 1) identify the parameters that play a dominant role in large-scale confined pillar destress blasting;, 2) quantify their relative importance; and, 3) develop a design technique based upon these parameters.

Because the basic mechanisms behind the complex mechanics of destress blasting are still neither fully understood nor universally agreed upon, it is difficult to envision how the identification and weighing of the many parameters at play in the process could be done in a formal manner. Instead, the identification of these parameters will be pursued conceptually, based upon basic blasting considerations. The weighing of these parameters will be subsequently attempted through the application of the relatively new Rock Engineering Systems (RES) methodology developed by Hudson (1992). The option of using neural networks for this task was briefly considered at this stage of the project – it was however deemed that there are not enough solid data available to train such a network with a high degree of confidence.

The next chapter will introduce and describe the Rock Engineering Systems methodology, and review its application to blasting. This approach will be later shown to have the potential to satisfactorily describe the interactions between the many parameters at play in large-scale choked pillar destress blasts.

CHAPTER VI

6. ROCK ENGINEERING SYSTEMS AND THEIR APPLICATION TO BLASTING

RÉSUMÉ DU CHAPITRE. Les Systèmes d'ingénierie du roc ("Rock Engineering Systems" ou "RES") sont une méthodologie d'ingénierie basée sur le calcul matriciel selon laquelle les interactions entre un nombre fini de paramètres interdépendants jouant un rôle dans le système d'ingénierie étudié sont quantifiées. La méthode, originalement proposée par John Hudson au début des années 1990, a montré un potentiel d'application à une grande variété de problèmes géotechniques. La matrice d'interaction dans laquelle les paramètres sont regroupés constitue la fondation de la méthodologie des RES. Une fois codée, elle permet de quantifier l'effet qu'a chacun des paramètres dans le système sur tous les autres paramètres, ainsi que l'effet qu'a sur lui chacun des autres paramètres du système.

Les principes de base des RES sont présentés dans ce chapitre. Un exemple d'application concernant la détermination de l'index de "Blastability" d'un massif rocheux, telle que développée par Latham & Lu (1999), est également présenté. Les principes de base décrits seront appliqués dans le prochain chapitre aux tirs confinés à grande échelle de relâchement des contraintes dans des piliers de mine.

CHAPTER SUMMARY. Rock Engineering Systems (RES) are a matrix-based engineering methodology whereby the interactions between a finite number of interdependent parameters that play a role in a particular engineering system are quantified. This approach, originally introduced in the early 1990's by John Hudson, has shown a broad applicability to a wide variety of geotechnical problems. The interaction matrix, in which all the parameters are organised, constitutes the basis of the RES approach. Once coded, it

allows to quantify the effect each parameter in the system has on all the other parameters, as well as the effect each of the other parameters in the system has on it.

The basic principles of the RES approach are introduced in this chapter. An example of its application for the determination of the "Blastability" of a rock mass, as developed by Latham & Lu (1999), is also presented. The basic principles described will be applied in the next chapter to large-scale choked panel destress blasts.

6.1. General description of the Rock Engineering Systems approach

The Rock Engineering Systems (RES) methodology was developed in the early 1990's by Professor John Hudson of the Imperial College in London, England. It is a methodical and highly organised technique designed to determine the relative importance of the parameters at play in a given rock engineering system. Figure 27 illustrates the basic principle of the "interaction matrix", which constitutes the foundation of the RES methodology, as derived by Hudson (1992).

As with every matrix, the data are arranged in boxes tagged (*i*,*j*), *i* referring to the position along the vertical axis (i.e., the row number), and *j* referring to the position along the horizontal axis (i.e., the column number), the reference (*1*,*1*) being located in the upper left corner of the matrix. With this approach, various engineering parameters of interest are located along the leading diagonal of the matrix, i.e., in boxes(*i*,*i*) and (*j*,*j*) in Figure 27.

The upper path between Parameter A in box (*i*,*i*) and Parameter B in box (*j*,*j*) corresponds to the influence Parameter A has on Parameter B. On the other hand, the lower path between Parameter B in box (*j*,*j*) and Parameter A in box (*i*,*i*) corresponds to the reciprocal influence Parameter B has on Parameter A. This approach essentially recognises that every pair of parameters influences each other: changing one alters the other, which, once adjusted consequently, affects the initial parameter back again.

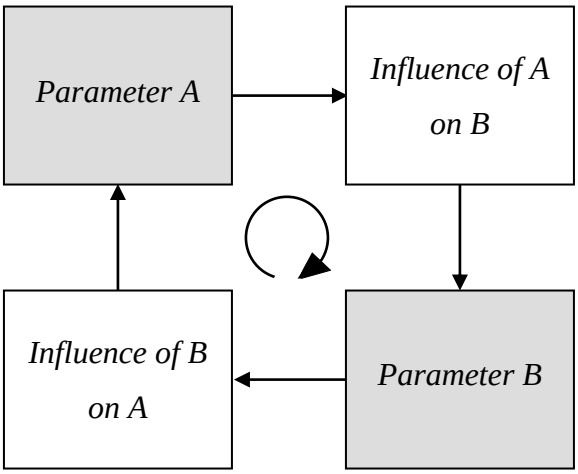

Figure 27. The basic principle of the interaction matrix. (Adapted from Hudson, 1992.)

One simple example of the usage of this approach is provided by Hudson – it concerns construction projects in hard rock and is shown in Figure 28. In this particular conceptual case, four engineering parameters are retained, which are located along the leading diagonal of the matrix, and highlighted in light grey. These are: the structure of the rock mass; the ground stresses; the quantitative hydrology; and, the construction itself.

The qualitative interactions between the various parameters are shown in the off-diagonal boxes. As shown in Figure 28, each of the four parameters affects all the other ones to some extent. For example, considering the rock structure and water inflow parameters, the following relationships are stated – from rock structure to water inflow: "the fracture network governs the secondary permeability" [box (1,3)]; and, from water inflow to rock structure: "continual water flow in fractures affects their properties" [box (3,1)]. The interaction matrix is, by nature, non-symmetrical.

In practice, such interaction matrices are normally larger that four by four – there is conceptually no limit on the number of parameters that one can include in a single matrix, although it becomes impractical to consider too many. An alternative way to building a difficult to handle single large matrix is to build a number of sub-matrices. With this approach, a given parameter in a matrix can be related to another matrix that deals specifically with it.

Rock Structure **F_{ij}** Box (1,1)	Fractures affect the values and orientations of the stresses Box (1,2)	The fracture network governs the secondary permeability Box (1,3)	Fractures can influence the size and orientation of excavations Box (1,4)
Stresses can open or close fractures, and also create them Box (2,1)	***Rock Stress*** **σ_{ij}** Box (2,2)	In general, the higher the normal stress, the lower the permeability Box (2,3)	High rock stresses can cause construction failures Box (2,4)
Continual water flow in fractures affects their properties Box (3,1)	Normal stresses are reduced by water pressure Box (3,2)	***Water Flow*** **K_{ij}** Box (3,3)	Grouting and drainage may be required during construction Box (3,4)
Blasting can damage old fractures and create new ones Box (4,1)	In the vicinity of excavations the principal stresses are altered Box (4,2)	An excavation will always become a sink for the water flow Box (4,3)	***Construction*** **C_{ij}** Box (4,4)

Figure 28. Four by four interaction matrix for a construction project in hard rock, with four leading diagonal terms: rock structure, rock stress, water flow and construction. (After Hudson, 1992.)

In order to have practical value, the interactions between the various parameters need to be quantified – assigning numerical values to the interaction boxes (*i*,*j*) is referred to as "coding" the matrix. There are essentially three procedures that can be used to perform this task, which are as follows, by order of increasing complexity.

1. The binary approach, whereby the values can be either 0 (no interaction) or 1 (interaction).
2. The "Expert Semi-Quantitative" (ESQ) method, whereby the interaction between parameters is ranked on a 0 to 4 scale, 0 representing no interaction, 1 representing a 'weak' interaction, 2 representing a 'medium' interaction, 3 representing a 'strong' interaction and 4 representing a 'critical' interaction.

3. Continuous quantitative coding schemes, based, for example, upon the slope of the P_i *vs*. P_j relationship, or on relationships derived from analytical or numerical analyses.

Figure 29 illustrates the results of this coding task. The sum of each row *i*, called the *cause* C of parameter P_i, quantifies the way in which P_i affects the entire system, while the sum of each column *j*, called the *effect* E of parameter P_j, quantifies the way in which the entire system affects P_j.

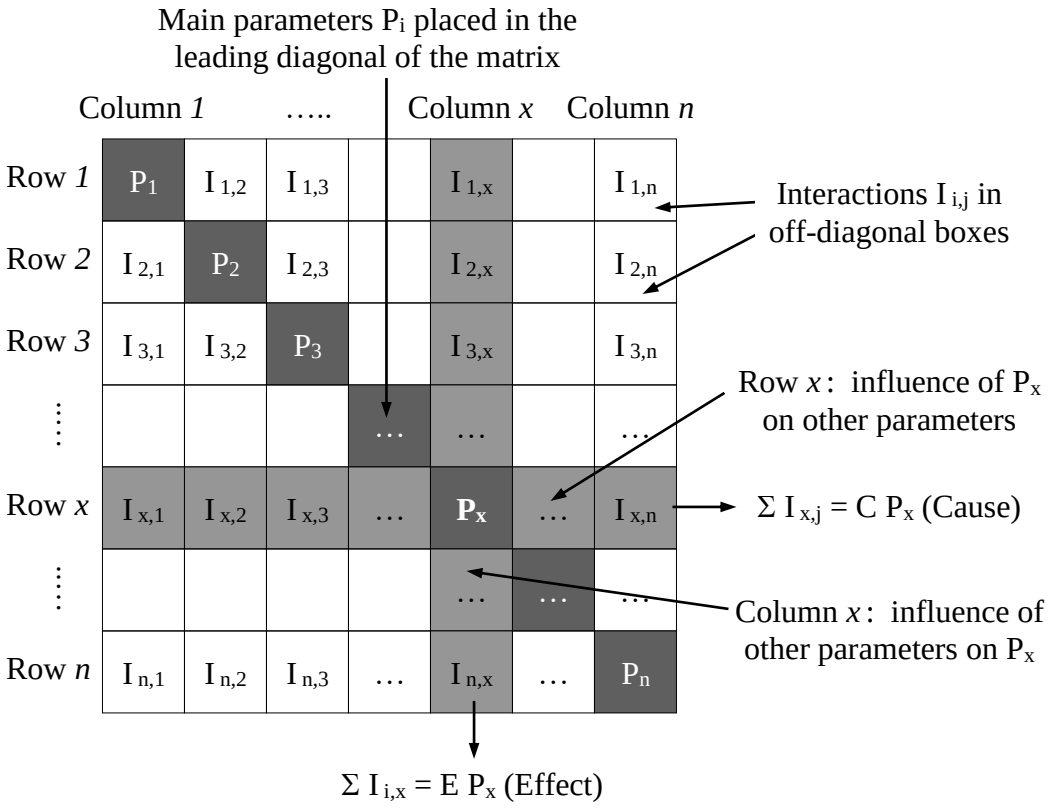

Figure 29. Coding of the interaction matrix, and cause and effect coordinates. (Adapted from Latham & Lu, 1999.)

These cause and effect values can be subsequently plotted against each other in a Cause *vs*. Effect (C–E) plot, which readily identifies the major contributing parameters and the principal interactions within the system. The C–E plot can be used, in turn, to assess various values, such as the *dominance* of each parameter (defined as the perpendicular distance of a given parameter's C–E point from the C = E line), or the *intensity* of each parameter (defined by how large a given parameter's C and E values are). Figure 30

conceptually illustrates how the C–E plot can be used to readily assess which parameters affect a given system the most, and which parameters are affected the most by a given system.

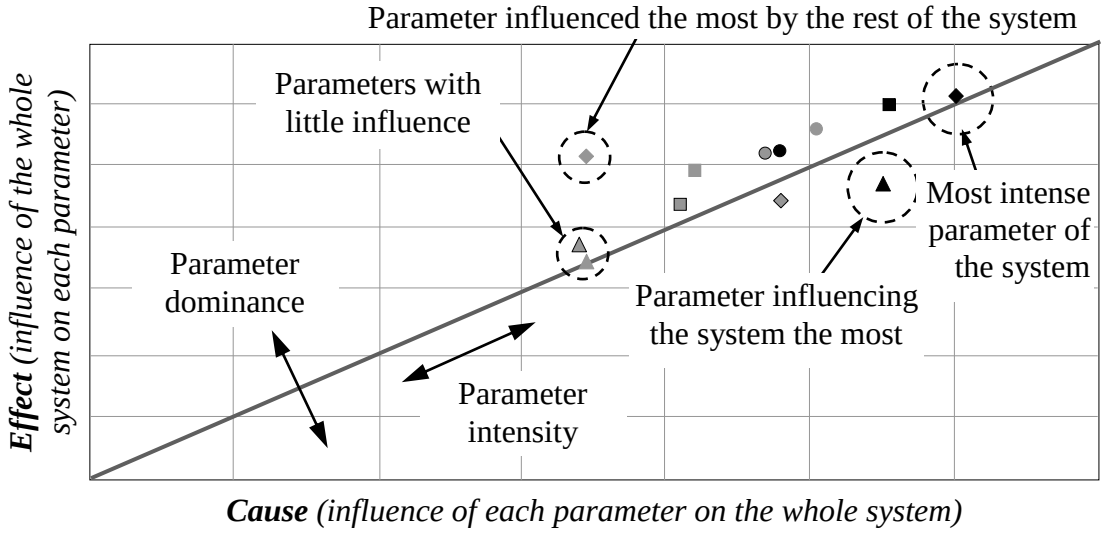

Figure 30. Generic example of a C–E plot. (Adapted from Latham & Lu, 1999.)

Parameters lying on, or near, the C = E line are essentially non-influential in the overall system because they have as much influence on the rest of the system as the rest of the system has on them. The parameter furthest away from the C = E line on the "effect" side is the one that the rest of the system (i.e., the other parameters) influences the most. Ideally, the end result of the process being analysed, for example the stress level in the rock mass if destressing was being considered, should be the most dominant parameter on the effect side (i.e., on the upper side of the C = E line), because it would thus be the parameter that would be affected the most by changing the other parameters. This would confirm that the choice of parameters was well adapted to the problem at hand.

Alternatively, the parameter furthest away from the C = E line on the "cause" side is the parameter influencing the rest of the system (i.e., all the other parameters) the most. In other words it is the parameter with the single largest influence on the entire system. The practical consequence is that special attention must be paid to this particular parameter in any attempt to engineer the system described.

6.2. APPLICATION OF THE RES APPROACH TO BLASTING – THE WORK OF LATHAM & LU

As discussed in Andrieux & Hadjigeorgiou (2001 and 2002), this engineering approach intuitively seems quite adequate to represent the general blasting process, whereby pairs of parameters do influence each other reciprocally. For example, one can consider the lowering of the explosive strength with respect to the required burden. Selecting a weaker explosive product does require the burden to be reduced accordingly. Once the burden has been diminished, it may influence, in turn, the effective strength of the explosive product by changing the amount of confinement the charges are subjected to. Indeed, reducing the confinement reduces the amount of time before the high-pressure detonation gases find a free face and vent back to atmospheric pressure, effectively reducing the amount of useful work done.

Latham & Lu (1999) have demonstrated that the "blastability" of a rock mass can be well described by means of an interactive RES approach. Blastability is an empirical concept that was originally introduced by Lilly (1986), which is defined as the ease with which a rock mass can be fragmented by blasting. Blastability is interesting because it aims at also considering the overall mechanical properties of the rock mass, which are often a large oversight of many common empirical blast design approaches.

A basic premise with blastability is that the blasting process changes the size distribution of the rock from a natural in situ block size distribution to a fragmented size distribution. This intuitively sound concept, suggested by Hudson & Harrison (1997), is illustrated in Figure 31.

Grenon *et al*. (1998) have validated this approach by presenting case studies from an underground hard rock mine where the processes that control the passage from the in situ block size distribution to the post-blast size distribution were investigated. In this work the in situ block size distribution was determined by using the results of scanline mapping and

a joint generator scheme (Stereoblock). This provided a realistic three-dimensional representation of the local pre-blasting joint network.

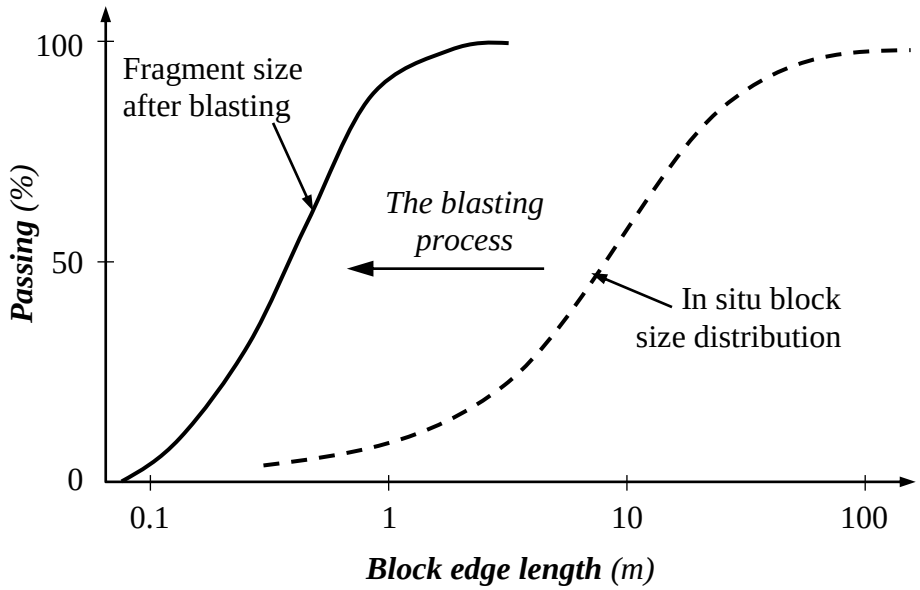

Figure 31. The blasting process in rock. (Adapted from Hudson & Harrison, 1997.)

Figure 32 shows the in situ block size distribution (represented by the "Stereoblock" curve) of a rock mass at the Noranda, Inc. Heath Steele Mine, and the post-blast block size distribution of the same rock mass, as determined by two image analysis software packages (the Split and the CANMET systems). These results clearly show that the blasting process involved a reduction in the block size distribution, from a coarse in situ state to a finer post-blast one.

Latham & Lu (1999) have investigated the opportunity of using Rock Engineering Systems to specifically describe the overall interactive mechanisms of rock blasting, and explored, in particular, the possibility of employing RES specifically for the assessment of the blastability of a rock mass. As shown in Figure 33, Latham & Lu suggested that two rock masses having identical natural in situ block size distributions (referred to as the In situ Block Size Distribution-Common, or IBSD-C) subject to the same blast design can have two distinct blasted rock size distributions (Blasted Block Size Distribution-1 and -2, or BBSD-1 and BBSD-2, respectively).

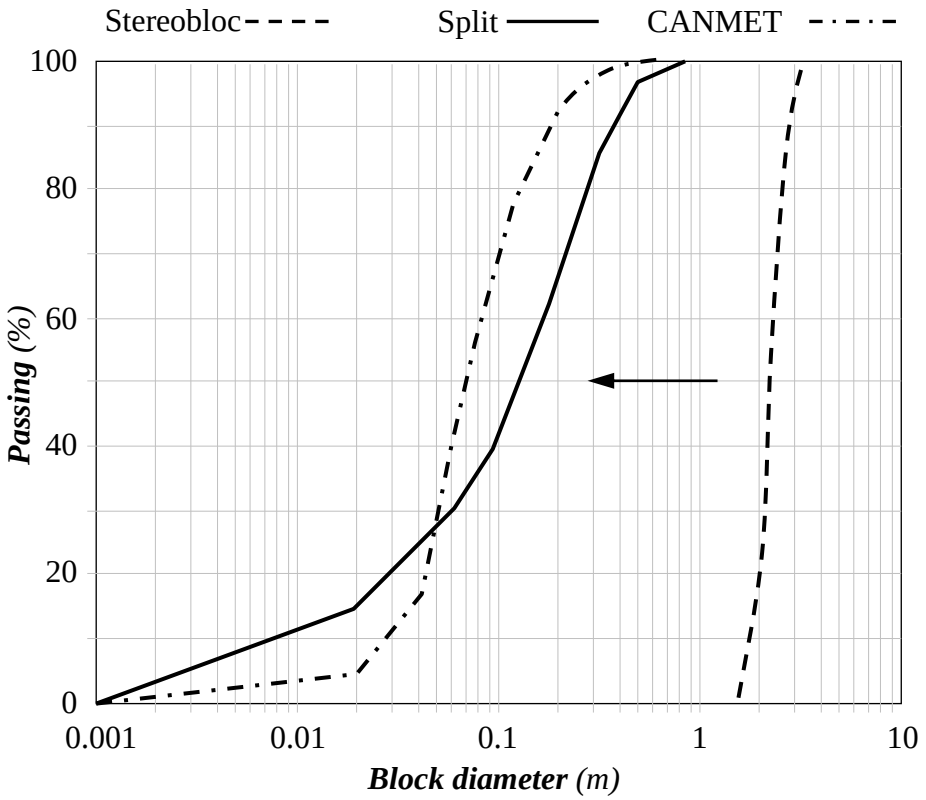

Figure 32. The change of the rock mass block size distribution prior to ("Stereoblock" curve), and after ("Split" and "CANMET") blasting. (After Grenon *et al*., 1998.)

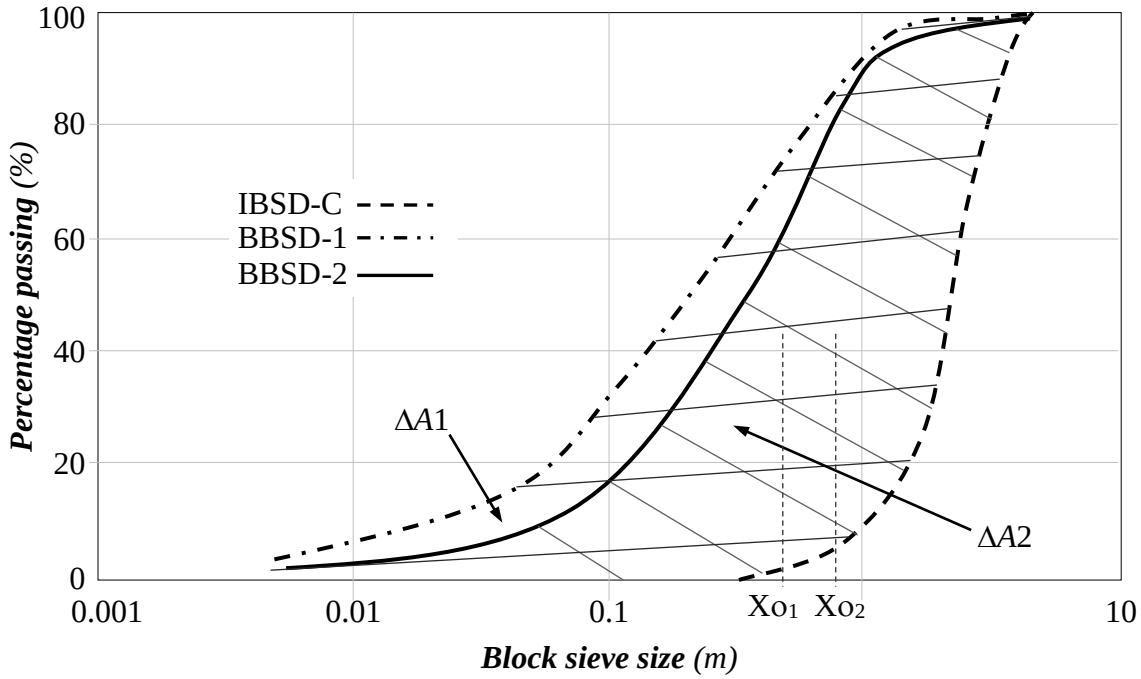

Figure 33. The concept of blastability. (After Latham & Lu, 1999.)

Since both rock masses are blasted the same way and, hence, are subject to identical amounts of explosive energy, then the resulting distinct fragmentations can be argued to be necessarily controlled by the inherent blastability of each rock mass. This is a powerful approach since it considers the properties of the rock mass to the extent that they can significantly affect the predicted results, even if the explosive products used and the blast design implemented are similar.

The quantities $\Delta A1$ and $\Delta A2$ in Figure 33 are the transformation areas for the two different rock masses subjected to the same amount of explosive energy and the same blast design. In the example shown, rock mass #2 is intrinsically more difficult to blast than rock mass #1 as indicated by $\Delta A2$ being smaller than $\Delta A1$, which results in curve BBSD-2 being coarser than curve BBDS-1.

The difference between $\Delta A1$ and $\Delta A2$ indicates the difference in blastability between the two rock masses. The values Xo_1 and Xo_2 shown along the x-axis of Figure 33 represent the centres of gravity of the transformation areas of rock mass #1 and #2, respectively. As the value of Xo_i moves left towards finer material, the blastability of the rock mass improves.

The explosive energy input per unit rock mass that is consumed in reducing the rock mass from its in situ block size distribution IBSD to a finer blasted fragment size distribution BBSD has been shown by Latham & Lu to be related to the transformation area ΔA and, hence, to Xo.

This approach thus not only considers an all-encompassing blasting-relevant property of the rock mass, but also the explosive energy input per unit rock mass, which is dependent upon the explosive products used and the blast design implemented.

In developing a blasting interaction matrix to construct a rock mass Blastability Index, Latham & Lu identified a series of relevant parameters P_i, as shown in Table 3.

Table 3. Coding values of the blastability interaction matrix. (After Latham & Lu, 1999.)

P_i	Factors affecting blastability	Depicting parameter(s)
P_1	Strength	Uniaxial compressive strength
P_2	Resistance to fracturing	Uniaxial tensile strength
P_3	Sturdiness	Density
P_4	Elasticity	Young's Modulus
P_5	Resistance to dynamic loading	P-wave velocity
P_6	Hardness of the rock	Schmidt hardness value
P_7	Deformability	Poisson's ratio
P_8	Resistance to breaking	Fracture toughness
P_9	In situ block size	Mean block size (K_{50})
P_{10}	Fragility of the rock mass	Fractal dimension of the in situ rock mass
P_{11}	Integrity of the rock mass	Ratio of the in situ P-wave velocity over the P-wave velocity in laboratory samples
P_{12}	Discontinuity's plane strength	Cohesion and friction angle

Based upon the RES principles discussed earlier, these parameters are placed along the leading diagonal of a 12 by 12 interaction matrix. Using a normalised scaled continuous quantitative scheme, Latham & Lu (1999) have coded this matrix with the values shown in Figure 34. (They have acknowledged that in this case, and due to the complexity of the process, some of the coding ended up being carried out by means of objective measurements, whereas other coding was done instead by subjective judgement.) The summation of each line (the cause of each parameter) and column (the effect of each parameter) has also been calculated and is shown in Figure 34.

The practical meaning of the matrix can be readily shown using any pair of parameters. Consider, for example, the interaction between parameters P_3 (the sturdiness) and P_6 (the hardness of the rock). The influence of P_3 on P_6 is represented by the grey arrows in Figure 34, and was given a value of 0.80. The reciprocal influence of P_6 on P_3 is represented by the black arrows, and was given a lower value of only 0.75. This indicates that, according to Latham & Lu, the sturdiness P_3 influences the hardness P_6 slightly more than it is influenced by it.

P_1	0.65	0.70	0.85	0.65	0.55	0.40	0.75	0.50	0.55	0.30	0.40	6.30
0.75	P_2	0.40	0.45	0.65	0.50	0.40	0.65	0.60	0.45	0.50	0.50	5.85
0.90	0.75	P_3	0.80	0.70	0.80	0.45	0.50	0.25	0.25	0.20	0.20	5.80
0.80	0.50	0.70	P_4	0.60	0.60	0.55	0.25	0.45	0.30	0.45	0.15	5.35
0.45	0.65	0.70	0.45	P_5	0.50	0.25	0.45	0.45	0.40	0.25	0.45	5.00
0.70	0.50	0.75	0.40	0.50	P_6	0.25	0.45	0.35	0.35	0.45	0.40	5.10
0.40	0.20	0.40	0.65	0.25	0.45	P_7	0.50	0.20	0.25	0.25	0.15	3.70
0.50	0.70	0.20	0.20	0.15	0.50	0.35	P_8	0.40	0.25	0.20	0.30	3.75
0.25	0.30	0.25	0.50	0.35	0.25	0.30	0.40	P_9	0.80	0.65	0.45	4.50
0.65	0.60	0.30	0.35	0.25	0.35	0.40	0.55	0.65	P_{10}	0.80	0.20	5.10
0.45	0.45	0.20	0.60	0.60	0.45	0.20	0.15	0.50	0.55	P_{11}	0.25	4.40
0.25	0.65	0.10	0.30	0.45	0.25	0.15	0.50	0.55	0.25	0.30	P_{12}	3.75
6.10	5.95	4.70	5.55	5.15	5.20	3.70	5.15	4.90	4.40	4.35	3.45	

Figure 34. Results of the blastability interaction matrix coding. (After Latham & Lu, 1999.)

Figure 35 shows the cause-effect plot associated with this example, and highlights which parameters are the most and the least intense, and which ones are influencing, and are being influenced by, the system the most. As mentioned previously, the parameter that influences the rest of the system the most is the one that lies the furthest away from the C = E line, below it, whereas the parameter that is influenced the most by the rest of the system is the one that lies the furthest away from this line, but above it.

The interest of this approach lies essentially in identifying the critical factors that affect blastability. Whether the selected parameters are adequate or even whether they include redundant elements can undoubtedly be the topic of lengthy discussions. In reviewing existing literature it certainly can be argued that there is no consensus regarding exactly which parameters should be considered in rock blasting engineering.

An important question lies with how the selected parameters are defined. In certain cases, as with the uniaxial compressive strength the authors have chosen to represent the strength parameter P_1, values are easy to determine. In other instances, however, representing a

parameter value is not so easy. The rock mass fragility parameter P_{10} is a good example, whereby the authors suggested using the fractal dimension of the in situ rock mass to represent it.

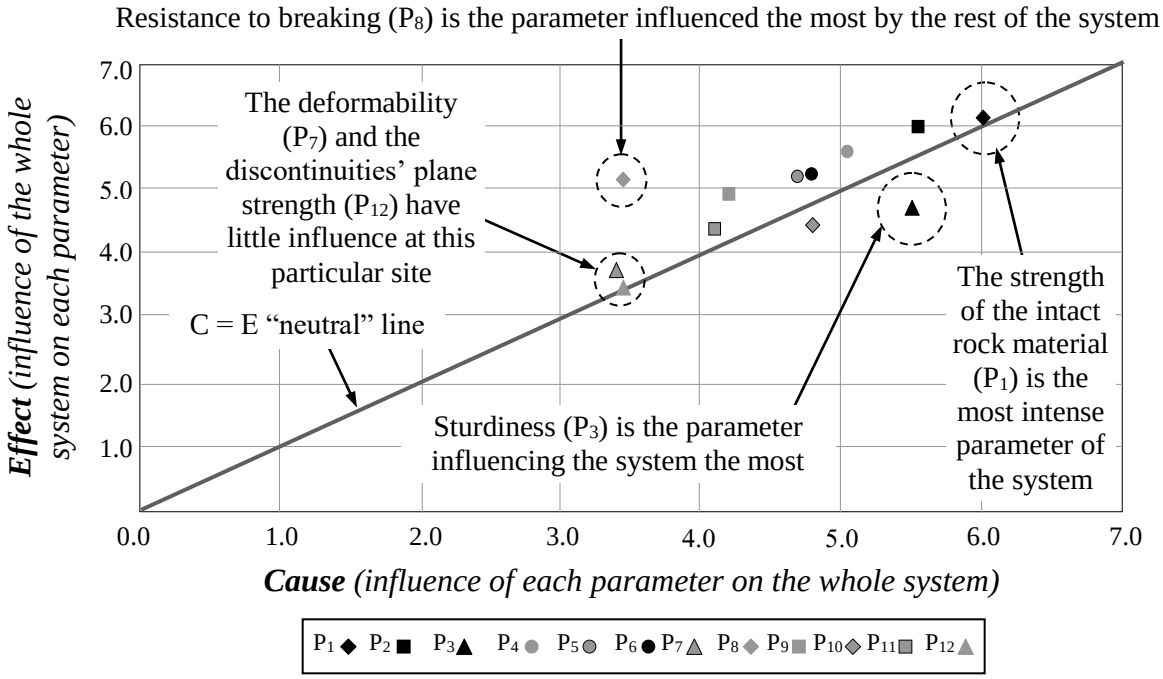

Figure 35. The cause-effect plot for the interaction matrix-coding example described by Latham & Lu (1999) and shown in Figure 34.

One significant advantage of this approach is its usage of matrices, which, besides being highly flexible, have the ability to systematically and methodically manage large amounts of data. The RES methodology is also modular by nature, and, hence, well adapted to further enhancements – such as adding, removing or merging parameters, for example – as various aspects of the engineering system being analysed become better understood.

CONCLUSION DU CHAPITRE. Les Systèmes d'ingénierie du roc ("Rock Engineering Systems" ou "RES") sont une méthodologie d'ingénierie basée sur le calcul matriciel selon laquelle les interactions entre un nombre fini de paramètres interdépendants jouant un rôle dans le système d'ingénierie étudié sont quantifiées. Cette approche, qui a démontré un potentiel d'application à une grande variété de problèmes géotechniques, a l'avantage

significatif d'utiliser des matrices, qui, en plus d'être hautement flexibles, ont la capacité intrinsèque de gérer de grandes quantités d'information de manière systématique et méthodique. L'approche des RES est également modulaire et, ainsi, bien adaptée à des améliorations ultérieures lorsqu'une meilleure compréhension de certains aspects du domaine d'ingénierie étudié est atteinte.

Le prochain chapitre va examiner l'applicabilité au domaine des sautages confinés à grande échelle de relaxation des contraintes dans des piliers de mine de la méthodologie des Systèmes d'ingénierie du roc, qui a démontré suite aux travaux de Latham & Lu (1999) le potentiel de décrire les opérations de sautage "standard".

CHAPTER CONCLUSION. Rock Engineering Systems (RES) are a matrix-based engineering methodology whereby the interactions between a finite number of interdependent parameters that play a role in a particular engineering system are quantified. This approach, which has shown broad applicability to a wide range of geotechnical topics, has the significant advantage of using matrices. These, besides being highly flexible, have the ability to systematically and methodically manage large amounts of data. The methodology is also modular and, hence, well adapted to further enhancements as various aspects of the engineering system being analysed become better understood.

The next chapter will investigate the applicability to the field of large-scale choked panel destress blasting of the Rock Engineering Systems methodology, which has been shown by Latham & Lu (1999) to have the potential to describe the "standard" blasting process.

CHAPTER VII

7. LARGE-SCALE CONFINED PILLAR DESTRESS BLASTING AND ROCK ENGINEERING SYSTEMS

SOMMAIRE DU CHAPITRE. Le Chapitre VII applique la méthodologie des Systèmes d'ingénierie du roc discutée au chapitre précédent au cas des tirs confinés à grande échelle de relaxation des contraintes dans des piliers de mine. La première étape dans l'élaboration d'une matrice d'interaction consiste à identifier les divers paramètres qui jouent un rôle dans le processus étudié. Dans le cadre de ces travaux, ces paramètres peuvent être regroupés en deux catégories: 1) ceux reliés au comportement mécanique du massif rocheux sous hautes contraintes; et, 2) ceux reliés aux tirs de relaxation des contraintes. L'identification de ces paramètres est effectuée dans ce chapitre basée sur ceux qui contrôlent la rupture violente du roc sous hautes contraintes, ainsi que sur des considérations fondamentales d'ingénierie des sautages aux explosifs.

Une fois ces paramètres identifiés et la matrice construite, l'interaction entre chaque paire de paramètres est décrite et justifiée qualitativement. L'étape suivante consiste à choisir des propriétés largement disponibles ou faciles à obtenir qui représentent ces paramètres – cela est effectué aussi bien à l'échelle du matériel rocheux intact qu'à celle du massif rocheux puisqu'il n'est pas possible a priori de déterminer laquelle sera la plus appropriée.

Le codage des matrices d'interaction, à l'échelle du roc intact et à celle du massif rocheux, est ensuite effectué, basé sur des considérations fondamentales de mécanique des roches et de sautage, des études de cas et, dans une certaine mesure, l'expérience et l'intuition de l'auteur. Ces valeurs de codage ont été déterminées incrémentallement et de manière itérative en considérant deux paramètres à la fois et en évaluant leur degré

d'interdépendance en fonction de valeurs de codage préalablement assignées, d'une manière globale. Le processus a été répété de nombreuses fois pour toutes les paires d'interactions possibles, jusqu'à ce qu'un niveau de confiance soit atteint que les interactions quantifiées soient consistantes les unes envers les autres. Des graphes cause-effet ont ensuite été préparés, aux deux échelles considérées.

CHAPTER SUMMARY. Chapter VII applies the Rock Engineering Systems methodology discussed in the previous chapter to large-scale choked pillar destress blasting. The first step in elaborating a RES interaction matrix consists in identifying the parameters that play a role in the process of interest. Within the frame of this work, these parameters can be grouped in two categories: 1) those that relate to the mechanical behaviour of the rock mass under high stress conditions; and, 2) those that pertain to the destress blasting process itself. The identification of these parameters is completed in this chapter based upon those that control violent rock failure under high stress conditions and fundamental blast engineering considerations.

Once these parameters are identified and the interaction matrix is constructed, the interaction between each pair of parameters is described and justified in a qualitative manner. The next step consists in choosing readily available or obtainable properties to represent these parameters – importantly, this will be done at both the intact rock material and the rock mass scales, since it cannot be inferred beforehand which scale is most appropriate.

The coding of the interaction matrices, at both the intact rock material and the rock mass scales, is then done, based upon fundamental rock mechanics and blasting considerations, case histories, and, to a certain extent, the experience and intuition of the author. The coding values were determined incrementally and in an iterative manner by considering two parameters at a time, and assessing their degree of interdependence based upon previously assigned values, in a global manner. The process was repeated numerous times for all the interaction combinations, until a level of confidence was attained that all the interactions derived were consistent with each other. The C–E plots were then derived, at both scales.

7.1. ADVANTAGES OF THE APPLICATION OF THE RES METHODOLOGY

As mentioned, one of the principal advantages of the RES methodology is its usage of matrices, which, by nature, are a highly organised system in which the data are systematically and methodically structured. It can become very difficult to consider in a rational manner all the parameters that play a role in a given engineering system without

resorting to some method to organise and manage them, particularly when a large number of such parameters have been identified. Certainly, alternative empirical methods commonly employed to describe blasting become more cumbersome and difficult to use as the number of parameters considered increases.

As noted in the previous chapter, the RES approach also has the advantage of being highly modular. Any of its components can be individually modified, improved and refined as more understanding into the system investigated is gained, and more calibration data become available. Changes in individual components improve the overall system without disturbing its other components. New modules, either matrices or sub-matrices better suited at dealing with a particular aspect of the process, can also be added reasonably easily once a sound overall architecture has been constructed. This modular aspect of the technique allows for its improvement with time and usage.

7.2. PARAMETERS THAT CONTROL VIOLENT ROCK MASS FAILURE UNDER HIGH STRESS CONDITIONS

A number of well documented parameters play a role in governing the violent failure of massive to sparsely jointed and moderately jointed hard rock masses subjected to high stress levels. These rock mass conditions are of particular interest within the frame of this work because they represent the most likely situations in which destress blasting will be attempted in Canadian underground hard rock metal mines. Massive to sparsely jointed rock masses correspond to situations where the spacing between discontinuities is wider than the excavation width. A moderately jointed rock mass is one that exhibits a low number (two to three) of relatively widely spaced (in the order of more than 20% the excavation width) joint sets – even though some of the structures might be joining, they are generally not continuous and exhibit a rough surface, usually without in-filling material (Hoek, 1998).

Highly jointed rock masses – which exhibit a high number (typically four or more) of tightly spaced (in the order of less than 20% the excavation width) major joint sets – are usually too soft and too fractured to accumulate the large amounts of strain energy that can lead to violent failure situations. Such rock masses, whereby discontinuities are both persistent and continuous, are essentially networks of small interlocking discrete blocks and wedges that can move substantially along each other and dissipate strain in a progressive non-violent manner. Very high levels of confining stress, which effectively prevent any of this movement to occur, can sometimes result in violent failure conditions – under such circumstances a part of a highly stressed and highly confined pillar core typically fails suddenly, causing in turn the ejection of loose material around the periphery of nearby excavations. This failure mechanism is however not very common, and most rockbursts occur in massive to moderately jointed hard rock masses.

Parameters known to play a role in the violent failure of massive to moderately jointed hard rock masses subjected to high stress levels are as follows:

- *The mining method*. The mining method controls how the ground stresses will be modified and where they will be diverted as mining progresses, whether certain regions will be subjected to high mining-induced stress levels, whether or not pillars will be created, the shape and size of such pillars, etc.
- *The characteristics of the excavations*. Parameters such as the location of the excavations (including their depth and position relative to each other), as well as their size, orientation and geometry, largely control whether or not high stress levels are likely to build up in their vicinity and between them, and whether or not conditions of violent failure can develop around them.
- *The in situ stress regime*. This parameter controls the stress magnitudes that can be induced around the various excavations and in the various pillars as mining progresses.
- *The mechanical properties of the rock*. The stiffness, strength and brittleness of the various geological units comprised in the rock mass constitute an important aspect in determining the response of the rock mass to the stress regime and the potential for violent failure.

- *The stiffness of the loading system*. All other parameters remaining constant, as the stiffness of the loading system decreases the potential for violent failure increases.

All these parameters are related, either directly or indirectly, to the geomechanical aspects of violent rock mass failure previously discussed in detail. As mentioned earlier, the stress path to failure (the evolution of the stress regime from virgin conditions to the encounter of the failure envelope) also controls to a certain extent the type of failure to expect. The stress path is however essentially a result of the combination of the parameters just discussed.

7.3. PARAMETERS PLAYING A ROLE IN DESTRESS BLASTING

As pointed out in Chapter IV, the case studies describing large-scale confined pillar destress blasts do not systematically document and discuss the exact same parameters – as a result, it can be argued that "all" the pertinent data were not collected in a methodical and complete way in each reported case study. This renders direct comparisons between all the case studies difficult, the extrapolation from one to the other hard, and the elaboration of a single "unifying" design approach arduous. Nonetheless, their study, combined with rock mechanics and blasting engineering considerations, clearly indicates that only a limited number of parameters play a dominant role in governing how successful a large-scale choked panel destress blast can be. These parameters can be argued to be related 1) to the rock mass properties and its stress state; and, 2) to the drilling and blasting design implemented.

7.3.1. Rock- and stress-related parameters

The state of the rock mass at the time of the destress blast – in terms of its mechanical properties, its degree of fracturing and the stress regime it is subjected to – has a significant influence on the outcome of the destress blasting procedure.

7.3.1.1.Stiffness, strength and brittleness

The stiffness, strength and brittleness of the rock mass in which a choked destress blast is attempted are critical parameters as they largely dictate how much of a shattering effect the blasting energy will have. Figure 8 illustrated these components. Stiffness is represented by the Young's modulus, strength (or peak strength) by the maximum compressive load the rock mass can bear, and brittleness by how steep and pronounced the brittle response is. As mentioned previously, a stiff, strong and brittle rock mass results in: 1) more strain energy being accumulated for a given deformation (caused either by the local static ground stresses, or the dynamic blasting process itself); 2) more strain energy being accumulated prior to failure; and, 3) larger amounts of accumulated strain energy being suddenly released at failure. Such rock masses are hence easier to literally break apart – provided that enough energy is inputted into the system to fail them –, and their brittleness tends to make them reach their residual strength shortly after failure, which is beneficial with respect to destressing as it rapidly reduces their load bearing capacity.

7.3.1.2.Degree of fracturing

The degree of fracturing of the rock mass is a very important parameter as it affects its overall mechanical properties, including stiffness. The degree of fracturing can be used to downgrade the strength and brittleness parameters of the intact rock material, which can be more easily measured in the laboratory on intact samples than in the field directly at the rock mass scale. One could argue that how jointed the rock mass is also affects the amount of explosive energy required to carry out a destress blast. A more jointed rock mass might actually require *more* explosive energy to compensate for the decreased blasting efficiency associated with a softer and more ductile ("absorbing") medium.

For the purpose at hand, the degree of fracturing can conceivably be represented in a number of ways, such as by the RQD (described in Appendix D), RMR (described in Appendix E), GSI (Geological Strength Index, defined by Hoek *et al*. [1995] and described in Appendix F) or Q (developed by Barton *et al*., [1974] and described in Appendix G) ratings, or the spacing of the joint sets, or the block size distribution, for example. Both

natural features and mining-induced fractures, which result from high stress conditions, need to be considered.

7.3.1.3.Proximity to static failure

The proximity to failure from a static stress point of view, either in the ($\sigma_1 - \sigma_3$) or the ($\tau - \sigma_N$) space, provides an estimate of how far the rock mass stands from its failure envelope. This, in turn, dictates how much explosive energy is required in order to "tip it over" its peak strength and achieve a destressing effect. Figure 36 illustrates this point, for a non-linear Hoek-Brown failure envelope expressed in the ($\sigma_1 - \sigma_3$) space.

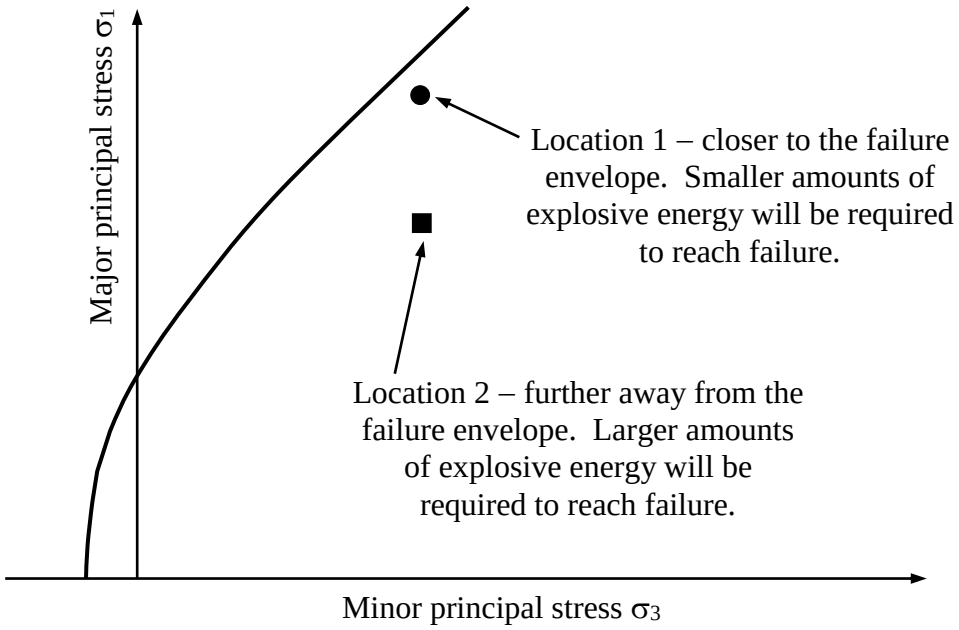

Figure 36. The concept of distance away from the failure envelope. (After Andrieux *et al*., 2004.)

There undoubtedly exists a relationship between the optimum amount of explosive energy required per quantity of targeted rock mass and how far this rock mass stands from its failure envelope, which depends on its mechanical properties and the stress regime it is subjected to at the time of the blast. Please note that the absolute stress levels that prevail in and around the targeted zone are not considered to be a governing parameter – this is

because it is assumed that they are high enough to warrant considering destress blasting in the first place.

7.3.1.4.Additional comments on the rock-related parameters

The five rock-related parameters considered here to play a role in large-scale choked pillar destress blasting are somewhat different from those identified as playing a role in the occurrence of violent rock mass failure under high stress conditions. In particular, only the properties of the rock horizon in which the destress blast is attempted are considered, and not those of the adjacent rock units. Although a soft loading system would further promote the failure of the targeted region, this has not been considered within the scope of this work.

7.3.2. Blasting-related parameters

The parameters related to the explosive products selected and the way they are used are also critical with respect to the effectiveness of a large-scale confined pillar destress blast. Although, and as mentioned previously, some debate still exists concerning the exact detailed mechanisms taking place during destress blasting, the blasting process is likely to result in the following main events occurring:

1. *The crushing of the periphery of the blastholes*. This effect, due to its limited geometrical extent, is not likely to play a significant destressing role.

2. *The creation of new fractures*, preferentially aligned with (and promoted by) the major principal stress component σ_1. As described in Andrieux & Brummer (2002), timing the blast "diagonally" with respect to the major principal stress component can help promote fracture creation in shear as well. Figure 37 illustrates this point. As can be seen in Figure 37d, maximum shear theoretically occurs along a plane oriented at 45° to the major principal stress vector σ_1.

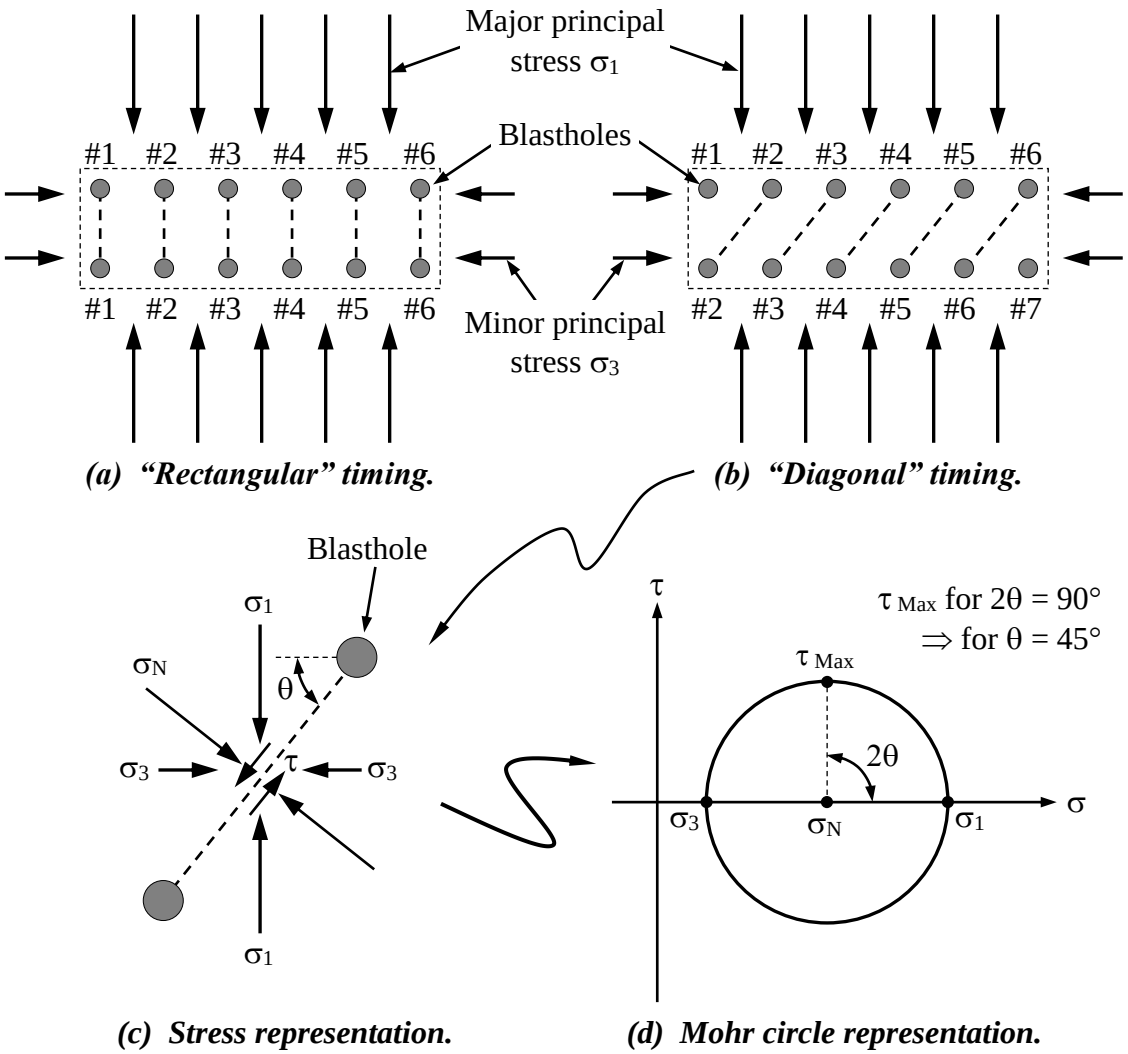

Figure 37. The theoretical potential of a diagonal blasting sequence to promote shear fractures in the destressed zone. (Adapted from Andrieux & Brummer, 2002.)

The fracture creation effect probably plays a more important role in the case of a more massive rock mass with fewer natural fractures in it.

3. *The extension of existing fractures*, also preferentially aligned with (and promoted by) the major principal stress component. This fracture extension effect probably plays a more dominant role in the case of a more jointed rock mass where it may be easier for the explosive gaseous energy to exploit pre-existing fractures than it is to create new ones.

The rapid and very large pressure build-up of the detonation gases within the fracture networks inside the rock mass also causes a near-instantaneous reduction of the normal stress acting upon these fractures. This reduction, although of short duration, results in any shear strain stored along these fractures being near-instantaneously released by allowing movement to occur along them. This can be inferred to constitute a dominant effect if high levels of strain energy have been accumulated within the rock mass, which could not be statically dissipated due to a high level of confinement, a high friction angle value on the discontinuities, and/or the presence of discrete "lock-up" points along their surface. In this case, a highly gaseous explosive product would be advantageous with respect to destress blasting.

7.3.2.1.Orientation of the destress blast

If the targeted volume – which, for large-scale choked panel destress blasts typically has a long and narrow shape – is sub-parallel to σ_1, it will represent a small "obstacle" for the ground stresses to go around, similarly to a narrow excavation oriented sub-parallel to the major principal stress, and the destress blast will probably not be very effective. On the other hand, if the targeted volume is perpendicular to σ_1, it will then have a maximum effect of diverting the stress away from the blasted region. Figure 38, a schematic view through a conceptual destress blast showing the amount of blocking effect achieved as a function of its orientation with respect to the major principal stress component, illustrates these points.

The orientation of σ_1 can generally be derived from field observations (if the stress level is high enough), or from instrumentation or numerical stress modelling.

Please note that the combination of this sixth parameter with the fifth one (the proximity to failure) accounts for both the orientation and the magnitude of the mining-induced principal stress vectors.

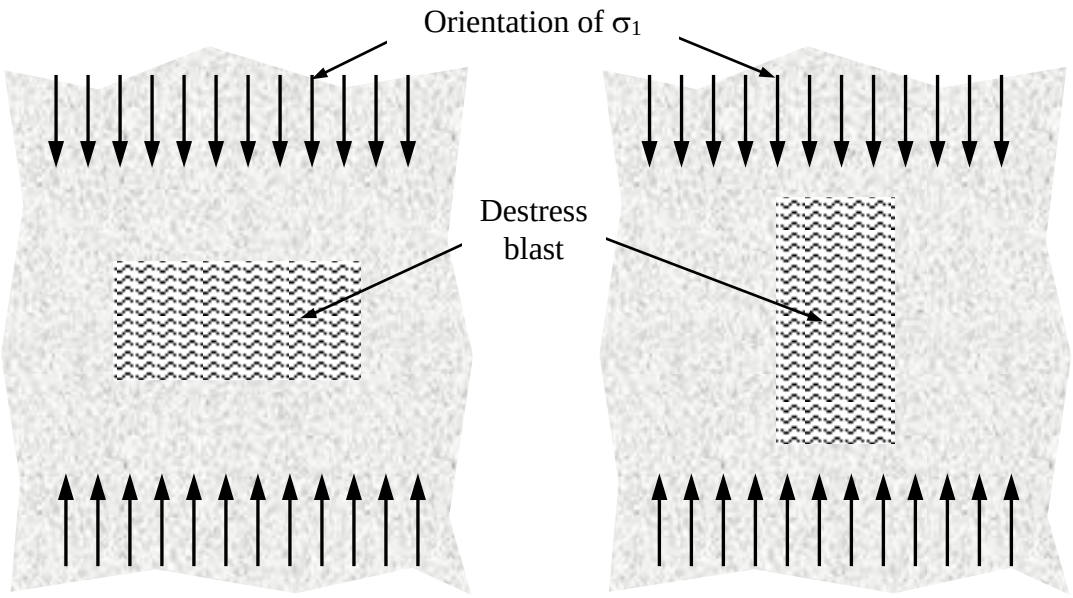

Figure 38. Schematic illustration of the amount of stress blocking effect achieved as a function of the blast orientation with respect to σ_1. (After Andrieux *et al*., 2004.)

7.3.2.2.Width of the destress blast

The width of the targeted zone, measured in a direction parallel to σ_1, is also important as it is easier to achieve an effective destressing effect when this width is large. The reason is that as the number of blasting rings increases, a wider internal volume of rock is surrounded by explosive charges, which results in a larger thickness of rock being fractured and disturbed.

As disturbances – in terms of discrete blasted blocks having moved, rotated and shifted relative to each other – occurs over a wider thickness of material, a better immediate destressing result is obtained, and any stress re-mobilisation effect is further delayed and reduced in magnitude. Figure 39 schematically illustrates this concept of disturbance width.

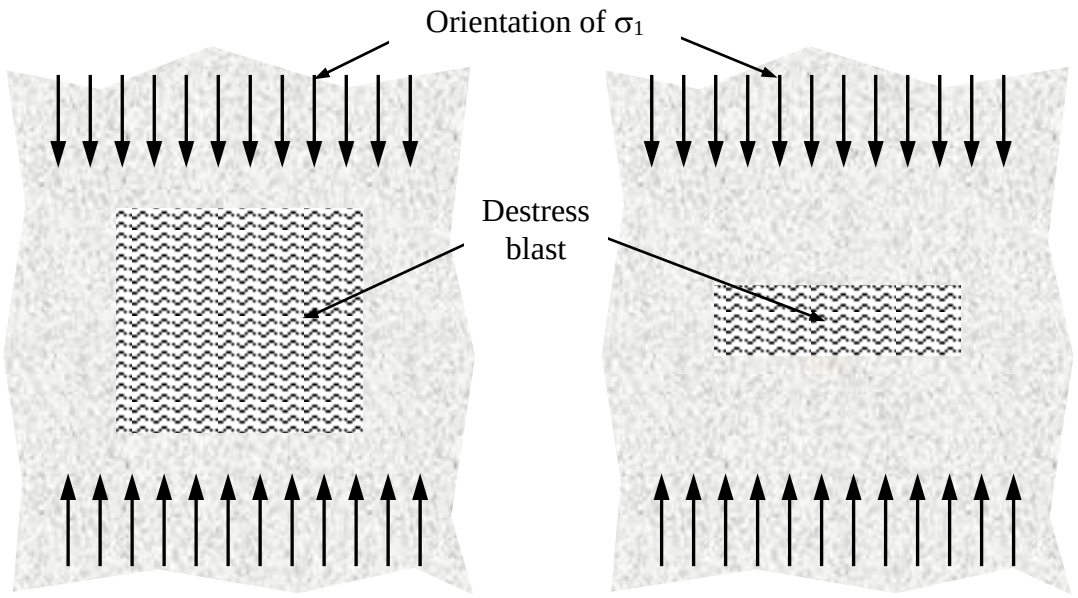

Figure 39. Schematic cross-section through a conceptual destress blast showing the concept of disturbance width. (Adapted from Andrieux *et al*., 2004.)

7.3.2.3.Amount of explosive energy

The total amount of explosive energy per quantity of targeted rock (either in terms of volume or mass), which will be referred to in this thesis as the "unit explosive energy", is obviously an important parameter: as more explosives are used in a given volume, more unit energy is introduced into the system, and more fracturing and disturbance can be expected to occur throughout the volume of rock to destress.

7.3.2.4.Confinement of the explosive charges

The confinement of the explosive charges is also an important parameter as it has a large effect on the amount of useful work the detonation gases will provide. The behaviour of the detonation gases of an explosive product is characterised by their equation of state, which relates pressure, volume and temperature. As time elapses, the gases drive further inside the fracture networks and occupy an increasingly larger volume. They simultaneously cool down as well. This combined reduction of temperature and increase of

occupied volume translates into a reduction of the pressure exerted by the detonation gases onto the fracture walls. However, once the detonation gases reach a free face, they rapidly vent to atmospheric pressure, quickly stopping any further useful work inside the rock mass. Figure 40 schematically illustrates this mechanism.

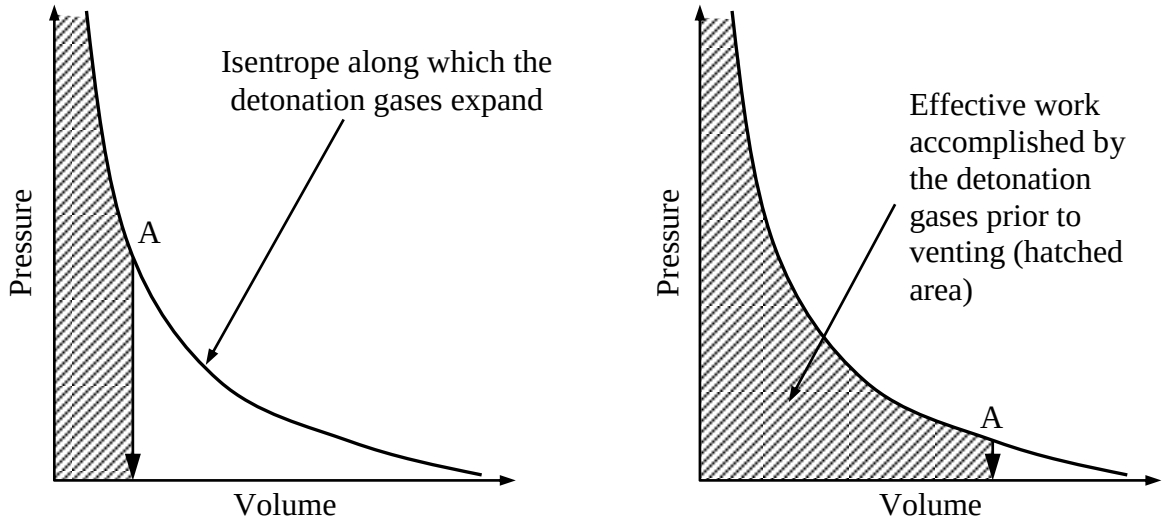

Once a free face is reached (at Point A), venting occurs and the pressure rapidly drops to atmospheric pressure, effectively ending the amount of useful work performed by the detonation gases inside the blasted rock mass.

Figure 40. Amount of useful work performed by the detonation gases in the case of early (left hand side) and late (right hand side) venting. (After Andrieux *et al*., 2004.)

As the level of confinement of the explosive charges increases, the point in time at which the gases will encounter a free face is postponed, which maximises the effective work they will accomplish inside the rock mass.

Also, the confinement of an explosive charge – in terms of its decoupling ratio inside the hole, the stiffness and strength properties of the surrounding rock mass, and, to a certain extent, its proximity to a free face – affects its velocity of detonation (VOD). Typically, and with all other parameters remaining unchanged, as the degree of charge confinement increases, the VOD increases as well (up to a certain maximum value), and vice-versa. Since the borehole pressure generated by a detonating explosive charge is related to the square of the VOD, the reduction in VOD that accompanies a reduction in charge

confinement can significantly lower the borehole pressure and, hence, the shock effect of the explosive charge. This, in turn, lowers the amount of effective work performed by the charge.

7.4. ROCK ENGINEERING SYSTEMS AND LARGE-SCALE CONFINED PILLAR DESTRESS BLASTING

As discussed, and based upon case histories and engineering concepts, a total of nine (9) parameters can be identified as playing a role with respect to large-scale choked panel destress blasting. In accordance with the RES methodology, a tenth parameter, P_{10}, must also be added, which represents the result of the destress blast, in terms of the stress reduction it achieved. The necessity to include a results parameter in this particular case could be argued. Although in a continuous or cyclic process such as mining, for example, the excavations previously created do modify the system and affect the conditions under which future excavations will be completed, this may not be so relevant with a "single event" such as destress blasting. In any case, this parameter has been included at this early stage in order to comply with standard RES methodology. As a result, the initial interaction matrix constructed for large-scale choked pillar destress blasting is as shown in Figure 41, with: P_1 the stiffness of the rock; P_2 the strength of the rock; P_3 the brittleness of the rock; P_4 the degree of fracturing of the rock mass; P_5 the proximity to (static) stress-induced failure; P_6 the orientation of the destress blast; P_7 the width of the destress blast; P_8 the unit explosive energy; P_9 the confinement of the explosive charges; and, P_{10} the result of the destress blast. Please refer to Figure 29 for a detailed description of the nomenclature used in Figure 41.

Looking at the matrix in Figure 41 one will notice that the strength of the rock appears twice: once directly in parameter P_2, and once indirectly in parameter P_5. This raises the question of whether or not this constitutes "double accounting" of the rock strength, which would artificially boost the cause of this parameter.

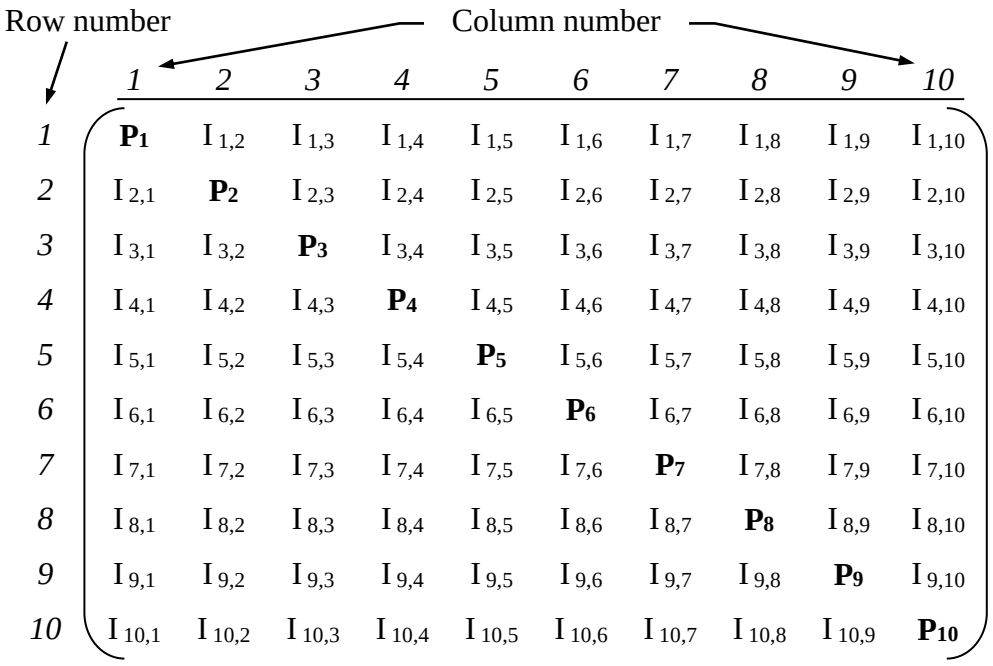

Figure 41. Initial interaction matrix constructed for large-scale confined panel destress blasting.

Within the frame of this work, it is argued that every effort should be made to reduce the RES matrix to the bare minimum number of parameters, while still capturing all the relevant ones. This approach ensures that only the fundamental components at play in large-scale confined panel destress blasts are considered and that the process is reduced to its most basic elements. Another advantage of this approach is the simplification it allows, which is not negligible if the method is to eventually be used in a practical manner by practitioners.

Based upon these considerations, parameters P_2 was removed from the matrix – as a result, the strength of the rock remains in only one place, under parameter P_5. Figure 42 shows the simplified 9 by 9 matrix, in which the numbering has been revised in order to remain sequential, with, now: P_1 the stiffness of the rock; P_2 the brittleness of the rock; P_3 the degree of fracturing of the rock mass; P_4 the proximity to (static) stress-induced failure; P_5 the orientation of the destress blast; P_6 the width of the destress blast; P_7 the unit explosive energy; P_8 the confinement of the explosive charges; and, P_9 the result of the destress

blast. This 9 by 9 interaction matrix structure will be retained throughout the remainder of this work.

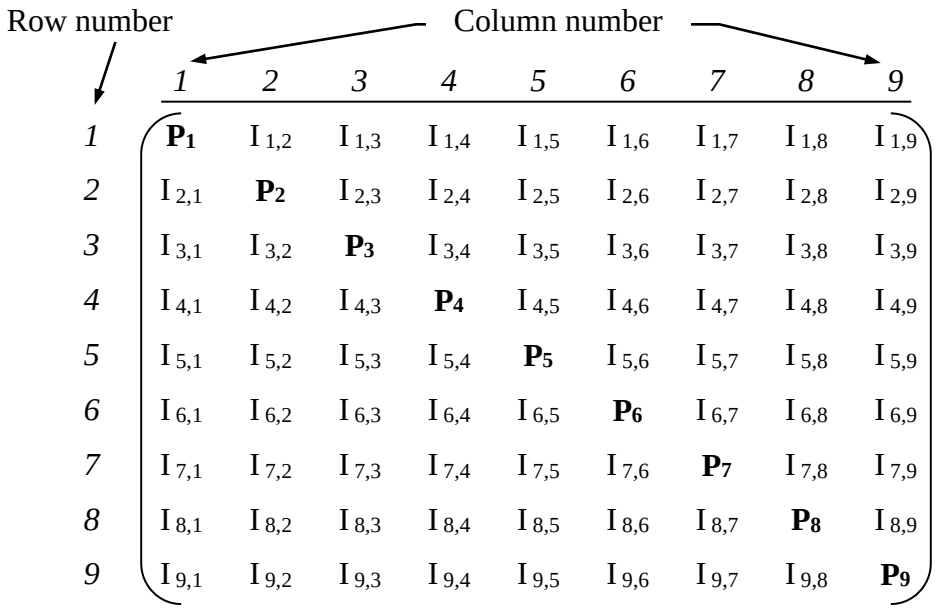

Figure 42. Final interaction matrix constructed for large-scale confined panel destress blasting.

The next step consists in examining how the various parameters of the matrix shown in Figure 42 interact.

7.4.1. Global interaction between each pair of parameters

The examination in a qualitative manner of how the various parameters of the RES matrix, taken two at a time, interact can provide a valuable feel for its internal mechanics. This first pass assessment consists in determining whether an increase in a given parameter leads to an increase or a decrease in another given parameter. For this purpose the following convention is proposed:

- When two parameters work in the same direction, i.e., when an increase in a parameter will result in an increase of another parameter, or when a decrease in a parameter will result in a decrease of another parameter, the symbol U-U (for “Up-Up”) will be used to describe this interaction.

- On the other hand, when two parameters work in opposite directions, i.e., when an increase in a parameter will result in a decrease of another parameter, or when a decrease in a parameter will result in an increase of another parameter, the symbol U-D (for "Up-Down") will be used to describe this interaction.

Importantly, two types of interactions can be encountered. One can be stated as "parameter P_i will result in parameter P_j to increase (or decrease)", the other one as "parameter P_i will allow for parameter P_j to be increased (or decreased)". In this application, certain parameters have no real direct effect on other parameters, but have nevertheless some influence on them. For example, the proximity to failure of the rock mass does not have a direct effect on the number of blasthole rings. However, a closer proximity to failure may allow to reduce the number of blasting rings for the same destressing result to be attained. This second type of interaction represents a subtle change from the standard RES methodology, which allowed to consider a greater number of interactions between the various parameters in the system. Based upon the proposed convention, a qualitative interaction can be derived for each pair of parameters, as shown in Figure 43.

P_1	U-U	U-D	U-U	U-D	U-D	U-D	U-D	U-U
U-U	**P_2**	U-D	U-U	U-D	U-D	U-D	U-D	U-U
U-D	U-D	**P_3**	U-U	U-U	U-U	U-U	U-U	U-D
U-D	U-D	U-U	**P_4**	U-D	U-D	U-D	U-D	U-U
U-D	U-D	U-U	U-D	**P_5**	U-D	U-D	U-D	U-U
U-D	U-D	U-U	U-D	U-D	**P_6**	U-U	U-D	U-U
U-D	U-D	U-U	U-U	U-D	U-D	**P_7**	U-D	U-U
U-D	U-D	U-D	U-U	U-D	U-D	U-D	**P_8**	U-U
U-D	U-D	U-U	U-U	U-U	U-U	U-U	U-U	**P_9**

Figure 43. General qualitative interactions between each pair of parameters in the large-scale confined panel destress blasting interaction matrix.

The global interactions shown in Figure 43 are discussed, explained and justified in a qualitative manner in the following sections. (In these sections the interaction $I_{i,j}$ referenced in each case is as shown in Figure 42.)

7.4.1.1.Effects of P_1 – the stiffness of the rock, on all the other parameters

- *Effect on P_2, the brittleness of the rock (interaction $I_{1,2}$).* As the stiffness of the rock increases, its brittleness usually increases as well.
- *Effect on P_3, the degree of fracturing of the rock mass (interaction $I_{1,3}$).* As the stiffness of the rock increases, its degree of homogeneity also generally increases, which, in turn, results in its degree of fracturing to decrease.
- *Effect on P_4, the proximity to failure of the rock (interaction $I_{1,4}$).* As the stiffness of the rock increases, with all the other parameters remaining the same, more load is generated for the same amount of imposed strain, which brings the rock closer to its failure envelope.
- *Effect on P_5, the orientation of the destress blast (interaction $I_{1,5}$).* As the stiffness of the rock increases, it becomes more amenable to destress blasting, which, in turn, lowers the requirement for the destress blast to be oriented perpendicularly to the major principal stress component.
- *Effect on P_6, the width of the destress blast (interaction $I_{1,6}$).* As just mentioned, as the stiffness of the rock increases, it becomes easier to destress, which, in turn, lowers the requirement for the destress blast to encompass a wide zone.
- *Effect on P_7, the unit explosive energy in the destress blast (interaction $I_{1,7}$).* Again, as the stiffness of the rock increases, it becomes easier to destress, which, in turn, lowers the requirement for more unit explosive energy to be used. From another point of view, a softer rock mass tends to require more unit explosive energy in order to compensate for the decreased blasting efficiency associated with a softer and more ductile (“absorbing”) medium.
- *Effect on P_8, the confinement of the explosive charges in the destress blast (interaction $I_{1,8}$).* As the stiffness of the rock increases, it becomes easier to destress, which, in turn, lowers the requirement for the explosive charges to be confined and for all the available explosive energy to be used.

- *Effect on P_9, the result of the destress blast (interaction $I_{1,9}$).* As the stiffness of the rock increases and it becomes easier to destress – and with all other parameters remaining constant –, the destressing effect increases as well.

7.4.1.2.Effects of P_2 – the brittleness of the rock, on all the other parameters

- *Effect on P_1, the stiffness of the rock (interaction $I_{2,1}$).* As the brittleness of the rock increases, its stiffness usually increases as well.
- *Effect on P_3, the degree of fracturing of the rock mass (interaction $I_{2,3}$).* As the brittleness of the rock increases, its degree of fracturing generally decreases.
- *Effect on P_4, the proximity to failure of the rock (interaction $I_{2,4}$).* As the brittleness of the rock increases, its stiffness usually increases as well, which, in turn, results in more load being generated for the same amount of imposed strain, and in the rock being closer to its failure envelope. Hence, a more brittle rock generally results in it being closer to its failure envelope for a given applied load.
- *Effect on P_5, the orientation of the destress blast (interaction $I_{2,5}$).* As the brittleness of the rock increases and its destressing becomes inherently easier, the necessity to orient the destress blast at 90° to the σ_1 component is alleviated.
- *Effect on P_6, the width of the destress blast (interaction $I_{2,6}$).* As the brittleness of the rock increases and it becomes easier to destress, the requirement to target a wide zone is lessened.
- *Effect on P_7, the unit explosive energy in the destress blast (interaction $I_{2,7}$).* As the brittleness of the rock increases and it becomes easier to shatter, the amount of unit explosive energy required to achieve a given level of destressing is lowered.
- *Effect on P_8, the confinement of the explosive charges in the destress blast (interaction $I_{2,8}$).* As the brittleness of the rock increases and it becomes easier to break, the necessity to maximise the use of the available explosive energy through maximum confinement decreases.

- *Effect on P_9, the result of the destress blast (interaction $I_{2,9}$).* With all other parameters remaining unchanged, as the brittleness of the rock increases, its becomes easier to shatter, which, in turn, increases the level of destressing achieved.

7.4.1.3.Effects of P_3 – the degree of fracturing of the rock mass, on all the other parameters

- *Effect on P_1, the stiffness of the rock (interaction $I_{3,1}$).* As the degree of fracturing of the rock mass increases, the stiffness (at the rock mass scale) tends to decrease. This effect is due to the increase in the degrees of liberty the more numerous blocks that comprise the rock mass have to move relative to each other in a progressive manner, in response to strain.

- *Effect on P_2, the brittleness of the rock (interaction $I_{3,2}$).* As the degree of fracturing of the rock mass increases, the brittleness (again at the rock mass scale) tends to decrease, for the same reason just discussed.

- *Effect on P_4, the proximity to failure of the rock (interaction $I_{3,4}$).* As the degree of fracturing of the rock mass increases, it becomes intrinsically weaker, which, for a given stress regime, brings the failure envelope closer. Figure 44 illustrates this point, with Hoek-Brown failure criteria in the (σ_1 , σ_3) space.

- *Effect on P_5, the orientation of the destress blast (interaction $I_{3,5}$).* As the degree of fracturing of the rock mass increases, it can be argued to become more difficult to blast because: 1) its stiffness and brittleness are reduced; and, 2) some of the blasting energy will be dissipated in the fracture networks. As a result, an augmentation in the degree of fracturing of the rock mass results in an increased need to orient the destress blast perpendicularly to the major principal stress component to achieve results.

  On the other hand, however, and as discussed for interaction $I_{3,4}$, as the degree of fracturing of the rock mass increases, it becomes intrinsically weaker, which lowers the need to orient the destress blast perpendicularly to the major principal stress component. This latter effect is however perceived as lesser than the former, and a “U-U” rating was chosen for interaction $I_{3,5}$.

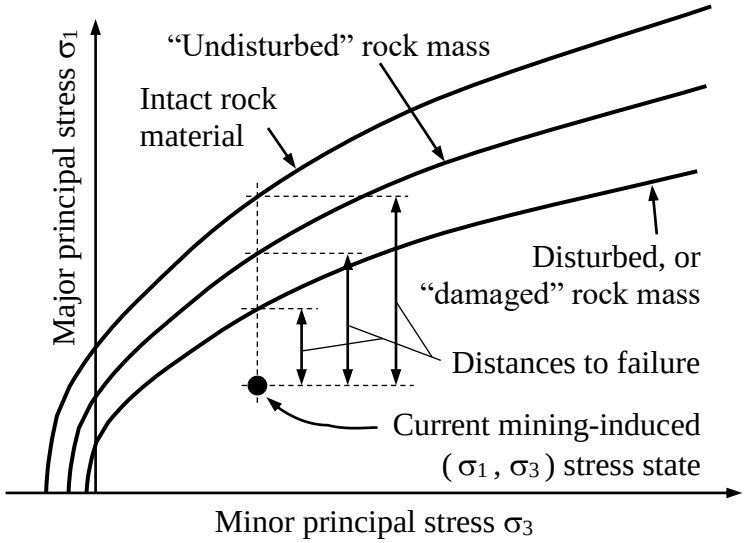

Figure 44. Conceptual representation of the failure envelopes associated with various degrees of rock mass fracturing, and how they change the proximity to failure for a given stress state.

- *Effect on P_6, the width of the destress blast (interaction $I_{3,6}$).* As just mentioned, as the degree of fracturing of the rock mass increases, it becomes more difficult to blast – as a result, an increase in the degree of fracturing should result in an increased need to widen the targeted zone. The counter-argument formulated for interaction $I_{3,5}$, based upon the fact that as its degree of fracturing increases the rock mass becomes weaker, can again be made, which lowers the requirement to have a wider destress zone. However, the former effect is seen as more pronounced, and a "U-U" rating was assigned to interaction $I_{3,6}$.

- *Effect on P_7, the unit explosive energy in the destress blast (interaction $I_{3,7}$).* As the degree of fracturing of the rock mass increases, it becomes more jointed and requires more unit explosive energy to compensate for the decreased blasting efficiency associated with a softer and more ductile ("absorbing") medium. However, the same counter-argument as before can be made again: as the degree of fracturing increases, the rock mass becomes weaker, which requires less unit explosive energy to push it to failure. The increased ductility of a more fractured rock mass was ultimately deemed the dominant factor, and a "U-U" rating was assigned to interaction $I_{3,7}$.

- *Effect on P_8, the confinement of the explosive charges in the destress blast (interaction $I_{3,8}$).* Again, as the degree of fracturing of the rock mass increases, it becomes more broken and requires more explosive energy to compensate for the decreased blasting efficiency associated with a softer and more ductile medium. This, in turn, warrants more confinement to be applied to the explosive charges in order to maximise the usage of their energy.

  The same counter-argument as before can however be made yet again, whereby an increased degree of fracturing makes the rock mass intrinsically weaker, which requires less explosive energy to push it to failure and reduces the requirement for a high level of charge confinement. As for the previous three interactions, the former argument was deemed dominant, and a "U-U" rating was retained for interaction $I_{3,8}$.

- *Effect on P_9, the result of the destress blast (interaction $I_{3,9}$).* The same arguments as previously made apply here again. As the degree of fracturing of the rock mass increases, it becomes softer and more ductile. This, in turn, makes it less amenable to destressing by blasting due to the decreased efficiency of detonating explosives in such a material. On the other hand, as the degree of fracturing of the rock mass increases, it becomes weaker and, as a result, sits closer to failure. Overall, it was decided in this first approach that the former effect is dominant, which resulted in a "U-D" rating to be assigned to interaction $I_{3,9}$.

7.4.1.4.Effects of P_4 – the proximity to failure of the rock, on all the other parameters

- *Effect on P_1, the stiffness of the rock (interaction $I_{4,1}$).* As the rock approaches its failure envelope, previously existing fractures extend and new micro-fractures develop, which soften the rock mass. Hence, a closer proximity to failure results in a decrease of the rock mass stiffness.

- *Effect on P_2, the brittleness of the rock (interaction $I_{4,2}$).* As the rock mass approaches static stress-induced failure there might conceptually be a somewhat reduced need for it

to be brittle for a given destress blast design to be successful. This interaction is however probably quite weak.

- *Effect on P_3, the degree of fracturing of the rock mass (interaction $I_{4,3}$).* The increase in macro- and micro-fracturing associated with the approach towards the failure envelope increases parameter P_3.
- *Effect on P_5, the orientation of the destress blast (interaction $I_{4,5}$).* As the rock approaches its failure envelope, the necessity to orient the destress blast at 90° to σ_1 is somewhat lessened.
- *Effect on P_6, the width of the destress blast (interaction $I_{4,6}$).* As the rock approaches failure, the requirement to target a wider zone is decreased to a certain extent.
- *Effect on P_7, the unit explosive energy in the destress blast (interaction $I_{4,7}$).* As the rock approaches its failure envelope, less unit explosive energy is required to push it to failure.
- *Effect on P_8, the confinement of the explosive charges in the destress blast (interaction $I_{4,8}$).* Again, as the rock approaches failure, less explosive energy is required to push it to failure, which lowers the need to confine the explosive charges in the destress blast.
- *Effect on P_9, the result of the destress blast (interaction $I_{4,9}$).* A closer proximity to the static failure envelope will result, for a given destress blast design, in a more pronounced destressing effect, as less of the explosive energy will be needed to push the rock mass to failure, which, in turn, will leave more energy available to cause additional damage in the rock mass.

7.4.1.5.Effects of P_5 – the orientation of the destress blast, on all the other parameters

Within the frame of this work, the angle representing the orientation of the destress blast is defined as shown in Figure 45, as the angle between the destress blast azimuth and the direction of the targeted stress component (usually σ_1, but also conceivably σ_2 or σ_v, for example). Please note that the orientation of the destress blast, combined with its geometry

and size, greatly influences where the regions of high and low stress will be located, as well as their extent.

- *Effect on P_1, the stiffness of the rock (interaction $I_{5,1}$).* As the orientation of the destress blast becomes more perpendicular to the direction of the targeted stress component, the stiffness of the rock can be less for a similar destressing effect to be achieved.

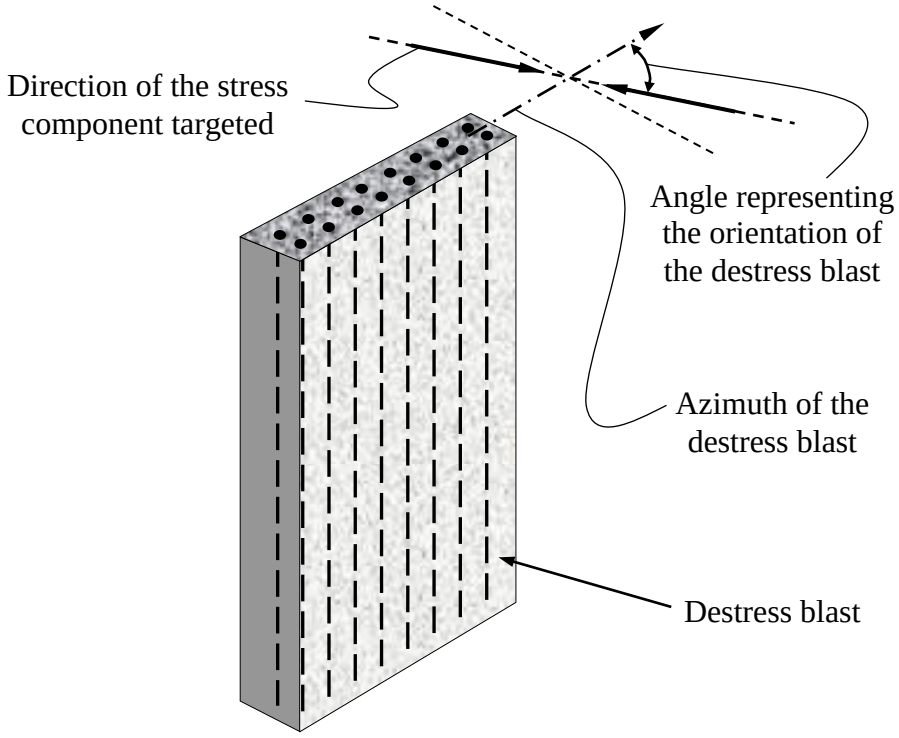

Figure 45. Schematic representation showing how the angle representing the orientation of the destress blast is defined.

- *Effect on P_2, the brittleness of the rock (interaction $I_{5,2}$).* Following the same logic as in the previous paragraph, as the orientation of the destress blast becomes more perpendicular to the direction of the targeted stress component, the brittleness of the rock can be less for a similar destressing effect to be achieved.

- *Effect on P_3, the degree of fracturing of the rock mass (interaction $I_{5,3}$).* As the orientation of the destress blast becomes more perpendicular to the direction of the targeted stress component, the length of "effective" fracturing in the rock mass (perpendicular to the direction of the stress component) increases. Figure 46 illustrates this effect.

- *Effect on P_4, the proximity to failure of the rock (interaction $I_{5,4}$).* As the orientation of the destress blast becomes more perpendicular to the direction of the targeted stress component, the requirement for the rock mass to be nearing its failure envelope for the destress blast to be successful is (slightly) reduced.

- *Effect on P_6, the width of the destress blast (interaction $I_{5,6}$).* Following the same logic, as the orientation of the destress blast becomes more perpendicular to the direction of the targeted stress component, the requirement for the destressed zone to be wide is lessened.

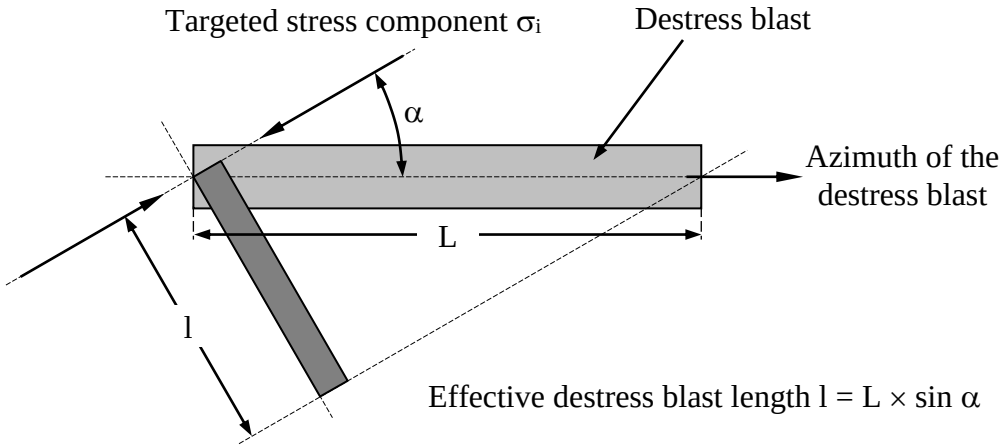

Figure 46. Schematic view showing how the effective length of the destress blast increases as the orientation of the destress blast becomes more perpendicular to the direction of the targeted stress component.

- *Effect on P_7, the unit explosive energy in the destress blast (interaction $I_{5,7}$).* The amount of unit explosive energy required in the destress blast is lowered as the orientation of the destress blast becomes more perpendicular to the direction of the targeted stress component. In other words, as the azimuth of the destress blast becomes more parallel to the targeted stress component, more unit explosive energy is required in an attempt to maximise the damage zone and compensate for the less favourable orientation.

- *Effect on P_8, the confinement of the explosive charges in the destress blast (interaction $I_{5,8}$).* Following the same logic as for interaction $I_{5,7}$, the level of confinement of the explosive charges can be lowered as the orientation of the destress blast becomes more perpendicular to the direction of the targeted stress component. Again, as the azimuth of

the destress blast becomes more parallel to the stress component targeted, the amount of useful explosive energy needs to be exploited to its fullest in an attempt to maximise the damage zone and compensate for the less favourable orientation – one way of achieving this is by increasing the confinement of the charges.

- *Effect on P_9, the result of the destress blast (interaction $I_{5,9}$).* As the orientation of the destress blast becomes more perpendicular to the direction of the targeted stress component, the zone effectively destressed will be enlarged and the destressing effect will be increased.

7.4.1.6.Effects of P_6 – the width of the destress blast, on all the other parameters

- *Effect on P_1, the stiffness of the rock (interaction $I_{6,1}$).* As the width of the destress blast increases, the potential destressing effect also increases, which lowers to some extent the requirement for the rock to be stiff.
- *Effect on P_2, the brittleness of the rock (interaction $I_{6,2}$).* Similarly, as the width of the destress blast increases and the potential destressing effect is enhanced, the requirement for the rock to be brittle is reduced to some extent.
- *Effect on P_3, the degree of fracturing of the rock mass (interaction $I_{6,3}$).* As the width of the destress blast increases, the rock mass can conceivably be more fractured (and, hence, more difficult to blast) for a similar destressing effect to be achieved. A counter-argument can however be formulated, whereby as the destress blast becomes wider and, hence, more effective, the requirement for the rock mass to be nearing its failure envelope is somewhat reduced. This results in a lowered need for the rock mass to have undergone the process of pre-existing crack extension and stress-induced fracture creation, which, in turn, results in a lower degree of fracturing. The former argument is taken to be more pronounced, and, as a result, a "U-U" rating was retained for interaction $I_{6,3}$.
- *Effect on P_4, the proximity to failure of the rock (interaction $I_{6,4}$).* As just mentioned, as the width of the destress blast increases – which makes the blast more effective – the requirement for the rock mass to be nearing its failure envelope is reduced.

- *Effect on P_5, the orientation of the destress blast (interaction $I_{6,5}$).* As the width of the destress blast increases, the same effective results can be achieved by orienting the destress blast at a shallower angle to the targeted stress component. Figure 47 illustrates this interaction.

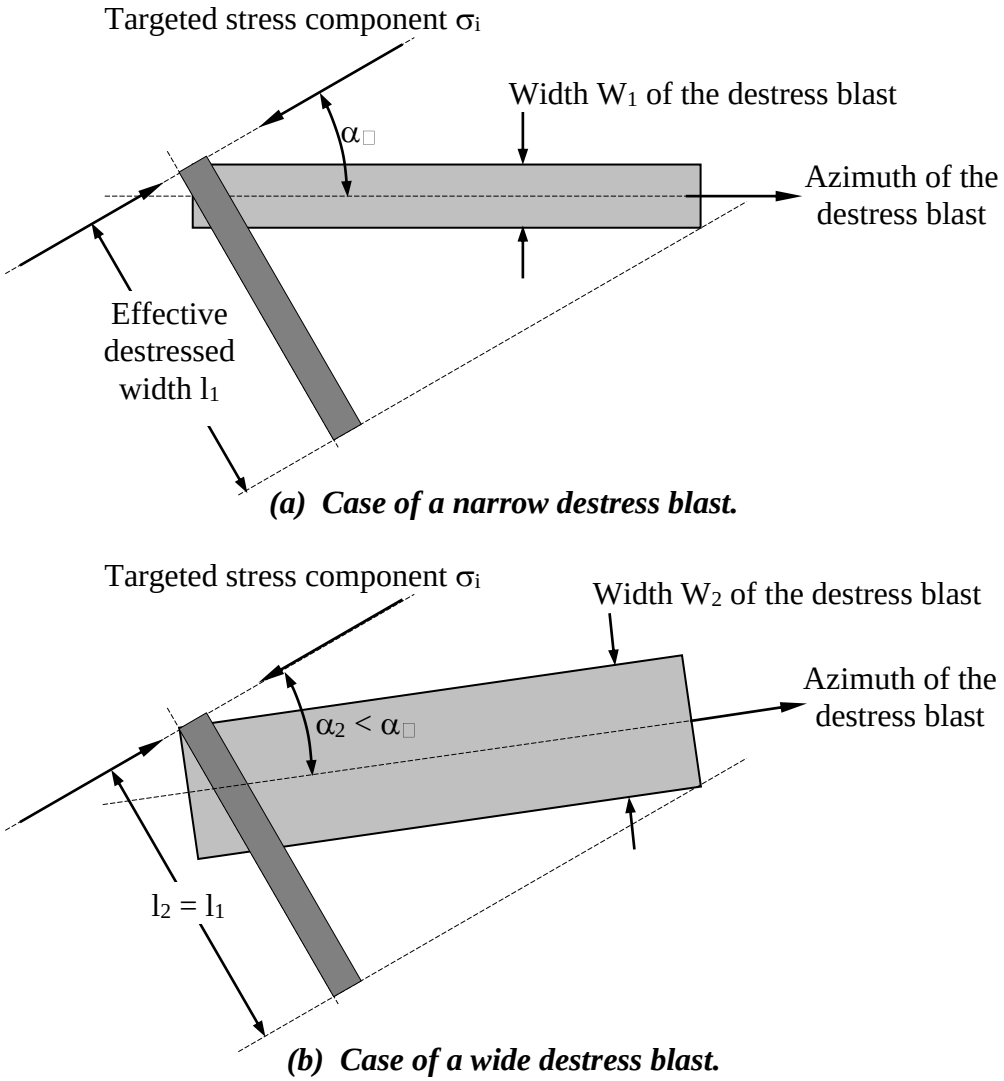

Figure 47. Schematic views showing how a wider destress blast (b) results in a smaller angle of incidence being required to achieve the same effective destressed width.

- *Effect on P_7, the unit explosive energy in the destress blast (interaction $I_{6,7}$).* Within the context of this work the width of the destress blast is increased by adding rows of blastholes, rather than by expanding their pattern. Adding rows of blastholes while keeping all other loading parameters the same results in a significant increase of the *total*

explosive energy in the destress blast, but only in a small increase of the *unit* explosive energy.

- *Effect on P_8, the confinement of the explosive charges in the destress blast (interaction $I_{6,8}$).* As the width of the destress blast increases and the destressing potential is intensified, similar results can be obtained while somewhat reducing the level of confinement of the explosive charges.

- *Effect on P_9, the result of the destress blast (interaction $I_{6,9}$).* As the width of the destress blast increases, the disturbance is applied over a wider zone, which, in turn, increases the destressing effect.

7.4.1.7.Effects of P_7 – the unit explosive energy in the destress blast, on all the other parameters

- *Effect on P_1, the stiffness of the rock (interaction $I_{7,1}$).* As the amount of unit explosive energy in the destress blast increases, the degree of fracturing – from both previously existing discontinuities that are extended and new ones that are generated – increases as well, which results in a reduction of the stiffness of the rock mass. However, and as mentioned before, it should be noted that if the *total* amount of explosive energy is increased solely by adding rows of blastholes, the *unit* energy of the blast (in calories of explosive energy per unit mass of targeted rock) increases only slightly.

- *Effect on P_2, the brittleness of the rock (interaction $I_{7,2}$).* As more unit explosive energy is used in a destress blast, the need for the rock mass to exhibit a brittle behaviour is somewhat alleviated for a given level of destressing to be achieved.

- *Effect on P_3, the degree of fracturing of the rock mass (interaction $I_{7,3}$).* As mentioned, as the amount of unit explosive energy in the destress blast increases, the degree of fracturing of the rock mass will increase as well. The comment made before on maintaining the *unit* explosive energy of the blast near constant does apply here again.

- *Effect on P_4, the proximity to failure of the rock (interaction $I_{7,4}$).* As discussed, the amount of unit explosive energy in the destress blast increases the degree of fracturing of the rock mass. This, similarly to what was described for interaction $I_{3,4}$ and

illustrated in Figure 44, weakens the rock mass, which, for a given stress regime, brings it closer to its failure envelope.

- *Effect on P_5, the orientation of the destress blast (interaction $I_{7,5}$).* As the amount of unit explosive energy in the destress blast increases, the necessity to orient it perpendicularly to the stress component to reduce is somewhat lowered.
- *Effect on P_6, the width of the destress blast (interaction $I_{7,6}$).* Similarly, as the amount of unit explosive energy in the destress blast increases, the requirement to target a wider zone is somewhat reduced.
- *Effect on P_8, the confinement of the explosive charges in the destress blast (interaction $I_{7,8}$).* As for the previous two interactions, as the amount of unit explosive energy in the destress blast increases, the requirement to highly confine the charges is somewhat reduced.
- *Effect on P_9, the result of the destress blast (interaction $I_{7,9}$).* As the amount of unit explosive energy in the destress blast increases, the destressing effect increases as well.

7.4.1.8.Effects of P_8 – the confinement of the explosive charges, on all the other parameters

- *Effect on P_1, the stiffness of the rock (interaction $I_{8,1}$).* As the level of confinement of the explosive charges in the destress blast increases, the extent of the damage they will cause can be expected to increase as well, which will further soften the rock mass.
- *Effect on P_2, the brittleness of the rock (interaction $I_{8,2}$).* As the explosive charges become more confined and more of their gas energy is effectively used in the destress blast, the need for the rock mass to exhibit a brittle behaviour is lowered to a certain extent for a given level of destressing to be achieved.
- *Effect on P_3, the degree of fracturing of the rock mass (interaction $I_{8,3}$).* Based upon the same reasoning, as the level of confinement of the explosive charges in the destress blast increases and they cause more damage, the degree of fracturing of the rock mass will increase too.

- *Effect on P_4, the proximity to failure of the rock (interaction $I_{8,4}$).* As just discussed, as the level of confinement of the explosive charges in the destress blast increases, the degree of fracturing of the rock mass increases too, which weakens it and, for a given stress regime, brings it closer to its failure envelope.

- *Effect on P_5, the orientation of the destress blast (interaction $I_{8,5}$).* As the level of confinement of the explosive charges increases, the destress blast becomes more effective, which lowers the requirement to orient it at 90° to the targeted stress component.

- *Effect on P_6, the width of the destress blast (interaction $I_{8,6}$).* Similarly, as the level of confinement of the explosive charges increases and the destress blast becomes more effective, its width can be somewhat reduced for similar destressing results to be attained.

- *Effect on P_7, the unit explosive energy in the destress blast (interaction $I_{8,7}$).* Following the same logic, when the level of confinement of the explosive charges increases and the destress blast becomes more effective, the unit explosive energy in it can be reduced to some extent for similar destressing results to be achieved.

- *Effect on P_9, the results of the destress blast (interaction $I_{8,9}$).* As the level of confinement of the explosive charges increases and the destress blast becomes more effective, the level of destressing achieved can be expected to increase.

7.4.1.9.Effects of P_9 – the results of the destress blast, on all the other parameters

- *Effect on P_1, the stiffness of the rock (interaction $I_{9,1}$).* As the level of destressing achieved by the destress blast increases, the stiffness of the rock mass decreases.

- *Effect on P_2, the brittleness of the rock (interaction $I_{9,2}$).* Similarly, as the level of destressing achieved by the destress blast increases and more damage has been done to it, the brittleness of the destressed rock mass decreases.

- *Effect on P_3, the degree of fracturing of the rock mass (interaction $I_{9,3}$).* As the level of destressing achieved by the destress blast increases, the degree of fracturing of the rock mass increases too.
- *Effect on P_4, the proximity to failure of the rock (interaction $I_{9,4}$).* As the level of success achieved by the destress blast increases and the degree of fracturing of the rock mass intensifies, the proximity to failure increases as well. (Ideally, the failure envelope should be reached.)
- *Effect on P_5, the orientation of the destress blast (interaction $I_{9,5}$).* As the level of success achieved by the destress blast increases and the rock mass becomes more fractured and damaged, any future destress blast in the same region will become more difficult, which will increase the requirement to orient it perpendicularly to the targeted stress component.
- *Effect on P_6, the width of the destress blast (interaction $I_{9,6}$).* Similarly, as the level of success achieved by the destress blast increases, any future destress blast in the same region will become more difficult and its width will hence need to be increased.
- *Effect on P_7, the unit explosive energy in the destress blast (interaction $I_{9,7}$).* Again, as the level of success achieved by the destress blast increases and the rock mass becomes more fractured and damaged, any future destress blast in the same region will become more difficult, which will increase its unit explosive energy requirements.
- *Effect on P_8, the confinement of the explosive charges in the destress blast (interaction $I_{9,8}$).* Once more, as the level of success achieved by the destress blast increases, any future destress blast in the same area will become more difficult and the confinement of its explosive charges will need to be increased.

7.4.2. Properties that describe the RES interaction matrix parameters

Each of these nine parameters now needs to be quantitatively represented by tangible and well defined properties that can be either obtained from laboratory specimens, measured reliably in the field, or looked up in explosives manufacturers product specification sheets

or technical literature. It is important at this stage to clearly establish the difference between a *parameter*, which is an entity used in the interaction matrix to account for a particular behaviour of the system, and a *property*, which is a quantity that can be obtained unequivocally and is used to quantify one or more parameters.

7.4.2.1.Intact rock material scale vs. rock mass scale

Those parameters that are related to the rock (parameters P_1 [the stiffness of the rock], P_2 [its brittleness] and P_4 [its proximity to static stress-induced failure]) can conceivably be considered either at the intact rock material scale, or at that of the rock mass. The first approach is intrinsically simpler because these parameters can then be represented by properties that are easily, directly and unequivocally measured in the laboratory – they however need to be adjusted and corrected for the fact that the rock mass properties are what is ultimately pertinent in the case of large-scale confined panel destress blasts. The second approach is more complex because it requires these parameters to be represented by properties either extrapolated to, or measured directly at, the rock mass scale – its main advantage however resides in the scientific relevance of this larger scale to the problem at hand. Parameter P_3 (the degree of fracturing of the rock mass), although also related to the rock, is not subjected to this scale distinction – it will however need to be weighed differently in the interaction matrix at each scale because, at the rock mass scale, its effects are already considered to a certain extent in the other three rock-related parameters.

Because it is not known beforehand whether the simpler approach at the intact rock material scale is adequate, or whether the more complex rock mass scale approach is required, both will be retained and developed in parallel in the remainder of this work, and both will be tested against detailed case histories in chapters IX and X. As a result, *two* interaction matrices will be formally developed, which will be coded differently.

7.4.2.2.Parameter P_1 – stiffness of the rock

Parameter P_1, which characterises the stiffness of the rock in which the destress blast is to be implemented, can be represented simply by the Young's modulus (or elastic modulus) of

the rock. The issue of intact rock material scale *vs*. rock mass scale just discussed does apply to this rock-related parameter.

Deriving the Young's modulus at the intact rock material scale is simple – Figure 8 showed graphically how $E_{Laboratory}$ can easily be obtained from a simple unconfined compressive test (ASTM, 2002) performed on an intact sample of the material. The other approach, whereby the Young's modulus at the rock mass scale is retained to represent parameter P_1, adds some complexity to the approach. A number of well established empirical procedures can be used to extrapolate the easily obtainable $E_{Laboratory}$ to the rock mass scale. For example, the following relation, suggested by Nicholson & Bieniawski (1990), can be used:

$$E_{Rock\ mass} = E_{Laboratory} \times (0.000028\ RMR^{2} + 0.009\ e^{[\ RMR\ /\ 22.82\ ]}) \quad \text{….. Eq. (20)}$$

With RMR the Rock Mass Rating developed in South Africa by Bieniawski (1976, 1989) – a description of the RMR methodology is provided in Appendix E. Other empirical relationships have been proposed, amongst which the following ones summarised by Barton (2002):

$$E_{Rock\ mass} = (2 \times RMR) - 100, \text{ for RMR values greater than 50} \quad \text{….. Eq. (21)}$$

$$E_{Rock\ mass} = 10^{([\ RMR - 10\ ]\ /\ 40\ )}, \text{ for RMR values lower than 50} \quad \text{….. Eq. (22)}$$

$$E_{Rock\ mass} = 10 \times (Q \times [\ \sigma_c\ /\ 100\ ])^{1/3} \quad \text{….. Eq. (23)}$$

Note: Equation (21) is from Bieniawski (1989); Equation (22) is from Serafim & Pereira (1983); and, Equation (23) is from Barton (1988).

With: RMR as previously defined; Q the rock Tunnelling Quality Index proposed in 1974 at the Norwegian Geomechanics Institute (Barton *et al*., 1974 – a description of the Q methodology is provided in Appendix G); and, σ_C the compressive strength of the intact rock material. These scaling relationships are however all somewhat limited by the lack of sensitivity associated with the RMR and Q methodologies. The fact that the level of confidence in such scaling approaches increases for good quality rocks (in which case it is easier to define a reliable value of RMR and Q) is beneficial for the topic at hand, because destress blasting is usually conducted in good quality rock masses.

Within the frame of this work Equation (20) was retained to derive the elastic modulus of the rock mass from that of the intact rock material. The reasons for this choice are that: 1) only RMR and $E_{Laboratory}$ are required; 2) it covers a wider range of RMR values than equations (21) and (22); and, 3) RMR is easier to obtain, and less dependent upon the skills of the person doing the mapping, than Q is.

Alternatively, and preferably if at all possible, the stiffness of the rock mass can be measured directly with a dilatometer, or from a large-scale in situ jacking test.

7.4.2.3.Parameter P_2 – brittleness of the rock

Parameter P_2 is meant to account for the brittleness of the rock in which the destress blast is to be implemented – the brittleness of the rock is thus an obvious property to describe it. Even though there are disagreements between some members of the rock engineering community on whether brittleness is a material property or, rather, merely describes a type of fracture (Denkhaus, 2003 [a, b]; Altindag, 2003 [a]), it will be assumed within the frame of this thesis that it is a material property. Bates & Jackson (1987) of the American Geological Institute define brittleness as a property of materials that rupture or fracture with little or no plastic flow. Brittleness can also be seen as a measure of the relative susceptibility of a material to the two competing ductile and fragile mechanical responses.

Contrary to the Young's modulus, brittleness is an arduous property to measure – at the time this thesis was written there was in fact no standardised and universally-accepted method for defining and measuring it at any scale.

At the scale of the intact material the Brittleness Index Modified (BIM) approach, described by Simon *et al*. (1998) and described in Section 2 of Appendix A, was retained. The reason for this choice is the simplicity of the method and its relative consistency – in particular, it does not require to test brittle samples in the post-peak domain, which is often associated with great practical difficulties. As when $E_{Laboratory}$ is retained to represent the stiffness of the rock, parameter P_3 (the degree of fracturing of the rock mass) will need to have a heavy

influence on parameter P_2 in the intact rock material properties-based RES interaction matrix, in order to appropriately downgrade it to the rock mass scale.

At the rock mass scale, the ratio B_1 of the uniaxial strength of the rock mass to its tensile strength proposed by Altindag (2003 [b]) was retained for this work, as follows:

$$B_1 = \sigma_{c\ Rock\ Mass} / \sigma_{T\ Rock\ Mass} \quad \text{..... Eq. (24)}$$

With: B_1 the brittleness of the material (dimensionless); $\sigma_{c\ Rock\ Mass}$ the uniaxial compressive strength of the rock mass; and, $\sigma_{T\ Rock\ Mass}$ the tensile strength of the rock mass. This index was retained because it is widely used in the literature (Walsh & Brace [1964], Vardoulakis [1984], Inyang [1991], Kahraman [2002], amongst others), and relatively simple to derive at the rock mass scale. For this purpose the following equations (Hoek & Brown, 1988) can be used in the case of a moderately jointed and undisturbed (which is generally the case when a large-scale choked pillar destress blast is being contemplated) rock mass:

$$\sigma_{c\ Rock\ Mass} = \sigma_3 + [(m_{\ Rock\ Mass} \times \sigma_c \times \sigma_3) + (s_{\ Rock\ Mass} \times \sigma_c^{\ 2})]^{0.5} \quad \text{..... Eq. (25)}$$

$$\sigma_{T\ Rock\ Mass} = [(m_{\ Rock\ Mass}\ \sigma_c) - (\{m_{\ Rock\ Mass}^{\ 2}\ \sigma_c^2\} - \{4\ s_{\ Rock\ Mass}\ \sigma_c^2\})^{0.5}] / 2 \quad \text{..... Eq. (26)}$$

With: $\sigma_{c\ Rock\ Mass}$ and $\sigma_{T\ Rock\ Mass}$ as defined in Equation (24); $m_{\ Rock\ Mass}$ the value of the Hoek-Brown constant m at the rock mass scale; $s_{\ Rock\ Mass}$ the value of the Hoek-Brown constant s at the rock mass scale; σ_c the uniaxial compressive strength of the intact rock material; and, σ_3 the minor principal stress component (set at zero in Equation [25]). Please note that Equation (26) is simply the quadratic formulae for $\sigma_1 = 0$ of the Hoek-Brown failure envelope. Parameters $m_{\ Rock\ Mass}$ and $s_{\ Rock\ Mass}$, in turn, are calculated as follows (Hoek *et al.*, 1995) for rock masses of good to reasonable quality (which, again, is generally the case when large-scale confined pillar destress blasts are attempted):

$$m_{\ Rock\ Mass} = m_{\ Laboratory} \times e^{([\ GSI - 100] / 28)} \quad \text{..... Eq. (27)}$$

$$s_{\ Rock\ Mass} = s_{\ Laboratory} \times e^{([\ GSI - 100] / 9)} = e^{([\ GSI - 100] / 9)} \quad \text{..... Eq. (28)}$$

$$GSI = RMR_{89} - 5 \quad \text{..... Eq. (29)}$$

With: $m_{Rock\ Mass}$ and $s_{Rock\ Mass}$ as defined previously; $m_{Laboratory}$ and $s_{Laboratory}$ the values of the Hoek-Brown constants m and s at the laboratory rock sample scale, respectively (please note that $s_{Laboratory}$ is equal to one); GSI the Geological Strength Index (more details on this rating are provided in Appendix F); and, RMR_{89} the 1989 version of the Bieniawski RMR classification system (Bieniawski, 1989), where the Groundwater rating is set to 15 and the Adjustment for Joint Orientation is set to zero. (The RMR classification system, as mentioned previously, is described in detail in Appendix E.)

As was the case for P_1, both approaches have merit: using the BIM methodology to represent parameter P_2 at the scale of the intact rock material has the advantage of being simple, whereas using index B_1 at the scale of the rock mass has the advantage of already considering this more relevant scale. In each case, again, the influence of parameter P_3 (the degree of fracturing of the rock mass) will have to be adjusted differently: this influence will need to be greater at the scale of the intact rock material than at that of the rock mass (where brittleness has already been downgraded).

7.4.2.4.Parameter P_3 – degree of fracturing of the rock mass

Parameter P_3 is intended to account for the degree of fracturing of the rock mass in which the destress blast is to be detonated. There are numerous ways that can be retained to represent this parameter based upon: 1) empirical characterisation methodologies such as the Rock Mass Rating, Geological Strength Index or Q rating (please refer to appendices E, F and G, respectively, for a description of these approaches); 2) the spacing of the joint sets; or, 3) the block size distribution. The simple ratio RQD/Jn (RQD and Jn are described in detail in appendices D and G, respectively), which effectively represents the structure of the rock mass, could also be used.

Considering that one of the functions of P_3 is to downgrade the rock parameters in the case where these are represented by intact rock properties, it should ideally be represented by a property that readily allows this extrapolation between the intact and the rock mass scales. As a result, the selection of an empirical characterisation methodology would be

advantageous because numerous such scaling laws have been developed for these approaches, as shown earlier in equations (20) through to (23) and (27) through to (29). As can be seen in these equations, both the RMR and Q approaches can be used to downgrade the Young's modulus, whereas the GSI methodology can be used to downgrade the strength of the rock. Although these techniques are not perfect, they have the advantage of being well documented and widely used to extrapolate mechanical properties between the intact and the rock mass scales.

Within the frame of this work the Rock Mass Rating was chosen to represent parameter P_3, mainly because it is easy to obtain, and can be used to scale both the Young's modulus (with equations [20], [21] or [22]) and the strength of the rock (with equations [27] and [28], and the conversion between the GSI and the RMR provided by Equation [29]).

Contrary to what was the case with P_1 and P_2 before, parameter P_3 will be represented by the RMR regardless of the scale at which these were considered – only its interactions with both will vary depending on this scale.

7.4.2.5.Parameter P_4 – proximity to failure of the rock mass

Parameter P_4, the proximity to static stress-induced failure, is probably best represented by the static stress regime that prevails at the time of the blast (in the form of the magnitude of $\sigma_{1\ actual}$ and $\sigma_{3\ actual}$ – please note that the orientation of $\sigma_{1\ actual}$ and $\sigma_{3\ actual}$ will be accounted for later by parameter P_6, the orientation of the destress blast) and the failure envelope of the rock unit in which the destress blast is attempted.

The static magnitude of the major and minor principal stress components $\sigma_{1\ actual}$ and $\sigma_{3\ actual}$ at the time of the blast can be evaluated either analytically for simple geometries (from the stress gradient, the depth and an adequate stress representation approach such as the equation proposed by Kirsch [1898] for circular openings subjected to biaxial stresses, for example), or numerically with an adequate code for more complex geometries and/or high extraction ratios.

As far as the failure envelope is concerned, any criterion that adequately captures the behaviour of the rock mass under stress can conceivably be employed, such as the linear Mohr-Coulomb or the non-linear Hoek-Brown criteria, for example. Within the frame of this work it was decided to use the Hoek-Brown criterion. The main reasons for this choice are that 1) it is commonly used in the mining industry; 2) it is relatively easily obtained from triaxial laboratory tests; and, 3) a methodology – based upon the GSI – has been developed that allows to extrapolate the strength from laboratory samples to the rock mass scale. (It is well recognised that this extrapolation is not perfect, but it has the advantage of being relatively widely used and well documented.)

In order to remain consistent, and depending upon the scale at which the properties that represent parameters P_1 and P_2 are considered, the Hoek-Brown criterion needs to be taken either at the intact material scale or at that of the rock mass. At the intact rock material scale parameters m and s are as directly fitted from triaxial tests (ASTM, 2002) completed under various confining pressures on intact samples of the rock material. (At this scale, and as mentioned before, parameter s is equal to 1.) At the rock mass scale parameters m and s can be modified using equations (27), (28) and (29).

Equations (30) and (31) from Hoek *et al*. (1995) will be used in the remainder of this work to represent the proximity to static failure (parameter P_4) at the intact rock material and the rock mass scales, respectively:

$$PTF_{Intact} = \sigma_{1\ actual} / (\sigma_{3\ actual} + [m_{Laboratory}\ \sigma_c\ \sigma_{3\ actual} + s_{Laboratory}\ \sigma_c^{\ 2}]^{0.5}) \quad \text{..... Eq. (30)}$$

$$PTF_{Rock\ Mass} = \sigma_{1\ actual} / (\sigma_{3\ actual} + [m_{Rock\ Mass}\ \sigma_c\ \sigma_{3\ actual} + s_{Rock\ Mass}\ \sigma_c^{\ 2}]^{0.5}) \text{..... Eq. (31)}$$

With: PTF the proximity to static stress-induced failure (i.e., the proximity to the static failure envelope), expressed in percentage; $\sigma_{1\ actual}$ and $\sigma_{3\ actual}$ the local major and minor principal stress components acting at the time of the destress blast, respectively; σ_c the unconfined compressive strength of the intact rock material; and, $m_{Laboratory}$, $m_{Rock\ Mass}$, $s_{Laboratory}$ and $s_{Rock\ Mass}$ the values of the Hoek-Brown constants m and s, either at the laboratory rock sample or the rock mass scales. (Please note that $m_{Rock\ Mass}$ and $s_{Rock\ Mass}$ are given by equations [27] and [28], respectively.)

7.4.2.6.Parameter P_5 – orientation of the destress blast

Parameter P_5, the orientation of the destress blast with respect to the stress component to reduce, can be derived from the mining-induced stress tensor that prevails locally at the time of the destress blast. Numerical methods could be used to derive this information with a good level of confidence, although field indications on the direction of the principal stresses – such as breakouts along excavations and inside boreholes – become more obvious as the volume of interest becomes subjected to higher stress levels, which is normally the case when destress blasting is being contemplated. Instrumentation, such as stress cells, for example, can also be used for this purpose.

7.4.2.7.Parameter P_6 – width of the destress blast

Parameter P_6, the width of the destress blast, can be easily obtained from the blasting engineer – all that is required is the number of blasthole rings and the distance between them.

7.4.2.8.Parameter P_7 – unit explosive energy

Similarly to parameter P_6, parameter P_7 can be easily obtained from the blasting engineer based upon the burdens and spacings throughout the blast, the diameter and length of the blastholes, the characteristics of the explosive products used, the charge coupling ratios implemented, and the toe and collar lengths retained. Please note that the outside zone of influence of the peripheral blastholes – as per Figure 23 and Figure 24, and the accompanying comments – must be accounted for when calculating the volume of rock targeted by the destress blast for the purpose of establishing the unit explosive energy.

7.4.2.9.Parameter P_8 – confinement of the explosive charges

Parameter P_8, which relates to the confinement of the explosive charges in the destress blast, was chosen to be represented by the ratio of the total unloaded collar and toe length over the blasthole diameter.

7.4.2.10. Parameter P_9 – result of the destress blast

As discussed earlier in Section 3.3, parameter P_9, which characterises the results achieved by the destress blast, can be assessed qualitatively based upon how "easier" mining became after the blast, or how much "quieter" the local seismicity became. These are however difficult to include in a RES interaction matrix. The quantitative monitoring of the microseismic activity in the region of interest can also provide insight into the success achieved by the blast, but it is difficult to summarise this activity into a single number that can be readily inserted into a RES matrix.

In a more qualitative manner, the destressing results achieved by the blast could conceivably be represented by any of the properties previously shown in Figure 20, which all vary with the compressive stress the rock mass is subjected to. But, as pointed out in Section 3.3, resistivity, permeability, sonic velocity and acoustic emission are not well-suited to routine measurements by mine site personnel.

Convergence measurements can also be performed with contractometers (extensometers that can measure both extension and contraction) across the targeted zone, to check for movement between the hanging wall and footwall at blast time. Load cells can also be used, that provide a direct assessment of the stress levels in the region of interest.

Within the frame of this work, load cells will be retained and the average stress drop measured at various points near the blasted zone will be taken to represent parameter P_9. As it will be discussed later in the case histories of chapters IX and X, Geokon vibrating wire load cells have proven both relatively easy to install (due to their wedge anchoring mechanism) and reliable.

7.4.2.11. Summary of the properties retained to represent the parameters of the RES matrix at the intact rock material and the rock mass scales

The nine parameters included in the large-scale confined pillar destress blasting Rock Engineering Systems interaction matrix and their corresponding properties are summarised

in Table 4 and Table 5, for the cases where the rock properties are considered at the intact rock material scale and at the rock mass scale, respectively. As mentioned, parameters P_1 through to P_4 relate to the rock mass (either at the intact material scale [Table 4] or at the rock mass scale [Table 5]) and stress conditions, whereas parameters P_5 through to P_8 relate to blasting issues. These latter ones remain identical regardless of the scale at which the rock-related properties are defined.

Table 4. Properties used to characterise the parameters used in the large-scale choked pillar destress blasting RES interaction matrix. Case where the rock properties are at the intact material scale.

Parameter	Description	Associated measurable properties
P_1	Stiffness of the intact rock material	$E_{Laboratory}$
P_2	Brittleness of the intact rock material	BIM
P_3	Degree of fracturing of the rock mass	RMR
P_4	Proximity to failure of the intact rock material	$\sigma_{1\ actual}$, $\sigma_{3\ actual}$, Hoek-Brown failure criterion (intact material)
P_5	Orientation of the destress blast	$\sigma_{1\ actual}$, azimuth of the destress blast
P_6	Width of the destress blast	Burden, blasthole diameter and number of blasthole rings used
P_7	Unit explosive energy	Explosive density, AWS, blasthole length and diameter, collar length, burden and spacing
P_8	Confinement of the explosive charges	Toe breakthrough, collar and toe lengths, collar and toe stemming
P_9	Result of the destress blast	Stress level reduction, based upon instrumentation and measurements

Table 5. Properties used to characterise the parameters used in the large-scale choked pillar destress blasting RES interaction matrix. Case where the rock properties are at the rock mass scale.

Parameter	Description	Associated measurable properties
P_1	Stiffness of the rock mass	$E_{Laboratory}$, RMR
P_2	Brittleness index of the rock mass	$B_1 = \sigma_{c\ Rock\ Mass} / \sigma_{T\ Rock\ Mass}$
P_3	Degree of fracturing of the rock mass	RMR
P_4	Proximity to failure of the rock mass	$\sigma_{1\ actual}$, $\sigma_{3\ actual}$, Hoek-Brown failure criterion (rock mass)

Table 5 (continued). Properties used to characterise the parameters used in the large-scale choked pillar destress blasting RES interaction matrix. Case where the rock properties are at the rock mass scale.

Parameter	Description	Associated measurable properties
P_5	Orientation of the destress blast	$\sigma_{1\ actual}$, azimuth of the destress blast
P_6	Width of the destress blast	Burden, blasthole diameter and number of blasthole rings used
P_7	Unit explosive energy	Explosive density, AWS, blasthole length and diameter, collar length, burden and spacing
P_8	Confinement of the explosive charges	Toe breakthrough, collar and toe lengths, collar and toe stemming
P_9	Result of the destress blast	Stress level reduction, based upon instrumentation and measurements

Generally accepted means of quantifying the nine parameters chosen for inclusion in the large-scale confined pillar destressing RES interaction matrix have been suggested in this section. It is well recognised at this stage that the formulations proposed to represent the various parameters involved are neither exhaustive nor necessarily the "best" (i.e., the most scientifically robust) ways to quantify each one. The objective is however not so much to argue which are the best possible choices, but rather 1) to show that ways do exist to describe the interaction matrix parameters using readily available properties; and, 2) to select the simplest possible such properties. At any rate, a major advantage of the RES approach is that at any point in the process the method of quantifying the parameters can be improved as more data or information become available.

7.4.3. Coding of the RES interaction matrices at the intact rock material and the rock mass scales

The next step now consists of coding the two interaction matrices (the one that considers the intact rock properties and the one that considers the rock mass properties). As discussed, the weighing of the matrix interactions needs to be different for the two scales.

The degree of fracturing of the rock mass (parameter P_3) must weigh more heavily in the case where the properties of the rock are considered at the scale of the intact rock material than in the case where they are considered at the scale of the rock mass. (In the latter case the macroscopic fabric of the rock mass is already taken into account in parameters P_1, P_2 and P_4.)

The ESQ ("Expert Semi-Quantitative") matrix coding approach proposed by Hudson (1992) and previously discussed in Section 6.1 was chosen for this purpose, whereby a value of 0 is allocated where it is deemed that no interaction exists between two parameters, and values of 1, 2, 3 and 4 are allocated for 'weak', 'medium', 'strong' and 'critical' interactions, respectively. It is difficult to formally discuss and justify each of the 64 values eventually chosen in each matrix, as was done, for example, for the qualitative interactions between each pair of parameters summarised in Figure 43. The coding values in both matrices were initially all arbitrarily set at 2, then incrementally adjusted in an iterative manner by considering two parameters at a time and assessing their degree of inter-dependence based upon previously assigned values, in a global manner. For each matrix, the process was repeated over three hundred times until a level of confidence was attained that all the interactions derived were consistent with each other, both intuitively and globally considering the case histories examined. This was deemed sufficient at this stage considering that the formal validation was going to be done subsequently by systematically testing all the interactions obtained against recent well-document case studies.

Figure 48 shows an example of the iterative methodology for the case of the intact rock material scale early in the process, when many interactions were still set at the initial value of 2. Consider for example interaction $I_{2,3}$, between the brittleness of the intact rock material and the degree of fracturing of the rock mass – this value was initially set at 2 (grey circle in the matrix in Figure 48a). Considering that interaction $I_{1,3}$, between the stiffness of the intact rock material and the degree of fracturing of the rock mass, has been set at 3 in a previous iteration, and also considering that the relation between the brittleness of the intact rock material and the degree of fracturing of the rock mass is likely to be comparable, interaction $I_{2,3}$ is set at 3 as well (grey circle in the matrix in Figure 48b).

Similarly, assuming that interaction $I_{1,4}$, between the stiffness and the proximity to failure of the intact rock material, is 2, then interaction $I_{2,4}$, between the brittleness and the proximity to failure of the intact rock material, also initially set at 2 (grey square in Figure 48b) must be downgraded to at least 1 (grey square in Figure 48c). The rationale is that brittleness is a post-peak property that is only indirectly linked to the pre-peak proximity to failure, via the stiffness, as discussed previously. Continuing the process, and considering that 1) interaction $I_{3,1}$ between the degree of fracturing of the rock mass and the stiffness of the intact rock material has been previously adjusted at 3, and 2) interaction $I_{3,2}$ between the degree of fracturing of the rock mass and the brittleness of the intact rock material must be comparable, this value is adjusted from 2 (grey circle in Figure 48c) to 3 (grey circle in Figure 48d). As mentioned, this process was repeated until all the interactions appeared to be qualitatively consistent with each other. Note in Figure 49 that interactions $I_{3,1}$ and $I_{3,2}$ were eventually set at 4 as the process was repeated and more interactions were assessed.

P1	2	3	2	2	2	2	2	2
2	**P2**	(2)	2	2	2	2	2	2
3	2	**P3**	2	2	2	2	2	2
1	2	2	**P4**	2	2	2	2	2
2	2	2	2	**P5**	2	2	2	2
2	2	2	2	2	**P6**	2	2	2
2	2	2	2	2	2	**P7**	2	2
2	2	2	2	2	2	2	**P8**	2
2	2	2	2	2	2	2	2	**P9**

Figure 48a. Iteration i.

P1	2	3	2	2	2	2	2	2
2	**P2**	(3)	[2]	2	2	2	2	2
3	2	**P3**	2	2	2	2	2	2
1	2	2	**P4**	2	2	2	2	2
2	2	2	2	**P5**	2	2	2	2
2	2	2	2	2	**P6**	2	2	2
2	2	2	2	2	2	**P7**	2	2
2	2	2	2	2	2	2	**P8**	2
2	2	2	2	2	2	2	2	**P9**

Figure 48b. Iteration i+1.

P1	2	3	2	2	2	2	2	2
2	**P2**	3	[1]	2	2	2	2	2
3	(2)	**P3**	2	2	2	2	2	2
1	2	2	**P4**	2	2	2	2	2
2	2	2	2	**P5**	2	2	2	2
2	2	2	2	2	**P6**	2	2	2
2	2	2	2	2	2	**P7**	2	2
2	2	2	2	2	2	2	**P8**	2
2	2	2	2	2	2	2	2	**P9**

Figure 48c. Iteration i+2.

P1	2	3	2	2	2	2	2	2
2	**P2**	3	1	2	2	2	2	2
3	(3)	**P3**	2	2	2	2	2	2
1	2	2	**P4**	2	2	2	2	2
2	2	2	2	**P5**	2	2	2	2
2	2	2	2	2	**P6**	2	2	2
2	2	2	2	2	2	**P7**	2	2
2	2	2	2	2	2	2	**P8**	2
2	2	2	2	2	2	2	2	**P9**

Figure 48d. Iteration i+3.

Figure 48. Iteration example for the coding of the interaction matrix at the intact rock material scale, early in the process.

Figure 49 and Figure 50 show the final results of the coding exercise completed for the cases where the rock properties are considered at the intact rock material scale and at the rock mass scale, respectively.

									Causes
P_1	2	3	2	1	1	2	1	2	14
2	**P_2**	3	1	1	2	2	2	2	15
4	4	**P_3**	2	1	2	2	2	2	19
1	1	2	**P_4**	1	1	3	1	4	14
2	2	2	1	**P_5**	1	1	1	3	13
3	2	4	2	2	**P_6**	1	1	3	18
4	3	4	4	3	3	**P_7**	3	4	28
2	2	3	2	1	2	2	**P_8**	3	17
3	3	4	4	2	1	2	1	**P_9**	20
Effects	21	19	25	18	12	13	15	12	23	158

Figure 49. Coding of the interaction matrix for large-scale choked pillar destress blasts. Case where the rock properties are considered at the intact rock material scale.

									Causes
P_1	2	2	2	1	1	2	1	2	13
2	**P_2**	1	1	1	2	2	2	2	13
1	1	**P_3**	2	1	2	2	2	3	14
1	1	2	**P_4**	1	1	3	1	4	14
2	2	2	1	**P_5**	1	1	1	3	13
3	2	4	2	2	**P_6**	1	1	3	18
4	3	4	4	1	1	**P_7**	3	4	24
2	2	3	2	1	2	2	**P_8**	3	17
3	3	4	4	2	1	2	1	**P_9**	20
Effects	18	16	22	18	10	11	15	12	24	146

Figure 50. Coding of the interaction matrix for large-scale choked pillar destress blasts. Case where the rock properties are considered at the rock mass scale.

This constitutes a somewhat intuitive effort at coding the two interaction matrices retained at this stage of the work, and it is acknowledged that extensive and spirited discussions could be carried out regarding the numbers eventually chosen. It will however be demonstrated in chapters IX and X, through the detailed analysis of well-documented case histories, that these numbers are reasonable.

A cause-effect plot was constructed for each interaction matrix based upon these coding results, which are shown in Figure 51 and Figure 52 for the intact rock material scale and the rock mass scale, respectively.

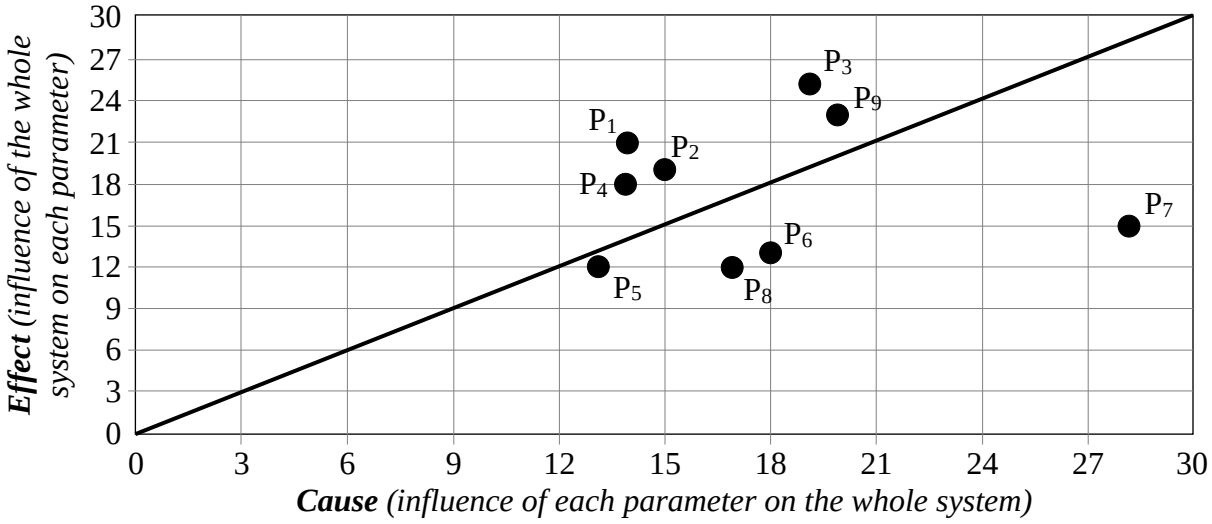

Figure 51. C–E plot for the interaction matrix for large-scale choked panel destress blasting. Case where the rock properties are considered at the intact rock material scale.

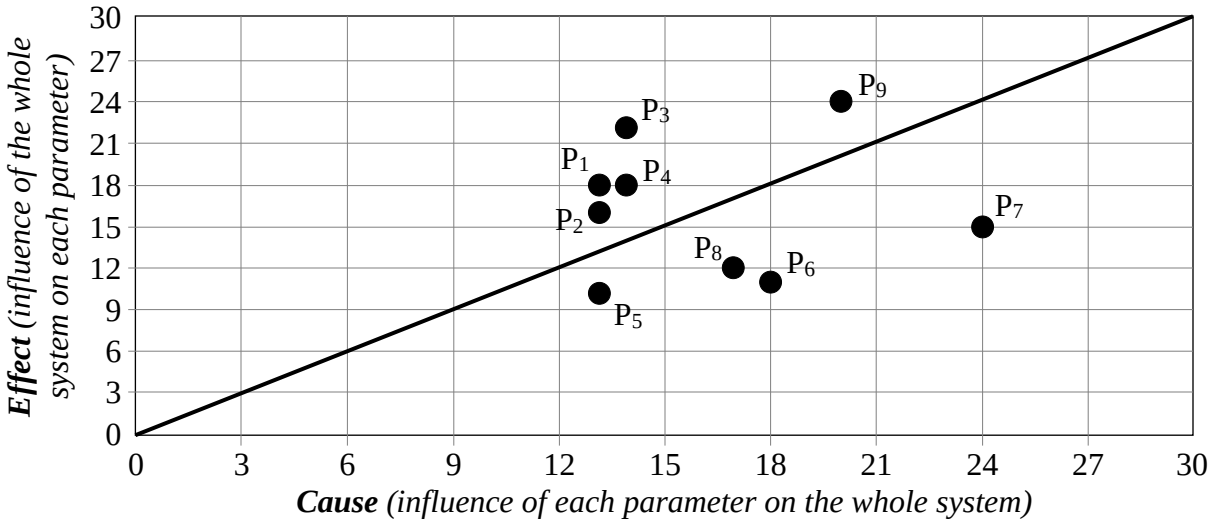

Figure 52. C–E plot for the interaction matrix for large-scale choked panel destress blasting. Case where the rock properties are considered at the rock mass scale.

The diagonal C=E line in a C–E plot essentially represents a state of equilibrium – a parameter that would land on this line has as much influence on the rest of the system as

the rest of the system has on it. In the case where the rock properties are considered at the intact material scale (Figure 51) and based upon the coding values shown in Figure 49, the most intense parameter (the one that weighs the most on the entire system) is P_7, the unit explosive energy. The least intense parameter (the one that weighs the least on the entire system) is P_5, the orientation of the destress blast. The parameter that influences the entire system the most is again P_7, the unit explosive energy, whereas the one that is influenced the most by the rest of the system is P_1, the stiffness of the rock.

In the case where the rock properties are considered at the rock mass scale (Figure 52) and based upon the coding values shown in Figure 50, the most intense parameter is again P_7, the unit explosive energy, but not by as much of a margin as in the previous case. The least intense parameter is again P_5, the orientation of the destress blast, but also by a margin smaller than in the previous case. The parameter that influences the entire system the most is once more P_7, the unit explosive energy, closely followed by P_6, the width of the destress blast. The parameter that is influenced the most by the rest of the system is in this case P_3, the degree of fracturing of the rock mass.

The influence and dominance of the various parameters are clearly the direct result of the coding values chosen in the interaction matrices. Although largely intuitive, the results at this stage do make some instinctive sense. At both scales, the most intense parameter and the one that influences the entire system the most is P_7, the unit explosive energy. Considering that destress blasting is about using explosives to damage the rock mass, this result is hardly arguable and well within the logic set forth.

At the scale of the intact rock material the parameter that is influenced the most by the rest of the system is P_1, the stiffness of the rock, followed by P_3 and P_2, the degree of fracturing and the brittleness of the rock, respectively. At the scale of the rock mass this parameter is P_3, the degree of fracturing of the rock mass, with this influence being quite dominant, as the other parameters lie significantly closer to the C=E line. Logically, if one accepts that the unit explosive energy is the most intense parameter, then the parameter most influenced by the rest of the system should be the degree of fracturing of the rock mass, which is what

the explosive energy directly affects. It is however not irrational for the stiffness to be the parameter most influenced by the rest of the system at the intact material scale, because 1) at this scale the degree of fracturing of the rock mass plays less of a role and 2) it is the stiffness of the material that controls the amount of stress that can be attained in a small sample under load.

As a footnote, it should be pointed out that the system at hand is quite "tight", with no parameters, except perhaps for the unit explosive energy, being truly dominant. Instead, all parameters play a significant role in the confined destress blasting process, which is indicative that the choice of parameters was reasonable. It also suggests that it would have been very difficult to rank their relative contributions to the process without the help of a systematic and highly structured methodology such as the RES approach.

Overall, the interactions derived with the RES approach are in accordance with the logic that supports the large-scale confined pillar destress blast design methodology that has been proposed by Andrieux & Brummer (2002), and described earlier.

CONCLUSION DU CHAPITRE. Cet important chapitre a appliqué la méthodologie des Systèmes d'ingénierie du roc aux sautages confinés à grande échelle de relâchement des contraintes dans des piliers de mine. Les paramètres qui jouent un rôle dans le processus ont d'abord été identifiés, à partir desquels la matrice d'interaction a été construite. Des propriétés largement disponibles ou faciles à obtenir ont également été choisies dans ce chapitre, aussi bien à l'échelle du matériel intact qu'à celle du massif rocheux. Le codage de la matrice, aux deux échelles considérées, a ensuite été complété d'une manière incrémentale et itérative jusqu'à ce que toutes les combinaisons d'interactions soient consistantes les unes envers les autres.

Bien que critique pour déterminer les paramètres d'importance dans le processus des tirs confinés à grande échelle de relaxation des contraintes dans des piliers de mine, la matrice d'interaction comme telle a une valeur pratique limitée pour le technicien confronté au design d'un tel tir. Le prochain chapitre va adresser cette question et présenter le nouveau concept de l' "Index de relâchement" ("Destressability Index" en anglais), qui est un nombre unique qui quantifie les chances de réussite d'un tir confiné à grande échelle de relaxation des contraintes dans un pilier de mine.

CHAPTER CONCLUSION. This important chapter has applied the methodology of the Rock Engineering Systems to large-scale choked pillar destress blasting. The parameters that play a role in the process were first identified, from which the interaction matrix was constructed. Readily available or obtainable properties to represent these parameters were also chosen in this chapter, at both the intact rock material and the rock mass scales. The coding of the interaction matrices, also at both the intact rock material and the rock mass scales, was then completed in an incremental and iterative manner until all the interaction combinations were consistent with each other.

Although critical in order to determine the parameters of importance in the large-scale choked panel destress blasting process, the interaction matrix as such is of limited practical value to the field practitioner faced with designing such a blast. The next chapter will address this issue and introduce the new concept of the "Destressability Index", which is a single number that quantifies the likelihood of success of a given large-scale choked pillar destress blast.

CHAPTER VIII

8. DESTRESSABILITY INDEX FOR LARGE-SCALE CONFINED DESTRESS BLASTS IN UNDERGROUND MINE PILLARS

SOMMAIRE DU CHAPITRE. Tel que discuté dans le chapitre précédent, l'influence sur les résultats d'un tir confiné à grande échelle de relâchement des contraintes dans un pilier de mine qu'a chacun des paramètres identifiés comme jouant un rôle dans le processus peut être rationnellement établie avec l'approche des Systèmes d'ingénierie du roc. Bien qu'essentielles, cette identification et pondération des paramètres impliqués ont toutefois une valeur pratique limitée pour le technicien confronté au design d'un tel tir.

Cette question est adressée dans ce chapitre par le développement de l' "Index de relâchement" ("Destressability Index"), une valeur calculée unique qui quantifie les chances de succès d'un design de tir donné, dans un massif rocheux donné soumis à un régime de contraintes donné. L'Index de relâchement, qui peut varier de zéro (chances de succès extrêmement faibles) à un (très hautes chances de succès), est largement basé sur les interactions identifiées et quantifiées avec la méthode des Systèmes d'ingénierie du roc décrite dans le chapitre précédent. Des plages de valeurs pour chacune des propriétés sélectionnées pour représenter les paramètres de la matrice d'interaction ont d'abord été établies, ainsi que leur cote de "destressabilité". Celles-ci, combinées avec la cause de chacun des paramètres (telle que déterminée dans le chapitre précédent), ont permis de quantifier leur aptitude à favoriser une relaxation des contraintes, de les regrouper et de calculer la valeur de l'Index de relâchement associée à une situation donnée.

La méthodologie a été développée (encore une fois aux échelles du matériel intact et du massif rocheux) à partir de considérations fondamentales de mécanique des roches et de

forage-sautage, d'études de cas documentées, et, dans une certaine mesure, de l'expérience et de l'intuition de l'auteur. De gros chiffriers ont été construits dans le cadre de ces travaux, qui permettent de recalculer rapidement et automatiquement l'Index de relâchement pour n'importe quelle combinaison de valeurs de codage de la matrice d'interaction, diverses plages de valeurs des propriétés et des cotes de "destressabilité" correspondantes, ainsi que diverses combinaisons de valeurs pour les propriétés d'input.

En plus de décrire en détail la méthodologie de l'Index de relâchement, ce chapitre présente un exemple d'application à chacune des échelles considérées.

CHAPTER SUMMARY. As shown in the previous chapter, the influence on the outcome of a large-scale confined pillar destress blast of each of the various parameters identified as playing a role in the process can be established rationally with the Rock Engineering Systems approach. Although essential, this identification and weighing of the contributing parameters is nevertheless of limited practical value to the field practitioner faced with designing such a blast.

This issue is addressed in this chapter by the development of the "Destressability Index", a single calculated number that quantifies the likelihood of success of a given large-scale choked pillar destress blast design, in a given rock mass under a given state of stress. The Destressability Index, which can vary between zero (extremely low chance of success) and one (very high chance of success), is largely based upon the interactions identified and quantified with the RES approach in the previous chapter. Ranges of values for each of the properties selected to represent the parameters of the interaction matrix were first established, along with their "destressability" rating. These, combined with the cause of each parameter (as derived in the previous chapter), allow to quantify the conduciveness to destress blasting of each of these parameters, merge them, and calculate a Destressability Index value.

The methodology was developed (again at both the intact rock material scale and at that of the rock mass) from fundamental rock mechanics and drilling & blasting engineering considerations, documented case histories, and, to a certain extent, the experience and intuition of the author. To aid in this work, large spreadsheets were constructed that rapidly and automatically recalculate the Destressability Index for any combination of interaction matrix coding values, any modification in the property ranges and corresponding ratings, as well as various combinations of property input values.

Besides describing the Destressability Index methodology in detail, this chapter provides a generic example at each scale.

8.1. General description of the Destressability Index methodology

The general process behind the development of the Destressability Index methodology can be summarised as follows. First, three ranges of values were established for the property chosen to represent each parameter, within which the degree of conduciveness to destress blasting is either poor, average or good. Only the first eight parameters of the RES interaction matrix were considered, with the ninth parameter (the one describing the results of the destress blast) being dropped. Only three ranges of values were considered at this point to keep the methodology simple while its foundations are being established. For each parameter these three ranges were established in an iterative manner based upon relevant case studies from Chapter IV, fundamental rock mechanics and blasting engineering considerations, as well as the personal insight and experience of the author. The choices eventually made were later validated through the back-analysis of detailed case studies – this aspect will be discussed in detail in chapters IX and X.

Secondly, a "destressability" rating of zero, 1 or 2 was assigned to each range ('not conducive', 'somewhat conducive' and 'conducive'), respectively. With this approach, a range within which a property is poorly conducive to successful confined destress blasting was assigned a rating of '0'. This rating was increased to '1' for the range within which this property is somewhat conducive to successful choked destress blasting, and to '2' for the range within which it is conducive to it.

Thirdly, for each of the eight retained RES interaction matrix parameters a score was associated with each range, by multiplying the rating (0, 1 or 2) by the cause of this parameter (its influence on the rest of the system), as identified in the previous chapter with the RES methodology – a higher score hence means that the parameter plays a more important role in the process. This score is essentially a representation of the individual importance each of these eight parameters has on the destress blasting process. This is the stage where the relative weighing of each parameter on the entire choked destress blasting process was established, using the systematic RES method.

Fourthly, the maximum possible score of each parameter (its cause multiplied by 2, for the situation where it would be very conducive to destress blasting) was added to produce a maximum possible total score, i.e., the score that would be attained in a "perfect" case whereby each parameter would be very conducive to an efficient destress blasting process and yield a rating of 2. This maximum possible score was used at the end of the process to normalise the overall score of a given situation (i.e., a given combination of rock mass properties, stress state and destress blast design) and produce a single Destressability Index value.

Once the property ranges are established, the Destressability Index is obtained as follows. For a given situation the value of the property selected to describe a RES interaction matrix parameter is obtained or derived (from laboratory tests, mapping, field measurements, numerical modelling, geometrical parameters, blasting parameters, explosives properties, etc.) and compared to the threshold values established. Depending upon the value obtained, a rating of 0, 1 or 2 is assigned to each parameter. This rating is then multiplied by the cause of this parameter to obtain a score, which provides a quantified measure of how favourable it is to a successful confined destress blast. All eight scores (from the eight parameters retained) are then added to produce a total score for the situation being examined, which is normalised by dividing it by the maximum possible total score – this produces the Destressability Index, a number between zero and one. Four categories of Destressability Index values have been established at this stage, based upon the normalised total score obtained: 'Low' (overall normalised score of between 0.00 and 0.40), 'Medium' (overall normalised score of between 0.40 and 0.70), 'Good' (overall normalised score of between 0.70 and 0.85) and 'Excellent' (overall normalised score of between 0.85 and 1.00).

This methodology is not a direct design procedure, but rather an assessment of the likelihood of success of a proposed design in a given situation. Although one cannot modify the intrinsic rock parameters, one can choose to a certain extent the stress state that will prevail at the time of the destress blast (by choosing the step in the mining sequence at which the destress blast will be implemented), and one can alter the blasting parameters.

Once a design has been modified, the Destressability Index can be re-assessed – this allows the design to be eventually optimised, in an iterative manner.

As was done in the previous chapter for the coding of the large-scale confined pillar destress blasting Rock Engineering Systems interaction matrix, the rock-related parameters were considered at both the scale of the intact rock material and at that of the rock mass. Both approaches were again considered separately during the elaboration of the methodology – both will be assessed in the next two chapters through the back-analysis of well-documented recent case histories.

A key aspect in the development of the Destressability Index methodology is the elaboration of the ranges of the various properties for the establishment of the "destressability" score. Equally important is the adjustment of the ranges of normalised scores associated with the various Destressability Index categories ('Poor', 'Average', 'Good' and 'Excellent'). These issues, summarised in the following sections, were tackled through the extensive use of Microsoft Excel spreadsheets (one at the scale of the intact rock material and one at that of the rock mass), which regroup the RES interaction matrix coding values, as well as the entire Destressability Index methodology. These spreadsheets allowed to quickly and automatically recompile the entire Destressability Index system for 1) any change in the RES interaction matrix coding values; 2) any modification in the property ranges and their corresponding destressability ratings; and, 3) various combinations of example values. Appendix H describes these spreadsheets in detail, at both the intact rock material scale (Figure 147 and Figure 148) and the rock mass scale (Figure 149 and Figure 150).

Overall, the methodology was developed in an incremental manner over many iterations, whereby the various property ranges and their corresponding destressability ratings were varied and tested against documented case histories. It would be unpractical and tedious to describe in detail each of the many combinations tested during this work. Instead, the final results of this exercise will be described at each scale in the following sections, along with an application example – these final results will be validated later in chapters IX and X.

8.2. ASSESSMENT OF THE DESTRESSABILITY INDEX AT THE INTACT ROCK MATERIAL SCALE

The ranges of values eventually retained for the properties that describe the interaction matrix parameters at the intact rock material scale will first be presented in detail. How they are used for the determination of the Destressability Index value will then be illustrated with a generic example.

8.2.1. Ranges of property values for the rating of each parameter and scoring system

Table 6 through to Table 13 show ranges of values for the property that describes each of the first eight parameters in the RES interaction matrix at the intact rock material scale, for the rating of these parameters in terms of how conducive they are to choked destress blasting. Please refer to Table 4 for a detailed list of the properties retained to characterise the parameters at that scale.

In each table a higher rating value corresponds to a situation that is more conducive to successful choked destress blasting. In these tables the cause is taken directly from the RES interaction matrix at the intact rock material scale (shown in Figure 49) and the score is simply the rating multiplied by the cause.

Table 6. Range of rock elastic modulus values for the rating of parameter P_1 (stiffness of the rock), for the interaction matrix at the intact rock material scale.

Range of values		Rating	Cause	Score	Maximum score for P_1
Below	45	0	14	0	
Between	45 and 85	1	14	14	
Over	85	2	14	28	28

Note: values of $E_{Laboratory}$ are expressed in GPa.

Table 7. Range of BIM values for the rating of parameter P_2 (brittleness of the rock), for the interaction matrix at the intact rock material scale.

Range of values		Rating	Cause	Score	Maximum score for P_2
Between	1.00 and 1.20	2	15	30	
Between	1.20 and 1.50	1	15	15	
Over	1.50	0	15	0	30

Note: values of BIM are dimensionless.

Table 8. Range of RMR values for the rating of parameter P_3 (degree of fracturing of the rock mass), for the interaction matrix at the intact rock material scale.

Range of values		Rating	Cause	Score	Maximum score for P_3
Between	0 and 60%	0	19	0	
Between	60 and 80%	1	19	19	
Between	80 and 100%	2	19	38	38

Note: values of RMR are expressed in percentage.

Table 9. Range of proximity to failure values for the rating of parameter P_4 (proximity to failure of the rock), for the interaction matrix at the intact rock material scale.

Range of values		Rating	Cause	Score	Maximum score for P_4
Between	0 and 10%	0	14	0	
Between	10 and 25%	1	14	14	
Between	25 and 100%	2	14	28	28

Notes: proximity to failure is represented by $\sigma_1 / \sigma_3 + [\, m\, \sigma_c\, \sigma_3 + s\, \sigma_c^2 \,]^{0.5}$, and expressed in percentage.

Parameters m and s are expressed at the laboratory scale.

Table 10. Range of angle values for the rating of parameter P_5 (orientation of the destress blast with respect to σ_1), for the interaction matrix at the intact rock material scale.

Range of values		Rating	Cause	Score	Maximum score for P_5
Between	0 and 30°	0	13	0	
Between	30 and 60°	1	13	13	
Between	60 and 90°	2	13	26	26

Note: angles are between the azimuth of the destress blast plane and the direction of σ_1, and are expressed in degrees.

Table 11. Range of number of blasting rings for the rating of parameter P_6 (width of the target zone), for the interaction matrix at the intact rock material scale.

Range of values		Rating	Cause	Score	Maximum score for P_6
Below	2	0	18	0	
Between	2 and 4	1	18	18	
Above	4	2	18	36	36

Note: the width of the target zone is expressed in number of blasting rings.

Table 12. Range of explosive energy per unit mass values for the rating of parameter P_7 (unit explosive energy), for the interaction matrix at the intact rock material scale.

Range of values		Rating	Cause	Score	Maximum score for P_7
Between	0 and 200	0	28	0	
Between	200 and 350	1	28	28	
Between	350 and 500	2	28	56	56

Note: values of explosive energy per unit mass are expressed in calories of explosive energy per kilogram of rock.

Table 13. Range of charge confinement ratios for the rating of parameter P_8 (confinement of the explosive charges), for the interaction matrix at the intact rock material scale.

Range of values		Rating	Cause	Score	Maximum score for P_8
Between	0 and 25	0	17	0	
Between	25 and 45	1	17	17	
Over	45	2	17	34	34

Note: values of charge confinement ratios are expressed as a ratio of the blasthole diameter.

The maximum total score possible (the sum of the maximum score of each parameter in Table 6 through to Table 13) is 276.

For a given situation (i.e., a given destress blast design to be implemented in a given rock mass under a given set of stress conditions), the property assigned to represent each parameter is categorised using the proper table between Table 6 and Table 13. Depending upon its value, each property will fall within one of the three categories (‘not conducive’, ‘somewhat conducive’ or ‘conducive’ to destress blasting) and will be assigned a rating of

either 0, 1 or 2, which will, in turn, yield a certain score. At the end of the process all eight scores are added to produce the total score associated with the situation being examined. This total score is then normalised, by dividing it by 276 (the maximum total score possible). The last step consists in assessing the Destressability Index with Table 14.

Table 14. Assessment of the Destressability Index as a function of the overall normalised parameter score at the intact rock material scale.

Overall normalised score	Destressability Index
From 0.00 to 0.40	Low
From 0.40 to 0.70	Medium
From 0.70 to 0.85	Good
From 0.85 to 1.00	Excellent

Table 15 lists the properties and quantities that are required to establish the score of each parameter for the purpose of deriving a Destressability Index at the intact rock material scale for a given destress blast design. An example value is provided for each entry, which will be used in an example provided to illustrate the approach.

Table 15. List of the basic properties and quantities required for the assessment of the Destressability Index at the intact rock material scale.

Properties	Symbol	Unit	Example value
Density of the rock	ρ_r	*kg/m³*	3,600
Young's modulus of the intact rock material	$E_{Laboratory}$	*GPa*	125
Unconfined compressive strength of the intact rock material	$\sigma_{c\ Laboratory}$	*MPa*	190
Brittleness Index Modified ratio	BIM	–	1.30
Rock Mass Rating of the rock mass	RMR	*%*	80
Hoek-Brown parameter m of the intact rock material	$m_{Laboratory}$	–	10.000
Hoek-Brown parameter s of the intact rock material	$s_{Laboratory}$	–	1.000
Effective σ_1 component at the time of the destress blast	$\sigma_{1\ Actual}$	*MPa*	75
Effective σ_3 component at the time of the destress blast	$\sigma_{3\ Actual}$	*MPa*	25

Table 15 (continued). List of the basic properties and quantities required for the assessment of the Destressability Index at the intact rock material scale.

Properties	Symbol	Unit	Example value
Angle of incidence of the blast with respect to the σ_1 component	θ	*degrees*	75
Length of the pillar to destress	L	*m*	50.00
Height of the pillar to destress	H	*m*	30.00
Number of blasting rings in the destress blast	N	*#*	3
Diameter of the blastholes	D	*mm*	165.1
Distance between blasthole rings	B	*m*	3.70
Distance between blastholes on the same ring	S	*m*	3.70
Unloaded toe length in the blastholes *****	T	*m*	0.00
Unloaded collar length in the blastholes	C	*m*	5.00
Usage of inert stemming material ******	–	*Yes* or *No*	Yes
Density of the explosive product	ρ_e	*g/cm³*	1.25
Absolute weight strength of the explosive	AWS	*cal/g*	866

***** *use zero for non-breakthrough holes.*
****** *add 50% confinement if stemming material is used.*

The various geometrical properties of Table 15 are shown schematically in Figure 53.

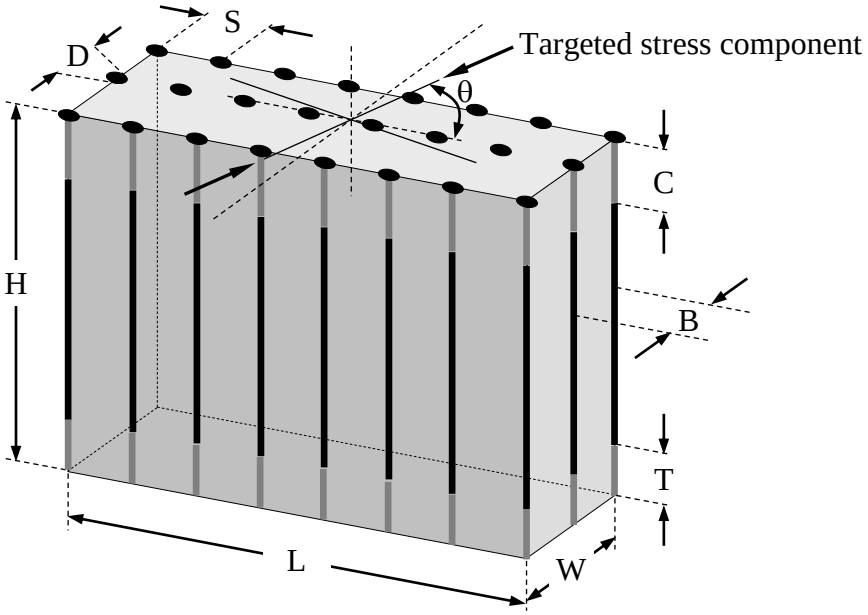

Figure 53. Schematic isometric illustration (not to scale) of the various properties and quantities shown in Table 15.

8.2.2. Calculation example

Following is a calculation example of the Destressability Index based upon the values shown in the last column of Table 15, and as per the geometry shown in Figure 53. Please note that, although a generic situation can be envisioned for the purpose of providing an example, each situation is really its own case and the geometrical parameters must be adjusted consequently.

8.2.2.1.Step I – Calculation of the required design values

Proximity to static failure = $\sigma_1 / (\sigma_3 + [m_{Laboratory} \sigma_c \sigma_3 + s_{Laboratory} \sigma_c^{\,2}]^{0.5}) = 23.9\%$

Effective width of the targeted pillar $W_{Eff.} = ([N - 1] \times B) + (2 \times 16 \times D / 1000) \sim 12.7m$

Effective length of the targeted pillar $L_{Eff} = L = 50.0m$. (The destress blast is considered in this example to be abutting against mined-out areas, as per the situation shown in Figure 24c – as a result, no outside zone of influence needs to be considered in this direction in this particular case.)

Effective volume of the targeted pillar $V_{Eff.} = W_{Eff.} \times L_{Eff} \times H = 19{,}025\ m^3$. (Detailed calculations would be required for irregular shapes.)

Effective mass of the targeted pillar $M_{Eff.} = V_{Eff.} \times \rho_r / 1000 \sim 68{,}490$ tonnes

Effective energy per hole $E_{Eff.} = \pi D^2\, 0.25\, (H - T - C)\, \rho_e\, AWS\, 10^{-9} = 0.579$ Gcal/hole. (A 100% charge coupling ratio is assumed here, which is generally the case with large-scale confined destress blasts in pillars, where large amounts of explosive energy are sought after.)

In the case of fanned blastholes with variable collar lengths, a detailed calculation would be required for each hole.

Charge confinement ratio = $(T + C) / (D / 1000) = (0 + [5 \times 1.5]) / (0.1651) = 45.4$. (50% was added to "C" because of the presence of inert stemming material in the collar in this example.) In the case of fanned blastholes with variable collar lengths, an average collar length would have to be used.

Total number of blastholes $N_b = ([L / S] + 1)_{\text{rounded to the nearest unit below}} \times N = 42$. (The actual number of blastholes, as per the drilling layout, should be used directly instead, if available.)

Total explosive energy in the blast $E_{Blast} = E_{Eff.} \times N_b = 0.579 \times 42 = 24.3$ Gcal. In the case of fanned blastholes with variable collar lengths, the energy value of each individual hole would have to be added.

Unit energy in the blast $E_{Unit} = (E_{Blast} / M_{Eff.}) \times 10^6 = 355$ cal/kg of rock. (E_{Unit} should be checked for values over 500, which would be indicative of very high energy levels, outside of those experimented in the industry.)

8.2.2.2.Step II – Rating of the parameters

Rating for parameter P_1 – Stiffness of the intact rock material:

$E_{Laboratory} = 125$ GPa. Using Table 6, the corresponding rating is 2, for a score of 28.

Rating for parameter P_2 – Brittleness of the intact rock material:

BIM = 1.30. Using Table 7, the corresponding rating is 1, for a score of 15.

Rating for parameter P_3 – Degree of fracturing of the rock mass:

RMR = 80%. Using Table 8, the corresponding rating is 2, for a score of 38.

Rating for parameter P_4 – Proximity to failure:

Proximity to static failure = 23.9%. Using Table 9, the corresponding rating is 1, for a score of 14.

Rating for parameter P_5 – Orientation of σ_1 :

$\theta = 75°$. Using Table 10, the corresponding rating is 2, for a score of 26.

Rating for parameter P_6 – Width of the target zone:

N = 3. Using Table 11, the corresponding rating is 1, for a score of 18.

Rating for parameter P_7 – Explosive energy per tonne of target zone:

E_{Unit} = 355 cal/kg of rock. Using Table 12, the corresponding rating is 2, for a score of 56.

Rating for parameter P_8 – Confinement of the explosive charges:

Charge confinement ratio = 45.4. Using Table 13, the corresponding rating is 2, for a score of 34.

8.2.2.3.Step III – Assessment of the Destressability Index value

Table 16 summarises the rating and score associated with each parameter for the example being considered for the assessment of the Destressability Index.

Table 16. Rating and score associated with each parameter for the example assessment of the Destressability Index at the intact rock material scale.

Parameter	Rating	Score
P_1 – Stiffness of the intact rock material	2	28
P_2 – Brittleness of the intact rock material	1	15
P_3 – Degree of fracturing of the rock mass	2	38
P_4 – Proximity to failure	1	14
P_5 – Orientation with respect to σ_1	2	26
P_6 – Width of the target zone	1	18
P_7 – Explosive energy per tonne of target zone	2	56
P_8 – Confinement of the explosive charges	2	34
	Total	229

The corresponding overall normalised score is (229 / 276) = 0.83, which, based upon Table 14, would correspond to a Destressability Index of ‘Good’. In other words, for the example provided the rock properties and stress conditions, combined with the proposed blast design, would be conducive to a successful destressing effect.

8.3. ASSESSMENT OF THE DESTRESSABILITY INDEX AT THE ROCK MASS SCALE

As was done in the previous section at the intact rock material scale, the methodology at the rock mass scale will first be described in detail, and then illustrated with the same example.

8.3.1. Ranges of property values for the rating of each parameter and scoring system

Table 17 through to Table 25 show ranges of values of the property that describes each of the first eight parameters in the RES interaction matrix at the rock mass scale, for the rating of these parameters in terms of how conducive they are to choked destress blasting. Please refer to Table 5 for a detailed list of the properties retained to characterise the parameters at that scale. As at the intact rock material scale, higher rating values correspond to a situation that is more conducive to successful confined destress blasting. The cause in these tables is taken directly from the RES interaction matrix at the rock mass scale (shown in Figure 50) and the score is again the rating multiplied by the cause.

Table 17. Range of rock mass elastic modulus values for the rating of parameter P_1 (stiffness of the rock), for the interaction matrix at the rock mass scale.

Range of values		Rating	Cause	Score	Maximum score for P_1
Below	25	0	13	0	
Between	25 and 50	1	13	13	
Over	50	2	13	26	26

Note: values of $E_{Rock\ Mass}$ are expressed in GPa.

Table 18. Range of B_1 values for the rating of parameter P_2 (brittleness of the rock), for the interaction matrix at the rock mass scale.

Range of values		Rating	Cause	Score	Maximum score for P_2
Below	10.0	0	13	0	
Between	10.0 and 18.0	1	13	13	
Over	18.0	2	13	26	26

Note: values of B_1 are dimensionless.

Table 19. Range of RMR values for the rating of parameter P_3 (degree of fracturing of the rock mass), for the interaction matrix at the rock mass scale.

Range of values		Rating	Cause	Score	Maximum score for P_3
Between	0 and 60%	0	14	0	
Between	60 and 80%	1	14	14	
Between	80 and 100%	2	14	28	28

Note: values of RMR are expressed in percentage.

Table 20. Range of proximity to failure values for the rating of parameter P_4 (proximity to failure of the rock), for the interaction matrix at the rock mass scale.

Range of values		Rating	Cause	Score	Maximum score for P_4
Between	0 and 33%	0	14	0	
Between	33 and 70%	1	14	14	
Between	70 and 100%	2	14	28	28

Notes: proximity to failure is represented by $\sigma_1 / \sigma_3 + [\, m\, \sigma_c\, \sigma_3 + s\, \sigma_c^2 \,]^{0.5}$*, and expressed in percentage.*
Parameters m and s are expressed at the rock mass scale.

One will notice that the rating thresholds shown in Table 20 for the range of values are quite different from those shown in Table 9, in order to account for the scale considered. This is because at the rock mass scale the stress level is compared to the rock mass strength, whereas at the intact rock material scale it is compared to the intact rock material strength. Regardless of the scale considered, the stress level must however have a comparable effect on the chance of success of a large-scale choked panel destress blast in the field, and, hence, provide a comparable rating for parameter P_4.

At this early stage the rock mass strength has been considered to be about a third of the intact rock material strength, in which case the stress level thresholds (in MPa) used for the rating of parameter P_4 at both scales are somewhat similar. Table 21 illustrates this point. Consider for example that the intact rock material strength is, say, 150 MPa, which, with no confinement and a RMR of 85, would correspond to a rock mass strength of about 50 MPa. As shown in columns 3 and 5 of Table 21, the stress levels (in MPa) associated with the various ratings of parameter P_4 are comparable.

Table 21. Comparison between the ranges of proximity to failure values for the rating of parameter P_4 at the intact material and rock mass scales, with no confinement.

Range of values	At the intact material scale		At the rock mass scale		Rating
	(% of strength [1])	*(MPa)*	*(% of strength [2])*	*(MPa)*	
Below	10%	15	33%	17	0
Between	10 and 25%	15 and 38	33 and 70%	17 and 35	1
Over	25%	38	70%	35	2

Notes: [1] *percentage of the intact rock material strength (150 MPa in this example).*
[2] *percentage of the rock mass strength (50 MPa in this example).*

Although this similarity in the threshold stress levels between the two scales diminishes as more confinement is applied, which is usually the case when destress blasts are attempted, the ranges shown in Table 9 and Table 20 were retained as a first approach, which will be evaluated with the case studies.

Table 22. Range of angle values for the rating of parameter P_5 (orientation of the destress blast with respect to σ_1), for the interaction matrix at the rock mass scale.

Range of values		Rating	Cause	Score	Maximum score for P_5
Between	0 and 30°	0	13	0	
Between	30 and 60°	1	13	13	
Between	60 and 90°	2	13	26	26

Note: angles are between the azimuth of the destress blast plane and the direction of σ_1, and are expressed in degrees.

Table 23. Range of number of blasting rings for the rating of parameter P_6 (width of the target zone), for the interaction matrix at the rock mass scale.

Range of values		Rating	Cause	Score	Maximum score for P_6
Below	2	0	18	0	
Between	2 and 4	1	18	18	
Above	4	2	18	36	36

Note: the width of the target zone is expressed in number of blasting rings.

Table 24. Range of explosive energy per unit mass values for the rating of parameter P_7 (unit explosive energy), for the interaction matrix at the rock mass scale.

Range of values		Rating	Cause	Score	Maximum score for P_7
Between	0 and 200	0	24	0	
Between	200 and 350	1	24	24	
Between	350 and 500	2	24	48	48

Note: values of explosive energy per unit mass are expressed in calories of explosive energy per kilogram of rock.

Table 25. Range of charge confinement ratios for the rating of parameter P_8 (confinement of the explosive charges), for the interaction matrix at the rock mass scale.

Range of values		Rating	Cause	Score	Maximum score for P_8
Between	0 and 25	0	17	0	
Between	25 and 45	1	17	17	
Over	45	2	17	34	34

Note: values of charge confinement ratios are expressed as a ratio of the blasthole diameter.

The maximum total score possible (the sum of the maximum score of each parameter in Table 17 through to Table 20 and Table 22 through to Table 25) is 252.

For a given situation (a given destress blast design to be implemented in a given rock mass under a given set of stress conditions), the property assigned to represent each parameter is categorised using the proper table between Table 17 and Table 25. As was the case at the intact rock material scale and depending upon its value, each property will fall within one of three categories (‘not conducive’, ‘somewhat conducive’ or ‘conducive’ to destress blasting) and will be assigned a rating of either 0, 1 or 2, which will, in turn, yield a certain score.

At the end of the process all eight scores are added to produce the total score associated with the situation being examined. This total score is then normalised, by dividing it by 252 (the maximum total score possible). The last step of the process consists in assessing the Destressability Index with Table 26.

Table 26. Assessment of the Destressability Index as a function of the overall normalised parameter score at the rock mass scale.

Overall normalised score	Destressability Index
From 0.00 to 0.40	Low
From 0.40 to 0.70	Medium
From 0.70 to 0.85	Good
From 0.85 to 1.00	Excellent

Table 27 summarises the properties and quantities that are needed to establish the score of each parameter for the purpose of deriving a Destressability Index value at the rock mass scale. An example value is again provided for each entry, in order to illustrate the approach (this example is the same one used at the intact rock material scale in the previous section).

Table 27. List of the basic properties and quantities required for the assessment of the Destressability Index at the rock mass scale.

Properties	Symbol	Unit	Example value
Density of the rock	ρ_r	*kg/m³*	3,600
Young's modulus of the intact rock material	$E_{Laboratory}$	*GPa*	125
Unconfined compressive strength of the intact rock material	$\sigma_{c\ Laboratory}$	*MPa*	190
Rock Mass Rating of the rock mass	RMR	*%*	80
Hoek-Brown parameter m of the intact rock material	$m_{Laboratory}$	–	10.000
Hoek-Brown parameter s of the intact rock material	$s_{Laboratory}$	–	1.000
Effective σ_1 component at the time of the destress blast	$\sigma_{1\ Actual}$	*MPa*	75
Effective σ_3 component at the time of the destress blast	$\sigma_{3\ Actual}$	*MPa*	25
Angle of incidence of the blast with respect to the σ_1 component	θ	*degrees*	75
Length of the pillar to destress	L	*m*	50.00
Height of the pillar to destress	H	*m*	30.00
Number of blasting rings in the destress blast	N	*#*	3
Diameter of the blastholes	D	*mm*	165.1
Distance between blasthole rings	B	*m*	3.70

Table 27 (continued). List of the basic properties and quantities required for the assessment of the Destressability Index at the rock mass scale.

Properties	Symbol	Unit	Example value
Distance between blastholes on the same ring	S	*m*	3.70
Unloaded toe length in the blastholes *****	T	*m*	0.00
Unloaded collar length in the blastholes	C	*m*	5.00
Usage of inert stemming material ******	–	*Yes* or *No*	Yes
Density of the explosive product	ρ_e	*g/cm³*	1.25
Absolute weight strength of the explosive	AWS	*cal/g*	866

***** *use zero for non-breakthrough holes.*
****** *add 50% confinement if stemming material is used.*

8.3.2. Calculation example

A calculation example of the Destressability Index at the rock mass scale is presented in this section, based upon the example values shown in the last column of Table 27, and as per the geometry shown in Figure 53. As for the example at the intact rock material scale of Section 8.2.2, please note that each situation is its own case and that the geometrical parameters must be adjusted consequently.

8.3.2.1.Step I – Calculation of the required design values

$E_{Rock\ Mass} = E_{Laboratory} \times ([\ 0.000028 \times RMR^{2}\ ] + [\ 0.009 \times e^{\{RMR/22.82\}}]) = 59.9$ GPa

$GSI = RMR - 5 = 80 - 5 = 75$

$m_{Rock\ Mass} = m_{Laboratory} \times e^{([GSI - 100]/28)} = 4.095$ (undisturbed, before the destress blast)

$s_{Rock\ Mass} = s_{Laboratory} \times e^{([GSI - 100]/9)} = 0.062$ (undisturbed, before the destress blast). It is again assumed that the GSI will be higher than 25 in all cases where destress blasting will be attempted. Please refer to Equation (67) in Appendix F.

$\sigma_{c\ Rock\ Mass} = \sigma_3 + ([\ m_{Rock\ Mass}\ \sigma_c\ \sigma_3\ ] + [\ s_{Rock\ Mass}\ \sigma_c^{2}\ ])^{0.5}$, for $\sigma_3 = 0$, which is 47.4 MPa.

Exponent *a* of the generalised Hoek-Brown failure criterion for jointed rock masses is

set at 0.5 because, again, it is assumed that the GSI will be higher than 25 when destress blasting will be attempted. Please refer to Equation (68) in Appendix F.

$\sigma_{T\ Rock\ Mass} = (m_{Rock\ Mass}\ \sigma_c - [m_{Rock\ Mass}^{2}\ \sigma_c^{2} - 4\ s_{Rock\ Mass}\ \sigma_c^{2}]^{0.5}) /2$ (quadratic formulae for $\sigma_1 = 0$), which is 2.90 MPa

$B_1 = \sigma_{c\ Rock\ Mass} / \sigma_{T\ Rock\ Mass} = (47.4 / 2.90) = 16.3$

Proximity to failure $= \sigma_1 / (\sigma_3 + [m_{Rock\ Mass}\ \sigma_c\ \sigma_3 + s_{Rock\ Mass}\ \sigma_c^{2}]^{0.5}) = 43.5\%$

Effective width of the targeted pillar $W_{Eff.} = ([N - 1] \times B) + (2 \times 16 \times D / 1000) \sim 12.7$m

Effective length of the targeted pillar $L_{Eff} = L = 50.0$m. (The destress blast is considered in this example to be abutting against mined-out areas, as per the situation shown in Figure 24c – as a result, no outside zone of influence needs to be considered in this direction in this particular case.)

Effective volume of the targeted pillar $V_{Eff.} = W_{Eff.} \times L_{Eff.} \times H = 19{,}025$ m³. As at the intact rock material scale, detailed calculations would be required for irregular shapes.

Effective mass of the targeted pillar $M_{Eff.} = V_{Eff.} \times \rho_r / 1000 \sim 68{,}490$ tonnes

Effective energy per hole $E_{Eff.} = \pi\ D^{2}\ 0.25\ (H - T - C)\ \rho_e\ AWS\ 10^{-9} = 0.579$ Gcal/hole. (A 100% charge coupling ratio is again assumed, as in the example at the intact rock material scale.) In the case of fanned blastholes with variable collar lengths, a detailed calculation would be required for each hole.

Charge confinement ratio $= (T + C) / (D / 1000) = 45.4$. (50% was added to C because of the presence of inert stemming material in the collar.) In the case of fanned blastholes with variable collar lengths, an average collar length would be used at this stage.

Total number of blastholes $N_b = ([L / S] + 1)_{Rounded\ to\ the\ nearest\ unit\ below} \times N = 42$. (The actual number of holes, as per the layout, should be used directly instead, if available.)

Total explosive energy in the blast $E_{Blast} = E_{Eff.} \times N_b = 0.579 \times 42 = 24.3$ Gcal. In the case of fanned blastholes with variable collar lengths, the energy value of each individual hole would have to be added.

Unit energy in the blast $E_{Unit} = (E_{Blast} / M_{Eff.}) \times 10^{6} = 355$ cal/kg of rock. (As mentioned before, E_{Unit} should be checked for values over 500, which would be indicative of very high energy levels, outside of those experimented in the industry.)

8.3.2.2.Step II – Rating of the parameters

Rating for parameter P_1 – Stiffness of the rock mass:

$E_{Rock\ Mass}$ = 59.9 GPa. Using Table 17, the corresponding rating is 2, for a score of 26.

Rating for parameter P_2 – Brittleness of the rock mass:

B_1 = 16.3. Using Table 18, the corresponding rating is 1, for a score of 13.

Rating for parameter P_3 – Degree of fracturing of the rock mass:

RMR = 80%. Using Table 19, the corresponding rating is 2, for a score of 28.

Rating for parameter P_4 – Proximity to failure:

Proximity to failure = 43.5%. Using Table 20, the corresponding rating is 1, for a score of 14.

Rating for parameter P_5 – Orientation of σ_1 :

$\theta = 75°$. Using Table 22, the corresponding rating is 2, for a score of 26.

Rating for parameter P_6 – Width of the target zone:

N = 3. Using Table 23, the corresponding rating is 1, for a score of 18.

Rating for parameter P_7 – Explosive energy per tonne of target zone:

E_{Unit} = 355 cal/kg of rock. Using Table 24, the corresponding rating is 2, for a score of 48.

Rating for parameter P_8 – Confinement of the explosive charges:

Charge confinement ratio = 45.4. Using Table 25, the corresponding rating is 2, for a score of 34.

8.3.2.3.Step III – Assessment of the Destressability Index value

Table 28 summarises the rating and score associated with each parameter for the example assessment of the Destressability Index at the rock mass scale.

Table 28. Rating and score associated with each parameter for the example assessment of the Destressability Index at the rock mass scale.

Parameter	Rating	Score
P_1 – Stiffness of the rock mass	2	26
P_2 – Brittleness of the rock mass	1	13
P_3 – Degree of fracturing of the rock mass	2	28
P_4 – Proximity to failure	1	14
P_5 – Orientation with respect to σ_1	2	26
P_6 – Width of the target zone	1	18
P_7 – Explosive energy per tonne of target zone	2	48
P_8 – Confinement of the explosive charges	2	34
	Total	207

The corresponding overall normalised score is (207 / 252) = 0.82, which, based upon Table 26, would correspond to a Destressability Index of 'Good'.

CONCLUSION DU CHAPITRE. La méthodologie de l'Index de relâchement – une valeur calculée unique qui quantifie les chances de succès d'un tir confiné à grande échelle de relaxation des contraintes dans un pilier de mine, tiré dans un massif rocheux donné soumis à un régime de contraintes donné – a été décrite dans ce chapitre.

Bien que développée à partir de considérations fondamentales d'ingénierie, cette méthode comprend un certain degré de jugement, notamment au niveau 1) du choix des paramètres inclus dans la matrice d'interaction et de leur influence sur les résultats du tir; 2) du choix des propriétés qui représentent ces paramètres; 3) du codage des matrices d'interaction aux diverses échelles; et, 4) de l'établissement des plages de propriétés et des cotes correspondantes pour le calcul de la valeur de l'Index de relâchement. En conséquence, la méthodologie – c'est-à-dire la capacité de l'Index de relâchement à prédire les résultats d'un tir confiné à grande échelle de relaxation des contraintes dans un pilier – doit être vérifiée et validée avec des études de cas bien instrumentées et documentées. Cela va être

fait dans les deux prochains chapitres aux échelles du matériel intact et du massif rocheux afin de tenter d'évaluer laquelle est la plus appropriée.

CHAPTER CONCLUSION. The Destressability Index methodology has been described in this chapter, which is a unique calculated number that quantifies the likelihood of success of a given large-scale choked pillar destress blast design, in a given rock mass and under a given state of stress.

Although developed based upon fundamental engineering considerations, it encompasses a certain degree of judgement, including 1) in the choice of the parameters that were retained in the RES interaction matrix and how they influence the destress results; 2) in the choice of properties that represent these parameters; 3) in the coding of the RES interaction matrices at the various scales; and, 4) in the establishment of the property ranges and their corresponding ratings for the assessment of the Destressability Index value. As a result, the methodology – i.e., the ability of the Destressability Index to predict the results of a given large-scale confined pillar destress blast design under a given set of circumstances – must be tested and validated against well-instrumented and fully-documented case histories. This will be done in the next two chapters, at both the intact rock material and the rock mass scales in an attempt to assess which is the most appropriate.

CHAPTER IX

9. FIRST CASE STUDY – DESTRESS BLAST IN THE 29-9 PILLAR AT BRUNSWICK MINE

SOMMAIRE DU CHAPITRE. Le développement de la méthodologie de l'Index de relâchement décrit au chapitre précédent comprend un élément de jugement qui, bien qu'il soit basé sur un processus de raisonnement logique, doit être testé et validé avec des études de cas bien instrumentées et documentées. Deux telles études sont présentées dans cette thèse, la première dans ce chapitre et la seconde au chapitre suivant.

La première étude de cas provient de la Mine Brunswick de Noranda où un tir confiné à grande échelle de relaxation des contraintes a été détoné en octobre 1999 dans le pilier de sulfures stériles No. 29-9. L'historique et le raisonnement ayant conduit à la décision de tenter un tel sautage sont brièvement présentés dans un premier temps, ainsi que les contraintes et les restrictions pratiques qui étaient associées au projet. Le design du tir, ainsi que les divers types d'instrumentation utilisés pour évaluer son comportement sur le terrain et ses résultats sont ensuite décrits.

Les résultats obtenus sont ensuite présentés et discutés, des points de vue des performances sur le terrain, des observations visuelles post-tir et des résultats provenant des instruments installés. Cette section est détaillée car le degré de succès atteint par le tir doit être clairement établi afin de pouvoir évaluer avec confiance l'exactitude de la prévision que l'Index de relâchement aurait faite.

Deux valeurs de l'Index de relâchement sont par la suite calculées: une à l'échelle du matériel intact et une à l'échelle du massif rocheux. Suite à cela, la performance du

sautage, telle qu'observée sur le terrain et mesurée avec les instruments, est comparée aux deux valeurs obtenues pour l'Index de relâchement, de manière à évaluer dans quelle mesure et avec quelle précision cet outil aurait pu prédire les résultats du tir.

Veuillez noter qu'une description de cette étude de cas a déjà été effectuée dans un article technique intitulé "Large-Scale Panel Destress Blast at Brunswick Mine" (*Sautage à grande échelle de relaxation d'un pilier à la mine Brunswick*) par Andrieux, Brummer, Liu, Mortazavi et Simser. Cette publication a été originalement présentée en novembre 2000 à la 23^{ième} Session d'étude sur les techniques de sautage organisée par la SEEQ à Québec (Québec, Canada). Cet article a été subséquemment publié sous le même nom dans l'édition de novembre/décembre 2003 du Bulletin de l'Institut canadien des mines, de la métallurgie et du pétrole. La contribution spécifique de l'auteur aux travaux décrits dans cet article est telle que suit. D'abord, en tant qu'Ingénieur senior en contrôle de terrain à la mine Brunswick jusqu'à la fin de mars 2000, il a largement contribué à la décision de tenter un tir confiné à grande échelle de relâchement des contraintes dans le pilier 29-9. Ensuite, en tant qu'ingénieur sur le site responsable de l'exécution de ce projet, l'auteur a conçu et chargé le sautage, et a supervisé tous les aspects du programme d'instrumentation. Subséquemment, en tant qu'ingénieur en mécanique des roches à Consultation Itasca Canada, l'auteur a analysé et interprété une grande partie des données et a co-rédigé le rapport à CAMIRO ainsi que l'article en question. Veuillez toutefois noter que la description donnée dans cette thèse est plus détaillée que celle de l'article, et offre un meilleur aperçu des travaux. La section 9.6, sur l'évaluation de l'Index de relâchement, est entièrement inédite et a été développée spécifiquement dans le cadre des travaux de doctorat rapportés dans ce document.

CHAPTER SUMMARY. The development of the Destressability Index methodology described in the previous chapter encompassed an element of judgement, which, although based upon a logical thinking process, requires to be tested and validated against well-instrumented and fully-documented case histories. Two such case histories are presented in this thesis, the first one in this chapter and the second one in the next chapter.

The first case study was carried out at the Noranda Brunswick Mine in October 1999 in the 29-9 waste sulphides pillar. The background and rationale behind the decision to implement a large-scale choked destress blast are briefly presented first, along with associated practical constraints and limitations. The design of the blast, as well as the instrumentation used to assess its field behaviour and results are described next.

The results achieved are then presented and discussed, from the viewpoints of field performance, visual post-blast observations and instrumentation results. This section needs to be quite detailed because the degree of success achieved by the destress blast must be clearly established in order to reliably ascertain the accuracy of the prediction the Destressability Index methodology would have made.

Two Destressability Index values are subsequently calculated: one at the scale of the intact rock material and one at that of the rock mass. Following this, the field performance of the

destress blast is compared with the two Destressability Index values obtained, in order to assess how valuable a tool each would have been to predict the outcome of the blast.

Please note that a description of this case study was previously provided in a paper entitled *Large-Scale Panel Destress Blast at Brunswick Mine* by Andrieux, Brummer, Liu, Mortazavi and Simser, which was presented in November 2000 at the 23rd Study Session on Blasting Techniques organised by the SEEQ in Quebec City (Quebec, Canada). This paper was subsequently published under the same name in the November/December 2003 issue of the Bulletin of the Canadian Institute of Mining, Metallurgy and Petroleum. The specific contribution of the author to the work described in this paper was as follows. Firstly, as Senior Ground Control Engineer at Brunswick Mine until the end of March 2000, he was instrumental in the decision to implement a large-scale choked destress blast in the 29-9 Pillar. Secondly, as the on site engineer responsible for the implementation of this project, the author designed and loaded the blast, and supervised all aspects of the field instrumentation programme. Subsequently, as a rock mechanics engineer at Itasca Consulting Canada, the author analysed and interpreted much of the data, and co-wrote the report to CAMIRO, as well as the paper aforementioned. Please note, however, that the description provided in this work goes much further than the one in the article, and offers significantly more insight. Section 9.6, on the assessment of the Destressability Index, is entirely original and was developed specifically within the framework of this thesis.

9.1. INTRODUCTION AND BACKGROUND

A large-scale choked panel destress blast was detonated at the Noranda, Inc. Brunswick Mine in October 1999 in an attempt to reduce the ground stresses in a critically important mining region. This work, sponsored by the Mining Division of CAMIRO and Brunswick Mine, consisted in heavily choke-blasting – and subsequently leaving in place – the large 29-9 massive sulphides pillar on the southwest side of the 1000m Level. The objective of this blast was to maximise breakage in the area to destress, while minimising collateral damage to critical infrastructures in the vicinity.

Back in 1999, future success at Brunswick Mine was critically dependent upon the successful extraction of the south end of the 1000m Level, which turned out to be one of the most difficult to engineer. This region was situated in the lower part of the mine and in the late 1990's constituted its southern abutment, which resulted in high stress conditions.

Complex local geological settings and numerous identified structures further increased both the likelihood and the anticipated severity of the ground control-related problems expected during extraction. These conditions had resulted in this difficult region being designed for pillarless pyramidal mining in order to leave behind no ground in which stresses could accumulate. This three-dimensional pyramid was designed to start in the expected most difficult region, on the south abutment near a plunging waste metasediments structure, and to progress north, east and up.

One of the identified keys to the successful extraction of this region was to stress-shadow both the Bulk Zone and the Main Ore Zone South (MOZ South), where most of the reserves were located, by first mining the #9 hanging wall lens, also referred to as the West Ore Zone (WOZ), in order to cut off the major principal stress. (The σ_1 stress component at Brunswick Mine was sub-horizontal and oriented perpendicular to the strike of the ore body, in an east-west direction.) Figure 54 shows a plan view of the south end of the 1000m Level at the Sill elevation – the grid is 50m and the areas already mined out in 1999 are shaded in grey.

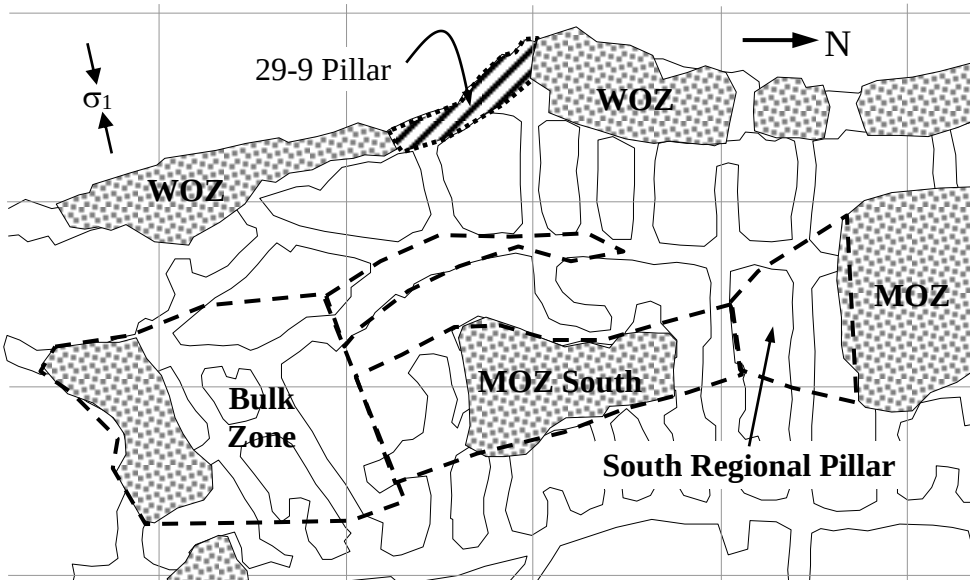

Figure 54. Plan view of the south end of the 1000 Sill level showing the various mining zones. (After Andrieux *et al*., 2000.)

Figure 55 shows the significant level of seismic activity that was recorded in this region between 28 April 1999 and 28 October 1999, i.e., during the six month period before the destress blast. (Note that only events located within 30m above and below the 1000 Sill elevation are shown in this view.) This figure shows only a snapshot of the heavy seismicity the south end of the mine was sustaining, which was affecting mining operations by causing delays and requiring reconditioning work to be conducted on a routine basis.

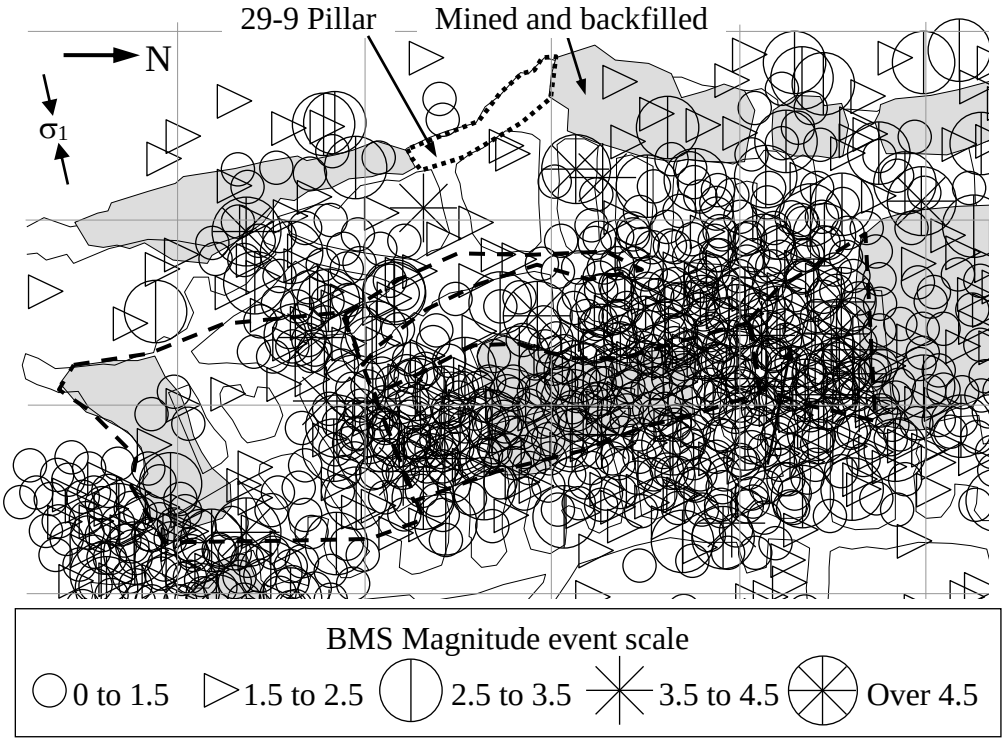

Figure 55. Plan view of the south end of 1000 Sill showing the seismic activity recorded in this region between 28 April 1999 and 28 October 1999 within 30m of the level.

(Please note in Figure 55 that the BMS Magnitude scale corresponds approximately to the Richter Magnitude scale plus 4. For example, a BMS Magnitude event 4 corresponds approximately to a Richter Magnitude event 0.)

As can be seen in Figure 54 and Figure 55, a gap existed in the WOZ in the form of the 29-9 Pillar, which was originally going to be extracted as a stope. Further exploration showed it to be waste sulphides, i.e., massive sulphides with a metal content below the cut-off grade. Its mechanical properties were however quite similar to those of ore-grading

massive sulphides (dense, stiff, strong and brittle). This pillar had a squat shape with a high width-to-height ratio, which resulted in it being extremely strong and unlikely to fail early in a natural manner as mining was to progress.

Even though not ore, the 29-9 Pillar could not be left intact as it would have provided a long-term "window" through which the major principal stress could have flowed and affected mining of the Bulk Zone and MOZ South. Besides being uneconomical, the mining (i.e., the removal with mucking equipment) of this waste material would have taken time and resources, thus further delaying the extraction of the WOZ, which was already behind schedule. In light of these considerations, it was decided to break this pillar with explosives in order to prevent it from carrying and transferring load, and leave it in place.

9.2. DESTRESS BLAST SITE AND ASSOCIATED CONSTRAINTS

As can be seen in Figure 56 the 29-9 Pillar sat between the 1000 Sill elevation (overcut) and the 1125-5 sub elevation (undercut), and fully bridged the gap between the 28-9 Stope to the South and the 30-9 Stope to the North, which were both mined and backfilled. (In this figure solid light grey indicates remaining ore, dotted light grey indicates backfill and dark grey shows the 29-9 waste sulphides pillar.)

The scheduling of such a large destress blast in the centre of the high priority WOZ brought a few challenges. In particular, two production stopes were active at the time in the immediate vicinity of the destress blast: the 160,000 tonne 130-9 Stope, between 1000-1 sub and 1000 Sill, and the remainder of the smaller 128-9 Stope, also between the 1000-1 sub and 1000 Sill. Figure 56 shows the location of the destress blast relative to these two active stopes. Ideally, the 29-9 Pillar would have been blasted first – that way, its destressing effect would have been easier to assess, with no other large-scale mining activity occurring elsewhere in the vicinity. The problem was that the 130-9 Stope had 160,000 tonnes of ore at risk in it. Its back on 1000 Sill, despite the installation of cablebolts and numerous shotcrete pillars, had already caved about 5m and it was feared

that the highly confined destress blast in the nearby 29-9 had the potential to induce enough vibrations to further damage the back. This would have meant weeks of remotely breaking and cleaning-up large ore slabs, which would have further delayed the critical and already late sequence in the WOZ.

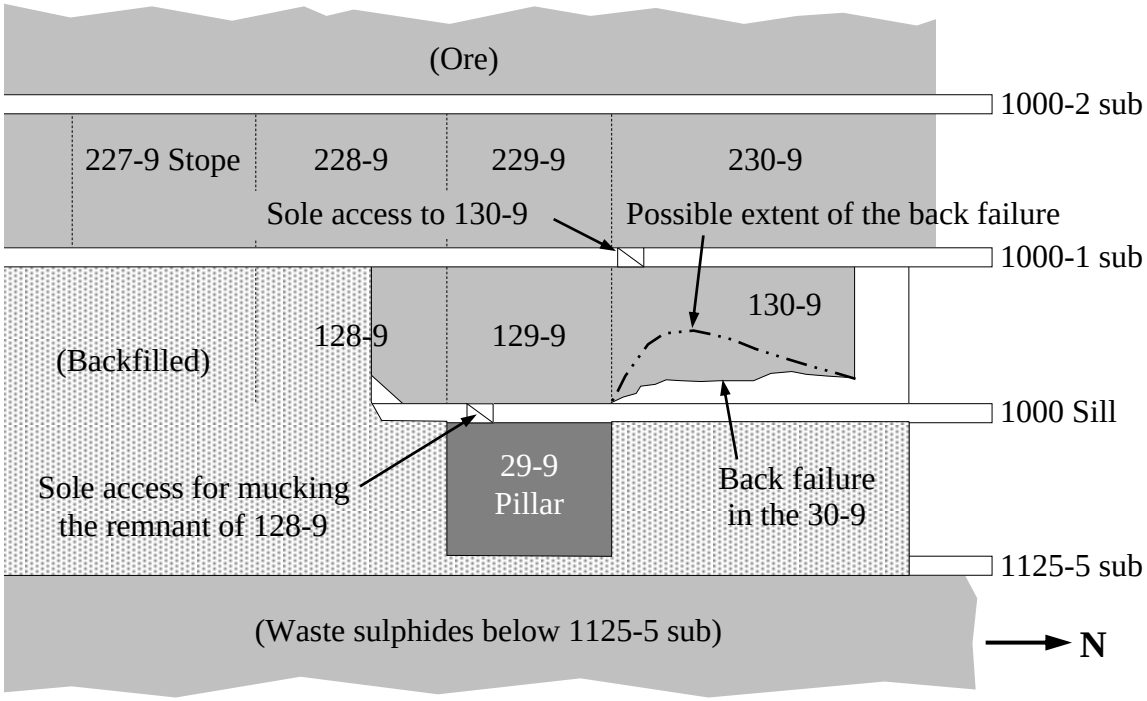

Figure 56. Schematic longitudinal section (not to scale) of the WOZ lens looking west, showing the 29-9 Pillar where the destress blast took place. (After Andrieux *et al*., 2000.)

Furthermore, the ore in the 130-9 Stope was scheduled for November and no contingency ore was available to replace it. Besides production delays and shortcomings, significant caving inside the undercut of the 130-9 Stope would have put the sole access to this stope on 1000-1 sub at risk. In light of these considerations, it was decided to blast the 130-9 Stope prior to the 29-9 Pillar. Blasting this large stope first was expected to shed additional stress towards the 29-9 Pillar, which was deemed a possible advantage from a technical point of view, as destressing was thus anticipated to create even more of a stress drop, possibly making it easier to measure. This decision also meant that there was a sizeable risk of damaging the 29-9 Pillar area due to the large blast-induced vibrations that were expected from the 160,000 tonne mass-blast in the 130-9 Stope. To alleviate the need for potential reconditioning work, it was decided to load the destress blast prior to firing the

130-9 Stope blast, and to protect it from possible ground falls by burying it under a 1m-thick cap of 7% cement paste backfill.

The next question was whether to blast the 29-9 Pillar before the remnant of the 128-9 Stope. As seen in Figure 56, the brow in this stope on 1000 Sill had already caved (it had actually caved to this shape after each successive blast). Firing the over-confined 29-9 destress blast right next to it had a large potential to further damage this brow, resulting in even more unstable ground conditions and large slabs of ore obstructing the already difficult to muck draw-point. Furthermore, the only access to muck the 128-9 Stope on 1000 Sill was through the 29-9 Pillar access, which was likely going to be damaged by the destress blast. Sequence-wise, the 128-9 Stope was holding the 227-9 Stope between 1000-2 sub and 1000-1 sub, which was already drilled. In turn, the extraction of the 227-9 Stope was needed to provide stress shadowing to the lead stope of the pillarless pyramidal mining front in the Bulk Zone.

However, blasting the 128-9 Stope before the 29-9 Pillar had the potential to damage the 29-9 region. To overcome this problem, the destress blast would again have had to be pre-loaded, which would have made the remote mucking of the 128-9 Stope right by it hazardous. The risks of damaging the surface blast connections would also have been significant. Because “only” 6,000 tonnes of ore were at risk and the destress blast could not be indefinitely delayed, it was decided to fire the destress blast before the 128-9 Stope. The area would then be cleaned-up and graded, and the 29-9 Access reconditioned in order to remotely muck the 128-9 Stope as fast as possible. This meant that the vibration levels from the destress blast had to be controlled.

9.3. DESIGN OF THE DESTRESS BLAST

The design of the destress blast was done with two objectives in mind. Firstly, to sufficiently break the rock mass to obtain an adequate destressing effect, and, secondly, to

cause as little collateral damage as possible to the surrounding regions, particularly to the critical nearby haulage ways serving the south end of the 1000m Level. Some general design guidelines were identified early, as follows: 1) re-pumpable bulk emulsion explosives; 2) 165 mm diameter blastholes; 3) 20m average charge length; 4) 2.4m by 2.4m blasthole pattern (at the toe of the holes – the rationale behind this choice is discussed later); 5) non-breakthrough blastholes (only one blasthole was broken through to the level below, to allow for water drainage during the drilling phase – no other holes broke through, in order to maximise charge confinement); and, 6) no free face.

The explosive product used was the Explosives Technologies International (ETI) Fragmite Plus, an underground permissible glass micro-balloon sensitised 1.25 g/cm³ density re-pumpable bulk emulsion. It was selected because already well implemented at the mine site, high energy, water resistant (important because the non-breakthrough destress blastholes were going to wait pre-loaded, until the neighbouring 130-9 Stope was mass-blasted), capable of sinking down wet holes during loading, associated with a high and consistent VOD, and not overly shock desensitisation-prone. This product has a nominal VOD of 5,800 m/s, a relative weight strength (RWS) of 0.71, and an absolute weight strength (AWS) of 0.71×912 cal/g (for AnFO) $\approx$ 645 cal/g. The destressing effect was expected to be mainly the result of shock energy. The relative lack of gas generation associated with emulsion products – not ideal as gas pressure is helpful in further driving fractures and displacing blocks of broken rock – was deemed acceptable overall.

Larger 165 mm (6-1/2 in) diameter blastholes were retained with the objective of maximising damage, as they contain over twice the amount of explosives per metre that can be fitted in the regular 115 mm (4-1/2 in) size production blastholes. The pattern was fixed at 2.4m by 2.4m at the toe of the holes, which corresponded to about 14.5 times the blasthole diameter of 165 mm. This drill hole density was almost double that of a regular blasting pattern for longhole stoping, and close to the “16 times the hole diameter” rule-of-thumb discussed previously (Blake *et al.*, 1998). This over-loading was intentional and aimed at increasing damage in the targeted region.

To further assess the blasting design, the VCR (for "Vibration Contour in Rock") software (Heilig & McKenzie, 1995) was used to estimate the damage zone around a proposed fully-loaded blasthole. This software graphically illustrates the vibration contours around a charged blasthole based upon the near-field Holmberg-Persson equation (Holmberg & Persson, 1980). The input parameters include the properties of the surrounding rock mass and of the explosives loaded in the blasthole. As a first-pass estimation, the following parameters were used: rock density of 4.30 t/m^3; P-wave velocity of 6,000 m/s; s-wave velocity of 3,500 m/s; and, the site-specific coefficients K and α of 800 and 0.75, respectively.

Figure 57 shows the computed vibration contours obtained for the bulk emulsions considered, when loaded in a 165 mm diameter blasthole in massive sulphides. As illustrated, the vibration level at a distance of 4m from the charge was calculated to be close to 4.0 m/s, which is still sufficient to fracture rock (please refer to Table 30).

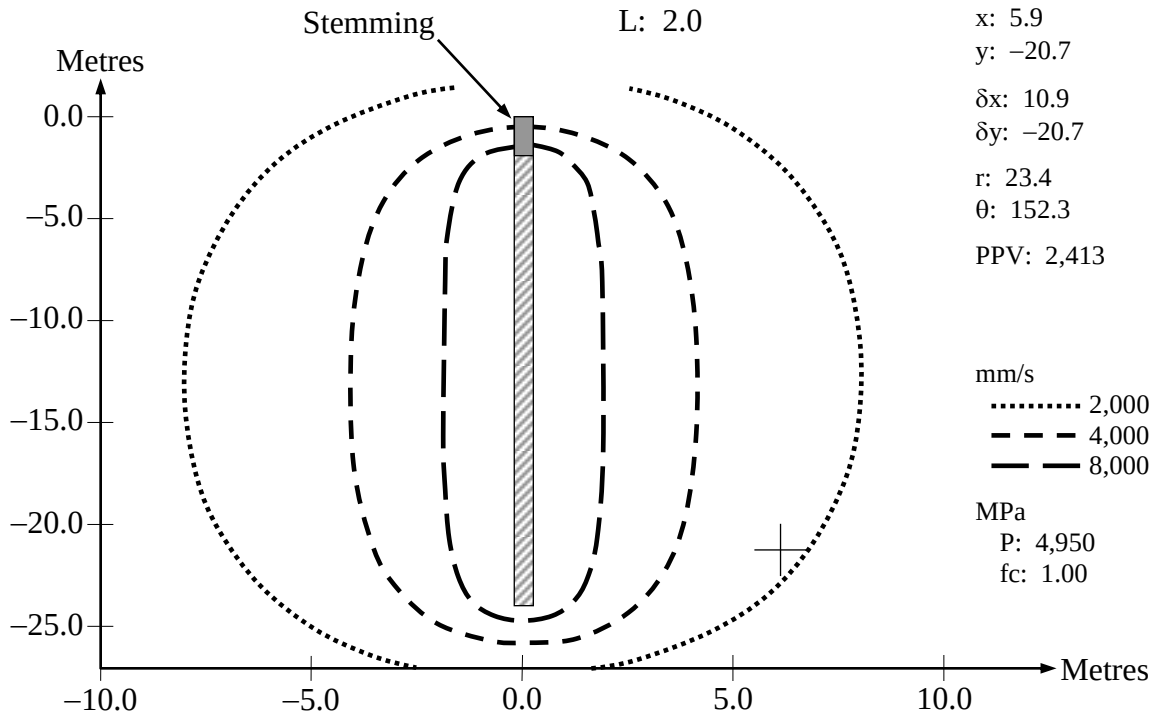

Figure 57. Vibration contours obtained with the VCR software. (After Andrieux *et al*., 2000.)

Based upon the volume and geometry of the pillar to destress, and the proposed drilling pattern, thirty-two (32) blastholes were required, two per ring, along sixteen (16) rings.

The longitudinal section in Figure 58a shows how the rings towards the north side of the blast had to be fanned northwards due to the back failure inside the 130-9 Stope, by the north edge of the 29-9 Pillar. Drilling vertical blastholes in this region would have meant having collars immediately next to a ground fall, with any further deterioration of the 130-9 Stope back resulting in the loss of these holes. Ensuring the safety of the driller was also a major issue.

The destress blastholes also needed to be dipped westwards in order to follow the sulphides-metasediments contact, as shown in Figure 58b.

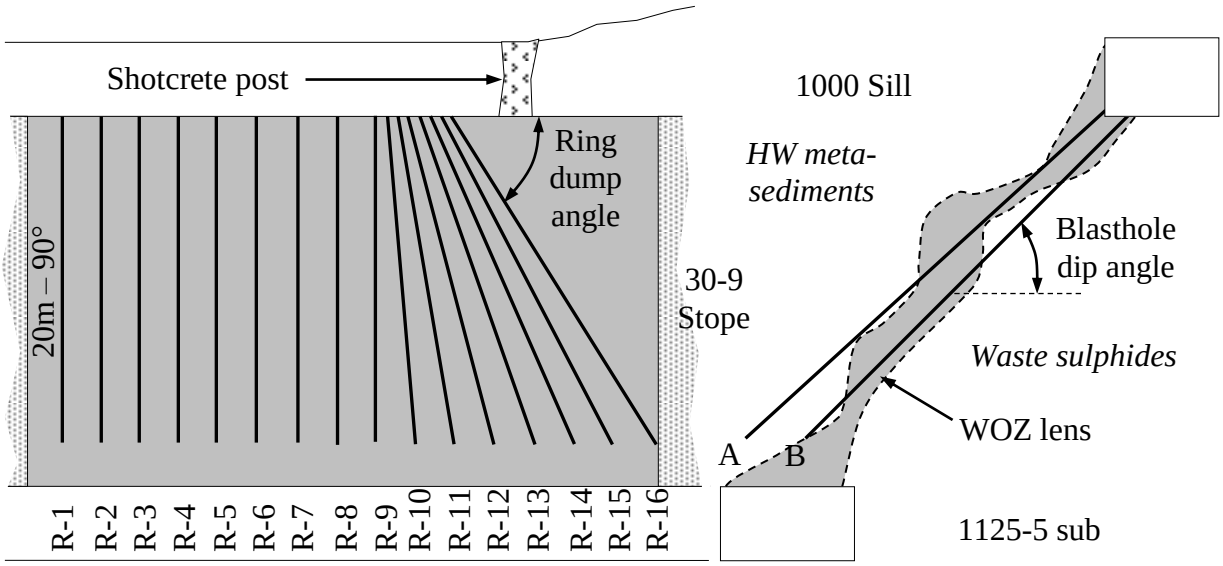

(a) Long section looking west. ***(b) Cross-section looking north (R-8).***

Figure 58. (a) Longitudinal section of the 29-9 Pillar looking west; and, (b) cross-section at Ring 8 looking north. (After Andrieux *et al*., 2000.)

Table 29 summarises the drilling parameters implemented for the destress blast in the 29-9 Pillar. In all, a total of 877.7m of drilling were required.

Table 29. Drilling data summary for the destress blast in the 29-9 Pillar at Brunswick Mine.

Ring *(#)*	Dump angle	Hole *(#)*	Dip angle	Length *(m)*
R-1	90°	A	55°	24.4
		B	55°	24.4
R-2	90°	A	54°	25.3
		B	54°	25.3
R-3	90°	A	52°	25.0
		B	52°	25.0
R-4	90°	A	50°	25.6
		B	50°	25.6
R-5	90°	A	47°	27.1
		B	48°	26.5
R-6	90°	A	44°	28.7
		B	46°	27.1
R-7	90°	A	43°	29.0
		B	46°	27.1
R-8	90°	A	43°	29.0
		B	45°	27.4
R-9	90°	A	43°	28.7
		B	46°	26.8
R-10	85°	A	43°	28.7
		B	46°	26.8
R-11	80°	A	42°	29.0
		B	46°	27.1
R-12	75°	A	43°	29.0
		B	46°	27.4
R-13	71°	A	43°	31.4
		B	46°	29.9
R-14	66°	A	45°	29.0
		B	48°	27.4
R-15	62°	A	46°	29.0
		B	49°	27.7
R-16	58°	A	47°	29.3
		B	50°	28.0

As mentioned, the destress blast had to be designed to also minimise collateral damage to crucial nearby infrastructure on 1000 Sill and 1000-1 sub. This was addressed through a simple square root scaling relationship that links the amplitude of the blast-induced vibrations to the distance away from the blast. By knowing the distance between the blast and the various infrastructures of concern, the level of blast-induced vibrations at each of these locations could be assessed, as a function of the charge weight fired per delay. This square root scaling relationship, developed by the USBM for cylindrical charges (as defined previously towards the end of Section 4.2), is as follows:

$$PPV = K\,[\,R / (W)^{0.5}\,]^{-\beta} \qquad \text{..... Eq. (32)}$$

With PPV the peak particle velocity (in mm/s) anticipated at a distance R (in metres) away from the blast due to the instantaneous detonation of an explosive charge weighting W (in

kg); *K* the constant site-specific amplitude factor (assumed at 800); and, β the constant site-specific attenuation factor (assumed at 1.5). Equation (32) thus becomes:

$$PPV = 800 [R / (W)^{0.5}]^{-1.5} \quad \text{..... Eq. (33)}$$

With PPV, R and W as defined in Equation (32). Equations (32) and (33) were expected to under-estimate vibrations by at least 20% due to the fact that they do not consider the over-confinement of the charges in a choked destress blast.

As mentioned, 32 blastholes were required in the blast, each one initially assumed to be loaded with an approximately 20m-high column of explosives. With a 1.25 g/cm³ density emulsion, this corresponded to about 17.1 tonnes of explosives for the whole blast assuming all the holes were to be loaded identically. Several sequencing options were considered. The best approach destressing-wise was to fire all the charges simultaneously in order to generate maximum damage. Using Equation (33), the instantaneous detonation of the 17,100 kg in all the 32 charges would have yielded a blast-induced vibration in excess of 3.3 m/s at a distance of 50m away, and of approximately 855 mm/s 125m away. Table 30 shows the effects on a "typical" rock mass of various vibration levels, as reported by Chiappetta *et al*. (1987) – 250 mm/s seems to be the limit below which no fracturing of intact rock occurs.

Table 30. Effects on a "typical" rock mass of various vibration levels.
(After Chiappetta *et al*., 1987.)

Particle velocity		Effects on "typical" rock
(mm/s)	*(in/s)*	
< 250	< 10	No fracturing of intact rock
250 to 635	10 to 25	Minor tensile slabbing
635 to 2,500	25 to 100	Strong tensile and some radial cracking
> 2,500	> 100	Complete break-up

In light of these figures, the potential to cause damage to critical areas in the vicinity was considered too high to allow the simultaneous detonation of all the destress charges. A threshold of 250 mm/s at a distance of 50m away was set, as this distance encompassed most of the identified critical areas (128-9 Stope, 29-8 Stope, the two south draw points in

the 30-9 Stope, the 130-9 Access and the 129-9 area). This corresponded to the detonation of only one (1) destress blasthole loaded with 535 kg of emulsion per delay.

Vibrations from sequential blasting were also thought about in light of their potential to dead-press neighbouring charges during the blast. Although the chances of such occurrences were deemed moderate at the vibration levels anticipated and with the use of emulsion, it was decided to increase the distance between successive destress charges to further reduce the risk. One way to achieve this could have been to drill only every second hole out of the initial pattern. Instead, the "discarded" blastholes were still drilled but turned into lightly charged presplit holes, between destress holes. These not only allowed to maintain greater distance between adjacent destress blastholes, they also provided the opportunity to attempt to crack the rock mass ahead of these, in order to provide a surface across which part of the vibrational energy from the large destress charges would be reflected back to the area to fracture. Furthermore, the presplit lines were designed to cut off as much as possible potential gas penetration from the previously detonated large destress charges, which could have affected the next pair of destress charges. Figure 59 schematically shows the final sequence retained. Light grey circles correspond to the lightly charged presplit blastholes and black circles correspond to the heavily loaded destress blastholes. The number next to each blasthole corresponds to its sequential position in the firing sequence.

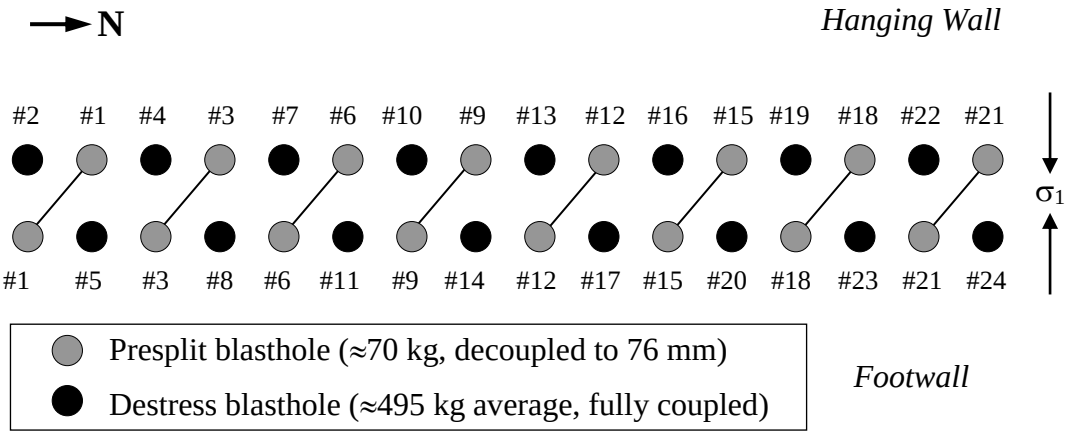

Figure 59. Schematic plan view (not to scale) showing the blasting sequence retained in the 29-9 Pillar at Brunswick Mine. (After Andrieux *et al*., 2000.)

As shown in Figure 59, pairs of presplit blastholes were fired simultaneously ahead of each pair of destress blastholes, which were then fired individually. The en-echelon progression of the destress holes was also aimed at breaking the rock mass at as sharp an angle as possible to the local major principal stress component. The angled presplit lines were also deemed advantageous with regard to the orientation of the major principal stress component, which was expected to facilitate the creation and extension of shear fractures along these planes. Table 31 shows the actual Primadet MS detonator numbers used to achieve the designed firing sequence, as well as the resulting delays, in milliseconds (the shaded cells correspond to the destress blastholes, whereas the white cells correspond to the presplit blastholes).

Table 31. Detonator numbers and resulting delays used to achieve the blasting sequence retained. (After Andrieux *et al*., 2000.)

Sequence	*(#)*	1	2	3	4	5	6	7	8
Detonator	*(#)*	1	2	3	4	5	6	7	8
Delay	*(ms)*	25	50	75	100	125	150	175	200

Sequence	*(#)*	9	10	11	12	13	14	15	16
Detonator	*(#)*	8½	9	9½	10	10½	11	11½	12
Delay	*(ms)*	225	250	275	300	325	350	375	400

Sequence	*(#)*	17	18	19	20	21	22	23	24
Detonator	*(#)*	12½	13	13½	14	14½	15	16	17
Delay	*(ms)*	425	450	475	500	525	600	700	800

The destress blastholes were designed fully coupled, with a 4 to 5m collar length, or roughly 25 to 30 times their diameter, with no decking being implemented. The presplit blastholes were designed to be decoupled to 76 mm (3 inches), using ABS tubing. After being cut to length, the bottom end of these decoupling tubes was plugged and the tube lowered in the blasthole, with double Cari straps being used to secure the tubes at the collar of the holes. Each destress blasthole collar was plugged immediately above the top of the explosive column using wood wedges, and topped with 0 to 3/4 inch crushed rock along the entire remaining length of the borehole, to provide charge confinement. In contrast, an air deck was maintained in each presplit blasthole, by leaving an 8m-long air gap between the top of the decoupled charge and the wood wedge holding a 4m-high column of 0-3/4 inch

crushed rock stemming inside the ABS pipe. The explosive charges in the blastholes sitting in rings 10 through to 16 had to be adjusted due to their dumped angles, in order to avoid excessive proximity between neighbouring charges, which could have resulted in charge cut-offs and other malfunctions. Table 32 summarises the measured loading data for each blasthole in the destress blast.

Table 32. Loading data for the destress blast in the 29-9 Pillar at Brunswick Mine.

Ring *(#)*	Hole *(#)*	Hole *(type)*	Charge *(kg)*	Ring *(#)*	Hole *(#)*	Hole *(type)*	Charge *(kg)*
1	A	Destress	495	9	A	Destress	585
	B	Presplit	68		B	Presplit	68
2	A	Presplit	68	10	A	Presplit	45
	B	Destress	457		B	Destress	443
3	A	Destress	480	11	A	Destress	298
	B	Presplit	68		B	Presplit	45
4	A	Presplit	68	12	A	Presplit	68
	B	Destress	470		B	Destress	577
5	A	Destress	575	13	A	Destress	400
	B	Presplit	68		B	Presplit	57
6	A	Presplit	68	14	A	Presplit	45
	B	Destress	588		B	Destress	482
7	A	Destress	607	15	A	Destress	320
	B	Presplit	68		B	Presplit	45
8	A	Presplit	68	16	A	Presplit	68
	B	Destress	591		B	Destress	528

Based upon all the individual explosive charges in the destress blast, which added to close to 8.9 tonnes (just under 7.9 tonnes in the destress holes, and 985 kg in the presplit holes), and considering the 645 cal/g AWS of the bulk emulsion, the total energy for the entire blast was $5{,}740 \times 10^6$ calories, or about 5.7 Gcal. The volume directly targeted was 27.2m high (20.0m vertically, as shown in Figure 58a, but considering the 47° average dip of the blastholes), by 30m long (in the north-south direction, corrected for the trapezoidal shape of the block), by 2.4m wide (in the east-west direction), for approximately 1,960 m^3. Considering the outside zones of influence of about 16 blasthole diameters on both sides of the panel added $2 \times (16 \times 0.165) \times 30 \times 27.2 \approx 4{,}310$ m^3, for a total volume of close to 6,275 m^3. At a rock density of 4.3 t/m^3, the total targeted mass was about 26,980 tonnes.

Hence, the energy ratio of the proposed destress blast was ($5{,}740 \times 10^6$ cal / 26,980,000 kg) = 212 cal/kg. This ratio fell within the 200 to 500 cal/kg guideline previously discussed. Figure 60 shows where this design lied in comparison with documented destress blast case studies, as reported by Brummer (2001).

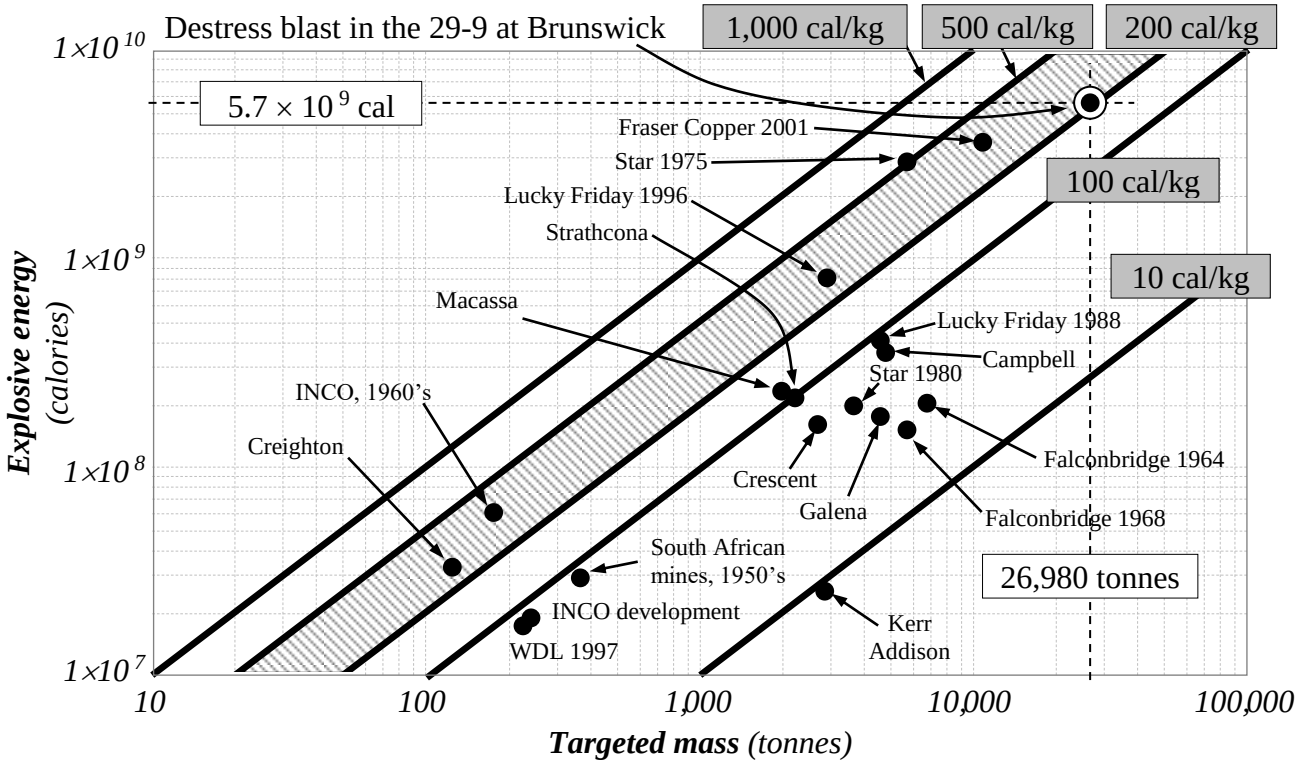

Figure 60. Designed explosive energy input per tonne of targeted rock mass in the 29-9 Pillar at Brunswick Mine.

Table 33 summarises the principal statistics associated with the field implementation of the large-scale choked destress blast in the 29-9 Pillar at Brunswick Mine.

Table 33. Principal final field statistics of the destress blast in the 29-9 Pillar at Brunswick Mine.

Parameter	Values and units
Number of blastholes	32
Total drilling length	877.7m (2,879 ft)
Total explosives loaded	8,880 kg (19,535 lb)
Explosive type	Bulk emulsion
Total explosive energy	5.73×10^9 cal

Table 33 (continued). Principal final field statistics of the destress blast in the 29-9 Pillar at Brunswick Mine.

Parameter	Values and units
Maximum charge per blasthole	607 kg (1,335 lb), for Hole A on Ring #7
Maximum charge per delay	607 kg (1,335 lb), on delay #10 (at 250 ms)
Full targeted rock volume	6,275 m^3 (221,415 ft^3)
Targeted rock tonnage (massive sulphides at 4.30 t/m^3)	26,980 tonnes
Effective Powder factor *	0.329 kg/t (1.415 kg/m^3)
Actual energy ratio	212.3 cal/kg

* *relative to the targeted mass and volume.*

As mentioned, the destress blast was designed to wait, fully loaded, and not be detonated until the mass-blast in the neighbouring 130-9 Stope was fired, which involved 160,000 tonnes of ore being shot in a little over 10% void. The vibration levels from this blast were anticipated to be sufficiently high to cause shake damage and ground falls in the areas immediately adjacent to it, which included the destress blast. In particular, it was recognised that a large potential existed to damage its surface connections.

To address this concern, the entire destress blast area, once loaded and connected, was buried under 1m of 7% cement paste backfill. Besides protecting the surface lines from loose rocks, this paste backfill cap further confined the charges.

Twenty-five pound bags of crushed rock were used to protect the surface connections of the initiation system from the paste backfill during placement, as shown in Figure 61. The top of some of the crushed rock bags that were not yet buried in paste fill is visible in the background. Great care had to be taken to flatten as much as possible and strategically arrange these 25 lb bags, in order to prevent the thick paste fill from flowing underneath, lifting and carrying them downstream, which could have resulted in damage to the surface connections.

Figure 61. Photograph looking northwest from the pillar access showing the placement of the 7% cement paste backfill. (After Andrieux *et al*., 2000.)

9.4. INSTRUMENTATION USED

The instrumentation aspect of the project was undertaken as a follow-up to a previous CAMIRO Mining Division project on destressing, which had been completed in 1998. The overall objective was to derive further insight into the field behaviour and effects of a large choked panel destress blast. The specific objectives of this work were to 1) instrument the destress area; 2) measure the field behaviour and the effects of the destress blast in several different ways; and, 3) numerically model the effects of the blast. This aspect of the project was sponsored jointly by CAMIRO – Mining Division, through its industry sponsors, and Brunswick Mine.

The following instrumentation was used to assess the reaction of the rock mass to the destress blast. (Figure 64 shows on a cross-section looking north and cut through the 29-9 Pillar the location of the various instruments. These locations are projected onto the cross-section plane, for simplification – the instrumentation holes were actually spread over a few metres in the third dimension [in the north-south direction].)

9.4.1. Mine-wide seismic monitoring system

The seismic response in the region following the destress blast was observed with the mine-wide Integrated Seismic System International (ISS) surveillance network installed at the mine site. The dense array of 25 triaxial and 18 uniaxial accelerometers allowed for the monitoring of seismic events as small as about −3 Richter Magnitude, with an average accuracy of 5 to 10 metres, just about anywhere in and around the mine. All events being manually processed at Brunswick Mine, much reliable information can be extracted from the recorded seismicity, in terms of both the spatial and temporal distribution of the activity, and also in terms of source parameter data. (Please refer to Section B.3.4 in Appendix B for a discussion on source parameter analyses.)

9.4.2. Vibrating wire stress cells

Vibrating wire stress cells, which utilise a vibrating wire transducer to measure the deformation of a cylinder preloaded into a borehole by a wedge-and-platen assembly, were the primary instruments used for monitoring stress changes. Figure 62 shows the various components of this type of stress cell, as well as the orientation of the vibrating wire in reference to the stress component being measured (these devices can measure stress in only one direction).

More specifically, vibrating wire stress cells track local variations in the stress field by measuring the frequency at which a tensioned wire vibrates inside its shell. As the stress varies the shell deforms (either expands or compresses), which causes the steel wire inside it to vibrate at different frequencies. This type of gauge needs to be pre-stressed inside its

borehole in order to be able to measure stress drops as well – the amount of pre-stressing is governed by how far the wedge is driven between the stress cell and the platen at installation time.

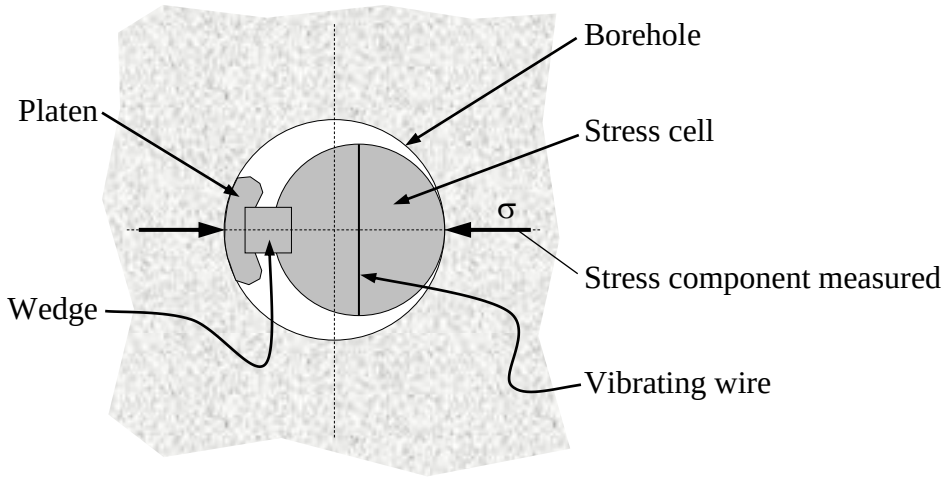

Figure 62. Schematic view (not to scale) down an installation borehole showing the various components of a vibrating wire stress cell.

Figure 64 shows the location of the two 76 mm (3 inch) diameter Geokon stress cells used. These gauges were installed inside NQ-size (75.7 mm diameter) diamond drill holes located on the footwall side from the #5 draw point of 130-9 Stope just north of the 29-9 Pillar, on the 1000 Sill elevation. One was installed towards 1000-1 sub inside an upwards 65°-dipping hole, at a depth of 10.8m.

The other was installed towards 1125-5 sub in a downwards 50°-dipping hole, at a depth of 4.5m (the original plan was to install it deeper, but stress-induced movement in the hole blocked the way). In both cases the instruments were oriented in order to measure changes in the major principal (sub-horizontal and oriented east-west) stress component. The instrument in the uphole was pre-stressed to 12 MPa, while the one in the downhole was pre-stressed to 17 MPa.

These instruments were wedged inside their boreholes and connected to a datalogger on 17 August 1999. Both then recorded continuously – in the form of one automatic reading every 10 minutes (the acquisition frequency was increased the day prior to the 130-9 mass-

blast to one measurement every five minutes) – the changes in stress caused at their respective locations by various mining activities. These activities included all production blasts, recorded seismic events, and some unknown events that affected the stress regime. Since the destress blast was not going to be fired first and the large blast in the 130-9 Stope was expected to significantly change the stress regime in the region, early monitoring was mandatory in order to provide a time-based record of how each blast affected this regime.

9.4.3. Multi-point extensometers

Two (2) six-point extensometers were used to measure the movement caused by the destress blast within the rock mass. These instruments consisted in six (6) independent fibreglass rods of varying length that were mounted inside sleeves and free to slide in them. When this type of instrument is installed inside a borehole, one end of these rods (the anchor) becomes embedded in the grout and attached to the rock mass. The other end of the rods, towards the collar of the hole (the reference point), is connected to a reading unit that measures the movement of the corresponding rod. As movement occurs inside the rock mass it displaces the rods that are embedded past the location of the movement, and this movement is read at the collar of the hole. The location of the anchors along the instrument hence dictates where movement can be detected inside the rock mass.

The instruments used in the 29-9 Pillar could read movement in both directions (extension and contraction). As shown in Figure 64, one extensometer was grouted inside a 30°-dipping downhole that intersected the targeted pillar, whereas the other one was installed inside a 30° uphole that intersected the ore zone directly above the 29-9 Pillar. The lower instrument was designed to measure the rock mass dilation that was expected to be caused by the damage from the destress blast (this dilation would result in the measurement of a contraction by the extensometer). The other instrument, located behind the overcut of the blast, was designed to detect the damage that was expected to be induced by the stress redistribution above the targeted region. Table 34 shows the location of the anchors along each extensometer and inside each borehole. As can be seen, these instruments were recessed inside the boreholes.

Table 34. Location of the anchors along the two extensometers installed in the 29-9 Pillar at Brunswick Mine.

Downhole extensometer		
Anchor *(#)*	Anchor depth ***** *(m)*	Location inside the hole ***** *(m)*
1	15.0	27.0
2	12.5	24.5
3	10.0	22.0
4	7.5	19.5
5	5.0	17.0
6	2.5	14.5
Head	0.0	12.0

Uphole extensometer		
Anchor (#)	Anchor depth ***** *(m)*	Location inside the hole ***** *(m)*
1	10.0	14.5
2	8.3	12.8
3	6.7	11.2
4	5.0	9.5
5	3.3	7.8
6	1.7	6.2
Head	0.0	4.5

***** *all depths and distances are relative to the collar of the boreholes.*

Both multi-point extensometers were manually read at regular intervals, including just hours prior to the destress blast on 28 October 1999, and again on 2 November 1999.

9.4.4. Borehole camera survey holes

Borehole camera surveys were used to provide a direct visual assessment of the pre- and post-destress blast conditions within the rock mass. As shown in Figure 64, two holes were used for this purpose: one 40°-dipping downhole that extended past the 29-9 Pillar, and one uphole that was parallel to the local dip of the West Ore Zone lens. The downhole was designed to observe the damage caused by the destress blast, whereas the uphole was designed to supplement the data from the nearby stress cell. Both observation holes were HQ-size diamond drill holes, with a diameter of 96.0 mm.

A borehole camera was used for the surveys, which were recorded on videotape for subsequent detailed analyses. Pre- and post-blast surveys were compared to identify new fractures, detect the extension of previously existing ones and assess the damage caused by the destress blast.

9.4.5. Two-dimensional seismic tomographic imaging

Seismic cross-hole surveys were also performed before and after the destress blast in order to investigate the damage it caused to the rock mass. Interestingly, and contrary to the other instrumentation used, geophysics-based imaging techniques consider volumes of rock rather than discrete points of observation. Blast-induced damage will typically cause 1) a decrease in the velocity of propagation of a seismic wave, which, in turn, will result in an increase in its arrival time; and, 2) an increase in its rise time due to increased attenuation of the seismic energy by the newly-created fractures in the rock mass. (The arrival time is defined as the time it takes for a seismic signal to travel from its source to the point of observation, whereas the rise time is defined as the time between the first arrival and the first peak of a signal. Figure 63 illustrates these concepts.)

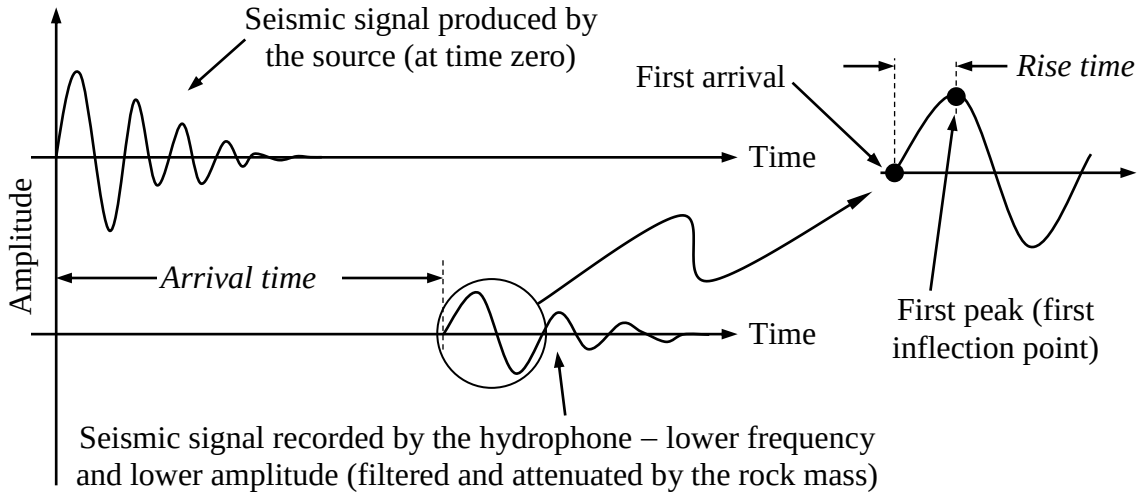

Figure 63. The definition of rise time and arrival time.

By comparing signals recorded along similar raypaths during the pre- and post-blast surveys, rock mass damage can theoretically be fairly precisely characterised. Constant vibrations were generated repetitively inside a water-filled borehole by an Oyo-Wappa mechanical seismic source in which a series of parallel steel disks are propelled against each other at high speed, expelling the water between them fast enough to create a strong vibrational impulse that is transferred to the rock mass and propagates in it.

Figure 64 shows the location of the two holes used for the seismic surveys, on both sides of the ore lens in order to detect changes in the destress blast region. The hole on the hanging wall side was drilled from 1000-1 sub due to access constraints. Series of vibrations were generated at 5m intervals down the hanging wall borehole in front of the 29-9 Pillar, and seismic recordings were done with a string of hydrophones located on the footwall side of the pillar. These measurements were repeated twice: once before, and once after the destress blast. Table 35 summarises the characteristics of the holes used for these surveys.

Table 35. Description of the boreholes used for the cross-hole seismic surveys.

Borehole	Dip *(degrees)*	Dip direction * *(degrees)*	Depth *(m)*
Source hole (hanging wall side)	50.5	234.2	84.0
Receiver hole (footwall side)	50.5	234.2	23.0

***** *clockwise from the North.*

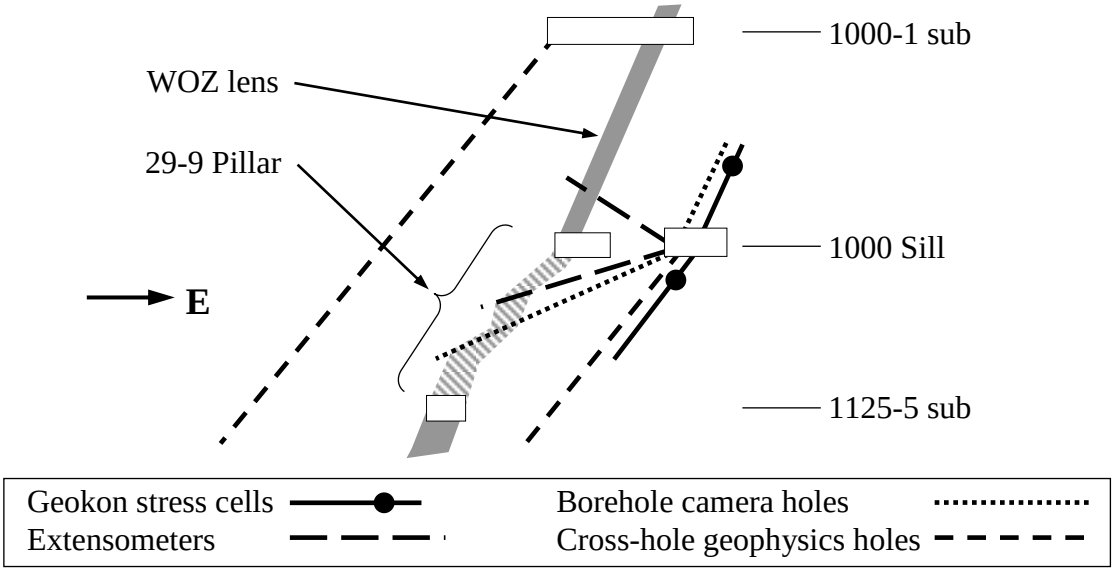

Figure 64. Cross-section through the 29-9 Pillar looking north and showing the projected location of the various instrumentation. (After Andrieux *et al*., 2000.)

9.4.6. High frequency geophones

The ground vibrations from the destress blast were also measured as a means to assess its field behaviour, compare how closely to their designed firing time each set of charges detonated, and evaluate whether the larger explosive charges in the blast detonated and contributed consistent amounts of work to the breaking process. Four (4) wall-mounted surface triaxial high frequency geophone arrays were used, all of them located on the 1000 Sill elevation. Figure 65 shows their location with respect to the destress blast. Each monitoring station comprised three (3) individual high frequency omni-directional OYO GeoSpace LT-101 geophones oriented at 90° to each other, in order to capture all the vibrational energy at their location. The stations were installed on drift walls with aluminium mounting blocks.

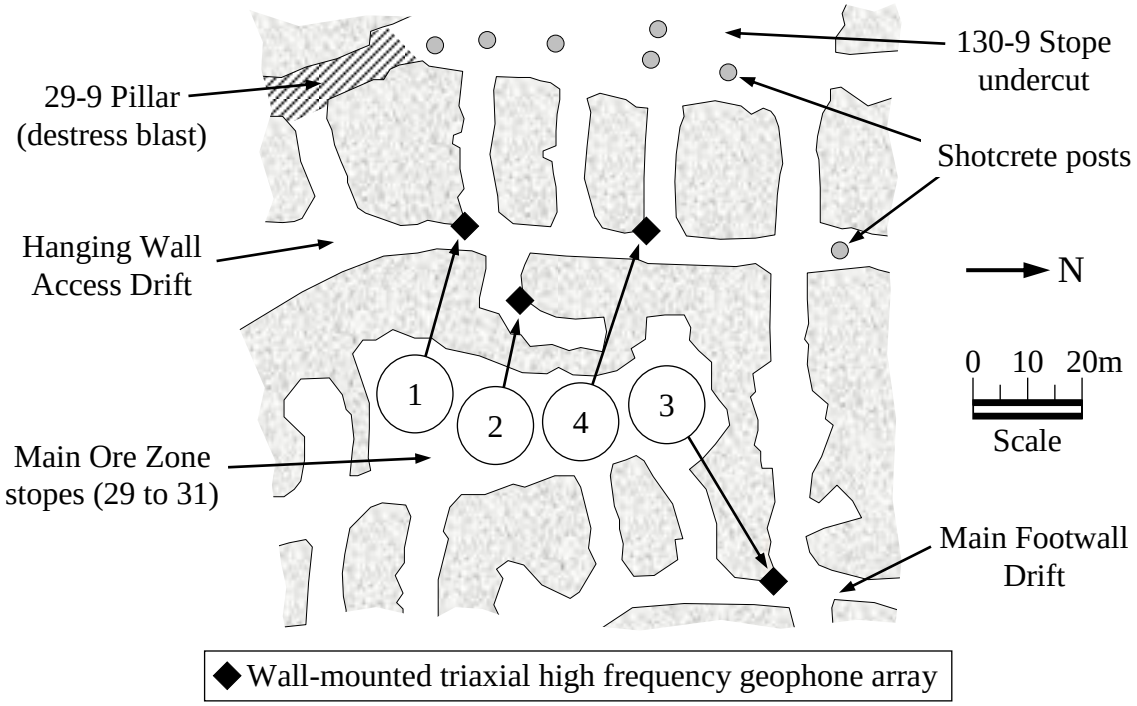

Figure 65. Plan view of the south end of the 1000 Sill level showing the location of the four wall-mounted triaxial high frequency geophone arrays around the 29-9 Pillar.

Table 36 shows the distance between the four geophone arrays and the destress blast in the 29-9 Pillar (the geophone array numbers correspond to those shown in Figure 65).

Table 36. Distance between the four high frequency geophones and the destress blast in the 29-9 Pillar at Brunswick Mine.

Geophone array *(#)*	(1)	(2)	(3)	(4)
Distance from the destress blast *(m)*	30	50	120	55

Three (3) 12 bit Instantel MiniMate digital seismographs (one eight channel unit, and two four channel systems) were used to monitor the destress blast, all set to record at a sampling rate of 8 kHz per channel. All three seismographs were triggered by a wirebreak loop attached to the detonating cord of the destress blast. The explosion of the cord broke the loop and simultaneously triggered all the seismographs, which were programmed to record for a duration of 2.5 seconds.

9.5. RESULTS OF THE DESTRESS BLAST

The 160,000 tonne production mass-blast in the 130-9 Stope was detonated 26 October 1999 at 17:52 AST, whereas the destress blast in the 29-9 Pillar was detonated 28 October 1999 at 17:57 AST. The following sections describe the results obtained from the various monitoring systems used.

9.5.1. Field performance of the destress blast

Figure 66 shows each of the three time-domain vibrational signals recorded at Station #1 (the nearest to the blast, as shown in Figure 65), as well as the nominal firing times, as designed (which are represented by the light vertical dashed lines visible on the seismogram).

Of the four surface-mounted triaxial blast vibration recording stations only two (stations #1 and #2) gave good results – Station #3 contained suspicious resonance-induced frequency components, while Station #4 loosened-up from the wall surface during the blast.

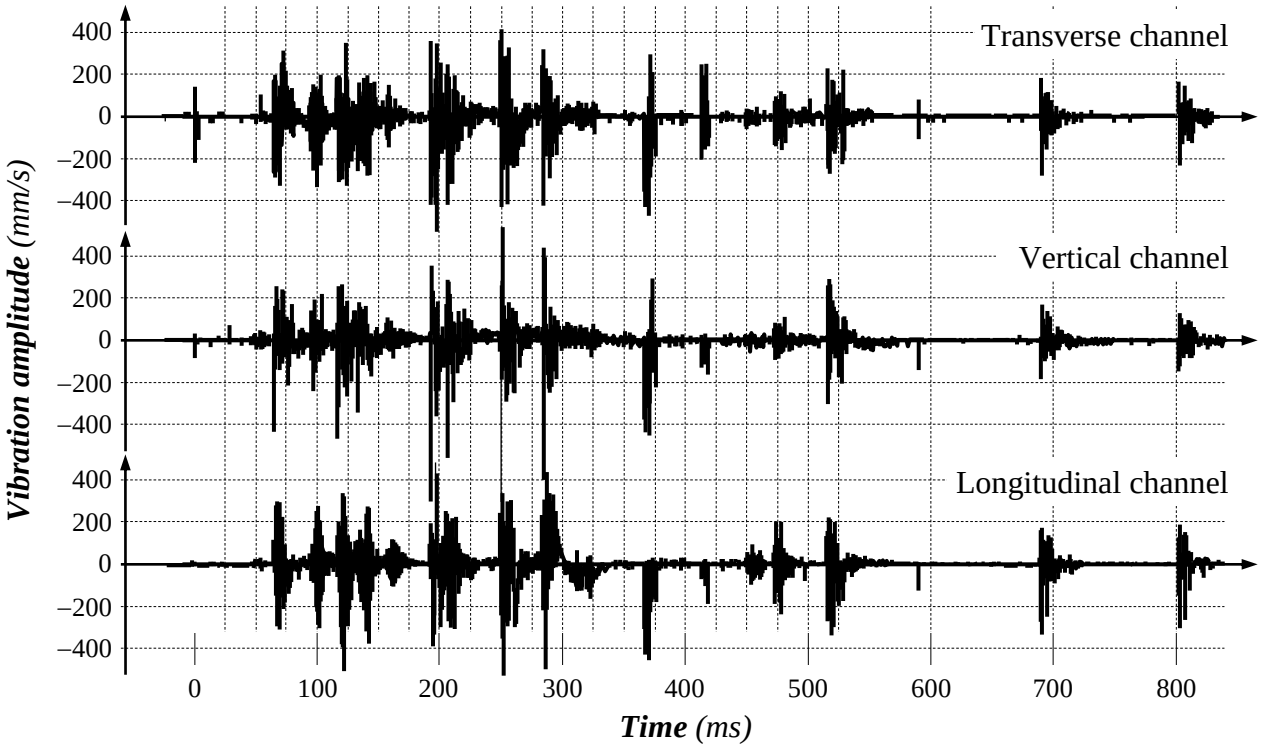

Figure 66. Blast vibration record for the station located 30m away from the destress blast in the 29-9 Pillar. (After Andrieux *et al*., 2000.)

As seen in Figure 66, out of a total of sixteen (16) heavily loaded destress charges (averaging 493 kg of emulsion each), ten (10) showed unequivocal traces on the seismograms. As for the other six, they did not appear at their respective nominal firing times on the seismograms, which means that they either fired out of sequence along with other charges, or did not fire at all. The overall similarities between the various wave packets on all channels suggest that most of the large destress charges contributed somewhat similar amounts of work to the breakage process.

These results imply that the panel destress blast went rather well, and did not suffer major malfunctions. Certainly, the vibration amplitudes obtained 30m away from the large destress charges, which average around 200 mm/s but instantaneously reach as much as 700 mm/s, are high enough to suggest that "some" damage was caused in the blasted region.

9.5.2. Visual post-blast assessments

Figure 67 through to Figure 69 are photographs taken shortly after the destress blast was fired in the 29-9 Pillar. Of particular interest was the severe overhead clearance reduction in the south part of the blast, partly due to floor heave and partly due to the accumulation there of material ejected during the blast – this ejected material came from the north end of the blast, where the rings were angled.

Figure 67 shows how severely the overhead clearance was reduced, from 3.5m after the paste backfill pour to about 1.2m after the destress blast. Shake damage associated with the blast can be seen at the bottom of the north wall, on the right hand side of the photograph. The material on the floor, better visible along the south wall on the left hand side, was paste backfill ejected during the blast. Both the walls and the back remained in good condition after the choked destress blast.

Figure 67. Photograph looking west taken on 1000 Sill in the access cross-cut to the 29-9 Pillar. (After Andrieux *et al*., 2000.)

The picture shown in Figure 68 was taken in the area from which the destress blastholes were drilled, loaded and buried under paste backfill, in front of the access shown in Figure 67, where the maximum overhead clearance reduction occurred. Please note how little damage was caused to the back and walls. The back in this area was supported with grouted 2.3m-long 20 mm steel rebars, #9 welded wiremesh screen, and dual 7m-long plated 15.9 mm cablebolts on a 1.8m by 1.8m pattern.

Figure 68. Photograph looking north in the 29-9 Pillar overcut on 1000 Sill. (After Andrieux *et al*., 2000.)

Figure 69 clearly shows the trench excavated in the north end of the blast, where the destress rings were angled. Please note how the trench shown in this figure is deepening going north, with decreasing charge confinement.

Also please note how much more damage was inflicted to the ground support by the ejected material – this material was projected mainly southwards, contributing to the overhead clearance reduction in the area.

Figure 69. Photograph looking north in the 29-9 Pillar overcut on 1000 Sill. This picture was taken further north from the area depicted in Figure 68. (After Andrieux *et al*., 2000.)

9.5.3. Seismic response to the destress blast

Figure 70 shows the seismic activity recorded in the south end of the mine within 30m of the 1000 Sill elevation (above and below) before (Figure 70a) and after (Figure 70b) the 28 October choked destress blast in the 29-9 Pillar. (Please note that Figure 70a is the same as Figure 55 – it has been repeated here to facilitate the comparison between the pre- and post-blast levels of seismic activity.) Figure 70 clearly shows that the seismicity recorded during the six month period after the destress blast was significantly lower than that recorded during the six month period before the blast. Some activity continued to affect the region, which was expected considering that the highly complex three-dimensional shape of the ore body in this region still provided remaining paths for the ground stresses to flow through. (A more complete stress cut-off and a further reduction of the level of seismicity were eventually achieved following the mass-blast fired in July 2001 higher up in the West Ore Zone, on 1000-3 sub and 1000-2 sub [Simser *et al*., 2002]. This mass-blast resulted in

a more complete cut-off of the path through which the sub-horizontal east-west stress component flowed towards the Bulk Zone.)

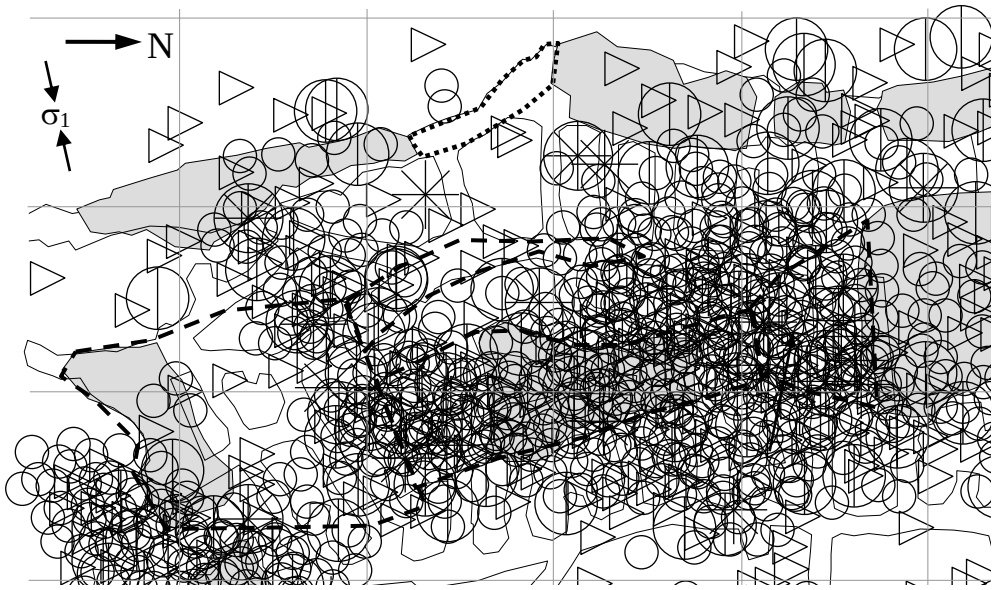

(a) Between 28 April 1999 and 28 October 1999.

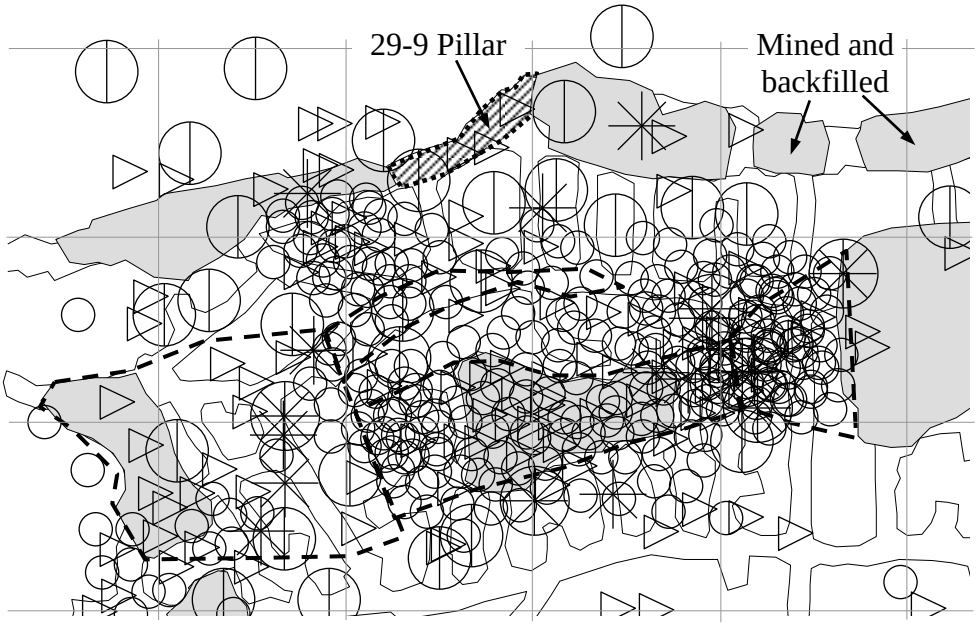

(b) Between 29 October 1999 and 28 April 2000.

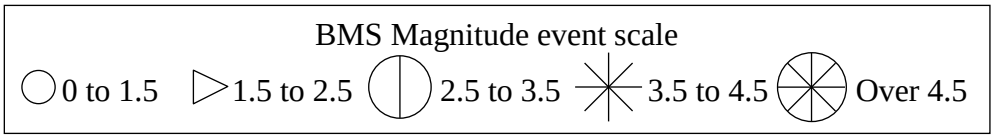

Figure 70. Plan view of the south end of 1000 Sill showing the seismic activity recorded in this region within 30m of the level between (a) 28 April 1999 and 28 October 1999; and, (b) 29 October 1999 and 28 April 2000.

Nevertheless, the substantial reduction in the seismicity after the choked destress blast in the 29-9 Pillar, both in terms of the total number of events and the number of large events (over a BMS Magnitude 4.5, or a Richter Magnitude of about +0.5) recorded, was interpreted as being an indication that the destress blast had achieved its objective of lowering the stress levels in the Bulk Zone to the East. Please note that Richter Magnitude events over about +1.8 are very rare at Brunswick Mine – the largest events are typically in the +0.5 to +1.2 Richter Magnitude range.

9.5.4. Borehole camera observations

The pre-blast survey in the most interesting downhole had to be stopped at a depth of 29.0m due to an accumulation of water and grease near the bottom of this hole. This accumulation could not be cleaned past this point due to a slip that partially obstructed the hole. The post-blast survey was carried out to a depth of 34.0m, where damage in the hole prevented further access. As a result, the last 5m of the downhole – where most of the interest lied – could not be compared before and after the destress blast. However, the sheer fact that the water drained is indicative of either a stress decrease (after the 130-9 Stope mass-blast, the destress blast, or both), or an increase in the fracture density, or both mechanisms.

The borehole camera surveys did not conclusively show that the destress blast fractured the rock mass. The dog-earing damage observed at the bottom of the hole, visible in Figure 71, could have been the result of high pre-destress blast static stresses, rather than the result of dynamic loading from the destress blast itself. It is difficult to conclude further, due to the absence of pre-blast information at the bottom of the observation hole.

An interesting point, however, is that the core from the downwards diamond drill hole at this depth did not show disking, which infers that the observed damage resulted in fact from a stress increase due to mining activity in the region, or the destress blast, or both. The uphole survey conducted before the destress blast revealed no damage along the entire length of the hole. The post-blast survey in this hole showed moderate damage starting 2m

from the collar, in the form of cracking. These observations are consistent with an increase in the stress levels, which was confirmed by the stress cell results.

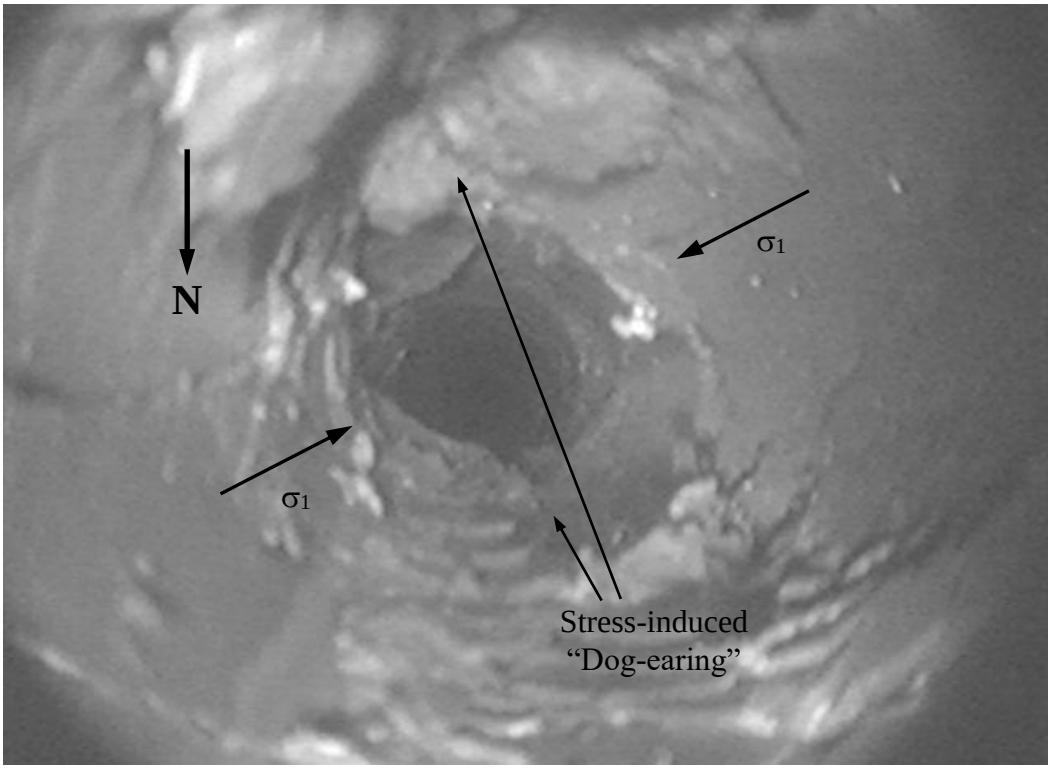

Figure 71. Photograph taken during the post-blast camera survey in the downhole, at a depth of 34.4m. (After Andrieux *et al*., 2000.)

9.5.5. Results from the stress cells

A complete history of the stress changes measured over the course of the project is given in Figure 72 – Table 37 provides a description of the mining events that are believed to have triggered the main stress jumps observed in this figure. The stress data associated with the 130-9 Stope mass-blast of 26 October and the 29-9 Pillar destress blast of 28 October are shown in more detail in Figure 73 (this figure is a zoomed view of the area highlighted in Figure 72.) It can be seen in Figure 72 and Figure 73 that the 26 October mass-blast in the 130-9 Stope led to a sizeable stress drop at the downhole gauge location, whereas it

resulted in a significant stress increase at the uphole gauge location, suggesting the wrapping of some of the ground stresses around the south abutment of the 130-9 Stope.

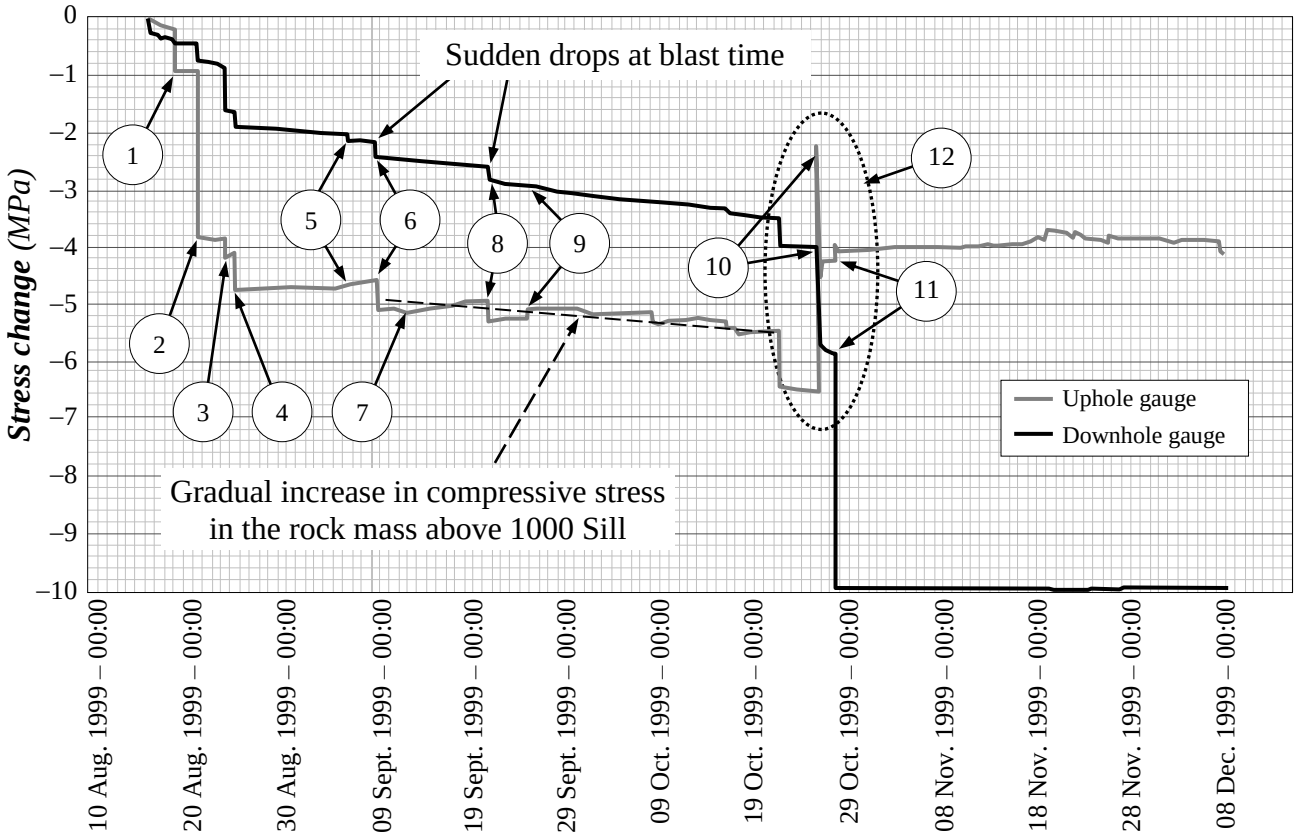

Figure 72. Complete datalogger results for the uphole and the downhole Geokon stress gauges. (After Andrieux *et al*., 2000.)

Table 37. Description of the mining events that triggered the selected stress jumps shown in Figure 72.

Event ID (as per Figure 72)	Date and time	Description
(1)	20 Aug. 1999, 06:16	M_R +1.6 event in the 130-7 Stope
(2)	22 Aug. 1999, ~18:00	22,025 tonne blast in the 131-7 Stope
(3)	25 Aug. 1999, ~18:00	Blast at end of dayshift
(4)	26 Aug. 1999, ~18:00	Blast at end of dayshift
(5)	06 Sept. 1999, ~18:00	33,000 tonne blast in the 124-4 Stope
(6)	09 Sept. 1999, ~18:00	500 tonne blast in the 324-8 Stope

Table 37 (continued). Description of the mining events that triggered the selected stress jumps shown in Figure 72.

Event ID (as per Figure 72)	Date and time	Description
⑦	12 Sept. 1999, ~04:00	*No explanation for this stress change*
⑧	21 Sept. 1999, ~18:00	42,335 tonne blast in the 229-7 Stope
⑨	25 Sept. 1999, ~21:00	*No explanation for this stress change*
⑩	26 Oct. 1999, 17:52	Mass-blast in the 130-9 Stope
⑪	28 Oct. 1999, 17:57	Destress blast in the 29-9 Pillar
⑫	Area zoomed in Figure 73	Detailed changes around the time of the destress blast

Notes: Events are arranged by sequential date of occurrence.
Event magnitudes are expressed in Local Richter Magnitude.

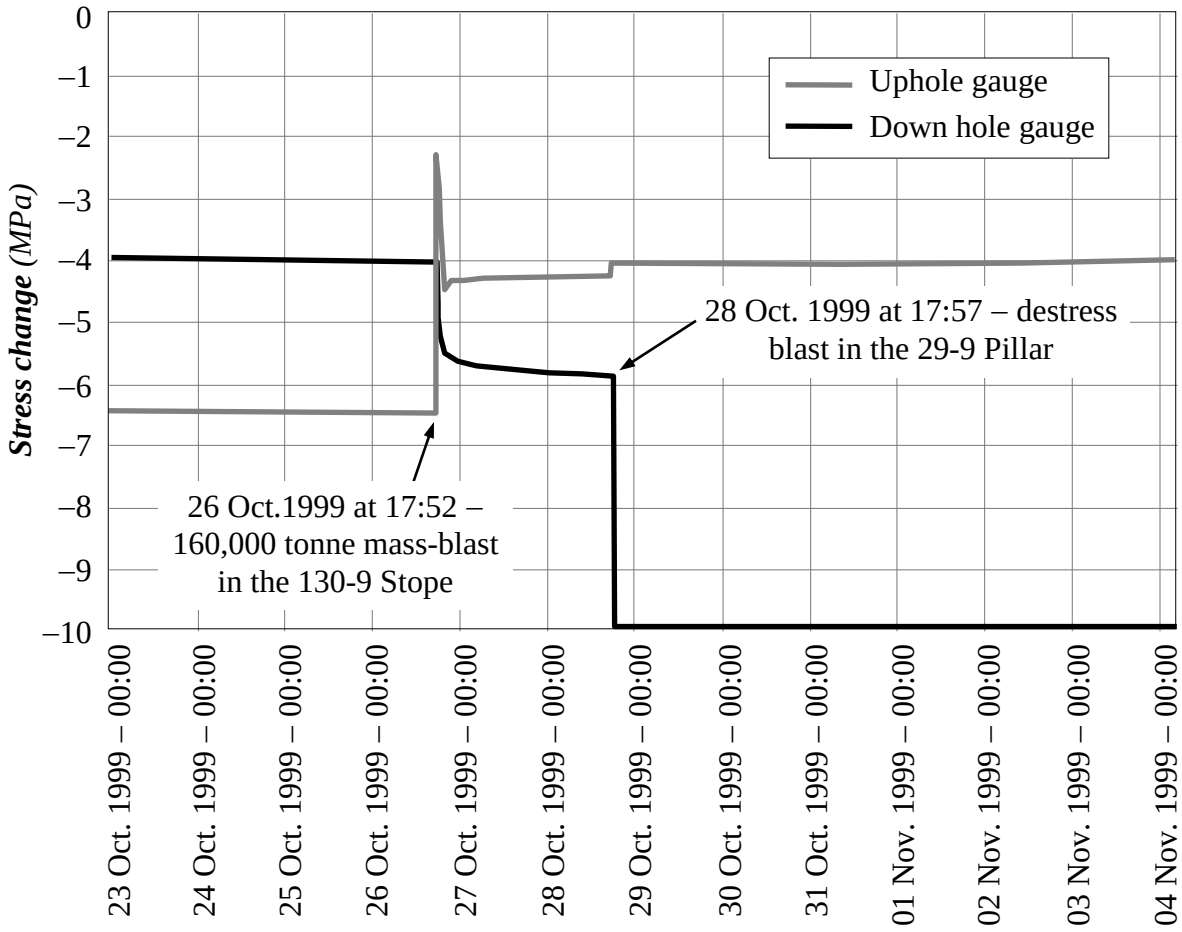

Figure 73. Datalogger results for the uphole and the downhole Geokon stress gauges from 23 October to 4 November 1999. (After Andrieux *et al*., 2000.)

As can be seen in Figure 73, the destress blast in the 29-9 Pillar led to a significant stress drop at the downhole gauge location and to a minor stress increase at the uphole gauge location, this time suggesting a significant destressing effect behind the pillar, as well as a stress wrapping effect above (and probably below) it.

This measured stress behaviour is entirely consistent with the results that would be expected from a successful destress blast in the 29-9 Pillar.

9.5.6. Results from the multi-point extensometers

Table 38 shows the values measured along the downhole multi-point extensometer, near the destress blast. Further to the values obtained on 28 October and 2 November (just before and after the 29-9 destress blast), the initial readings are also provided, for comparison purposes.

Table 38. Summary of the readings from the downhole extensometer. (After Andrieux *et al*., 2000.)

Anchor depth *(m)*	2 September 1999 *(ref.)*	28 October 1999	2 November 1999
27.0	+0.25 mm	+0.25 mm	–16.5 mm
24.5	+0.25 mm	+0.50 mm	–7.25 mm
22.0	+0.25 mm	+0.25 mm	+0.25 mm
19.5	+0.25 mm	+0.25 mm	0.00 mm
17.0	0.00 mm	0.00 mm	–1.50 mm
14.5	0.00 mm	0.00 mm	–1.50 mm

Further away from the destress blast ↓

Figure 74 shows the complete data recorded over the course of the project by all the anchors of the downhole instrument. As can be seen, very little change occurred prior to the destress blast. Significant changes were however observed following it, particularly at the lower two anchors (those nearest to the blast), which showed contractions of 16.75 mm at the bottom of the hole, and of 7.75 mm 2.5m higher.

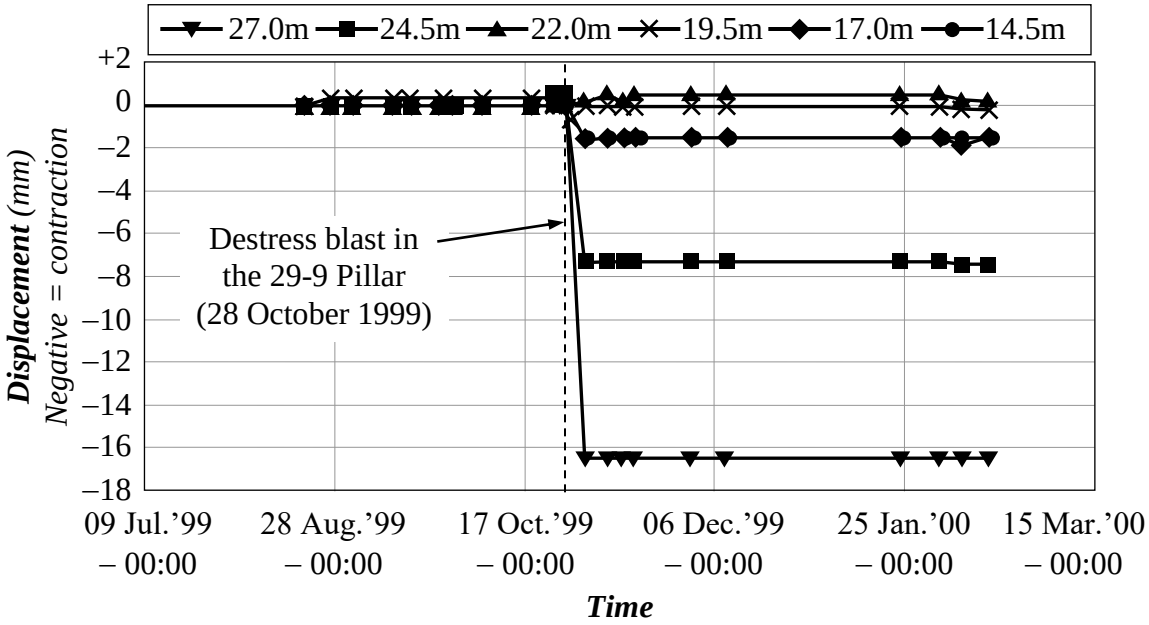

Figure 74. Displacements measured by the downhole multi-point extensometer. (After Andrieux *et al*., 2000.)

The contraction recorded indicates that the rock mass expanded in the vicinity of the destress blast, which, in turn, is indicative of an increase in the density of the fracture network. These are encouraging results, as they correspond to the effect the destress blast was expected to produce. As seen in Figure 74, the data are quite stable, and no significant further movement was recorded at any anchor in the downhole instrument after the destress blast was detonated.

The expansion measured in the destress blast region is interesting in light of the rationale that the hanging wall and footwall of the targeted zone must converge for destressing to occur. This highlights the requirement for some of the material to be ejected from the target region.

No movement was recorded along the other extensometer, in the uphole. It is believed that the stress increase above the 29-9 Pillar after the destress blast was insufficient to fracture and/or displace the rock mass at the location of the instrument.

9.5.7. Results from the cross-hole seismic surveys

As shown in Figure 75, series of vibrational signals were generated in the rock mass by a mechanical seismic source at 5m depth intervals (labelled in the figure by their depth from the collar on 1000-1 sub) in borehole "H", on the hanging wall side of the 29-9 Pillar. The advantage of using a mechanical seismic source, as compared to detonating seismic caps, is the higher degree of repeatability that can be achieved. These vibrations were recorded by a string of hydrophones in borehole "G", on the footwall side of the WOZ lens. Only the seismic source was incrementally lowered – the string of hydrophones, which covered the full length of the shorter footwall hole, remained stationary.

Please note that Figure 75 is schematic and was simplified for clarity: the distance between successive hydrophones on the string was in fact 1m, not 5m as suggested on the figure.

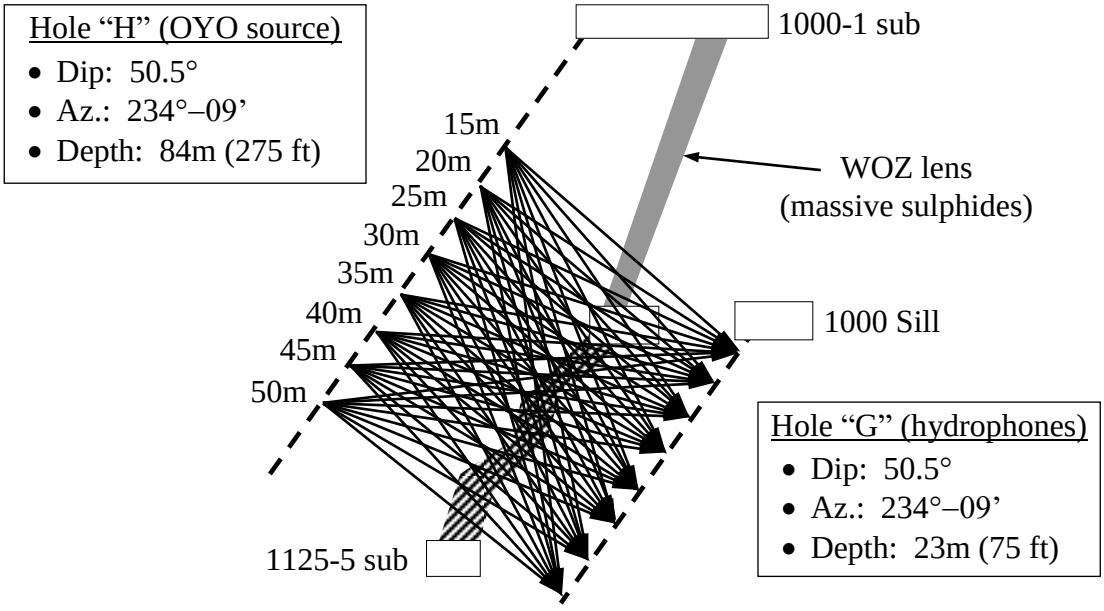

Figure 75. Cross-section looking north through the 29-9 Pillar showing the geometry of the cross-hole tomographic arrays.

The first series of analyses consisted in simply determining changes in P-wave rise times and arrival times for each of the parallel raypaths shown in Figure 76, and plotting them against source depth.

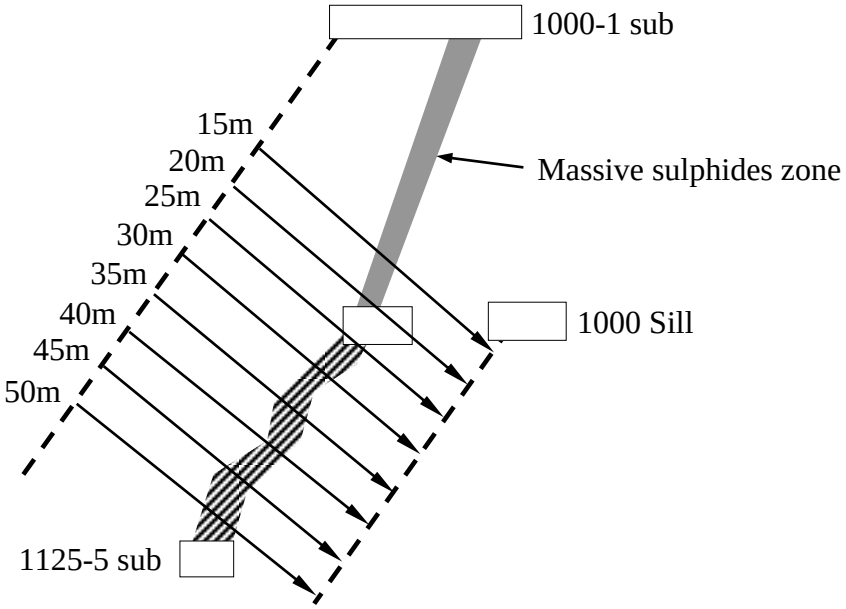

Figure 76. Cross-section looking north through the 29-9 Pillar showing the parallel raypaths used for the first series of seismic analyses. (After Andrieux *et al*., 2000.)

The results of these analyses are shown in Figure 77a for rise time changes, and Figure 77b for arrival time changes.

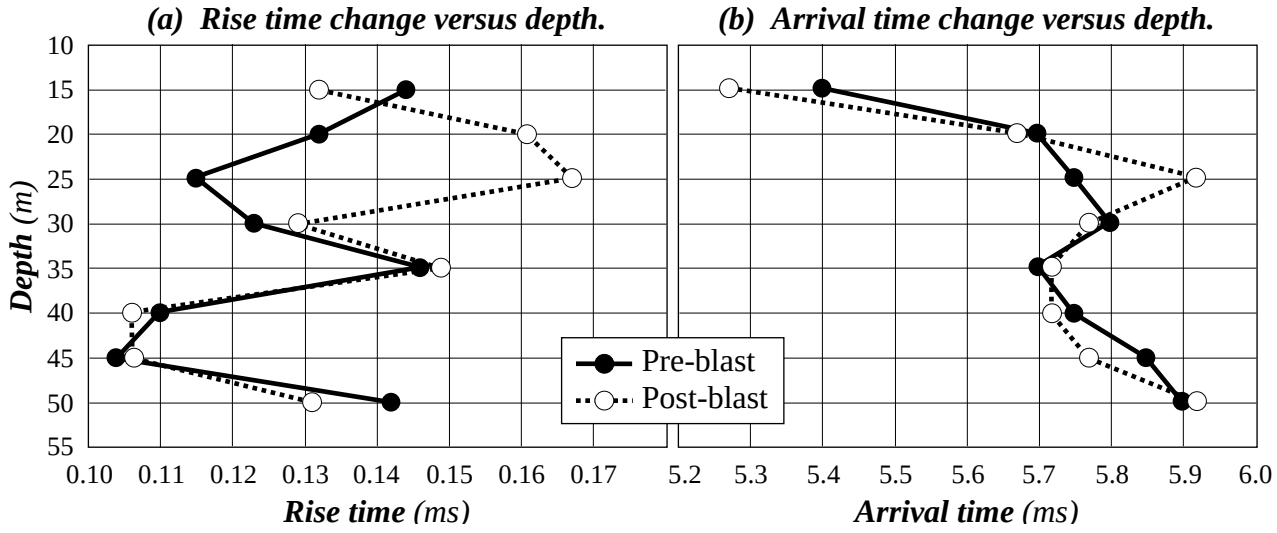

Figure 77. (a) Rise time change as a function of source depth; and, (b) arrival time change as a function of source depth. (After Andrieux *et al*., 2000.)

Rise time changes indicated a significant increase over a measured depth interval of 20-25m, with the rise time remaining near-constant below this depth. Arrival time data

remained quite constant, except at a depth of 25m where the signals were delayed in the post-blast survey, indicating a localised zone of damage, similarly to what was found with the rise time data.

Overall, the difference between the pre- and post-blast surveys suggested a region of localised damage immediately below the 1000 Sill elevation. No other regions were identified as having produced measurable changes in the seismic properties, suggesting relatively little measurable (by means of the analysis techniques used) blast-induced damage elsewhere.

The analyses were taken a step further by cross-correlating the pre- and post-destress blast P-wave velocity of propagation differences based upon all the raypaths shown in Figure 75. The cross-correlation of two complex functions $e(t)$ and $f(t)$ of a real variable t, denoted $e \star f$, is defined by:

$$e \star f = \bar{e}(-t) * f(t) \qquad \text{..... Eq. (34)}$$

Where * denotes convolution and $\bar{e}(t)$ is the complex conjugate of $e(t)$. Cross-correlation is essentially a statistical measure that times the movements and proximity of alignment between two data sets. Figure 78a shows the results of this analysis, which also highlighted a limited zone of rock mass damage in the same area as indicated by the previous analyses, immediately below the 1000 Sill elevation. The velocity change scale in Figure 78a is expressed relative to the average local east-west P-wave velocity of 5.2 m/ms, with negative change indicating a velocity reduction between the pre- and post-blast surveys.

The recorded data suggested that, with the experimental setup used, little detectable damage was caused to the rest of the rock mass comprising the 29-9 Pillar between 1000 Sill and 1125-5 sub. Interestingly, and as shown in Figure 78b, this zone of identified damage corresponded well to the volume of material that was ejected in the north end of the 29-9 Pillar during the destress blast, which was discussed in the caption of Figure 69. But, overall, the seismic surveys did not indicate that the destress blast resulted in significant measurable damage being inflicted to the bulk of the targeted pillar.

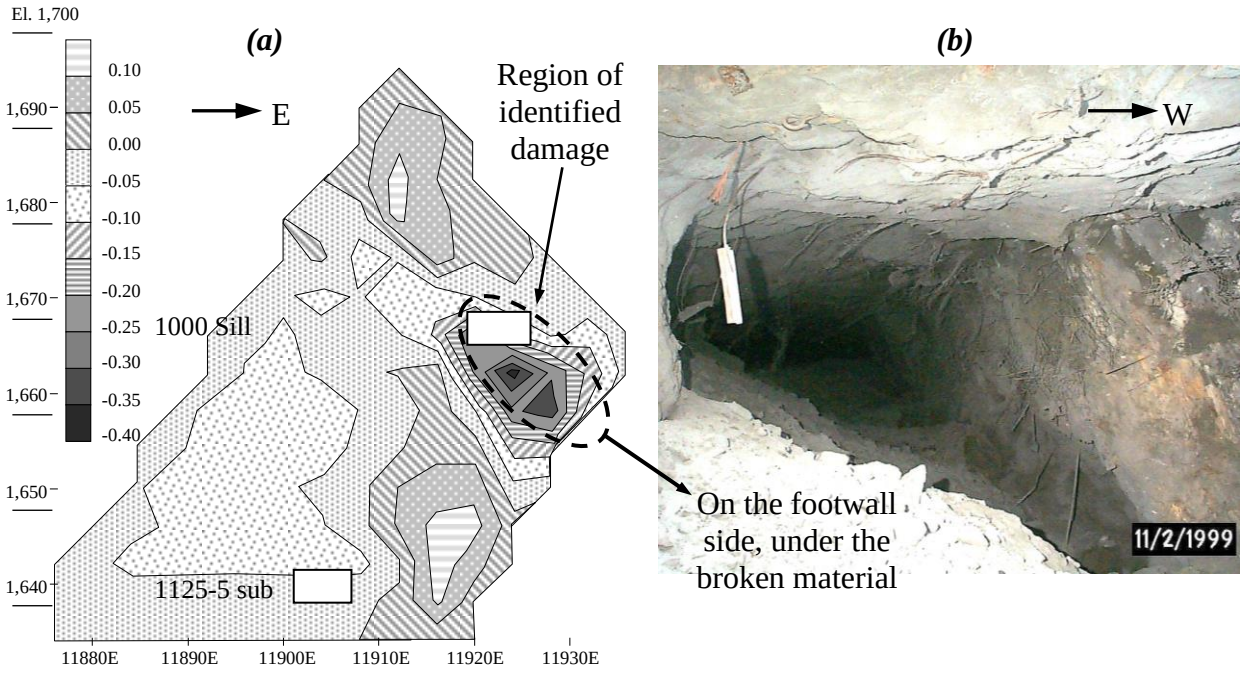

Figure 78. (a) Cross-correlated velocity difference image (cross-section looking north thought the 29-9 Pillar); and, (b) photograph looking south taken in the 29-9 Pillar overcut on 1000 Sill. (After Andrieux *et al*., 2000.)

Assuming that the destressing effect was to be the result of a blast-induced increase in the fracture network within the rock mass, this means that either the destress blast did not achieve this objective, or that the tomographic surveys were not sensitive enough to detect this change.

It should however be pointed out that the two holes used for the tomographic surveys were located quite far apart, due to access constraints. As a result, and as illustrated in Figure 79a, the difference between the pre- and post-blast mid-height raypath lengths that would have resulted from a "perfect" destress blast (through which no seismic energy would have propagated) would have been limited. On the other hand, and as shown in Figure 79b, this difference, in the case of more closely spaced holes, would have been much greater. In other words, it is possible that if the tomographic holes had been located closer together, more difference would have been detected between the pre- and the post-blast arrival time surveys.

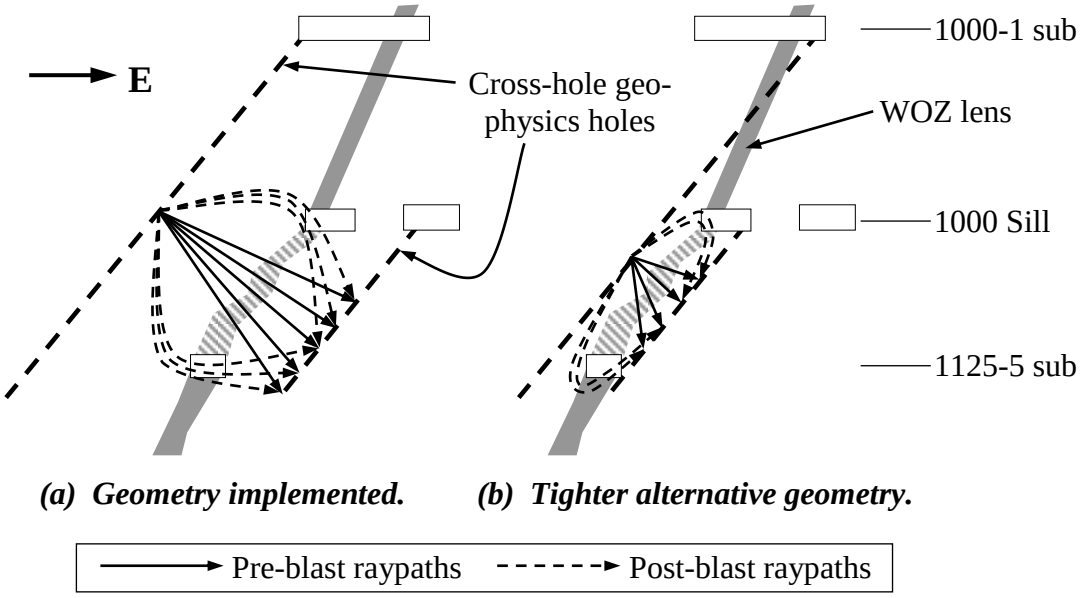

Figure 79. Influence of the distance between the tomographic holes on the assessment of the P-wave velocity of propagation difference before and after the destress blast.

An alternative way to look at this is as follows. Consider that the vibrational wave generated by a seismic source is forced to travel through a region of lower P-wave velocity in order to reach a receiver on the other side of this medium, as illustrated in Figure 80. Let Vp_A be the P-wave velocity of propagation in medium "A" and Vp_B the P-wave velocity of propagation in medium "B", with $Vp_A > Vp_B$.

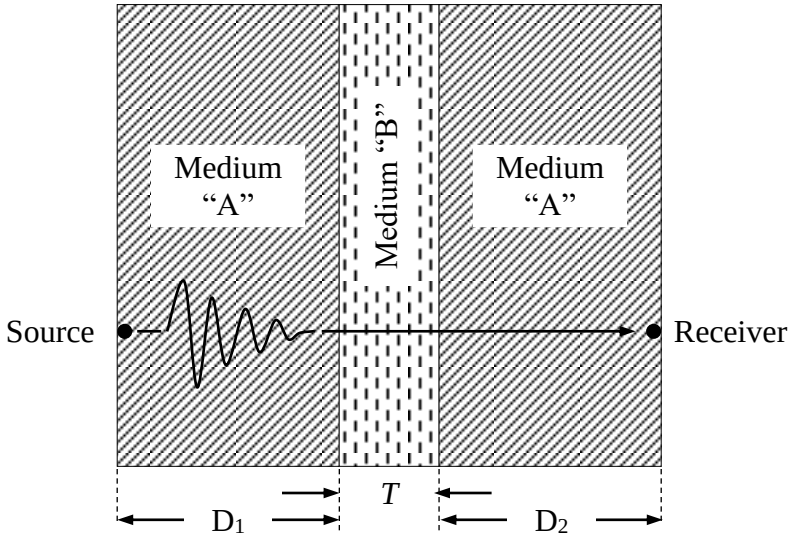

Figure 80. Schematic view showing a layer of lower P-wave velocity material (medium "B") sandwiched between two layers of a higher P-wave velocity medium (medium "A").

The vibrational wave will slow down while it travels through medium "B". The total travel time of the seismic wave between the source and the receiver will be $(D_1 / Vp_A) + (T / Vp_B) + (D_2 / Vp_A)$. As the relative thickness *T* of the central layer diminishes (as compared to that of the encasing medium "A"), the increase it causes in the total travel time becomes smaller, and, hence, more difficult to measure. For example, assume the values shown in Table 39, and assume that $D_1 = D_2 = 50$ metres and $Vp_A = 6{,}000$ m/s. As can be seen, as the thickness *T* of medium "B" decreases from 50m to 5m, and for the same P-wave velocity of propagation in this medium, the variation of the total travel time becomes significantly smaller, and, hence, more challenging to detect and measure.

Table 39. Theoretical variations in the travel time of a P-wave as a function of its velocity in medium "B" and the thickness of this medium.

P-wave velocity Vp_B in medium "B"	Thick-ness *T* of medium "B"	Total travel time from source to receiver	Total travel time variation	Thick-ness *T* of medium "B"	Total travel time from source to receiver	Total travel time variation
(km/s)	*(m)*	*(ms)*	*(%)*	*(m)*	*(ms)*	*(%)*
6.00	50.0	25.00	*Ref.*	5.0	17.50	*Ref.*
5.50	50.0	25.76	103	5.0	17.58	100
5.00	50.0	26.67	107	5.0	17.67	101
4.50	50.0	27.78	111	5.0	17.78	102
4.00	50.0	29.17	117	5.0	17.92	102
3.50	50.0	30.95	124	5.0	18.10	103
3.00	50.0	33.33	133	5.0	18.33	105
2.50	50.0	36.67	147	5.0	18.67	107
2.00	50.0	41.67	167	5.0	19.17	110
1.50	50.0	50.00	200	5.0	20.00	114
1.00	50.0	66.67	267	5.0	21.67	124
0.50	50.0	116.67	467	5.0	26.67	152
0.25	50.0	216.67	867	5.0	36.67	210

Note: Please refer to Figure 80 for a definition of the terminology used in this table.

These observations are summarised in Figure 81 – as can be seen, it is easier to measure changes in the P-wave velocity of propagation in medium "B" when its thickness is greater,

or, in other words, closer to that of the encasing layers. For example, for a value of Vp_B of 3,500 m/s, a 5m-thick layer of medium "B" would result in a 3.4% increase in the total travel time – a 50m-thick horizon would, on the other hand, yield a 23.8% increase in this travel time.

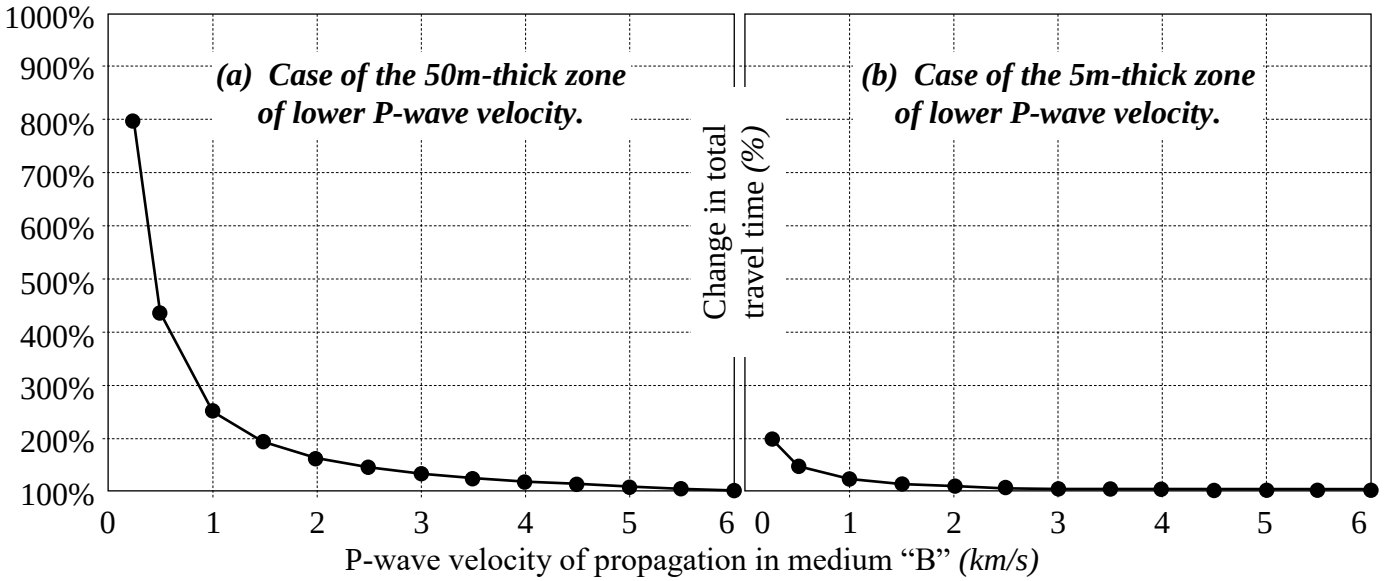

Figure 81. Theoretical variation of the P-wave travel time as a function of the relative thickness of the zone of interest.

In the case at hand, the thickness of the rock mass region targeted by the destress blast was much smaller than that of the massive sulphides layers on both sides of it. As a result, it would conceivably have been more difficult to measure the changes in the travel time of the P-waves that would have resulted from blast-induced damage in this region, as per Figure 81b. These comments also apply, to a certain extent, to the rise time measurements.

9.5.8. General conclusions from the observations and measurements

Based upon underground visual observations, there is little doubt that the destress blast caused extensive damage to the 29-9 Pillar. It is not possible to know in absolute terms to which levels the local ground stresses were reduced because no absolute stress measurements were available, neither before nor after the destress blast. However, in relative terms, a pair of uniaxial vibrating wire stress cells installed nearby provided strong

indication that the blast was successful in reducing the stress levels in the targeted region. The data from these particular instruments have been very reliable: in over six months of continuous measurements most changes in the records could be corroborated with either mining activities or significant seismic events. Multi-point extensometers also produced data consistent with those from the stress cells – a significant 16.75 mm contraction was measured at the bottom of the downhole unit (nearest to the destress blast), which indicates an expansion of the ground in the destress area, which, in turn, is indicative of an increase in the density of the fracture networks. Borehole camera observations made during the post-blast survey – mainly that the observed damage in the downhole was quite severe – were also indicative that the destress blast had affected the targeted region.

Overall, most observations and indications were consistent with a successful destress blast that effectively diverted the ground stresses away from the 29-9 Pillar and redistributed them above and below it.

9.6. DESTRESSABILITY INDEX ASSESSMENT

The previous section has demonstrated that the destress blast in the 29-9 Pillar did produce results consistent with a successful destressing effect. The Destressability Index that would have been associated with the rock mass conditions and the implemented blast design will now be evaluated, at both the intact rock material and the rock mass scales. The objectives are to assess how well this index would have "predicted" the outcome of the blast, and evaluate the scale at which it is the most accurate.

9.6.1. At the scale of the intact rock material

The first step in the calculation of the Destressability Index consists in quantifying the properties used to describe the first eight parameters of the RES interaction matrix at the intact rock material scale. Table 40 summarises the values associated with these properties.

Table 40. List of the basic properties and quantities required for the assessment of the Destressability Index at the intact rock material scale in the 29-9 Pillar.

Properties	Symbol	Unit	Value in 29-9
Density of the rock	ρ_r	*kg/m³*	4,300
Young's modulus of the intact rock material	$E_{Laboratory}$	*GPa*	130
Unconfined compressive strength of the intact rock material	$\sigma_{c\ Laboratory}$	*MPa*	235
Brittleness Index Modified ratio	BIM	–	1.10
Rock Mass Rating of the massive sulphides	RMR	*%*	85
Hoek-Brown parameter m of the intact rock material	$m_{Laboratory}$	–	16.000
Hoek-Brown parameter s of the intact rock material	$s_{Laboratory}$	–	1.000
Effective σ_1 component at the time of the destress blast	$\sigma_{1\ Actual}$	*MPa*	56 *
Effective σ_3 component at the time of the destress blast	$\sigma_{3\ Actual}$	*MPa*	30 *
Angle of incidence of the blast with respect to the σ_1 component	θ	*degrees*	90
Length of the pillar to destress	L	*m*	30.0 **
Height of the pillar to destress	H	*m*	27.2
Number of blasting rings in the destress blast	N	*#*	2
Diameter of the blastholes	D	*mm*	165.1
Distance between blasthole rings	B	*m*	2.40
Distance between blastholes on the same ring	S	*m*	2.40
Unloaded toe length in the blastholes ***	T	*m*	0.00
Unloaded collar length in the blastholes	C	*m*	5.0 ****
Usage of inert stemming material *****	–	*Yes* or *No*	Yes
Density of the explosive product	ρ_e	*g/cm³*	1.25
Absolute weight strength of the explosive	AWS	*cal/g*	645

* *as estimated with the 3DEC numerical stress simulations reported in Brummer* et al. *(2000).*

** *corrected to account for the geometrical shape of the blast (dumped rings on the north side).*

*** *use zero for non-breakthrough holes.*

**** *Minimum value – eventually irrelevant since already yielding the maximum charge confinement rating of 2.*

***** *add 50% confinement if stemming material is used.*

9.6.1.1.Step I – Calculation of the required design values

Proximity to static failure = $\sigma_1 / (\sigma_3 + [m_{Laboratory} \sigma_c \sigma_3 + s_{Laboratory} \sigma_c^{2}]^{0.5}) = 12.7\%$

Effective width of the targeted pillar $W_{Eff.} = ([N - 1] \times B) + (2 \times 16 \times D / 1000) \sim 7.7$m. (The 29-9 Pillar abutted against mined-out stopes, and, hence, no outside zone of influence needs to be considered in the north-south direction in this case.)

Effective length of the targeted pillar $L_{Eff.} = 30.0$m

Effective volume of the targeted pillar $V_{Eff.} = W_{Eff.} \times L_{Eff.} \times H = 6{,}275$ m³

Effective mass of the targeted pillar $M_{Eff.} = V_{Eff.} \times \rho_r / 1000 \sim 26{,}980$ tonnes

Charge confinement ratio = $(T + C) / (D / 1000) = (0 + [5 \times 1.5]) / (0.1651) = 45.4$. (50% is added to C because of the presence of inert stemming material in the collar.)

Total number of blastholes $N_b = 32$

Total explosive energy in the blast $E_{Blast} = 5.73$ Gcal

Unit energy in the blast $E_{Unit} = (E_{Blast} / M_{Eff.}) \times 10^{6} = 212.3$ cal/kg of rock

9.6.1.2.Step II – Rating of the parameters

Rating for parameter P_1 – Stiffness of the intact rock material:

$E_{Laboratory} = 130$. Using Table 6, the corresponding rating is 2, for a score of 28.

Rating for parameter P_2 – Brittleness of the intact rock material:

BIM = 1.10. Using Table 7, the corresponding rating is 2, for a score of 30.

Rating for parameter P_3 – Degree of fracturing of the rock mass:

RMR = 85%. Using Table 8, the corresponding rating is 2, for a score of 38.

Rating for parameter P_4 – Proximity to failure:

Proximity to static failure = 12.7%. Using Table 9, the corresponding rating is 1, for a score of 14.

Rating for parameter P_5 – Orientation of σ_1 :

$\theta = 90°$. Using Table 10, the corresponding rating is 2, for a score of 26.

Rating for parameter P_6 – Width of the target zone:

N = 2. Using Table 11, the corresponding rating is 1, for a score of 18.

Rating for parameter P_7 – Explosive energy per tonne of target zone:

E_{Unit} = 212.3 cal/kg of rock. Using Table 12, the corresponding rating is 1, for a score of 28.

Rating for parameter P_8 – Confinement of the explosive charges.

Charge confinement ratio = 45.4. Using Table 13, the corresponding rating is 2, for a score of 34.

9.6.1.3.Step III – Assessment of the Destressability Index

Table 41 summarises the rating and score associated with each parameter for the assessment of the Destressability Index at the intact rock material scale in the 29-9 Pillar at Brunswick Mine.

Table 41. Rating and score associated with each parameter for the assessment of the Destressability Index at the intact rock material scale in the 29-9 Pillar.

Parameter	Rating	Score
P_1 – Stiffness of the intact rock material	2	28
P_2 – Brittleness of the intact rock material	2	30
P_3 – Degree of fracturing of the rock mass	2	38
P_4 – Proximity to failure	1	14
P_5 – Orientation with respect to σ_1	2	26
P_6 – Width of the target zone	1	18
P_7 – Explosive energy per tonne of target zone	1	28
P_8 – Confinement of the explosive charges	2	34
	Total	216

The corresponding overall normalised score is thus (216 / 276) = 0.78, which, based upon Table 14, would correspond to a Destressability Index of 'Good'.

9.6.2. At the scale of the rock mass

As was done at the intact rock material scale, the first step in the calculation of the Destressability Index at the rock mass scale consists in quantifying the properties used to describe the first eight parameters of the RES interaction matrix at that particular scale. Table 42 summarises the values associated with these properties.

Table 42. List of the basic properties and quantities required for the assessment of the Destressability Index at the rock mass scale in the 29-9 Pillar.

Properties	Symbol	Unit	Value in 29-9
Density of the rock	ρ_r	*kg/m³*	4,300
Young's modulus of the intact rock material	$E_{Laboratory}$	*GPa*	130
Unconfined compressive strength of the intact rock material	$\sigma_{c\ Laboratory}$	*MPa*	235
Rock Mass Rating of the massive sulphides	RMR	*%*	85
Hoek-Brown parameter m of the intact rock material	$m_{Laboratory}$	–	16.000
Hoek-Brown parameter s of the intact rock material	$s_{Laboratory}$	–	1.000
Effective σ_1 component at the time of the destress blast	$\sigma_{1\ Actual}$	*MPa*	56 *
Effective σ_3 component at the time of the destress blast	$\sigma_{3\ Actual}$	*MPa*	30 *
Angle of incidence of the blast with respect to the σ_1 component	θ	*degrees*	90
Length of the pillar to destress	L	*m*	30.0 **
Height of the pillar to destress	H	*m*	27.2
Number of blasting rings in the destress blast	N	*#*	2
Diameter of the blastholes	D	*mm*	165.1
Distance between blasthole rings	B	*m*	2.40
Distance between blastholes on the same ring	S	*m*	2.40
Unloaded toe length in the blastholes ***	T	*m*	0.00
Unloaded collar length in the blastholes	C	*m*	5.0 ****

Table 42 (continued). List of the basic properties and quantities required for the assessment of the Destressability Index at the rock mass scale in the 29-9 Pillar.

Properties	Symbol	Unit	Value in 29-9
Usage of inert stemming material *****	–	*Yes* or *No*	Yes
Density of the explosive product	ρ_e	*g/cm³*	1.25
Absolute weight strength of the explosive	AWS	*cal/g*	645

* *as estimated with the 3DEC numerical stress simulations reported in Brummer* et al. *(2000).*

** *corrected to account for the geometrical shape of the blast (dumped rings on the north side).*

*** *use zero for non-breakthrough holes.*

**** *Minimum value – eventually irrelevant since already yielding the maximum charge confinement rating of 2.*

***** *add 50% confinement if stemming material is used.*

9.6.2.1.Step I – Calculation of the required design values

$E_{Rock\ Mass} = E_{Laboratory} \times ([\ 0.000028 \times RMR^{2}\ ] + [\ 0.009 \times e^{\{RMR/22.82\}}]) = 74.8$ GPa

$GSI = RMR - 5 = 85 - 5 = 80$

$m_{Rock\ Mass} = m_{Laboratory} \times e^{([GSI - 100]/28)} = 7.833$ (undisturbed, before the destress blast)

$s_{Rock\ Mass} = s_{Laboratory} \times e^{([GSI - 100]/9)} = 0.108$ (undisturbed, before the destress blast)

$\sigma_{c\ Rock\ Mass} = \sigma_3 + ([\ m_{Rock\ Mass}\ \sigma_c\ \sigma_3\ ] + [\ s_{Rock\ Mass}\ \sigma_c^{2}\ ])^{0.5}$, for $\sigma_3 = 0$, which is 77.4 MPa

$\sigma_{T\ Rock\ Mass} = (\ m_{Rock\ Mass}\ \sigma_c - [\ m_{Rock\ Mass}^{2}\ \sigma_c^{2} - 4\ s_{Rock\ Mass}\ \sigma_c^{2}\ ]^{0.5}\ )/2$ (quadratic formulae for $\sigma_1 = 0$), which is 3.3 MPa

$B_1 = \sigma_{c\ Rock\ Mass} / \sigma_{T\ Rock\ Mass} = (47.4 / 2.90) = 23.8$

Proximity to failure $= \sigma_1 / (\ \sigma_3 + [\ m_{Rock\ Mass}\ \sigma_c\ \sigma_3 + s_{Rock\ Mass}\ \sigma_c^{2}\ ]^{0.5}\ ) = 20.2\%$

Effective width of the targeted pillar $W_{Eff.} = ([N - 1] \times B) + (2 \times 16 \times D / 1000) \sim 7.7$m. (Again, the 29-9 Pillar abutted against mined-out stopes, and, hence, no outside zone of influence needs to be considered in the north-south direction in this case.)

Effective length of the targeted pillar $L_{Eff.} = 30.0$m

Effective volume of the targeted pillar $V_{Eff.} = W_{Eff.} \times L_{Eff.} \times H = 6{,}275$ m³

Effective mass of the targeted pillar $M_{Eff.} = V_{Eff.} \times \rho_r / 1000 \sim 26{,}980$ tonnes

Charge confinement ratio = (T + C) / (D / 1000) = 45.4. (50% was added to C because of the presence of inert stemming material in the collar.)

Total number of blastholes $N_b = 32$

Total explosive energy in the blast $E_{Blast} = 5.73$ Gcal

Unit energy in the blast $E_{Unit} = (E_{Blast} / M_{Eff.}) \times 10^6 = 212.3$ cal/kg of rock

9.6.2.2.Step II – Rating of the parameters

Rating for parameter P_1 – Stiffness of the rock mass:

$E_{Rock\ Mass} = 74.8$. Using Table 17, the corresponding rating is 2, for a score of 26.

Rating for parameter P_2 – Brittleness of the rock mass:

$B_1 = 23.8$. Using Table 18, the corresponding rating is 2, for a score of 26.

Rating for parameter P_3 – Degree of fracturing of the rock mass:

RMR = 85. Using Table 19, the corresponding rating is 2, for a score of 28.

Rating for parameter P_4 – Proximity to failure:

Proximity to failure = 20.2%. Using Table 20, the corresponding rating is 0, for a score of 0.

Rating for parameter P_5 – Orientation of σ_1 :

$\theta = 90°$. Using Table 22, the corresponding rating is 2, for a score of 26.

Rating for parameter P_6 – Width of the target zone:

N = 2. Using Table 23, the corresponding rating is 1, for a score of 18.

Rating for parameter P_7 – Explosive energy per tonne of target zone:

E_{Unit} = 212.3 cal/kg of rock. Using Table 24, the corresponding rating is 1, for a score of 24.

Rating for parameter P_8 – Confinement of the explosive charges:

Charge confinement ratio = 45.4. Using Table 25, the corresponding rating is 2, for a score of 34.

9.6.2.3.Step III – Assessment of the Destressability Index

Table 43 summarises the rating and score associated with each parameter for the calculation of the Destressability Index at the rock mass scale in the 29-9 Pillar.

Table 43. Rating and score associated with each parameter for the assessment of the Destressability Index at the rock mass scale in the 29-9 Pillar.

Parameter	Rating	Score
P_1 – Stiffness of the rock mass	2	26
P_2 – Brittleness of the rock mass	2	26
P_3 – Degree of fracturing of the rock mass	2	28
P_4 – Proximity to failure	0	0
P_5 – Orientation with respect to σ_1	2	26
P_6 – Width of the target zone	1	18
P_7 – Explosive energy per tonne of target zone	1	24
P_8 – Confinement of the explosive charges	2	34
	Total	182

The corresponding overall normalised score is thus (182 / 252) = 0.72, which, based upon Table 26, would again correspond to a Destressability Index of ‘Good’.

CONCLUSION DU CHAPITRE. Le calcul d’un Index de relâchement de ‘bon’ aux échelles du matériel intact et du massif rocheux est raisonnablement en accord avec les observations et les mesures faites sur le terrain suite à la détonation du tir confiné à grande échelle de relaxation des contraintes d’octobre 1999 dans le pilier 29-9 à la mine Brunswick. Toutes

les indications, excepté peut-être celles provenant des mesures géophysiques, ont indiqué clairement qu'une réduction significative du niveau de contraintes a eu lieu dans la région, d'une manière consistante avec un tir réussi pour lequel un 'bon' résultat aurait été prédit. Ce chapitre a donc établi que le sautage a fonctionné de manière satisfaisante et que la méthodologie de l'Index de relâchement aurait été utile dans la mesure où elle aurait prédit ce résultat correctement.

Ce chapitre a également démontré que les données requises par la méthodologie sont faciles à obtenir et que l'approche est relativement simple à utiliser.

Une autre étude de cas détaillée d'un sautage confiné à grande échelle de relaxation des contraintes dans un pilier de mine va être présentée dans le prochain chapitre de manière à davantage valider la méthode.

CHAPTER CONCLUSION. The calculation of a 'Good' Destressability Index at both the intact rock material and the rock mass scales is in reasonable accordance with the field results observed and measured underground following the detonation of the large-scale confined destress blast of October 1999 in the 29-9 Pillar at Brunswick Mine. All indications, except perhaps from the geophysics-based assessment techniques, clearly indicated that a significant stress reduction occurred in the region, consistent with a successful destress blast for which a 'Good' outcome would have been predicted. Hence, this chapter has established that the destress blast worked to a satisfactory extent, and that the Destressability Index methodology would have been useful in the sense that it would have correctly predicted this outcome.

This chapter also demonstrated that the input values required by the methodology are easily and readily obtainable, and that the approach is relatively simple to use.

Another detailed case history of a large-scale choked pillar destress blast will be presented in the next chapter in order to further validate the method.

CHAPTER X

10. SECOND CASE STUDY – DESTRESS BLAST IN THE 42-1-080 PILLAR AT THE FRASER COPPER MINE

SOMMAIRE DU CHAPITRE. Deux études de cas entièrement instrumentées et documentées sont présentées dans cette thèse afin de valider la méthodologie de l'Index de relâchement présentée au Chapitre VIII. La première étude de cas constituait le sujet du chapitre précédent – la seconde va être discutée en détail au Chapitre X. Le tir de relâchement des contraintes présenté dans cette deuxième étude de cas a été détoné en décembre 2001 dans le gisement de cuivre de la mine Fraser de Falconbridge limitée, dans un pilier de gneiss felsique à proximité de la lentille "A5-Right" et de l'accès 42-1-080. Comme pour la première étude de cas, l'historique et le raisonnement ayant conduit à la décision de tenter un tel sautage sont brièvement présentés dans un premier temps, ainsi que les contraintes et les restrictions pratiques qui étaient associées au projet. Le design du tir, ainsi que les divers types d'instrumentation utilisés pour évaluer son comportement sur le terrain et ses résultats sont ensuite décrits.

Les résultats obtenus sont ensuite présentés et discutés, des points de vue des performances sur le terrain, des observations visuelles post-tir et des résultats provenant des instruments installés. Comme pour l'étude de cas du Chapitre IX, cette section est assez détaillée car le degré de succès atteint par le tir doit être clairement établi afin de pouvoir évaluer avec confiance l'exactitude de la prévision que l'Index de relâchement aurait faite. Deux valeurs de l'Index de relâchement sont par la suite calculées – une à l'échelle du matériel intact et une à l'échelle du massif rocheux – auxquelles la performance du sautage est comparée de manière à évaluer dans quelle mesure et avec quelle précision cet outil aurait pu prédire les résultats du tir.

La description de cette étude de cas est largement basée sur le rapport de mars 2002 préparé pour Falconbridge limitée et intitulé “Report on the Destress Blast of 24 December 2001 in 42-1-1620 Stope, 080 Access, Fraser Copper Mine” (*Rapport sur le sautage de relaxation des contraintes du 24 décembre 2001 dans le chantier 42-1-1620, Accès 080, à la mine Fraser Copper*) par Sampson-Forsythe, Andrieux et Brummer. La contribution spécifique de l’auteur aux travaux décrits dans ce rapport est la suivante. En tant que consultant externe il a formulé la recommandation formelle d’aller de l’avant avec un tir confiné à grande échelle de relâchement des contraintes dans la lentille A5-Right. Une fois la décision prise par la direction de Falconbridge, l’auteur a conçu le sautage et a installé une partie de l’instrumentation (les cellules de contrainte et les géophones d’enregistrement des vibrations de sautage) sous terre avec les ingénieurs du site. Une fois le sautage effectué, il a d’abord analysé et interprété les données, puis a été le principal contributeur au rapport en question. La description des travaux est plus élaborée dans cette thèse que dans le rapport – elle offre ici des détails additionnels et un meilleur aperçu du projet. La section 10.6, qui traite de l’évaluation de l’Index de relâchement, est quant à elle entièrement originale et a été rédigée spécifiquement dans le cadre des travaux de doctorat rapportés dans cette thèse.

CHAPTER SUMMARY. Two well-instrumented and fully-documented case histories are presented in this thesis to validate the Destressability Index methodology described in Chapter VIII. The first case study was the topic of the previous chapter – the second one will be discussed in detail in Chapter X. The destress blast presented in this second case study was detonated on the Copper side of the Falconbridge Limited Fraser Mine in December 2001, in a felsic gneiss pillar by the A5-Right lens / 42-1-080 Access. As for the first case study, the background and rationale behind the decision to implement a large-scale choked panel destress blast in the first place are presented, along with the associated practical constraints and limitations. The design of the blast and the instrumentation used to assess its results are subsequently described.

The results achieved are then presented and discussed, from the perspectives of field performance, visual post-blast observations and instrumentation results. As for the case study of Chapter IX, this section is quite detailed because the degree of success achieved by the destress blast must be clearly established in order to reliably determine the accuracy of the prediction the Destressability Index methodology would have made. Two Destressability Index values are then calculated – one at the scale of the intact rock material and one at that of the rock mass – against which the field performance of the destress blast is compared in order to assess how valuable a tool each would have been to predict the outcome of the blast.

A description of this case study was previously provided in a March 2002 report to Falconbridge Limited entitled *Report on the Destress Blast of 24 December 2001 in 42-1-1620 Stope, 080 Access, Fraser Copper Mine* by Sampson-Forsythe, Andrieux and Brummer. The specific contribution of the author to the work that was described in this report is as follows. As the consulting engineer involved in this project, he made the formal recommendation to implement a large-scale choked destress blast in the A5-Right

lens. Once the decision to go ahead had been made by Falconbridge management, the author designed the blast and installed some of the instrumentation underground (the stress cells and the blast vibration monitors) with the site engineers. After the blast was fired, he analysed and interpreted the data, then was the principal contributor to the report aforementioned. As was the case with the Brunswick Mine case study presented in the previous chapter, the description provided in this thesis goes further than the one in the report, as it affords additional detail and offers more insight. Section 10.6, on the assessment of the Destressability Index, is entirely original and was developed specifically within the framework of this thesis.

10.1. INTRODUCTION AND BACKGROUND

A large-scale choked panel destress blast was fired 24 December 2001 at 15:56 EST in the A5-Right / 42-1-080 Access Pillar area on the Copper side of the Falconbridge Limited Fraser Mine, a region of the mine exploited by an overhand cut-and-fill method. This blast was extensively instrumented as it constituted the first such attempt in the highly stressed Fraser Copper Mine, and due to the fact that confined panel destress blasting had the potential to help in future sill pillar mining situations. The objective of this blast was to deflect the high mining-induced sub-horizontal north-south stress component in the 42-1-1620 Stope two to four cuts above Cut #22 (the next one to be exploited), away from mining activity. It was also expected that this stress increase in the sill pillar would be sufficient to fail it and result in easier mining conditions in the remaining cuts. Figure 82 shows a composite plan view of Cut #21 from the 42-1-080 and 42-1-133 accesses on the 42 Level, on which the largest rockbursts experienced between July 1999 and March 2001 in the 39 Sill (west of the 42-1-133 Ramp Access) are shown.

The mining of Cut #21 in the 42-1-1620 Stope took nearly two years to complete, between January 2000 and December 2001, which is twice as long as previous cuts in this region. (This time period however included a seven month labour dispute from August 2000 to February 2001.) The main reason why mining was so slow in this cut was the occurrence of heavy seismic activity, as shown in Figure 82. The events shown in this figure are described in more detail in Table 44.

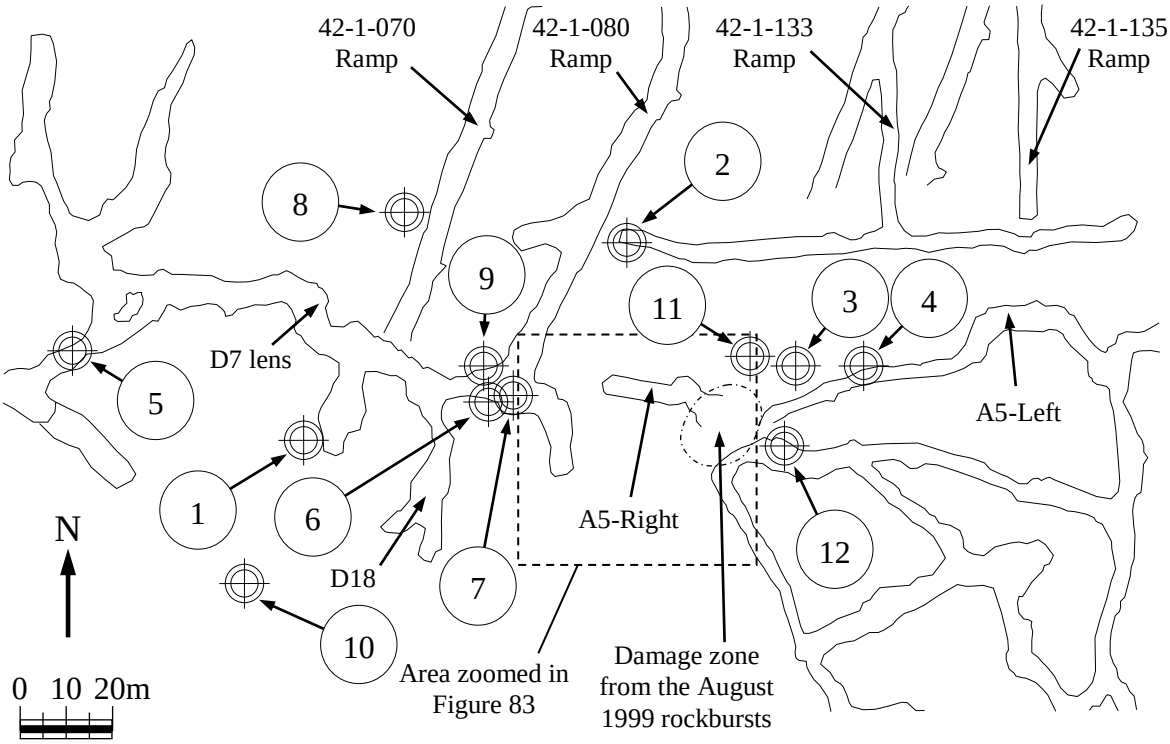

Figure 82. Composite plan view of the 42-1-1620 Stope, Cut #21, showing the location of the major rockbursts experienced in the 39 Sill west of the 42-1-133 Ramp Access, from July 1999 to March 2001.

Table 44. Summary of the largest seismic events recorded in the 39 Sill west of the 42-1-133 Ramp Access, from July 1999 to March 2001.

Event ID in Figure 82	Date and time	Nuttli Magnitude
1	09 Jul. 1999, 14:45	M_N +1.8
2	25 Jul. 1999, 14:52	M_N +2.5
3	04 Aug. 1999, 11:08	M_N +2.6
4	08 Aug. 1999, 09:07	M_N +1.3
5	27 Jan. 2000, 08:39	M_N +0.8
6	02 Feb. 2000, 11:15	M_N +1.0

Event ID in Figure 82	Date and time	Nuttli Magnitude
7	04 Feb. 2000, 15:31	M_N +1.1
8	07 Feb. 2000, 10:59	M_N +1.9
9	01 Mar. 2000, 23:13	M_N +1.9
10	21 Mar. 2000, 11:55	M_N +1.8
11	21 Mar. 2001, 14:31	M_N +2.5
12	01 Jul. 2000, 00:10	M_N +2.2

Please note that the Nuttli Magnitude (M_N) scale corresponds approximately to the Richter Magnitude (M_R) scale + 0.3. For example, a given M_R +1.0 event would be given more or less a +1.3 Nuttli Magnitude.

Several major rockbursts had occurred in the felsic gneiss and Sudbury breccia footwall rock units, near prominent waste pillars, as well as by the east and west abutments of the sill pillar. Historically, the largest seismic event in the region was a +2.6 Nuttli Magnitude rockburst, which occurred 4 August 1999 and resulted in about 80 tonnes of material being displaced. There were also other significant rockbursts in the 42-1-1620 Stope while mining Cut #21, but they located east of the 42-1-133 Access and were not in close proximity to the area eventually targeted for destress blasting.

The redistribution of ground stresses in the 42-1-1620 Stope as mining progressed was identified as the main contributor and triggering mechanism for the seismicity and rockbursting in the area. A diamond drill hole in the A5-Right / 080 Access pillar showed borehole breakouts indicative of high sub-vertical stresses in the immediate footwall of the ore lens, due to the wrapping of the mining-induced sub-horizontal north-south major principal stress component around the void created by the extracted cuts below. What made the narrow A5-Right ore lens particularly difficult was the absence of hanging wall stringers south of it (please refer to Figure 82), which provided a certain “softening” effect in other areas, and the presence of a large footwall waste pillar adjacent to the 42-1-080 Access, which had great energy storage capabilities. The potential for severe rockbursting in this region was likely to increase as each successive mining cut resulted in yet more stress being concentrated above the 42-1-1620 Stope, until the load would eventually become high enough to fail the sill pillar. This, based upon numerical modelling (Pierce & Board, 1999[a], 1999[b]), was not expected to occur until just one or two cuts remained.

Based upon all these considerations, a large-scale choked panel destress blast was attempted in order to facilitate the extraction of the next few cuts, and with the expectation that the sudden stress increase would accelerate the global failure of the sill pillar above.

10.2. DESTRESS BLAST SITE AND ASSOCIATED CONSTRAINTS

The 080 Access / A5-Right felsic gneiss pillar area on the footwall (north) side of the ore lenses was targeted for destress blasting. It was however unlikely that the pillar itself could be effectively destressed without causing significant collateral damage to the 42-1-080 access, which constituted a critical access to the high grade D7, D18 and A5-Right ore lenses. As a result, the approach retained consisted in firing a relatively narrow but still large-scale confined panel destress blast south of the A5-Right / 080 Access Pillar area, on the hanging wall side of the ore stringers complex.

The objective was to cut off some of the high mining-induced sub-horizontal north-south stress component in the sill pillar above Cut #21 (where full-entry mining needed to resume next), and redistribute it higher, away from active mining areas. Figure 83 shows a schematic plan view of the A5 stringer and the location of the destress blastholes.

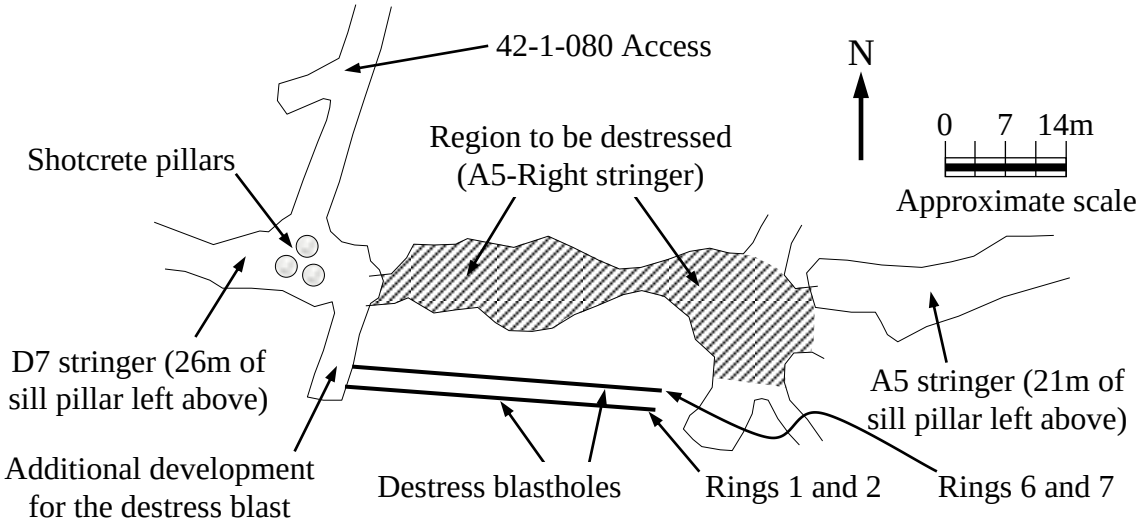

Figure 83. Schematic plan view showing the A5 stringers and the area targeted by the destress blast.

In order to perform the destress blast from outside the targeted area, four rounds of extra development (3.5m wide by 3.5m high) were taken in the immediate hanging wall, off the 42-1-080 Access, as shown in Figure 83. Two main constraints were considered during the

design of the destress blast: the preservation of the 42-1-080 Access for the next four cuts (or two years) and maximum ore recovery from the A5-Right stringer (i.e., minimum collateral damage in this area).

The benefits from the destress blast were expected to largely outweigh the overall cost of the project. The rockbursting activity that had occurred in the 42-1-080 Access and A5-Right pillar had caused significant damage to the mine openings, which resulted in production delays and losses, as well as in extensive rehabilitation work being required in the affected areas.

10.3. DESIGN OF THE DESTRESS BLAST

Several general assumptions and premises were established at an early stage relating to the rock mass, the drilling parameters and the explosive products to be used. Firstly, the destress blast was to be implemented in the felsic gneiss geological unit, on the hanging wall side of the A5 lens. As shown in Figure 83 and Figure 85, two parallel rows of fanned destress blastholes were to be drilled eastwards and upwards from the proposed hanging wall development – considering the amount of extra development that could be done in the allocated time window with the resources available, this was all that could be fitted. The blastholes were to be 114.3 mm (4.5 inches) in diameter, mainly because the mine was already equipped to drill this hole size. A 3m by 3m drilling pattern was retained, as measured at the toe of the blastholes. The maximum blasthole length was limited to 30m in order to maintain drilling accuracy with the selected drilling diameter. The blastholes were to be non-breakthrough.

Based upon the geometry of the volume targeted (which was controlled to a large extent by the 30m maximum drilling depth) and the proposed 3m by 3m drilling pattern, a total of 28 fanned blastholes were required (14 per row). As sketched in Figure 84 and in order to simplify the drilling operations and avoid overcrowding in the collar region, each of the

two rows of blastholes was drilled in a staggered manner, whereby every second blasthole along each row was offset by about 30 cm towards the centre of the volume to destress. As a result, the blastholes along the outside lines of each row were 3m apart, whereas those along the inside lines were approximately 2.4m apart.

The explosive product retained was Handi-Bulk, a booster-sensitive re-pumpable bulk emulsion supplied by Orica and routinely used at the time at all the Falconbridge Sudbury operations. This product has a density of 1.25 g/cm³, a velocity of detonation (VOD) of 6,000 m/s, a relative weight strength (RWS) of 0.95, and an absolute weight strength (AWS) of 0.95 × 912 cal/g (for AnFO) = 866 cal/g. The charges were to be fully coupled to the blastholes, and no decking was to be used.

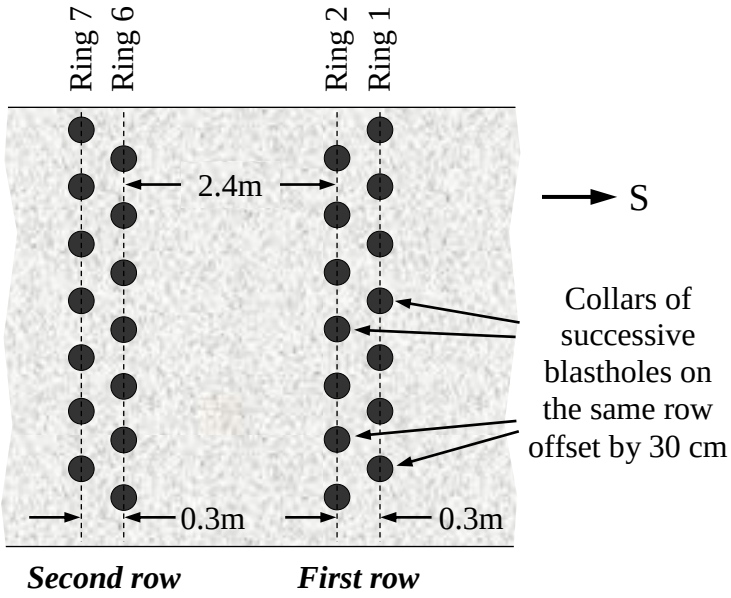

Figure 84. Schematic elevation view (not to scale) looking at the east wall of the proposed hanging wall drilling drift, and showing the offset blasthole collars.

Collar length adjustments were required due to the fanned nature of the drilling pattern, in order to evenly distribute the explosive energy throughout the blast, avoid cut-offs in the collar region and reduce the risk of product desensitisation. Each blasthole had an unloaded collar length of at least 5m, which corresponded to about twice what would be implemented for “normal” blasthole operations, or approximately twice 25 times the

blastholes diameter (which would correspond to 5.7m). This was meant to maximise the confinement of the explosive charges in order to provide the maximum destressing effect. Figure 85 shows the drilling pattern and the explosive loading design retained – rings #1 and #2, and #6 and #7 relate to the slightly offset series of blastholes on each row.

Based upon the individual charges designed for the destress blast, which added to nearly 4.4 tonnes of explosives, and considering the 866 cal/g AWS of the bulk emulsion product to be used, the total energy for the entire blast came to $3{,}790 \times 10^6$ calories, or about 3.8 Gcal.

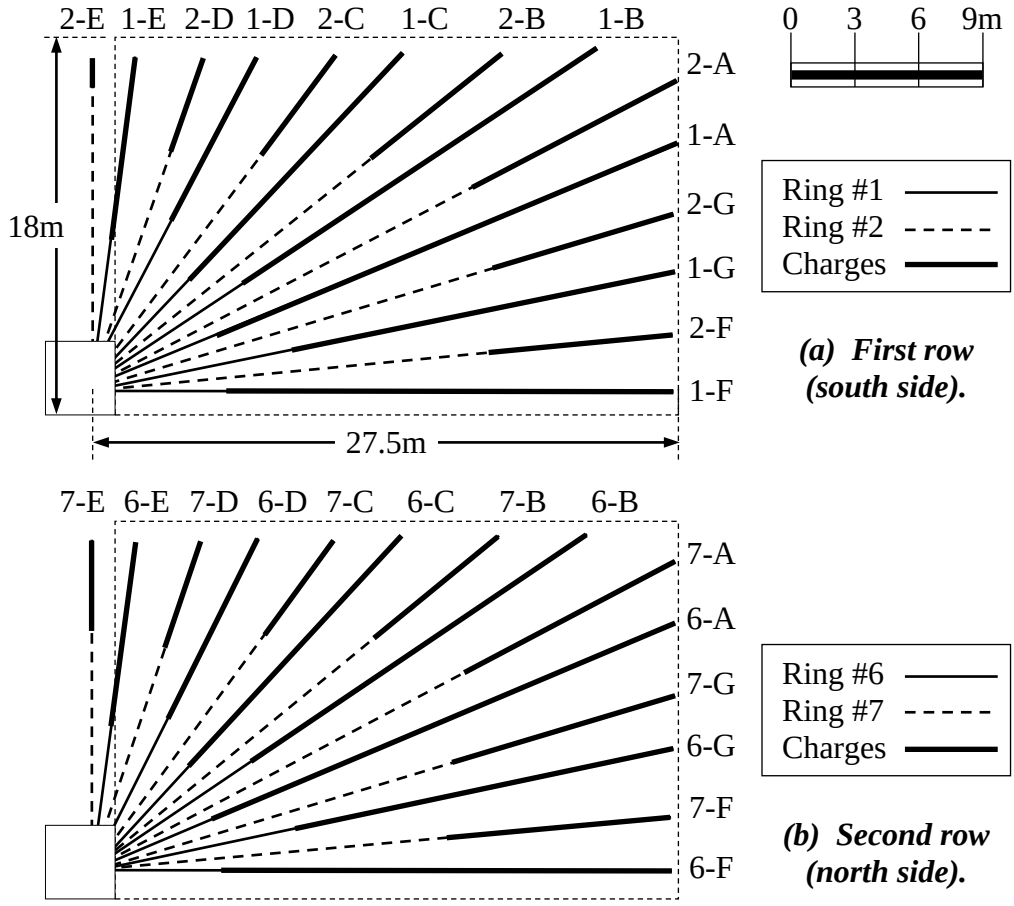

Figure 85. Elevation views looking north of (a) the south row; and, (b) the north row of destress blastholes, as designed.

As indicated in Figure 85a, the region to destress was 18.0m high, by 27.5m in the east-west direction, by 3m in the north-south direction, for a volume of 1,485 m^3. However, and

as discussed before, an external zone of influence needs to be considered to account for the damage that the outside explosive charges will cause to the surrounding rock mass. Initially, and as shown in Figure 23 and Figure 86a, the width and length (as defined by the orientation of the destress blastholes) of the targeted zone were each increased by twice 16 times the diameter of the blastholes and the effective volume was calculated based upon these larger values. This, however, results in quite a large effective volume that tends to artificially lower the important unit explosive energy value (this parameter has the highest cause in the RES matrix, at both scales). Furthermore, the four corners of this outside zone are located further away than 16 blasthole diameters. After conducting a sensitivity analysis of the effects of the shape of this external zone, it was found that dropping its four corners, as shown in Figure 86b, tended in some instances to yield a Destressability Index rating that matched a bit more closely the results reported in documented case histories.

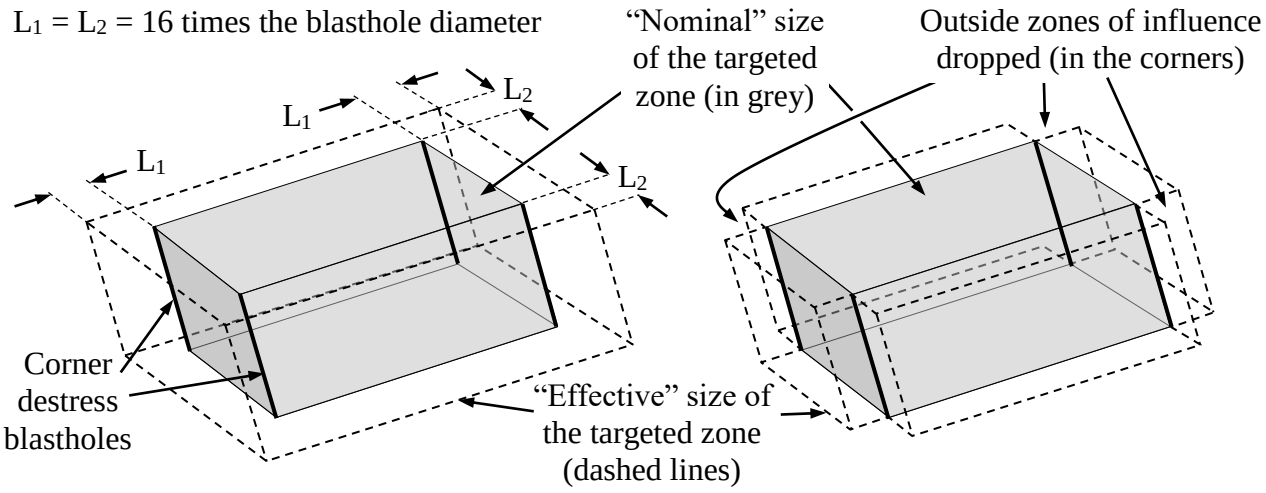

(a) Outside zones of influence initially considered.

(b) Outside zones of influence eventually considered.

Figure 86. Representation of the outside zones of influence retained around a large-scale choked pillar destress blast.

The approach of the reduced outside zone of influence will be used in Chapter X. It is however difficult in this particular case to assess which direction constitutes the length and which one constitutes the height of the target zone since the blastholes are fanned from a single drift. Eventually, one outside zone of influence was chosen in the north-south direction, and one was chosen in the vertical axis. Considering as per Figure 86b these four

outside zones of influence added $2 \times (16 \times 0.114) \times 18 \times 27.5 = 1{,}810$ m^3 in the north-south direction, and $2 \times (16 \times 0.114) \times 3 \times 27.5 = 300$ m^3 in the vertical direction, which gave a total effective volume of close to 3,600 m^3. At a rock density of 2.8 t/m^3, the total targeted mass was thus about 10,075 tonnes. In turn, the explosive energy ratio of the proposed destress blast was ($3{,}790 \times 10^6$ calories / 10,075,000 kg) = 376.2 cal/kg. This ratio fell within the 200 to 500 cal/kg guideline previously discussed. Figure 87 shows where this design lied in comparison with documented destress blast case studies, as reported by Brummer (2001). As mentioned, designs for fully-confined pillars should plot in the hatched 200 to 500 cal/kg zone.

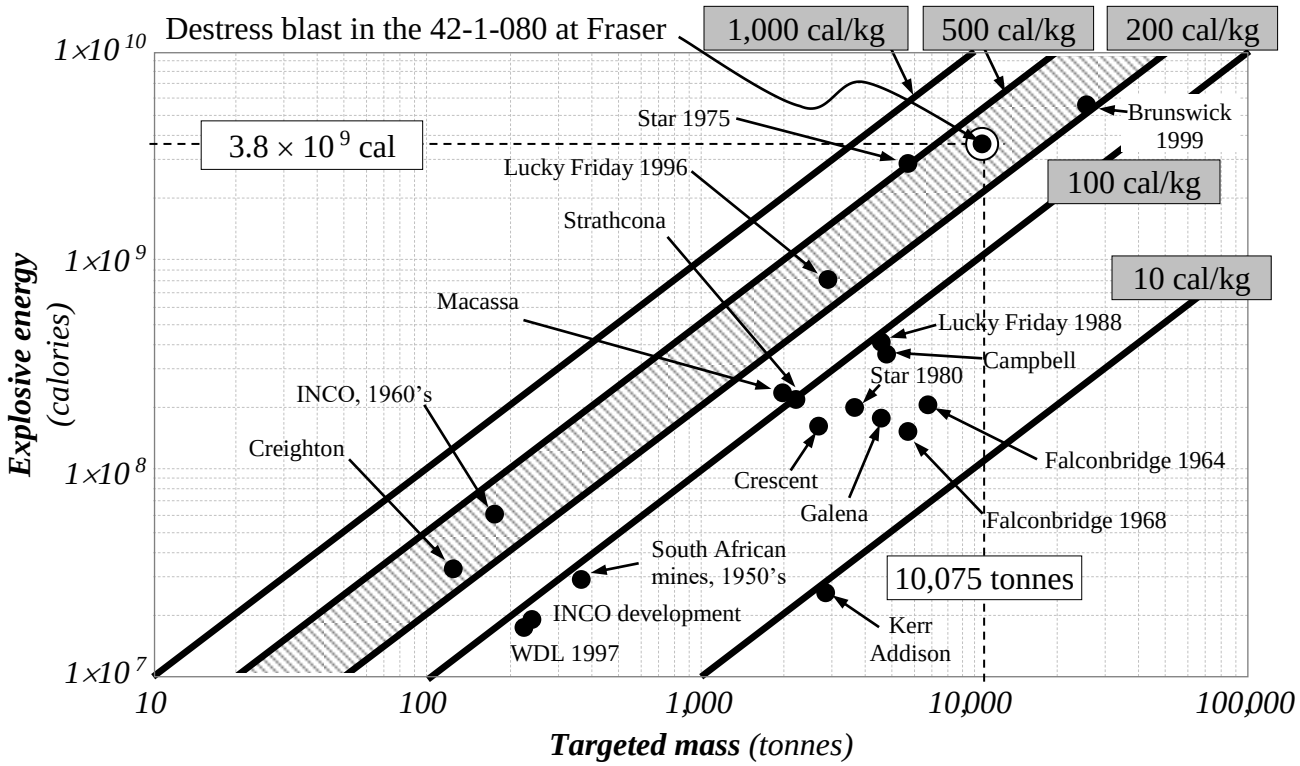

Figure 87. Designed explosive energy input per tonne of targeted rock in the 42-1-080 area.

As shown schematically in Figure 88 (which is a rotated view), an en-echelon firing sequence was retained in order to fracture the rock mass at some angle to the targeted stress component. The objective was to preferentially promote the formation of fractures at angle to σ_1, in order to allow shear movement to occur within the destressed volume. Each

blasthole was double-primed, with one primer located towards the toe, and the other one about one third of the way down from the collar.

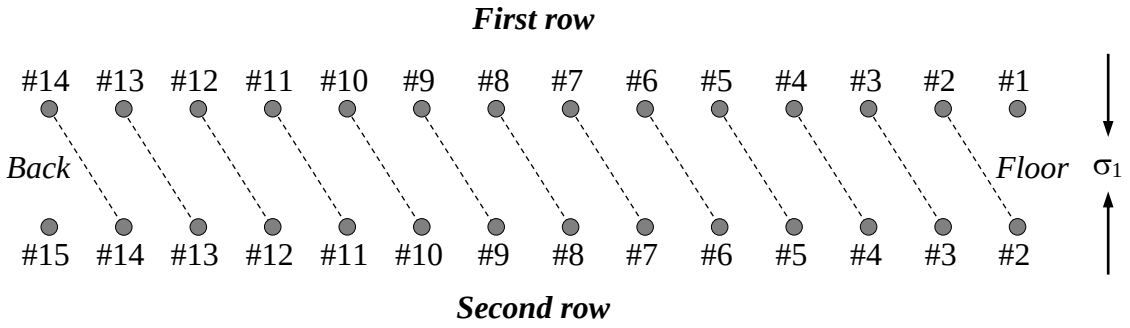

Figure 88. Sketch (not to scale) of the en-echelon firing sequence retained for the destress blast.

A blast-induced vibration level of 250 mm/s at a distance of 50m had been successfully used in the past (Andrieux *et al*., 2000) as a threshold value to limit the collateral damage inflicted in the surroundings of a large choked destress blast. This threshold was implemented again in this case. Based upon the explosive charges shown in Figure 85 and the sequence indicated in Figure 88, the maximum designed charge per delay was 454 kg, which corresponded to the fifth set of charges to detonate (holes 1-A and 7-G). Equation (32) was again used to predict blast-induced vibration levels – as before, values of K and β of 800 and 1.5, respectively, were retained for this evaluation. This time, however, an arbitrary increase of 25% was implemented in an attempt to account for the high level of confinement the explosive charges were going to be subjected to. At a distance of 50m, and for the maximum charge weight per delay of 454 kg, this yielded a PPV of 223 mm/s (8.8 in/s), and of 278 mm/s (11.0 in/s) once the 25% factor was applied. This being only about 11% over the self-imposed 250 mm/s limit, the en-echelon sequence shown in Figure 88 was adopted.

In light of the sizeable risks associated with the malfunction of a powerful and highly confined blast near production areas, stringent precautions were taken at every stage of the implementation phase in order to ensure compliance with the design and early detection of potential problems. The actual drilling depths were reported, as well as particular

occurrences, such as unexpected hole breakthroughs or jammed drill rods, for example. Table 45 through to Table 48 show the designed *vs*. actual (as reported by the drillers, and later confirmed during loading) drilling parameters.

Rings #1 and #2 pertain to the first row of blastholes (located at the far end of the dedicated drilling drift, on the south side), whereas rings #6 and #7 relate to the second row of blastholes (located near the entrance of the drilling drift, on the north side). The drilling depths were quite close to the designed ones. Occurrences of offsets and squeezing were observed along the length of most of the blastholes, indicative of high stress conditions approaching the local strength of the rock mass.

Table 45. Designed *vs*. actual drilling for Ring #1.

Ring - Hole	Dump angle *(degrees)*	Dip angle *(degrees)*	Design length *(m)*	Reported length *(m)*	Comments
1-A	90°	22.7°	29.2	29.2	Re-drilled
1-B	90°	33.7°	27.5	27.5	N/A
1-C	90°	46.6°	19.9	19.9	N/A
1-D	90°	62.8°	15.5	15.5	N/A
1-E	90°	82.0°	13.8	13.8	N/A
1-F	90°	00.0°	26.8	26.8	Broke into backfill
1-G	90°	11.6°	27.4	27.4	N/A

Table 46. Designed *vs*. actual drilling for Ring #2.

Ring - Hole	Dump angle *(degrees)*	Dip angle *(degrees)*	Design length *(m)*	Reported length *(m)*	Comments
2-A	90°	28.1°	30.6	29.2	N/A
2-B	90°	39.5°	24.0	27.5	N/A
2-C	90°	53.9°	17.7	19.9	N/A
2-D	90°	71.6°	14.4	15.5	N/A
2-E	90°	90.0°	13.5	13.8	N/A
2-F	90°	05.9°	27.0	26.8	Broke twice into Hole 1-G
2-G	90°	17.3°	25.0	27.4	N/A

Table 47. Designed *vs*. actual drilling for Ring #6.

Ring - Hole	Dump angle *(degrees)*	Dip angle *(degrees)*	Design length *(m)*	Reported length *(m)*	Comments
6-A	90°	22.9°	29.2	29.2*	* As re-drilled
6-B	90°	34.1°	27.4	27.4	N/A
6-C	90°	47.2°	20.0	20.0	N/A
6-D	90°	63.7°	15.4	15.4	N/A
6-E	90°	83.0°	13.8	13.8	N/A
6-F	90°	00.0°	26.8	26.8	Rods jammed at a depth of 21m
6-G	90°	11.7°	27.4	27.4	N/A

Table 48. Designed *vs*. actual drilling for Ring #7.

Ring - Hole	Dump angle *(degrees)*	Dip angle *(degrees)*	Design length *(m)*	Reported length *(m)*	Comments
7-A	90°	28.3°	30.6	30.6	N/A
7-B	90°	39.7°	23.9	23.9	N/A
7-C	90°	54.2°	17.7	17.7	N/A
7-D	90°	72.0°	14.4	14.4	N/A
7-E	90°	90.0°	13.8	13.8	N/A
7-F	90°	06.0°	27.0	27.0	N/A
7-G	90°	17.5°	28.2	28.2	N/A

Note: the dip angles shown in Table 45 through to Table 48 are positive upwards.

Although the drilling depths were close to the designed ones, none of the blastholes were breaking through into accessible areas from which their accuracy could have been verified. As a result they were surveyed by Borinfo, Inc. of Sudbury with specialised instrumentation. Only 20 of the 28 blastholes were surveyed as the near-vertical ones could not be covered due to angle limitations in the available Boretrak™ equipment. The longest blastholes (those with the largest potential to deviate and the largest explosive charges) were however all surveyed. These measurements showed that a significant number of blastholes had strongly curved northwards. What raised the most concern, however, was the location of most blastholes on Ring #6, which appeared to have been drilled on an

excessively southerly azimuth. This resulted in some important blastholes on that ring to intersect the plane of rings #1 and #2.

A number of corrective steps were taken based upon these data. Firstly, blasthole 6-A (located towards the centre of the panel to destress, designed to contain a critical 24m-long explosive column and surrounded by two blastholes also heavily loaded) and blasthole 6-G (also located towards the centre of the panel and designed to be loaded with a 19m-long explosive charge) were re-drilled. Secondly, blasthole 2-B (planned to be loaded with a 8m-long charge and sufficiently off-course to potentially disturb more important charges on rings #6 and #7) was abandoned. Thirdly, blasthole 2-C, although off-course, was primed with a #11 detonator instead of the initially planned #10 due to its proximity to two other charges also primed with a #11 cap. The three explosive charges initiated with a #11 detonator did not combine into the largest charge weight per delay, and, hence, were not deemed as having the potential to cause damaging ground vibrations.

The destress blast was loaded Friday 21 December 2001 by Orica personnel, under the supervision of the Fraser Mine blasting specialist. The final depth of each blasthole was measured and recorded, as well as the exact amount of bulk emulsion explosives pumped into it. Table 49 through to Table 52 compare the design and actual (as measured in the field) drilling and loading parameters for rings #1, #2, #6 and #7, respectively.

Please note that the charge lengths are calculated (not measured) based upon the actual charge weights and for fully-coupled 114.3 mm (4.5 in) diameter charges, and that the unloaded collar lengths are also calculated, by subtracting the calculated charge lengths from the measured blasthole depths.

The Orica EXEL MS series of non-electric short period detonators was used for the blast. The units obtained by Fraser Mine had shock tube lengths of 15 and 25m, which was too short to reach the end of the deepest blastholes and toe-prime their charges. This was however not deemed to be a critical problem, and these detonators were used nevertheless.

Table 49. Loading parameters for Ring #1.

Ring-Hole (#)	Design length (m)	Actual length (m)	Design charge (kg)	Actual charge (kg)	Charge length (m)	Design collar (m)	Actual collar (m)	Detonator / Delay (# / ms)
1-A	29.2	29.5	310	292	22.8	5.0	6.7	5 / 125
1-B	27.5	27.5	256	254	19.8	7.5	7.7	7 / 175
1-C	19.9	20.0	186	190	14.8	5.0	5.2	9 / 225
1-D	15.5	14.1	115	114	8.9	6.5	5.2	11 / 275
1-E	13.8	13.5	113	101	7.9	5.0	5.6	13 / 325
1-F	26.8	29.1	280	191	14.9	5.0	14.2	1 / 25
1-G	27.4	30.8	242	267	20.8	8.5	10.0	3 / 75

Table 50. Loading parameters for Ring #2.

Ring-Hole (#)	Design length (m)	Actual length (m)	Design charge (kg)	Actual charge (kg)	Charge length (m)	Design collar (m)	Actual collar (m)	Detonator / Delay (# / ms)
2-A	30.6	30.6	142	165	12.9	19.5	17.7	6 / 150
2-B	24.0	24.0	103	101	7.9	16.0	16.1	8 / 200
2-C	17.7	17.3	73	63	4.9	12.0	12.4	11 / 275
2-D	14.4	17.0	56	58	4.5	10.0	12.5	12 / 300
2-E	13.5	14.5	13	37	2.9	12.5	11.6	14 / 350
2-F	27.0	27.0	115	203	15.8	18.0	11.2	2 / 50
2-G	28.2	28.5	124	183	14.3	18.5	14.2	4 / 100

Table 51. Loading parameters for Ring #6.

Ring-Hole (#)	Design length (m)	Actual length (m)	Design charge (kg)	Actual charge (kg)	Charge length (m)	Design collar (m)	Actual collar (m)	Detonator / Delay (# / ms)
6-A	29.2	33.0	310	308	24.0	5.0	9.0	6 / 150
6-B	27.4	28.7	255	267	20.8	7.5	7.9	8 / 200
6-C	20.0	20.0	192	191	14.9	5.0	5.1	10 / 250
6-D	15.4	14.4	121	104	8.1	6.0	6.3	12 / 300
6-E	13.8	13.4	113	105	8.2	5.0	5.2	14 / 350
6-F	26.8	26.8	280	241	18.8	5.0	8.0	2 / 50
1-G	27.4	24.5	242	188	14.7	8.5	9.8	4 / 100

Note: the data for Hole 6-E are as loaded (please refer to the first paragraph after Table 52).

Table 52. Loading parameters for Ring #7.

Ring-Hole (#)	Design length (m)	Actual length (m)	Design charge (kg)	Actual charge (kg)	Charge length (m)	Design collar (m)	Actual collar (m)	Detonator / Delay (# / ms)
7-A	30.6	30.0	149	191	14.9	19.0	15.1	7 / 175
7-B	23.9	24.0	101	152	11.9	16.0	12.1	9 / 225
7-C	17.7	18.0	73	72	5.6	12.0	12.4	11 / 275
7-D	14.4	13.5	69	101	7.9	9.0	5.6	13 / 325
7-E	13.8	13.5	55	54	4.2	9.5	9.3	15 / 375
7-F	27.0	26.4	141	127	9.9	16.0	16.5	3 / 75
7-G	28.2	28.3	144	165	12.9	17.0	15.4	5 / 125

Vertical blasthole 6-E was observed Monday morning 24 December to have leaked. The plug meant to keep the explosive product in place had slipped, but because some of the emulsion pumped had remained inside the hole, it was fired without being reloaded. Table 53 summarises the principal statistics associated with the field implementation of the large-scale choked panel destress blast in the 42-1-1620 Stope.

Table 53. Principal final field statistics of the destress blast in the 42-1-1620 Stope.

Parameter	Values and units
Number of blastholes	28
Total drilling	638m (2,093 ft)
Total explosives loaded	4,485 kg (9,867 lb)
Explosive type	Bulk emulsion
Total explosive energy	3.884×10^9 cal
Maximum charge per blasthole	308 kg (678 lb), for Hole 6-A
Maximum charge per delay	473 kg (1,041 lb), on delay #6 (at 150 ms)
Targeted rock volume *	3,600 m^3 (127,035 ft^3)
Targeted rock tonnage (felsic gneiss at 2.80 t/m^3)	10,075 tonnes
Effective powder factor **	0.445 kg/t (1.247 kg/m^3)
Design energy ratio	376.2 cal/kg
Actual energy ratio	385.5 cal/kg

* *the blasthole deviations observed were not deemed sufficient to require changing this figure.*

** *relative to the effective targeted mass and volume.*

The blasthole collars would have been stemmed if possible, ideally with 0-20 mm (0-3/4 inch) crushed rock. This was however not possible to achieve since the blastholes were either horizontal or drilled upwards.

10.4. INSTRUMENTATION USED

A series of instruments were specifically installed in the vicinity of the destress blast in order to assess its results. These instruments were as follows.

- Three (3) Geokon vibrating wire stress cells to measure stress variations
- Two (2) MPBX multi-point extensometers to measure ground movement
- One (1) strain gauge embedded inside a shotcrete post to measure vertical displacement
- Three (3) surface-mounted triaxial geophone arrays to measure the vibrations from the blast

The mine-wide ESG seismic system was used as well to closely track the evolution of the seismic activity after the destress blast. Detailed underground inspections were also completed 27 and 28 December in the immediate vicinity of the blast and in the surrounding regions.

10.4.1. Vibrating wire stress cells

All three Geokon vibrating wire stress cells were similar to those used for the destress blast in the 29-9 Pillar at Brunswick Mine and described in Section 9.4.2 – they were the nominal 76 mm (3 inch) diameter model and were installed inside NQ-size (75.7 mm diameter) diamond drill holes. The location of each gauge is shown on plan view in Figure 89. As shown, two of the three instruments were installed along different orientations inside the same diamond drill hole off the east wall of the 42-1-080 Access, behind the area targeted for destressing – this diamond drill hole was dipping upwards at 45°.

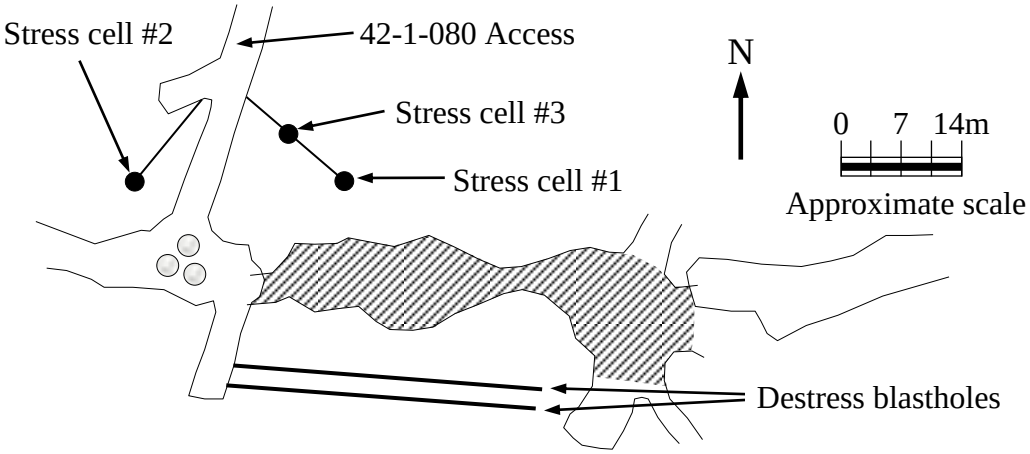

Figure 89. Schematic plan view showing the location of the three Geokon stress cells used to track stress changes following the destress blast.

The third sensor (named "Stress cell #2" in Figure 89) was located on the west side of the 42-1-080 Access, in a diamond drill hole off the remuck bay, with the objective of detecting a possible stress redistribution towards this area. This second diamond drill hole was also oriented upwards, but at an angle of only 30°. Each stress cell was set up as described below.

- Stress cell #1 was installed at a depth of 13.2m and oriented horizontally in order to measure the expected magnitude reduction in the major principal stress component following the destress blast. (At the location of this gauge, behind the footwall contact and about half way up the remaining sill pillar, this stress component was inferred to be locally sub-horizontal and oriented north-south.) The sensor was pre-stressed in place to 10 MPa. Based upon the observation of the core retrieved from the diamond drill hole, this sensor was installed in weak and broken ore.

- Stress cell #2 was installed at a depth of 10.4m, and was oriented about 45° off the vertical, sub-parallel to a direction along which a plunging stress component was expected to increase as the result of the regional major principal stress being pushed upwards and to the West by the destress blast. This gauge was pre-stressed in place to 15 MPa. Based upon observations of the core from the diamond drill hole, this sensor was installed in solid felsic gneiss.

- Stress cell #3 was installed vertically at a depth of 4.2m in the same diamond drill hole as stress cell #1, and pre-stressed in place to 14 MPa. Based upon the observation of the local core, this sensor was installed in solid felsic gneiss.

Figure 90 shows the orientation of each gauge inside its respective borehole. The stress component measured in each case is parallel to the axis defined by the centres of the stress cell and the platen, as represented by the black arrows.

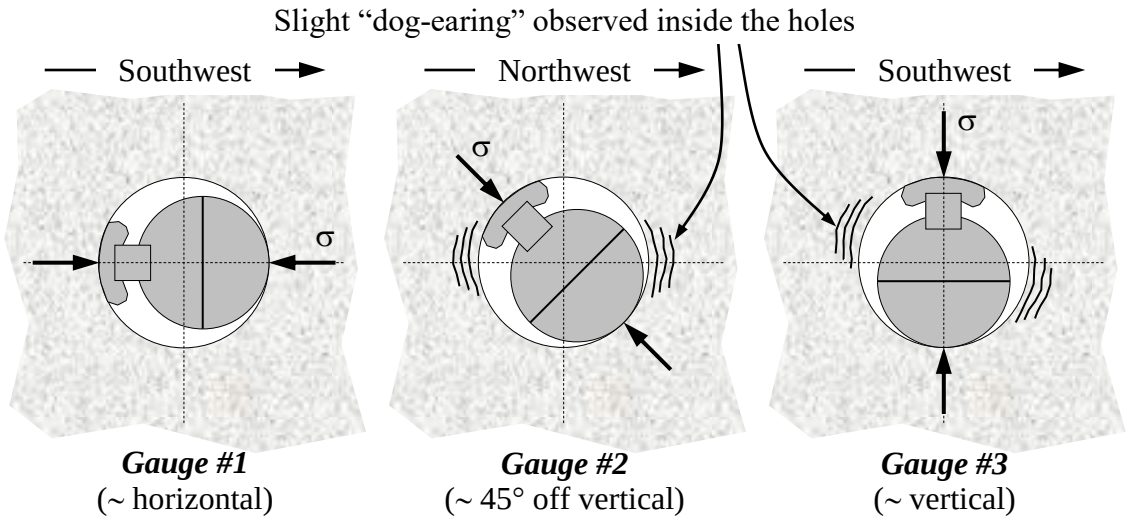

Figure 90. Installation of the three Geokon vibrating wire stress cells – schematic diagrams looking down the instrumented holes and showing the orientation of the gauges.

Stress cells #1 and #3 were connected to a datalogger programmed to automatically read them every two minutes and save to its internal memory every ten minutes the average of the last five readings. The datalogger was installed on the west wall of the 42-1-080 Access, just south of the remuck bay, and commissioned in the morning of 20 December. Stress cell #2 was not initially connected to the datalogger and was read manually (it was eventually connected to the automatic acquisition system during the morning of 28 December).

10.4.2. Multi-point extensometers

Two six-point extensometers fitted with 5 inch potentiometers were used to monitor possible ground movement following the destress blast. These instruments were similar to

those used at Brunswick Mine for the 29-9 Pillar destress blast, and previously described in Section 9.4.3. As shown in Figure 91, Unit #1 (5m-long) was located in the back of the intersection of the remuck bay and the 42-1-080 Access, while Unit #2 (10m-long) was located in the back of the 42-1-080 Access near the intersection with the A5 lens. Both units were installed in vertical 57 mm (2-1/4 in) diameter percussion holes and grouted in place – Sensor #1 was installed in a 6m-deep hole, whereas Sensor #2 was installed in an 11m-long one.

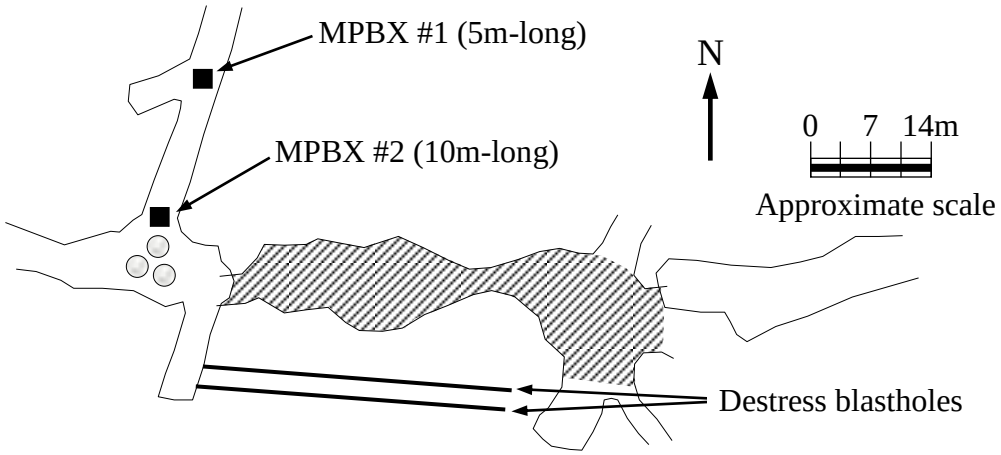

Figure 91. Schematic plan view showing the location of the two MPBX multi-point extensometers used to track ground movement following the destress blast.

Table 54 shows the location of each anchor along the two instruments, which were evenly spaced along their length.

Table 54. Location of the various anchors along the two multi-point extensometers installed in the back of the 42-1-080 Access.

MPBX #1	
Anchor *(#)*	Depth *(m)*
1	0.83
2	1.67
3	2.50
4	3.33
5	4.17
6	5.00

MPBX #2	
Anchor *(#)*	Depth *(m)*
1	1.67
2	3.33
3	5.00
4	6.67
5	8.33
6	10.00

Both extensometers were connected to the same datalogger that read the stress cells. They too were automatically read every two minutes, with the average of the last five readings being saved every ten minutes to the internal memory of the logger. Only five of the six anchors in each extensometer could be connected to the logger for automatic data acquisition due to the limited number of channels available on the system – as a result, the deepest anchor of each extensometer was left unconnected to the datalogger.

10.4.3. Strain gauge in the shotcrete pillar

A strain gauge was embedded inside a shotcrete post erected in the intersection of the 42-1-080 Access and A5 stringer, in order to measure vertical convergence in this area. Figure 92 shows the location of this instrumented shotcrete pillar.

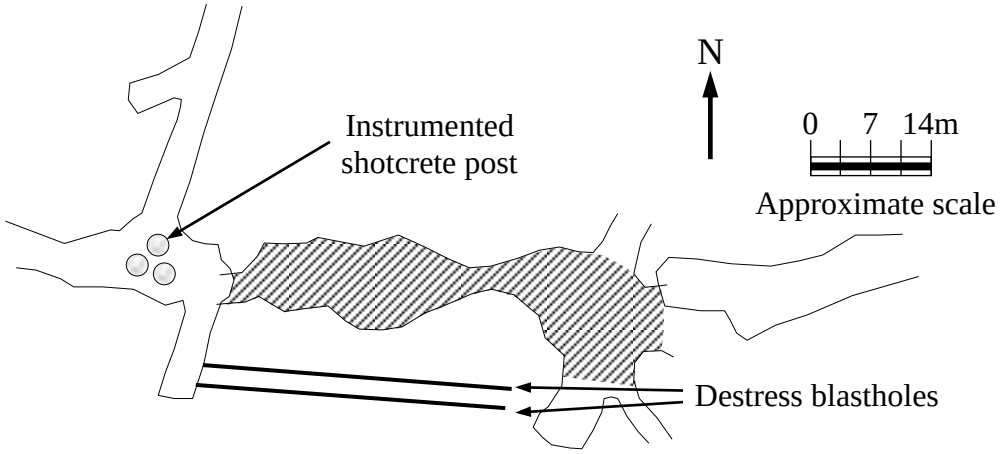

Figure 92. Schematic plan view showing the location of the shotcrete post instrumented with a strain gauge.

10.4.4. High frequency geophones

The ground vibrations produced by the destress blast were recorded at three locations, to examine the behaviour of the blast and check the vibration levels the surrounding areas were subjected to. Two (2) eight channel 12 bit Instantel MiniMate digital seismographs were used for this purpose, both capable of recording at a maximum sampling rate of 8 kHz per channel. All the sensors used were surface-mounted geophones. Grouting these

sensors inside boreholes would have provided more reliable readings but the objective was more to diagnose the behaviour of the blast and get a feel for the vibrations it produced, than record exact amplitude levels and frequency contents. Figure 93 shows the location of the two stations nearest to the destress blast. The third station was located 230m away in the 42-1 refuge station.

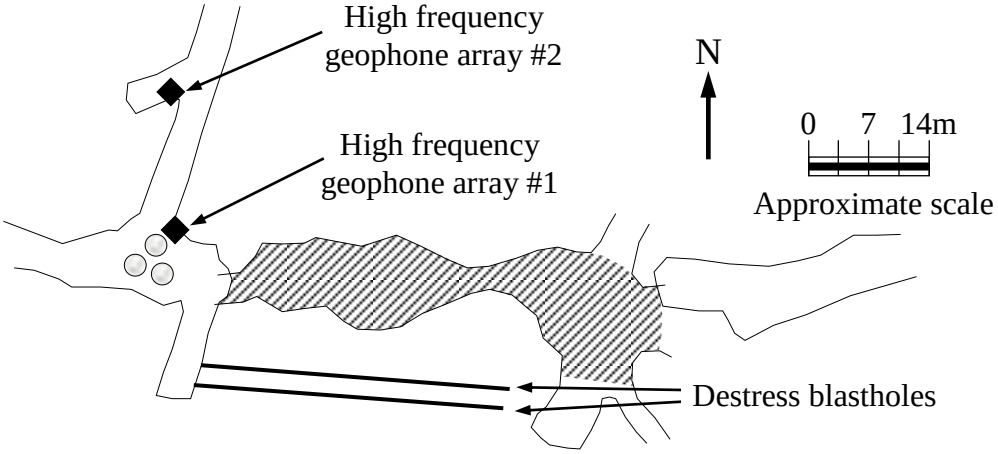

Figure 93. Schematic plan view showing the location of two of the three surface-mounted geophone stations. The third station was located in the 42-1 refuge station.

Table 55 shows the location of each of the three recording stations, as well as their distance from the destress blast.

Table 55. Distance from the destress blast of the three triaxial surface-mounted blast-induced vibration recording stations.

Station number	Number of recording axes	Location	Distance from the blast
Station #1	3	On the north side of the shotcrete post in the intersection of the 080 Access and the A5 lens	18m
Station #2	3	South wall of the 42-1-080 remuck bay	42m
Station #3	3	Floor of the 42-1 refuge station	230m

All the monitoring stations were triaxial, i.e., comprised three individual geophones oriented at 90° to each other, in order to capture all the vibrational energy at their location.

The individual sensors used at stations #1 and #2 were high frequency geophones (omni-directional OYO GeoSpace LT-101 gauges) wall-mounted using a two-component resin. Station #3, in the 42-1 refuge station, consisted of a directional triaxial far-field low frequency geophone that was kept in place against the concrete floor under a 25 kg sand bag. Both seismographs were triggered by a wirebreak loop attached to the detonating cord of the destress blast. The explosion of the cord severed the loop and instantaneously triggered both systems, which were programmed to record for a duration of three seconds. The extended recording duration was meant to try to detect nearby seismic events that would have been immediately triggered by the blast.

10.5. RESULTS OF THE DESTRESS BLAST

As mentioned, the blast was detonated 24 December 2001 at 15:56 EST. The following sections describe the results obtained with the various monitoring systems used, and provide a summary of the post-blast observations.

10.5.1. Field performance of the destress blast

Figure 94 shows the first 400 ms of the vibration record obtained at Station #2 on the south wall of the 080 Remuck Bay, 42m away from the blast. The x-axis represents time (in milliseconds) while the y-axis is particle velocity (in mm/s – please note that the y-axis scale is not the same on all four graphs). The first three graphs on the upper part of the figure represent the vibrations each individual axis recorded (transverse, longitudinal and vertical), while the fourth graph, at the bottom of the figure, is the vector sum of the first three. The vector sum of three signals recorded by orthogonally-oriented sensors located at a given point of interest is a time domain function defined as follows:

$$\text{Sum}(t) = [\, A_x(t)^2 + A_y(t)^2 + A_z(t)^2 \,]^{0.5} \qquad \text{..... Eq. (35)}$$

With Sum (t) the vector sum (the peak particle amplitude is the maximum of this function), which is the resultant amplitude at that point of interest at instant t, and $A_x(t)$, $A_y(t)$ and $A_z(t)$ the amplitudes measured at that same point at instant t by the three orthogonally-oriented gauges (units of displacement, velocity or acceleration must be consistent).

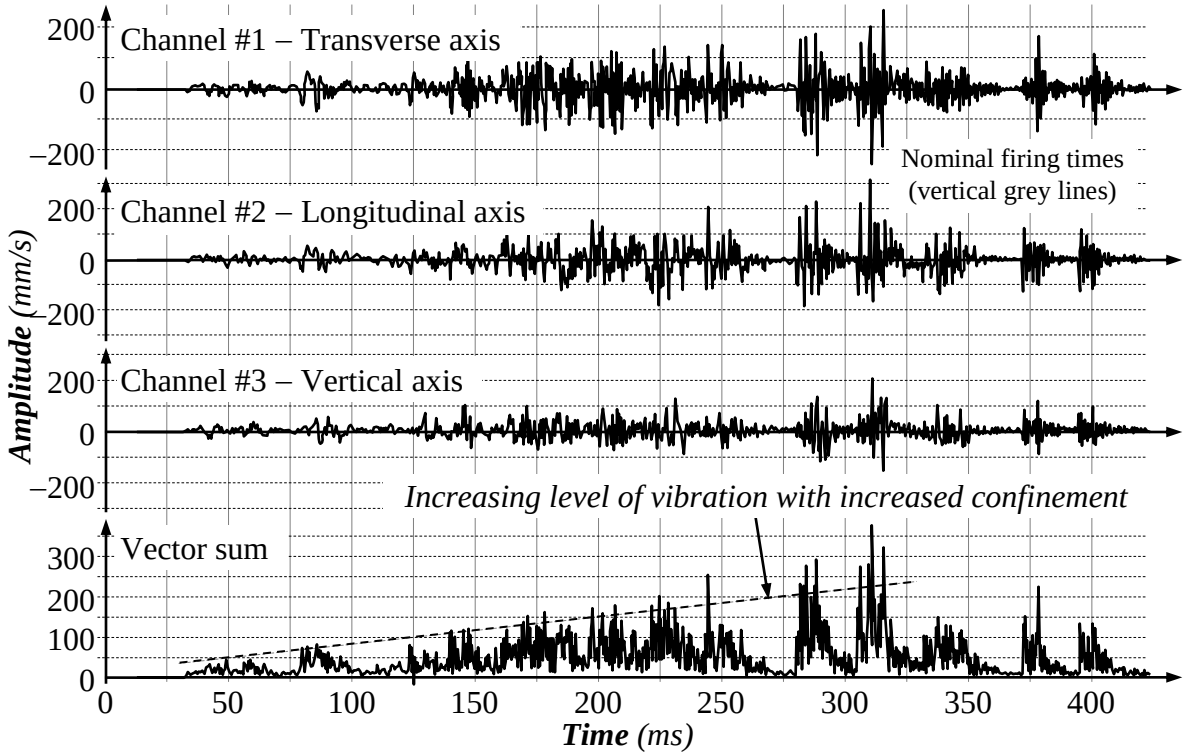

Figure 94. Blast-induced vibrations recorded on the south wall of the 080 Remuck Bay, 42m away from the blast.

The vibrational input in the rock mass matches the blasting sequence reasonably well: most vibration packets do occur near the expected detonation times indicated in Figure 94 by the vertical grey lines. Although the blast vibrations recorded cannot guaranty that each and every charge detonated, there are no obvious indications that holes did not fire. The amplitude of most of the packets is of the same order of magnitude. These observations are indicative that the blast, overall, progressed close to the way it was designed.

At a distance of 42m from the blast, the maximum peak particle velocity that was expected using Equation (33) – for the maximum charge per delay of 473 kg (as per Table 53), K = 800, β = 1.5 and an arbitrary 25% increase in amplitude to attempt to account for the state

of extreme confinement of the charges – was 373 mm/s (14.7 in/s). The PPV measured (the maximum of the vector sum trace) was 372 mm/s (14.6 in/s), for a difference of only about 0.3%. Despite this apparent match between the "predicted" and measured vibration levels, Figure 94 highlights the fundamental irrelevance of charge weight per delay in predicting vibration levels for highly confined charges. The PPV, which occurred at around 310 ms, was associated with either delay #12 or delay #13 (loaded with 162 and 202 kg of explosives, respectively) rather than with the maximum charge weight per delay of 473 kg associated with delay #6 (at 150 ms). Please note on Figure 94 how the vibration levels increased as the blast progressed and the choking effect increased.

Frequency analyses based upon Fast Fourier Transforms performed on the vibrational data recorded on the south wall of the 080 Remuck Bay were completed, which showed that the frequency content of the recorded signals lied well within the 1,250 Hz linear frequency response upper limit of the sensors used, which confirmed that a good match existed between the sensors used and the vibrations recorded. These analyses also indicated that no distorting resonance or oscillation effects, which can easily be introduced with poorly anchored surface-mounted gauges, affected the data.

Additional vibrations (not related to the detonation of explosive charges) were recorded within three seconds of the blast, which were inferred to be seismic events triggered as an immediate response of the rock mass to the blast and the stress redistribution it caused. Figure 95 shows the complete triaxial vibration record obtained on the south wall of the 080 Remuck Bay during the three seconds following the initiation of the destress blast. The x-axis is again time (in milliseconds) and the y-axis represents particle velocity (in mm/s – please note the different scales on the three channels). At least two distinct vibration packets unrelated with the detonation of explosive charges were recorded, which, as mentioned, were assumed to be seismic events. These events were of limited magnitude and likely too small to be recorded by the mine-wide ESG microseismic network.

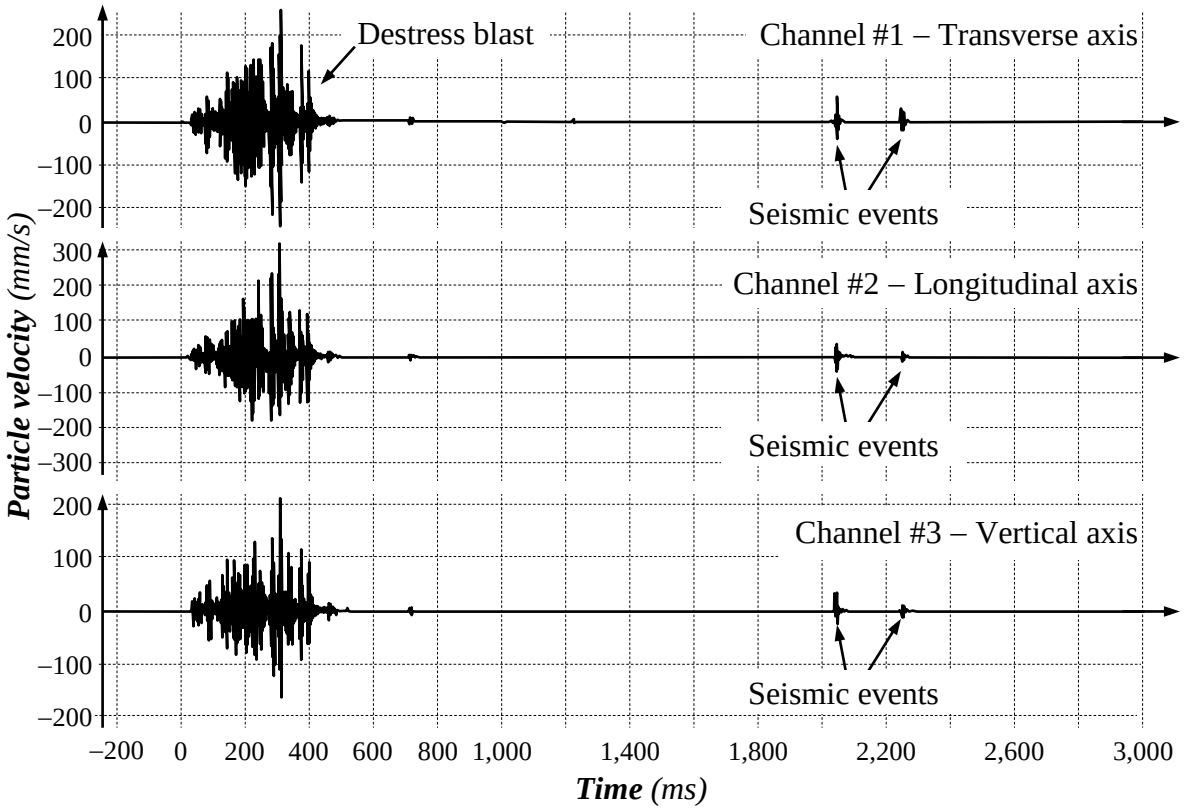

Figure 95. Vibrations recorded within 3 seconds of the destress blast on the south wall of the 080 Remuck Bay, 42m away.

The vibrational data recorded on the north side of the shotcrete post at the intersection of the 080 Access and the A5 lens showed a peak particle velocity of 428 mm/s associated with delay #7 (loaded with 405 kg of bulk emulsion). It is not particularly surprising that the peak particle velocity was associated with a different delay number than in the previous case because a shotcrete post is a man-made structure, which will respond to and dissipate vibrational energy in a manner particular to its shape, size, material, and coupling to the back and floor (rock and backfill, respectively, in this case). The frequency content of the vibrational signals recorded on the shotcrete pillar were also well within the capabilities of the sensors. The data recorded in the 42-1 refuge station, 230m away, yielded a peak vibration amplitude of 35 mm/s (1.4 in/s).

Overall, the blast-induced vibrational data can be summarised as follows: 1) these data were of good quality with clean signals; 2) the blast seems to have performed as planned, with no major blast malfunction being detected; and, 3) some vibrations were recorded

after the blast, inferred to be seismic events triggered by the blast and the associated stress redistribution.

10.5.2. Visual post-blast assessments

Detailed underground inspections were completed on the mornings of 27 and 28 December 2001 in order to visually assess the effects of the destress blast and check the surrounding areas for obvious signs of damage. Overall, ground conditions were good in all the areas inspected, with no excessive damage to mine openings and no failure of ground support systems being observed. In particular, the three shotcrete posts in the intersection remained intact. Blast damage was essentially restricted to the targeted area – Figure 96 gives an idea of the amount of material that was displaced by the destress blast.

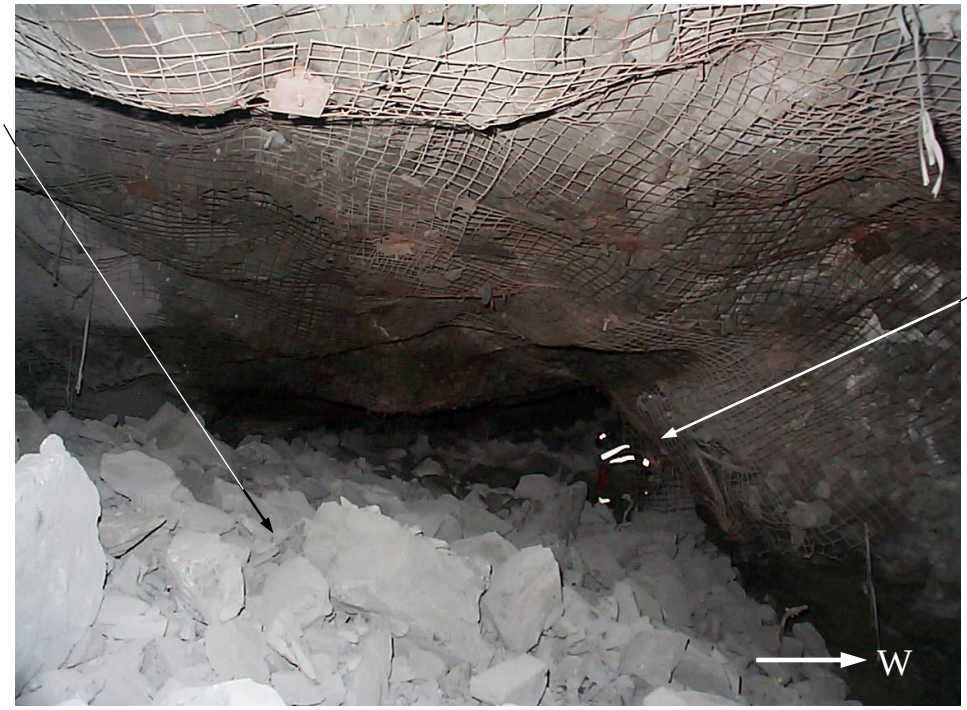

Figure 96. Photograph taken on the morning of 28 December 2001 looking south at the entrance of the destress blast drill drift.

As shown in Figure 96, a significant amount of energy was dissipated by the displacement of a relatively large volume of material up to 30m away. About 800 tonnes of material

were estimated to have been displaced into the destress drill drift and the main intersection with the 42-1-080 Access. (There is little doubt that a berm put in place at the entrance of the destress drill drift was instrumental in keeping most of the displaced material from reaching the A5 lens itself.) This expelled material was well fragmented, with the largest pieces being approximately 60 cm by 60 cm.

Importantly, the removal of nearly 800 tonnes of material from the collar region of the destress blast, which represents about 285 m^3 of rock, is ground through which stresses can no longer flow.

In addition, based upon field observations and discussions with miners in the 42-1-080 Access / A5-Right pillar (in February and early March 2002), it is evident that the ground immediately north of the destress blast location was heavily disturbed and fractured.

10.5.3. Seismic reaction to the destress blast

The response of the rock mass to the destress blast was also tracked through the seismic activity it triggered in the region. Figure 97 shows the activity recorded in Block 42-1620W (centred around the destress blast) by the mine-wide ESG Hyperion™ microseismic system between 24 December 2001 at 15:50 EST and 31 December 2001 at 01:00 EST.

Figure 97a is a plan view of the southwest region of the 42 Level (also showing the approximate location of the destress blast). Figure 97b is an elevation view looking north, while Figure 97c is an elevation view looking west. Both these elevation views are centred on the 42 Level where the destress blast was located.

It is clear from these data that a regional seismic reaction followed the destress blast, with the triggered seismicity being essentially concentrated on the footwall side of the destress blast, where most of the seismic activity generally occurs as a result of normal mining operations.

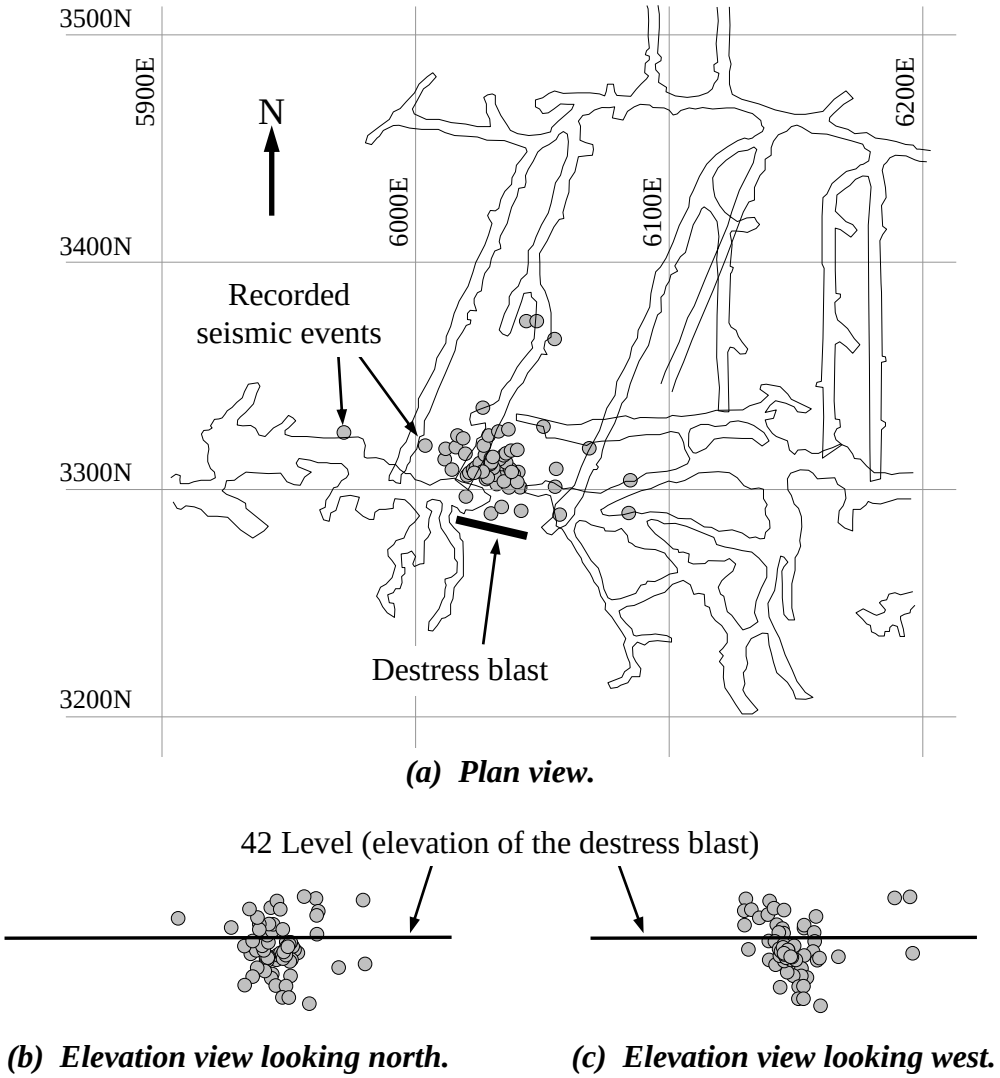

(a) Plan view.

(b) Elevation view looking north.

(c) Elevation view looking west.

Figure 97. Seismic response of the rock mass to the destress blast, between 15:50 24 December and 01:00 31 December 2001.

This reaction was however moderate in terms of the number of events generated, as shown by the activity rate recorded during the seven day period following the destress blast, which is plotted in Figure 98.

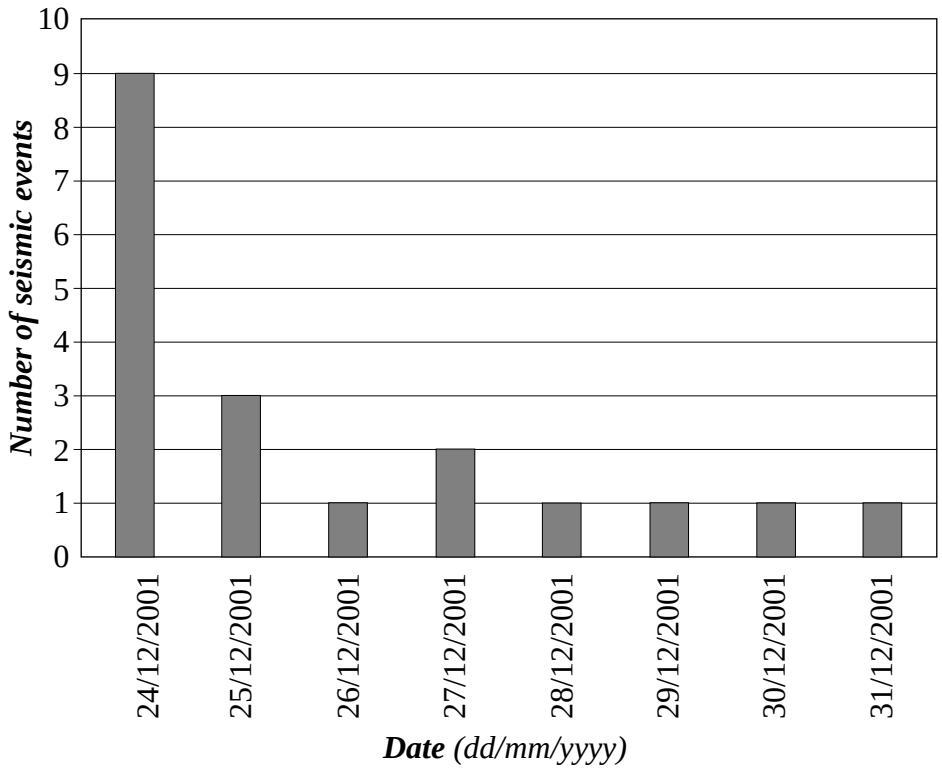

Figure 98. Seismic activity rate in the 42-1620W Block between the destress blast and 31 December 2001.

Figure 99 is perhaps a better way of showing the same data, in the form of the cumulative static stress drop inferred to have occurred in the region over the same period of time as a result of the seismic activity triggered by the destress blast. The static stress drop associated with a seismic event is given by the following equation (Madariaga, 1979):

$$\Delta\sigma = Mo / V \qquad \text{..... Eq. (36)}$$

With: $\Delta\sigma$ the static stress drop (in Pa); Mo the seismic moment (in N × m); and, V the source volume (in m^3). The seismic moment, in turn, is defined as:

$$Mo = G \times d \times A \qquad \text{..... Eq. (37)}$$

With: Mo the seismic moment (in N × m); G the bulk modulus of the rock mass (in Pa, assumed to be 30 GPa at the Fraser Copper Mine); and, d the average displacement (in m) over the source area A (in m^2). (Please refer to Mendecki [1997] for more detail on how quantitative seismic source parameters are derived from seismograms.)

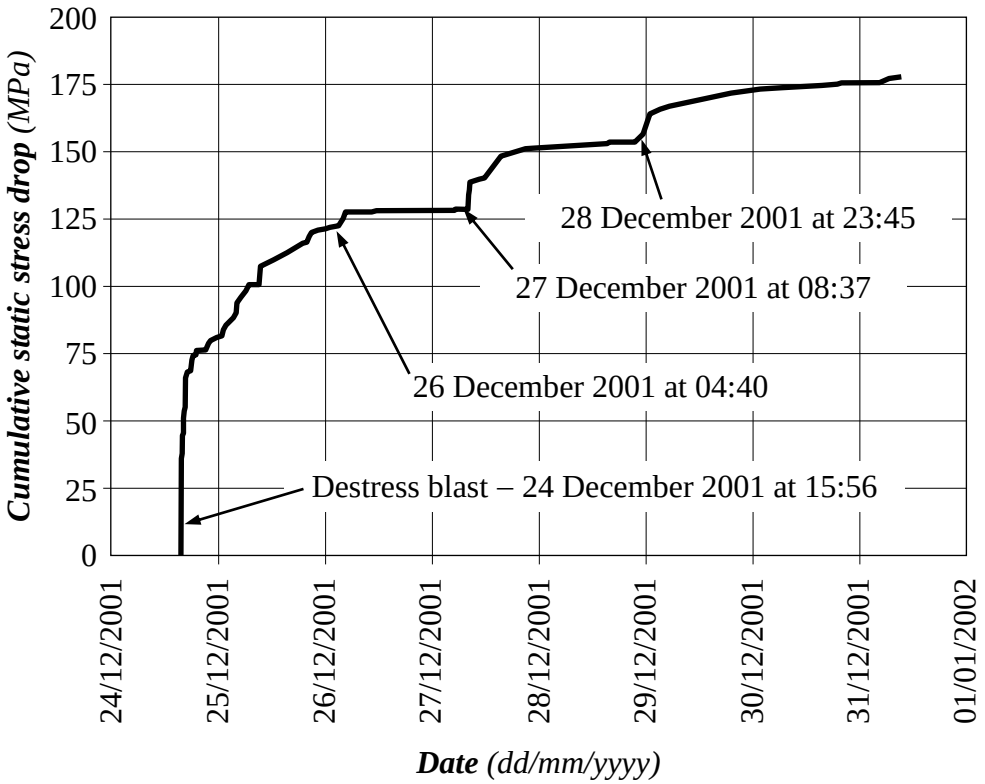

Figure 99. Cumulative static stress drop in the 42-1620W Block between the destress blast and 31 December 2001.

As shown in Figure 99, the cumulative static stress drop climbed sharply during the first four hours following the destress blast, principally as the result of a large seismic event (+0.9 Nuttli Magnitude) 28 seconds after the blast. The cumulative static stress drop continued to increase, although at a slower rate, until about 04:40 26 December. Further increases occurred 27 and 28 December as well, the result of relatively large seismic events.

The cumulative apparent volume of the seismic events recorded during the same time period was also computed from the ESG data using the following equation:

$$Va = (Mo^2) / (2 \times E \times G) \qquad \text{..... Eq. (38)}$$

With: Va the apparent volume of a given seismic event (in m^3); Mo its seismic moment (in $N \times m$); E its energy (in Joules); and, G the bulk modulus of the rock mass (in Pa). The summation of the apparent volume of each seismic event recorded in the volume and

time window of interest gives the cumulative apparent volume, which is a measure of the volume of rock that underwent coseismic inelastic strain as the result of the events considered. Figure 100 shows the evolution of the cumulative apparent volume as a function of time. This analysis suggests that a total volume of nearly 3,500m^3 of rock in the 42-1-080 Access and A5 lens region sustained irreversible damage due to the seismicity triggered by the destress blast.

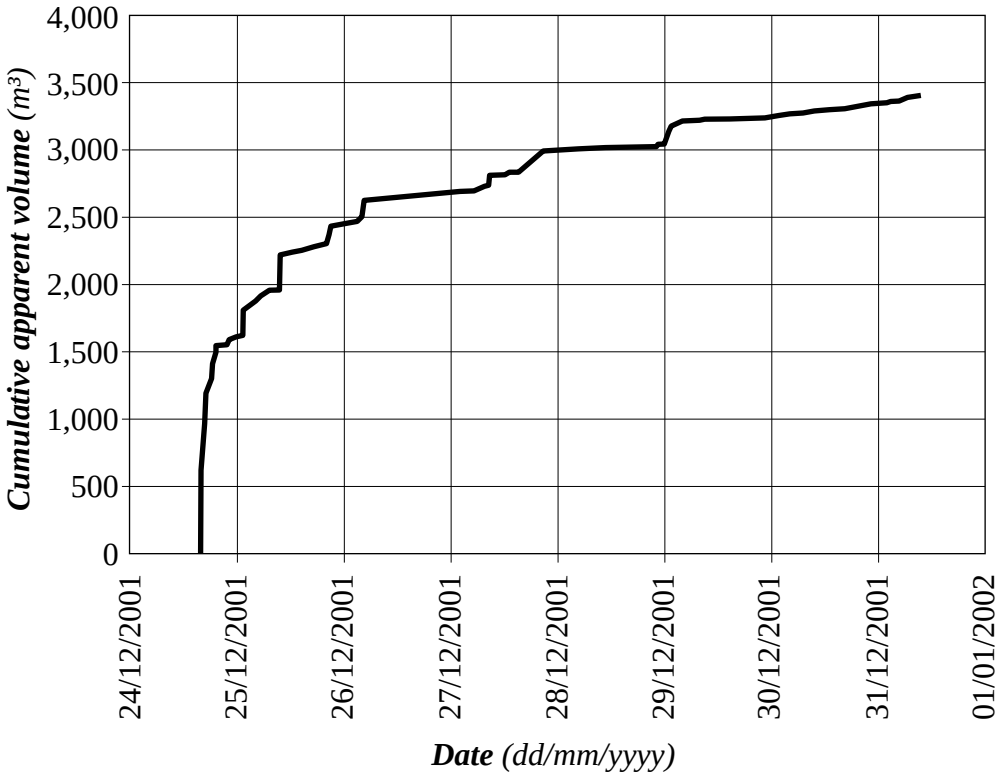

Figure 100. Cumulative apparent volume in the 42-1620W Block between the destress blast and 31 December 2001.

Based upon the seismic data recorded in the days following the destress blast, it can be inferred that it was successful at modifying the regional stress regime around the 42-1-080 Access.

10.5.4. Additional observations

Further insight was gained during the weeks that followed the destress blast. As mentioned previously, the mining of the previous cut (Cut #21) from the 42-1-080 Ramp Access had

started in early January 2000 and was only completed in December 2001, a few days before the 24 December destress blast. The actual mining time (excluding the seven month labour conflict) was about twice as long as for "normal" mining conditions in Zone 38. During the first two months of mining in Cut #21, at least five large events / rockbursts had occurred in the 080 Access area, resulting in several work interruptions. In comparison, the first two months of mining in the next cut (Cut #22) resulted in no large seismic events and minimal work stoppage. (The difficulties encountered in this case related to loose ground conditions rather than seismicity.)

In addition, the extraction of Cut #22 from the 135 Ramp was relatively quiet compared to that of Cut #21 from the 130 and 133 ramps, when over 100 tonnes of ore were lost due to the +2.6 Nuttli Magnitude event of 4 August 1999. Also, no significant seismic activity was recorded immediately behind the destress blast, in the A5 stringer just east of the 42-1-080 Access, during the two months following it.

All these observations are indicative that the destress blast significantly improved the general mining conditions.

By destressing to minimise stress problems in one area, one will generally cause a stress increase in another area, due to the redistribution of the loads. This was evident during the early stages of mining in D7 stringer (Cut #22), west of the 42-1-080 Ramp access, when significant seismic activity was observed ahead of the mining face after each blast. During this time the face was located in the abutment of the destress blast, where the stresses had been shed. These events were however of much lower energy than those recorded during the extraction of Cut #21, before the destress blast.

10.5.5. Results from the stress cells

Figure 101 shows the results obtained from the Geokon vibrating wire stress cells connected to the datalogger. The graph covers seven days of data collection, from 22 to 28 December 2001, inclusive.

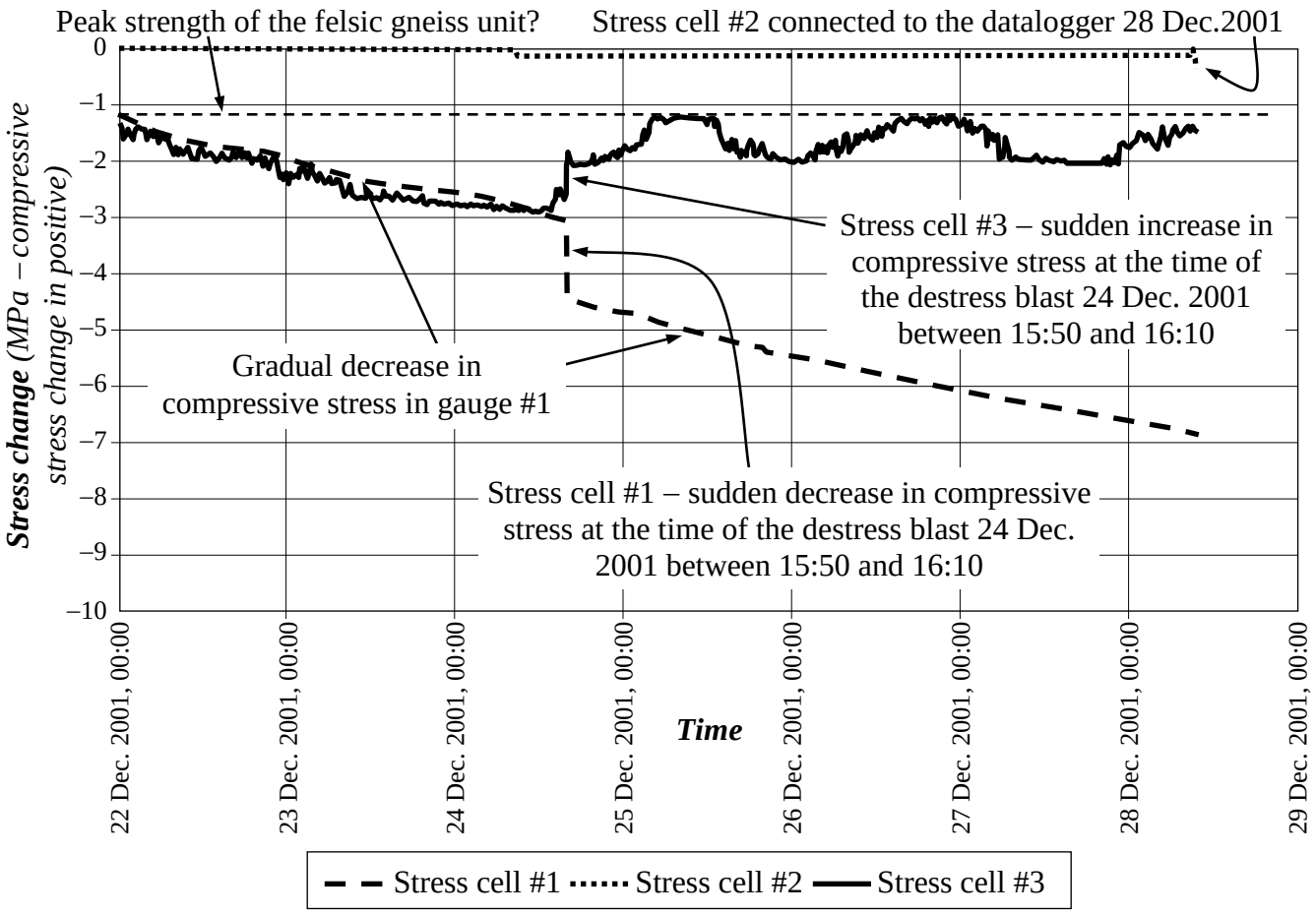

Figure 101. Results from the Geokon stress cells installed near the 42-1-080 Access.

Stress cell #1 recorded an overall decrease of the sub-horizontal north-south stress component of nearly 6 MPa. In particular, a sudden decrease of the order of 1.5 MPa occurred at blast time, 24 December between 15:50 and 16:10. Following the destress blast, the gradual reduction in the local sub-horizontal north-south compressive stress resumed, at about the same rate as before the destress blast. The fact that the stress relaxation rate did not change (accelerate and eventually stabilise) after the destress blast probably reflects the behaviour of the relatively weak ore where the gauge was installed, which is sufficiently soft to continually yield under the static stress-induced load rather than behave in a more brittle manner, as would be expected in granite for example.

Stress cell #3, located in a strong felsic gneiss, was showing a progressive reduction in the vertical stress component prior to the destress blast at a rate similar to that shown by stress

cell #1. Since it is highly unlikely that this was the result of the wedge of the instruments slipping between the platen and the cell (even if some slippage was indeed occurring, there was no reason for it to progress in the exact same manner in both instruments), it was assumed that this stress reduction was real. This could indicate that the area targeted for destressing had already reached its peak strength prior to the destress blast being fired, with this blast merely accelerating the yielding process. As shown in Figure 101, a sudden increase in the magnitude of the vertical compressive stress was measured by stress cell #3 at the time of the destress blast. This behaviour is in accordance with what was expected. As illustrated by the thick arrows in Figure 102, the reduction of the sill pillar effective thickness (through which stress can flow) that would result from a successful destress blast would cause a regional re-orientation of the stress flow, which would rotate upwards at the point of interest shown in the figure. (This point can be taken to correspond approximately to the location of gauge #3.)

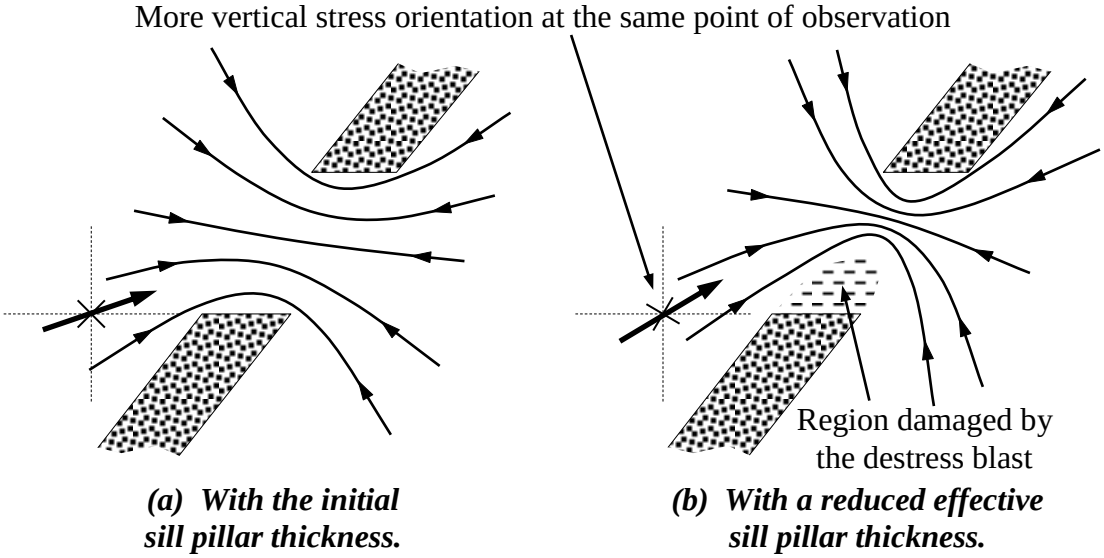

Figure 102. Conceptual cross-section (not to scale) looking west through the destressed pillar, showing how a reduction of the sill pillar effective thickness effectively results in a stress re-orientation at a given point of observation.

The behaviour of stress cell #3 after the destress blast is quite interesting. As shown in Figure 101, its readings oscillated between –1 and –2 MPa during the three days following the blast, with a period of about 36 hours. This behaviour is not entirely understood. One

possible explanation could be that the felsic gneiss yielded incrementally as the vertical stress component progressively increased. Assuming this to be the case, the peak compressive strength of the felsic gneiss at the point of observation would correspond to the horizontal dashed line superimposed on top of the figure. A mechanism that could explain the stress magnitude oscillation observed in gauge #3 is as follows: 1) the sill pillar yields; 2) the major principal stress component σ_1 is rotated more vertically and further concentrates in the shrinking intact core of the pillar; and, 3) this increased stress concentration quickly exceeds the local strength of the rock mass, which, in turn, yields further.

One point to keep in mind when looking at the data from the stress cells is the relatively large distance between these instruments and the destress blast, which results in less "spectacular" stress amplitude changes to be observed. Nevertheless, the data clearly showed a jump in the stress regime at blast time, consistent with a reduction in the sub-horizontal north-south component and an increase in the sub-vertical one.

10.5.6. Results from the multi-point extensometers

Figure 103 shows the results obtained from the multi-point extensometers. No anchor on extensometer #1 exhibited any movement – it was later found that the power lead on this unit was not connected to the datalogger due to the breakage of the wire in its socket. Extensometer #2, which was located much closer to the destress blast and in a relatively wide area, did however record movement. Due to inversions in the channel colour code, only data from anchors #1, #2 and #3, the furthermost from the rock surface, were logged. A displacement of 2 mm (0.08 inch) was recorded at these three anchors at blast time, followed by a series of small sudden jumps over a period of three and a half days after the destress blast. None of these small jumps could be reliably related to recorded seismic events.

The fact that permanent deformations were measured at blast time is indicative that it did result in some damage in the region. Because the three deepest anchors were affected to

about the same extent, it can be inferred that the movement occurred within 6.7m of the surface. This can conceivably be the result of either a stress relaxation (which would have caused a reduction in confinement and the sagging of the previously stress-fractured back), or a stress increase (caused by the dynamic load from the blast itself, which would have caused additional fracturing in the back and a resulting volume increase in this region).

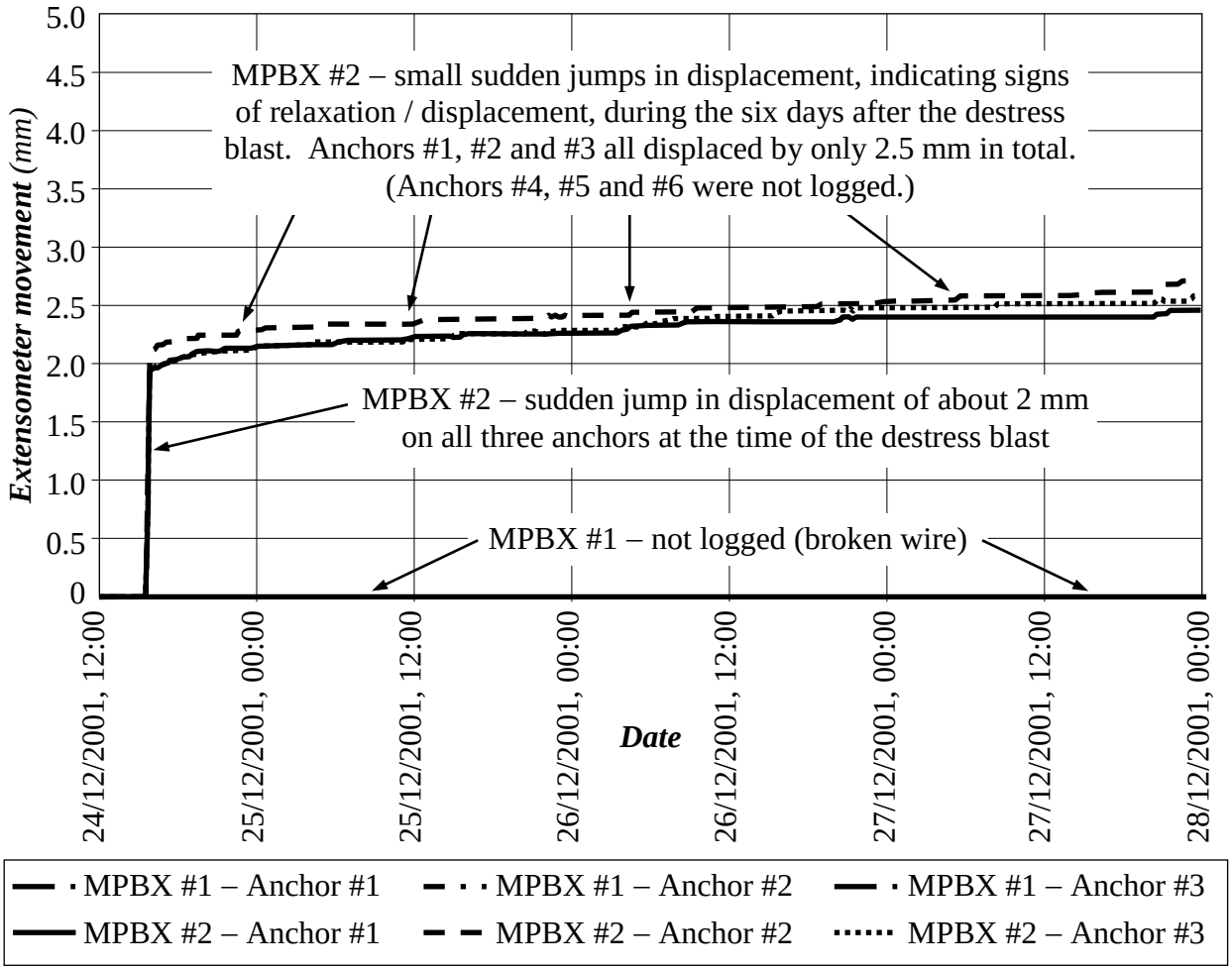

Figure 103. Results from the MPBX extensometers installed near the 42-1-080 Access.

It is difficult to further elaborate on the stress changes that could have resulted in the deformations measured by the extensometers – overall, however, indications are that a stress change did occur in the vicinity of extensometer #2 at blast time.

10.5.7. Results from the strain gauge in the instrumented shotcrete pillar

The strain gauge embedded in the shotcrete post at the entrance to the A5 lens indicated a load increase of approximately 20 tonnes over the three-day period following the blast. This was the result of a vertical convergence between the back and floor, due to the downwards movement of the strata in the back in response to the destress blast (as measured by extensometer #2).

Interestingly, a significant load relief followed after the backfilling cycle was completed in the area, probably due to the combined effect of the stiff ground support in the back and the compaction of the floor under the weight of the added backfill.

10.5.8. General conclusions from the observations and measurements

Based upon field observations, subsequent mining conditions, instrumentation results and seismic activity records, it can be concluded that the destress blast was successful in diverting at least some of the ground stresses away from the next cuts in the A5 stringer, and concentrating them instead higher up in the sill pillar and in the abutments. These effects were the fundamental objectives pursued by the project.

10.6. DESTRESSABILITY INDEX ASSESSMENT

The previous sections have shown that the destress blast in the A5-Right pillar produced results that are consistent with a successful destressing effect. As was done in Chapter IX for the destress blast in the 29-9 Pillar at Brunswick Mine, the Destressability Index that would have been associated with the rock mass conditions and the blast design implemented in the A5-Right pillar will be evaluated in this section, at both the intact rock material and the rock mass scales. Again, the objective of this task is to assess how accurately this index would have "predicted" the outcome of the blast, as well as lay the

ground for the evaluation of the scale at which this prediction would have been the most precise.

10.6.1. At the scale of the intact rock material

Table 56 summarises the values associated with the properties used to describe the first eight parameters of the RES interaction matrix at the intact rock material scale in the case of the A5-Right pillar at Fraser Copper Mine.

Table 56. List of the basic properties and quantities required for the assessment of the Destressability Index at the intact rock material scale in the A5-Right pillar.

Properties	Symbol	Unit	Value in A5-Right
Density of the rock	ρ_r	*kg/m³*	2,800
Young's modulus of the intact rock material	$E_{Laboratory}$	*GPa*	75
Unconfined compressive strength of the intact rock material	$\sigma_{c\ Laboratory}$	*MPa*	318
Brittleness Index Modified ratio	BIM	–	1.25
Rock Mass Rating of the felsic gneiss	RMR	*%*	85
Hoek-Brown parameter m of the intact rock material	$m_{Laboratory}$	–	7.500
Hoek-Brown parameter s of the intact rock material	$s_{Laboratory}$	–	1.000
Effective σ_1 component at the time of the destress blast	$\sigma_{1\ Actual}$	*MPa*	90
Effective σ_3 component at the time of the destress blast	$\sigma_{3\ Actual}$	*MPa*	35
Angle of incidence of the blast with respect to the σ_1 component	θ	*degrees*	85
Length of the pillar to destress	L	*m*	27.5
Height of the pillar to destress	H	*m*	18.0
Number of blasting rings in the destress blast	N	*#*	2
Diameter of the blastholes	D	*mm*	114.3
Distance between blasthole rings	B	*m*	3.00
Distance between blastholes on the same ring	S	*m*	3.00
Unloaded toe length in the blastholes *****	T	*m*	0.00

Table 56 (continued). List of the basic properties and quantities required for the assessment of the Destressability Index at the intact rock material scale in the A5-Right pillar.

Properties	Symbol	Unit	Value in A5-Right
Unloaded collar length in the blastholes	C	*m*	6.5 **
Usage of inert stemming material	–	*Yes* or *No*	No
Density of the explosive product	ρ_e	*g/cm³*	1.25
Absolute weight strength of the explosive	AWS	*cal/g*	866

***** *use zero for non-breakthrough holes.*
****** *derived from average values in the fanned blastholes.*

No numerical modelling work was done specifically within the scope of this project for the purpose of estimating the pre-blast stress levels because visual field observations left little doubt that these levels were nearing the strength of the rock mass. The seismic activity shown in Figure 82, the borehole breakouts described in Section 10.1 and the occurrences of offset and squeezing observed inside the destress blastholes are all indicative of these high levels of stress. Instead, the magnitude of the sub-vertical minor principal stress component σ_3 at the time of the destress blast was analytically estimated at 35 MPa based upon the depth of 1,260m and the known local vertical stress gradient of 0.028 MPa per metre of depth. The mining-induced major principal stress component at the Fraser Copper Mine is sub-horizontal and oriented north-south (the in situ major principal stress component is oriented east-west, but rotates to the north-south direction near the abutments of mined cuts in east-west-oriented lenses), with its magnitude about twice that of the vertical stress component. However, considering the sill pillar situation and based upon evidence of borehole breakouts in the instrumentation holes, the magnitude of σ_1 in this case was increased to 2.5 times the magnitude of σ_v, which corresponds to about 88 MPa (rounded to 90 MPa) before the destress blast.

This stress level is in agreement with the 70–80 MPa σ_1 magnitude computed a bit further east in the same sill pillar, but with one more cut still in place, by Pierce & Board (1999 [a]) with a 3DEC model.

10.6.1.1. Step I – Calculation of the required design values

Proximity to static failure = $\sigma_1 / (\sigma_3 + [m_{Laboratory} \sigma_c \sigma_3 + s_{Laboratory} \sigma_c^2]^{0.5}) = 19.4\%$

Effective volume of the targeted pillar $V_{Eff.} = 3{,}600\ m^3$ (as per Table 53)

Effective mass of the targeted pillar $M_{Eff.} = 10{,}075$ tonnes (as per Table 53)

Charge confinement ratio = (T + C) / (D / 1000) = (0 + [6.5 × 1.0]) / (0.1143) = 56.9

Total number of blastholes $N_b = 28$

Total explosive energy in the blast $E_{Blast} = 3.884$ Gcal (as per Table 53)

Unit explosive energy in the blast $E_{Unit} = 385.5$ cal/kg of rock

10.6.1.2. Step II – Rating of the parameters

Rating for parameter P_1 – Stiffness of the intact rock material:

$E_{Laboratory} = 75$ GPa. Using Table 6, the corresponding rating is 1, for a score of 14.

Rating for parameter P_2 – Brittleness of the intact rock material:

BIM = 1.25. Using Table 7, the corresponding rating is 1, for a score of 15.

Rating for parameter P_3 – Degree of fracturing of the rock mass:

RMR = 85%. Using Table 8, the corresponding rating is 2, for a score of 38.

Rating for parameter P_4 – Proximity to failure:

Proximity to static failure = 19.4%. Using Table 9, the corresponding rating is 1, for a score of 14.

Rating for parameter P_5 – Orientation of σ_1 :

$\theta = 85°$. Using Table 10, the corresponding rating is 2, for a score of 26.

Rating for parameter P_6 – Width of the target zone:

N = 2. Using Table 11, the corresponding rating is 1, for a score of 18.

Rating for parameter P_7 – Explosive energy per tonne of target zone:

E_{Unit} = 385.5 cal/kg of rock. Using Table 12, the corresponding rating is 2, for a score of 56.

Rating for parameter P_8 – Confinement of the explosive charges:

Charge confinement ratio = 56.9. Using Table 13, the corresponding rating is 2, for a score of 34.

10.6.1.3. Step III – Assessment of the Destressability Index

Table 57 summarises the rating and score associated with each parameter for the assessment of the Destressability Index at the intact rock material scale in the A5-Right pillar at Fraser Mine.

Table 57. Rating and score associated with each parameter for the assessment of the Destressability Index at the intact rock material scale in the A5-Right pillar.

Parameter	Rating	Score
P_1 – Stiffness of the intact rock material	1	14
P_2 – Brittleness of the intact rock material	1	15
P_3 – Degree of fracturing of the rock mass	2	38
P_4 – Proximity to failure	1	14
P_5 – Orientation with respect to σ_1	2	26
P_6 – Width of the target zone	1	18
P_7 – Explosive energy per tonne of target zone	2	56
P_8 – Confinement of the explosive charges	2	34
	Total	215

The corresponding overall normalised score is thus (215 / 276) = 0.78, which, based upon Table 14, would correspond to a Destressability Index of ‘Good’.

10.6.2. At the scale of the rock mass

Table 58 summarises the values associated with the properties used to describe the first eight parameters of the RES interaction matrix at the rock mass scale in the case of the A5-Right pillar at Fraser Copper.

Table 58. List of the basic properties and quantities required for the assessment of the Destressability Index at the rock mass scale in the A5-Right pillar.

Properties	Symbol	Unit	Value in A5-Right
Density of the rock	ρ_r	*kg/m³*	2,800
Young's modulus of the intact rock material	$E_{Laboratory}$	*GPa*	75
Unconfined compressive strength of the intact rock material	$\sigma_{c\ Laboratory}$	*MPa*	318
Rock Mass Rating of the felsic gneiss	RMR	*%*	85
Hoek-Brown parameter m of the intact rock material	$m_{Laboratory}$	–	7.500
Hoek-Brown parameter s of the intact rock material	$s_{Laboratory}$	–	1.000
Effective σ_1 component at the time of the destress blast	$\sigma_{1\ Actual}$	*MPa*	90
Effective σ_3 component at the time of the destress blast	$\sigma_{3\ Actual}$	*MPa*	35
Angle of incidence of the blast with respect to the σ_1 component	θ	*degrees*	85
Length of the pillar to destress	L	*m*	27.5
Height of the pillar to destress	H	*m*	18.0
Number of blasting rings in the destress blast	N	*#*	2
Diameter of the blastholes	D	*mm*	114.3
Distance between blasthole rings	B	*m*	3.00
Distance between blastholes on the same ring	S	*m*	3.00
Unloaded toe length in the blastholes *****	T	*m*	0.00
Unloaded collar length in the blastholes	C	*m*	6.5 ******
Usage of inert stemming material	–	*Yes* or *No*	No
Density of the explosive product	ρ_e	*g/cm³*	1.25
Absolute weight strength of the explosive	AWS	*cal/g*	866

***** *use zero for non-breakthrough holes.*
****** *derived from average values in the fanned blastholes.*

The magnitudes of σ_1 and σ_3 were derived as described immediately following Table 56 for the case of the Destressability Index at the intact rock material scale.

10.6.2.1. Step I – Calculation of the required design values

$E_{Rock\ Mass} = E_{Laboratory} \times ([\ 0.000028 \times RMR^{2}\ ] + [\ 0.009 \times e^{\{RMR/22.82\}}]) = 43.2$ GPa

$GSI = RMR - 5 = 85 - 5 = 80$

$m_{Rock\ Mass} = m_{Laboratory} \times e^{([GSI - 100]/28)} = 3.672$ (undisturbed, before the destress blast)

$s_{Rock\ Mass} = s_{Laboratory} \times e^{([GSI - 100]/9)} = 0.108$ (undisturbed, before the destress blast)

$\sigma_{c\ Rock\ Mass} = \sigma_3 + ([\ m_{Rock\ Mass}\ \sigma_c\ \sigma_3\ ] + [\ s_{Rock\ Mass}\ \sigma_c^{2}\ ])^{0.5}$, for $\sigma_3 = 0$, which is 104.7 MPa

$\sigma_{T\ Rock\ \ Mass} = (\ m_{Rock\ \ Mass}\ \sigma_c - [\ m_{Rock\ \ Mass}^{2}\ \sigma_c^{2} - 4\ s_{Rock\ \ Mass}\ \sigma_c^{2}\ ]^{0.5}\ )/2$ (the quadratic formulae for $\sigma_1 = 0$), which is about 9.5 MPa

$B_1 = \sigma_{c\ Rock\ Mass} / \sigma_{T\ Rock\ Mass} = (104.7 / 9.5) = 11.0$

Proximity to failure $= \sigma_1 / (\ \sigma_3 + [\ m_{Rock\ Mass}\ \sigma_c\ \sigma_3 + s_{Rock\ Mass}\ \sigma_c^{2}\ ]^{0.5}\ ) = 34.3\%$

Effective volume of the targeted pillar $V_{Eff.} = 3{,}600\ m^3$ (as per Table 53)

Effective mass of the targeted pillar $M_{Eff.} = 10{,}075$ tonnes (as per Table 53)

Charge confinement ratio $= (T + C) / (D / 1000) = 56.9$

Total number of blastholes $N_b = 28$

Total explosive energy in the blast $E_{Blast} = 3.884$ Gcal (as per Table 53)

Unit energy in the blast $E_{Unit} = (E_{Blast} / M_{Eff.}) \times 10^{6} = 385.5$ cal/kg of rock

10.6.2.2. Step II – Rating of the parameters

Rating for parameter P_1 – Stiffness of the rock mass:

$E_{Rock\ Mass} = 43.2$. Using Table 17, the corresponding rating is 1, for a score of 13.

Rating for parameter P_2 – Brittleness of the rock mass:

$B_1 = 11.0$. Using Table 18, the corresponding rating is 1, for a score of 13.

Rating for parameter P_3 – Degree of fracturing of the rock mass:

RMR = 85. Using Table 19, the corresponding rating is 2, for a score of 28.

Rating for parameter P_4 – Proximity to failure:

Proximity to failure = 34.3%. Using Table 20, the corresponding rating is 1, for a score of 14.

Rating for parameter P_5 – Orientation of σ_1 :

$\theta = 85°$. Using Table 22, the corresponding rating is 2, for a score of 26.

Rating for parameter P_6 – Width of the target zone:

N = 2. Using Table 23, the corresponding rating is 1, for a score of 18.

Rating for parameter P_7 – Explosive energy per tonne of target zone:

E_{Unit} = 385.5 cal/kg of rock. Using Table 24, the corresponding rating is 2, for a score of 48.

Rating for parameter P_8 – Confinement of the explosive charges:

Charge confinement ratio = 56.9. Using Table 25, the corresponding rating is 2, for a score of 34.

10.6.2.3. Step III – Assessment of the Destressability Index

Table 59 summarises the rating and score associated with each parameter for the assessment of the Destressability Index at the rock mass scale in the A5-Right pillar.

Table 59. Rating and score associated with each parameter for the assessment of the Destressability Index at the rock mass scale in the A5-Right pillar.

Parameter	Rating	Score
P_1 – Stiffness of the rock mass	1	13
P_2 – Brittleness of the rock mass	1	13

Table 59 (continued). Rating and score associated with each parameter for the assessment of the Destressability Index at the rock mass scale in the A5-Right pillar.

Parameter	Rating	Score
P_3 – Degree of fracturing of the rock mass	2	28
P_4 – Proximity to failure	1	14
P_5 – Orientation with respect to σ_1	2	26
P_6 – Width of the target zone	1	18
P_7 – Explosive energy per tonne of target zone	2	48
P_8 – Confinement of the explosive charges	2	34
	Total	194

The corresponding overall normalised score is thus (194 / 252) = 0.77, which, based upon Table 26, corresponds again to a Destressability Index of 'Good'.

CONCLUSION DU CHAPITRE. Le calcul d'un Indice de relâchement de 'bon' est raisonnable vis-à-vis des résultats observés et mesurés sous terre en décembre 2001 suite à la détonation du tir confiné à grande échelle de relaxation des contraintes dans le pilier 42-1-080 à la mine Fraser Copper. Comme pour l'étude de cas précédente du Chapitre IX, les deux approches – aux échelles du roc intact et du massif rocheux - ont donné des résultats comparables.

Certainement, toutes les observations faites sous terre ainsi que les résultats obtenus des instruments installés à proximité du sautage ont indiqué qu'une redistribution significative des contraintes de terrain a eu lieu dans la région, d'une manière consistante avec un tir réussi de relaxation des contraintes pour lequel un 'bon' résultat aurait été prévu. Donc, similairement au Chapitre IX, ce chapitre a établi que le tir de relaxation des contraintes a fonctionné de manière adéquate, et que la méthodologie de l'Index de relâchement aurait été utile puisqu'elle aurait correctement prédit ce résultat.

Ce chapitre a également démontré une nouvelle fois que les données et paramètres requis par la technique sont largement disponibles ou faciles à déterminer en suivant la méthodologie suggérée, et que l'approche générale est relativement simple à utiliser.

CHAPTER CONCLUSION. The calculation of a 'Good' Destressability Index rating is reasonable in light of the field results observed and measured underground following the detonation of the large-scale confined destress blast of December 2001 in the 42-1-080

pillar at the Fraser Copper Mine. As with the previous case study of Chapter IX, both approaches, at the intact rock material and the rock mass scales, gave comparable results.

Certainly, all the observations made underground and the results obtained from the instrumentation installed in the vicinity of the destress blast indicated that a significant stress redistribution occurred in the region, consistent with a successful destress blast for which a 'Good' outcome would have been predicted. Hence, similarly to Chapter IX, this chapter has established that the destress blast worked adequately, and that the Destressability Index methodology would have been useful because it would have predicted this outcome correctly.

This chapter also further demonstrated that the input values required by the technique are readily obtainable or easy to determine by following the suggested methodology, and that the approach is overall relatively simple to use.

CHAPTER XI

11. CONCLUDING REMARKS AND FUTURE WORK

This final chapter is divided into three parts. The first part provides an overview and a general summary of the work undertaken within the framework of this thesis, and recapitulates the essential phases of the research. The second part provides some conclusions on this work, highlights the innovations it contained and identifies the contributions it has made to the field of large-scale confined destress blasting engineering. The third part discusses further perspectives, and suggests possible future work 1) in the application of Rock Engineering Systems to large-scale confined destress blasts in underground mine pillars; and, 2) for the refinement of the Destressability Index methodology.

11.1. SUMMARY OF THE WORK AND ESSENTIAL PHASES OF THE RESEARCH

Considering that the trend in the Canadian underground mining industry is towards greater depths, major technical challenges must be met. One of them is associated with the

stability of the workings: as depth increases the stress levels increase as well, which are exacerbated by the load concentrations that result from mining. Hence, as mining goes deeper, the risk of the openings collapsing increases as well. Depending upon the rock mass properties and the geological settings, this failure can be either progressive, or sudden and violent, the latter case representing the worst situation. There are a number of proactive measures that can be implemented to alleviate the ground control issues associated with mining at depth, or under high stress levels. Mining methods can be changed, mining sequences can be altered, alternative ground support systems can be implemented, and preconditioning and destressing techniques can be applied. Reactive measures can also be considered, essentially by supplementing the ground support elements already installed, and/or attempting destressing.

This thesis has focused on the destressing option – either proactive or reactive – and, in particular, on large-scale confined destress blasts in underground mine pillars. One specific aspect of this work has been the application of Rock Engineering Systems to the development of a rational destress blast design methodology that would be both accessible and useful to practitioners such as site engineers, technologists and consultants.

The principal objective of this work has been to provide a methodology to quantify the chance of success of large-scale confined destress blasts in underground mine pillars. Since such blasts are generally attempted in highly stressed ground that is likely to fail violently over time, issues related to the violent failure of rock masses were discussed first. The various types of rockbursts were also reviewed, to establish in some detail which types of problems destressing is meant to address. A review of the methods most commonly used to assess the bursting potential of a rock mass was then completed with the objective of providing some means of assessing how urgent it is to take action at a given time, under a given set of circumstances. Possible measures to alleviate violent rock mass failure were then presented, which include, as a last resort, destress blasting. From this point onwards, the dissertation focused on destress blasting issues. General definitions and mechanisms were first presented, followed by the review of the various types of destress blasting that exist and the specific objectives pursued by each. Numerous case histories were

subsequently reviewed, which demonstrated the lack of well-established guidelines for the engineering and design of large-scale confined destress blasts in underground mine pillars, as well as for the reporting of the relevant data. The discussion then concentrated on the various choked destress blast design philosophies encountered in the literature. Following this, a review of the various general blasting engineering methodologies was conducted, which showed that none is readily capable of satisfactorily addressing large-scale confined destress blasts, nor of considering all the parameters involved.

Having recognised this lack of well-established guidelines for, and the limited direct applicability of the existing blast design techniques to, large-scale confined panel destress blasts, a novel alternative approach was proposed. It consisted in the application of the Rock Engineering Systems methodology to sort out in a rational manner the extent to which a number of parameters play a role in large-scale confined pillar destress blasting. (The RES approach uses a matrix-based technique to quantify in a systematic way the interaction between each pair of parameters known to play a role in a given engineering process.) In essence, a complex process was subjected to a rigorous engineering approach in order to identify which parameters truly control the results. This step was seen as paramount to being able to understand and quantify the various mechanisms at play, in order to derive a sensible engineering and design methodology for this type of blasting.

The general concept of the Rock Engineering Systems was introduced first, followed by a discussion on their potential application to blasting at large, and destress blasting in particular. Eight parameters were argued to have a significant effect on the large-scale confined pillar destress blasting process and were eventually retained – the first four relate to the rock in which the destress blast is attempted, the last four to blasting issues. Two RES interaction matrices were subsequently developed and coded, which described the large-scale confined pillar destress blasting process – the first matrix considered the four rock-related parameters at the scale of the intact rock material, whereas the second one considered them at the scale of the rock mass. The first approach is simpler because the rock-related parameters in the matrix can be represented by properties that are relatively easily derived in the laboratory – it however needs to be adjusted since it is the rock mass

properties that are ultimately pertinent in the case of a large-scale destress blast. The second approach is more complex because the rock-related matrix parameters must then be represented by properties either extrapolated to, or measured directly at, the rock mass scale – the main advantage, however, resides in the scientific relevance of this larger scale to the problem at hand. Being unsure beforehand which scale would be more appropriate, both were developed and evaluated. In each interaction matrix the RES approach was applied to weigh the individual influence of the eight parameters retained. This weighing was then used to derive a new methodology to assess the likelihood of a given destress blast design – implemented in a given rock mass subjected to a given stress regime – being successful. This methodology, developed at both the intact rock material and the rock mass scales, was based upon the development of a new parameter called the "Destressability Index".

Overall, the Destressability Index approach can be summarised as follows. A measurable value is first assigned to each of the properties associated with the eight governing parameters retained in the large-scale choked pillar destressing RES interaction matrix. Each value is compared to various thresholds, in order to assess how conducive it is to a successful choked destress blast – a simple rating of 0 (not conducive), 1 (somewhat conducive) or 2 (conducive) is assigned. For each parameter this 0, 1 or 2 rating is then multiplied by its cause (which represents its influence on the whole system, as identified previously with the RES methodology) in order to provide a measure of how favourable it is to a successful destress blast. This provides a score for each parameter. All the scores are then added and divided by the maximum possible arithmetical score to produce a normalised total score from which a Destressability Index rating can be derived, which can land in one of four categories: 'Low', 'Medium', 'Good' or 'Excellent'.

This new procedure is not a direct design methodology, but rather an assessment of the likelihood of success of a proposed destress blast design in a given situation. Although one cannot modify the intrinsic rock parameters, one can choose to a certain extent the stress state that will prevail at the time of the destress blast (by choosing the step in the mining sequence at which the destress blast will be implemented) and alter the blasting parameters

in order to increase the Destressability Index and, hence, the chance of success. The blast parameters can be modified a number of times and the Destressability Index re-assessed, which allows the design to be eventually optimised, in an iterative manner. As it was demonstrated through the review of numerous case histories, there are currently no well-established guidelines to 1) decide at which point a large-scale confined destress blast should be attempted in an underground mine pillar; and, 2) design such a blast based upon rock mechanics *and* blasting considerations. In general, a simple trial and error approach is implemented at a given site, with the best "formula" being retained as the standard for subsequent blasts. It is therefore argued that the proposed approach has a high practical value in the sense that it can help properly design a large-scale confined destress blast simply by taking steps that result in an increase in the Destressability Index. A particular appeal of this approach is that it provides a series of easily implemented steps that result in a rational assessment of the chance of success of a given destress blast design in a given situation of rock mass conditions and stress regime.

11.2. GENERAL CONCLUSIONS AND INNOVATIVE CONTRIBUTION TO KNOWLEDGE

The detailed case studies presented in chapters IX and X led to the conclusion that the Destressability Index values obtained – at both the intact rock material and rock mass scales – were in overall accordance with the field results observed and the various measurements made. The approach at both scales gave comparable results in both instances – this is not too surprising given how carefully the scale issue was considered during the development of the methodology.

The results obtained from these two case histories can be examined to evaluate how far each of the four Destressability Index values calculated landed from the thresholds of the neighbouring ratings. Table 60 compares the normalised scores obtained for these two case studies.

Table 60. Normalised destressability scores obtained for both case histories, at both the intact rock material and rock mass scales.

Scale considered	Normalised destressability scores obtained	
	Brunswick Mine case study of Chapter IX	Fraser Mine case study of Chapter X
Intact rock material	0.78	0.78
Rock mass	0.72	0.77

Note: a destressability rating of 'Good' corresponds to a normalised score of between 0.70 and 0.85.

Based upon these values it appears as though the approach at the intact rock material scale is a bit more optimistic, with scores of 0.78 in both cases, which are closer to the 0.85 threshold required to yield an 'Excellent' Destressability Index rating. The fact that the score was similar for both case studies also indicates that the methodology is probably less sensitive at that scale, and not able to account for relatively small differences in the conditions. The scores achieved at the rock mass scale were more conservative (i.e., more pessimistic) and more sensitive as well, with a difference of about 6.5% between the normalised destressability scores obtained at Brunswick and Fraser. The methodology indicated that the conditions and blast design parameters were a bit more conducive to a successful large-scale confined destress blast at the Fraser site than at Brunswick Mine, which, on hindsight, was probably confirmed in the field. The Fraser Mine blast was certainly successful enough to allow full-entry cut-and-fill mining to successfully resume in its immediate vicinity. Based upon these early observations, the approach at the rock mass scale should be retained over that at the intact rock material scale. Overall, the Destressability Index approach seems to work adequately for the two detailed case histories presented – if used beforehand, it would have agreed with the decision to go ahead with both blasts.

A number of innovative contributions have been made through the completion of this work, as follows.

- A large database of documented destress blasting case histories was constructed, which showed that not all destress blasts are similar in nature. Whether such blasts are used for

development, in preparation to mining (with the objective of re-entering the area), for the destressing of remnant pillars (with no subsequent personnel re-entry), for inducing slippage along faults, etc., has a large effect on the design implemented. As a result, not all destress blasts can be directly compared. Out of all these types of destress blasting, one – large-scale confined pillar destress blasts – was chosen as the point of focus of this thesis.

- The lack of well-established engineering guidelines for this type of blasting, as well as the general "art" connotation associated with it were not deemed satisfactory, and the process was investigated scientifically. Considering that 1) large-scale confined pillar destress blasts are usually a last resort endeavour with no possible second attempt; 2) the cost associated with their implementation can be in the hundreds of thousands of dollars; and, 3) the consequences of failure generally lead to significant ore losses and lost production (these blasts are only considered in the first place when large amounts of valuable ore are at risk, either directly or indirectly), this type of blast deserves sound engineering in order to maximise its chances of success. The work done in this thesis is thus not trivial.

- The Rock Engineering Systems approach was shown to be a valuable tool to help with the understanding of the complex mechanisms and interactions at play in the destressing problem examined. A comprehensive RES-based strategy was developed to 1) quantify the interactions between the various parameters involved; and, 2) assess both their individual and combined effects on the overall success of a given destress blast. With this approach the destress blasting process was considered simultaneously from *both* the blasting and the rock mechanics perspectives, which was a major innovation of this work.

- It was found that large-scale confined pillar destress blasts are not a routine endeavour, and that those mentioned in the literature were generally not reported in great detail – still, two very reliable and fully-documented case histories were found, on which the Destressability Index methodology was tested.

- The framework for building this type of project – in which interactions identified and quantified with RES-based analyses are subsequently used to derive an empirical engineering methodology – was laid-out.

Overall, this work led to the development of a scientific and engineered tool to assess the likelihood of success of a given large-scale choked pillar destress blast design implemented in a given rock mass subjected to a given stress regime. This tool was shown to be easy to use and based upon input data that are either easily available or readily obtainable with limited efforts. The case was also made that the Destressability Index methodology can be applied to future major large-scale confined pillar destress blasts, and adequately predict their outcome. As mentioned previously, the system developed in this work is modular in nature – as technology and knowledge advance, certain modules can be improved (without having to re-visit all the other ones) and increase the reliability of the entire approach.

11.3. FURTHER PERSPECTIVES AND POSSIBLE FUTURE WORK

It is well acknowledged that some limitations are associated with this work, and that further development would be beneficial. As far as such future work is concerned, it is the opinion of the writer that it should focus on the approach at the rock mass scale, which was shown by the back-analysis of the two detailed case studies to be somewhat more sensitive to the input parameters and more conservative in its assessment of the expected outcome of a given destress blast design.

Although significant progress has been achieved, there are a number of issues that would benefit from further work. In particular, the detailed back-analysis of more case studies would be useful – as with any new applied engineering methodology, the broader the array of cases tested, the more reliable and robust it becomes. This is certainly true of the Destressability Index technique. Various other issues that could gain from further investigation are discussed in the following sections.

11.3.1. Parameters of the RES interaction matrix

The eight parameters retained in the methodology could be revisited – in particular, other researchers should investigate whether the approach could be further simplified, by astutely combining some parameters together. During the course of the work described in this thesis, one parameter – addressing the strength of the rock –, was eliminated when found redundant since addressed in two places. It is possible that further simplifications could be made, which would render the technique that much easier to apply.

11.3.2. Coding of the RES interaction matrix

The coding of the RES interaction matrix could also be revised, particularly considering that the one proposed in this work was entirely based upon the perception, logic and experience of the writer. Not only would it be interesting to see how other researchers would code this matrix, it would also provide some sense on the degree of subjectivity involved in this important step.

11.3.3. Properties chosen to represent the system parameters

The next area where further work could be useful concerns the properties chosen to represent the parameters selected for inclusion in the methodology. Even though generally accepted means of quantifying the eight parameters have been retained, it is acknowledged that the chosen formulations are not necessarily the best ones, and that better properties could conceivably be selected.

Furthermore, and even if the global choice of properties remains unchanged, refinements should be sought after in their formulation. For example, one parameter that warrants further work is parameter P_8, the confinement of the explosive charges. As indicated previously, this parameter is represented by the "charge confinement ratio", which has been defined as the unloaded collar length plus the unloaded toe length, divided by the diameter of the blasthole – as a greater length is left unloaded inside a blasthole, the degree of

longitudinal charge confinement is taken to increase. One will have noticed that for non-breakthrough blastholes, the unloaded toe length is set to zero. This simplified the calculation in the development spreadsheets of the charge weight per blasthole, as well as the computation of the total and unit explosive energy in the blast during the elaboration of the methodology. However, the bottom portion of a non-breakthrough blasthole is more confined than that of a breakthrough hole – this should be reflected in the value of the charge confinement ratio. Figure 104 suggests an alternative approach for the calculation of the charge confinement ratio, which does take this consideration into account.

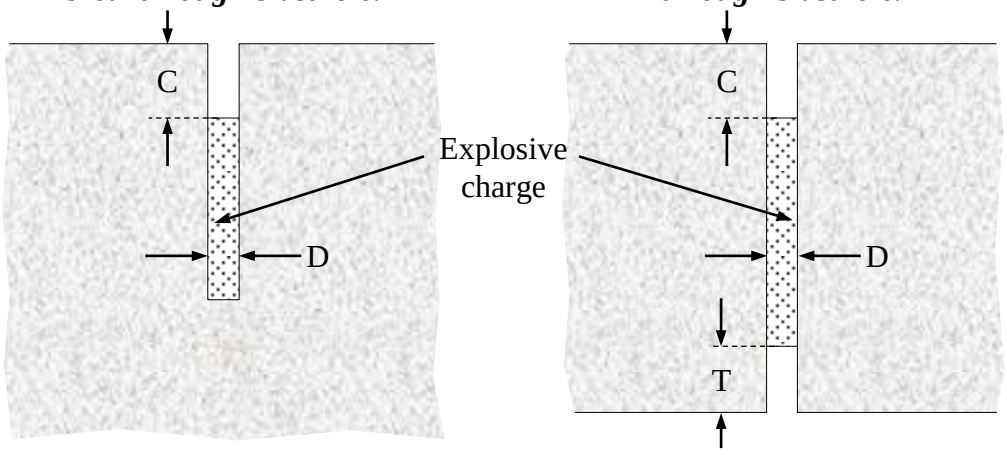

Then, in both cases, charge confinement ratio = (T + C) / D

Again, add 50% to C if inert stemming material is used, but up to a maximum value of C equal to 35 times the blasthole diameter.

Figure 104. Suggested alternative methodology for the calculation of the charge confinement ratio.

This suggestion is based upon the basic rule-of-thumb that states that the unloaded collar length of a blasthole should be between 20 and 25 times its diameter. The threshold of "35" times the blasthole diameter essentially recognises that past a certain degree of

longitudinal confinement no further gain in the amount of effective work performed by the explosive charge is gained.

11.3.4. Rating of the parameters

The rating of the various parameters, based upon the value of their associated property, should be examined further, particularly in terms of the range criteria applied for this rating. For example, the rating of parameter P_7 (the explosive energy per kg of targeted rock) shown in Table 24 should logically not only consider straight calories per kilogram, but also encompass some consideration of the rock mass strength and prevailing stress regime.

Another interesting aspect that should eventually be investigated as well concerns the system used to establish the rating of the various parameters from the value of their corresponding property. In this work finite property ranges have been established, bounded by threshold values and within which the rating of the parameter has been kept constant (at either 0, 1 or 2). A *continuous* rating scheme could conceivably be implemented instead, whereby the rating of each parameter would vary proportionally to the value of its corresponding property. With this approach, instead of being limited to integer values between 0 and 2, the rating of each parameter could be any real number between 0.00 and 2.00 (this range could also conceivably be changed). The multiplication of this rating by the cause of the parameter would allow, in turn, the calculation of a more precise parameter score. Although the establishment of simple discrete ranges was adequate as a first pass, it is not very sensitive, and directly affected by the threshold values chosen to establish these ranges. The back-analysis of more case histories would however be required to pursue such refinements, in order for them to be reliably backed-up by real data.

11.3.5. Evaluation of the destressability rating

Further improvements could also be made concerning the assessment made on the Destressability Index value obtained, and particularly on the normalised total destressability score. In the work presented herein the ‘Poor’, ‘Medium’, ‘Good’ and ‘Excellent’

Destressability Index ranges have been distributed in a certain manner between 0 and 1. These boundaries could quite conceivably be revisited and refined (and some ranges added too), again provided that more relevant case histories are analysed so it can be done reliably. Essentially, this would result in a revision of Table 26.

Furthermore, a continuous destressability rating system could be developed instead of fitting the results of the process to pre-established ranges. This would result in a system more sensitive to smaller changes in the input parameters.

11.3.6. Parametric analysis

An interesting project would consist in conducting a thorough parametric analysis to determine whether a normalised total parameter score of one can be achieved in practice. Some of the parameters might be acting in sufficiently opposite directions to preclude a "perfect" score from ever being attained. For example, for a given blasthole size, drilling pattern and explosive product, as parameter P_8 (the confinement of the explosive charges) improves (i.e., increases), less room remains available inside the blasthole for the explosives, which, in turn, would *worsen* (reduce) parameter P_7 (the unit explosive energy of the destress blast). Another example concerns the behaviour of the rock-related parameters, and particularly how stiffness, brittleness and strength interact for various geological formations, and how their combination affects the possible total parameter score in practice. Should the practical limits of the total parameter score be better defined, its normalisation could be modified to render the approach more precise (the normalisation could be done over a smaller interval).

11.3.7. Other further perspectives and potential future work

Other relevant issues are not considered at this point in the Destressability Index methodology. For example, the effects of the distribution in time of the explosive energy have not been addressed so far. This aspect could conceivably be tackled through the consideration of the timing sequence adopted for the blast. Intuitively, a quicker input of

explosive energy into the targeted rock mass should result in more shattering and, thus, in a more pronounced destressing effect. (When a fixed amount of energy is injected into a system over a shorter period of time, more power is provided.)

Also, the stiffness of the loading system acting upon a pillar targeted for destressing is not accounted for in the methodology at this stage. The additional energy released by a soft loading system once failure is initiated (at the instant of the blast) would contribute to the breakage process, and could lower to a certain extent the amount of explosive energy actually required to achieve a given destressing effect. Also considering the mechanical properties of the rock units adjacent to the targeted zone could thus potentially further improve the methodology.

Besides the issue of sufficiently breaking the rock mass to produce an adequate destressing effect, the question of how far away from an ore lens (where mining is to resume) a destress blast should be attempted will eventually need to be addressed as well. When destress blasting is pursued with the objective of stress-shadowing a particular ore lens, it can be done either within the lens itself, or outside of it in the host rock. It is generally not attractive to fire a destress blast directly in the ore lens sought after, as this would result in the loss of some of it. Furthermore, any stope coming into production against this destressed area would likely have to be drilled remotely, as live explosives could conceivably still be present in the destress blast. Also, the wall conditions encountered against this destressed area would likely be quite unstable. This leaves destressing from outside the lens, in the host rock – the question is how far away. If done too close to the ore lens, potential wall instability might develop in the nearby stopes, due to damage from the destress blast. If done too far, the destressing effect will be reduced, and a larger destress panel (covering a wider area) will be required. The elaboration of an additional parameter that would consider the distance between a large-scale confined destress blast and a zone of interest (where ground stresses need to be reduced in order for mining to resume under better conditions) would be useful. Ideally, this parameter should be rated against the net destressing effect achieved in the region of interest and subsequent wall control issues.

APPENDICES

Appendix A – Methodologies at the intact rock material scale for the assessment of the rockburst potential.

Appendix B – Methodologies at the rock mass scale for the assessment of the rockburst potential.

Appendix C – Selected case histories of destress blasting.

Appendix D – The Rock Quality Designation index (RQD).

Appendix E – The Rock Mass Rating system (RMR).

Appendix F – The Geological Strength Index (GSI).

Appendix G – The rock tunnelling Quality index (Q rating).

Appendix H – Destressability Index development spreadsheets.

APPENDIX A

A. METHODOLOGIES AT THE INTACT ROCK MATERIAL SCALE FOR THE ASSESSMENT OF THE ROCKBURST POTENTIAL

A.1. The Bursting Liability Index

The Bursting Liability Index W_{et} was proposed by Neyman *et al*. (1972) for the Polish coal fields. It is determined from a simple uniaxial compressive test as follows:

$$W_{et} = E_R / E_D \qquad \text{….. Eq. (39)}$$

With: W_{et} the Bursting Liability Index; E_R the elastic energy recovered (as determined from the area below the unloading curve); and, E_D the dissipated energy (as determined by the area between the loading and unloading curves). Figure 105 illustrates these energy values. As the value of W_{et} increases the sample exhibits less ability to dissipate energy in a stable manner by progressively propagating fractures through it, and the risk of violent failure increases.

In order for the test to be valid the compressive load must be brought to about 80 to 90% of the unconfined compressive strength of the sample – this threshold is both difficult to establish beforehand and achieve during the test. The value derived for W_{et} is thus dependent upon the compressive load that was eventually attained during the test.

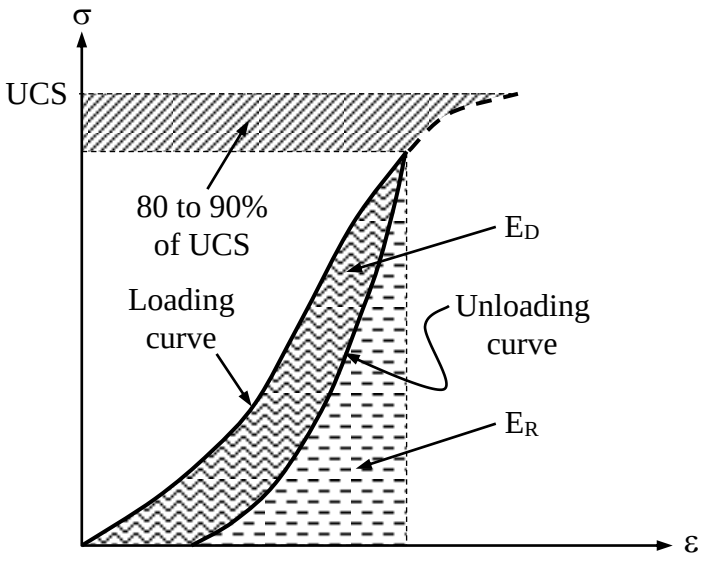

Figure 105. Determination of the W_{et} index from an unconfined compressive test. (Adapted from Simon *et al*.,1998.)

A.2. <u>The Brittleness Index Modified (BIM)</u>

The Brittleness Index Modified, or BIM, was described by Simon *et al*. (1998) as a way to address the intrinsic variability associated with the W_{et} index just discussed. The BIM, derived from a uniaxial compressive test carried out until failure of the sample is reached, is defined as follows:

$$BIM = A_2 / A_1 \qquad \text{….. Eq. (40)}$$

With: A_2 the total area under the loading curve; and, A_1 the area under the line that corresponds to the elastic modulus of the sample, as determined when the compressive load reaches 50% of the UCS. Figure 106 shows these values. As the value of the BIM increases, the amount of energy dissipated during the loading phase increases as well, which results in less energy being available at failure, and, hence, in a smaller potential for violent failure. This method eliminates the uncertainty associated with the determination of the W_{et} index (i.e., whether or not 80 to 90% of the UCS was indeed reached during the test) – in this case, failure is unequivocally attained and the parameters A_1 and A_2 are thus more reliable.

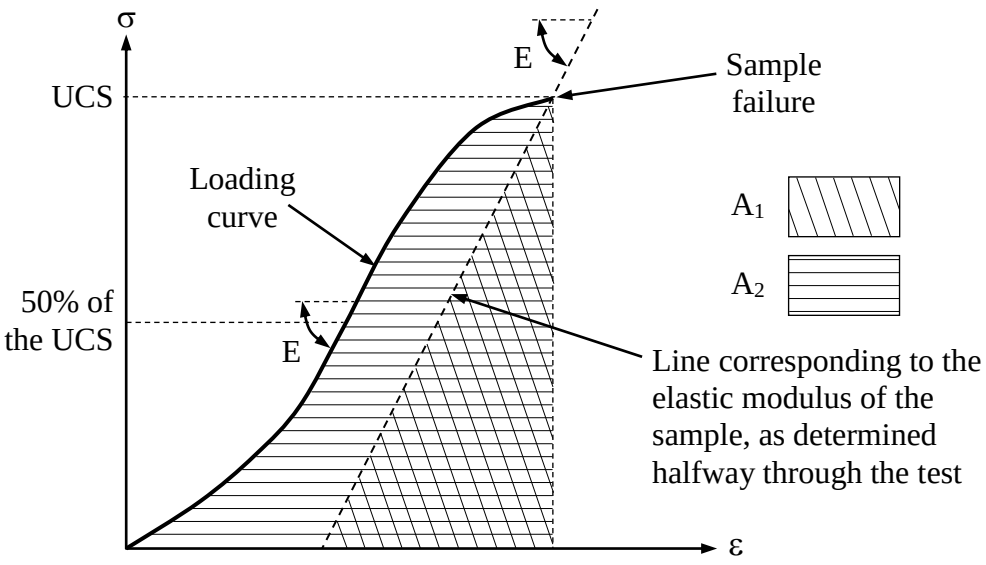

Figure 106. Determination of the BIM from a uniaxial compressive test. (After Simon *et al*., 1998.)

Aubertin *et al*. (1994) have derived a relation between the BIM and the potential for the rock to undergo violent failure – Table 61 summarises this relation.

Table 61. Relation between the BIM and the potential for violent rock failure. (After Aubertin *et al*., 1994.)

Range of BIM values	Potential for violent failure
1.00 < BIM < 1.20	High
1.20 < BIM < 1.50	Moderate
BIM > 1.50	Low

The BIM approach essentially implies that the brittleness of an intact sample of rock is closely related to its stiffness in the elastic domain.

A.3. The Decrease Modulus Index

Homand *et al*. (1988) proposed the Decrease Modulus Index, which is based upon the ratio of the elastic modulus of the intact rock material over the slope of its uniaxial compressive stress-strain curve in the post-peak domain, as follows.

$$D_{mi} = \left| E / E' \right| \qquad \text{..... Eq. (41)}$$

With: E the Young's modulus of the intact rock material; and, E' the slope of its uniaxial compressive stress-strain curve in the post-peak domain. As the value of D_{mi} increases the rock becomes less fragile and less likely to sustain violent failure.

A.4. The fragility of the intact rock

Hucka & Das (1974) have described two rules-of-thumb that provide a simple representation of the fragility of an intact rock sample, as follows:

$$B_I = (\sigma_C - T_o) / (\sigma_C + T_o) \qquad \text{..... Eq. (42)}$$

$$B_{II} = \sin \phi \qquad \text{..... Eq. (43)}$$

With: σ_C the uniaxial compressive strength of the intact rock material; T_o the tensile strength of the intact rock material; and, ϕ the friction angle. Both B_I and B_{II} are taken to give a representation of the fragility of the intact rock material – as this fragility increases the potential for violent failure increases as well. This approach is somewhat simplistic.

A.5. The Burst Efficiency Ratio

The Burst Efficiency Ratio B_{er}, originally was derived by Motyczha, was later described by Kidybinski (1981). It is defined as:

$$B_{er} = \phi_1 / \phi_0 \qquad \text{..... Eq. (44)}$$

With: ϕ_1 the energy of the particles ejected at failure from a sample subjected to a uniaxial compressive test; and, ϕ_0 the maximum energy stored in the sample during loading. The quantity ϕ_0 is given empirically by:

$$\phi_0 \approx (\sigma_C \times \varepsilon_r) / 2 \qquad \text{..... Eq. (45)}$$

With: σ_C the uniaxial compressive strength of the sample (i.e., the compressive load at failure); and, ε_r the axial deformation of the sample at failure. As the value of B_{er} increases

more of the energy accumulated in the sample is instantaneously liberated at failure, which results in a higher potential for violent failure. The main practical difficulty with the B_{er} approach is the reliable determination of ϕ_1 .

APPENDIX B

B. METHODOLOGIES AT THE ROCK MASS SCALE FOR THE ASSESSMENT OF THE ROCKBURST POTENTIAL

The approaches described in Appendix A merely indicate whether or not the intact rock material has a tendency to fail violently. They however do not account for the stress conditions and loading system characteristics known to play an important role in the violent failure of a rock mass. They also do not account for the geological structures within the rock, which can affect the behaviour of the rock mass. Following are a number of techniques that have been proposed to estimate the susceptibility of a rock mass to violent failure and rockbursting, and which consider various in situ conditions.

B.1. Activity Index

Tao (1988) proposed the Activity Index A_i , which he defined as follows:

$$A_i = \sigma_C / \sigma_1 \qquad \text{..... Eq. (46)}$$

With: σ_C the uniaxial compressive strength of the intact rock material (obtained in the laboratory); and, σ_1 the magnitude of the major principal in situ stress component acting upon the rock mass (derived from measurements or numerical modelling). Based upon his experience in Chinese mines, Tao suggested the following range of A_i values.

Table 62. Classes of Activity Index A_i and their effects on the behaviour of the rock mass. (After Tao, 1988.)

Class	Range of A_i	Seismic activity	Rock mass noises
I	Over 13.5	None	None
II	From 13.5 to 5.5	Limited	Weak
III	From 5.5 to 2.5	Significant	Loud
IV	Less than 2.5	Elevated	Very loud

Even though this approach is largely qualitative, it is relatively easy to apply, and has the merit of incorporating a stress component.

B.2. Seismic techniques

Seismic techniques can provide a good indication of the loading state of a rock mass. A number of approaches can be used, ranging from simple seismic velocity tests, to cross-holes seismic and full tomographic surveys. The basic principle behind these approaches is that a stress increase will close the many fractures and discontinuities inside a rock mass, which will facilitate the propagation of seismic energy through it. Inversely, a stress reduction can result in these discontinuities opening, which will impair the propagation of seismic energy through the rock mass.

As discussed by Telford *et al*. (1994), as the stress level acting on a given rock mass increases, the velocity of propagation of a seismic wave travelling in it will increase as well. This behaviour is shown schematically in Figure 107 as a function of axial deformation in an intact sample of brittle hard rock subjected to a uniaxial compression. As can be seen, the sonic velocity initially increases as the axial load becomes greater, and eventually starts to decrease rapidly as damage accumulates inside the sample.

Conducting successive seismic velocity of propagation surveys as mining progresses may thus indicate whether the stress is increasing or decreasing in a given region. (Many other parameters – such as damage and voids, for example – also influence the velocity of propagation of seismic waves, which can make the interpretation of such velocity surveys

difficult.) This information, combined with the proneness of the intact rock material to fail violently, can provide an assessment of the likelihood of the rock mass to burst in response to mining.

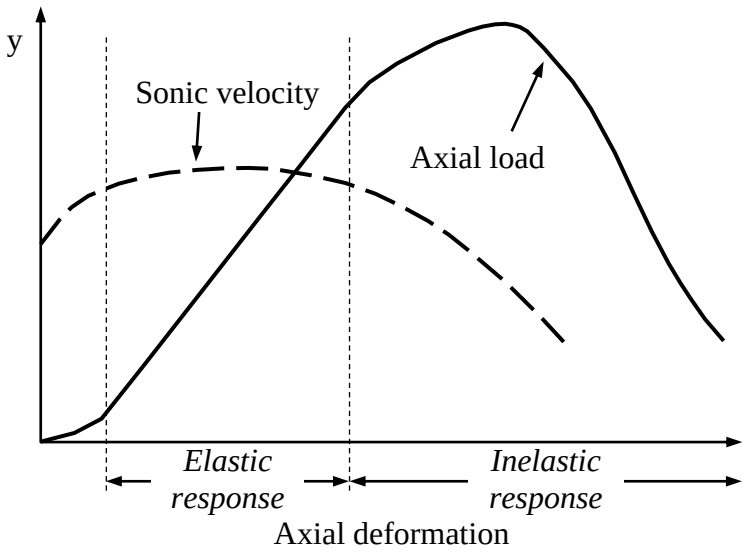

Figure 107. Schematic representation of the behaviour of the sonic velocity as a function of axial deformation in an intact sample of brittle hard rock. (After Bieniawski, 1967.)

A number of seismic techniques exist to measure the velocity of propagation of seismic waves in a rock mass. The simplest way consists in a single raypath test. As shown in Figure 108a, a seismic wave is generated (either by a small explosive charge, or a mechanical or piezoelectric device) at one location along a borehole, travels through the rock mass of interest, and is recorded at one location along another borehole by a seismic sensor. A synchronisation circuit between the source and the receptor allows to accurately measure the travel time of the pulse between the two points, from which velocity is deduced. As shown in Figure 108b, a series of successive measurements can be performed along the length of the boreholes, which yield one velocity at each elevation – this technique provides a more detailed rendering of the seismic velocity of propagation along the plane between the two boreholes. Tomographic seismic velocity surveys, illustrated in Figure 108c, provide yet more detail. In this technique the seismic source is again moved along the length of the source borehole, but the signal is simultaneously captured on the

other side by a string of receptors. The signals recorded at each sensor are cross-correlated, which allows a detailed composite image of the seismic velocity of propagation everywhere towards the centre of the plane to be produced.

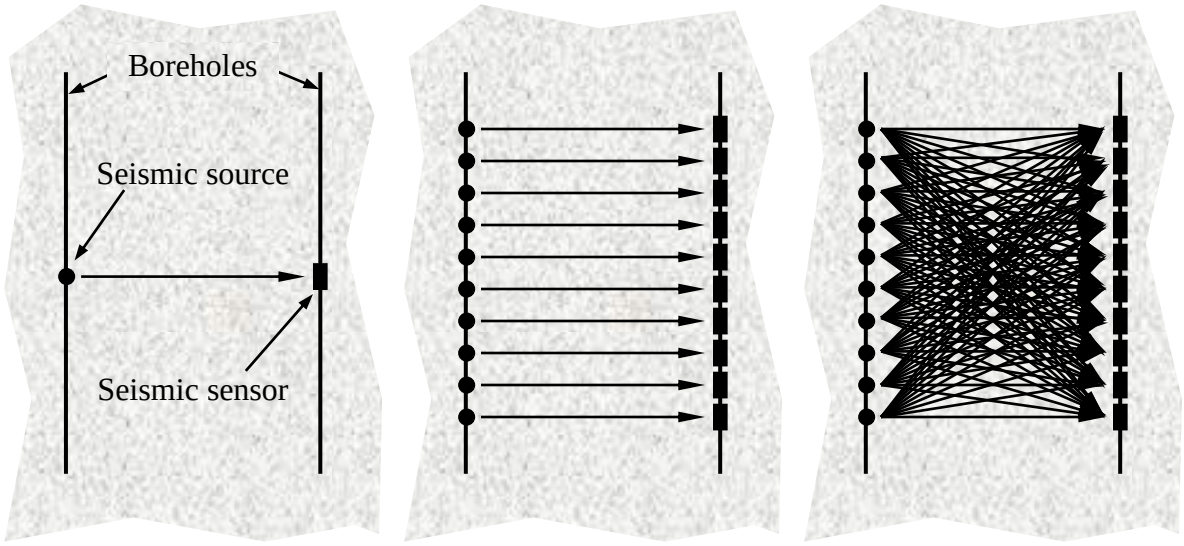

(a) Simple seismic velocity test. ***(b) Cross-hole seismic velocity survey.*** ***(c) Tomographic seismic velocity survey.***

Figure 108. Various types of seismic surveys for assessing the stress state of the rock mass.

These tests are generally performed in wet boreholes. Water, which is uncompressible, provides a much better coupling medium between the seismic source and the rock than air. At the other end of the path, immersed hydrophones are the most commonly used receptors. Measurements are usually done twice, by reversing the source and receptor holes.

These seismic techniques can be very effective at detecting relatively small changes in the stress regime (providing that no other phenomena are at play that can also influence the seismic velocity of propagation in the rock mass of interest), and have the advantage of operating at the rock mass scale, rather than as point measurements. As mentioned, they are however affected by a large number of parameters, such as the presence of water, large-scale discontinuities, geological contacts, anisotropic effects, etc., that can make interpretation difficult by non-specialised personnel. They are also somewhat cumbersome and not always easy to implement (generally due to access constraints between the boreholes). They also require highly specialised equipment.

B.3. Microseismic monitoring

Mine-wide microseismic monitoring can also provide valuable insight into the prevailing stress regime and on where violent rock mass failure is occurring. This type of monitoring uses a dispersed array of seismic sensors (either geophones or accelerometers) to record and locate the seismic energy liberated by the rock mass as it fails violently. By tracking how this seismicity evolves, the effect mining has on the rock mass can be assessed, and regions that are likely to sustain heavy seismicity (and potentially rockbursting) can be identified. Microseismic monitoring can be done with a number of techniques, some of which will be described in the following sections.

B.3.1. Magnitudes, and distribution in space and time

The simplest way to use microseismic data consists in examining their magnitude, as well as their spatial and temporal distributions, as shown in Figure 109. Figure 109a is a plot of the seismic activity recorded in 1999 on the north side of the 1000m Level at Brunswick Mine. Each sphere in this figure represents a seismic event, the diameter being scaled to the Richter Magnitude. Highly stressed regions that are undergoing violent failure (secondary stopes “A” and sill pillar “B”), yielded regions that carry relatively little load (secondary stope “C”), as well as regions where the stress is rising but not yet causing significant problems (abutment “D”) are all clearly visible.

Figure 109b shows the temporal distribution of the seismicity recorded in the same region between 1992 and 1999. The rise in the number of yearly seismic events clearly shows how the stress level in this region increased as mining progressed and the extraction ratio became larger. (This rise was however also linked to the fact that mining was accelerated significantly in this region starting in 1998, and that no mining was carried out in it during 1997.)

These data, although very useful, only show what is *currently* happening within the volume monitored – their use is thus essentially limited to making short-term decisions, on the closure and reopening of problem areas, for example. Sudden rises in the rate of activity can be indicative of imminent seismic flurries (and of potential rockbursting), but there is not always such a precursory trend.

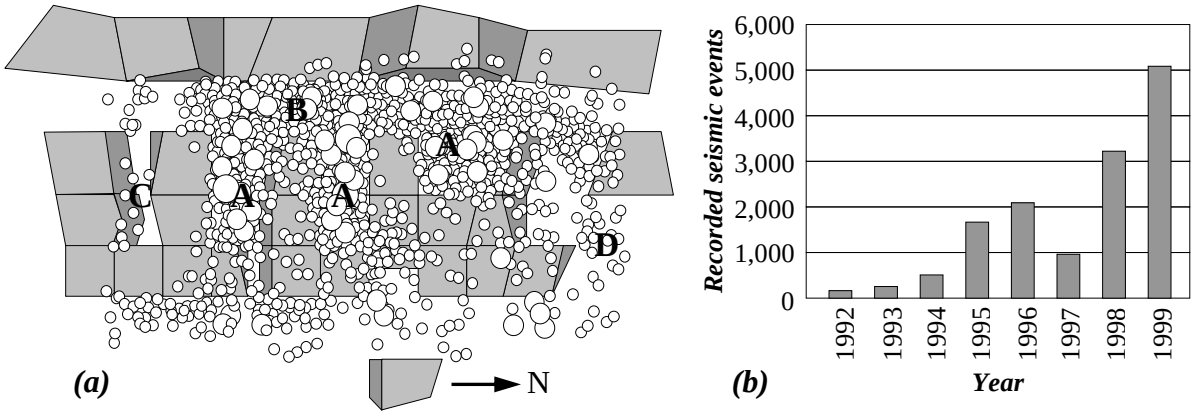

Figure 109. (a) Longitudinal section showing the seismic activity recorded in 1999 on the north side of the 1000m Level at Brunswick Mine; and, (b) number of seismic events recorded yearly from 1992 to 1999 in the same region. (After Andrieux & Simser, 2001.)

B.3.2. Scale invariance and fractal-based approaches

Entities that have a similar appearance regardless of the scale at which they are observed are said to present scale invariant characteristics. A snowflake, for example, exhibits such features: as a view of it is zoomed in, the shapes observed remain similar. Scale invariance is characterised by a power law relation between the number of objects and their linear size – this relation is referred to as a fractal (Mandelbrot, 1982). Mathematically, fractals are geometric objects generated by some infinitely repeated process and possessing self-similarity, i.e., each point of the set is contained in a scaled-down copy of the entire set (Nelson, 1998). Interestingly, a self-similar fractal distribution S_f in a space of dimension d_f can be attributed a similarity dimension D_f, where $0 \leq D_f \leq d_f$. As this similarity dimension D_f increases and approaches d_f, the degree of self-similarity between the elements in the data set increases as well.

Seismic activity presents scale invariant characteristics. In particular, the distribution in time and space of the microseismic events in a given cluster of activity, as well as the distribution of their magnitude relatively to their number, often exhibit these characteristics and are fractal (Gaudreau, 1997[a]). The potential to use fractals to identify possible precursory trends to imminent severe seismic activity and rockbursting has been investigated by a number of researchers, such as Xie & Pariseau (1992) and Eneva & Young (1993), for example. Typically, a sphere of radius r is considered, which is centred in the spatial centre of gravity of the seismic cluster considered, and the total number of seismic events $M(r)$ within this sphere is counted. There is a relationship between the number of events inside this sphere and its radius, in the form $M(r) \alpha r^{df}$, with d_f the dimension of the fractal distribution. This type of analyses can provide some indication on the propagation of damage inside the rock mass – as the dimension d_f of the distribution becomes smaller and the events are hence clustered inside a smaller sphere, the likelihood of severe seismicity – and possibly rockbursting – increases.

Furthermore, the clustering of seismic events in space and time can be quantified with a clustering index called Pn (Gaudreau, 1997[b]). This approach was first used in rock mechanics by Shah & Labuz (1995) for the characterisation of the acoustic emissions in stressed rock samples. Essentially, the Pn value represents the number of normalised space-time clustered pairs (a cluster, in this context, is a group of events with nearest-neighbour links to other events), for a given distance and delay between events. As the Pn value increases the probability that successive events separated by the corresponding distance and delay are part of the same cluster (and related to the same mechanisms) increases as well.

Figure 110 shows the example of a Pn-based analysis completed for the seismic events recorded 19 February 1997 after a production blast on the 1000m Level at Brunswick Mine. As can be seen, Pn values were derived for four distances and nine time increments between events. The highest Pn value (about 5.5) was encountered for a distance of approximately 400m and a delay of about 4.5 hours (270 minutes) between successive

events, which indicates that, for this particular seismic flurry, the events were dominantly clustered with these distance and delay.

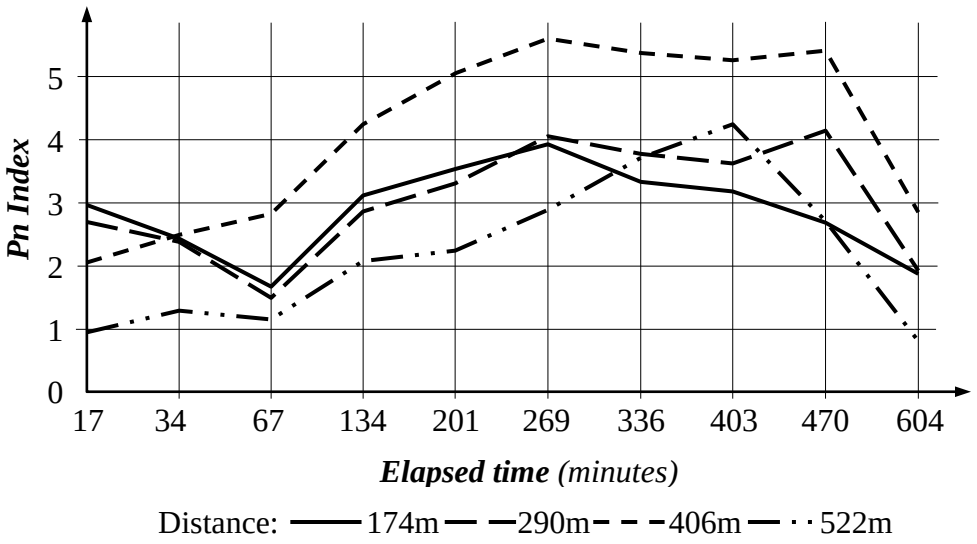

Figure 110. Pn space-time clustering analysis of seismic events recorded 19 February 1997 on the 1000m Level at Brunswick Mine. (After Gaudreau, 1997 [a].)

As the maximum Pn value increases and corresponds to decreasing distances and delays between successive events, the severity (in terms of the spatial and temporal concentration of the seismic events) of the resulting damage can be expected to increase as well.

Although it is not widely used, this approach has shown a certain potential to characterise a given seismic flurry, assess its potential to cause major damage to the mine infrastructure and – to a certain extent – estimate the likelihood of rockbursting.

B.3.3. Gutenberg-Richter plots

As more data are accumulated the response of the rock mass to mining becomes better understood, which provides invaluable qualitative insight into how it is likely to react to future mining. Large amounts of recorded seismic data can also be used to evaluate the probability of experiencing large seismic events and provide a measure of the seismic risk (and, indirectly, of the rockbursting risk as well).

If a straight line is fitted to a Gutenberg-Richter plot (a plot of the logarithm of the number of seismic events larger than a certain magnitude [on the y-axis], against the local Richter Magnitude M_R [on the x-axis]), it can be defined by two parameters. Firstly, the slope (or "b-value"), which governs the relationship between large and small seismic events; and, secondly, the intercept (or "a-value") on the vertical axis for $M_R = 0$, which governs the seismic event rate. Figure 111 shows an example for the case of 17,883 seismic events recorded between 1999 and 2002 in the 1000 South Bulk Zone at Brunswick Mine.

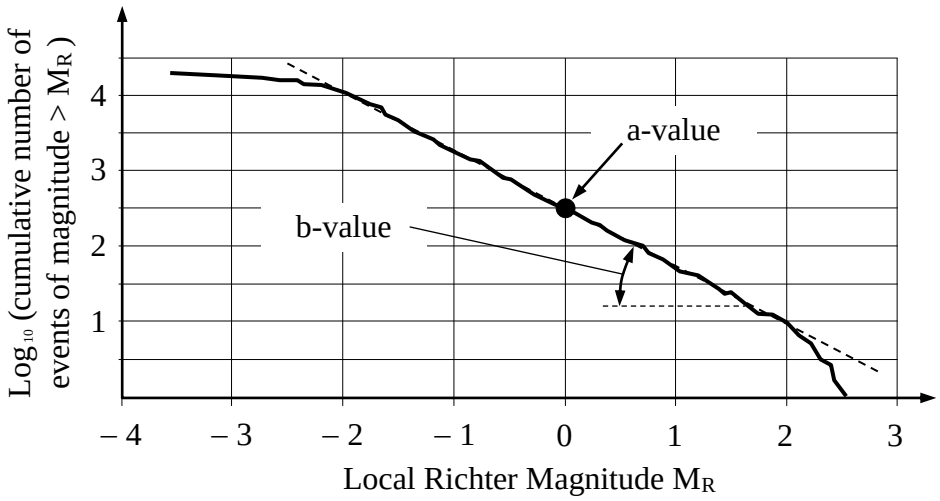

Figure 111. Example of a Gutenberg-Richter plot – case of the 1000 South Bulk Zone at Brunswick Mine. (Adapted from Simser & Falmagne, 2004.)

This relationship is usually expressed by the following equation:

$$\text{Log}_{10} N = a - b M_R \qquad \text{..... Eq. (47)}$$

With N the number of seismic events larger than a certain magnitude M_R. This relation between small and large events applies over a wide range of magnitudes, from small microseismic events to large tectonic earthquakes. This allows Equation (47) to determine the likely frequency of occurrence of large events from a complete record of smaller events.

A statistical analysis can be used to determine recurrence times and probability of occurrence of events, and particularly for those of interest (the larger ones). In other words, it allows to quantify the probability that a seismic event of a given magnitude will occur

during a given time period. Benjamin (1968) showed that the unconditional probability of occurrence of a seismic event E larger than a magnitude M (Richter or Nuttli), during a future time period Δt, is given by:

$$P[E > M, \Delta t] = 1 - [t_R / (t_R + \{\Delta t \times P[E > M]\})]^{n+1} \quad \text{..... Eq. (48)}$$

With: Δt the future time period of interest; t_R the monitoring period over which data have been collected; $P[E > M]$ the probability that a seismic event E has a magnitude greater than M; and, n the number of seismic events in the data set. Assuming that there are upper and lower bounds to the range of magnitudes of interest, and, hence, that the double truncated Gutenberg-Richter frequency-magnitude relationship described by Cosentino *et al*. (1977) is appropriate, the probability $P[E > M]$ is given by:

$$P[E > M] = (e^{-\beta M} - e^{-\beta M_{max}}) / (e^{-\beta M_{min}} - e^{-\beta M_{max}}) \quad \text{..... Eq. (49)}$$

With: $\beta = (b \times \ln[10])$, or $(2.3 \times b)$, b being the b-value discussed previously; and, $P[E > M] = 1$ for $M < M_{min}$, and zero for $M > M_{max}$. Although this approach can be used to quantify the risk of a seismic event of a given magnitude to occur over a given period of time, it only provides a limited indication of the risk of actual rockbursting, which is defined by the amount of ejection and the degree of damage a violent failure causes (damage is not systematically linked to magnitude).

B.3.4. Seismic source parameter analyses

Seismic source parameter analyses, pioneered in South Africa in the mid 1980's, have provided yet more insight into how the rock mass responds to mining. Seismic source parameters are based upon the energy and the moment associated with a single seismic event – they are calculated from seismic traces recorded with triaxial sensors. (Seismic source parameters can sometimes be derived from a uniaxial sensor array if a large enough number of sufficiently widely spaced transducers are available.) As described by Mendecki (1997), seismic energy is defined as the portion of the energy released by the seismic event in the form of seismic waves, whereas seismic moment is defined as a measure of the permanent deformation imparted at the seismic source by the seismic event. One seismic

source parameter of particular interest is the apparent stress of a seismic event, which provides an assessment of the stress level that prevails in the region where the seismicity occurs (Mendecki, 1997). Apparent stress is defined as follows:

$$\sigma_a = (Es \times G) / Mo \qquad \text{..... Eq. (50)}$$

With: σ_a the apparent stress (in Pa); Es the seismic energy liberated by the seismic event (in Joules); Mo the seismic moment of this event (in $N \times m$) – the ratio (Es / Mo) relates to the stress drop at the seismic source (Butler, 1997) –; and, G the rigidity of the rock mass (in Pa). As the apparent stress increases, more energy is released for a given seismic moment and higher stress conditions prevail at the source – as discussed by Simser & Andrieux (1999) this could be due to a lockup on a particular geological structure, or high stress levels. Furthermore, higher stress levels clamp the ground and result in less deformation occurring at the source for the same released energy, which further increases the apparent stress. Low apparent stress events, on the other hand, are generally indicative of lower stress levels, or post-failure conditions whereby the rock mass has fractured and softened – relatively higher seismic moments (which result in lower apparent stresses) are usually observed under these conditions.

The July 2001 mass-blast fired in the South West Ore Zone (South WOZ) at Brunswick Mine provides a good example of how apparent stress can be used to assess the response of the rock mass to mining. The objective of this 350,000 tonne mass-blast was to cut-off the high driving stresses that were affecting the recovery of a six million tonne block of ore on the south side of the mine. This blast was not a destress blast in the sense that it was entirely mucked – as a result (and as confirmed by various instrumentation and significantly easier subsequent mining conditions), there is no doubt that the stress reduction effect it had was substantial.

As shown in Figure 112, comparing the average pre- and post-blast apparent stress of the seismic events recorded in this region clearly reveals a significant shift in the distribution of $\log_{10}(\sigma_a)$, which reflects the stress reduction achieved in the region. The post-blast conditions were much less conducive to the rock mass undergoing violent failure.

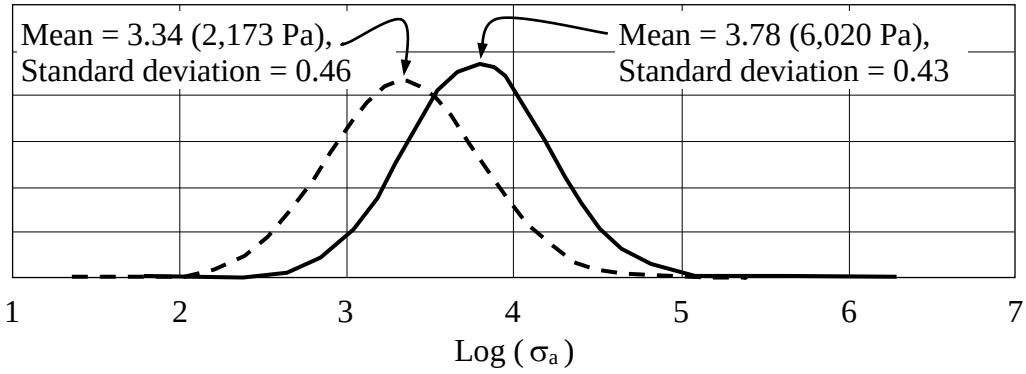

(a) South Bulk Zone.

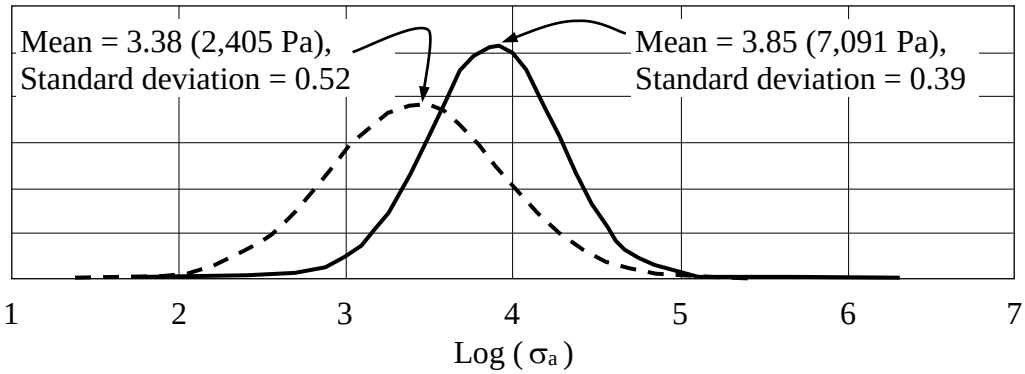

(b) South Regional Pillar.

Figure 112. Shift in the average apparent stress of the seismic events recorded (a) in the South Bulk Zone ; and, (b) in the South Regional Pillar, before and after the July 2001 mass-blast in the South WOZ at Brunswick Mine. (After Simser & Falmagne, 2004.)

Interestingly, the mass-blast had little immediate effect on the seismic event rate and average magnitudes recorded, and advanced seismic source parameter analyses were required to properly assess the effect it had on the rock mass (Simser, 2004).

Another source parameter-based analysis that has shown good potential at anticipating large-scale violent rock mass failure consists in tracking Energy Index *vs*. cumulative apparent volume. The Energy Index EI of a seismic event is a source parameter that can be calculated either for individual events or averaged over multiple consecutive events – it is particularly useful at providing an indication of the relative stress levels within the rock

mass (van Aswegen & Butler, 1993). The Energy Index is defined as the ratio of the seismic energy Es liberated by a seismic event divided by the average seismic energy Ea liberated by a seismic event of the same seismic moment Mo. The average seismic energy Ea in a given region is derived from the linear orthogonal fit of a $\log_{10}(Es)$ *vs*. $\log_{10}(Mo)$ plot, as shown in Figure 113.

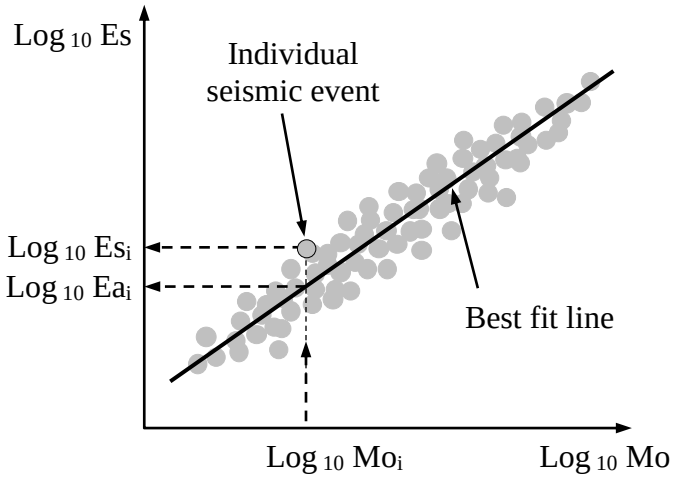

Figure 113. The concept of the seismic energy and the average seismic energy for a given seismic moment. (Adapted from Simser *et al*., 1998.)

A value of the Energy Index of 1.0 corresponds to an event that has an average stress level for the area – values above 1.0 correspond to higher-than-average stress levels, whereas values under 1.0 correspond to lower-than-average stress levels.

The apparent volume Va of an individual seismic event, on the other hand, is a measure of the volume of rock that sustained inelastic strain as a result of this event (Mendecki, 1997) – it is essentially a seismic strain indicator. The equation used to derive Va is:

$$Va = Mo / (2 \times \sigma_a) \qquad \text{..... Eq. (51)}$$

With: Va the apparent volume of the seismic event (in m^3); Mo the seismic moment of the seismic event (in $N \times m$); and, σ_a the apparent stress of the seismic event (in Pa).

A plot of Energy Index *vs*. cumulative apparent volume over a given period of time can be used to assess how the stress-strain state of a rock mass is evolving. In order to smooth the

Energy Index curve and provide a more reliable trend for how ground stresses are behaving, the Energy Index plotted is generally a moving average in which the value associated with a given event is averaged with those obtained for a number of previous events in the region (typically 5 or 10). Such a plot is referred to as a time history plot. There has been several well-documented occurrences in South Africa (Butler, 1997) and Canada (Simser, 2000) of severe seismicity occurring following a sudden raise in the cumulative apparent volume combined with a sharp drop in the Energy Index. This behaviour has been compared to that of a rock sample failing in compression, whereby the volume rapidly increases and the load is quickly shed. With this analogy the average Energy Index corresponds to stress, whereas the cumulative apparent volume corresponds to strain. It is the precursory nature of this trend that makes it particularly interesting.

Figure 114 is an example reported by Simser (2000) of a time history plot computed between January 1999 and July 2000 for the South Pyramid on the 850m Level at Brunswick Mine.

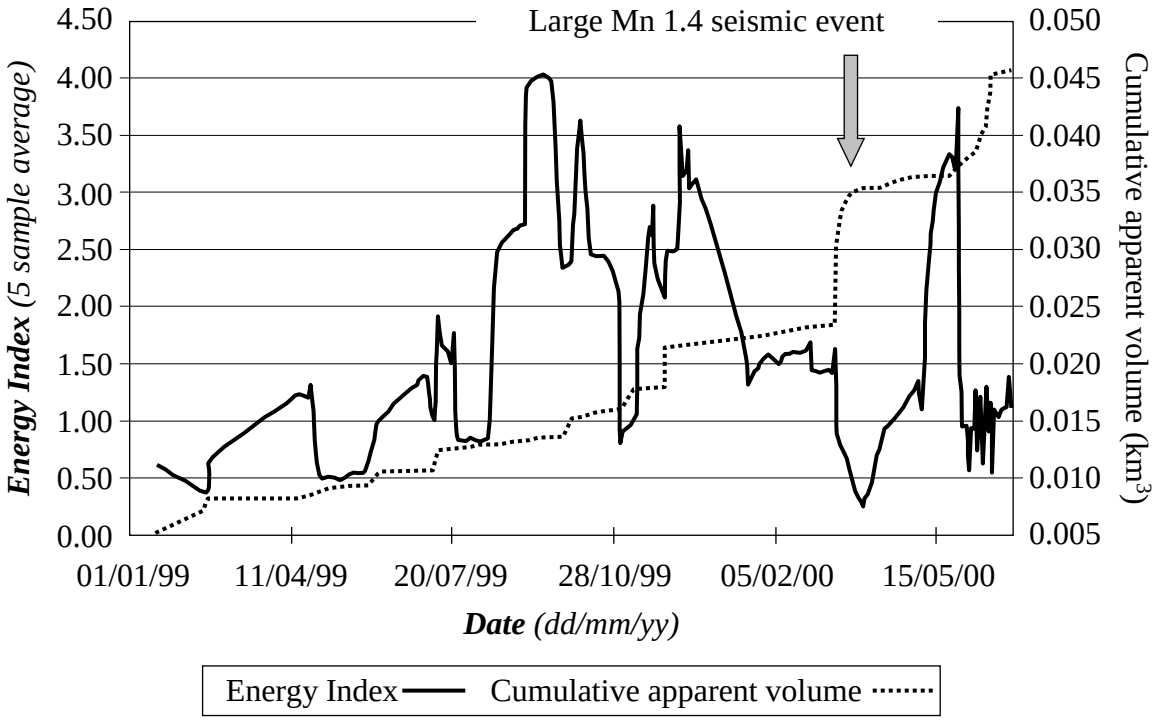

Figure 114. Moving average Energy Index *vs*. cumulative apparent volume in the South Pyramid on the 850m Level at Brunswick Mine. (After Simser, 2000.)

In this example the Energy Index moving average includes the previous five events. As can be seen, a sharp rise in the cumulative apparent volume, combined with a sudden and pronounced drop in the average Energy Index occurred just prior to a significant bout of seismicity.

Seismic source parameter-based analyses have the advantage of taking into account both the number and size of the events, which provides considerably more insight than merely considering an event frequency histogram similar to the one shown in Figure 109b.

Overall, the monitoring of the microseismicity can be an invaluable tool to understand the reaction of a rock mass to mining, and, to a certain extent, anticipate episodes of severe bouts of seismicity, possibly associated with rockbursting. Although promising for violent stress-driven pillar failures, these analyses have not been as successful with fault-slip mechanisms. Also, this approach is heavily dependent upon the quality of the seismic data. In particular, quantitative source parameter seismology can only be attempted on good quality data, in terms of both seismic coverage and processed triaxial seismic seismograms. These techniques also need considerable resources in both equipment and manpower (in order to process and analyse the data).

B.4. Energy-based approach

As discussed by Salamon (1974, 1984) any change in the size and/or geometry of a void inside a solid body, or in the external stress field it is subjected to, will result in a change of the energy balance of this body. This modification of the energy state and the transitory unbalance it can produce can be used to evaluate how much energy can become available to drive a violent failure around this void (Cook *et al*., 1966). According to Brady & Brown (1993) seismic events and rockbursts are the result of unstable energy changes in a system, between the pre- and post-excavation states. As shown in Figure 115a for a simplified two-dimensional example, prior to excavation every point along the surface S of a future void is subjected to traction forces (t_x, t_y) that provide equilibrium. Upon excavation these

traction forces are removed, which results in a redistribution of the static stresses around the excavation. As illustrated in Figure 115b, the regions of stress concentration, in particular, cause strain increases that consume the excess static energy.

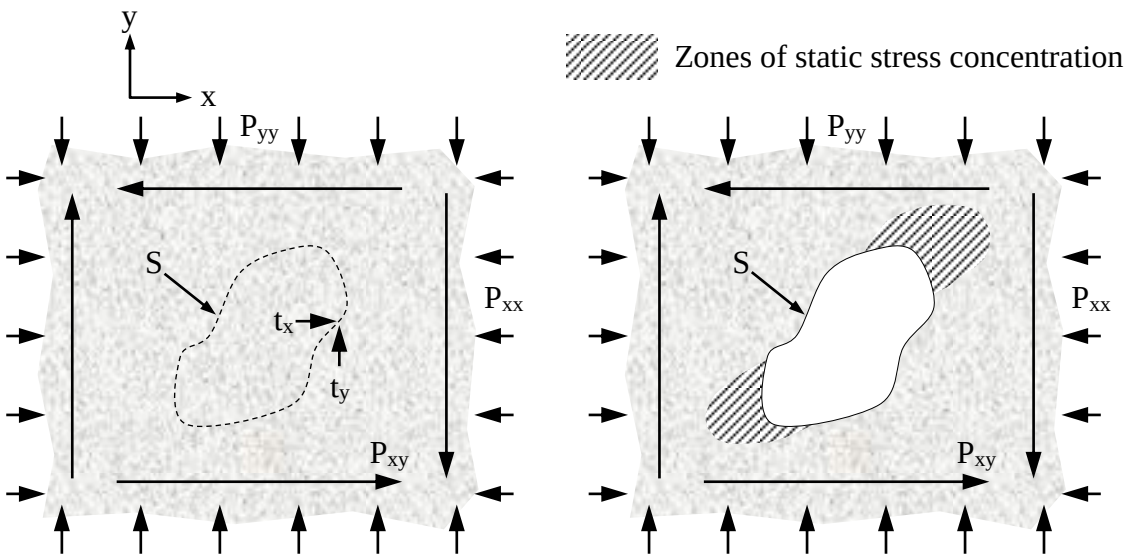

(a) Pre-mining state. ***(b) Post-mining state.***

Figure 115. (a) Pre-mining; and, (b) post-mining static states in a conceptual 2-D solid medium subjected to a biaxial stress field. (After Brady & Brown, 1993.)

To remain consistent with previous terminology, let U_c be the total static strain energy increase in the surrounding rock due to the excavation. If the excavation is done progressively (i.e., if the traction forces along surface S are removed very slowly and the stress redistribution is gradual) in a purely elastic medium, and if no ground support elements are considered, which would contribute to the energy balance by deforming, then U_c constitutes all the energy Ur released by the excavation process. These conditions are however seldom encountered in practice. Firstly, the rock is not elastic and fracturing generally occurs in the immediate vicinity of the void. This fracturing energy, U_f, will consume some of the energy released by the excavation. Statically, we have:

$$Ur = U_c + U_f + Us \qquad \text{….. Eq. (52)}$$

With: Ur the total energy released by the excavation process; U_c the total static strain energy increase in the surrounding (remaining) rock; U_f the energy dissipated by rock fracturing; and, Us the energy absorbed by the ground support system, if any.

Secondly, in the case of hard rock mining rapid excavation techniques are usually implemented by means of blasting. In this case the energy change in the system is not progressive and the displacement of the new surfaces is not restrained by the slow and incremental removal of material. This restraining work, which would have been performed in the case of the slow and progressive excavation process described previously, becomes excess transient energy when the excavation is sudden. This excess energy Ue at the excavation surface is near-instantaneously dissipated in the system in the form of transient dynamic loading, which can be larger than the final static stresses in the system. Some of this transient loading is absorbed by the ground support system (if any), and some is spent as seismic waves (vibrational energy). Hence, in the case of a rapid excavation, we have:

$$Ur = U_c + U_f + Us + Uv \qquad \text{..... Eq. (53)}$$

With: Ur, U_c, U_f and Us as defined for Equation (52), and Uv the vibrational energy released in the rock mass. In the case of seismicity- and rockburst-prone rock masses their stiff and strong pre-failure characteristics, combined with their brittle post-peak behaviour, exacerbates the dynamic loading component issue (Ortlepp, 1983).

Numerical methods are generally used to assess energy changes in a system. Certain components, such as the total energy released by the excavation process and the total static strain energy increase in the surrounding rock are readily obtainable with simple elastic codes. The energy dissipated by the fracturing of the rock in the vicinity of the excavation can be derived with inelastic numerical methods. The assessment of the energy absorbed by the ground support system can be done with advanced codes, but is generally performed using analytical methods.

The energy-based assessment of the potential a rock mass has to fail violently is interesting from a theoretical point of view, but not very practical. Besides the difficulties associated with assessing the various energy components involved, it does not account for time effects whereby seismicity nucleates in a region a starts in a delayed manner.

B.5. ERR – Energy Release Rate

The Energy Release Rate (ERR) approach is based upon the energy considerations discussed in the previous section. As an excavation is incrementally enlarged the energy Ur it releases can be related to its size increase. If the geometry of the excavation is regular (such as in the case of a longwall extraction approach, for example), this energy release can be conveniently related to the surface increase by the following expression:

$$ERR = Ur / \Delta S \qquad \text{..... Eq. (54)}$$

With: ERR the Energy Release Rate (in J/m^2); Ur the energy release (in Joules); and, ΔS the excavation area increase (in m^2). For an irregular excavation geometry, or one that cannot be "considered" two-dimensional, this energy release must be related to the volume increase by the following expression:

$$ERR_{volumetric} = Ur / \Delta V \qquad \text{..... Eq. (55)}$$

With: $ERR_{volumetric}$ the Energy Release Rate (in J/m^3); Ur the energy release (in Joules); and, ΔV the excavation volume increase (in m^3). The ERR value can be used to assess the rockburst potential of an excavation.

As shown in Figure 116 Cook (1977) reported the development of a rockburst risk ranking methodology (adjusted to South African deep longwall conditions) based upon the volumetric ERR described by Equation (55), as follows: A ('Negligible'); B ('Low'); C ('Moderate'); D ('High'); and, E ('Extreme').

Numerical methods are generally used to derive values of the ERR. This approach is ordinarily used to assess the potential for pillar bursting, whereby volumes of rock are subjected to large compressive stresses – it has shown limitations in the case of fault-slipping bursts.

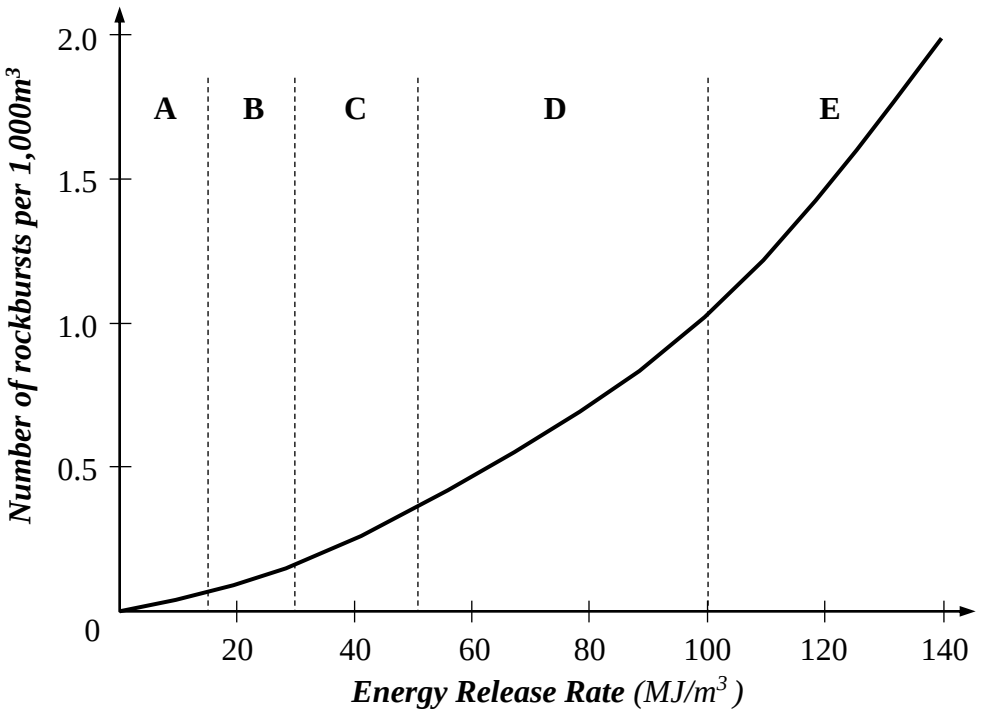

Figure 116. Relationship between the volumetric Energy Release Rate, the number of rockbursts and the danger associated with them. (After Cook, 1977.)

B.6. ESS – Excess Shear Stress

The Excess Shear Stress (ESS) methodology is another energy-based methodology used to assess the rockburst potential in a volume of rock. However, this particular approach is meant to address specifically the issue of fault-slip events, for which the ERR method has not produced good results. Ryder (1987, 1988) introduced this limit analysis-based approach whereby the static shear strength of a fault is compared to the dynamic shear stress acting upon it once slippage occurs, as follows:

$$\tau_s = c + (\mu_s \times \sigma_N) \quad \text{..... Eq. (56)}$$

$$\tau_d = \mu_d \times \sigma_N \quad \text{..... Eq. (57)}$$

$$ESS = \tau_e = \tau_s - \tau_d = [c + (\mu_s \times \sigma_N)] - (\mu_d \times \sigma_N) \quad \text{..... Eq. (58)}$$

With: τ_s the static shear strength of the fault (at the point of slippage); τ_d the dynamic shear stress along the fault once slippage has been initiated; τ_e the excess shear stress; c

the cohesion of the fault; μ_s and μ_d the static and dynamic coefficients of friction, respectively; and, σ_N the normal stress acting on the fault. The coefficient μ_s is usually around 0.6, which corresponds to a friction angle of about 30°. Ryder (1988) has suggested threshold ESS values above which fault slippage is likely to occur – these are 5 to 10 MPa for existing weakness planes, and 20 MPa for failure through intact rock bridges.

This method has been shown to produce conservative results in the sense that high ESS values often do not result in seismic events (Ryder, 1987). As pointed out by Simon *et al*. (1998), this approach does not take into account the post-peak stiffness of the fault and the stiffness of the loading system (i.e., that of the rock mass on both sides of the fault).

B.7. ERP – Evaluation of Rockburst Potential

The Evaluation of Rockburst Potential (ERP) methodology described by Simon *et al*. (1998) has been developed in an effort to provide underground mines in the Canadian Shield with an adapted and economical means of assessing the rockburst potential in their excavations. This approach, largely qualitative, encompasses up to four tasks.

The first task is the identification of the design sectors and their boundaries. This consists in subdividing the rock mass into sectors, or zones, in which a similar mechanical behaviour is expected. The boundaries between these zones are often major geological discontinuities along which large fault-slip type seismic events can occur – it is thus important to properly identify them and accurately locate them in space.

The second task is the identification of the excavations prone to rockbursting. These are often those located near, across or along the zone boundaries. The BIM approach discussed earlier in Section A.2 can be used to assist in this identification. The third task is a stability analysis of these excavations. At this step of the process the mining-induced stress regime (usually assessed by means of numerical methods) is compared to the rock mass strength. Depending upon the inferred risk, this stability analysis is aimed towards assessing either

the slipping potential along a discrete geological feature ("Type I" rockburst), or the failure potential of the rock mass under compressive load ("Type II" rockburst).

In the case of "Type I" rockbursts the fourth task consists in comparing the stiffness values. Firstly, the equivalent post-peak stiffness of the pillar is estimated, as follows:

$$k'_{pr} = (E'_m \times B) / (H \times [1 - \upsilon^2]) \quad \text{..... Eq. (59)}$$

With: k'_{pr} the equivalent post-peak stiffness of the pillar per unit length in the third dimension (in N/m) – k'_{pr} was defined in Figure 12; E'_m the post-peak stiffness of the encasing rock mass (in Pa); B and H the width and height of the pillar, respectively (in m); and, υ Poisson's ratio. Equation (59) applies to pillars in mines that are moderately deep (and, hence, subjected to a near uniaxial compressive load [Coates, 1981]) and with a squat shape (Simon *et al*., 1998). For pillars with a near square cross-section and considering perfectly elastic conditions, Equation (59) becomes:

$$k'_{pr} = (E'_m \times A) / H \quad \text{..... Eq. (60)}$$

With k'_{pr} again expressed in N/m, and A the cross-area of the pillar (in m^2). The equivalent post-peak stiffness of the pillar, k'_{pr}, is then compared with the stiffness of the loading system, k_e, as follows:

$$\text{If } |k'_{pr}| > |k_e|, \text{ there is a rockburst potential} \quad \text{..... Eq. (61)}$$

$$\text{With, } |k_e| = \Delta P / \Delta u \quad \text{..... Eq. (62)}$$

With: ΔP the peak load attained by the pillar (between points A and D in Figure 12); and, Δu the deformation of the loading system between points D and C in Figure 12. To aid in this approach the concept of the Bursting Potential Ratio (BPR) described by Simon *et al*. (1995) was developed, as follows:

$$BPR = |k'_{pr} / k_e| \quad \text{..... Eq. (63)}$$

With k'_{pr} and k_e as defined previously. As the value of BPR increases above one, the rockburst potential increases as well.

It has been postulated that the ERP approach can also be used to assess the strain-bursting potential of exposed surfaces. This is again done by calculating k'_{pr} with Equation (59), but by substituting B and H by the width and depth of the failure zone (as obtained by numerical modelling, or measurements).

The main practical difficulty associated with the ERP approach is determining the value of the various parameters required, particularly the post-peak properties at the rock mass scale.

B.8. Numerical stress modelling

Numerical stress modelling can also be used to assess rockburst potential. Besides information on the state of the ground stresses, which is an important contributing factor to this type of failure, it provides insight into the stress path a pillar is subjected to as mining progresses. As discussed earlier in Section 2.2.1, the manner in which the stress regime ($\sigma_1 - \sigma_3$) – or ($\tau - \sigma_N$) – evolves and approaches the failure envelope as mining advances can be indicative of the type of failure to expect. Figure 7 showed various possible such paths to failure, along with the potential for violent failure each one carries. As mentioned, this stress path-based analysis can provide fairly good insight into the potential for rockbursting to occur inside solid volumes of rock as a result of stress build-up. It has however shown limitations for the assessment of fault-slip bursting potential.

APPENDIX C

C. SELECTED CASE HISTORIES OF DESTRESS BLASTING

As mentioned in Section 4.2 the case histories selected for review in this thesis do not constitute an exhaustive description of all the destressing field trials done in the world to date. Rather, they were chosen because they encompass a wide array of approaches and provide a reasonable chance of identifying which parameters govern the destressing process the most.

C.1. South Africa

Numerous destressing experiments have been carried out in the ultra-deep South African gold mines where narrow shallow-dipping sub-horizontal reefs are exploited by longwall mining methods at depths in excess of 3,000 metres. This full personnel entry method exposes the miners to the very high stress levels that are concentrated ahead of the mining fronts in the very strong and stiff quartzites that typically constitute the host rock – as discussed earlier, this combination of high stress levels, and strong, stiff and brittle rock mass properties is often associated with violent failure in the form of rockbursting, which can be quite dangerous to the personnel.

Elaborate trials were carried out in the 1950's at the ERPM Mine, which are described in Roux *et al*. (1957) and Hill & Plewman (1957). This work concluded that the efficiency of

destress blasting was “beyond reasonable doubt” and that the techniques tested lead to reductions of 35% in the incidence of rockbursting; 77% in the occurrence of “devastating” rockbursts; and, 92% in the incidence of rockbursts that occurred during dayshift, when the exposure of the miners was at its highest. In spite of this, it was later reported by Tyser (1982) that difficulties were often encountered in loading the destress blastholes ahead of the mining faces as a result of the severe stress-induced squeezing they were subjected to – this reportedly made it difficult to implement the technique on a regular basis.

A number of the initial findings were questioned a few years later by Cook *et al*. (1966). The key argument was that the seismic data recorded during the trials at the ERPM Mine, which were originally interpreted as showing seismic events triggered by the destress blasts, showed none of the vibrational characteristics typically associated with seismic events. Cook *et al*. (1966) suggested that these vibrations corresponded instead to the explosive energy released by the destress charges themselves. The initial conclusions were however confirmed in 1984 by Hill, then by Ortlepp, following further analyses of the original seismograms.

Additional work was carried out on destress blasting by the South African Chamber of Mines in the 1980’s.

Toper *et al*. (1997) have described more recent work performed at the Blyvooruitzicht and Western Deep Levels mines. In particular, they discussed a series of face-parallel preconditioning trials that were conducted at the Western Deep Levels Mine at a depth of 2,600 metres in a 1.5 metre thick gold-bearing conglomerate, with a quartzite footwall (with a UCS of 220 MPa) and an andesitic lava hanging wall (with a UCS of 250 MPa). Figure 117 shows a plan view of the test site. One important component of the study was the seismic data recorded by the tight array of seismic sensors shown in Figure 117. This array, installed in 1994, provided accurate event locations, as well as a reliable seismic background level that could be compared to the seismicity triggered locally as a result of the preconditioning test blasts.

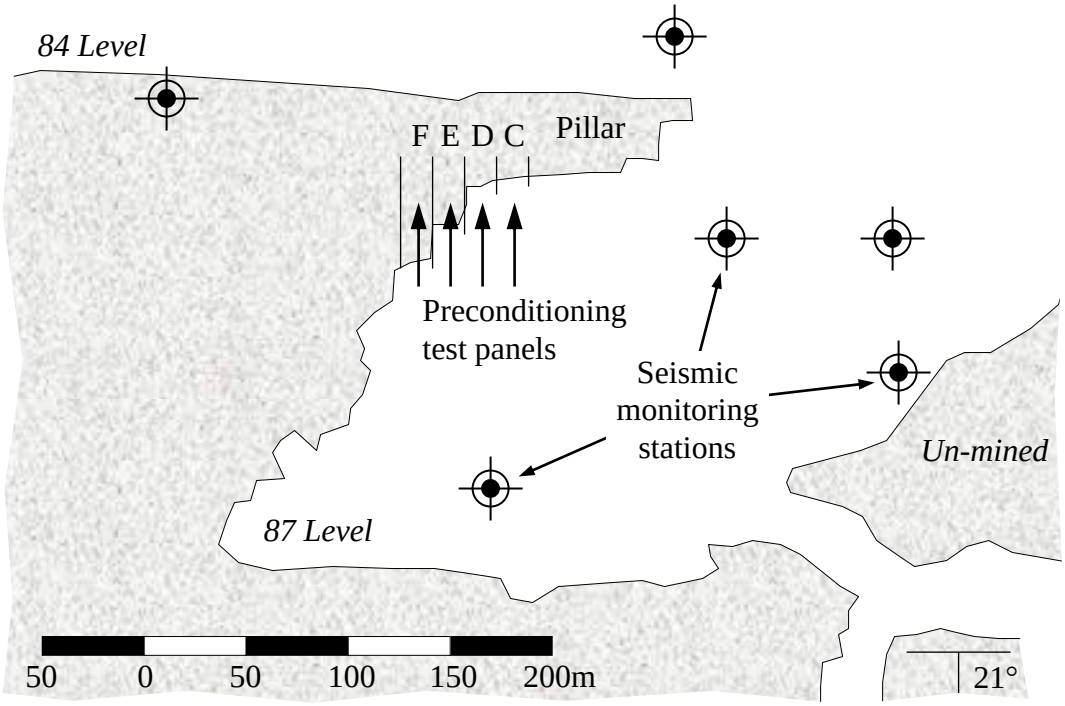

Figure 117. Plan view of the test stope at the Western Deep Levels Mine showing the location of the four preconditioning test panels, as well as the layout of the seismic system. (After Toper *et al*., 1997).

Table 63 summarises the seismic data recorded in each of the four panels shown in Figure 117. The seismic activity shown in this table is entirely associated with the preconditioning of Panel E – it pertains to seismic events recorded before and after the preconditioning blast that was fired in this panel.

Table 63. Summary of the seismic data recorded before and after the preconditioning of Panel E. (Adapted from Toper *et al*., 1997.)

Panel *(ID)*	Period	b-value *	Events recorded *(number)*	Events over a magnitude 0 ** *(%)*
C	Before	0.53	53	26.4
	After	0.47	30	30.0
	% change	–	–	+13.6
D	Before	0.48	29	20.7
	After	0.58	39	39.0
	% change	–	–	–13.5

Table 63 (continued). Summary of the seismic data recorded before and after the preconditioning of Panel E. (Adapted from Toper *et al*., 1997.)

Panel *(ID)*	Period	b-value *	Events recorded *(number)*	Events over a magnitude M_R 0 ** *(%)*
E	Before	0.42	28	53.6
	After	0.60	58	24.1
	% change	–	–	–55.0
F	Before	0.55	25	32.0
	After	0.51	109	33.0
	% change	–	–	+3.1

Notes:

***** *the b-value is defined as the slope of the* $\log_{10}$ *of the cumulative number of events* vs. *the Richter event magnitude plot. It governs the relationship between large and small seismic events, and can be used to estimate the number of events of a given Richter Magnitude that can be expected to occur. For example, a decrease in the b-value implies a greater proportion of large events, and, therefore, an increased risk of large seismic events occurring over a given period of time. Please refer to Section B.3.3 and Figure 111 for additional insight into the b-value.*

****** *Richter Magnitude.*

The significant reduction in the seismic activity in the immediate vicinity of Panel E (represented by a sizeable increase in the b-value and a large reduction in the percentage of events over a Richter Magnitude 2.0) is indicative of a successful destressing effect – Panel D seems to also have beneficiated from the destress blast in Panel E. Interestingly, an increase in the level of seismicity was observed in neighbouring panels F and, to a greater extent, C, after the destress blast was detonated in Panel E and as a result of the resulting stress transfer.

One particularly interesting measurement carried out during these tests consisted in the detailed mapping of the fractures in the face of the test panels, before and after each preconditioning blast. The dominant fracture group was parallel to the face and steeply diping, which is not surprising considering that the major principal stress component at the mine was oriented vertically. Interestingly, the main structural effect of the destress blasts was reportedly not the creation of new sets of fractures, but rather a change in the relative

distribution of each of the sets identified initially – in particular, the relative proportion of steeply-dipping fractures was observed to increase by as much as 25%, whereas the relative incidence of shallow-dipping features was noted to decrease by over 60%. This increase in the occurrence of face-parallel structures reportedly enhanced the advance rate of the face, which resulted in a production increase.

A change in the characteristics of the steeply dipping fractures was often noted after a destress blast, with gouge-filled shear fractures being often observed. There were also signs that shearing was occurring on the hanging wall reef contact. Cross-sectional observations of the rock mass ahead of the test faces were also possible due to the en-echelon geometry of the longwall panels in the test area – these observations indicated that a 3 metre-thick zone of intensified face-parallel fractures was typically created ahead of the face by the preconditioning blasts. It was also noted that the radius of influence of a "typical" 38 mm (1.5 inch) diameter destress blasthole was in the order of 1.5 metre.

These field trials lead to the conclusion that the practice could significantly improve mining conditions as, with over 8,000 m^2 of mining carried out with preconditioning, no face bursts had been reported and a 40% increase in face advance had been achieved.

C.2. United States

A number of documented large-scale confined destress blasts have been detonated in mine pillars in the United States, and particularly in the deep silver mines of the Coeur d'Alene mining district of northern Idaho (Blake, 1972; Blake, 1982; Board & Fairhurst, 1983). Jenkins & McMahon (1987) have compiled a review of the related research work performed by the U.S. Bureau of Mines (USBM) in the Coeur d'Alene district.

Prior to 1970, pillar destressing attempts consisted essentially in detonating a few long holes drilled past these pillar walls and loaded with a few cartridges of dynamite. These attempts were reportedly not very successful at reducing stress levels and improving mining conditions.

The first reported real attempt at destressing large mine pillars took place in 1970 in a sill pillar underneath the 3700 Level at the Galena Mine, at a depth of about 1,135m below surface. The targeted pillar was 30m in length by 6m in height and comprised the full 3m width of the ore lens.

As shown in Figure 118, eighteen (18) nearly 20 ft (6m) deep 1-7/8 inch (48 mm) diameter blastholes, drilled on a 5 ft (1.5m) spacing, were detonated with close to 500 lb (230 kg) of ANFO explosives in them. This destressing attempt was reportedly successful and resulted in the pillar being mined without any rockburst occurring.

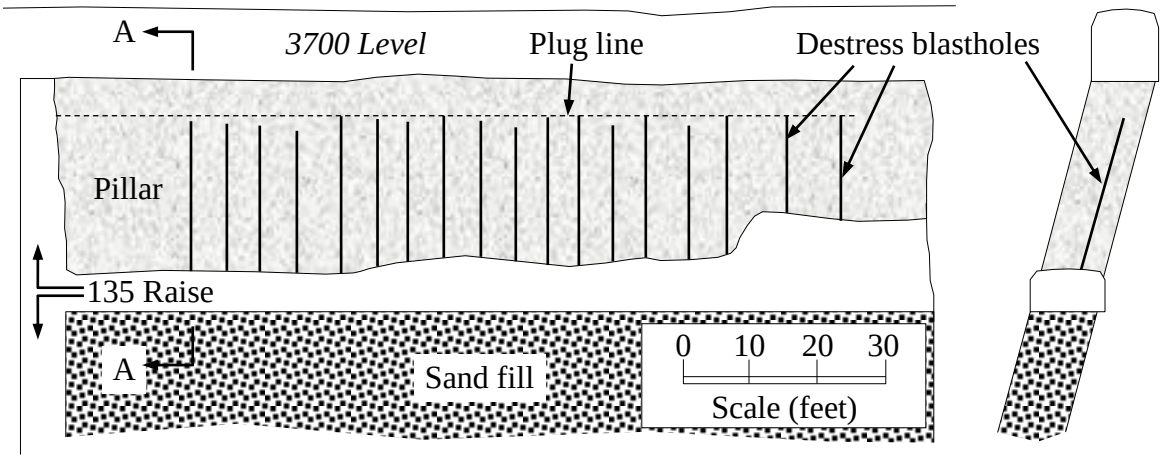

(a) Longitudinal section. ***(b) Cross section A-A.***

Figure 118. Destress blast pattern used in 1970 in the 40-135 overhand cut-and-fill test stope at the Galena Mine. (After Blake, 1972).

Interestingly, velocity surveys were conducted in this pillar before and after the destress blast by firing small explosive charges at the base of the stope and recording wave arrivals at a number of geophone locations in the sill drift above.

Figure 119 shows the results of this work – the much lower velocity contours recorded after the blast are indicative of considerable damage having been done to the pillar.

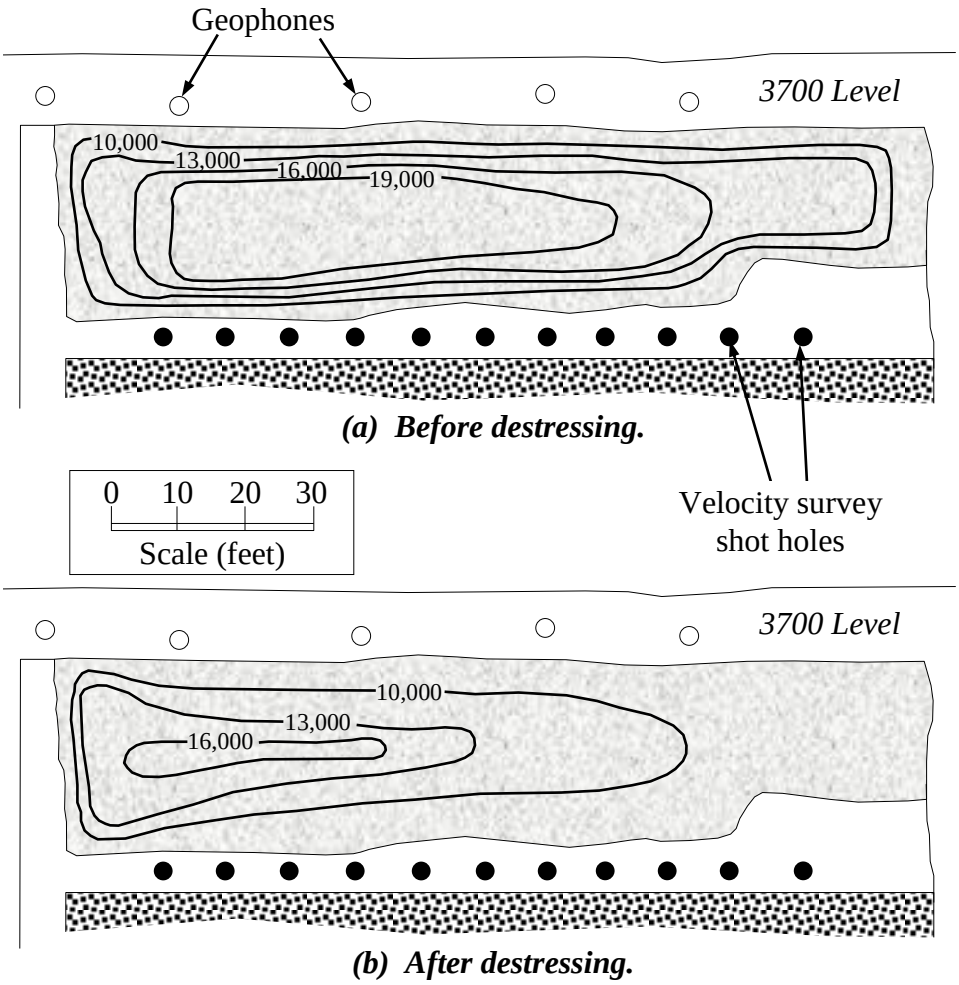

Figure 119. Results of a seismic velocity survey conducted by firing a number of small charges at the stope back while monitoring wave arrivals at a number of geophone locations in the sill drift above. (After Blake, 1972.)

The ground stresses in a series of relatively small but highly stressed sill pillars were also reportedly reduced at the Crescent Mine in 1972, by means of two separate destress blasts. Figure 120 shows a longitudinal view of the situation, where a total of 73 blastholes 1-5/8 inch (41 mm) in diameter drilled to a depth of 7 feet (2.1m) and along a spacing of also 7 ft (2.1m) were used, for a total ANFO charge of nearly 605 lb (275 kg). Post-blast convergence measurements (as described in Section 3.3) reportedly confirmed that the procedure had been successful.

Figure 120. Longitudinal view of the destress blastholes used in 1972 in two destress blasts in numerous sill pillars at the Crescent Mine. (After Board & Fairhurst, 1983.)

A number of destress blasts were detonated in remnant pillars at the Lucky Friday Mine in 1974 and 1975, with blastholes drilled 10 ft (3m) apart – no further details were recorded concerning the size and depth of these holes, the explosive products used, or the degree of success achieved.

A relatively large-scale destress blast was fired at the Lucky Friday Mine in 1985 when the sill pillar between the 4600 Level and the approaching overhand cut-and-fill stopes from

the 4900 Level started to be affected by significant seismic activity and rockbursting. As shown in Figure 121, nineteen (19) destress blastholes were drilled in this sill pillar at 70° on the footwall side of the lead stope on a 10 ft (3m) spacing.

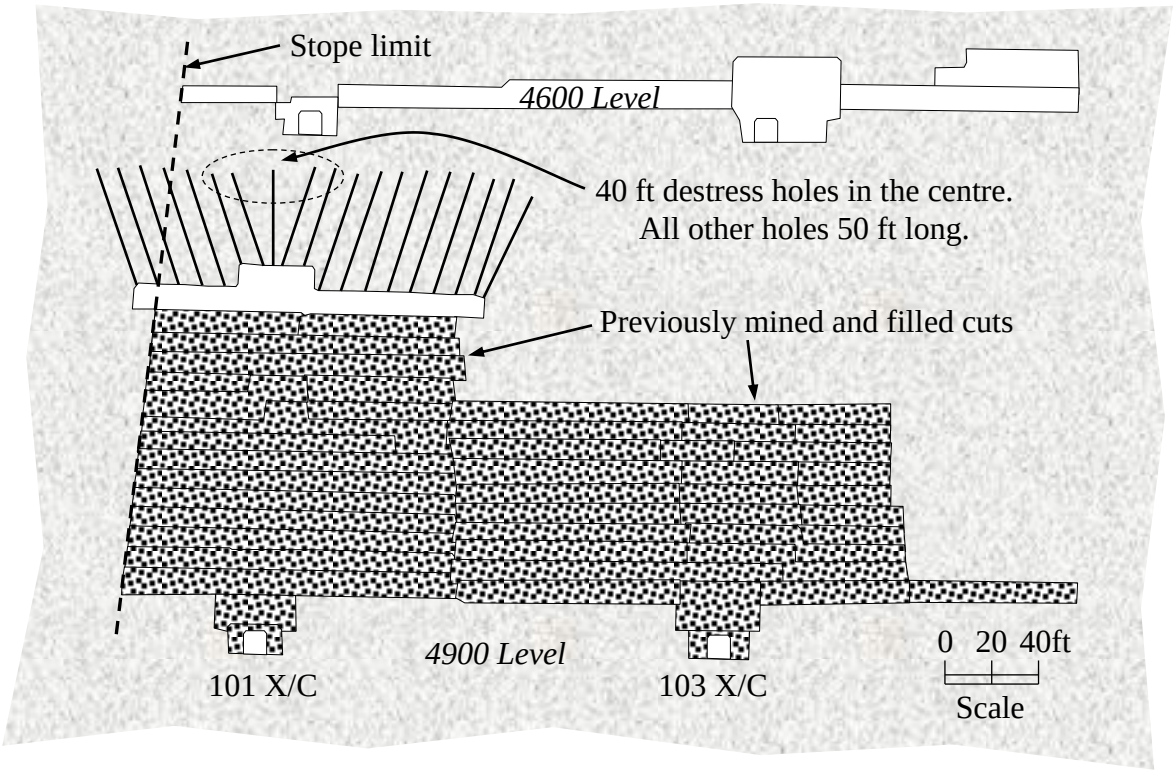

Figure 121. Longitudinal view of the 101 and 103 stopes showing the typical sill pillar destressing layout used at the Lucky Friday Mine. (After Jenkins & McMahon, 1987.)

These destress holes – 2-1/2 inches (63.5 mm) in diameter and 40 to 50 ft (12 to 15m) in depth – were loaded with nearly 880 lb (400 kg) of ANFO. This blast reportedly reduced the level of seismic activity in the targeted regions and achieved its objective, even though it pushed the seismically active high stress fronts towards more virgin ground.

The Lucky Friday Mine continued to implement large-scale confined destress blasts in highly stressed pillars and acquired for this purpose a Cubex drill fitted with a 5 in (127 mm) diameter bit. With this new hole size, the drilling pattern was expanded to 10 ft by 10

ft (3m by 3m), and the blastholes were loaded leaving 20 ft (6m) long collars and blasted 100 milliseconds and up apart.

The largest choked pillar destress blast ever attempted at the Lucky Friday Mine – detonated in December 1990 – was located in the 5100-106 Stope at a depth of 4,920 ft (1,500m), was 590 ft (180m) in strike length and 92 ft (28m) in height. It comprised 58 destress blastholes, 5 in (127 mm) in diameter and drilled 10 ft (3m) apart to a depth of 82 ft (25m) – each hole was loaded with a 50 ft (15m) long column of APEX 340 and stemmed. A total of nearly 13,860 lb (6.3 tonnes) of explosives were detonated in this blast.

A Richter Magnitude 2.0 seismic event occurred at blast time, followed by an intense bout of seismic activity for about twelve hours. The pillar was subsequently recovered over a two year period during which some rockbursts occurred, but in regions that could not have been reached by the destress blast. Another large-scale confined destress blast fired in a pillar at the Lucky Friday Mine in 1996 was also reportedly successful.

The Star Mine, in partnership with the USBM, initiated a destress blasting programme in 1975 with the objective of assessing the possibility of lowering the ground stresses in a production block located at a depth of 7,700 ft (2,350m) prior to its extraction. The main objective was to assess whether it was possible to destress an entire stoping block prior to mining it, in order to avoid the long production delays associated with drilling and blasting smaller scale destress rounds. This work was done using blastholes between 3-5/8 and 4 inches (92 to 102 mm) in diameter.

Two preparatory destress blasts were detonated in a first phase. As shown in Figure 122, ring-drilled blastholes were first fired in 1976 from cross-cuts #7 and #10 on the 7700 Level in order to destress the first lifts of the #7 and #10 stopes. Ring-drilled blastholes were subsequently detonated in 1979 from the #8 and #12 cross-cuts on the 7900 Level below, with the objective of destressing the #8 and #12 stopes.

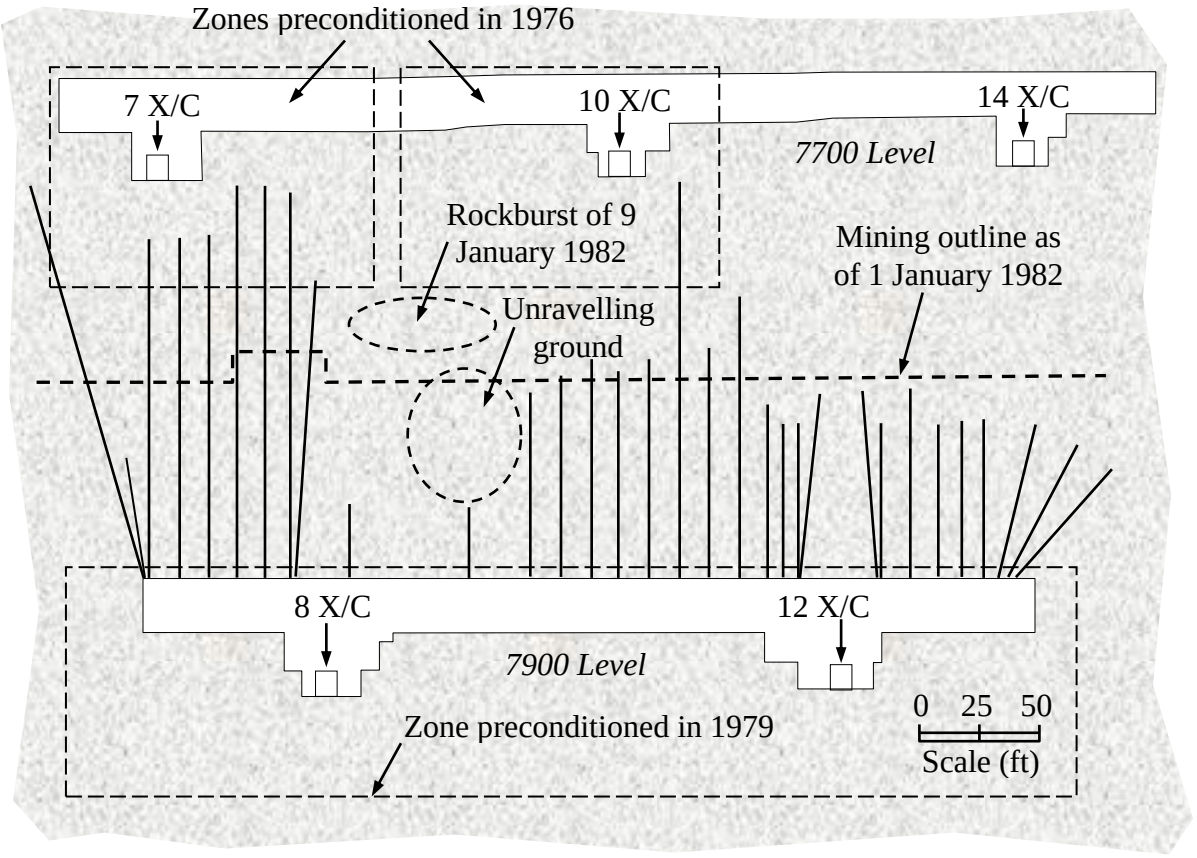

Figure 122. Longitudinal view of the large panel preconditioning blast at the Star Mine. (After Board & Fairhurst, 1983.)

Details of the preconditioning rings blasted off the various cross-cuts on the 7700 and 7900 levels are shown in Figure 123. Although these fanned blastholes were drilled with an in-the-hole hammer, serious difficulties were encountered during drilling, which resulted in many holes being lost. The first blast, detonated off the 7700 Level, required 4,500 ft (nearly 1,370m) of drilling and over 8,800 lb (4 tonnes) of explosives. As a result of this blast the raises and the first few lifts were reportedly mined without the occurrence of major seismicity, except in the gap between the two targeted zones. The second blast, fired off the 7900 Level, needed over 7,200 ft (2,200m) of drilling and about 9,900 lb (4.5 tonnes) of Tovex 5000 emulsion explosives. The third and final destress blast was fired in 1982, which encompassed approximately 3,000 ft (915m) of long upholes drilled off the floor of the second cut in the #8 and #12 cut-and-fill stopes – the objective was to complete the destressing of the entire stope panels. Nearly 4,000 lb (close to 1.8 tonne) of explosives were detonated in this final destress blast.

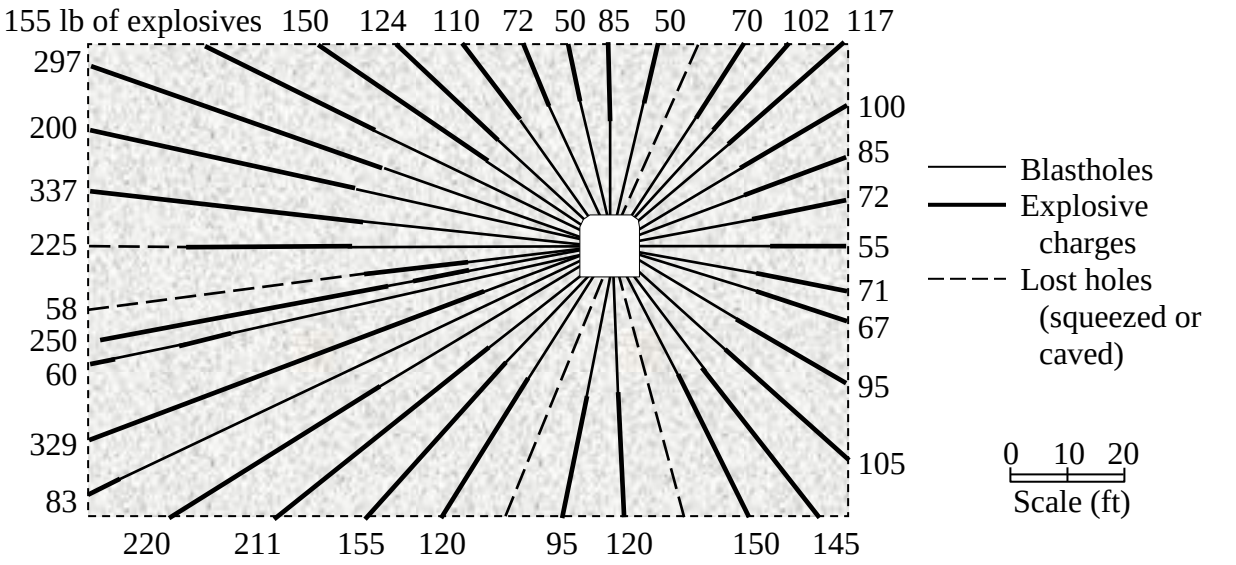

(a) #10 Cross-cut on the 7700 Level.

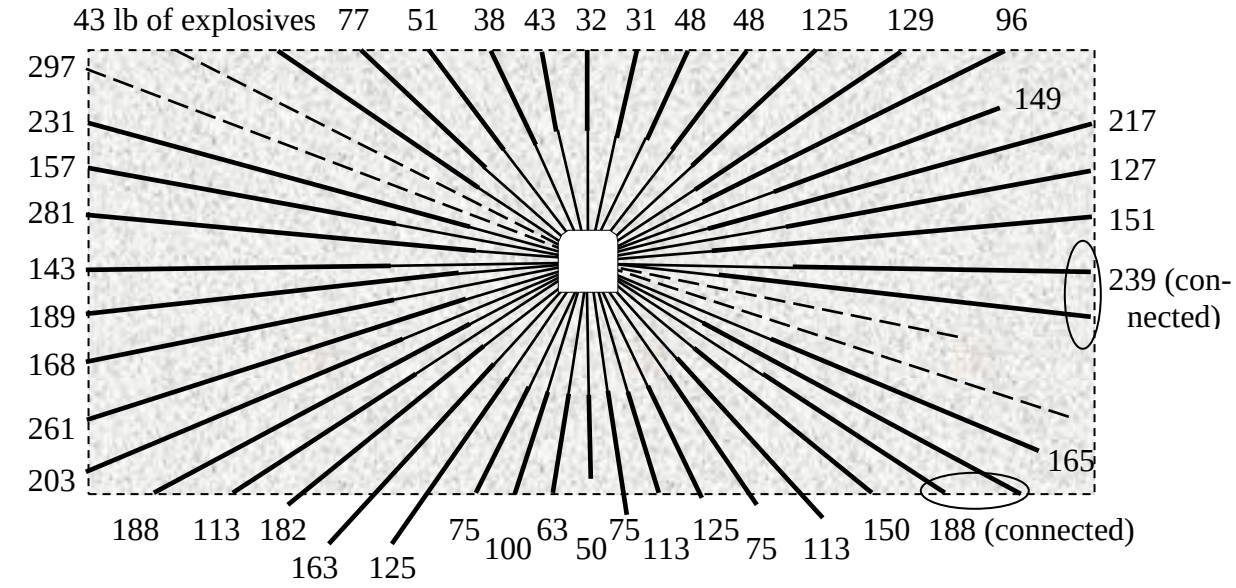

(b) #8 Cross-cut on the 7900 Level.

Figure 123. Preconditioning blasthole rings drilled off (a) the #10 X/C on Level 7700; and, (b) the #8 X/C on Level 7900 at the Star Mine. (After Board & Fairhurst, 1983.)

The mining front off the 7900 Level was reportedly affected by very little seismicity, but the one above the zone destressed from the 7700 Level was hit by some twenty (20) rockbursts. Large rockbursts also occurred in gaps between the destressed zones – Figure 122 shows the location of one such event, which happened 9 January 1982.

The Star Mine was closed in May 1982 before the mining of this block was completed, and, hence, the full effect of this destressing experiment is difficult to assess. However, the practice of detonating large-scale choked destress blasts in ore pillars, implemented for six years, was reportedly quite efficient overall at reducing the level of seismicity experienced and the number of rockbursts sustained.

The destressing of the next cut-and-fill lift was routinely carried out at the Star Mine. The timber sets used for ground support precluded the implementation of blasts with very heavy powder factors. As a result, a relatively light destressing approach was developed in order for successive lifts to be mined in destressed ground. Figure 124 shows the staggered design eventually retained.

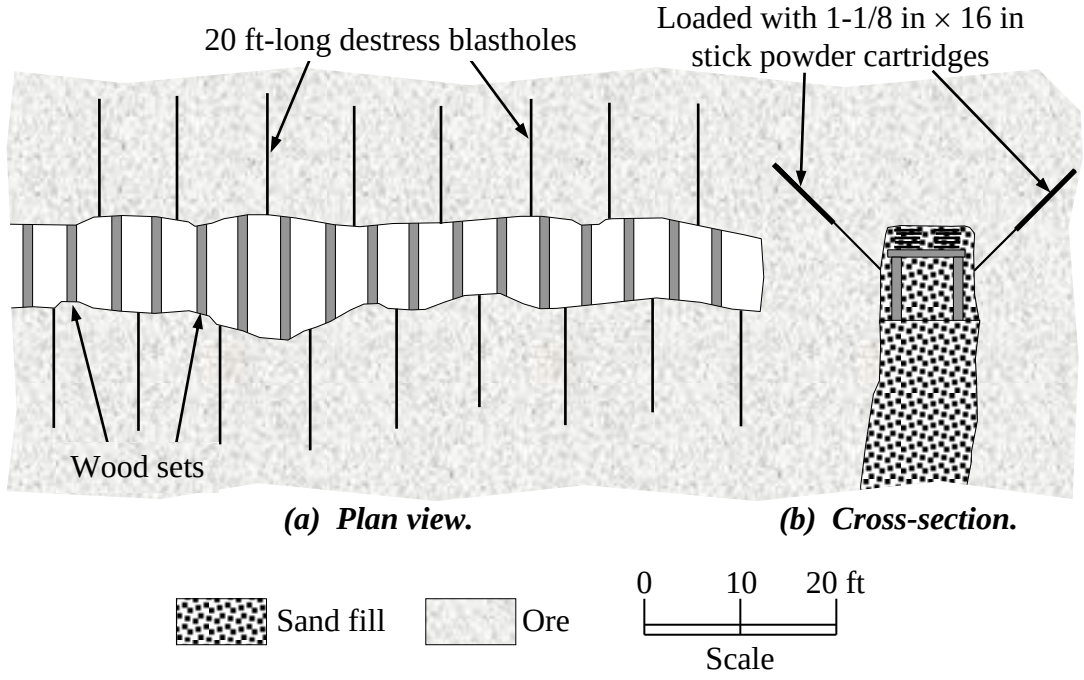

Figure 124. (a) Plan view; and, (b) cross-section of the destressing method implemented at the Star Mine in timbered cut-and-fill stopes. (After Jenkins & McMahon, 1987.)

Once mining was completed on a lift, 20 ft (6m) long destress blastholes were drilled upwards every metre in alternating walls with jacklegs. The last 10 ft (3m) of each hole was subsequently loaded with a charge of about 10 lb (4.5 kg) consisting of stick powder cartridges 1-1/8 inch in diameter by 16 inches in length (28.6 mm by 40.6 cm). The lift was then backfilled, with the objective of minimising damage to its walls (which could

have undercut the walls of the next cut), and the destress blastholes were detonated – a few small bursts were typically triggered at that time. Fifty-four (54) cut-and-fill lifts in burst-prone stopes were successfully destressed in this manner between 1974 and 1977 at the Star Mine. Rockbursts however still reportedly occurred once the remaining sill pillar became over-stressed.

A large-scale destressing attempt – described in detail by Board & Fairhurst (1983) – was made at the Star Mine in 1979-1980 in a 50 ft (15m) high sill pillar located in the Grouse Vein at a depth of 6,700 ft (2,040m). This destressing attempt was aimed at reducing the severe rockbursting activity that was typically associated with sill pillars of about 15 metres in height. As shown in Figure 125, the destress blast comprised 29 blastholes 2 to 2-1/4 inches (50 to 57 mm) in diameter and 16 to 26 feet (5 to 8m) in depth drilled with jacklegs and stopers directly in the centre of the pillar with a spacing of 6.5 to 10 feet (2 to 3m).

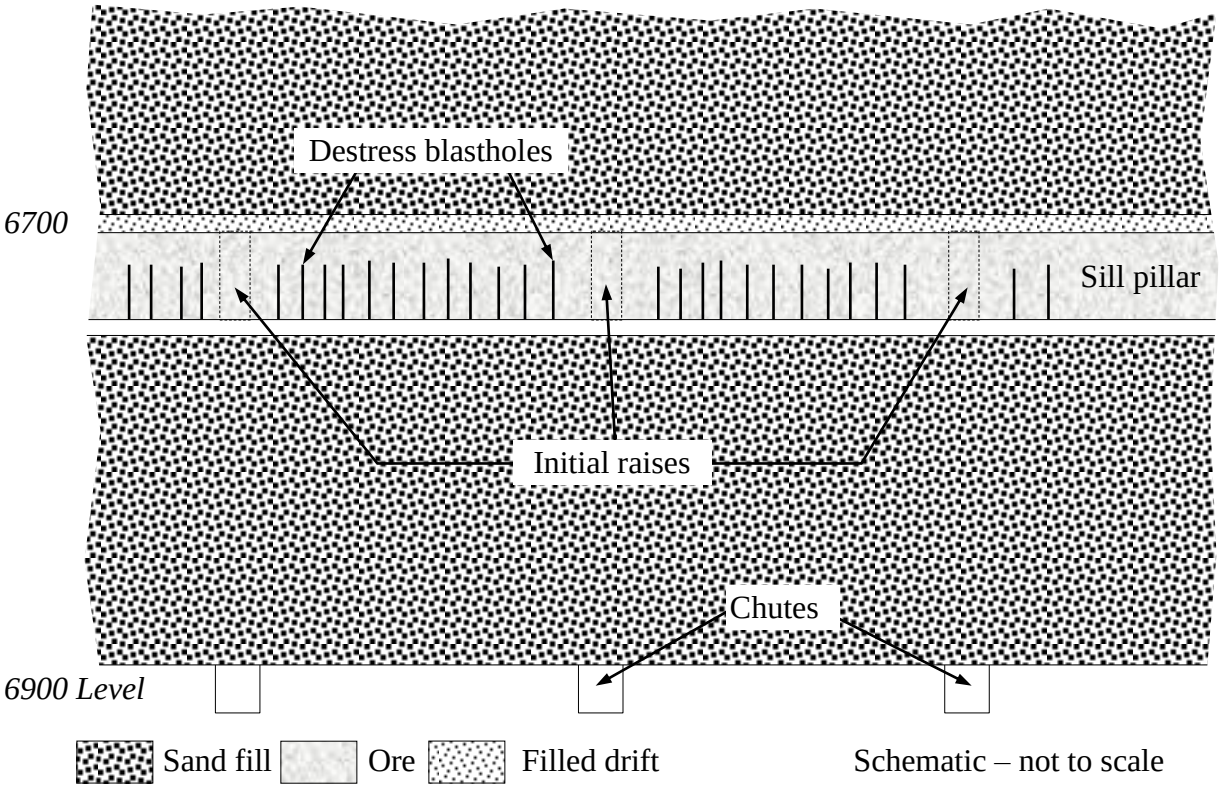

Figure 125. Schematic longitudinal view through the Grouse Vein at the Star Mine showing the location of the destress blastholes. (After Board & Fairhurst, 1983.)

Depending upon the presence of water these blastholes were loaded with either ANFO or Tovex. The charges were primed with a booster located near their toe and sequenced with short period nonel detonators. One metre-long collars were left unloaded, which were stemmed with clay. A total of only 395 lb (180 kg) of explosives were eventually used due to loading difficulties, which translated into a charge density of only about 1.0 lb per foot of blasthole (about 1.5 kg per metre of blasthole).

The blast was instrumented extensively with convergence cells located on both sides of the pillar, as well as three IRAD load cells (oriented in order to measure variations in the stress component perpendicular to the ore lens). Pressure cells were installed on the 6700 Level inside the lightly-consolidated classified tailings backfill that had been placed there prior to the blast. These pressure cells were meant to measure an increase in the stress within the backfill as a result of the wall convergence that was expected to occur as the pillar was destressed.

Despite the small quantities of explosives used, and as shown in Figure 126 and Figure 127, the instruments recorded immediately after the destress blast a convergence of the pillar walls of between 0.3 and 1.5 inch (8 to 38 mm), an average reduction of 7.5 MPa of the stress component acting perpendicularly to the pillar (in this case over a period of weeks), and a stress increase inside the backfill of nearly 130 psi (900 kPa). This strong response is interesting considering the relatively light design of the destress blast and the fact that no major seismicity was reportedly triggered by the destress blast.

As shown in Figure 127, all three stress meters showed a significant drop – from 600 to as much as 1,600 psi (4 to 11 MPa) – during the weeks following the destress blast. The sill pillar itself was recovered without major difficulties being reported, with the development of the three initial raises (shown in Figure 125) being carried out with little difficulty.

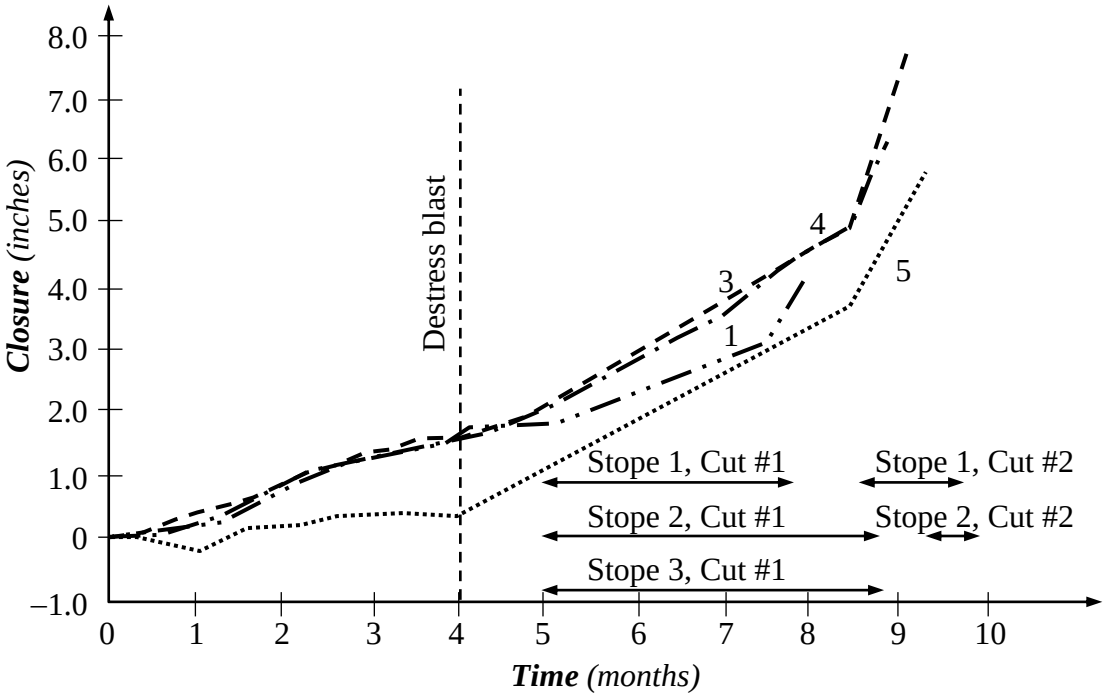

Figure 126. Closure measurements in the sill pillar region of the Grouse Vein at the Star Mine before and after the destress blast. (After Board & Fairhurst, 1983.)

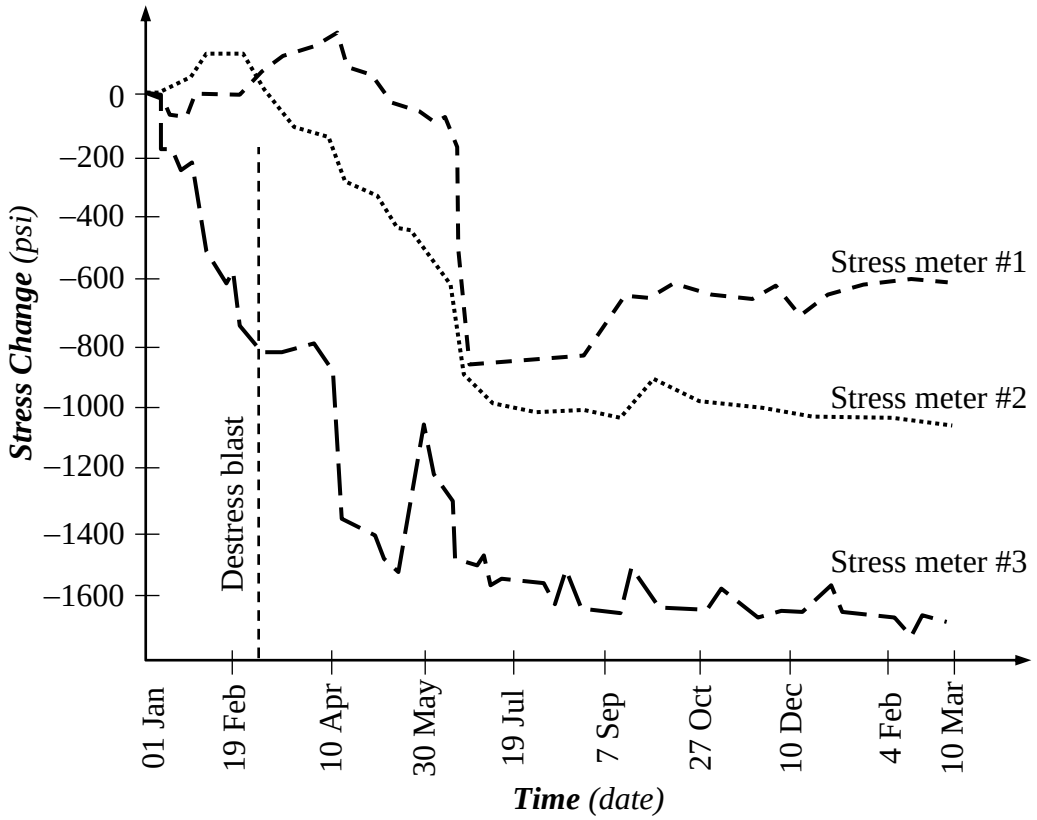

Figure 127. IRAD stress cell measurements in the sill pillar region of the Grouse Vein at the Star Mine before and after the destress blast. (After Board & Fairhurst, 1983.)

The Galena Mine, in association with the USBM, fired in February 1990 a large-scale confined destress blast in a pillar located at a depth of 4,300 feet (about 1,310m). The drilling pattern and quantities of explosives used were reportedly too wide and insufficient for the size of the pillar, and the blast did not trigger any major seismic event and failed to reduce the stress levels in it. Figure 128 shows the layout used, and highlights the small proportion of the pillar that was targeted.

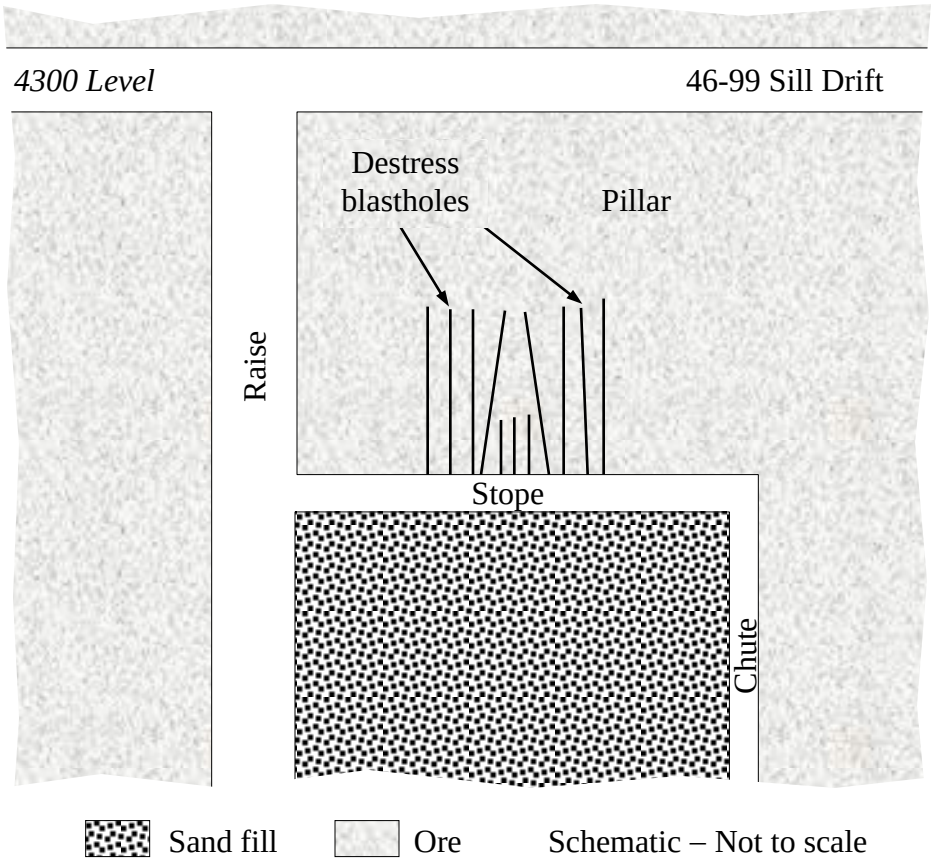

Figure 128. Schematic longitudinal view (not to scale) showing the layout of the unsuccessful 1990 pillar destress attempt at Galena Mine. (After Board & Fairhurst, 1983.)

Overall, large-scale confined destress blasts have been implemented in numerous pillars for many years in the United States in the Coeur d'Alene silver mining district, and have been associated with various levels of success. Often, the explosive energy levels of these blasts have been maintained relatively low in an attempt to preserve the integrity of the ground not targeted by the blasts.

C.3. Canada

Most of the deep mining and highly stressed operations in Canada have experimented with destress blasting, in both development headings and production stopes. Since the 1960's INCO Limited has experimented with, and implemented, destress blasting techniques in development faces in many of its underground mines, in both horizontal headings (drifts and tunnels) and vertical development (raises and shafts), as reported by Garood (1984). Figure 129 is a plan view showing the typical destress blast design implemented in development headings at INCO, as reported by Garood.

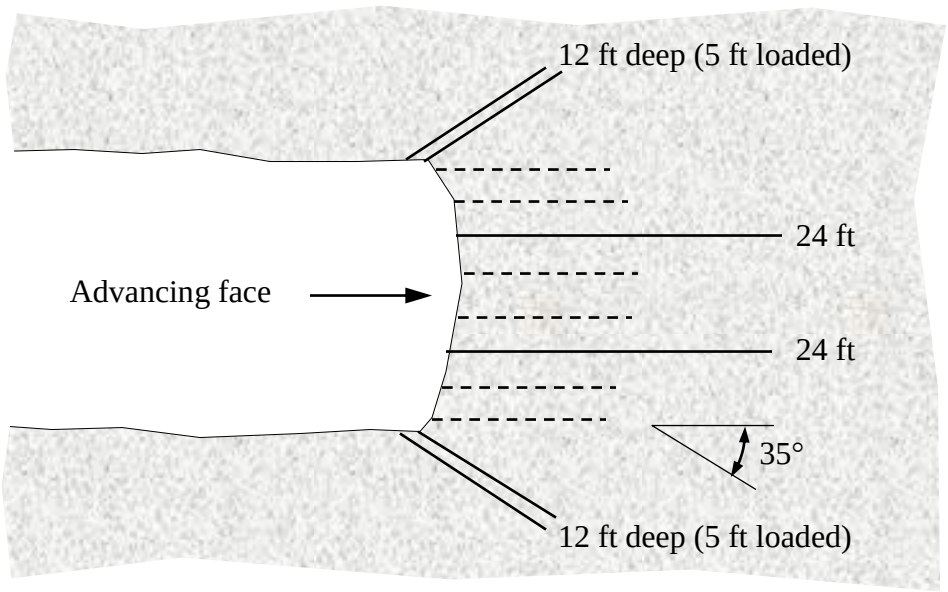

Figure 129. Plan view of a typical INCO destress blast design for drift rounds. (After Garood, 1984.)

As can be seen, a limited number of holes were drilled ahead of, as well as away from, the face. One of the two 35° side holes on each side of the drift was drilled upwards, whereas the other one was drilled downwards. The two horizontal destress blastholes and the bottom 5 ft (1.5m) of the inclined destress holes were loaded with ANFO and blasted with the face. Figure 130 shows the typical destress layout implemented during the sinking of the No. 11 Shaft at the Creighton Mine – as can be seen, relatively small quantities of explosives were used.

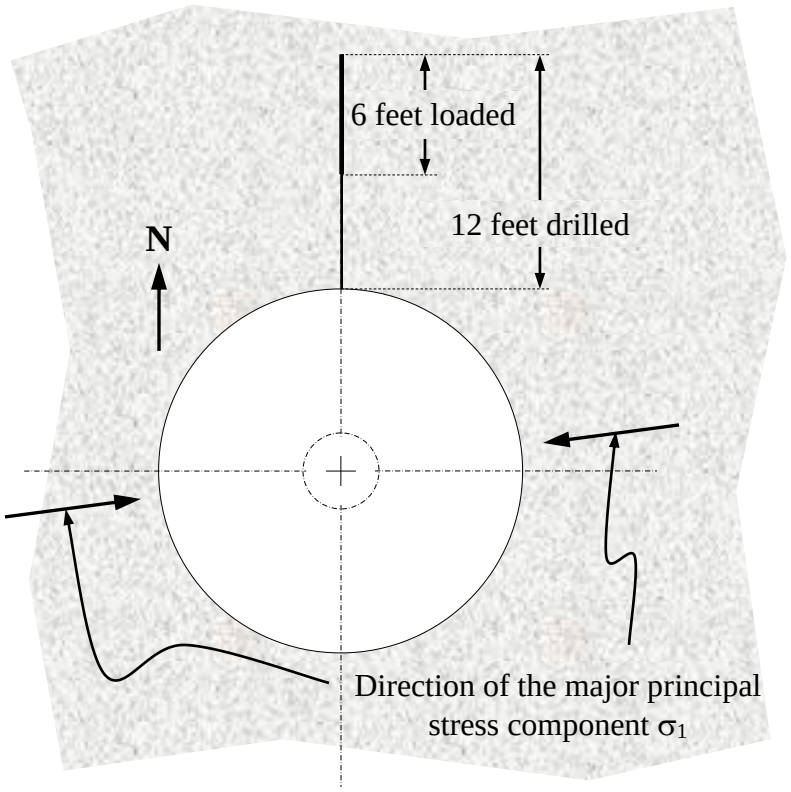

Figure 130. Plan view of the typical destress blasthole layout implemented in the Creighton No. 11 Shaft. (After Garood, 1984.)

O'Donnell (1992) also summarised a number of case studies from the INCO Creighton Mine, one of the deepest in Canada. In response to the increasingly difficult conditions encountered as development was carried out at depths in excess of 2,000 metres, the amount of destressing was progressively increased, to eventually reach the ten hole pattern shown in Figure 131. In this layout, 1.5 metre-long columns of ANFO were loaded in the toe of the face holes, whereas 0.6 metre-long charges of ANFO were detonated in the bottom of the wall and corner holes.

O'Donnell mentioned that much of the success attained was attributed to the fact that 85% of all rockbursts occurred at blast time. This is an interesting indication that destress blasting not only alters the fracture pattern and promotes deformation, it also triggers seismic events – which can release significant amounts of accumulated strain energy – at blast time.

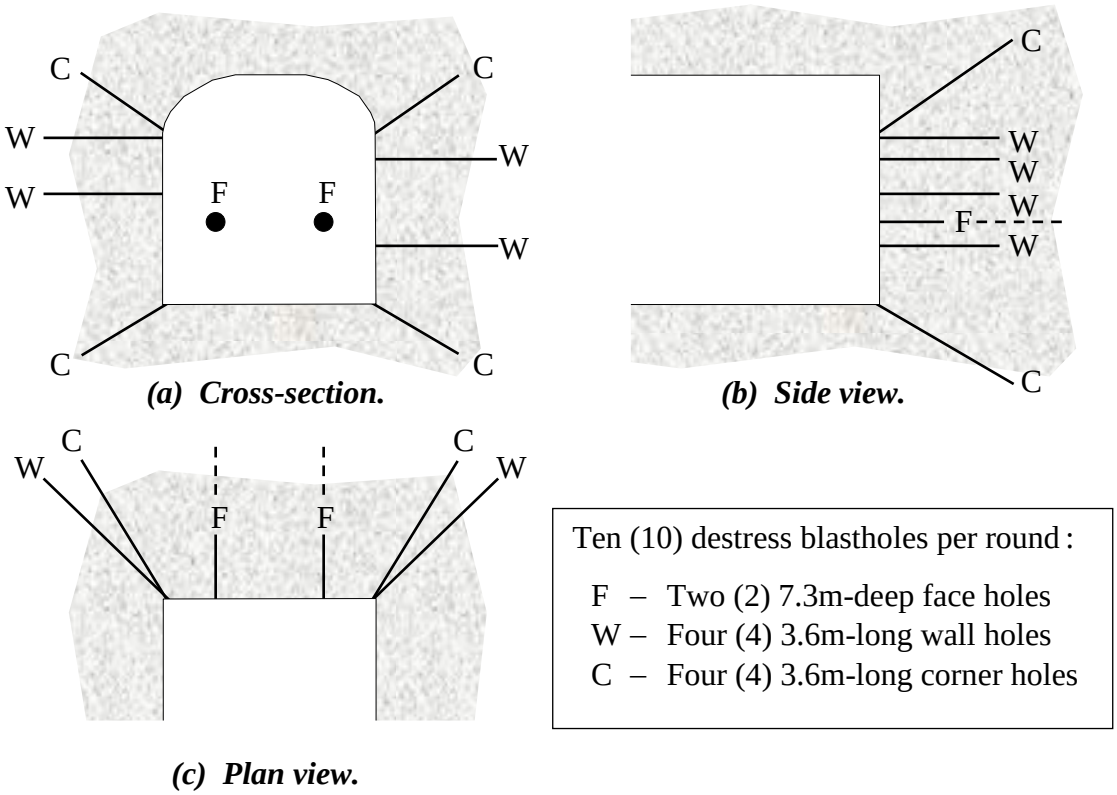

Figure 131. Schematic views of the typical destressing pattern implemented on the 2195m Level at the Creighton Mine. (Adapted from O'Donnell, 1992.)

O'Donnell (1992) reported that destress blasting in both the development headings and the ore blocks themselves – combined with an adequate mining sequence and appropriate ground support systems – have allowed the successful recovery of significant blocks of ore at depths of between 2,000 and 2,200 metres at the Creighton Mine. These pillars had historically been very difficult to mine and had in some cases been previously abandoned due to poor ground conditions and rockbursting.

In particular, a destress slot was blasted at Creighton Mine below the 6600 Level, in an area that had been converted from cut-and-fill to vertical retreat mining (VRM) in light of the high stress conditions that had developed as the sill pillar reached a thickness of only 30m. Hedley (1992) describes how this small 6m-wide transverse slot was mined across the sill pillar by a series of five blasts. A 6m by 6m central panel was taken first with 6-1/4 in (159 mm) blastholes drilled on a 3m by 3m pattern – this initial panel was mined retreating upwards with successive 3m thick slices, as would be done with a drop raise, and backfilled

with cemented tailings. Larger panels were subsequently extracted, towards the footwall first, then towards the hanging wall. This approach – which, as discussed earlier, cannot be considered as destress blasting *per se* because the material was not left in place but mined-out – was reportedly successful at relieving the high stress conditions that prevailed in the sill pillar. Thousands of microseismic events occurred in the sill pillar region as the successive panels were mined, most of them within two hours of the blasts. Large rockbursts were also induced, which caused damage, but these took place near blast time, when no miners were underground.

O'Donnell (1999) has provided a detailed account of a large-scale destress blast that was implemented in May 1998 in a large regional pillar at the INCO Stobie Mine in Sudbury. The 25 Pillar was a highly stressed large piece of ground located above the 550m Level, in which substantial ore reserves were tied up. In order to facilitate the recovery of these reserves, INCO engineers decided to destress this pillar by means of a large-scale destress slot. This slot comprised two parallel rows of blastholes drilled 1.5 to 1.8m apart, which were also parallel to the strike of the hanging wall ore-waste contact. As shown in Figure 132, two sections of fanned blasthole rings were drilled at each end of the destress slot, in order to provide relief to the centre destress blastholes and concentrate stress further towards the slot region. (Please note that not all the blastholes are shown in Figure 132.)

A series of upper blastholes, 102 mm (4 inches) in diameter and averaging a length of 21.3m, were drilled 85° from the horizontal. These blastholes had a spacing of 2.4m on the north half of the 2170 Destress Drift, whereas this spacing was reduced to 1.8m in the south half of this drift – the spacing was tightened to 1.2m in the central section. The emulsion product (Dyno Nobel RUS) routinely used at the mine was chosen for this blast. Collar lengths varied between 1.5 and 3.0m, and averaged 2.1m. As much as 10,045 kg of emulsion explosives were used in the destress blastholes – the rings on the south and north sides were blasted with 12,575 kg and 10,900 kg of emulsions, respectively. Because of the large number of blastholes involved, both short and long period Nonel detonators were used in the blast, with each blasthole being double primed.

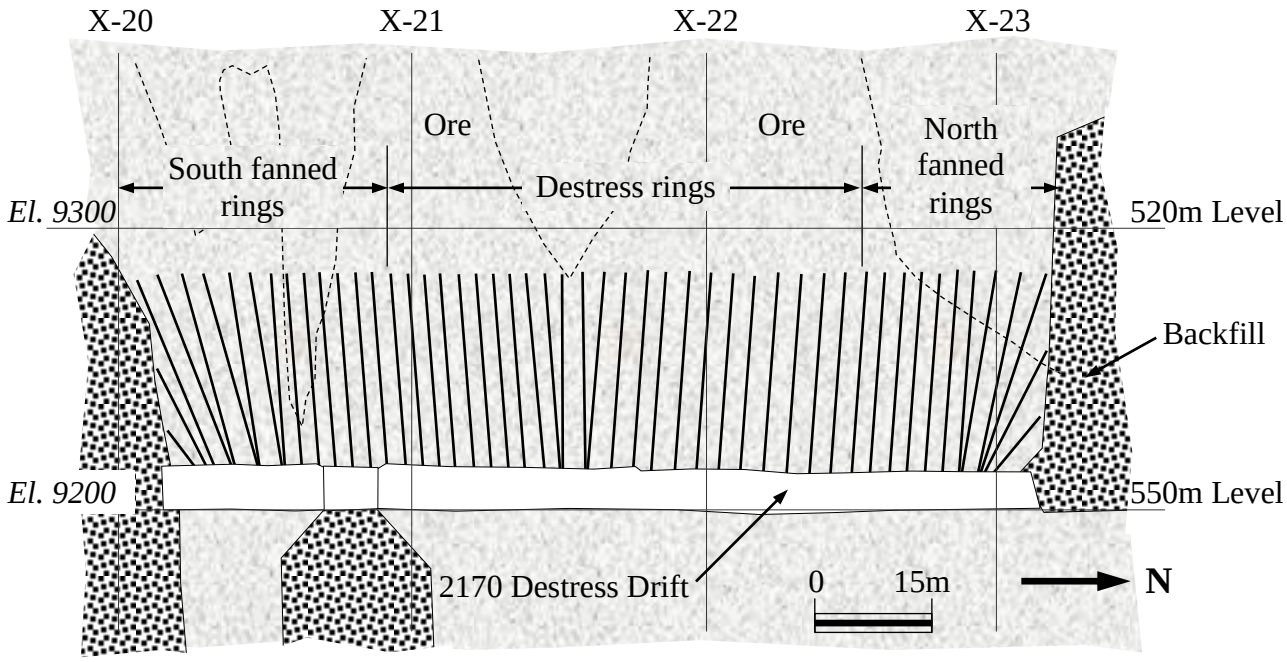

Figure 132. Longitudinal view looking west cut through the destress slot in the 25 Pillar at Stobie Mine. (After O'Donnell, 1999.)

The destress blast was instrumented with CSIRO stress cells, and the ground vibrations it produced were monitored. Microseismic monitoring, as well as visual observations before and after the blast, completed the array of collected data.

Of particular interest is a measured reduction of 8 MPa in the magnitude of the major principal stress component in the 2185 X/C on the 550 Level following the blast – this stress drop is of a similar order of magnitude as those recorded following large-scale panel destress blasts at Brunswick Mine in 1999 and Fraser Copper Mine in 2001, and described in detail in chapters IX and X, respectively. This destress blast was reportedly instrumental in the recovery of as much as 1.8 million tonnes of ore between the 520 and 550m levels.

Oliver *et al*. (1987) have summarised the three-fold strategy implemented by INCO Limited to alleviate the rockburst problem in deep remnant pillars, as follows: 1) locate such pillars in relatively weak ground that is subjected to the smallest possible level of lateral confinement; 2) modify their behaviour with preconditioning blasts; and, 3) attempt to trigger the sudden and violent failures at blast time, when no personnel is underground.

Falconbridge Limited has also experimented with various destress blasting techniques in remnant mine pillars in the Sudbury mining district, as reported by Moruzi & Pasieka (1964), including by detonating charges in the hanging wall of lenses mined with a cut-and-fill method. These trials were reportedly not successful due to insufficient levels of explosive energy having been used.

Slade (1968) described a series of destress blasts that were implemented at the Falconbridge #5 Mine in narrow cut-and-fill horizons where high levels of seismicity were being experienced in the hanging wall of production stopes. At the beginning of the mining cycle 3m-long percussion blastholes were drilled upwards 6 metres apart in the hanging wall from within the stopes. However, once the sill pillar became too thin, diamond drill holes were drilled downwards into the hanging wall from the upper level, as shown in Figure 133. This approach was reportedly successful and resulted in easier mining conditions inside the stopes.

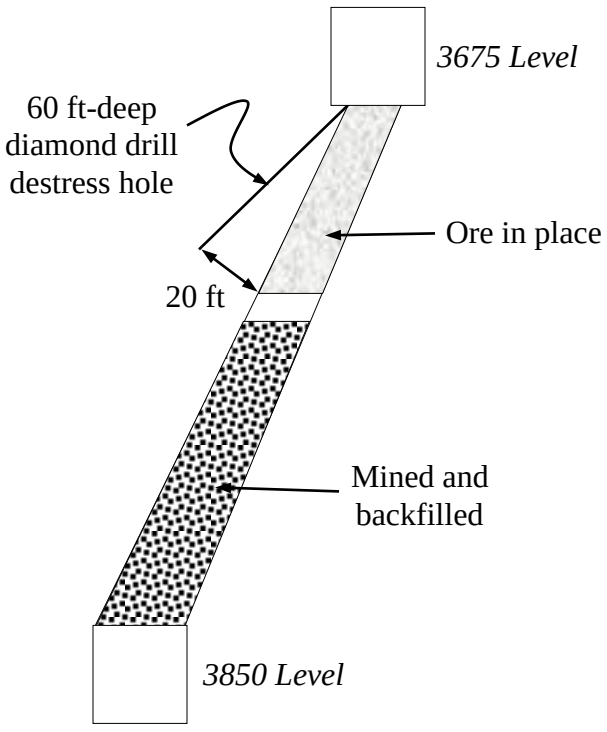

Figure 133. Destressing approach implemented at the Falconbridge #5 Shaft in narrow cut-and-fill veins. (After Slade, 1968.)

Hanson *et al*. (1992) also described a 1991 large-scale destress attempt at the Strathcona Mine in Stope 25-39-D4. This blast consisted of 66 blastholes, 64 mm in diameter and 5.5 metres in depth, and had the objective of lowering the stress levels in the stope. The blast itself triggered a +2.6 Nuttli Magnitude seismic event, which caused considerable damage in the neighbouring excavations. More recently, large-scale confined destress blasts were implemented in 2001 at the Fraser Deep Copper Mine (Strathcona Deep), mainly in relatively small and somewhat isolated remnant pillars – these blasts are reported in detail in Andrieux (2001), Sampson-Forsythe & Andrieux (2001) and Sampson-Forsythe *et al*. (2002). Chapter X of this thesis focuses on one of these blasts.

Since the 1950's, the deep underground gold mines of the Kirkland Lake mining district have also experimented with destress blasting. In particular, and as described by Harling (1965), attempts have been made to destress remnant pillars at both the Macassa and Lake Shore mines. The approach typically consisted in drilling long 38 to 57 mm diameter destress blastholes in the plane of the ore body, generally with a diamond drill for increased accuracy and easier loading of the smoother holes. The holes were generally loaded with ANFO, leaving a 3m-long empty collar, and detonated simultaneously. The hole spacing was usually about 7.5 metres.

Harling (1965) describes in detail a large-scale destress blast that was done in the remnant of the 40026-2 Stope at the Lake Shore Mine in which particularly difficult ground conditions prevailed, accompanied by seismic activity. As shown in Figure 134, a 30 metre-long raise was driven from the undercut of the stope, in the abutment region of the pillar, from which a first series of long diamond drill 38 mm diameter destress blastholes were drilled – another series of similar destress holes were drilled downwards from the overcut in order to complete the coverage of the pillar.

Although a number of successive destress blasts were ultimately required in the area, a sufficient level of stress reduction was reportedly achieved in the end, and the remnant of the 40026-2 Stope was successfully mined.

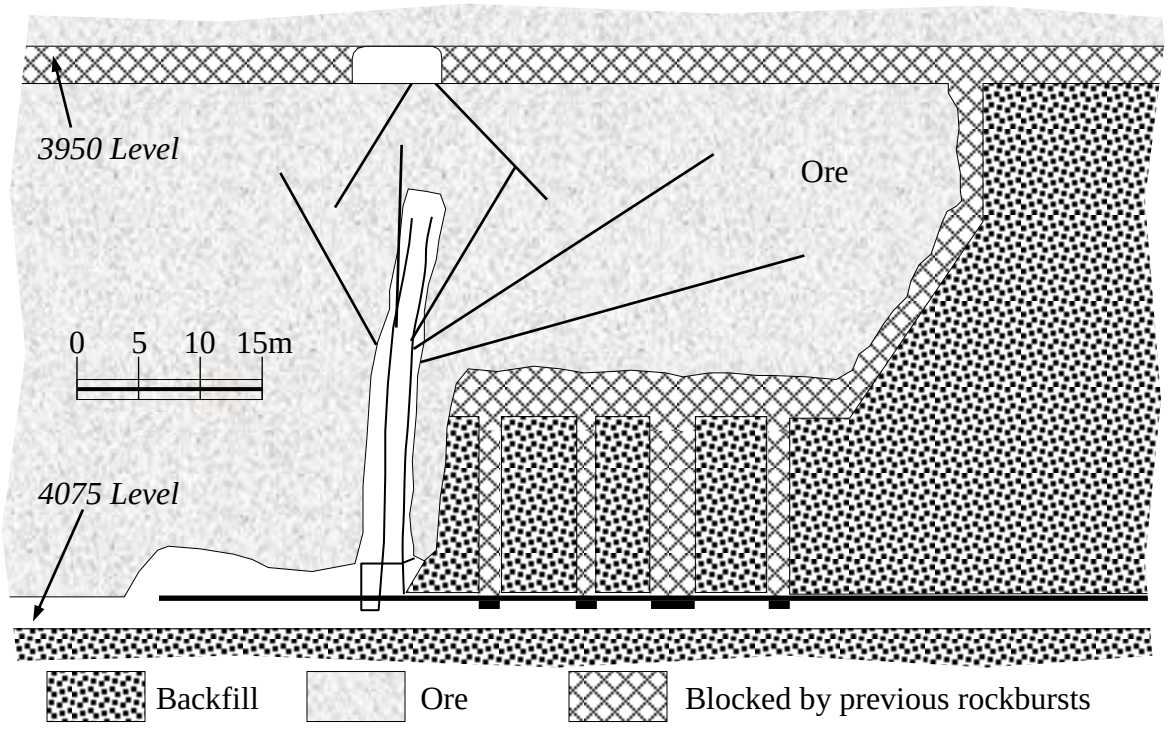

Figure 134. Longitudinal view of the destress blast layout implemented at the Lake Shore Mine in 1962 for the recovery of the remnant 40026-2 Pillar. (After Harling, 1965.)

Fault destressing has also been attempted at the Lake Shore Mine in the Kirkland Lake mining district when approaching known active faults. Figure 135 shows the design implemented in 1958 in the vicinity of the notoriously problematic Lake Shore Fault.

Intuitively, and also based upon the experience acquired since with this type of blasting, the few destress holes were located quite far apart, and their destressing effect was probably not significant. (In fact, a massive Nuttli Magnitude 4.3 fault-slip seismic event occurred in this region three years later, in March 1961.)

Despite the marginal results obtained with the few tests done, fault destressing at both the Lake Shore and Macassa mines was considered, from a qualitative point of view, to have a beneficial effect. It should however be noted that none of these tests has been reported to have triggered a fault-slip event at blast time.

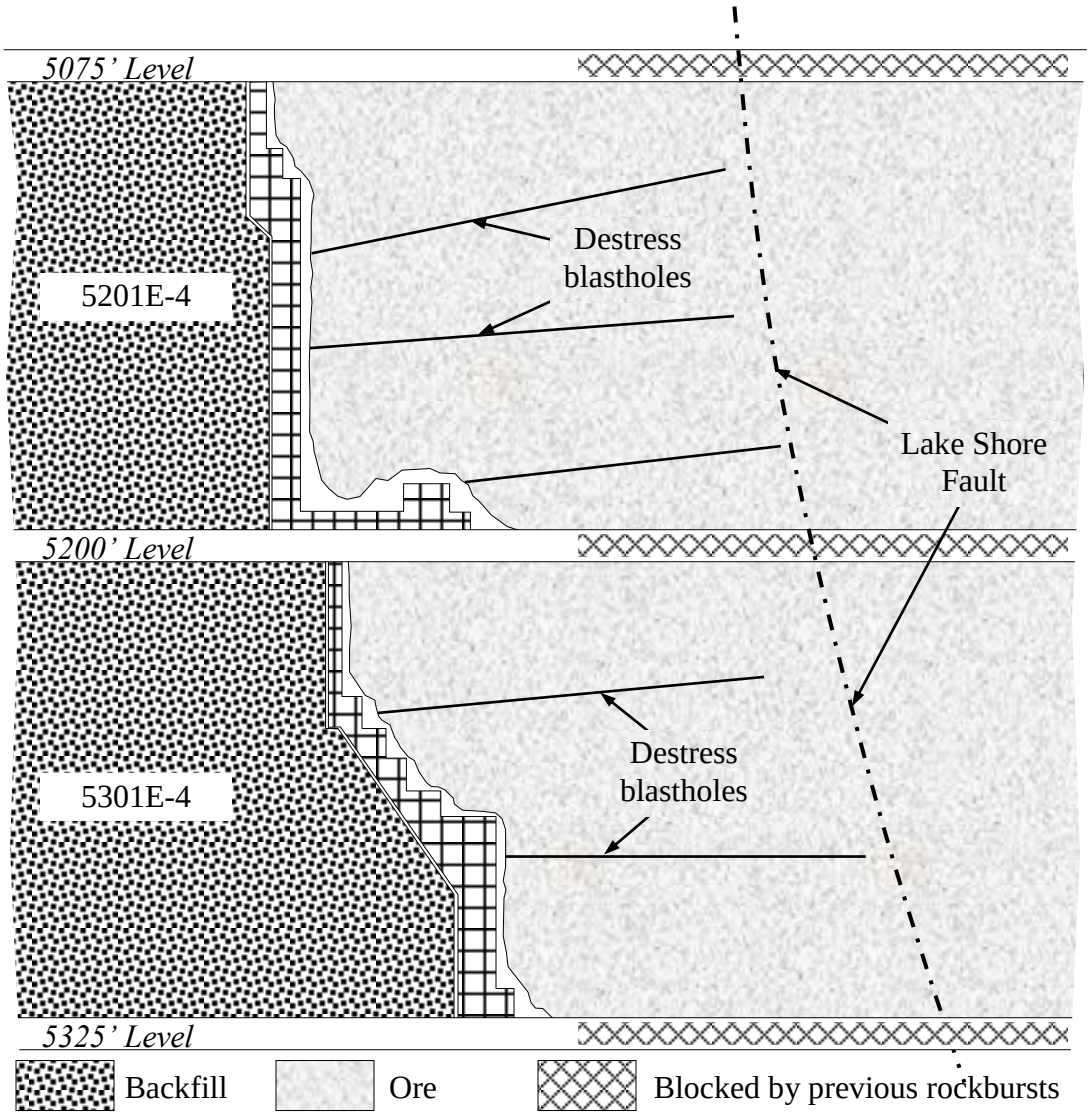

Figure 135. Longhole destressing approach implemented at the Lake Shore Mine when approaching the active Lake Shore Fault. (After Harling, 1965.)

A large-scale destress blast was implemented at Macassa Mine in an attempt to destress a burst-prone horizontal pillar, as described by Hanson *et al*. (1987). Cut-and-fill mining was used at this operation to recover narrow (2 to 6m wide) 75°-dipping gold-bearing lenses located at a depth ranging from 1,400 to 2,150 metres. Once the extraction ratio reached 60%, which corresponded to a sill pillar thickness of about 18m, bursting conditions started to develop inside the stopes and mining became hazardous. An attempt was made in 1987 to destress the 5480 Sill Pillar, located at a depth of about 1,750 metres. A region 70m long by 20m high was targeted by this destress blast, in which 630 kg of ANFO were detonated

for a powder factor of 0.15 kg of explosives per cubic metre of rock. A spacing of 3.0m was maintained between the 64 mm (2-1/2 in) blastholes, which were drilled to a depth of between 16 and 21 metres. An unloaded 2.5m-long collar was maintained in each blasthole. Figure 136 shows the general destress layout implemented in this sill pillar.

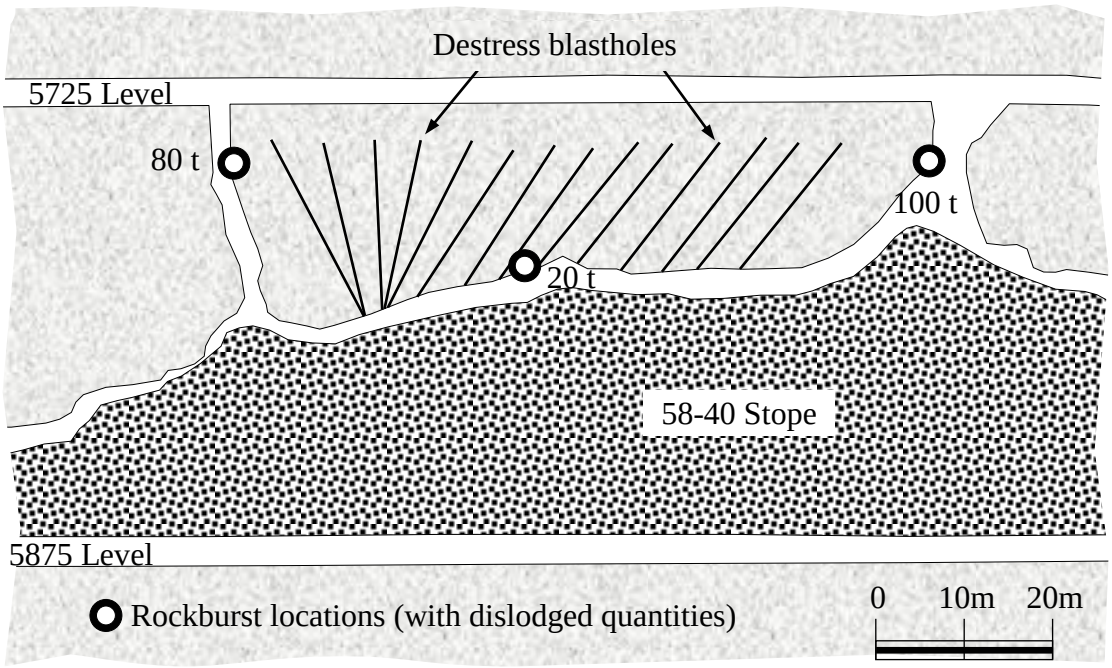

Figure 136. Longitudinal section showing the destress layout in the 58-40 Sill Pillar at Macassa Mine. (After Hanson *et al*., 1987.)

The results of this destress blast were assessed using blast-induced vibration monitoring, seismic monitoring and convergence metres installed inside the stope. Of particular interest are the convergence readings: 25 mm were recorded immediately after the blast, and an additional 8 mm was observed later, when a small rockburst occurred in the stope. Practical results were reportedly only partially successful, as, only twelve months later, a series of rockbursts violently dislodged over 1,000 tonnes of rock and caused significant damage.

Blake *et al*. (1998) mention that the Kerr Addison Mine also resorted intensively to destress blasting, although little detailed information is available on the designs implemented, other

than the fact that the blastholes were 38 to 57 mm in diameter and were drilled on a 5.5 metre spacing. These blasts were reportedly successful and resulted in a reduction of the occurrence of rockbursts.

The Abitibi mining camp of northwest Quebec has also experimented with destress blasting. In particular, the Sigma Mine located in Val d'Or did a test in 1996 in the abandoned 55°-dipping 3420 East Stope to assess the potential of the approach to reduce the occurrence of violent rock failure in highly stressed regions. Labrie *et al*. (1996) and Aubertin *et al*. (1997) have described this experiment, carried out at a depth of 1,500m in a region of good quality rock prone to violently failure. Fifteen (15) 8.5m-long 38 mm upper blastholes were drilled parallel to the ore vein in a 17m-long area, along two rows located 1.2m apart – the spacing between successive blastholes on the same row was 1.8m, with the blastholes being staggered on each row. One line of destress blastholes was drilled along the footwall contact, whereas the other was located near the centre of the drift. The destress blastholes were pneumatically loaded with ANFO, leaving 3m-long unloaded collars that were subsequently stemmed with cement plugs. All the holes were double-primed and fired simultaneously to provide the maximum instantaneous energy input possible. Figure 137 shows the approach implemented.

Seismic velocity surveys were used to assess the results of this destress blast – a decrease in this velocity was observed, which is indicative of damage having been done to the rock mass. The field stresses were also measured using the doorstopper method – these measurements indicated an astounding stress drop in the centre of the target zone, from 104 to 59 MPa, with, as intuitively expected, a significant stress increase being measured on the west side of the pillar. Despite these indications, it was reportedly not possible to relate this large stress drop to a precise change in rock mass properties. Measurements were also carried out inside N size diamond drill holes with a dilatometer before and after the blast, which indicated a reduction of about 10% of the deformation modulus. Labrie *et al*. (1996) concluded that these measurements were still insufficient to firmly decide whether or not the destress blast had reduced the local stress levels to acceptable levels. (This pillar has

not been mined, and, hence, no additional qualitative data are available to assess the degree of success achieved by this blast.)

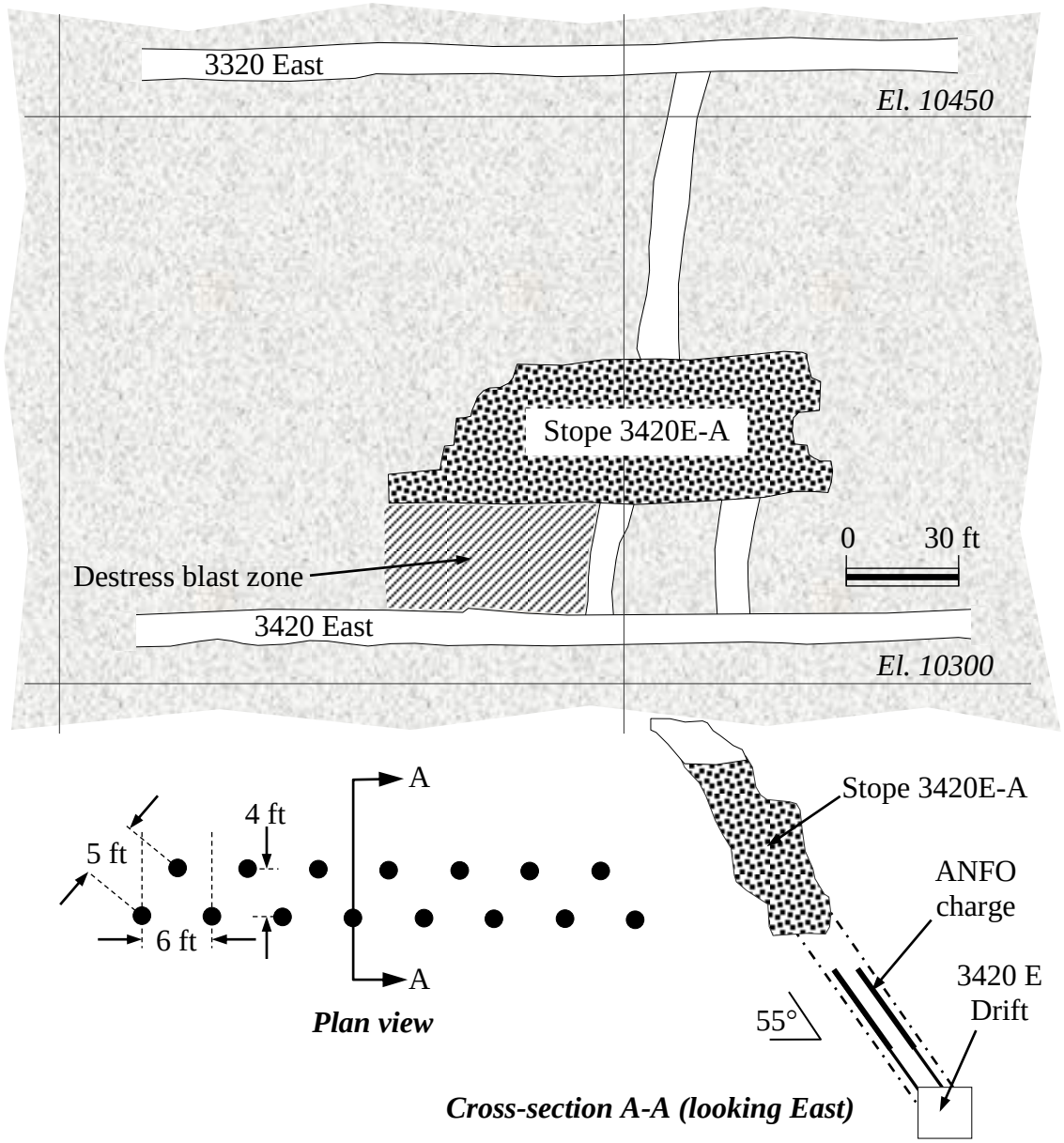

Figure 137. Longitudinal (top) and plan views, and cross-section showing the destress blast layout implemented in the 3420E Stope at Sigma Mine. (After Labrie *et al*., 1996.)

Some of the mines of the Red Lake mining district, where the extraction of relatively narrow sub-vertical gold lenses has been accompanied by significant seismic activity since the 1960's, have also experimented with destress blasting. Typically, the seismic activity was concentrated in the andesite geological unit, which is relatively strong and fragile. As

described by Scoble *et al*.(1987), destress blasting techniques have been used successfully in the middle of the 1980's at the Campbell Red Lake Mine, which involved the usage of 45 mm diameter blastholes loaded with ANFO. Figure 138 shows the reportedly most successful choked panel destress blast taken at the Campbell Red lake Mine in a sill pillar in the 1604 East Stope on the 18 Level.

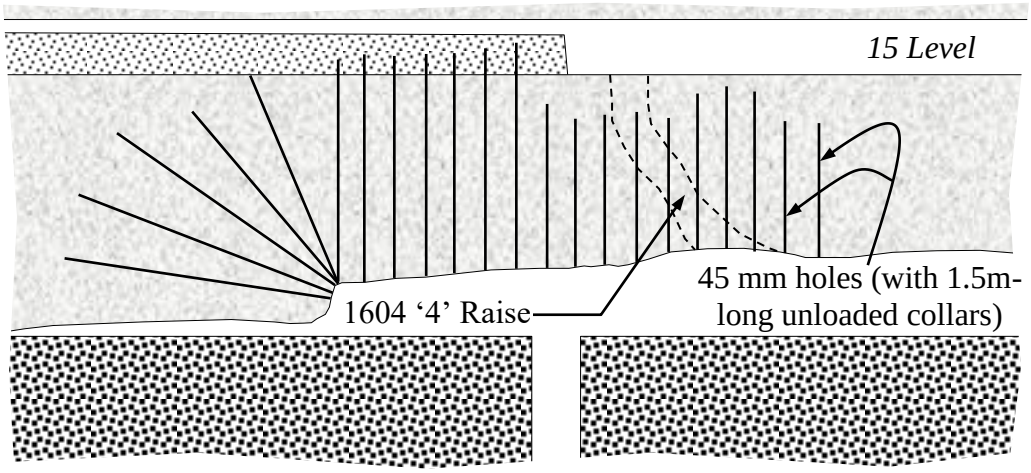

(a) Composite B-B longitudinal section.

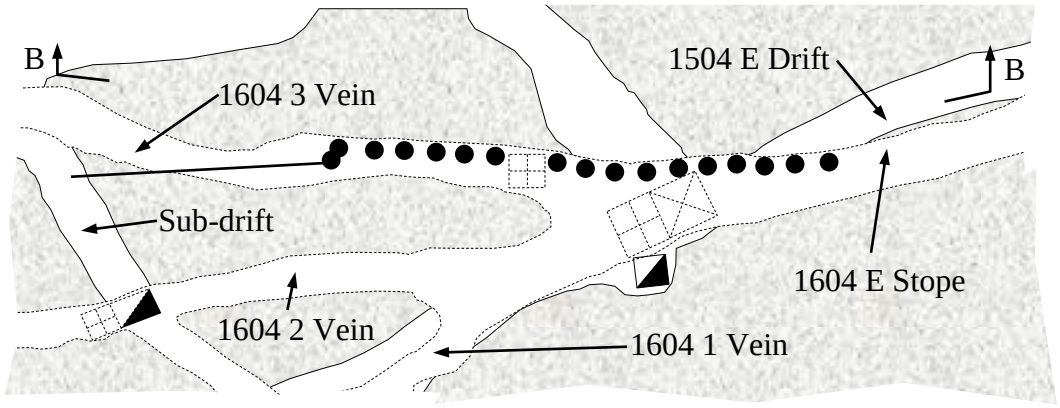

(b) Plan view.

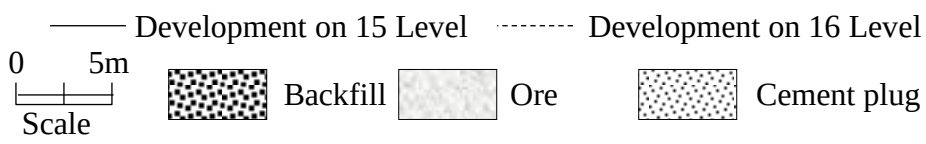

Figure 138. Destress layout implemented in the remnant of the 1604 East Stope at the Campbell Red Lake Mine. (After Blake *et al*., 1998.)

Interestingly, these tests have indicated that the zone affected by these ANFO-loaded 2.5m-long 45 mm diameter parallel blastholes was of the order of 1 metre, and that some effects were observed as far as 1.6 metre away. One important conclusion reached following these trials is that the maximum distance within which new fractures can be initiated and the elastic modulus of the rock mass can be significantly lowered does not exceed about 16 times the diameter of the blastholes used.

In October 1999 the Noranda Inc. Brunswick Mine successfully detonated a large-scale confined destress blast in a large massive sulphides pillar, as described by Andrieux *et al*. (2000) and Brummer *et al*. (2000). This particular blast constitutes the case study that is discussed in detail in Chapter IX of this thesis.

C.4. Australia

The Australian underground mining industry has historically not been renowned for particularly high stress conditions. This has however started to change in recent years, and seismicity and rockbursting have become problems at a number of underground operations, and particularly in Western Australia. One example is the Mount Charlotte Mine, located near Kalgoorlie, which exploits large gold-bearing lenses that are hosted in a massive, strong and stiff dolerite formation, with major faults nearby. These lenses are near-vertical, with a thickness of between 30 and as much as 80m, and a strike length as high as 200 to 300m. The longhole open stoping method implemented at the mine results in the creation of highly stressed rib and sill pillars, some of which are prone to violent failure.

Mikula *et al*. (1995) described a destress blast that was carried out between the 900 and 950 levels in the form of choked charges fired in a narrow slot along the hanging wall contact of a large highly-stressed rib pillar located adjacent to the un-mined I2 Stope. The zone targeted for destressing was 36m in strike length, 55m in height and 3 to 4m in width. Figure 139 shows the general location of the destress slot next to the I2 Stope, as well as the location of the nearby excavations and major geological features.

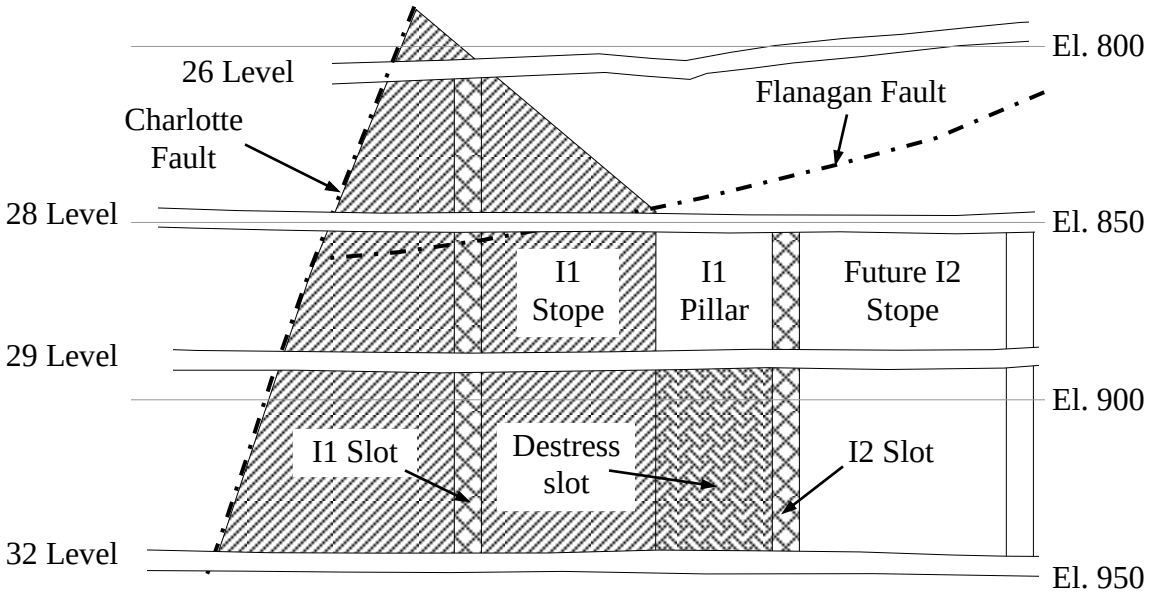

(a) Longitudinal section cut at 19800E, looking East.

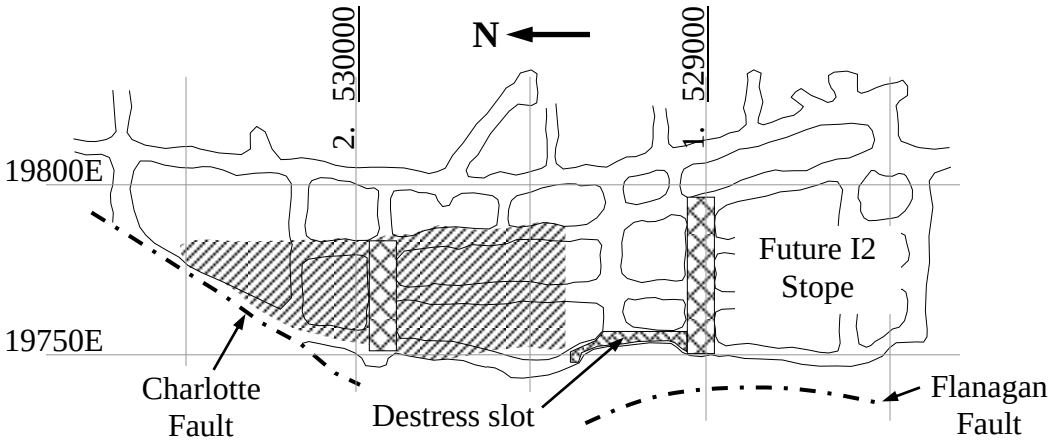

(b) Plan view cut at the 29 Level.

Figure 139. (a) Longitudinal section; and, (b) plan view showing the general location of the destress slot next to the I2 Stope at Mount Charlotte Mine. (Adapted from Mikula *et al*., 1995.)

Seventeen (17) vertical 140 mm (5-1/2 in) blastholes were drilled downwards to a depth of 53 metres from the 29 Level. (Because of the great depth in relation to the hole diameter, each blasthole was surveyed for accuracy, to ensure deviation was less than 1.0m). As shown in Figure 140a, twelve of these holes (coloured in grey in the figure) were pairs of presplit holes, drilled in between five actual destress blastholes (shown in black in the figure), and meant to enhance their effect. The destress blastholes were loaded with four

decks, each comprising 150 kg of Powergel emulsion explosives and fitted with two primers. Each deck was separated from its neighbours by a 4.5m-long column of crushed rock (a 4.5m collar stemming length was also maintained). The presplit blastholes were lightly loaded with one 40 kg deck of emulsion explosives (with only one primer) located in the centre of the blasthole. Figure 140b shows the loading details for each type of blasthole.

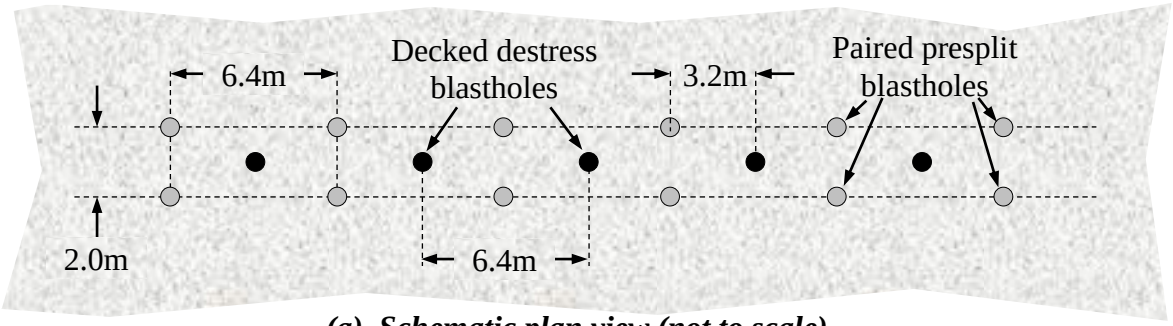

(a) Schematic plan view (not to scale).

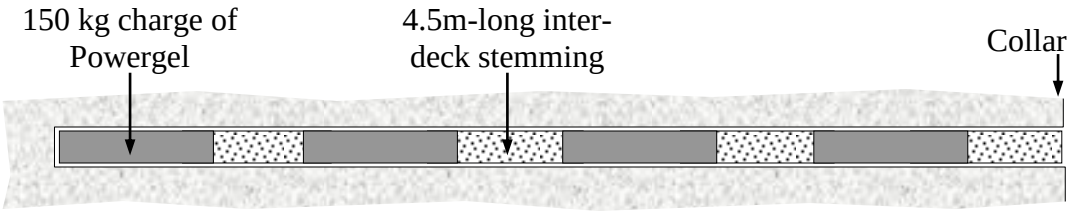

(b) Schematic loading of a destress blasthole (not to scale).

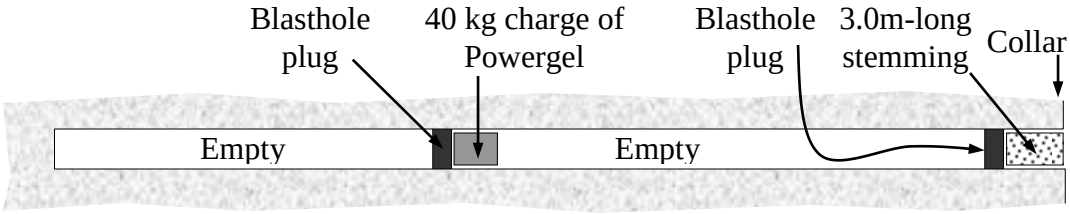

(c) Schematic loading of a presplit blasthole (not to scale).

Figure 140. Schematic views (not to scale) showing (a) the general arrangement of the destress and presplit blastholes; and, (b & c) their loading parameters. (After Mikula *et al*., 1995.)

The destress blast was instrumented with a CSIRO stress cell and a vibrating wire gauge (both located about one-third of the way down the destress slot, and near it), extensometers located across large-scale geological features, and closure stations located on the 29 Level.

The vibrations induced by the blast were also monitored, both underground and on surface. Data from the mine 32 channel full waveform microseismic system were also used to assess the response of the rock mass to the destress blast.

Stress changes following the blast were measured at +9 MPa and +21MPa in the east-west direction (perpendicular to the destress slot), and at +2 MPa and –4 MPa in the north-south direction (parallel to the destress slot). One would have intuitively expected a stress drop in the east-west direction, and, overall, more negative differential readings. The extensometers detected up to 21 mm of displacement along the instrumented geological structures, whereas the closure stations measured a 7 mm closure across the destress slot – these readings are consistent with a successful destressing effect. The destress blast was qualitatively described by the authors as successful.

C.5. Sweden

Some of the underground mines exploited in Sweden by Boliden AB are also subjected to seismic activity, which can, on occasions, lead to unstable ground conditions. Within the Swedish context, the problem is not so much the risk of major devastating rockbursts occurring, but rather the stability of the excavation surfaces, at the relatively small scale. Under the mining-induced stress levels encountered in many Boliden mines spalling can occur at the lead corners of stopes advancing in the relatively high sub-horizontal stress field that generally prevails. (Even though the depth of most Boliden underground mines is relatively shallow [averaging 400 metres], the in situ horizontal stress components are often comparable to those encountered in Canadian mines at depths of around 1,000 metres [Borg, 1983].) This spalling effect has the potential to progress vertically along the ore-waste contacts, and particularly on the footwall side where the stress concentration tends to be more intense due to the geometry of the stopes (Krauland *et al.*, 2001). As a result, the destress blasts implemented are generally small and carried out in the corner between the back and the footwall of the excavations. The objective sought after is to create a fracture zone in order to shed the ground stresses a bit further inside the rock mass.

Figure 141 shows the effect on the stress levels ahead of a cut-and-fill stope subjected to a high sub-horizontal stress field of a 2.5, 5 and 10% reduction in the elastic modulus of a destressed zone located on the footwall side of this stope, as computed by an elastic numerical model. As can be seen in the figure, as the destressed zone becomes softer a significant reduction in the stress levels is achieved in the immediate location of the blastholes.

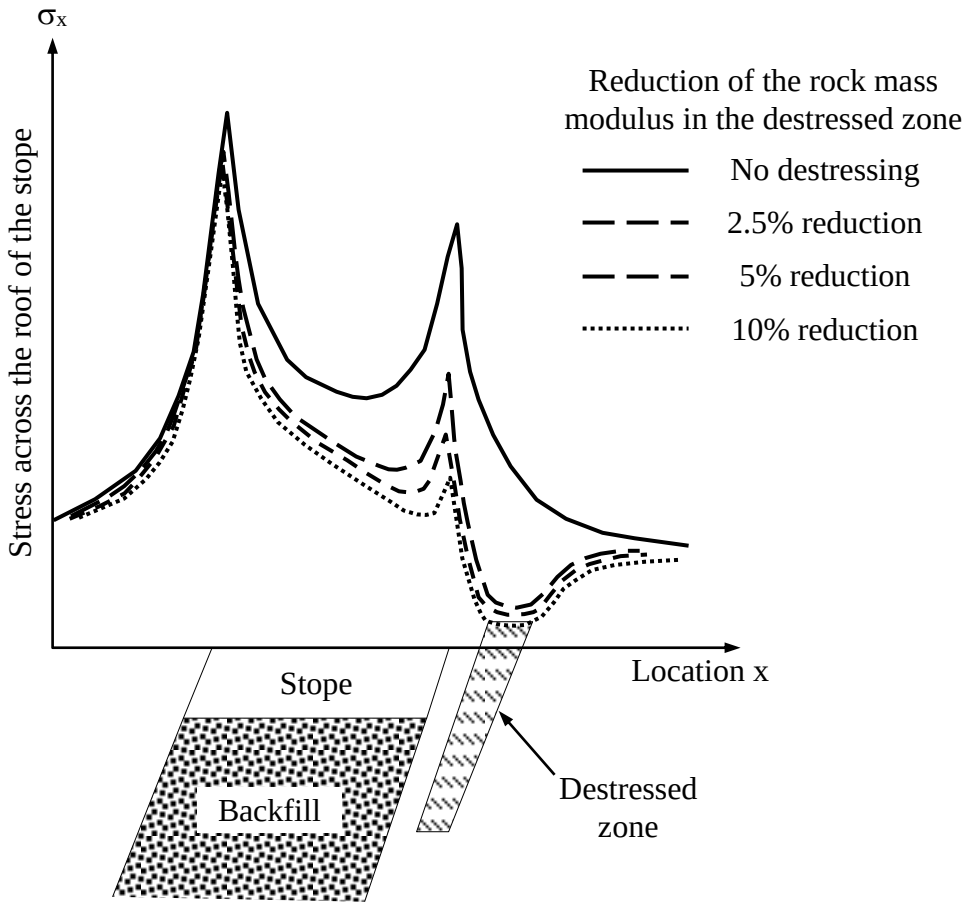

Figure 141. Schematic illustration (not to scale) showing the modelled effect of a 2.5, 5 and 10% reduction in the elastic modulus of a destressed zone located on the footwall side of a cut-and-fill stope in a high sub-horizontal stress field. (After Blake *et al*., 1998).

Numerous Boliden underground mines use small-scale destress blasts for local stress relaxation in excavations. The technique used generally consists of drilling two or three blastholes 2 to 3 metres in depth of which only the bottom 0.5 to 1.0 metre is loaded with 1.0 to 1.5 kg of explosives – the procedure is typically repeated with each new development or breast round. In most cases, the destress blastholes are detonated

simultaneously with the round itself, but destressing is also sometimes carried out before the advance round is taken. Boliden engineers have reported good success with this approach, even stating that proper destress blasting can be more effective, faster and cheaper in addressing difficult high stress conditions than increasing the rock bolting density or shotcrete thickness.

Blake *et al*. (1998) reported that three principles are implemented in the planning of destress blasts at the Boliden operations, which can be summarised as follows:

1. the explosive charges must crush as much as possible the rock surrounding the destress blastholes, which is best achieved using a high velocity of detonation explosive (due to the accompanying high detonation pressure);
2. the destress blast must be fired in highly-stressed rock that is approaching its ultimate strength – the targeted rock must also be brittle in order for the destress blast to fail a volume of material as large as possible; and,
3. the magnitude and orientation of the adverse stress component must be known so that the destress blast can be laid out (located and oriented) appropriately in relation to critically-loaded rock.

Even though the objective at Boliden is not the large-scale destressing of mining panels, the principles used are quite consistent with those involved with this type of destressing. Because the scale at which destressing is typically done in Sweden is much smaller than would be pertinent to this thesis, additional case histories will not be discussed here.

C.6. Germany

Deep underground coal mines, including in France (in the Alsace-Lorraine region), Germany (in the Ruhr coal fields) and Poland, are prone to rockbursts – the French mines are also subjected to gas outbursts. Water injection and destress blasting are routinely carried out in these countries to control rockbursting (Bräuner, 1994; Blake *et al*., 1998) – the blasting approach has the added advantage of creating fracture patterns, which also

allow highly flammable organic gases to escape from the coal mass. Due to similarities in their configuration, it is now generally inferred that deep flat tabular coal mines and South African gold mines are probably affected by the same major rockburst mechanisms. These mechanisms, discussed previously, are: 1) fault-slipping, whereby sudden and violent slip occurs along a persistent large-scale sub-planar geological structure; 2) pillar bursting, whereby the rock mass is crushed under high levels of both driving stress and confinement; and, 3) face bursting. Pillar bursting and face bursting in deep highly-stressed narrow shallow-dipping tabular coal seams typically occur in the form of the foundation beneath a pillar failing suddenly, and in the form of the rock on or near the mining face suddenly crushing and ejecting material into the stope, respectively. The former mechanism usually occurs when a hard geological layer is located in the immediate vicinity of the coal seam roof or floor.

The most often encountered rockburst mechanism in the western underground coal fields of Germany is strain bursting, usually in the form of a sudden and violent crushing of the coal seam itself, ahead of the mining face. These events can be quite powerful, and typically result in a sudden expulsion of coal from the face, a strong air displacement and a seismic event. The largest rockburst-related seismic event recorded to date in the Ruhr coal fields had a Richter Magnitude of as much as 3.4.

Some German underground coal mining operations have adopted a strategy to address the rockburst hazard. The first step consists in determining whether or not a given coal seam will be burst-prone during its extraction. For this end, a standard laboratory test has been developed by Bräuner (1983), whereby a 11 mm-diameter borehole is drilled inside a 320 cm^3 sample of the coal subjected to a 156 MPa initial stress inside a stiff testing machine, as shown in Figure 142. The load inside the sample is monitored during and immediately after the drilling of the 11 mm test hole – if the vertical stress gradually decreases, the coal is categorised as non burst-prone. On the other hand, if the vertical load drops by sudden and large successive increments, the seam is categorised as burst-prone. Figure 143 shows the typical behaviour associated with each of the three types of coal – Type I is burst-prone, whereas types II and III are not.

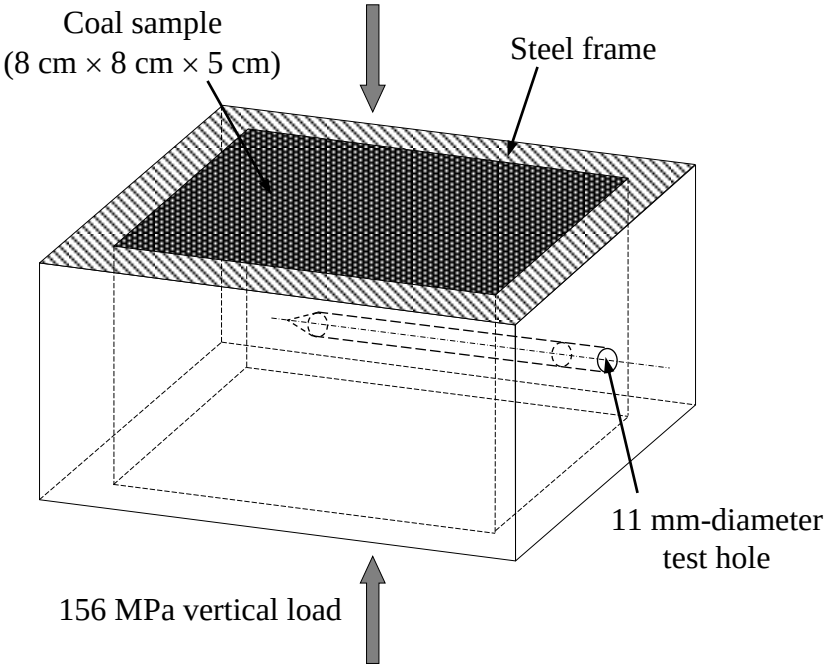

Figure 142. Standardised coal sample test for the assessment of burst-proneness in the German Ruhr coal fields. (After Bräuner, 1994.)

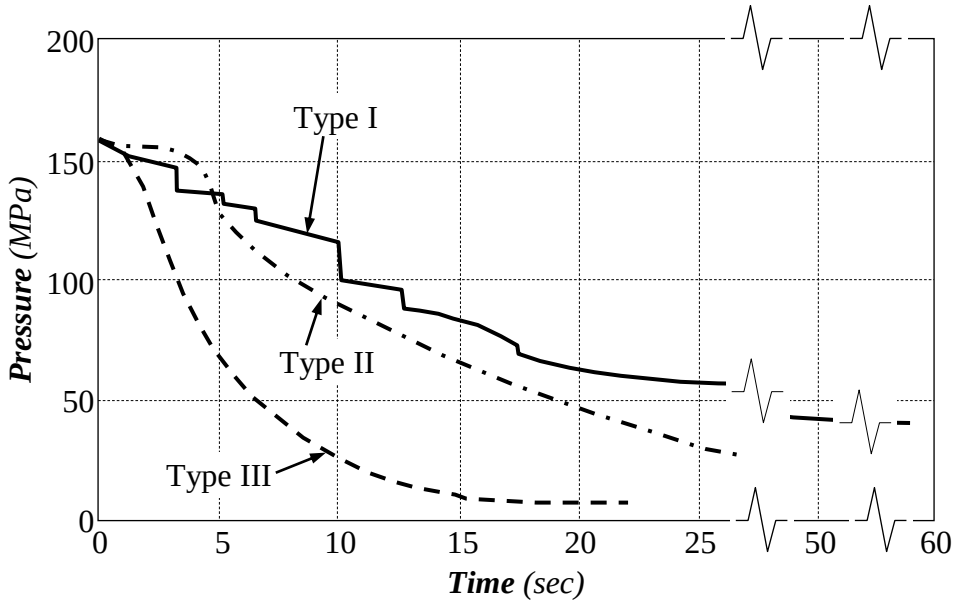

Figure 143. Typical results of the standardised coal sample test showing burst-prone (Type I) and non-burst prone (types II and III) seams. (After Bräuner, 1994.)

Test drilling is routinely carried out ahead of the mining front inside burst-prone seams by specially trained miners. In this procedure 50 mm-diameter test holes are drilled with small hand-held drills, as shown in Figure 144.

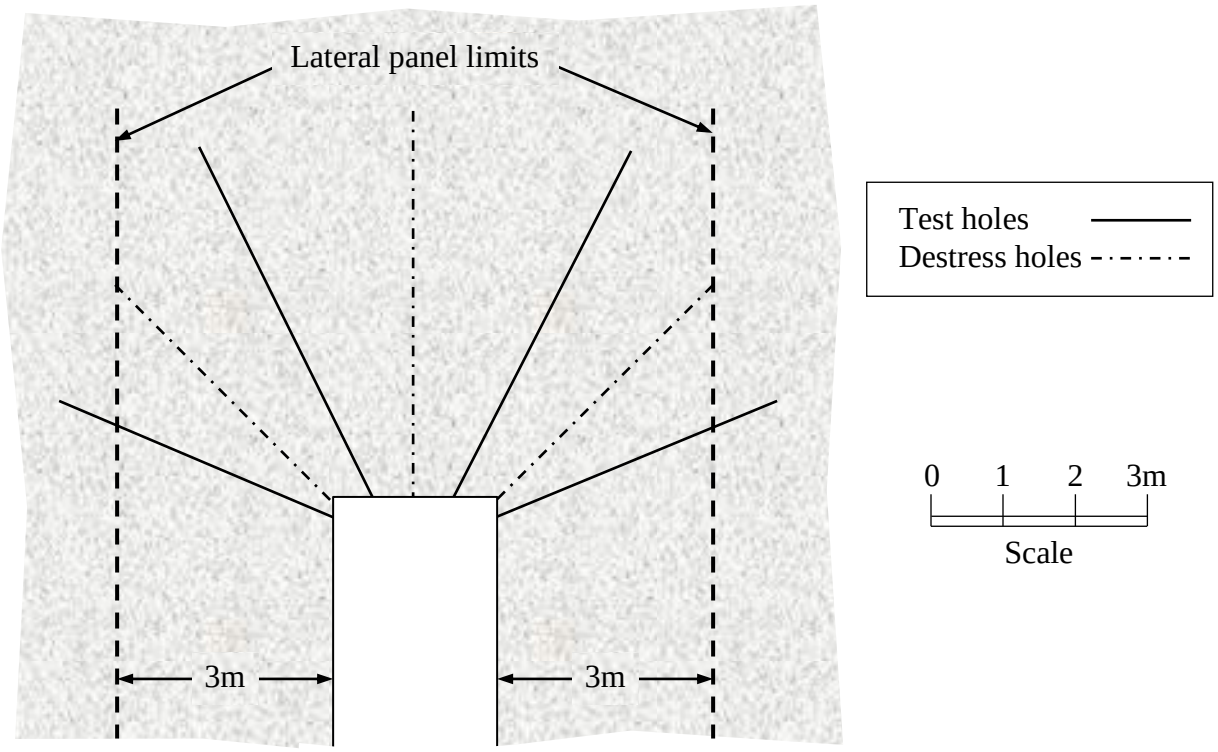

Figure 144. Schematic plan view showing the typical test and destress hole layout ahead of a German burst-prone underground coal mine panel. (Adapted from Will, 1982.)

The amount of cuttings generated by the drilling of the test holes is measured and compared to the theoretical volume expected based upon the size of the holes. Excess cuttings are indicative of the coal fracturing into the test hole as it is drilled, which, in turn, is indicative of a stress regime nearing the strength of the seam. Microseismic activity is typically associated with such caving holes, which indicates violent failure as well. As shown in Figure 145 for a typical test hole inside a burst-prone seam, the location of the stress peak ahead of the face generally coincides with the area that produces the largest volume of cuttings. (In this case, the stress cell that measured the pressure inside the 2.5m-thick seam had been installed 4.7m deep inside a dedicated hole parallel to the test hole and located 1m away from it.)

Once the location of the peak stress front has been determined ahead of the face in a burst-prone seam, the overall strategy consists in keeping this stress peak a certain distance ahead of the face, which is generally three times the seam thickness, plus a constant amount.

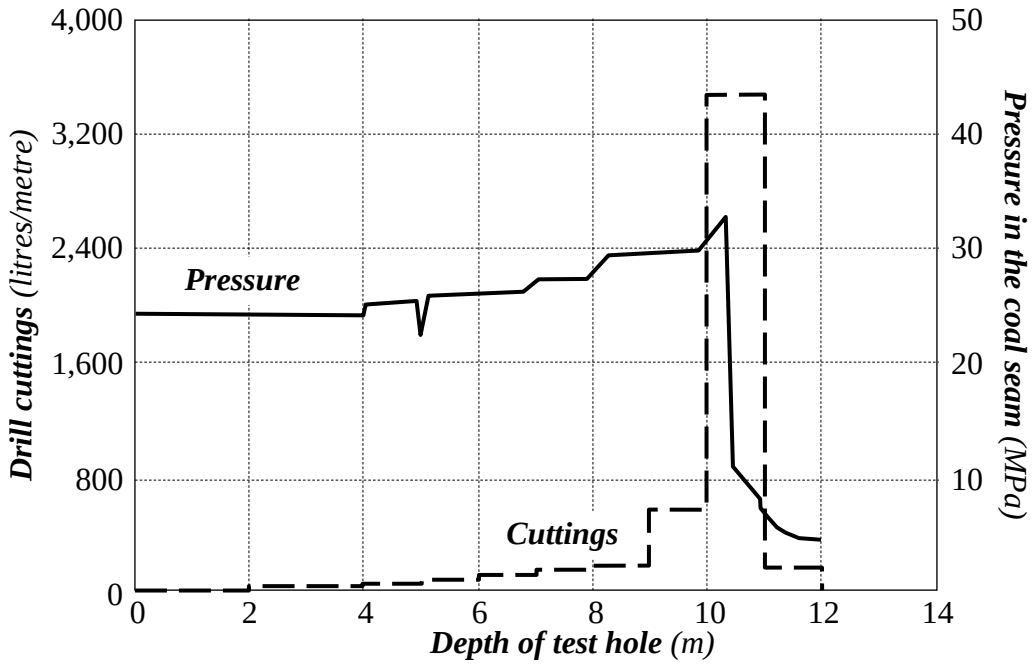

Figure 145. Results of a typical test hole ahead of the coal face – the volume of cuttings is highest near the peak stress region. (After Bräuner, 1994.)

In the case where the stress peak is found to be closer to the face than the safe distance, mining is then halted until preconditioning is carried out. This is usually done by drilling 100 mm-diameter holes into the seam, as shown in Figure 144, without blasting them. Additional holes are drilled until no excess cuttings are produced within the required safe distance from the face, at which point mining can resume. Will (1982) reported that some coal mines carry out preconditioning by detonating strongly-confined explosive charges inside the test holes. In this case, the success of the blast in moving the high stress front further away inside from the face is assessed with new test holes.

C.7. Poland

The occurrence of rockbursting in Polish underground coal mines is quite common. Thirty-eight (38) of the sixty-nine (69) underground coal mines in operation in Poland in 1986 were classified as burst-prone (Blake *et al*., 1998) – these burst-prone coal mines produced 93 million tonnes in 1984, which represented about 54% of the total output. Because rockbursts are relatively common in Polish coal mines, research into the phenomenon has

been carried out for some time. This work has suggested that rockbursts generally occur if the following three factors are present: 1) a coal seam that tends to accumulate elastic energy and release it violently; 2) high stress conditions; and, 3) thick, stiff, strong and brittle encasing strata (Blake *et al*., 1998).

The Polish approach to dealing with burst-prone coal seams is quite similar to the one implemented in Germany in similar situations, whereby test holes are drilled ahead of the face with hand-held drills and volumes of cuttings are measured. Forty-two (42) millimetre holes are however typically used, instead of the larger 50 mm holes generally used in Germany. As what is commonly observed in Germany, microseismic activity is typically triggered by the drilling of the test holes. The rockburst hazard is assessed based upon the proximity between the peak stress zone and the mining face, with the risk rating increasing with smaller distances. A proximity of less than 1.5 times the coal seam thickness results in a 'very burst-prone' rating, whereas the rating is lowered to 'burst-prone' in situations where this proximity is between 1.5 and 3.4 times the seam thickness. As much as possible bursting hazards are mitigated by modifying the mining sequence in order to alleviate stress concentrations near active mining areas and stress-shadow problematic seams by mining neighbouring panels (Zipf & Heasley, 1990). Mining scenarios whereby stresses are pinched inside shrinking pillars are also avoided as much as possible.

Active destressing is however also done when other approaches cannot be implemented or are not giving the expected results. Drilling relief holes into the seam is one option. It is however not as commonly done as in Germany because of the inherent risk to the driller at the face – the amount of dust produced during the process is also reportedly an issue.

Detonating explosive destressing charges in the burst-prone seam is more commonly done, and accounts for nearly 60% of all the active destressing work implemented in Polish underground coal mines. The destress blastholes are usually between 6 and 12m deep, loaded with significant charges – hundreds of kilograms of explosives are sometimes used to fracture the seam. Care is however taken to not completely destroy the seam during the process.

Saturating the targeted seam with fluids accounts for about 30% of all the active destressing work. Water is generally used for that purpose, pumped into the seam under pressures of up to about 15 MPa. Hybrid methods are used in the remaining 10% of the case, which target the encasing strata rather than the seam itself. These techniques generally combine choked longhole blasting on the floor side and hydraulic fracturing on the roof side.

APPENDIX D

D. THE ROCK QUALITY DESIGNATION INDEX (RQD)

Note: this appendix is the near-integral excerpt of pages 29 and 30 of the book "Support of Underground Excavations in Hard Rock" by Hoek et al. *(1995). Reproduced with the permission of A. A. Balkema.*

The RQD (Rock Quality Designation) index was originally developed by Deere (Deere *et al*., 1967) in order to provide a simple quantitative assessment of the rock mass quality from drill core. The RQD is defined as the percentage of intact core pieces longer than 100 mm (4 inches) in the total length of core. Because smaller core is more fragile and more likely to be artificially broken upon recovery, the smallest core size on which RQD should be logged is NX (54.7 mm, or 2.15 inches). The core should also be drilled with a double tube core barrel, for the same reason. Figure 146 shows the procedure suggested by Deere & Deere (1988) for the measurement and determination of the RQD index from a run of core.

Artificial fractures (caused by the drilling process itself, or the handling of the core) must be ignored when logging fractures in the core for the purpose of determining RQD. The RQD value obtained is very dependent upon the orientation of the borehole – fracture sets

that are parallel to the axis of the borehole cannot be reliably identified and taken into account.

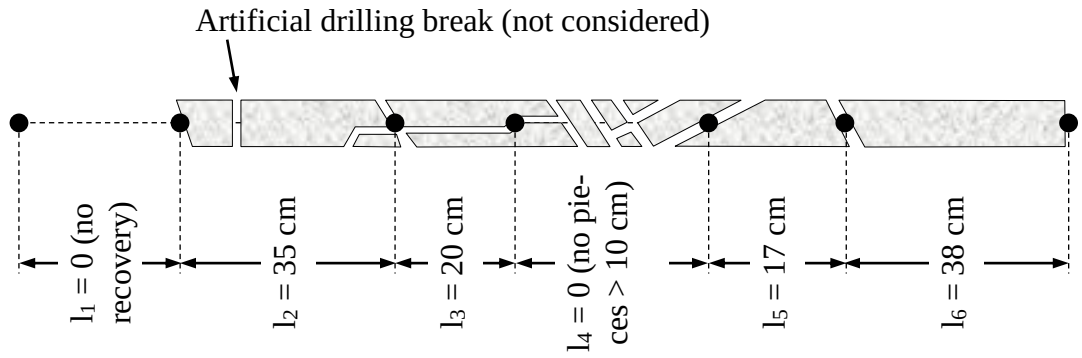

Total length of core run = 200 cm

RQD = ([Σ Length of core pieces > 10 cm in length] / [Total length of core run]) × 100%

In this example, RQD = ([35 + 20 +17 +38] / [200]) × 100% = 55%

Figure 146. Schematic view (not to scale) illustrating the procedure for the determination of the RQD index. (Adapted from Deere & Deere, 1988.)

RQD can also be derived in the absence of core, if discontinuities are visible in surface exposures or exploration drifts. Palmström (1982) suggested the following relationship for clay-free rock:

$$RQD = 115 - 3.3\ Jv \qquad \text{..... Eq. (64)}$$

With Jv the volumetric joint count, defined as the sum of the number of joints per unit length, for all joint sets. Blast-induced and other artificial breaks must be ignored when assessing Jv. The use of Jv can help reduce the directional dependence associated with logging RQD from core.

APPENDIX E

E. THE ROCK MASS RATING SYSTEM (RMR)

Note: this appendix is the near-integral excerpt of pages 33 through to 35 of the book "Support of Underground Excavations in Hard Rock" by Hoek et al. *(1995). Reproduced with the permission of A. A. Balkema.*

Bieniawski (1976) published the details of a rock mass classification method called the Geomechanics Classification or the Rock Mass Rating (RMR) system. Over the years, this system has been successively refined as more case records have been examined and the reader should be aware that Bieniawski has made significant changes in the ratings assigned to different parameters. The discussion that follows is based upon the 1989 version of the classification (Bieniawski, 1989).

The following six parameters are used to classify a rock mass using the RMR system: 1) the uniaxial compressive strength of the rock material; 2) the Rock Quality Designation [RQD]; 3) the spacing of the discontinuities; 4) the condition of the discontinuities; 5) the groundwater conditions; and, 6) the orientation of the discontinuities.

In applying this classification system, the rock mass is divided into a number of structural regions and each region is classified separately. The boundaries of the structural regions

usually coincide with a major structural feature such as a fault or with a change in rock type. In some cases, significant changes in discontinuity spacing or characteristics, within the same rock type, may necessitate the division of the rock mass into a number of small structural regions.

The Rock Mass Rating system is presented in Table 64, giving the ratings for each of the six parameters previously listed. These ratings are summed to give a value of RMR.

Table 64. The Rock Mass Rating system. (After Bieniawski, 1989.)

A. CLASSIFICATION PARAMETERS AND THEIR RATINGS									
Parameter			Range of values						
1	Strength of the intact rock material (MPa)	Point-load strength index	> 10	4 to 10	2 to 4	1 to 2	Uniaxial compressive testing is preferred for this low strength range		
		Uniaxial compressi-ve strength	> 250	100 to 250	50 to 100	25 to 50	5 to 25	1 to 5	< 1
	Rating		15	12	7	4	2	1	0
2	Drill core quality RQD		90 to 100%	75 to 90%	50 to 75%	25 to 50%	Less than 25%		
	Rating		20	17	13	8	3		
3	Spacing of discontinuities		> 2.0 m	0.6 to 2.0 m	200 to 600 mm	60 to 200 mm	< 60 mm		
	Rating		20	15	10	8	5		
4	Condition of discontinuities (See E)		Very rough surfaces Not continuous No separation Unweathered walls	Slightly rough surfaces Separation <1mm Slightly weathered walls	Slightly rough surfaces Separation <1mm Highly weathered walls	Slickensided surfaces Or Gouge < 5 mm thick Or Separation 1-5mm Continuous	Soft gouge > 5 mm thick Or Separation > 5 mm Continuous		
	Rating		30	25	20	10	0		
5	Ground water	Inflow per 10 m tunnel length (l/m)	None	< 10	10 to 25	25 to 125	> 125		
		(Joint water pressure) / (Major principal σ)	0	< 0.1	0.1 to 0.2	0.2 to 0.5	> 0.5		
		General conditions	Completely dry	Damp	Wet	Dripping	Flowing		
	Rating		15	10	7	4	0		
B. RATING ADJUSTMENT FOR DISCONTINUITY ORIENTATION (See F)									
Strike and dip orientations			Very favourable	Favourable	Fair	Unfavourable	Very unfavourable		
Ratings	Tunnels and mines		0	–2	–5	–10	–12		
	Foundations		0	–2	–7	–15	–25		
	Slopes		0	–5	–25	–50	–––		
C. ROCK MASS CLASSES DETERMINED FROM THE TOTAL RATINGS									
Rating			100 to 81	61 to 80	41 to 60	21 to 40	< 21		
Class number			I	II	III	IV	V		
Description			Very good rock	Good rock	Fair Rock	Poor rock	Very poor rock		
D. MEANING OF ROCK CLASSES									
Class number			I	II	III	IV	V		
Average stand-up time			20 years for 15 metre span	1 year for 10 metre span	1 week for 5 metre span	10 hours for 2.5 metre span	30 minutes for 1 metre span		
Cohesion of rock mass (kPa)			> 400	300 to 400	200 to 300	100 to 200	< 100		
Friction angle of rock mass			> 45°	35 to 45°	25 to 35°	15 to 25°	< 15°		

Table 64 (continued). The Rock Mass Rating system. (After Bieniawski, 1989.)

E. GUIDELINES FOR CLASSIFICATION OF DISCONTINUITY CONDITIONS *					
Discontinuity length (persistence) Rating	< 1 m 6	1 to 3 m 4	3 to 10 m 2	10 to 20 m 1	> 20 m 0
Separation (aperture) Rating	None 6	< 0.1 mm 5	0.1 to 1.0 mm 4	1.0 to 5.0 mm 1	> 5.0 mm 0
Roughness Rating	Very rough 6	Rough 5	Slightly rough 3	Smooth 1	Slickensided 0
Infilling (gouge) Rating	None 6	Hard filling <5 mm 4	Hard filling >5 mm 2	Soft filling < 5 mm 2	Soft filling > 5 mm 0
Weathering Rating	Unweathered 6	Slightly weathered 5	Moder. weathered 3	Highly weathered 1	Decomposed 0

F. EFFECT OF DISCONTINUITY STRIKE AND DIP ORIENTATION IN TUNNELLING **			
Strike perpendicular to tunnel axis		Strike parallel to tunnel axis	
Drive with dip – Dip 45 to 90°	Drive with dip – Dip 20 to 45°	Dip 45 to 90°	Dip 20 to 45°
Very favourable	Favourable	Very favourable	Fair
Drive against dip – Dip 45 - 90°	Drive against dip – Dip 20 - 45°	Dip 0 to 20° – Irrespective of strike angle	
Fair	Unfavourable	Fair	

* Some conditions are mutually exclusive. For example, if in-filling is present, the roughness of the surface will be overshadowed by the influence of the gouge. In such cases use A.4 directly.

** Modified after Wickham *et al.*, 1972.

The following example illustrates the use of these tables to arrive at an RMR value. A tunnel is to be driven through a slightly weathered granite with a dominant joint set dipping at 60° against the direction of the drive. Index testing and logging of diamond drilled core give typical point-load strength index values of 8 MPa and average RQD values of 70%. The slightly rough and slightly weathered joints with a separation of less than 1 mm, are spaced at 300 mm. Tunnelling conditions are anticipated to be wet. The RMR value is determined as shown in Table 65.

Table 65. RQD determination example.

Table	Item	Value	Rating
Table 64 – A.1	Point load index	8 MPa	12
Table 64 – A.2	RQD	70%	13
Table 64 – A.3	Spacing of discontinuities	300 mm	10
Table 64 – E.4	Condition of discontinuities	Note 1	22
Table 64 – A.5	Groundwater	Wet	7
Table 64 – B	Adjustment for joint orientation	Note 2	–5
		Total	59

Note 1. For slightly rough and altered discontinuity surfaces with a separation of less than 1 mm, Table 64.A.4 gives a rating of 25. When more detailed information is available, Table 64.E can be used to obtain a more refined rating. Hence, in this

case, the rating is the sum of: 4 (1 to 3 m discontinuity length), 4 (separation of 0.1 to 1.0 mm), 3 (slightly rough), 6 (no in-filling) and 5 (slightly weathered), for a total of 22.

Note 2. Table 64.F gives a description of ‘Fair’ for the conditions assumed where the tunnel is to be driven against the dip of a set of joints dipping at 60°. Using this description for ‘Tunnels and Mines’ in Table 64.B gives an adjustment rating of –5.

APPENDIX F

F. THE GEOLOGICAL STRENGTH INDEX (GSI)

Note: this appendix consists of selected near-integral excerpts between pages 161 and 175 of the manual "Rock Engineering Course Notes" by Hoek (1998). Reproduced with the permission of the University of Toronto.

Reliable estimates of the strength and deformation characteristics of rock masses are required for almost any form of analysis used for the design of slopes, foundations and underground excavations. Hoek & Brown (1980) proposed a method for obtaining estimates of the strength of jointed rock masses, based upon an assessment of the interlocking of rock blocks and the condition of the surfaces between these blocks. This method was modified over the years in order to meet the needs of users who were applying it to problems that were not considered when the original criterion was developed (Hoek, 1983; Hoek & Brown, 1988). The application of the method to very poor quality rock masses required further changes (Hoek *et al*., 1992) and, eventually, the development of a new classification called the Geological Strength Index, or GSI (Hoek, 1994; Hoek *et al*., 1995; Hoek & Brown, 1997).

The strength of a jointed rock mass depends upon the properties of the intact rock pieces and also upon the freedom of these pieces to slide and rotate under different stress

conditions. This freedom is controlled by the geometrical shape of the intact rock pieces, as well as the condition of the surfaces separating the pieces. Angular rock pieces with clean, rough discontinuity surfaces will result in a much stronger rock mass than one which contains rounded particles surrounded by weathered and altered material. The GSI provides a system for estimating the reduction in rock mass strength for different geological conditions. This system is presented in Table 66 and Table 67. Experience has shown that Table 66 is sufficient for field observations since the letter code that identifies each rock mass category can be entered into a field log. Later, these codes can be used to estimate the GSI value from Table 67.

In earlier versions of Table 66 the terms BLOCKY/SEAMY and CRUSHED were used, following the terminology used by Terzaghi (1946). However, these terms proved to be misleading and they have been replaced, in this table, by BLOCKY/DISTURBED, which more accurately reflects the increased mobility of a rock mass that has undergone some folding and/or faulting, and DISINTEGRATED, which encompasses a wider range of particle shapes.

The Generalised Hoek-Brown failure criterion for jointed rock masses is defined by:

$$\sigma'_1 = \sigma'_3 + \sigma_{ci} \times ([\{ m_b \times \sigma'_3 \} / \sigma_{ci}] + s)^a \qquad \text{..... Eq. (65)}$$

With: σ'_1 and σ'_3 the maximum and minimum effective stresses at failure, respectively; σ_{ci} the uniaxial compressive strength of the intact rock pieces; m_b the value of the Hoek-Brown constant m (associated with the degree of block interlocking in the rock mass) at the rock mass scale; s the Hoek-Brown constant associated with the degree of fracturing of the rock mass; and, *a* an exponent that depends upon the rock mass characteristics.

Once the Geological Strength Index GSI has been estimated, the parameters that describe the rock mass strength characteristics are calculated as follows:

$$m_b = m_i \times e^{([GSI - 100] / 28)} \qquad \text{..... Eq. (66)}$$

With: m_b as defined in Equation (65); m_i the value of the Hoek-Brown constant m at the laboratory rock sample scale; and, GSI the Geological Strength Index.

Table 66. Characterisation of rock masses on the basis of interlocking and joint alteration. (After Hoek *et al*., 1995.)

ROCK MASS CHARACTERISTICS FOR STRENGTH ESTIMATES Based upon the appearance of the rock, choose the category that you think gives the best description of the 'average' undisturbed in situ conditions. Note that exposed rock faces that have been created by blasting may give a misleading impression of the quality of the underlying rock. Some adjustment for blast damage may be necessary and examination of diamond drill core or of faces created by pre-split or smooth blasting may be helpful in making these adjustments. It is also important to recognize that the Hoek-Brown criterion should only be applied to rock masses where the size of individual blocks is small compared with the size of the excavation under consideration. STRUCTURE		SURFACE CONDITIONS DECREASING SURFACE QUALITY ⇨	VERY GOOD Very rough, fresh unweathered surfaces	GOOD Rough, slightly weathered, iron stained surfaces	FAIR Smooth, moderately weathered or altered surfaces	POOR Slickensided, highly weathered surfaces with compact coatings or fillings of angular fragments	VERY POOR Slickensided, highly weathered surfaces with soft clay coatings or fillings
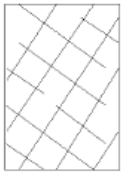	BLOCKY - very well interlocked undisturbed rock mass consisting of cubical blocks formed by three orthogonal discontinuity sets	DECREASING INTERLOCKING OF ROCK PIECES ⇩	**B/VG**	**B/G**	**B/F**	**B/P**	**B/VP**
	VERY BLOCKY - interlocked, partially disturbed rock mass with multifaceted angular blocks formed by four or more discontinuity sets		**VB/VG**	**VB/G**	**VB/F**	**VB/P**	**VB/VP**
	BLOCKY/DISTURBED- folded and/or faulted with angular blocks formed by many intersecting discontinuity sets		**BD/VG**	**BD/G**	**BD/F**	**BD/P**	**BD/VP**
	DISINTEGRATED - poorly interlocked, heavily broken rock mass with a mixture or angular and rounded rock pieces		**D/VG**	**D/G**	**D/F**	**D/P**	**D/VP**

Table 67. Estimate of Geological Strength Index GSI based upon geological descriptions. (After Hoek *et al*., 1995.)

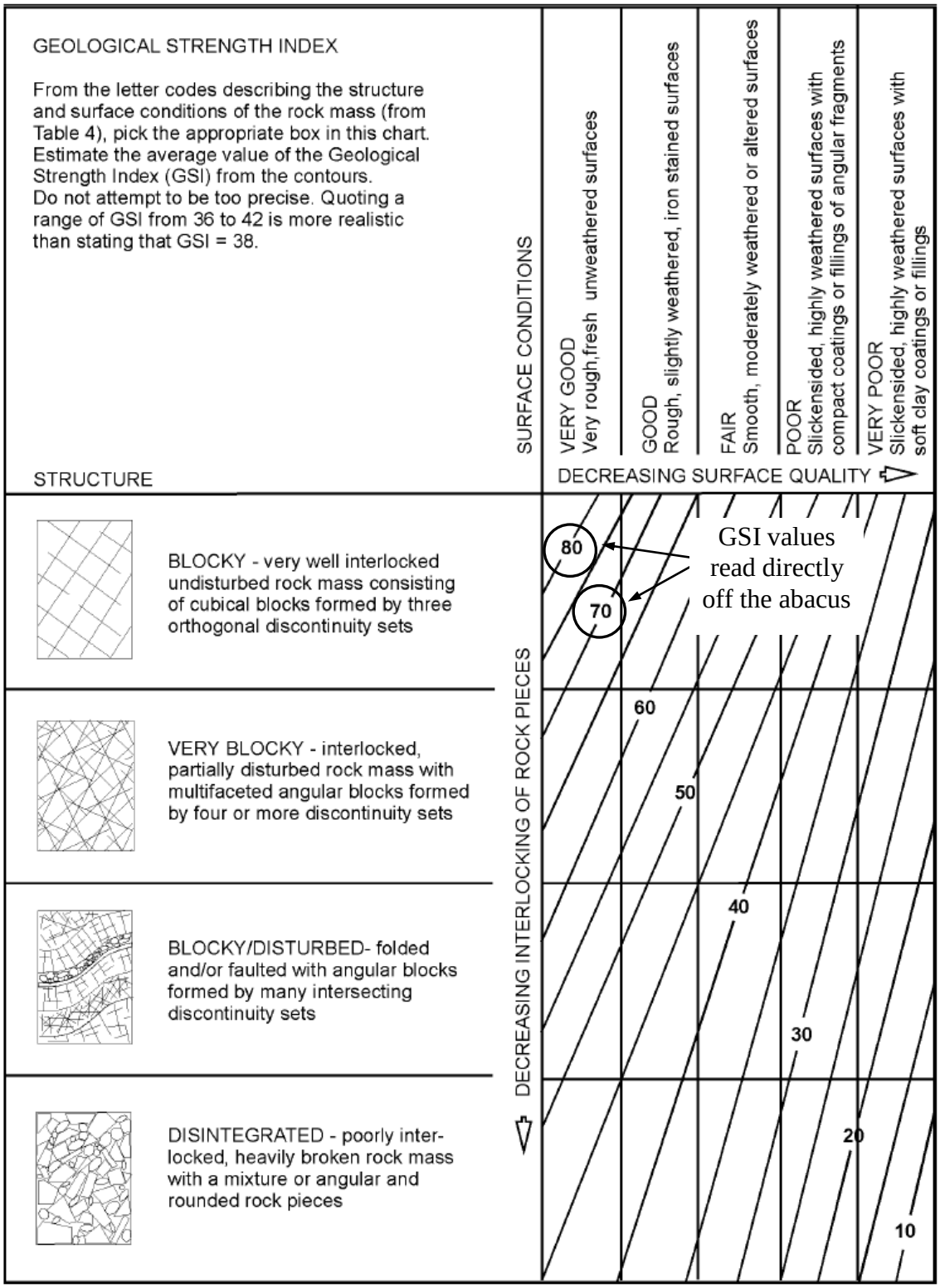

For GSI values larger than 25, i.e., for rock masses of good to reasonable quality, the original Hoek-Brown criterion (Hoek & Brown, 1980) is applicable with:

$$s = e^{([GSI - 100] / 9)} \quad \text{..... Eq. (67)}$$

$$a = 0.5 \quad \text{..... Eq. (68)}$$

With s and *a* as defined in Equation (65). For GSI values below 25, i.e., for rock masses of very poor quality, the modified Hoek-Brown criterion applies with:

$$s = 0 \quad \text{..... Eq. (69)}$$

$$a = 0.65 - (GSI / 200) \quad \text{..... Eq. (70)}$$

The choice of GSI = 25 for the switch between the original and modified criteria is purely arbitrary. It could be argued that a switch at GSI = 30 would not introduce a discontinuity in the value of *a*, but extensive trials have shown that the exact location of this switch has negligible practical significance.

For better quality rock masses (GSI over 25), the value of GSI can be estimated directly from the 1976 version of the Bieniawski Rock Mass Rating (Bieniawski, 1976), with the Groundwater rating set to 10 (dry) and the Adjustment for Joint Orientation set to 0 (very favourable). For very poor quality rock masses the value of RMR is very difficult to estimate and the balance between the ratings no longer gives a reliable basis for estimating rock mass strength. Consequently, the Bieniawski RMR classification should not be used for estimating the GSI values for poor quality rock masses.

If the 1989 version of the Bieniawski RMR classification (Bieniawski, 1989) is used, then GSI = $RMR_{89} - 5$, where RMR_{89} has the Groundwater rating set to 15 and the Adjustment for Joint Orientation set to zero.

One of the practical problems that arises when assessing the value of GSI in the field is related to blast damage – there can be a considerable difference in the appearance of a rock face that has been excavated by controlled blasting *vs*. damaged by bulk blasting. Wherever possible, the undamaged face should be used to estimate the value of GSI since

the overall aim is to determine the properties of the undisturbed rock mass. Where all the visible faces have been damaged by blasting, some attempt should be made to compensate for the lower values of GSI obtained from such faces. In recently blasted faces, new discontinuity surfaces will have been created by the blast and these will give a GSI value that may be as much as 10 points lower than that for the undisturbed rock mass. In other words, severe blast damage can be allowed for by moving up one row in Table 66 and Table 67.

Where blast damaged faces have been exposed for a number of years, it may also be necessary to step as much as one column to the left in order to allow for surface weathering, which will have occurred during this exposure. Hence, for example, a badly blast damaged weathered rock surface which has the appearance of a BLOCKY/DISTURBED and FAIR (BD/F in Table 66) rock mass may actually be VERY BLOCKY and GOOD (VB/G) in its unweathered and undisturbed in situ state.

An additional practical question is whether diamond drill core can be used to estimate the GSI value behind the visible faces. For reasonable quality rock masses (GSI over 25) the best approach is to evaluate the core in terms of the Bieniawski RMR classification and then, as described above, to estimate the GSI value from RMR. For poor quality rock masses (GSI under 25), relatively few intact core pieces longer than 100 mm are recovered and it becomes difficult to determine a reliable value for RMR. Under these circumstances, the physical appearance of the material recovered in the core should be used as a basis for estimating GSI.

APPENDIX G

G. THE ROCK TUNNELLING QUALITY INDEX (Q RATING)

Note: this appendix is the near-integral excerpt of pages 37 through to 43 of the book "Support of Underground Excavations in Hard Rock" by Hoek et al. *(1995). Reproduced with the permission of A. A. Balkema.*

G.1. Standard rock tunnelling Quality index, Q

On the basis of an evaluation of a large number of case histories of underground excavations, Barton *et al*. (1974) of the Norwegian Geotechnical Institute (NGI) proposed a tunnelling Quality index (Q) for the determination of rock mass characteristics and tunnel support requirements. The numerical value of the index Q varies on a logarithmic scale from 0.001 to a maximum of 1,000, and is defined by:

$$Q = (RQD \times Jr \times Jw) / (Jn \times Ja \times SRF) \qquad \text{..... Eq. (71)}$$

Where RQD is the Rock Quality Designation; Jr is the joint roughness number; Jw is the joint water reduction factor; Jn is the joint set number; Ja is the joint alteration number;

and, SRF is the stress reduction factor. In explaining the meaning of the parameters used to determine the value of Q, Barton *et al*. (1974) offer the following comments:

- The first quotient (RQD/Jn), representing the structure of the rock mass, is a crude measure of the block or particle size, with the two extreme values (100/0.5 and 10/20) differing by a factor of 400. If the quotient is interpreted in units of centimetres, the extreme "particle sizes" of 200 to 0.5 cm are seen to be crude but fairly realistic approximations. Probably the largest blocks should be several times this size and the smallest fragments less than half the size. (Clay particles are excluded.)

- The second quotient (Jr/Ja) represents the roughness and frictional characteristics of the joint walls or filling materials. This quotient is weighted in favour of rough, unaltered joints in direct contact. It is to be expected that such surfaces will be close to peak strength, that they will dilate strongly when sheared, and they will therefore be especially favourable to tunnel stability.

- When rock joints have thin clay mineral coatings and fillings, the strength is reduced significantly. Nevertheless, rock wall contact after small shear displacements have occurred may be a very important factor for preserving the excavation from ultimate failure.

- Where no rock wall contact exists, the conditions are extremely unfavourable to tunnel stability. The "friction angles" (given in Table 68) are a little below the residual strength values for most clays, and are possibly down-graded by the fact that these clay bands or fillings may tend to consolidate during shear, at least if normal consolidation or if softening and swelling has occurred. The swelling pressure of montmorillonite may also be a factor here.

- The third quotient (Jw/SRF) consists of two stress parameters. SRF is a measure of: 1) loosening load in the case of an excavation driven through shear zones and clay-bearing rock, 2) rock stress in competent rock; and, 3) squeezing loads in plastic incompetent rocks. It can be regarded as a total stress parameter. The parameter Jw is a measure of water pressure, which has an adverse effect on the shear strength of joints due to a reduction in effective normal stress.

Water may, in addition, cause softening and possible out-wash in the case of clay-filled joints. It has proved impossible to combine these two parameters in terms of inter-block effective stress, because paradoxically a high value of effective normal stress may sometimes signify less stable conditions than a low value, despite the higher shear strength. The quotient (Jw/SRF) is a complicated empirical factor describing the "active stress".

- It appears that the rock tunnelling quality Q index can now be considered to be a function of only three parameters, which are crude measures of: 1) block size (RQD/Jn); 2) inter-block shear strength (Jr/Ja); and, 3) active stress (Jw/SRF). Undoubtedly, there are several other parameters that could be added to improve the accuracy of the classification system.

  One of these would be the joint orientation. Although many case records include the necessary information on structural orientation in relation to excavation axis, it was not found to be the important general parameter that might be expected. Part of the reason for this may be that the orientations of many types of excavations can be, and normally are, adjusted to avoid the maximum effect of unfavourably oriented major joints. However, this choice is not available in the case of tunnels, and more than half the case records were in this category. The parameters Jn , Jr and Ja appear to play a more important role than orientation, because the number of joint sets determines the degree of freedom for block movement (if any), and the frictional and dilatational characteristics can vary more than the down-dip gravitational component of unfavourably oriented joints.

  If joint orientations had been included the classification would have been less general, and its essential simplicity lost.

Table 68 gives the classification of individual parameters used to obtain the tunnelling Quality index Q for a rock mass.

Table 68. Description and rating of the individual parameters used in the tunnelling Quality index Q. (After Barton *et al*., 1974.)

DESCRIPTION	VALUE	NOTES
1. ROCK QUALITY DESIGNATION	***RQD***	
A. Very poor	0 - 25	1. Where *RQD* is reported or measured as ≤ 10 (including 0),
B. Poor	25 - 50	a nominal value of 10 is used to evaluate *Q*.
C. Fair	50 - 75	
D. Good	75 - 90	2. *RQD* intervals of 5, i.e. 100, 95, 90 etc. are sufficiently
E. Excellent	90 - 100	accurate.
2. JOINT SET NUMBER	J_n	
A. Massive, no or few joints	0.5 - 1.0	
B. One joint set	2	
C. One joint set plus random	3	
D. Two joint sets	4	
E. Two joint sets plus random	6	
F. Three joint sets	9	1. For intersections use $(3.0 \times J_n)$
G. Three joint sets plus random	12	
H. Four or more joint sets, random,	15	2. For portals use $(2.0 \times J_n)$
heavily jointed, 'sugar cube', etc.		
J. Crushed rock, earthlike	20	
3. JOINT ROUGHNESS NUMBER	J_r	
a. Rock wall contact		
b. Rock wall contact before 10 cm shear		
A. Discontinuous joints	4	
B. Rough and irregular, undulating	3	
C. Smooth undulating	2	
D. Slickensided undulating	1.5	1. Add 1.0 if the mean spacing of the relevant joint set is
E. Rough or irregular, planar	1.5	greater than 3 m.
F. Smooth, planar	1.0	
G. Slickensided, planar	0.5	2. $J_r = 0.5$ can be used for planar, slickensided joints having
c. No rock wall contact when sheared		lineations, provided that the lineations are oriented for
H. Zones containing clay minerals thick	1.0	minimum strength.
enough to prevent rock wall contact	(nominal)	
J. Sandy, gravely or crushed zone thick	1.0	
enough to prevent rock wall contact	(nominal)	
4. JOINT ALTERATION NUMBER	J_a	ϕr degrees (approx.)
a. Rock wall contact		
A. Tightly healed, hard, non-softening,	0.75	1. Values of ϕr, the residual friction angle,
impermeable filling		are intended as an approximate guide
B. Unaltered joint walls, surface staining only	1.0	25 - 35 to the mineralogical properties of the
C. Slightly altered joint walls, non-softening	2.0	25 - 30 alteration products, if present.
mineral coatings, sandy particles, clay-free		
disintegrated rock, etc.		
D. Silty-, or sandy-clay coatings, small clay-	3.0	20 - 25
fraction (non-softening)		
E. Softening or low-friction clay mineral coatings,	4.0	8 - 16
i.e. kaolinite, mica. Also chlorite, talc, gypsum		
and graphite etc., and small quantities of swelling		
clays. (Discontinuous coatings, 1 - 2 mm or less)		

Table 68 (continued). Description and rating of the individual parameters used in the tunnelling Quality index Q. (After Barton *et al*., 1974.)

DESCRIPTION	VALUE	NOTES	
4, JOINT ALTERATION NUMBER	J_a	ϕr degrees (approx.)	
b. Rock wall contact before 10 cm shear			
F. Sandy particles, clay-free, disintegrating rock etc.	4.0	25 - 30	
G. Strongly over-consolidated, non-softening clay mineral fillings (continuous < 5 mm thick)	6.0	16 - 24	
H. Medium or low over-consolidation, softening clay mineral fillings (continuous < 5 mm thick)	8.0	12 - 16	
J. Swelling clay fillings, i.e. montmorillonite, (continuous < 5 mm thick). Values of J_a depend on percent of swelling clay-size particles, and access to water.	8.0 - 12.0	6 - 12	
c. No rock wall contact when sheared			
K. Zones or bands of disintegrated or crushed	6.0		
L. rock and clay (see G, H and J for clay	8.0		
M. conditions)	8.0 - 12.0	6 - 24	
N. Zones or bands of silty- or sandy-clay, small clay fraction, non-softening	5.0		
O. Thick continuous zones or bands of clay	10.0 - 13.0		
P. & R. (see G.H and J for clay conditions)	6.0 - 24.0		
5. JOINT WATER REDUCTION	J_w	approx. water pressure (kgf/cm^2)	
A. Dry excavation or minor inflow i.e. < 5 l/m locally	1.0	< 1.0	
B. Medium inflow or pressure, occasional outwash of joint fillings	0.66	1.0 - 2.5	
C. Large inflow or high pressure in competent rock with unfilled joints	0.5	2.5 - 10.0	1. Factors C to F are crude estimates; increase J_w if drainage installed.
D. Large inflow or high pressure	0.33	2.5 - 10.0	
E. Exceptionally high inflow or pressure at blasting, decaying with time	0.2 - 0.1	> 10	2. Special problems caused by ice formation are not considered.
F. Exceptionally high inflow or pressure	0.1 - 0.05	> 10	
6. STRESS REDUCTION FACTOR		***SRF***	
a. Weakness zones intersecting excavation, which may cause loosening of rock mass when tunnel is excavated			
A. Multiple occurrences of weakness zones containing clay or chemically disintegrated rock, very loose surrounding rock any depth)		10.0	1. Reduce these values of *SRF* by 25 - 50% but only if the relevant shear zones influence do not intersect the excavation
B. Single weakness zones containing clay, or chemically disintegrated rock (excavation depth < 50 m)		5.0	
C. Single weakness zones containing clay, or chemically disintegrated rock (excavation depth > 50 m)		2.5	
D. Multiple shear zones in competent rock (clay free), loose surrounding rock (any depth)		7.5	
E. Single shear zone in competent rock (clay free). (depth of excavation < 50 m)		5.0	
F. Single shear zone in competent rock (clay free). (depth of excavation > 50 m)		2.5	
G. Loose open joints, heavily jointed or 'sugar cube', (any depth)		5.0	

Table 68 (continued). Description and rating of the individual parameters used in the tunnelling Quality index Q. (After Barton *et al*., 1974.)

DESCRIPTION	VALUE			NOTES
6. STRESS REDUCTION FACTOR			***SRF***	
b. Competent rock, rock stress problems				
	σ_c/σ_1	σ_t/σ_1		2. For strongly anisotropic virgin stress field
H. Low stress, near surface	> 200	> 13	2.5	(if measured): when $5 \leq \sigma_1/\sigma_3 \leq 10$, reduce σ_c
J. Medium stress	200 - 10	13 - 0.66	1.0	to $0.8\sigma_c$ and σ_t to $0.8\sigma_t$. When σ_1/σ_3 > 10,
K. High stress, very tight structure	10 - 5	0.66 - 0.33	0.5 - 2	reduce σ_c and σ_t to $0.6\sigma_c$ and $0.6\sigma_t$, where
(usually favourable to stability, may				σ_c = unconfined compressive strength, and
be unfavourable to wall stability)				σ_t = tensile strength (point load) and σ_1 and
L. Mild rockburst (massive rock)	5 - 2.5	0.33 - 0.16	5 - 10	σ_3 are the major and minor principal stresses.
M. Heavy rockburst (massive rock)	< 2.5	< 0.16	10 - 20	3. Few case records available where depth of
c. Squeezing rock, plastic flow of incompetent rock				crown below surface is less than span width.
under influence of high rock pressure				Suggest *SRF* increase from 2.5 to 5 for such
N. Mild squeezing rock pressure			5 - 10	cases (see H).
O. Heavy squeezing rock pressure			10 - 20	
d. Swelling rock, chemical swelling activity depending on presence of water				
P. Mild swelling rock pressure			5 - 10	
R. Heavy swelling rock pressure			10 - 15	

ADDITIONAL NOTES ON THE USE OF THESE TABLES

When making estimates of the rock mass Quality (*Q*), the following guidelines should be followed in addition to the notes listed in the tables:

1. When borehole core is unavailable, *RQD* can be estimated from the number of joints per unit volume, in which the number of joints per metre for each joint set are added. A simple relationship can be used to convert this number to *RQD* for the case of clay free rock masses: $RQD = 115 - 3.3\ J_v$ (approx.), where J_v = total number of joints per m^3 ($0 < RQD < 100$ for $35 > J_v > 4.5$).
2. The parameter J_n representing the number of joint sets will often be affected by foliation, schistosity, slaty cleavage or bedding etc. If strongly developed, these parallel 'joints' should obviously be counted as a complete joint set. However, if there are few 'joints' visible, or if only occasional breaks in the core are due to these features, then it will be more appropriate to count them as 'random' joints when evaluating J_n.
3. The parameters J_r and J_a (representing shear strength) should be relevant to the weakest significant joint set or clay filled discontinuity in the given zone. However, if the joint set or discontinuity with the minimum value of J_r/J_a is favourably oriented for stability, then a second, less favourably oriented joint set or discontinuity may sometimes be more significant, and its higher value of J_r/J_a should be used when evaluating *Q*. The value of J_r/J_a should in fact relate to the surface most likely to allow failure to initiate.
4. When a rock mass contains clay, the factor *SRF* appropriate to loosening loads should be evaluated. In such cases the strength of the intact rock is of little interest. However, when jointing is minimal and clay is completely absent, the strength of the intact rock may become the weakest link, and the stability will then depend on the ratio rock-stress/rock-strength. A strongly anisotropic stress field is unfavourable for stability and is roughly accounted for as in note 2 in the table for stress reduction factor evaluation.
5. The compressive and tensile strengths (σ_c and σ_t) of the intact rock should be evaluated in the saturated condition if this is appropriate to the present and future in situ conditions. A very conservative estimate of the strength should be made for those rocks that deteriorate when exposed to moist or saturated conditions.

Note : *Nickson* et al. *(2001) have proposed a simplified way of qualifying the joint roughness number Jr when characterising the rock mass from core data. When a joint feels like baby skin it can be considered "polished/smooth". When it feels like fine sandpaper it can be considered "slightly rough", whereas it can be considered "rough" when it feels like coarse sandpaper. In the case where a joint feels like coarse sandpaper and has small-scale undulations (up to a few*

millimetres) it can be considered "very rough". This simplified rating can be useful in determining a proper Jr value from the limited joint exposure provided by a core.

Potvin & Hadjigeorgiou (2001) mention a simplified approach to determine the joint alteration number Ja from core data. If the joint cannot be scratched with a knife, Ja can be taken as 0.75. If it can be scratched with a knife, it can be considered to be between 1.0 and 1.5. In the case where a joint has a slippery touch and can be scratched with a fingernail, Ja can be taken as 2 – when the joint can be indented with a fingernail, Ja can be set at 4.

The use of Table 68 is illustrated in the following example. A 15m span crusher chamber for an underground mine is to be excavated in a norite at a depth of 2,100m below surface. The rock mass contains two sets of joints controlling stability. These joints are undulating, rough and unweathered with very minor surface staining. RQD values range from 85% to 95%, and laboratory tests on core samples of intact rock give an average uniaxial compressive strength of 170 MPa. The principal stress directions are approximately vertical and horizontal, and the magnitude of the horizontal principal stress is approximately 1.5 times that of the vertical principal stress. The rock mass is locally damp but there is no evidence of flowing water.

The numerical value of RQD is used directly in the calculation of Q and, for this rock mass, an average value of 90 will be used. Table 68.2 shows that, for two joint sets, the joint set number, Jn, is 4. For rough or irregular joints that are undulating, Table 68.3 gives a joint roughness number, Jr, of 3. Table 68.4 gives a joint alteration number, Ja, of 1.0, for unaltered joint walls with surface staining only. Table 68.5 shows that, for an excavation with minor inflow, the joint water reduction factor, Jw, is equal to 1.0. For a depth below surface of 2,100m the overburden stress will be approximately 57 MPa and, in this case, the magnitude of the major principal stress σ_1 will be around 85 MPa. Since the uniaxial compressive strength of the norite is approximately 170 MPa, this gives a ratio (σ_C / σ_1) = 2. Table 68.6 shows that, for competent rock with rock stress problems, this value of (σ_C / σ_1) can be expected to produce heavy rockbursting conditions and that the value of SRF

should lie between 10 and 20. A value of SRF = 15 will be assumed for this calculation. Using these values gives Q = (90 × 3 × 1) / (4 × 1 × 15) = 4.5.

Table 69 summarises the relationship between the value obtained for the Q index and the quality of the rock mass.

Table 69. Relationship between the Q rating and the quality of the rock mass. (After Barton *et al*., 1974).

Quality Index Q	Corresponding rock mass quality
0.001 – 0.01	Exceptionally poor
0.01 – 0.1	Extremely poor
0.1 – 1	Very poor
1 – 5	Poor
5 – 10	Fair
10 – 50	Good
50 – 100	Very good
100 – 500	Extremely good
500 – 1,000	Exceptionally good

G.2. Modified rock tunnelling Quality index, Q'

A modified rock tunnelling Quality index, Q' (Mathews *et al*., 1980), is also used, generally to assess the quality of open stope walls and backs in mining applications. Q' is defined as follows:

$$Q' = (RQD \times Jr \times Jw) / (Jn \times Ja) \qquad \text{..... Eq. (72)}$$

Where, as in Equation (71), RQD is the Rock Quality Designation; Jr is the joint roughness number; Jw is the joint water reduction factor; Jn is the joint set number; and, Ja is the joint alteration number. The only difference between the Q and Q' ratings is that the stress reduction factor SRF has been dropped in the modified Rock Tunnelling Quality Index –

the determination of the five remaining parameters is exactly as described in Table 68 for the original Q rating.

Mathews *et al*. (1980) have justified the removal of the stress reduction factor in the Q' rating by the fact that the standard Q methodology was based upon tunnelling case histories – which generally involve relatively shallow and small underground openings – and does not accurately reflect the effect stress has on larger and deeper underground excavation surfaces. Q' is generally used in the Stability Graph method developed by Mathews *et al*. (1980), in which a dedicated Rock Stress Factor, A, is used instead of the SRF to account for the stresses acting upon the free surfaces of open stopes at depth.

APPENDIX H

H. DESTRESSABILITY INDEX DEVELOPMENT SPREADSHEETS

Microsoft Excel spreadsheets were extensively used in the development of the Destressability Index methodology, with one spreadsheet being constructed for the intact rock material scale case and one for the rock mass scale case. Each spreadsheet consisted of two main worksheets: one that addressed the coding of the 9 by 9 RES interaction matrix (shown in Figure 147 and Figure 149 at the intact rock material and the rock mass scales, respectively) and one that addressed the Destressability Index (shown in Figure 148 and Figure 150, also at the intact rock material and the rock mass scales, respectively). The second worksheet took the parameter, property and cause values directly from the first one. In both worksheets only those cells in light grey could be modified, all the other cells being protected and automatically calculated based upon these input cells and according to the various formulae shown in the body of the thesis – the manual override of protected cells was however done in certain instances to simulate specific case histories.

This approach allowed to quickly and automatically recompile the entire Destressability Index system for 1) any change in the interaction matrix coding values in the first worksheet; and, 2) any modification in the property ranges and corresponding ratings, as well as for various combinations of example values in the second worksheet. In all, well over three hundred different combinations ended up being evaluated in a relatively short period of time, for various combinations of input data.

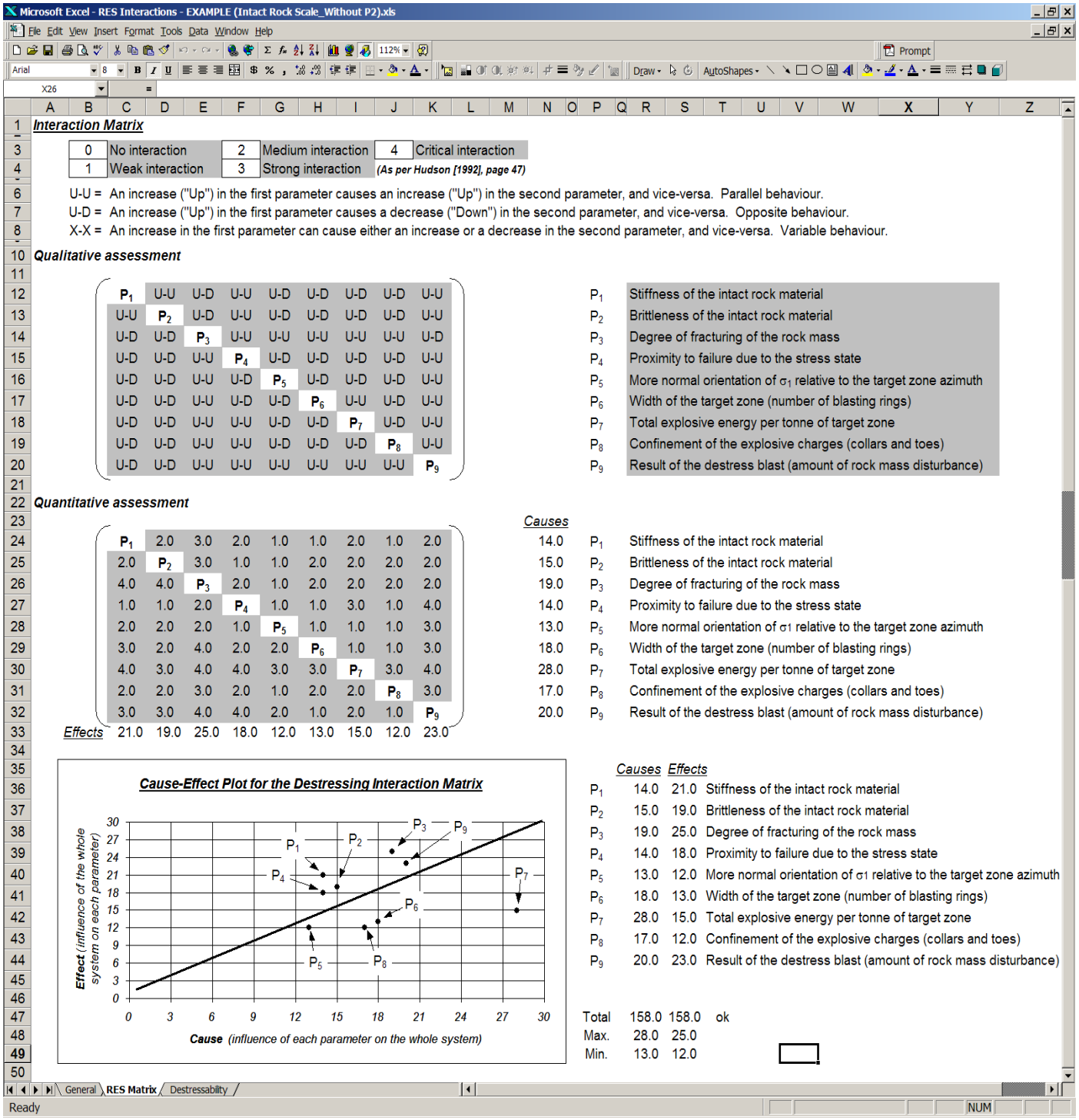

P1	U-U	U-D	U-U	U-D	U-D	U-D	U-D	U-U
U-U	**P2**	U-D	U-U	U-D	U-D	U-D	U-D	U-U
U-D	U-D	**P3**	U-U	U-U	U-U	U-U	U-U	U-D
U-D	U-D	U-U	**P4**	U-D	U-D	U-D	U-D	U-U
U-D	U-D	U-U	U-D	**P5**	U-D	U-D	U-D	U-U
U-D	U-D	U-U	U-D	U-D	**P6**	U-U	U-D	U-U
U-D	U-D	U-U	U-U	U-D	U-D	**P7**	U-D	U-U
U-D	U-D	U-U	U-U	U-D	U-D	U-D	**P8**	U-U
U-D	U-D	U-U	U-U	U-U	U-U	U-U	U-U	**P9**

P1	Stiffness of the intact rock material
P2	Brittleness of the intact rock material
P3	Degree of fracturing of the rock mass
P4	Proximity to failure due to the stress state
P5	More normal orientation of σ_1 relative to the target zone azimuth
P6	Width of the target zone (number of blasting rings)
P7	Total explosive energy per tonne of target zone
P8	Confinement of the explosive charges (collars and toes)
P9	Result of the destress blast (amount of rock mass disturbance)

										Causes		
P1	2.0	3.0	2.0	1.0	1.0	2.0	1.0	2.0	14.0	P1	Stiffness of the intact rock material
2.0	**P2**	3.0	1.0	1.0	2.0	2.0	2.0	2.0	15.0	P2	Brittleness of the intact rock material
4.0	4.0	**P3**	2.0	1.0	2.0	2.0	2.0	2.0	19.0	P3	Degree of fracturing of the rock mass
1.0	1.0	2.0	**P4**	1.0	1.0	3.0	1.0	4.0	14.0	P4	Proximity to failure due to the stress state
2.0	2.0	2.0	1.0	**P5**	1.0	1.0	1.0	3.0	13.0	P5	More normal orientation of σ1 relative to the target zone azimuth
3.0	2.0	4.0	2.0	2.0	**P6**	1.0	1.0	3.0	18.0	P6	Width of the target zone (number of blasting rings)
4.0	3.0	4.0	4.0	3.0	3.0	**P7**	3.0	4.0	28.0	P7	Total explosive energy per tonne of target zone
2.0	2.0	3.0	2.0	1.0	2.0	2.0	**P8**	3.0	17.0	P8	Confinement of the explosive charges (collars and toes)
3.0	3.0	4.0	4.0	2.0	1.0	2.0	1.0	**P9**	20.0	P9	Result of the destress blast (amount of rock mass disturbance)
Effects	21.0	19.0	25.0	18.0	12.0	13.0	15.0	12.0	23.0		

	Causes	*Effects*	
P1	14.0	21.0	Stiffness of the intact rock material
P2	15.0	19.0	Brittleness of the intact rock material
P3	19.0	25.0	Degree of fracturing of the rock mass
P4	14.0	18.0	Proximity to failure due to the stress state
P5	13.0	12.0	More normal orientation of σ1 relative to the target zone azimuth
P6	18.0	13.0	Width of the target zone (number of blasting rings)
P7	28.0	15.0	Total explosive energy per tonne of target zone
P8	17.0	12.0	Confinement of the explosive charges (collars and toes)
P9	20.0	23.0	Result of the destress blast (amount of rock mass disturbance)
Total	158.0	158.0	ok
Max.	28.0	25.0	
Min.	13.0	12.0	

Figure 147. Destressability Index development spreadsheet at the intact rock material scale – RES interaction matrix worksheet.

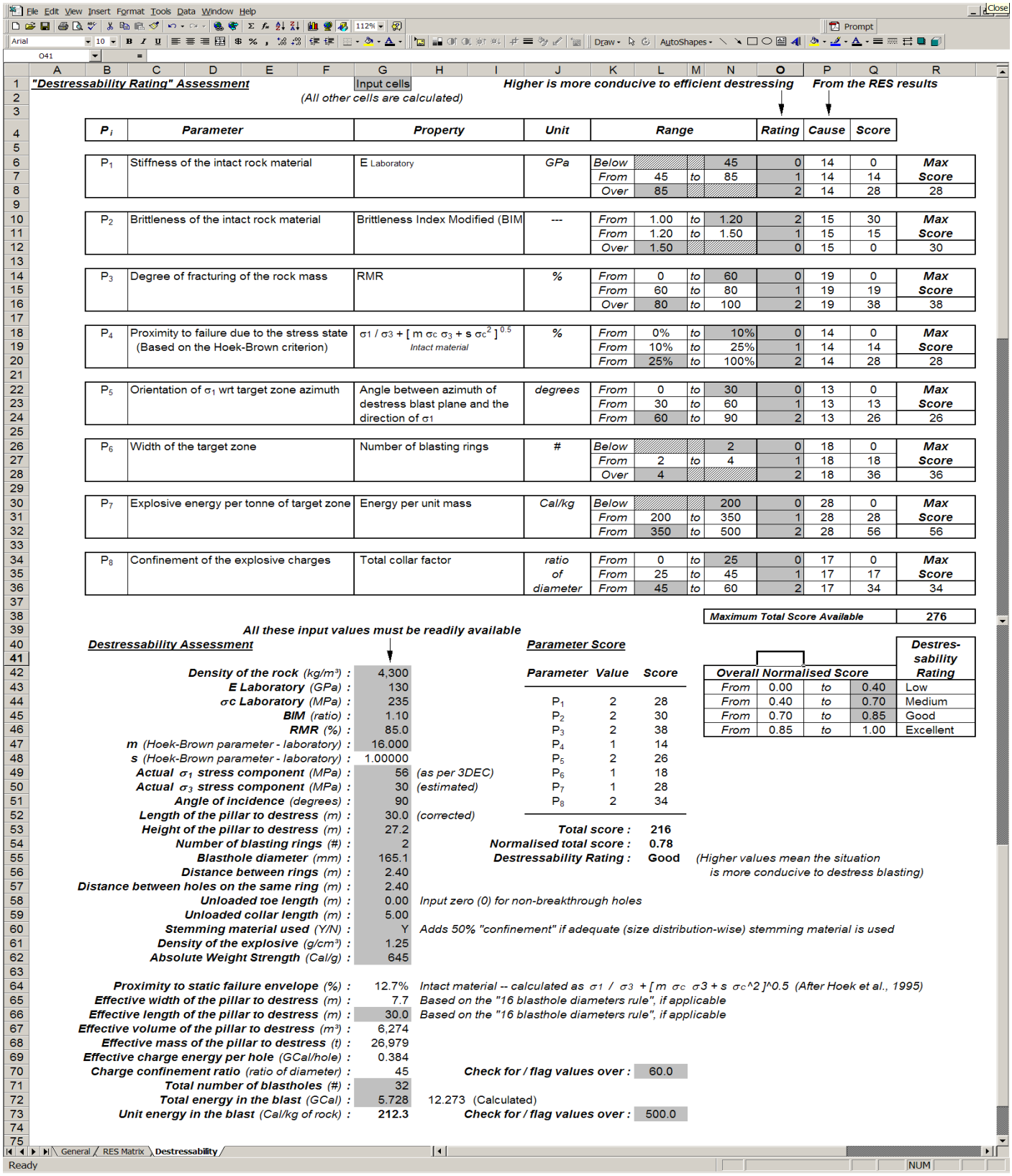

"Destressability Rating" Assessment — Input cells — *(All other cells are calculated)* — *Higher is more conducive to efficient destressing* — *From the RES results*

P_i	Parameter	Property	Unit	Range				Rating	Cause	Score	
P_1	Stiffness of the intact rock material	E Laboratory	GPa	Below			45	0	14	0	Max
				From	45	to	85	1	14	14	Score
				Over	85			2	14	28	28
P_2	Brittleness of the intact rock material	Brittleness Index Modified (BIM	---	From	1.00	to	1.20	2	15	30	Max
				From	1.20	to	1.50	1	15	15	Score
				Over	1.50			0	15	0	30
P_3	Degree of fracturing of the rock mass	RMR	%	From	0	to	60	0	19	0	Max
				From	60	to	80	1	19	19	Score
				Over	80	to	100	2	19	38	38
P_4	Proximity to failure due to the stress state (Based on the Hoek-Brown criterion)	$\sigma_1 / \sigma_3 + [\, m\, \sigma_c\, \sigma_3 + s\, \sigma_c^2\,]^{0.5}$ *Intact material*	%	From	0%	to	10%	0	14	0	Max
				From	10%	to	25%	1	14	14	Score
				From	25%	to	100%	2	14	28	28
P_5	Orientation of σ_1 wrt target zone azimuth	Angle between azimuth of destress blast plane and the direction of σ_1	degrees	From	0	to	30	0	13	0	Max
				From	30	to	60	1	13	13	Score
				From	60	to	90	2	13	26	26
P_6	Width of the target zone	Number of blasting rings	#	Below			2	0	18	0	Max
				From	2	to	4	1	18	18	Score
				Over	4			2	18	36	36
P_7	Explosive energy per tonne of target zone	Energy per unit mass	Cal/kg	Below			200	0	28	0	Max
				From	200	to	350	1	28	28	Score
				From	350	to	500	2	28	56	56
P_8	Confinement of the explosive charges	Total collar factor	ratio of diameter	From	0	to	25	0	17	0	Max
				From	25	to	45	1	17	17	Score
				From	45	to	60	2	17	34	34

Maximum Total Score Available 276

All these input values must be readily available

Destressability Assessment

Density of the rock (kg/m³) :	4,300	
E Laboratory (GPa) :	130	
σc Laboratory (MPa) :	235	
BIM (ratio) :	1.10	
RMR (%) :	85.0	
m (Hoek-Brown parameter - laboratory) :	16.000	
s (Hoek-Brown parameter - laboratory) :	1.00000	
Actual σ_1 stress component (MPa) :	56	(as per 3DEC)
Actual σ_3 stress component (MPa) :	30	(estimated)
Angle of incidence (degrees) :	90	
Length of the pillar to destress (m) :	30.0	(corrected)
Height of the pillar to destress (m) :	27.2	
Number of blasting rings (#) :	2	
Blasthole diameter (mm) :	165.1	
Distance between rings (m) :	2.40	
Distance between holes on the same ring (m) :	2.40	
Unloaded toe length (m) :	0.00	Input zero (0) for non-breakthrough holes
Unloaded collar length (m) :	5.00	
Stemming material used (Y/N) :	Y	Adds 50% "confinement" if adequate (size distribution-wise) stemming material is used
Density of the explosive (g/cm³) :	1.25	
Absolute Weight Strength (Cal/g) :	645	
Proximity to static failure envelope (%) :	12.7%	Intact material -- calculated as σ1 / σ3 + [m σc σ3 + s σc^2]^0.5 (After Hoek et al., 1995)
Effective width of the pillar to destress (m) :	7.7	Based on the "16 blasthole diameters rule", if applicable
Effective length of the pillar to destress (m) :	30.0	Based on the "16 blasthole diameters rule", if applicable
Effective volume of the pillar to destress (m³) :	6,274	
Effective mass of the pillar to destress (t) :	26,979	
Effective charge energy per hole (GCal/hole) :	0.384	
Charge confinement ratio (ratio of diameter) :	45	Check for / flag values over : 60.0
Total number of blastholes (#) :	32	
Total energy in the blast (GCal) :	5.728	12.273 (Calculated)
Unit energy in the blast (Cal/kg of rock) :	212.3	Check for / flag values over : 500.0

Parameter Score

Parameter	Value	Score
P_1	2	28
P_2	2	30
P_3	2	38
P_4	1	14
P_5	2	26
P_6	1	18
P_7	1	28
P_8	2	34

Total score : 216
Normalised total score : 0.78
Destressability Rating : Good

(Higher values mean the situation is more conducive to destress blasting)

Overall Normalised Score				Destressability Rating
From	0.00	to	0.40	Low
From	0.40	to	0.70	Medium
From	0.70	to	0.85	Good
From	0.85	to	1.00	Excellent

Figure 148. Destressability Index development spreadsheet at the intact rock material scale – Destressability Index calculation worksheet.

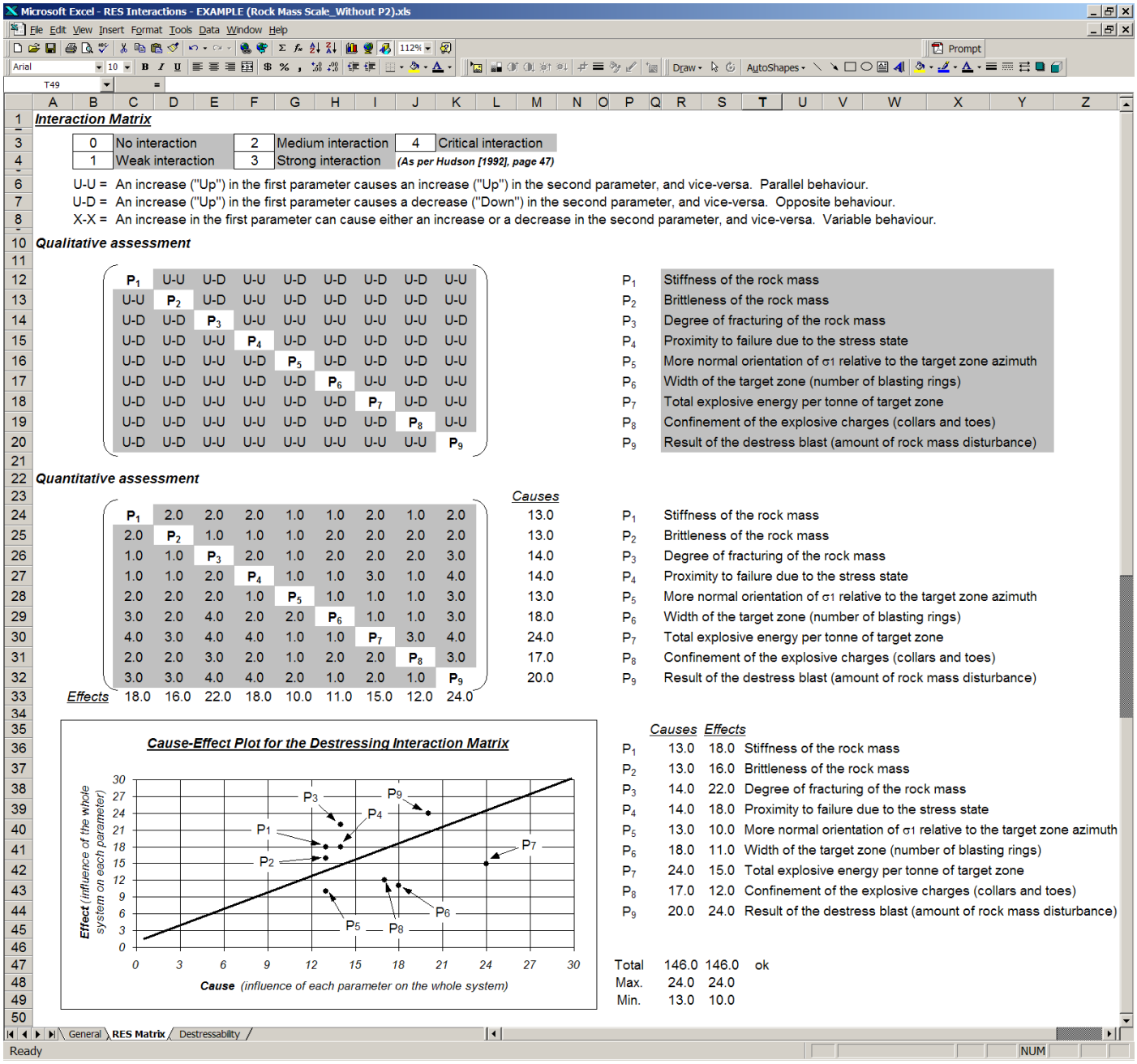

Figure 149. Destressability Index development spreadsheet at the rock mass scale – RES interaction matrix worksheet.

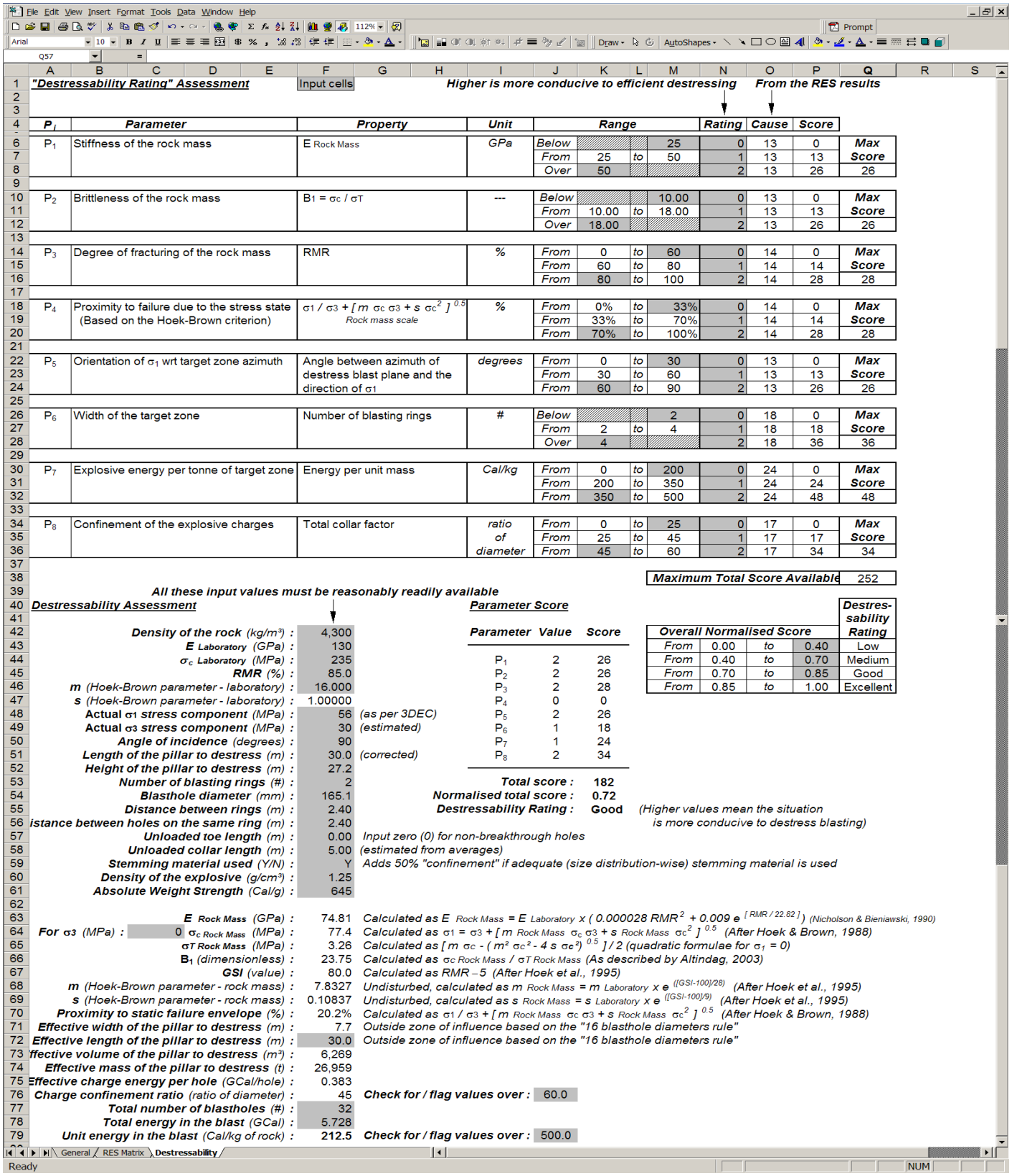

"Destressability Rating" Assessment — Input cells — Higher is more conducive to efficient destressing — From the RES results

P_i	Parameter	Property	Unit	Range				Rating	Cause	Score	
P_1	Stiffness of the rock mass	E Rock Mass	GPa	Below		to	25	0	13	0	Max Score
				From	25	to	50	1	13	13	
				Over	50			2	13	26	26
P_2	Brittleness of the rock mass	$B_1 = \sigma_c / \sigma_T$	---	Below		to	10.00	0	13	0	Max Score
				From	10.00	to	18.00	1	13	13	
				Over	18.00			2	13	26	26
P_3	Degree of fracturing of the rock mass	RMR	%	From	0	to	60	0	14	0	Max Score
				From	60	to	80	1	14	14	
				From	80	to	100	2	14	28	28
P_4	Proximity to failure due to the stress state (Based on the Hoek-Brown criterion)	$\sigma_1 / \sigma_3 + [\, m\ \sigma_c\ \sigma_3 + s\ \sigma_c^2\ ]^{0.5}$ Rock mass scale	%	From	0%	to	33%	0	14	0	Max Score
				From	33%	to	70%	1	14	14	
				From	70%	to	100%	2	14	28	28
P_5	Orientation of σ_1 wrt target zone azimuth	Angle between azimuth of destress blast plane and the direction of σ_1	degrees	From	0	to	30	0	13	0	Max Score
				From	30	to	60	1	13	13	
				From	60	to	90	2	13	26	26
P_6	Width of the target zone	Number of blasting rings	#	Below		to	2	0	18	0	Max Score
				From	2	to	4	1	18	18	
				Over	4			2	18	36	36
P_7	Explosive energy per tonne of target zone	Energy per unit mass	Cal/kg	From	0	to	200	0	24	0	Max Score
				From	200	to	350	1	24	24	
				From	350	to	500	2	24	48	48
P_8	Confinement of the explosive charges	Total collar factor	ratio of diameter	From	0	to	25	0	17	0	Max Score
				From	25	to	45	1	17	17	
				From	45	to	60	2	17	34	34

Maximum Total Score Available: 252

All these input values must be reasonably readily available

Destressability Assessment

Density of the rock (kg/m³) :	4,300	
E Laboratory (GPa) :	130	
σ_c Laboratory (MPa) :	235	
RMR (%) :	85.0	
m (Hoek-Brown parameter - laboratory) :	16.000	
s (Hoek-Brown parameter - laboratory) :	1.00000	
Actual σ_1 stress component (MPa) :	56	(as per 3DEC)
Actual σ_3 stress component (MPa) :	30	(estimated)
Angle of incidence (degrees) :	90	
Length of the pillar to destress (m) :	30.0	(corrected)
Height of the pillar to destress (m) :	27.2	
Number of blasting rings (#) :	2	
Blasthole diameter (mm) :	165.1	
Distance between rings (m) :	2.40	
istance between holes on the same ring (m) :	2.40	
Unloaded toe length (m) :	0.00	Input zero (0) for non-breakthrough holes
Unloaded collar length (m) :	5.00	(estimated from averages)
Stemming material used (Y/N) :	Y	Adds 50% "confinement" if adequate (size distribution-wise) stemming material is used
Density of the explosive (g/cm³) :	1.25	
Absolute Weight Strength (Cal/g) :	645	

Parameter Score

Parameter	Value	Score
P_1	2	26
P_2	2	26
P_3	2	28
P_4	0	0
P_5	2	26
P_6	1	18
P_7	1	24
P_8	2	34
Total score :		182
Normalised total score :		0.72
Destressability Rating :		Good

(Higher values mean the situation is more conducive to destress blasting)

Overall Normalised Score				Destressability Rating
From	0.00	to	0.40	Low
From	0.40	to	0.70	Medium
From	0.70	to	0.85	Good
From	0.85	to	1.00	Excellent

E Rock Mass (GPa) :	74.81	Calculated as E Rock Mass = E Laboratory x (0.000028 RMR² + 0.009 e [RMR / 22.82]) (Nicholson & Bieniawski, 1990)
For σ_3 (MPa) : 0	77.4	σ_c Rock Mass (MPa) : Calculated as $\sigma_1 = \sigma_3 + [\, m$ Rock Mass $\sigma_c\ \sigma_3 + s$ Rock Mass $\sigma_c^2\ ]^{0.5}$ (After Hoek & Brown, 1988)
σ_T Rock Mass (MPa) :	3.26	Calculated as $[\, m\ \sigma_c - (m^2\ \sigma_c^2 - 4\ s\ \sigma_c^2)^{0.5}\ ] / 2$ (quadratic formulae for $\sigma_1 = 0$)
B_1 (dimensionless) :	23.75	Calculated as σ_c Rock Mass / σ_T Rock Mass (As described by Altindag, 2003)
GSI (value) :	80.0	Calculated as RMR – 5 (After Hoek et al., 1995)
m (Hoek-Brown parameter - rock mass) :	7.8327	Undisturbed, calculated as m Rock Mass = m Laboratory x e ([GSI-100]/28) (After Hoek et al., 1995)
s (Hoek-Brown parameter - rock mass) :	0.10837	Undisturbed, calculated as s Rock Mass = s Laboratory x e ([GSI-100]/9) (After Hoek et al., 1995)
Proximity to static failure envelope (%) :	20.2%	Calculated as $\sigma_1 / \sigma_3 + [\, m$ Rock Mass $\sigma_c\ \sigma_3 + s$ Rock Mass $\sigma_c^2\ ]^{0.5}$ (After Hoek & Brown, 1988)
Effective width of the pillar to destress (m) :	7.7	Outside zone of influence based on the "16 blasthole diameters rule"
Effective length of the pillar to destress (m) :	30.0	Outside zone of influence based on the "16 blasthole diameters rule"
ffective volume of the pillar to destress (m³) :	6,269	
Effective mass of the pillar to destress (t) :	26,959	
Effective charge energy per hole (GCal/hole) :	0.383	
Charge confinement ratio (ratio of diameter) :	45	Check for / flag values over : 60.0
Total number of blastholes (#) :	32	
Total energy in the blast (GCal) :	5.728	
Unit energy in the blast (Cal/kg of rock) :	212.5	Check for / flag values over : 500.0

Figure 150. Destressability Index development spreadsheet at the rock mass scale – Destressability Index calculation worksheet.

REFERENCES

Adams, T. , R. Demuth, L. Margolin, and B. Nichols, 1983. *Simulation of Rock Blasting With the SHALE Code*. In the proceedings of the First International Symposium on Rock Fragmentation by Blasting (FRAGBLAST'1 – P.-A. Persson, editor), pages 361 to 373. Luleå, Sweden. Published by A. A. Balkema, Rotterdam, Netherlands.

Aimone, C., 1982. *Three-Dimensional Wave Propagation Model of Full Scale Rock Fragmentation*. Ph.D. Thesis, Department of Civil Engineering, Northwestern University, 295 pages. Evanston, Illinois, U.S.A.

Altindag, R., 2003[a]. *Reply to H. G. Denkhaus "Brittleness and Drillability"*. In the Journal of the South African Institute of Mining and Metallurgy, Vol. 103, No. 8, page 525. Johannesburg, Republic of South Africa.

Altindag, R., 2003[b]. *Correlation of Specific Energy with Rock Brittleness Concepts on Rock Cutting*. In the Journal of the South African Institute of Mining and Metallurgy, Vol. 103, No. 4, pages 163 to 171. Johannesburg, Republic of South Africa.

Andrieux, P., J. Hadjigeorgiou, and R. Brummer, 2004. *A Rock Engineering Systems Approach to Destress Rock Blasting*. In the proceedings of the Second International Seminar on Deep and High Stress Mining, pages 277 to 291. Symposium Series S37, published by the South African Institute of Mining and Metallurgy. Johannesburg, Republic of South Africa.

Andrieux, P., H. Zhu, and R. Brummer, 2003. *Advanced Numerical Stress Analyses for the Recovery of the 680 Sill Pillar at Louvicourt Mine*. Itasca Consulting Canada, Inc.

internal report to Aur Resources, Ltd., Louvicourt Mine, 155 pages. Sudbury, Ontario, Canada.

Andrieux, P., and J. Hadjigeorgiou, 2002. *The Potential Application of Rock Engineering Systems to Rock Blasting*. In the proceedings of the 104th Annual General Meeting of the Canadian Institute of Mining, Metallurgy and Petroleum. On CD-ROM, 9 pages. Vancouver, British Columbia, Canada.

Andrieux, P., and R. Brummer, 2002. *Large-Scale Choked Destress Blasts in Mine Pillars*. In French. In the proceedings of the 17th Colloquium on Ground Control of the Quebec Mining Association, 17 pages. Val d'Or, Quebec, Canada.

Andrieux, P., and J. Hadjigeorgiou, 2001. *Rock Engineering Systems and Rock Blasting*. In the proceedings of the 24th Study Session on Blasting Techniques, SEEQ, 12 pages. Quebec City, Quebec, Canada.

Andrieux, P., and R. Brummer, 2001. *Assessment of the West Ore Zone Mass-Blast and of Future Mining in the 1000m Level Bulk Zone at Brunswick Mine*. Itasca Consulting Canada, Inc. internal report to Noranda, Inc., Brunswick Mine, 109 pages. Sudbury, Ontario, Canada.

Andrieux, P., 2001. *General Pillar Destressing Considerations at the Fraser Copper Mine*. Technical memorandum from Itasca Consulting Canada, Inc. to Falconbridge, Ltd., Fraser Mine, 7 pages. Sudbury, Ontario, Canada.

Andrieux, P., and B. Simser, 2001. *Ground Stability-Based Mine Design Guidelines at Brunswick Mine*. In the "Underground Mining Methods – Engineering Fundamentals and International Case Studies" Handbook of the Society of Mining Engineers (W. Hustrulid & R. Bullock, editors), pages 207 to 214. Published by the American Institute of Mining and Exploration. Littleton, Colorado, U.S.A.

Andrieux, P., R. Brummer, Q. Liu, A. Mortazavi, and B. Simser, 2000. *Large-Scale Panel Destress Blast at Brunswick Mine*. In the proceedings of the 23rd Study Session on Blasting Techniques, SEEQ. Quebec City, Quebec, Canada. Paper published under the same name in the Bulletin of the Canadian Institute of Mining, Metallurgy and

Petroleum, Vol. 96, No. 1075 (November/December 2003), pages 78 to 87. Montreal, Quebec, Canada.

ASTM International, 2002. *D2938-95(2002) – Standard Test Method for Unconfined Compressive Strength of Intact Rock Core Specimens*. 3 pages. West Conshohocken, Pennsylvania, U.S.A.

Aubertin, M., R. Simon, L. Auer, and D. E. Gill, 1997. *A Study on the Rockburst Potential at the Sigma Mine in Relation With the Effects of the Pre-Fracturing Blast*. In French. Report to the Quebec Ministry of Natural Resources, CDT P1848, 186 pages. École Polytechnique de Montréal, Mineral Engineering Department. Montreal, Quebec, Canada.

Aubertin, M., D. E. Gill, and R. Simon, 1994. *On the Use of the Brittleness Index Modified (BIM) to Estimate the Post-Peak Behaviour of Rocks*. In the proceedings of the First North American Rock Mechanics Symposium – NARMS'94 (P. Nelson & S. Laubach, editors), pages 945 to 952. Austin, Texas, U.S.A. Published by A. A. Balkema, Rotterdam, Netherlands.

Barton, N., 2002. *Some New Q Value Correlations to Assist in Site Characterisation and Tunnel Design*. International Journal of Rock Mechanics & Mining Sciences, Vol. 39 (2002), pages 185 to 216.

Barton, N., 1988. *Rock Mass Classification and Tunnel Reinforcement Selection Using the Q-System*. In "Rock Classification Systems for Engineering Purposes" (L. Kirkaldie, editor), pages 159 to 184. ASTM STP-984, American Society for Testing and Materials. West Conshohocken, Pennsylvania, U.S.A.

Barton, N., R. Lien, and J. Lunde, 1974. *Engineering Classification of Rock Masses for the Design of Tunnel Support*. Norwegian Geomechanics Institute. In "Rock Mechanics", Vol. 6, No. 4, pages 189 to 236.

Bates, R., and J. A. Jackson, 1987. *Glossary of Geology*. Third Edition, published by the American Geological Institute, 788 pages. Washington, D.C., U.S.A.

Bawden, W., and P. Lausch, 2000. *The Use of SMART Cable Bolt Instruments Towards the Design and Design Optimization of Underground Rock Support Systems*. In the

proceedings of the 53rd Annual General Meeting of the Canadian Geotechnical Society. On CD-ROM, 9 pages. Montreal, Quebec, Canada.

Benjamin, J., 1968. *Probabilistic Models for Seismic Force Design*. In the Journal of the Structural Division of the ASCE, pages 1175 to 1196.

Bieniawski, Z., 1989. *Engineering Rock Mass Classifications: A Complete Manual for Engineers and Geologists in Mining, Civil, and Petroleum Engineering*. John Wiley & Sons publishers, 272 pages. New York, New York, U.S.A.

Bieniawski, Z., 1976. *Rock Mass Classification in Rock Engineering*. In the proceedings of the "Exploration for Rock Engineering" symposium (Z. Bieniawski, editor), pages 97 to 106. Cape Town, Republic of South Africa. Published by A. A. Balkema, Rotterdam, Netherlands.

Bieniawski, Z., 1967. *Mechanism of Brittle Fracture of Rock. Part I: Theory of the Fracture Process; Part II: Experimental Studies; Part III: Fracture in Tension and Under Long-Term Loading*. International Journal of Rock Mechanics & Mining Sciences, Vol. 4, pages 395 to 430.

Blake, W., M. Board, and R. Brummer, 1998. *Destress Blasting Practices – A Review of the Literature and Current Industrial Practice*. Report from the Itasca Consulting Group and Richard Brummer Associates to CAMIRO – Mining Division, 96 pages. Sudbury, Ontario, Canada.

Blake, W., 1982. *Rock Preconditioning as a Seismic Control Measure in Mines*. In the proceedings of the First International Congress on Rockbursts and Seismicity in Mines, organised by the South African Institute of Mining and Metallurgy (N. Gay & E. Wainwright, editors), pages 225 to 229. Johannesburg, Republic of South Africa.

Blake, W., 1972. *Destressing Test at the Galena Mine, Wallace, Idaho*. Journal of the SME of the AIME, Vol. 252, No. 3, pages 294 to 299. Keystone, Colorado, U.S.A.

Board, M., and R. Brummer, 1998. *Risk Assessment of Deep Mining at Kidd Mine – A Technical Evaluation*. Joint report by the Itasca Consulting Group and Richard Brummer Associates to Falconbridge, Ltd., Kidd Mine Division, 16 pages. Published internally by Falconbridge, Ltd. Sudbury, Ontario, Canada.

Board, M., A. Rorke, G. Williams, and N. Gay, 1992. *Fluid Injection for Rockburst Control in Deep Mining*. In the proceedings of the 33rd U.S. Symposium on Rock Mechanics (J. Tillerson & W. Wawersik, editors), pages 111 to 120. Santa Fe, New Mexico, USA. Published by A. A. Balkema, Rotterdam, Netherlands.

Board, M., and C. Fairhurst, 1983. *Rockburst Control Through Destressing – A Case Example*. In the proceedings of the "Rockbursts : Prediction and Control" conference organised by the British Institution of Mining and Metallurgy, pages 147 to 161. London, England.

Borg, T., 1983. *Prediction of Rock Failures in Mines With Application to the Näsliden Mine in Northern Sweden*. Doctoral Thesis, 1983:26D, Luleå University, 167 pages. Luleå, Sweden.

Brady, B., and E. T. Brown, 1993. *Rock Mechanics for Underground Mining – Second Edition*. Published by Chapman & Hall, 571 pages. London, England.

Braithwaite, M., W. Brown, and A. Minchinton, 1996. *The Use of Ideal Detonation Computer Codes in Blast Modelling*. In the proceedings of the Fifth International Symposium on Rock Fragmentation by Blasting (FRAGBLAST'5 – B. Mohanty, editor), pages 37 to 44. Montreal, Quebec, Canada. Published by A. A. Balkema, Rotterdam, Netherlands.

Bräuner, G., 1994. *Rockbursts in Coal Mines and Their Prevention*. 144 pages. Published by A. A. Balkema, Rotterdam, Netherlands.

Bräuner, G., 1983. *Nature of Rockbursts in the Ruhr Coal Fields and Measures to Eliminate the Hazard*. Unpublished notes – personal communication reported by M. Board.

Brummer, R., and P. Andrieux, 2002. *Destress Blasting – A Design Methodology Based on Case Studies*. In the proceedings of the Fifth North American Rock Mechanics Symposium ("NARMS–TAC 2002: Mining and Tunnelling Innovation and Opportunity" – R. Hammah, W. Bawden, J. Curran, and M. Telesnicki, editors), Vol. 1, pages 165 to 172. Published by the University of Toronto Press. Toronto, Ontario, Canada.

Brummer, R., 2001. *Destress Blasting*. Notes of a CAMIRO – Itasca Canada short course on destress blasting held 11 February 2001. Sudbury, Ontario, Canada.

Brummer, R., A. Mortazavi, P. Andrieux, and B. Simser, 2000. *Report to Canadian Mining Industry Research Organisation, Mining Division – Destress Blasting: A Monitored Field Trial at Brunswick Mine*. Report from Itasca Consulting Canada, Inc., to CAMIRO – Mining Division, 120 pages. Sudbury, Ontario, Canada.

Brummer, R., and A. Rorke, 1988. *Case Studies on Large Rockbursts in South African Gold Mines*. In the proceedings of the Second International Congress on Rockbursts and Seismicity in Mines (C. Fairhurst, editor), pages 323 to 329. Minneapolis, Minnesota, U.S.A. Published by A. A. Balkema, Rotterdam, Netherlands.

Brummer, R., 1987. *Fracturing and Deformation at the Edges of Tabular Gold Mining Excavations and the Development of a Numerical Model Describing Such Phenomena*. Doctoral Thesis, Rand Afrikaans University, 204 pages. Johannesburg, Republic of South Africa.

Butler, A., 1997. *Application of Weighted Energy Index for Routine Evaluation of Rockburst Potential*. In the proceedings of the Fourth International Congress on Rockbursts and Seismicity in Mines (S. Gibowicz, editor), pages 317 to 323. Krakow, Poland. Published by A. A. Balkema, Rotterdam, Netherlands.

Chiappetta, F., D. Borg, and V. Sterner, 1987. *Explosives and Rock Blasting*. Published by Atlas Powder Co., 662 pages. Dallas, Texas, U.S.A.

Chung, S., 1997. *Explosive Technology – Open Pit and Underground Blasting*. In the notes of the Continuing Education Course, Part D, Vol. I. Queen's University, Department of Mining Engineering. Kingston, Ontario, Canada.

Coates, D., 1981. *Rock Mechanics Principles*. Published by CANMET – Energy, Mines and Resources Canada, Monograph 874, 452 pages. Ottawa, Ontario, Canada.

Cook, N. (editor), 1977. *An Industry Guide to the Amelioration of the Hazards of Rockbursts and Rock Falls*. Report to the High Level Committee on Rockbursts and Rock Falls, South African Chamber of Mines, P.R.D. Series 216, 178 pages. Johannesburg, Republic of South Africa.

Cook, N., E. Hoek, J. Pretorius, D. Ortlepp, and M. Salamon, 1966. *Rock Mechanics Applied to the Study of Rockbursts*. In the Journal of the South African Institute of Mining and Metallurgy, Vol. 66, pages 435 to 528. Johannesburg, Republic of South Africa.

Cosentino, P., V. Ficara, and D. Luzio, 1977. *Truncated Exponential Frequency-Magnitude Relationship in the Earthquake Statistics*. In the Bulletin of the Seismological Society of America, Vol. 67, pages 1615 to 1623.

Crouch, S., 1974. *Analysis of Rockbursts in Cut-and-Fill Stopes*. In the Journal of the SME of the AIME, Vol. 256, pages 298 to 303. Littleton, Colorado, U.S.A.

Cundall, P., 2002. Personal communication, Itasca Consulting Group. Minneapolis, Minnesota, U.S.A.

Cundall, P., and R. Hart, 1993. *Numerical Modelling of Discontinua*. In "Comprehensive Rock Engineering: Principles, Practices and Projects" (J. Hudson, editor), Vol. 2, Chapter 9, pages 231 to 243. Pergamon Press.

Cundall, P., 1988. *Formulation of a Three-Dimensional Distinct Element Model – Part I: A Scheme to Detect and Represent Contacts in a System Composed of Many Polyhedral Blocks*. International Journal of Rock Mechanics, Mining Sciences and Geomechanics Abstracts, Vol. 25, pages 107 to 116.

Cunningham, C. V. B., 1987. *Fragmentation Estimations and the Kuz-Ram Model – Four Years On*. In the proceedings of the Second International Symposium on Rock Fragmentation by Blasting (FRAGBLAST'2 – W. Fourney, editor), pages 475 to 487. Keystone, Colorado, U.S.A. Published by A. A. Balkema, Rotterdam, Netherlands.

Cunningham, C. V. B., 1983. *The Kuz-Ram Model for Prediction of Fragmentation from Blasting*. In the proceedings of the First International Symposium on Rock Fragmentation by Blasting (FRAGBLAST'1 – P.-A. Persson, editor), pages 439 to 454. Luleå, Sweden. Published by A. A. Balkema, Rotterdam, Netherlands.

Da Gama, C., 1983. *Use of Comminution Theory to Predict Fragmentation of Jointed Rock Masses Subjected to Blasting*. In the proceedings of the First International

Symposium on Rock Fragmentation by Blasting (FRAGBLAST'1 – P.-A. Persson, editor), pages 565 to 579. Luleå, Sweden. Published by A. A. Balkema, Rotterdam, Netherlands.

Deere, D. U., and D. W. Deere, 1988. *The Rock Quality Designation (RQD) Index in Practice*. In "Rock Classification Systems for Engineering Purposes" (L. Kirkaldie, editor), pages 91 to 101. ASTM STP-984, American Society for Testing and Materials. West Conshohocken, Pennsylvania, U.S.A.

Deere, D. U., A. Hendron, F. Patton, and E. Cording, 1967. *Design of Surface and Near-Surface Construction in Rock*. In "Failure and Breakage of Rock" (C. Fairhurst, editor), proceedings of the 8th U.S. Symposium on Rock Mechanics, pages 237-302. Minneapolis, Minnesota, U.S.A. Published by the SME of the AIME. Littleton, Colorado, U.S.A.

Denkhaus, H., 2003[a]. *Brittleness and Drillability – Comment on "The Evaluation of Rock Brittleness Concept on Rotary Blasthole Drills" and "Correlation of Specific Energy With Rock Brittleness Concepts on Rock Cutting" by R. Altindag*. In the Journal of the South African Institute of Mining and Metallurgy, Vol. 103, No. 8, page 523. Johannesburg, Republic of South Africa.

Denkhaus, H., 2003[b]. *Brittleness and Drillability – Second Reply to R. Altindag*. In the Journal of the South African Institute of Mining and Metallurgy, Vol. 103, No. 8, page 527. Johannesburg, Republic of South Africa.

Eneva, M., and R. P. Young, 1993. *Evaluation of Spatial Patterns in the Distribution of Seismic Activity in Mines: a Case Study of Creighton Mine, Northern Ontario (Canada).* In the proceedings of the Third International Congress on Rockbursts and Seismicity in Mines (P. Young, editor), organised by Queen's University, pages 175 to 180. Kingston, Ontario, Canada. Published by A. A. Balkema, Rotterdam, Netherlands.

Falmagne, V., B. Simser, P. Andrieux, D. Ouellet, and G. Gagnon, 2003. *Bell-Allard Mine – Risk Assessment in the Retreat Zone*. In French. Joint report by the Noranda

Technology Centre and Itasca Consulting Canada, Inc., to the Noranda, Inc., Bell-Allard Mine, 50 pages. Pointe-Claire (Montreal), Quebec, Canada.

Favreau, R. F., and P. Favreau, 2002. *How to Design a Blast With Computer Simulations*. In the Bulletin of the Canadian Institute of Mining, Metallurgy and Petroleum, Vol. 95, No. 1066, pages 100 to 101. Montreal, Quebec, Canada.

Garood, P., 1984. *Ground Control Aspects of the Development at Creighton No. 11 Shaft*. In the Canadian Institute of Mining, Metallurgy and Petroleum Special Volume 30 "Rock Breaking and Mechanical Excavation" (P. Baumgartner, editor), pages 91 to 95. Montreal, Quebec, Canada.

Gaudreau, D., 1997 [a]. *Characterisation of Mine Seismicity at Brunswick Mining Division*. Annual Noranda Chief Engineers Meeting. Noranda Technology Centre. Pointe-Claire (Montreal), Quebec, Canada.

Gaudreau, D., 1997 [b]. *Rockburst Risk Assessment Literature Review*. Internal Noranda Technology Centre report, 48 pages. Pointe-Claire (Montreal), Quebec, Canada.

Grady, D., and M. Kipp, 1980. *Continuum Modelling of Explosive fracture in Oil Shale*. International Journal of Rock Mechanics, Mining Sciences and Geomechanics Abstracts, Vol. 17, pages 147 to 157.

Grenon, M., J. Hadjigeorgiou, and Q. Liu, 1998. *Quantifying In Situ Rock Block Size and Resulting Fragment Size Distributions Due to Blasting*. FRAGBLAST – The International Journal of Blasting and Fragmentation, Vol. 2, pages 205 to 218.

Haghighi, R., R. Briton, and D. Skidmore, 1988. *Modelling Gas Pressure Effects on Explosive Rock Breakage*. International Journal of Mining and Geological Engineering, Vol. 6, pages 73 to 79.

Han, S., T. Kyoya, Y. Ichikawa, and T. Kawamoto, 1986. *A Dynamic Analysis of Jointed Rock Mass*. In the proceedings of the International Symposium on Engineering in Complex Rock Formations, pages 338 to 344. Beijing, People's Republic of China. Published by Science Press.

Hanson, D., D. Malinski, V. Kazakidis, L. Laverdure, and R. Brummer, 1992. *The Design and Evaluation of a Destress Blast at Strathcona Mine*. In the proceedings of the 16th Canadian Symposium on Rock Mechanics, pages 35 to 42. Laurentian University. Sudbury, Ontario, Canada.

Hanson, D., W. Quesnel, and R. Hong, 1987. *Destressing a Rockburst-Prone Crown Pillar – Macassa Mine*. CANMET, Mining Research Laboratories, Report #MRL 87-82 (TR), 66 pages. Elliot Lake, Ontario, Canada.

Harling, J., 1965. *Report on Longhole Destressing in the Kirkland Lake Camp*. Ground Control Principles, RB-12, 22 pages.

Harries, G., 1983. *The Modelling of Long Cylindrical Charges of Explosives*. In the proceedings of the First International Symposium on Rock Fragmentation by Blasting (FRAGBLAST'1 – P.-A. Persson, editor), pages 419 to 431. Luleå, Sweden. Published by A. A. Balkema, Rotterdam, Netherlands.

Harries, G., 1973. *A Mathematical Model of Cratering and Blasting*. National Symposium on Rock Fragmentation, pages 41 to 54. Adelaide, Australia.

Hart, R., M. Board, B. Brady, B. O'Hearn, and G. Allan, 1988. *Examination of Fault-Slip-Induced Rockbursting at the Strathcona Mine*. In "Key Questions in Rock Mechanics", proceedings of the 29th U.S. Symposium on Rock Mechanics (P. Cundall, R. Sterling and A. Starfield, editors), pages 369-379. Minneapolis, Minnesota, USA. Published by A. A. Balkema, Rotterdam, Netherlands.

Hedley, D., 1992. *Rockburst Handbook for Ontario Hardrock Mines*. CANMET Special Report SP92-1E. Canada Centre for Mineral and Energy Technology, Mining Research Laboratories, 305 pages. Ottawa, Ontario, Canada.

Heilig, J., and C. McKenzie, 1995. *Estimating and Controlling Blast Vibration-Induced Damage Around Underground Excavations*. Report by BLM Blastronics Canada, Inc., to the CAMIRO Mining Division, 37 pages. Sudbury, Ontario, Canada.

Heuze, F., O. Walton, D. Maddix, R. Shafer, and T. Butkovich, 1990. *Analysis of Explosions in Hard Rocks: the Power of Discrete Element Modelling*. In

"Mechanics of Jointed and Faulted Rock" (H. Rossmanith, editor), pages 21 to 28. Published by A. A. Balkema, Rotterdam, Netherlands.

Hill, F., and R. Plewman, 1957. *Destressing : A Means of Ameliorating Rockburst Conditions – Part II. Implementing Destressing With a Discussion of the Results so Far Obtained.* Journal of the South African Institute of Mining and Metallurgy, pages 120 to 127. Johannesburg, Republic of South Africa.

Hoek, E., 1998. *Rock Engineering Course Notes*. University of Toronto, Department of Civil Engineering, 313 pages. Toronto, Ontario, Canada.

Hoek, E., and E. T. Brown, 1997. *Practical Estimates of Rock Mass Strength*. International Journal of Rock Mechanics, Mining Sciences and Geomechanics Abstracts, Vol. 34, No. 8, pages 1165 to 1186.

Hoek, E., P. Kaiser, and W. Bawden, 1995. *Support of Underground Excavations in Hard Rock.* 215 pages. Published by A. A. Balkema, Rotterdam, Netherlands.

Hoek, E., 1994. *Strength of Rock and Rock Masses*. International Society of Rock Mechanics News Journal, Vol. 2, No. 2, pages 4 to 16. Lisbon, Portugal.

Hoek, E., D. Wood, and S. Shah, 1992. *A Modified Hoek-Brown Criterion for Jointed Rock Masses.* In "Rock Characterisation", proceedings of the Eurock'92 symposium of the International Society of Rock Mechanics (J. Hudson, editor), pages 209 to 214. London, England.

Hoek, E., and E. T. Brown, 1988. *The Hoek-Brown Failure Criterion – a 1988 Update*. In "Rock Engineering for Underground Excavations" (J. Curran, editor), proceedings of the 15th Canadian Rock Mechanics Symposium, pages 31 to 38. Department of Civil Engineering, University of Toronto. Toronto, Ontario, Canada.

Hoek, E., 1983. *Strength of Jointed Rock Masses*. 23rd Rankine Lecture, published in Géotechnique, Vol. 33, No. 3, pages 187 to 223.

Hoek, E., and E. T. Brown, 1980. *Underground Excavations in Rock.* Published by the Institution of Mining and Metallurgy, 527 pages. London, England.

Holmberg, R., and P.-A. Persson, 1980. *Design of Tunnel Perimeter Blasthole Patterns to Prevent Rock Damage*. In the Transactions of the Institution of Mining and Metallurgy, Section A: Mineral Industry, Vol. 89, pages A37 to A40. London, England.

Homand, F., J.-P. Piguet, and R. Revalor, 1988. *Dynamic Phenomena in Mines and Characteristics of Rocks*. In the proceedings of the Second International Congress on Rockbursts and Seismicity in Mines (C. Fairhurst, editor), pages 139 to 142. Minneapolis, Minnesota, U.S.A. Published by A. A. Balkema, Rotterdam, Netherlands.

Hucka, V., and B. Das, 1974. *Brittleness Determination of Rocks by Different Methods*. International Journal of Rock Mechanics and Mining Sciences, Vol. 11, pages 389 to 392.

Hudson, J. A., and J. P. Harrison, 1997. *Engineering Rock Mechanics – An Introduction to the Principles*. Pergamon Press, 444 pages. London, England.

Hudson, J. A., 1992. *Rock Engineering Systems: Theory and Practice*. Ellis Horwood Series in Civil Engineering – Geotechnics, 185 pages. New York, New York, U.S.A.

Inyang, H., 1991. *Development of a Preliminary Rock Mass Classification Scheme for Near Surface Excavations*. International Journal of Surface Mining and Reclamation, Vol. 5, pages 65 to 74.

Jenkins, F., and T. McMahon, 1987. *A History of Rockburst Research in the Coeur d'Alene Mining District*. In the proceedings of the Sixth International Conference on Ground Control in Mines, pages 61 to 78. Conference organised by the U.S. Bureau of Mines, U.S. Department of the Interior,. Morgantown, West Virginia, U.S.A.

Kahraman, S., 2002. *Correlation of TBM and Drilling Machine Performances With Rock Brittleness*. In Engineering Geology, Vol. 65(h), pages 269 to 283.

Kaiser, P., D. McCreath, and D. Tannant, 1996. *Canadian Rockburst Support Handbook – Draft Version*. Published by the Geomechanics Research Centre, Laurentian University, 314 pages. Sudbury, Ontario, Canada.

Karwoski, W., W. McLaughlin, and W. Blake, 1979. *Rock Preconditioning to Prevent Rockbursts – Report on a Field Demonstration*. Report of Investigation RI 8381, U.S. Bureau of Mines, U.S. Department of the Interior, 47 pages. Spokane, Washington, U.S.A.

Katsabanis, P. D., 2001. *Application of Numerical Modelling to Practical Blast Design*. In the proceedings of the 24th Study Session on Blasting Techniques, SEEQ, 15 pages. Quebec City, Quebec, Canada.

Katsabanis, P. D., and L. Liu, 1998. *A Numerical Study of Some Aspects of the Spherical Charge Cratering Theory*. FRAGBLAST – The International Journal of Blasting and Fragmentation, Vol. 2, No. 2, pages 219 to 233.

Kidybinski, A., 1981. *Bursting Liability Indices in Coal*. International Journal of Rock Mechanics and Mining Sciences, Vol. 18, pages 295 to 304.

Kirsch, G., 1898. *The Theory of Elasticity and the Needs of the Strength Theory*. In German. Veit. Deut. Ing., Vol. 42, No. 28, pages 797 to 807.

Kleine, T., A. Cocker, and A. Kavetsky, 1990. *The Development and Implementation of a Three Dimensional Model of Blast Fragmentation and Damage*. In the proceedings of the Third International Symposium on Rock Fragmentation by Blasting (FRAGBLAST'3 – C. McKenzie, editor), pages 181 to 187. Brisbane, Queensland, Australia. Published by A. A. Balkema, Rotterdam, Netherlands.

Krauland, N., P.-I. Marklund, and M. Board, 2001. *Rock Support in Cut-and-Fill Mining at the Kristineberg Mine*. In the "Underground Mining Methods – Engineering Fundamentals and International Case Studies" Handbook of the Society of Mining Engineers (W. Hustrulid & R. Bullock, editors), pages 325 to 332. Published by the American Institute of Mining and Exploration. Littleton, Colorado, U.S.A.

Labrie, D., M. Plouffe, A. Harvey, and C. Major, 1996. *Destress Blast Testing at Sigma Mine: Experimentation and Results*. In the proceedings of the 19th Study Session on Blasting Techniques, SEEQ, 24 pages. Quebec City, Quebec, Canada.

Last, N., and T. Harper, 1990. *Response of Fractured Rock Subject to Fluid Injection – Part I: Development of a Numerical Model; Part II: Characteristic Behaviour; Part III: Practical Application*. In " Tectonophysics", Vol. 172, pages 1 to 65.

Latham, J.-P., and P. Lu, 1999. *Development of an Assessment System for the Blastability of Rock Masses*. International Journal of Rock Mechanics and Mining Sciences, Vol. 36, pages 41 to 55.

Lightfoot, N., and O. Goldbach, 1995. *Controlled Fault Slip: Water Injection*. SIMRAC report, Project GAP 030, 168 pages. Johannesburg, Republic of South Africa.

Lightfoot, N., 1993. *The Use of Numerical Modelling in Rockburst Control*. In the proceedings of the Third International Congress on Rockbursts and Seismicity in Mines (P. Young, editor), organised by Queen's University, pages 355 to 360. Kingston, Ontario, Canada. Published by A. A. Balkema, Rotterdam, Netherlands.

Lilly, P. A., 1986. *An Empirical Method of Assessing Rock Mass Blastability*. Large Open Pit Conference, Australasian Institute of Mining and Metallurgy, pages 89 to 92.

Madariaga, R., 1979. *Dynamics of an Expanding Circular Fault*. Bulletin of the Seismological Society of America, Vol. 66, pages 639 to 666.

Mandelbrot, B., 1982. *The Fractal Geometry of Nature*. 480 pages. Published by Freeman, Ltd. San Francisco, California, U.S.A.

Margolin, L., 1983. *Elastic Moduli of a Cracked Body*. International Journal of Fracture, Vol. 22, No. 1, pages 65 to 79.

Mathews, K., E. Hoek, D. Wyllie, and S. Stewart, 1980. *Prediction of Stable Excavations for Mining at Depths Below 1000m in Hard Rock*. CANMET Report 802-1571, MRL, 134 pages. Ottawa, Ontario, Canada.

McHugh, S., 1983[a]. *Computational Simulations of Dynamically-Induced Fractures and Fragmentation*. In the proceedings of the First International Symposium on Rock Fragmentation by Blasting (FRAGBLAST'1 – P.-A. Persson, editor), pages 407 to 418. Luleå, Sweden. Published by A. A. Balkema, Rotterdam, Netherlands.

McHugh, S., 1983[b]. *Crack Extension Caused by Internal Gas Pressure Compared With Extension Caused by Tensile Stress*. International Journal of Fracture, Vol. 21, pages 163 to 176.

Mendecki, A., 1997. *Seismic Monitoring in Mines*. Chapman & Hall, 262 pages. London, England.

Mikula, P., M. Lee, and K. Guilfoyle, 1995. *Preconditioning a Large Pillar at Mount Charlotte Mine*. In the proceedings of the Underground Operators Conference, pages 265 to 272. Kalgoorlie, Western Australia, Australia.

Minchinton, A., and P. Lynch, 1996. *Fragmentation and Heave Modelling Using a Coupled Discrete Element Gas Flow Code*. In the proceedings of the Fifth International Symposium on Rock Fragmentation by Blasting (FRAGBLAST'5 – B. Mohanty, editor), pages 71 to 80. Montreal, Quebec, Canada. Published by A. A. Balkema, Rotterdam, Netherlands.

Mitri, H., 2000. *Practitioner's Guide to Destress Blasting in Hard Rock Mines*. Technical study financed by the IRSST and published by McGill University, Faculty of Engineering, Department of Mining and Metallurgical Engineering, 201 pages. Montreal, Quebec, Canada.

Mortazavi, A., P. Andrieux, and R. Brummer, 2001. *Modelling of Blast-Induced Stress Wave Propagation and Fracturing in Hard Rock Material*. Itasca Consulting Canada, Inc. report to INCO Mines Research, 74 pages. Sudbury, Ontario, Canada.

Mortazavi, A., and P. D. Katsabanis, 1998. *Discontinuum Modelling of Blasthole Expansion and Explosive Gas Pressurisation in Jointed Media*. International Journal of Rock Mechanics and Mining Science, Vol. 35, Paper No. 48, pages 487 to 498.

Moruzi, G., and A. Pasieka, 1964. *Evaluation of a Blasting Technique for Destressing*. In the proceedings of the Sixth American Symposium on Rock Mechanics, pages 185 to 204. University of Missouri-Rolla. Rolla, Missouri, U.S.A.

Nelson, D. (editor), 1998. *The Penguin Dictionary of Mathematics – Second Edition*. Penguin Books, Ltd., 461 pages. New York, New York, U.S.A.

Neyman, B., Z. Szecowka, and W. Zuberek, 1972. *Effective Methods for Fighting Rockburst in Polish Collieries*. In the proceedings of the Fifth International Strata Control Conference, pages 23.1 to 23.9. Düsseldorf, Germany.

Nicholson, G., and Z. Bieniawski, 1990. *A Non-Linear Deformation Modulus Based on Rock Mass Classification*. International Journal of Mining and Geological Engineering, Vol. 8, No. 3, pages 181 to 202.

Nickson, S., A. Coulson, and J. Hussey, 2001. *Noranda's Approach to Evaluating a Competent Deposit for Caving*. In the "Underground Mining Methods – Engineering Fundamentals and International Case Studies" Handbook of the Society of Mining Engineers (W. Hustrulid & R. Bullock, editors), pages 521 to 534. Published by the American Institute of Mining and Exploration. Littleton, Colorado, U.S.A.

Nilson, R., W. Proffer, and R. Duff, 1985. *Modelling of Gas-Driven Fractures Induced by Propellant Combustion Within a Borehole*. International Journal of Rock Mechanics, Mining Sciences and Geomechanics Abstracts, Vol. 22, pages 3 to 19.

O'Donnell, D. (Sr.), 1999. *The Development and Application of Destressing Techniques in the Mines of INCO Limited, Sudbury, Ontario*. M. Sc. Thesis, Department of Mining Engineering, Laurentian University, 141 pages. Sudbury, Ontario, Canada.

O'Donnell, D. (Sr.), 1992. *The Use of Destressing at INCO's Creighton Mine*. In the proceedings of the MASSMIN'92 conference (organised by the South African Institute of Mining and Metallurgy), pages 71 to 74. Johannesburg, Republic of South Africa.

Oliver, P., T. Wiles, P. MacDonald, and D. O'Donnell (Sr.), 1987. *Rockburst Control Measures at INCO's Creighton Mine*. In the proceedings of the Sixth International Conference on Ground Control in Mines, pages 79 to 90. Conference organised by the U.S. Bureau of Mines, U.S. Department of the Interior. Morgantown, West Virginia, U.S.A.

Ortlepp, D., 1983. *The Mechanisms and Control of Rockbursts*. In the book "Rock Mechanics in Mining Practice" (S. Budavari, editor), published by the South African

Institute of Mining and Metallurgy, Mono Series No. 5, pages 257 to 282. Johannesburg, Republic of South Africa.

Palmström, A., 1982. *The Volumetric Joint Count – A Useful and Simple Measure of the Degree of Jointing*. In the proceedings of the Fourth Congress of the International Association of Engineering Geologists, pages 221 to 228. New Delhi, India.

Pierce, M., and M. Board, 1999 [a]. *Modelling of Sill Pillar Extraction in the Deep Copper Zone of Strathcona Mine*. Technical report from the Itasca Consulting Group to Falconbridge, Ltd., 30 pages. Minneapolis, Minnesota, U.S.A.

Pierce, M., and M. Board, 1999 [b]. *Modelling of Sill Pillar Extraction in the Deep Copper Zone of Strathcona Mine – Additional Recommendations*. Technical report from the Itasca Consulting Group to Falconbridge, Ltd., 27 pages. Minneapolis, Minnesota, U.S.A.

Potvin, Y., and J. Hadjigeorgiou, 2001. *The Stability Graph Method for Open Stope Design*. In the "Underground Mining Methods – Engineering Fundamentals and International Case Studies" Handbook of the Society of Mining Engineers (W. Hustrulid & R. Bullock, editors), pages 513 to 520. Published by the American Institute of Mining and Exploration. Littleton, Colorado, U.S.A.

Potyondy, D., and P. Cundall, 1996. *Modelling of Shock- and Gas-Driven Fractures Induced by a Blast Using Bonded Assemblies of Spherical Particles*. In the proceedings of the Fifth International Symposium on Rock Fragmentation by Blasting (FRAGBLAST'5 – B. Mohanty, editor), pages 55 to 61. Montreal, Quebec, Canada. Published by A. A. Balkema, Rotterdam, Netherlands.

Preece, D., S. Burchell, and S. Scovira, 1993. *Coupled Explosive Gas Flow and Rock Motion Modelling With Comparison to Bench Blast Field Data*. In the proceedings of the Fourth International Symposium on Rock Fragmentation by Blasting (FRAGBLAST'4 – H.-P. Rossmanith, editor), pages 239 to 245. Vienna, Austria. Published by A. A. Balkema, Rotterdam, Netherlands.

Roux, A., E. Leeman, and H. Denkhaus, 1957. *Destressing : A Means of Ameliorating Rockburst Conditions – Part I.* Journal of the South African Institute of Mining and Metallurgy, pages 101 to 119. Johannesburg, Republic of South Africa.

Ruest, M., 2001. Personal communication. Itasca Consulting Group. Minneapolis, Minnesota, U.S.A.

Ryder, J., 1988. *Excess Shear Stress in the Assessment of Geologically Hazardous Situations*. Journal of the South African Institute of Mining and Metallurgy, Vol. 88, No. 1, pages 27 to 39. Johannesburg, Republic of South Africa.

Ryder, J., 1987. *Excess Shear Stress (ESS) : An Engineering Criterion for Assessing Unstable Slip and Associated Rockburst Hazards*. In the proceedings of the Sixth International Conference on Rock Mechanics, Vol. 2, pages 1211 to 1215. Montreal, Quebec, Canada.

Salamon, M., 1984. *Energy Considerations in Rock Mechanics: Fundamental Results*. Journal of the South African Institute of Mining and Metallurgy, Vol. 84, No. 8, pages 233 to 246. Johannesburg, Republic of South Africa.

Salamon, M., 1974. *Rock Mechanics of Underground Excavations*. In the proceedings of the Third Congress of the International Society of Rock Mechanics, Vol. 1, Part B, pages 951 to 1099. Denver, Colorado, U.S.A.

Sampson-Forsythe, A., P. Andrieux, and R. Brummer, 2002. *Report on the Destress Blast of 24 December 2001 in 42-1-1620 Stope, 080 Access, Fraser Copper Mine*. Joint Falconbridge, Ltd. and Itasca Consulting Canada, Inc. internal report to Fraser Mine, 42 pages. Sudbury, Ontario, Canada.

Sampson-Forsythe, A., and P. Andrieux, 2001. *Destress Blasting in 42-1-1620 Stope, 080 Access – Project Update*. Joint Falconbridge, Ltd. and Itasca Consulting Canada, Inc. internal report to Fraser Mine, 10 pages. Sudbury, Ontario, Canada.

Scott, A., 1996. *"Blastability" and Blast Design*. In the proceedings of the Fifth International Symposium on Rock Fragmentation by Blasting (FRAGBLAST'5 – B. Mohanty, editor), pages 27 to 36. Montreal, Quebec, Canada. Published by A. A. Balkema, Rotterdam, Netherlands.

Serafim, J., and J. Pereira, 1983. *Considerations of the Geomechanical Classification of Bieniawski*. In the proceedings of the 12th Congress on Large Dams, pages 59 to 68. Mexico City, Mexico.

Shah, K., and J. Labuz, 1995. *Damage Mechanisms in Stressed Rock from Acoustic Emission*. In the Journal of Geophysics Research, Vol. 100, No. B8, pages 15527 to 15539.

Shi, G.-H., 1992. *Block System Modelling by Discontinuous Deformation Analysis*. WIT Press, 228 pages. Southampton, England.

Simon, R., M. Aubertin, and D. E. Gill, 1998. *Guide for the Evaluation of the Rockburst Potential in Mines With the ERP Methodology*. In French. Technical study financed by the IRSST and published by the École Polytechnique de Montréal, Department of Mineral Engineering, 122 pages. Montreal, Quebec, Canada.

Simon, R., M. Aubertin, and H. Mitri, 1995. *Evaluation of Rockburst Potential in Hard Rock Mines*. In the proceedings of the 97th Annual General Meeting of the Canadian Institute of Mining, Metallurgy and Petroleum, 10 pages. Halifax, Nova Scotia, Canada.

Simser, B., and V. Falmagne, 2004. *Seismic Source Parameters Used to Monitor Rockmass Response at Brunswick Mine*. In the Bulletin of the Canadian Institute of Mining, Metallurgy and Petroleum, Vol. 97, No. 1080, pages 58 to 63. Montreal, Quebec, Canada.

Simser, B., February 2004. Personal communication. Sudbury, Ontario, Canada.

Simser, B., P. Andrieux, V. Falmagne, A. Coulson, and M. Grenon, 2002. *The Rock Mechanics Design for a 352,800 Tonne Mass-Blast at the Brunswick Mine, Bathurst, New Brunswick*. In the proceedings of the 5th North American Rock Mechanics Symposium ("NARMS–TAC 2002: Mining and Tunnelling Innovation and Opportunity" – R. Hammah, W. Bawden, J. Curran, and M. Telesnicki, editors), Vol. 1, pages 815 to 823. Published by the University of Toronto Press. Toronto, Ontario, Canada.

Simser, B., 2000. *Seismic Source Parameters – An Engineering Perspective*. In the proceedings of the Mining Seismicity Workshop, CAMIRO – Mining Division. On CD-ROM, 19 pages. Sudbury, Ontario, Canada.

Simser, B., and P. Andrieux, 1999. *Seismic Source Mechanisms at Brunswick Mine*. In the proceedings of the 14th Mine Operators' Conference of the Canadian Institute of Mining, Metallurgy and Petroleum, 12 pages. Bathurst, New Brunswick, Canada.

Simser, B., P. Andrieux, D. Peterson, T. MacDonald, and J. Alcott, 1998. *Advanced Monitoring and Analysis of Microseismic Activity as an Aid to Mining at Brunswick Mine*. In the proceedings of the Third North American Rock Mechanics Symposium (NARMS'98), Paper No. CAN-310. On CD-ROM, 16 pages. Cancún, Quintana Roo, Mexico.

Singh, P., 1987. *Chemical Destressing to Alleviate Rockbursts*. In the proceedings of the Sixth International Conference on Ground Control in Mining, pages 70-78. Conference organised by the U.S. Bureau of Mines, U.S. Department of the Interior. Morgantown, West Virginia, U.S.A.

Slade, A., 1968. *Some Practical Aspects of Rock Mechanics in Falconbridge's Sudbury Operations*. In the Bulletin of the Canadian Institute of Mining, Metallurgy and Petroleum, Vol. 61, No. 678, pages 1161 to 1165. Montreal, Quebec, Canada.

Starfield, A., and J. Pugliese, 1968. *Compression Waves Generated in Rock by Cylindrical Explosive Charges: A Comparison Between Computer Model and Field Measurements*. International Journal of Rock Mechanics, Mining Sciences and Geomechanics Abstracts, Vol. 5, pages 65 to 77.

Tao, Z., 1988. *Support Design of Tunnels Subjected to Rockbursting*. In "Rock Mechanics and Power Plants" (M. Romana, editor), pages 407 to 411. Published by A. A. Balkema, Rotterdam, Netherlands.

Telford, W., L. Geldart, and R. Sheriff, 1994. *Applied Geophysics – Second Edition*. Published by the Cambridge University Press, 770 pages. Cambridge, England.

Terzaghi, K., 1946. *Rock Defects and Loads on Tunnel Support*. In "Rock Tunnelling With Steel Support" (R. Proctor & T. White, editors), Vol. 1, pages 17 to 99.

Published by the Commercial Shearing and Stamping Company. Youngston, Ohio, U.S.A.

Toper, A., 2002. *Destressing/Preconditioning to Control Rockbursts in South African Deep-Level Gold Mines*. In the proceedings of the First International Seminar on Deep and High Stress Mining, organised by the Australian Centre for Geomechanics, 27 pages. Perth, Western Australia, Australia.

Toper, A., M. Grodner, R. Stewart, and N. Lightfoot, 1997. *Preconditioning : A Rockburst Control Technique*. In the book "Rockbursts and Seismicity in Mines" (S. Gibowicz & S. Lasocki, editors), pages 267 to 272. Published by A. A. Balkema, Rotterdam, Netherlands.

Tran, H., and Q. Liu, 1997. *Literature review of Current Destressing Technology*. Noranda Technology Centre, Mines and Exploration Division – Geomechanics Programme, 27 pages. Pointe-Claire (Montreal), Quebec, Canada.

Tyser, J., 1982. *Panel discussion*. During the First International Congress on Rockbursts and Seismicity in Mines (organised by the South African Institute of Mining and Metallurgy). Johannesburg, Republic of South Africa.

Valliappan, S., and K. Ang, 1988. *Finite Element Analysis of Vibrations Induced by Propagating Waves Generated by Tunnel Blasting*. Rock Mechanics and Rock Engineering, Vol. 21, pages 53 to 78.

van Aswegen, G., and A. Butler, 1993. *Application of Quantitative Seismology in South African Gold Mines*. In the proceedings of the Third International Congress on Rockbursts and Seismicity in Mines (P. Young, editor), organised by Queen's University, pages 261 to 266. Kingston, Ontario, Canada. Published by A. A. Balkema, Rotterdam, Netherlands.

Vardoulakis, I., 1984. *Rock Bursting as a Surface Instability Phenomenon*. International Journal of Rock Mechanics, Mining Sciences and Geomechanics Abstracts, Vol. 21, pages 137 to 144.

Walsh, J., and W. Brace, 1964. *A Fracture Criterion for Brittle Anisotropic Rock*. In the Journal of Geophysics Research, Vol. 69, pages 3449 to 3456.

Wickham, G., H. Tiedemann, and E. Skinner, 1972. *Support Determination Based on Geologic Prediction*. In the proceedings of the North American Rapid Excavation and Tunnelling Conference (K. Lane & L. Garfield, editors), pages 43 to 64. Chicago, Illinois, U.S.A.

Will, M., 1982. *Seismic Observations During Test Drilling and Destressing Operations in German Coal Mines*. In the proceedings of the First International Congress on Rockbursts and Seismicity in Mines, organised by the South African Institute of Mining and Metallurgy (N. Gay & E. Wainwright, editors), pages 231 to 234. Johannesburg, Republic of South Africa.

Xie, H., and G. Pariseau, 1992. *Studies on Mechanism of Rockburst-Associated Seismicity in Mines by Using Fractals and Damage Mechanics*. In the proceedings of the 33rd U.S. Symposium on Rock Mechanics (J. Tillerson & W. Wawersik, editors), pages 745 to 754. Santa Fe, New Mexico, U.S.A. Published by A. A. Balkema, Rotterdam, Netherlands.

Yang, R., and A. Kavetsky, 1990. *A Three Dimensional Model of Muckpile Formation and Grade Boundary Movement in Open Pit Blasting*. In the International Journal of Mining and Geological Engineering, Vol. 8, pages 13 to 34.

Zipf, R., and K. Heasley, 1990. *Decreasing Coal Bump Risk Through Optimal Cut Sequencing With a Non-Linear Boundary Element Program*. In "Rock Mechanics – Contributions and Challenges", proceedings of the 31st U.S. Symposium on Rock Mechanics (W. Hustrulid & G. Johnson, editors), pages 77 to 84. Colorado School of Mines. Boulder, Colorado, U.S.A. Published by A. A. Balkema, Rotterdam, Netherlands.

INDEX OF TOPICS

INDEX OF REFERENCED AUTHORS